EVOLVING PICTURE OF CALCIUM HANDLING IN CARDIAC DISEASE

EDITED BY: Maria Fernandez-Velasco, Angélica Rueda, Gema Ruiz-Hurtado and Laetitia Pereira

PUBLISHED IN: Frontiers in Physiology

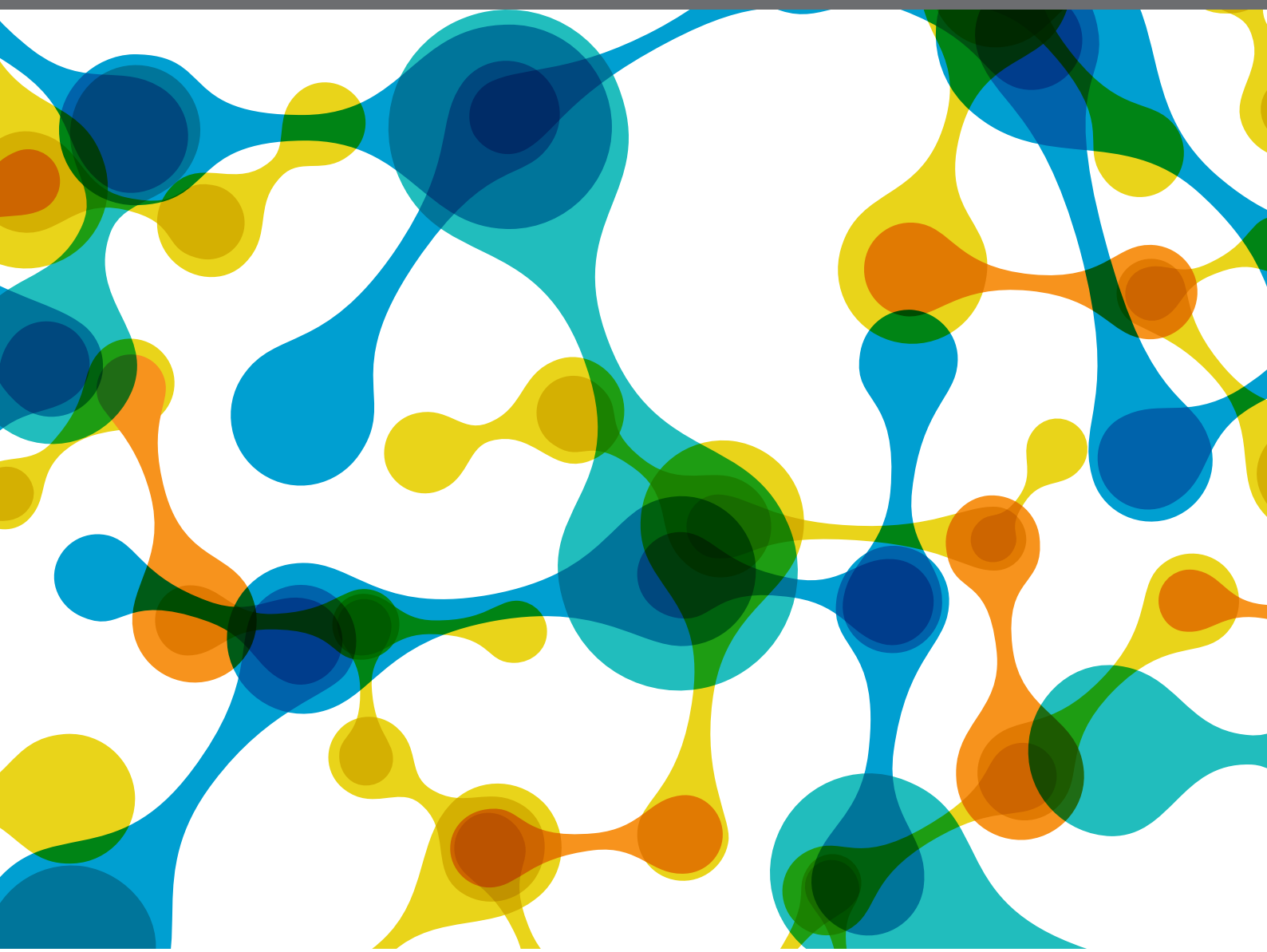

frontiers Research Topics

frontiers

ISSN 1664-8714
ISBN 978-2-88966-123-7
DOI 10.3389/978-2-88966-123-7

About Frontiers

Frontiers is more than just an open-access publisher of scholarly articles: it is a pioneering approach to the world of academia, radically improving the way scholarly research is managed. The grand vision of Frontiers is a world where all people have an equal opportunity to seek, share and generate knowledge. Frontiers provides immediate and permanent online open access to all its publications, but this alone is not enough to realize our grand goals.

Frontiers Journal Series

The Frontiers Journal Series is a multi-tier and interdisciplinary set of open-access, online journals, promising a paradigm shift from the current review, selection and dissemination processes in academic publishing. All Frontiers journals are driven by researchers for researchers; therefore, they constitute a service to the scholarly community. At the same time, the Frontiers Journal Series operates on a revolutionary invention, the tiered publishing system, initially addressing specific communities of scholars, and gradually climbing up to broader public understanding, thus serving the interests of the lay society, too.

Dedication to Quality

Each Frontiers article is a landmark of the highest quality, thanks to genuinely collaborative interactions between authors and review editors, who include some of the world's best academicians. Research must be certified by peers before entering a stream of knowledge that may eventually reach the public - and shape society; therefore, Frontiers only applies the most rigorous and unbiased reviews.
Frontiers revolutionizes research publishing by freely delivering the most outstanding research, evaluated with no bias from both the academic and social point of view. By applying the most advanced information technologies, Frontiers is catapulting scholarly publishing into a new generation.

What are Frontiers Research Topics?

Frontiers Research Topics are very popular trademarks of the Frontiers Journals Series: they are collections of at least ten articles, all centered on a particular subject. With their unique mix of varied contributions from Original Research to Review Articles, Frontiers Research Topics unify the most influential researchers, the latest key findings and historical advances in a hot research area! Find out more on how to host your own Frontiers Research Topic or contribute to one as an author by contacting the Frontiers Editorial Office: researchtopics@frontiersin.org

EVOLVING PICTURE OF CALCIUM HANDLING IN CARDIAC DISEASE

Topic Editors:
Maria Fernandez-Velasco, University Hospital La Paz, Spain
Angélica Rueda, National Polytechnic Institute of Mexico (CINVESTAV), Mexico
Gema Ruiz-Hurtado, Instituto de Investigación Hospital 12 de Octubre, Spain
Laetitia Pereira, Institut National de la Santé et de la Recherche Médicale (INSERM), France

Citation: Fernandez-Velasco, M., Rueda, A., Ruiz-Hurtado, G., Pereira, L., eds. (2020). Evolving Picture of Calcium Handling in Cardiac Disease. Lausanne: Frontiers Media SA. doi: 10.3389/978-2-88966-123-7

Table of Contents

frontiers in Physiology

EDITORIAL
published: 04 September 2020
doi: 10.3389/fphys.2020.01013

Editorial: Evolving Picture of Calcium Handling in Cardiac Disease

Gema Ruiz-Hurtado [1,2†], Angélica Rueda [3†], Laetitia Pereira [4†] and María Fernández-Velasco [5,6]*

[1] Cardiorenal Translational Laboratory, Institute of Research i+12, University Hospital 12 de Octubre, Madrid, Spain, [2] CIBER-CV, University Hospital 12 de Octubre, Madrid, Spain, [3] Department of Biochemistry, Center for Research and Advanced Studies of the National Polytechnic Institute (CINVESTAV-IPN), Mexico City, Mexico, [4] UMR-S1180, Université Paris-Saclay, Châtenay-Malabry, France, [5] La Paz University Hospital Health Research Institute, IdiPAZ, Madrid, Spain, [6] CIBER-CV, Alberto Sols Biomedical Research Institute, Madrid, Spain

Keywords: calcium handling, ryanodine, heart disease, ion channels, EC coupling

Editorial on the Research Topic

Evolving Picture of Calcium Handling in Cardiac Disease

Cardiovascular diseases (CVDs) underlie a high rate of mortality worldwide. Both acquired and inherited CVDs are closely related to ionic channelopathies, compromising the expression and function of a wide number of ion channels. Ca^{2+} mishandling has been associated with several CVDs, such as those involved in metabolic disorders, hypertrophy, heart failure, and several inherited heart diseases that implicate cardiac dysfunction and arrhythmias (Kushnir et al., 2018). Moreover, the archives of biomedical and life sciences are showing a multitude of contributions related to this topic, demonstrating the high interest of the scientific community in this specific research field. Indeed, Ca^{2+} is the key regulator of the Ca^{2+} induced Ca^{2+} release (CICR) process, the main actor in cardiac excitation-contraction coupling (ECC) (Fabiato, 1983). Briefly, ECC begins with membrane depolarization of cardiomyocytes, activating sarcolemmal L-type voltage-dependent Ca^{2+} channels, thus promoting an inward Ca^{2+} current (I_{CaL}) that activates the intracellular Ca^{2+} channel/ryanodine receptor type 2 (RyR2), located at the sarcoplasmic reticulum (SR), triggering a transient increase of cytosolic Ca^{2+} levels, and eliciting cell contraction. To get new insights into these processes, Aguilar-Sanchez et al. evaluated in an elegant study whether the autonomous system regulates ECC in endocardial and epicardial layers from intact beating mouse hearts. The authors recorded action potentials (APs), Ca^{2+} transients, and Ca^{2+} currents in whole hearts, demonstrating that the Ca^{2+} influx occurring in AP phase 1, and not in phase 2, triggers ECC (Aguilar-Sanchez et al.).

After contraction, relaxation takes place when cytosolic Ca^{2+} levels return to physiological resting levels by two main mechanisms, the Sarco/Endoplasmic Reticulum Ca^{2+} ATPase (SERCA2a pump) and the sarcolemma Na^{+}- Ca^{2+} exchanger (NCX) (Bers, 2002). More recently, other elements have been described as involved in the control of cardiac intracellular Ca^{2+} handling, such as transient receptor potential (TRP) channels or organelles such as the nucleus or mitochondria that also rely on transporters or channels for Ca^{2+} dynamics. The fine orchestration of all these elements results in adequate ECC and cell contraction.

Since its discovery (Inui et al., 1987), RyR2 has acquired special interest, and a large number of studies have analyzed whether changes in the structure, genetics, and function of this macro channel are involved in the pathogenesis of several CVDs. Post-translational modifications of RyR2, such as phosphorylation and oxidation, have gained major attention and have been related to channel dysfunction in some CVDs such as heart failure. Leading groups in the field have focused their interest in analyzing the physio-pathological regulation of RyR2 function by protein

OPEN ACCESS

Edited by:
Christoph Fahlke, Julich Research Center, Helmholtz Association of German Research Centers (HZ), Germany

Reviewed by:
Gabriel Stölting, Charité – Universitätsmedizin Berlin, Germany

***Correspondence:**
María Fernández-Velasco
maria.fernandez@idipaz.es;
mvelasco@iib.uam.es

† These authors have contributed equally to this work

Specialty section:
This article was submitted to Membrane Physiology and Membrane Biophysics, a section of the journal Frontiers in Physiology

Received: *01 June 2020*
Accepted: *24 July 2020*
Published: *04 September 2020*

Citation:
Ruiz-Hurtado G, Rueda A, Pereira L and Fernández-Velasco M (2020) Editorial: Evolving Picture of Calcium Handling in Cardiac Disease. Front. Physiol. 11:1013. doi: 10.3389/fphys.2020.01013

kinase A or calmodulin kinase type II-dependent phosphorylation. In this line, Federico et al. have performed an interesting review article that addresses the most relevant findings related to changes in SR-Ca^{2+} uptake and post-translational modifications in RyR2, such as the phosphorylation and oxidation both linked to arrhythmias and other cardiac disturbances. In the same line, Fernández-Miranda et al. demonstrated in a prediabetic rat model of metabolic syndrome an "*in situ*" impairment of RyR2 function elicited by reduced levels of RyR2 phosphorylation, together with depressed SR-Ca^{2+} uptake by SERCA2a, which are responsible for the poor cardiac outcome linked to this metabolic disorder.

In addition to phosphorylation, redox modifications of RyR2 such as S-nitrosylation and S-glutathionylation have emerged as new and potent modulators of channel function, demonstrating a crosslink between oxidation and phosphorylation changes. In many cases, changes in the redox state of RyR2 participate in the generation of abnormal Ca^{2+} diastolic release, supporting an additional pro-arrhythmogenic mechanism in several CVDs. Nikolaienko et al. recapitulate in a remarkable review article the most significant findings related to whether redox modifications of RyR2 can induce channel dysfunction. In this line, Hamilton et al. tested the efficacy of mitochondria-targeted pharmacological interventions to attenuate cardiac arrhythmia at the cellular level and in "*ex-vivo*" hypertrophied thoracic aortic-banded mouse hearts. The authors demonstrated that the abnormal mitochondrial Ca^{2+} accumulation induced an excessive production of reactive oxygen species that promoted the oxidation of RyR2 and enhanced its activity, inducing a pro-arrhythmic spontaneous Ca^{2+} release (Hamilton et al.).

Besides this, increased reactive oxygen species can also activate the inflammatory response. In many cases, pro-inflammatory mediators result in intracellular Ca^{2+} mishandling. In this regard, Val-Blasco et al. have determined whether the lack of the pro-inflammatory mediator NOD1 (a specific innate immune receptor) improves the β-adrenergic regulation of intracellular Ca^{2+} dynamics in failing hearts. NOD1 is a well-known activator of the inflammatory response. An increasing amount of evidences suggest that inflammatory mediators participate in the progression of CVDs (Adamo et al., 2020). Inflammation and metabolic disorders are closely related, and in many cases involve changes in cardiac Ca^{2+} homeostasis. A well-designed report, published by Delgado et al. has addressed the role of the inflammatory mediator tumor necrosis factor (TNF)-α in the modulation of intracellular Ca^{2+} handling in a mouse model of diabetes type II (*db/db*). The authors demonstrated a different regulation of Ca^{2+} handling mediated by TNF-α in male compared to female *db/db* mice, supporting the idea of a cardioprotective role of gender in the Ca^{2+} mishandling linked to a pro-inflammatory environment (Delgado et al.).

Another interesting contribution has been supported by Cagalinec et al. using a transgenic rat model with a mutation in the gene encoding the wolframin protein (*Wfs1*$^{-e5/-e5}$), linked to diabetic and neurological complications. These authors demonstrated that *Wfs1*$^{-e5/-e5}$ rats are euglycemic at 4 months old and ventricular cardiomyocytes isolated from *Wfs1*$^{-e5/-e5}$ animals showed a higher duration of Ca^{2+} release; conjecturing a prolongation of RyR2 channel openings and modification in the RyR2 gating mediated by *Wfs1* in cardiac cells (Cagalinec et al.).

All these functional studies and reviews have contributed to a better understanding of the basis of CVDs arising from ion channel dysfunction and intracellular Ca^{2+} mishandling. These advances have also helped in the design of new drugs targeting ion channels, looking for more effective CVD treatments. Monsalvo-Villegas et al. performed an interesting pharmacological study describing a protective role of pirfenidone administration in isolated cardiomyocytes through modulation of CICR, ECC, and cell contractility. This study provides new explanations regarding the cardioprotective actions of pirfenidone (Monsalvo-Villegas et al.).

As previously mentioned, TRP channels have emerged as key partners in the pathogenesis of several CVDs, such as hypertrophy. Falcón et al. compiled in a commendable and well-organized review article the involvement of various subtypes of TRPs in cardiac physiology and CVDs. The authors particularly described the involvement of these receptors in heart remodeling linked to cardiac hypertrophy, uncovering a new and interesting field of research (Falcón et al.).

In addition to cardiac function, Ca^{2+} regulates vascular function. In this setting, Gutiérrez et al. have demonstrated in a well-conducted study whether different signaling pathways (PI3K, MAPK, and PKC) modulate Ca^{2+} entry and intracellular Ca^{2+} mobilization coupled to α_1-adrenoceptor activation in the vascular smooth muscle of rat resistance arteries.

To conclude, the compendium of articles included in this Research Topic presents a new and interesting scenario for near future research related to novel actors in the picture of intracellular Ca^{2+} mishandling associated with CVDs.

AUTHOR CONTRIBUTIONS

All authors listed have made a substantial, direct and intellectual contribution to the work, and approved it for publication.

FUNDING

GR-H and MF-V are supported by Instituto de Salud Carlos III, [MSII16/00047, CP15/00129, PI17/01093, PI17/01344], *Sociedad Española de Cardiología* (SEC 2017 and 2019) the European Regional Development Fund (Fondos FEDER and FSE). AR was supported by Fondo SEP-Cinvestav project #601410 FIDSC 2018/2; and Fondo SEP-Conacyt Ciencia Básica A1-S-9082. LP was supported by Institut de France Bourse Lefoulon Delaland and the ANR-11-1DEX-0003-02 as member of the Laboratory of Excellence LERMIT.

REFERENCES

Adamo, L., Rocha-Resende, C., Prabhu, S. D., and Mann, D. L. (2020). Reappraising the role of inflammation in heart failure. *Nat. Rev. Cardiol.* 17, 269–285. doi: 10.1038/s41569-019-0315-x

Bers, D. M. (2002). Cardiac excitation-contraction coupling. *Nature* 415, 198–205. doi: 10.1038/415198a

Fabiato, A. (1983). Calcium-induced release of calcium from the cardiac sarcoplasmic reticulum. *Am. J. Physiol.* 245, C1–C14. doi: 10.1152/ajpcell.1983.245.1.C1

Inui, M., Saito, A., and Fleischer, S. (1987). Isolation of the ryanodine receptor from cardiac sarcoplasmic reticulum and identity with the feet structures. *J. Biol. Chem.* 262, 15637–15642.

Kushnir, A., Wajsberg, B., and Marks, A. R. B. (2018). Ryanodine receptor dysfunction in human disorders. *Biochim. Biophys. Acta* 1865(11 Pt B), 1687–1697. doi: 10.1016/j.bbamcr.2018.07.011

Conflict of Interest: The authors declare that the research was conducted in the absence of any commercial or financial relationships that could be construed as a potential conflict of interest.

frontiers in Physiology

ORIGINAL RESEARCH
published: 14 June 2018
doi: 10.3389/fphys.2018.00702

Deficiency of NOD1 Improves the β-Adrenergic Modulation of Ca^{2+} Handling in a Mouse Model of Heart Failure

Almudena Val-Blasco[1†], Jose A. Navarro-García[2‡], Maria Tamayo[3†‡], Maria J. Piedras[4‡], Patricia Prieto[3†‡], Carmen Delgado[3†], Gema Ruiz-Hurtado[2], Laura Rozas-Romero[1], Marta Gil-Fernández[1], Carlos Zaragoza[5†], Lisardo Boscá[3†] and María Fernández-Velasco[1†]*

[1] Innate Immune Response Group, Instituto de Investigación Hospital Universitario La Paz, La Paz University Hospital, Madrid, Spain, [2] Cardiorenal Translational Laboratory and Hypertension Unit, Institute of Research i+12, Hospital Universitario 12 de Octubre, Madrid, Spain, [3] Departamento de Bioquímica, Facultad de Medicina, Instituto de Investigaciones Biomédicas Alberto Sols, Consejo Superior de Investigaciones Científicas, Madrid, Spain, [4] Department of Anatomy, Faculty of Health Sciences, Francisco de Vitoria University (UFV), Pozuelo de Alarcón, Spain, [5] Unidad de Investigación Cardiovascular, Universidad Francisco de Vitoria, Hospital Universitario Ramón y Cajal (IRYCIS), CIBERCV, Madrid, Spain

OPEN ACCESS

Edited by:
Tarik Smani,
Universidad de Sevilla, Spain

Reviewed by:
Marcelo Catalan,
Arturo Prat University, Chile
Jian Wu,
University of Southern California, United States

***Correspondence:**
María Fernández-Velasco
mvelasco@iib.uam.es;
maria.fernandez@idipaz.es

[†]CIBER-CV from ISCIII

[‡]These authors have contributed equally to this work.

Specialty section:
This article was submitted to Membrane Physiology and Membrane Biophysics, a section of the journal Frontiers in Physiology

Received: *01 March 2018*
Accepted: *22 May 2018*
Published: *14 June 2018*

Citation:
Val-Blasco A, Navarro-García JA, Tamayo M, Piedras MJ, Prieto P, Delgado C, Ruiz-Hurtado G, Rozas-Romero L, Gil-Fernández M, Zaragoza C, Boscá L and Fernández-Velasco M (2018) Deficiency of NOD1 Improves the β-Adrenergic Modulation of Ca^{2+} Handling in a Mouse Model of Heart Failure. Front. Physiol. 9:702. doi: 10.3389/fphys.2018.00702

Heart failure (HF) is a complex syndrome characterized by cardiac dysfunction, Ca^{2+} mishandling, and chronic activation of the innate immune system. Reduced cardiac output in HF leads to compensatory mechanisms via activation of the adrenergic nervous system. In turn, chronic adrenergic overstimulation induces pro-arrhythmic events, increasing the rate of sudden death in failing patients. Nucleotide-binding oligomerization domain-containing protein 1 (NOD1) is an innate immune modulator that plays a key role in HF progression. NOD1 deficiency in mice prevents Ca^{2+} mishandling in HF under basal conditions, but its role during β-adrenergic stimulation remains unknown. Here, we evaluated whether NOD1 regulates the β-adrenergic modulation of Ca^{2+} signaling in HF. Ca^{2+} dynamics were examined before and after isoproterenol perfusion in cardiomyocytes isolated from healthy and from post-myocardial infarction (PMI) wild-type (WT) and *Nod1*$^{-/-}$ mice. Isoproterenol administration induced similar effects on intracellular $[Ca^{2+}]_i$ transients, cell contraction, and sarcoplasmic reticulum (SR)-Ca^{2+} load in healthy WT and *Nod1*$^{-/-}$ cells. However, compared with WT-PMI cells, isoproterenol exposure induced a significant increase in the $[Ca^{2+}]_i$ transients and cell contraction parameters in *Nod1*$^{-/-}$-PMI cells, which mainly due to an increase in SR-Ca^{2+} load. NOD1 deficiency also prevented the increase in diastolic Ca^{2+} leak (Ca^{2+} waves) induced by isoproterenol in PMI cells. mRNA levels of β1 and β2 adrenergic receptors were significantly higher in *Nod1*$^{-/-}$-PMI hearts vs WT-PMI hearts. Healthy cardiomyocytes pre-treated with the selective agonist of NOD1, iE-DAP, and perfused with isoproterenol showed diminished $[Ca^{2+}]_i$ transients amplitude, cell contraction, and SR-Ca^{2+} load compared with vehicle-treated cells. iE-DAP-treated

cells also presented increased diastolic Ca^{2+} leak under β-adrenergic stimulation. The selectivity of iE-DAP on Ca^{2+} handling was validated by pre-treatment with the inactive analog of NOD1, iE-Lys. Overall, our data establish that NOD1 deficiency improves the β-adrenergic modulation of Ca^{2+} handling in failing hearts.

Keywords: β-adrenergic response, heart failure, NOD1, Ca^{2+} handling, innate immune system

INTRODUCTION

Heart failure (HF) is a complex clinical disorder characterized by the inability of the heart to deliver blood and nutrients to metabolic tissues. Chronic HF is a progressive disease, with high morbidity and mortality, and poses a significant economic burden on the healthcare system. Given its poor prognosis, the identification of molecular pathways contributing to HF is a major research goal.

Compensatory activation of the adrenergic nervous system is a pathophysiological response to HF progression, which functions to maintain cardiac homeostasis through activation of neural hormones, mainly catecholamines (Gordan et al., 2015). Accordingly, sympathetic hyperactivity is a hallmark of HF, activating β-adrenergic receptors to increase heart rate and cardiac contractility via excitation–contraction (EC) coupling, in an attempt to counteract the decreased cardiac output. Chronic exposure of the heart to elevated levels of catecholamines may, however, ultimately lead to the desensitization of β-adrenergic receptors, exacerbating the loss of cardiac function and increasing the risk for triggered arrhythmias and sudden death (Feldman et al., 2005; Brum et al., 2006; Venetucci et al., 2008).

There is a growing body of evidence suggesting a link between the innate immune response and HF progression (Lin and Knowlton, 2014; Mann, 2015). Whether the myocardial inflammatory response impairs cardiac damage is a question of broad significance. Recent studies indicate that some receptors of the innate immune system, including nucleotide-binding oligomerization domain-like receptors (NLRs), play significant roles in the host response after cardiac damage (Bullón et al., 2016; Monnerat et al., 2016; Val-Blasco et al., 2017a). Nucleotide-binding oligomerization domain (NOD) receptors are NLR family members that recognize conserved motifs of bacterial peptidoglycans in many Gram-negative bacteria (Caruso et al., 2014). Beyond their role as microbial pattern recognition receptors, it has recently been described that NODs can also be activated by non-infectious factors such as endoplasmic reticulum stress (Keestra-Gounder et al., 2016). Ligand activation of NOD receptors induces a conformational change in the protein, leading to self-oligomerization and promoting the recruitment of its adaptor, receptor-interacting protein 2 (RIP2), which activates nuclear factor-κB and triggers the inflammatory response (Park et al., 2007). NOD-containing protein 1 (NOD1) is expressed in the heart, and is functional in resident fibroblasts and cardiomyocytes (Fernández-Velasco et al., 2012; Delgado et al., 2015). Several studies have demonstrated a role for NOD1 in the progression of cardiovascular diseases, including atherosclerosis and diabetic cardiomyopathy (Prieto et al., 2014; Kanno et al., 2015; Val-Blasco et al., 2017b). We have recently shown that NOD1 is upregulated in both mouse and human failing myocardium, and its genetic deletion or pharmacological blockade prevents cardiac dysfunction and deleterious remodeling in failing hearts principally by preventing the HF-related Ca^{2+} mishandling (Val-Blasco et al., 2017a). Conversely, activation of NOD1 promotes a dysregulation of the intracellular Ca^{2+} dynamics, similar to those observed in HF (Delgado et al., 2015).

Ca^{2+} plays a key role in cardiac EC coupling. During EC coupling, an action potential leads to a small increase in intracellular Ca^{2+} via activated sarcolemmal L-type Ca channels (I_{CaL}), and this is amplified by a greater release of Ca^{2+} from the sarcoplasmic reticulum (SR) by ryanodine receptors (RyR_2), increasing the intracellular Ca^{2+} concentration ($[Ca^{2+}]_i$) – a process known as Ca^{2+}-induced Ca^{2+} release. This elevation in $[Ca^{2+}]_i$ results in myofilament activation and cell contraction. During relaxation, Ca^{2+} is removed from the cytosol primarily by two mechanisms: Ca^{2+} re-uptake by the SR-ATPase (SERCA2a) and Na^+/Ca^{2+} exchanger activation.

Excitation–contraction coupling is modulated by the sympathetic nervous system through activation of the β-adrenergic receptor coupled to Gs-type G-proteins, promoting an elevation in the intracellular concentration of cAMP (Bers, 2002). In turn, cAMP activates protein kinase A (PKA), resulting in the phosphorylation of several EC coupling-Ca^{2+} transporters such as I_{CaL}, RyR_2, and phospholamban, among others (Mayourian et al., 2018).

Several lines of evidence have established a direct relationship between Ca^{2+} dysregulation and HF progression (Gómez et al., 1997; Heinzel et al., 2011; Ruiz-Hurtado et al., 2015). Depressed systolic Ca^{2+} release, the decline in the SR-Ca^{2+} load, and the increased Ca^{2+} diastolic leak seem to be key players in HF progression, and these changes worsen under chronic β-adrenergic activation. We recently showed that NOD1 modulates intracellular Ca^{2+} handling in human and experimental failing hearts (Val-Blasco et al., 2017a); however, the role of NOD1 in the modulation of Ca^{2+} handling under β-adrenergic stimulation has not been investigated. Using a mouse HF model, we determined whether the deficiency of NOD1 impairs the modulation of Ca^{2+} dynamics under β-adrenergic stimulation.

MATERIALS AND METHODS

Myocardial Infarction Model

Male *Nod1*$^{-/-}$ mice on a C57BL/6J (6B; 129P2-*Nod1*^{tm1Nnz}/J) background were used in this study (Chamaillard et al., 2003). As controls, we used wild-type (WT) C57BL/6J mice (The Jackson

Laboratory, Bar Harbor, ME, United States). Experiments involving mice were carried out in compliance with Spanish and European guidelines (2010/63/EU) regarding animal policy and welfare recommendations. The present study was performed in male mice because they have been reported to be more prone than female to develop cardiac injury and Ca^{2+} mishandling after isoproterenol administration in experimental models of HF (Cross et al., 2002).

Mice were anesthetized by intraperitoneal (i.p.) injection of a mixture of ketamine (Imalgene®, 70 mg/kg) and xylazine (Rompun®, 10 mg/kg). Unconscious mice were shaved in the anterior region of the neck and the chest, intubated by tracheostomy, and connected to a small animal ventilator (MiniVent type 845, Harvard Apparatus) for artificial ventilation at 150 strokes/minute and 230 μL stroke volume. A 2–3 mm incision parallel to the lower costal edge was made and the left pectoralis major muscle was dissociated until the ribs were exposed. Left thoracotomy was performed between the third and fourth ribs to visualize the anterior surface of the heart and left lung. A 1-mm-thick piece of gelatin sponge (Spongostan®), slightly moistened with saline, was inserted through the hollow thoracotomy to protect the lung. The ribs were separated with an eyelid-retractor and a branch of the left coronary artery was ligated with a blue polypropylene monofilament surgical non-absorbable suture 6/0. The Spongostan® sponge was then removed and the chest was closed with braided silk non-absorbable suture 4/0. Respiratory stimulation was performed to return the heart to spontaneous breathing. For postoperative analgesia, buprenorphine (Buprex®, 0.05 mg/kg) was applied subcutaneously. Mice were kept on a warm electric blanket until spontaneous recovery. Sham-operated mice were used as the control group and underwent the same procedure, but without coronary ligation.

Myocyte Isolation

Adult male mice (2 months of age) were anesthetized with sodium pentobarbital (100 mg/kg i.p.) and heparinized (4 UI/g i.p.). Hearts were rapidly removed and cannulated via the ascending aorta for Langendorff perfusion. Retrograde perfusion was initiated with a free calcium Tyrode solution containing 0.2 mM EGTA over 2–3 min at room temperature, and subsequently with Tyrode solution containing $CaCl_2$ (0.1 mM) and type II collagenase (1 mg/mL; Worthington Biochemical, Lakewood, NY, United States). Successful digestion was assumed when the flux rate increased and the heart color changed from red to pallor. The heart was then taken off the apparatus, and the ventricles were removed, minced into small pieces, and mechanically dissociated in a thermostatic bath at 37°C in the enzymatic solution. The cardiomyocyte cell suspension was filtered through a nylon mesh (250 μm) and centrifuged at 300 rpm for 3 min. The cell pellet was suspended in Tyrode solution containing $CaCl_2$ (0.5 mM) and centrifuged as before. Finally, the cells were suspended in Tyrode solution containing $CaCl_2$ (1 mM). The Tyrode solution contained (in mM): 130 NaCl, 5.4 KCl, 0.5 $MgCl_2$, 25 HEPES, 0.4 NaH_2PO_4, and 22 glucose, which was adjusted to pH 7.4 with NaOH.

Confocal Microscopy

Local increases in intracellular Ca^{2+} concentration, $[Ca^{2+}]_i$ transients, and Ca^{2+} waves were analyzed in intact isolated cardiomyocytes loaded with the fluorescent Ca^{2+} dye Fluo-3AM (5 μmol/L, Invitrogen). $[Ca^{2+}]_i$ transients were recorded in cells electrically excited at 2 Hz by field stimulation using two parallel platinum electrodes. Ca^{2+} waves were acquired in quiescent myocytes. SR Ca^{2+} load was assessed by rapid caffeine application (10 mM) in cells previously excited at 2 Hz.

Images were acquired by confocal microscopy (Meta Zeiss LSM 710, 40× oil immersion objective with a 1.2 NA), by scanning the cell with an argon laser every 1.54 ms. Fluo-3AM was excited at 488 nm and emitted fluorescence was collected at >505 nm. Data analysis was performed with homemade routines using software written on the IDL platform (Research System Inc., Boulder, CO, United States), designed by Dr. AM Gómez (Inserm, UMR-S 1180). Images were corrected for background fluorescence. The fluorescence values (F) were normalized by the basal fluorescence ($F0$) to obtain the fluorescence ratio ($F/F0$).

Drugs and Treatments

Isolated cardiomyocytes were perfused with 10^{-8} M isoproterenol (Sigma-Aldrich, Madrid, Spain) for 1–5 min and intracellular Ca^{2+} dynamics were recorded. In some experiments, cells were pretreated with the selective NOD1 agonist C12-iE-DAP (iE-DAP, InvivoGen, San Diego, CA, United States), which has significant cell membrane permeability and high potency (Fernández-Velasco et al., 2012; Delgado et al., 2015; Val-Blasco et al., 2017a), or iE-Lys (Invivogen), an inactive analog of NOD1. Nodinitib-1 (Cayman) was used as a selective NOD1 inhibitor and mice were injected IP with 5 μmol/L nodinitib-1 or vehicle (<0.01% DMSO) three times weekly for 6 weeks.

Real-Time PCR

Frozen heart tissue was pulverized to powder and then homogenized in TRIZOL Reagent® solution (Ambion) with a Polytron system (MWR). RNA (250 ng) was reverse transcribed to cDNA using the *High-Capacity cDNA Reverse Transcription Kit* (Applied Biosystems #4368813). This template cDNA was used in the qPCR reaction with *Power SYBR Green PCR Master* mix (Applied Biosystems #4367659) and specific primers in a 7900HT Fast Real Time PCR system (Applied Biosystems). 18s-RNA was used as a housekeeping gene. The primer sequences (5′-3′) for β1 and β2 adrenergic receptors and 18s-RNA were as follows:

β1-F	CGCTGATCTGGTCATGGGAT
β1-R	GAAGAAGGAGCCGTACTCCC
β2-F	AATAGCAACGGCAGAACGGA
β2-R	TCACAAAGCCTTCCATGCCT
18s-F	CCAGTAAGTGCGGGTCATAAGC
18s-R	CCTCACTAAACCATCCAATCGG

Statistical Analysis

Results are reported as mean ± SEM. Statistical analysis was performed using two-way analysis of variance, paired (two-sided) Student's t test or χ^2 test, as appropriate. All statistical

analyses were performed with Origin 8.0 software (OriginLab, Northampton, MA, United States). Significance was set at $P < 0.05$.

RESULTS

Hypertrophy Development in Mice Subjected to Myocardial Infarction

Compared with healthy WT mice, post-myocardial infarction (PMI)-mice 6 weeks after surgery showed significantly increased heart weight, heart weight/body weight ratio, and heart weight/tibia length ratio, consistent with the development of cardiac hypertrophy (**Table 1**). By contrast, *Nod1*$^{-/-}$-PMI mice showed similar heart weight, heart weight/body weight, and heart weight/tibia length values to *Nod1*$^{-/-}$ mice (**Table 1**). These data indicate that deficiency of NOD1 attenuates cardiac hypertrophy in our PMI mouse model.

Deficiency of NOD1 Improves the β-Adrenergic Modulation of Systolic Ca^{2+} Release and Sarcoplasmic Reticulum Ca^{2+} Load in PMI Cardiomyocytes

We first analyzed whether deficiency of NOD1 determined the β-adrenergic response to Ca^{2+} handling in healthy myocytes. Isoproterenol perfusion induced a similar increase in $[Ca^{2+}]_i$ transients amplitude (**Figure 1A**), cell contraction (**Figure 1B**), and SR-Ca^{2+} load (**Figure 1C**) in WT and *Nod1*$^{-/-}$ cardiomyocytes.

Given that β-adrenergic regulation of Ca^{2+} dynamics plays a key role in HF-related cardiac dysfunction, we next questioned whether NOD1 deficiency impacted isoproterenol-induced modulation of Ca^{2+} handling in cardiomyocytes after PMI. **Figure 1D** shows representative line-scan Ca^{2+} fluorescence images obtained after electric field stimulation at 2 Hz in all groups. Under β-adrenergic stimulation, both WT-PMI and *Nod1*$^{-/-}$-PMI cardiomyocytes exhibited increased $[Ca^{2+}]_i$ transients (**Figure 1E**), augmented cell contraction (**Figure 1F**), and faster time decay of $[Ca^{2+}]_i$ transients (**Figure 1G**), but all these changes were significantly greater in *Nod1*$^{-/-}$-PMI cells. These results reveal that, compared with WT-PMI cells, *Nod1*$^{-/-}$-PMI myocytes show a significant improvement in Ca^{2+} mishandling, which was mostly due to the increased amplitude of $[Ca^{2+}]_i$ transients (**Figures 1D,E**) and also higher cell contraction parameters (**Figure 1F**). In this line, mean values of the amplitude of $[Ca^{2+}]_i$ transients ($F/F0$) in cardiomyctes obtained under isoproterenol administration were 5.31 ± 0.52 (n/N = 13/5) in WT, 5.18 ± 0.32 (n/N = 14/4) in *Nod1*$^{-/-}$, 4.18 ± 0.22 (n/N = 12/4) in WT-PMI, and 5.41 ± 0.21 (n/N = 13/4) in *Nod1*$^{-/-}$-PMI (**Figures 1A,E**). Thus, $[Ca^{2+}]_i$ transients obtained in the *Nod1*$^{-/-}$-PMI group during isoproterenol perfusion were similar to those of equivalent healthy WT and *Nod1*$^{-/-}$ cardiomyocytes. Consistent with this finding, treatment of WT-PMI mice with the selective NOD1 inhibitor nodinitib-1 resulted in higher amplitude isoproterenol-induced $[Ca^{2+}]_i$ transients in isolated cardiomyocytes compared with cells isolated from vehicle-treated mice (Supplementary Figure S1).

Next, to question whether changes in $[Ca^{2+}]_i$ transients during β-adrenergic stimulation in PMI cardiomyocytes were related to modifications in SR-Ca^{2+} load, we measured caffeine-evoked $[Ca^{2+}]_i$ transients in all groups. **Figure 2A** shows examples of line-scan images of caffeine-evoked $[Ca^{2+}]_i$ transients obtained in each group. Mean values of the amplitude of caffeine-evoked $[Ca^{2+}]_i$ transients (F/F0) in cardiomyocytes during isoproterenol exposure was 7.07 ± 0.69 (n/N = 9/3) in WT, 7.34 ± 0.93 (n/N = 10/4) in *Nod1*$^{-/-}$ (**Figure 1C**), 5.77 ± 0.46 (n/N = 13/4) in WT-PMI, and 7.40 ± 0.50 (n/N = 12/4) in *Nod1*$^{-/-}$-PMI (**Figure 2B**). Thus, the amplitude of $[Ca^{2+}]_i$ transients triggered by caffeine was significantly higher in *Nod1*$^{-/-}$-PMI mice than in WT-PMI mice, both in the absence or the presence of isoproterenol (**Figure 2B**). Additionally, the high values of SR-Ca^{2+} load in the *Nod1*$^{-/-}$-PMI group treated with isoproterenol were similar to those found in healthy WT and *Nod1*$^{-/-}$ cells treated with isoproterenol.

Taken together, β-adrenergic stimulation induced better systolic Ca^{2+} release and cell contractility in *Nod1*$^{-/-}$-PMI cells than in WT-PMI cells. These effects correlated with the significant increase in the SR-Ca^{2+} load induced by isoproterenol in *Nod1*$^{-/-}$-PMI cells.

Deficiency of NOD1 Prevents the Increased Diastolic Ca^{2+} Release Induced by β-Adrenergic Stimulation in PMI Cardiomyocytes

Since SR-Ca^{2+} load impairment is closely related to changes in diastolic Ca^{2+} release, we analyzed spontaneous Ca^{2+} waves in quiescent cells.

TABLE 1 | Cardiac properties of wild-type and *Nod1-deficent* mice.

	WT (N = 5)	*Nod1*$^{-/-}$ (N = 5)	WT-PMI (N = 4)	*Nod1*$^{-/-}$-PMI (N = 4)
HW (mg)	187.20 ± 3.72	173.60 ± 4.79	272.00 ± 10.70***	193.5 ± 13.35$^{\&\&}$
BW (g)	29.71 ± 1.37	29.95 ± 1.14	31.47 ± 0.54	30.03 ± 1.14
TL (mm)	21.90 ± 0.40	21.50 ± 0.31	21.25 ± 0.47	21.50 ± 0.28
HW/TL (mg/mm)	8.56 ± 0.25	8.08 ± 0.27	12.81 ± 0.53***	9.01 ± 0.66$^{\&\&}$
HW/BW (mg/g)	6.35 ± 0.32	5.82 ± 0.22	8.65 ± 0.37**	6.36 ± 0.26$^{\&\&}$

*HW, heart weight; BW, body weight; TL, tibia length. **$P < 0.01$, ***$P < 0.001$ vs WT and $^{\&\&}P < 0.01$ vs WT-PMI.*

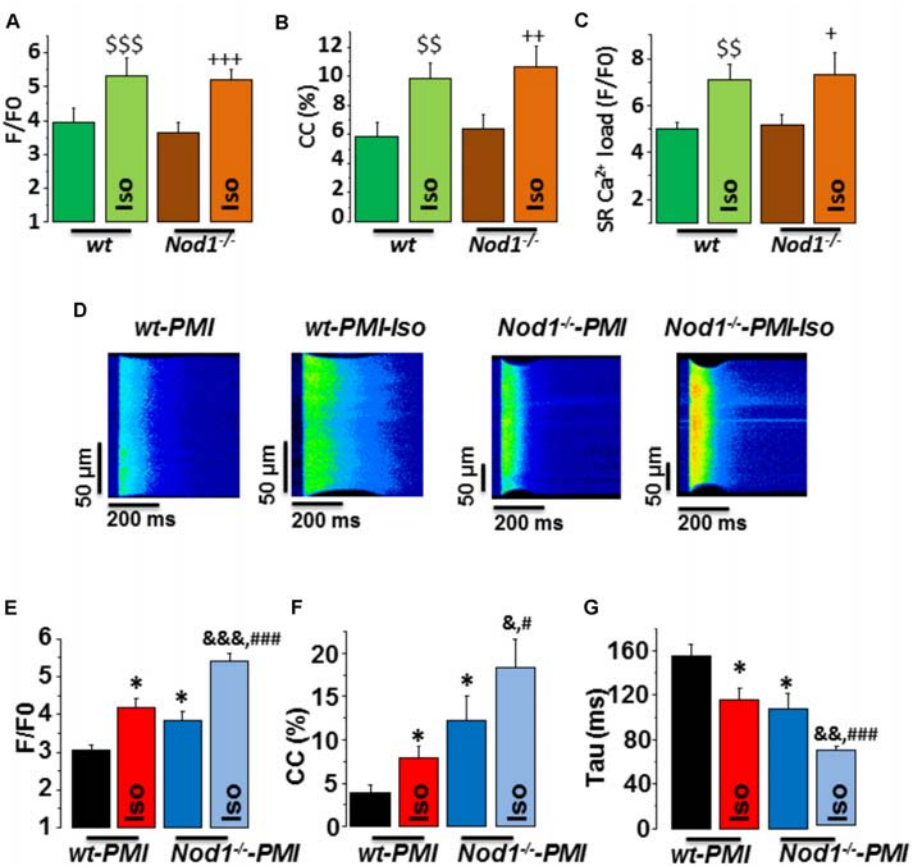

FIGURE 1 | Deficiency of NOD1 improves the modulation of systolic Ca^{2+} handling and SR-Ca^{2+} load by β-adrenergic stimulation in cardiomyocytes from failing mice. **(A–C)** Mean values of amplitude of $[Ca^{2+}]_i$ transients (*F*/*F*0, **A**), cell contractions (CC, %, **B**), and caffeine-evoked $[Ca^{2+}]_i$ transients amplitude (SR-Ca^{2+} load, *F*/*F*0, **C**) in WT (*n* = 13 cells/5 mice) and *NOD1*$^{-/-}$ cardiomyocytes (*n* = 14 cells/4 mice) with and without 10^{-8} M isoproterenol (Iso). **(D)** Representative line-scan confocal images of $[Ca^{2+}]_i$ transients obtained from WT-PMI and *NOD1*$^{-/-}$-PMI cardiomyocytes with and without Iso perfusion. **(E,F)** Mean values of peak fluorescence $[Ca^{2+}]_i$ transients (*F*/*F*0, **E**), cell contraction (CC, %, **F**), and decay time of $[Ca^{2+}]_i$ transients (tau, ms, **G**) in WT-PMI (*n* = 12 cells/4 mice) and *NOD1*$^{-/-}$-PMI (*n* = 13 cells/4 mice) cardiomyocytes with and without Iso. Histograms represent the mean ± SEM: $^{\$\$}P < 0.01$, $^{\$\$\$}P < 0.001$ vs WT; $^{+}P < 0.05$ vs *NOD1*$^{-/-}$, $^{++}P < 0.01$ vs *NOD1*$^{-/-}$, $^{+++}P < 0.001$ vs *NOD1*$^{-/-}$; $^{*}P < 0.05$ vs WT-PMI; $^{\&}P < 0.05$, $^{\&\&}P < 0.01$, $^{\&\&\&}P < 0.001$ vs *NOD1*$^{-/-}$-PMI; and $^{\#}P < 0.05$, $^{\#\#\#}P < 0.001$ vs WT-PMI treated with Iso.

Figure 3A shows a representative line-scan image of a Ca^{2+} wave recording from a WT-PMI myocyte. Ca^{2+} wave occurrence analysis (**Figure 3B**) revealed no statistically significant changes between WT-PMI (14.60%) and *Nod1*$^{-/-}$-PMI (10.50%) cells under basal conditions. By contrast, both groups showed a significant elevation in the Ca^{2+} wave rate after isoproterenol perfusion, but this was significantly higher in WT-PMI cardiomyocytes perfused with isoproterenol (**Figure 3**). Accordingly, the percentage of cells with Ca^{2+} waves during isoproterenol exposure was 34.07% in WT-PMI cells and 15.65% in *Nod1*$^{-/-}$-PMI cells ($P < 0.01$).

These results indicate that deficiency of NOD1 prevents the increase of Ca^{2+} diastolic leak induced by β-adrenergic stimulation in PMI cardiomyocytes, thus providing an explanation for the improvement in the SR-Ca^{2+} load and the resulting better systolic Ca^{2+} release in *Nod1*$^{-/-}$-PMI cells under isoproterenol administration.

mRNA Levels of the β1 and β2 Adrenergic Receptors Are Elevated in Nod1$^{-/-}$-PMI Hearts

Analysis of the mRNA levels of β1 and β2 adrenergic receptors in hearts from WT-PMI and *Nod1*$^{-/-}$-PMI mice revealed significantly increased expression of both receptors in *Nod1*$^{-/-}$-PMI hearts (**Figures 4A,B**). These increased β1 and β2 adrenergic receptor levels can explain at least in part the improvement in Ca^{2+} regulation observed in the *Nod1*$^{-/-}$-PMI group under isoproterenol administration.

Selective Activation of NOD1 Compromises the β-Adrenergic Regulation of Ca^{2+} Handling in Wild-Type Cardiomyocytes

We next addressed whether the selective activation of NOD1 impairs the β-adrenergic regulation of Ca^{2+} handling in

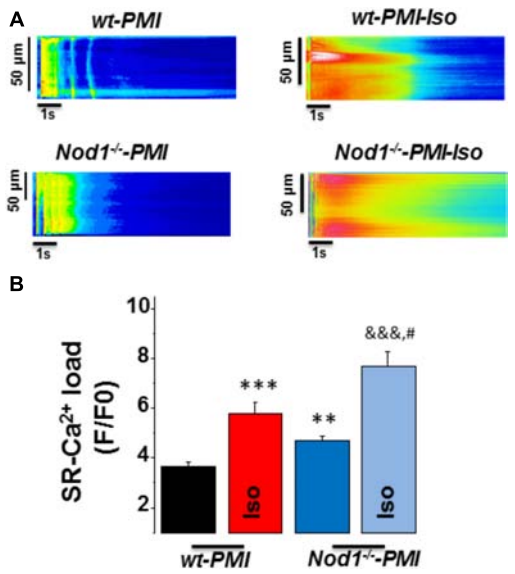

FIGURE 2 | Deficiency of NOD1 increases the β-adrenergic response on SR-Ca^{2+} load in cardiomyocytes from failing mice. **(A)** Representative line-scan confocal images of caffeine-evoked $[Ca^{2+}]_i$ transients obtained from WT-PMI and *NOD1*$^{-/-}$-PMI cardiomyocytes with and without Iso perfusion. **(B)** Mean values of caffeine-evoked $[Ca^{2+}]_i$ transients amplitude (SR-Ca^{2+} load, *F/F0*) in WT-PMI (n = 23 cells/4 mice), *NOD1*$^{-/-}$-PMI (n = 19 cells/4 mice), WT-PMI (n = 13 cells/4 mice), and *NOD1*$^{-/-}$-PMI (n = 12 cells/4 mice) cardiomyocytes treated with Iso. Histograms represent the mean ± SEM: $^{**}P < 0.01$, $^{***}P < 0.001$ vs WT-PMI; $^{\&\&\&}P < 0.001$ vs *NOD1*$^{-/-}$-PMI; and $^{\#}P < 0.05$ vs WT-PMI cardiomyocytes treated with Iso.

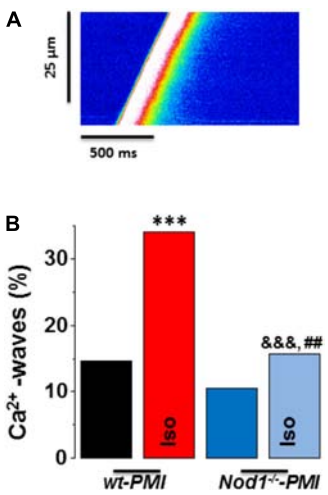

FIGURE 3 | Deficiency of NOD1 prevents the increase in diastolic Ca^{2+} release induced by isoproterenol in cardiomyocytes from failing mice. **(A)** A representative line-scan image of a Ca^{2+} wave recording from a WT-PMI myocyte. **(B)** The mean data for Ca^{2+} wave occurrence from WT-PMI (n = 9 cells/3 mice) and NOD1$^{-/-}$-PMI (n = 7 cells/3 mice) cardiomyocytes with and without Iso. Histograms represent the mean ± SEM: $^{*}P < 0.05$, $^{***}P < 0.001$, vs WT-PMI; $^{\&}P < 0.05$, $^{\&\&\&}P < 0.001$ vs *NOD1*$^{-/-}$-PMI; and $^{\#\#}P < 0.05$ vs WT-PMI cardiomyocytes treated with Iso.

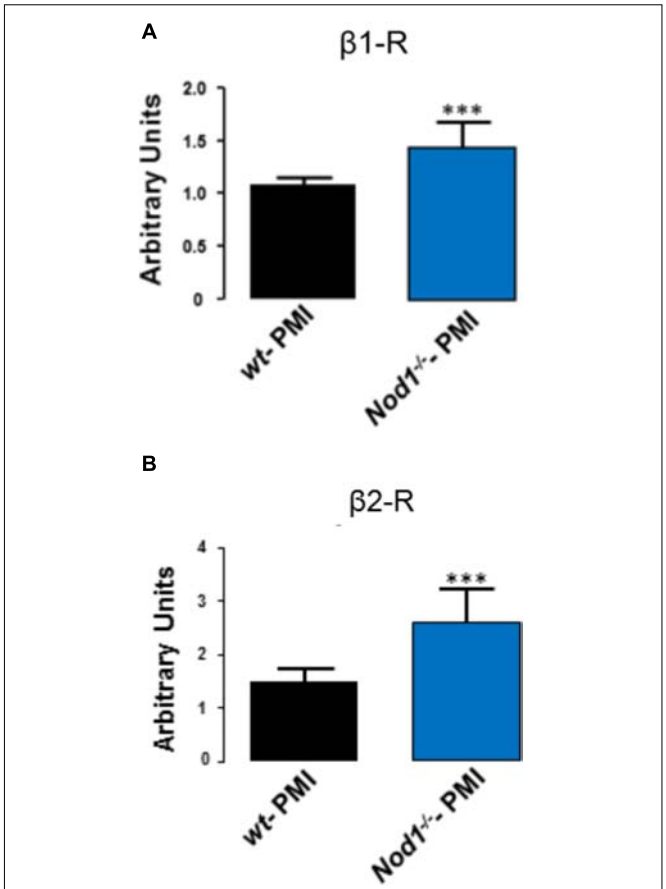

FIGURE 4 | Hearts from *Nod1*$^{-/-}$-PMI mice have elevated mRNA levels of β1 and β2 adrenergic receptors. Histograms illustrate mRNA levels of β1 **(A)** and β2 **(B)** adrenergic receptors normalized to 18s RNA levels obtained in WT-PMI (N = 6) and *Nod1*$^{-/-}$-PMI hearts (N = 6). Values are expressed in arbitrary units. $^{***}P < 0.001$ vs WT-PMI.

healthy cardiomyocytes. To do this, we pretreated WT cardiomyocytes for 1 h with the NOD1 ligand C12-iE-DAP (iEDAP; 20 μg/mL) and then we examined intracellular Ca^{2+} dynamics in the absence or presence of isoproterenol perfusion. Under isoproterenol stimulation, iE-DAP-treated cells showed reduced amplitude of $[Ca^{2+}]_i$ transients (**Figures 5A,B**), cell contraction (**Figure 5C**), and SR-Ca^{2+} load (**Figure 5D**) compared with vehicle-treated cardiomyocytes. Treatment of cells with the inactive analog of IE-DAP, iE-Lys (20 μg/mL), resulted in a similar isoproterenol response for Ca^{2+} handling to vehicle-treated cells, demonstrating the selective effect of iE-DAP on Ca^{2+} handling under β-adrenergic stimulation (**Figures 5A–D**).

Finally, we investigated whether the selective activation of NOD1 impairs diastolic Ca^{2+} release under β-adrenergic stimulation. As shown in **Figure 5E**, isoproterenol perfusion promoted a significant increase in Ca^{2+} waves in WT cells pretreated with iE-DAP as compared with vehicle- or iE-Lys-treated cells. Importantly, the percentage of Ca^{2+} waves in cells that were pretreated with iE-DAP and under

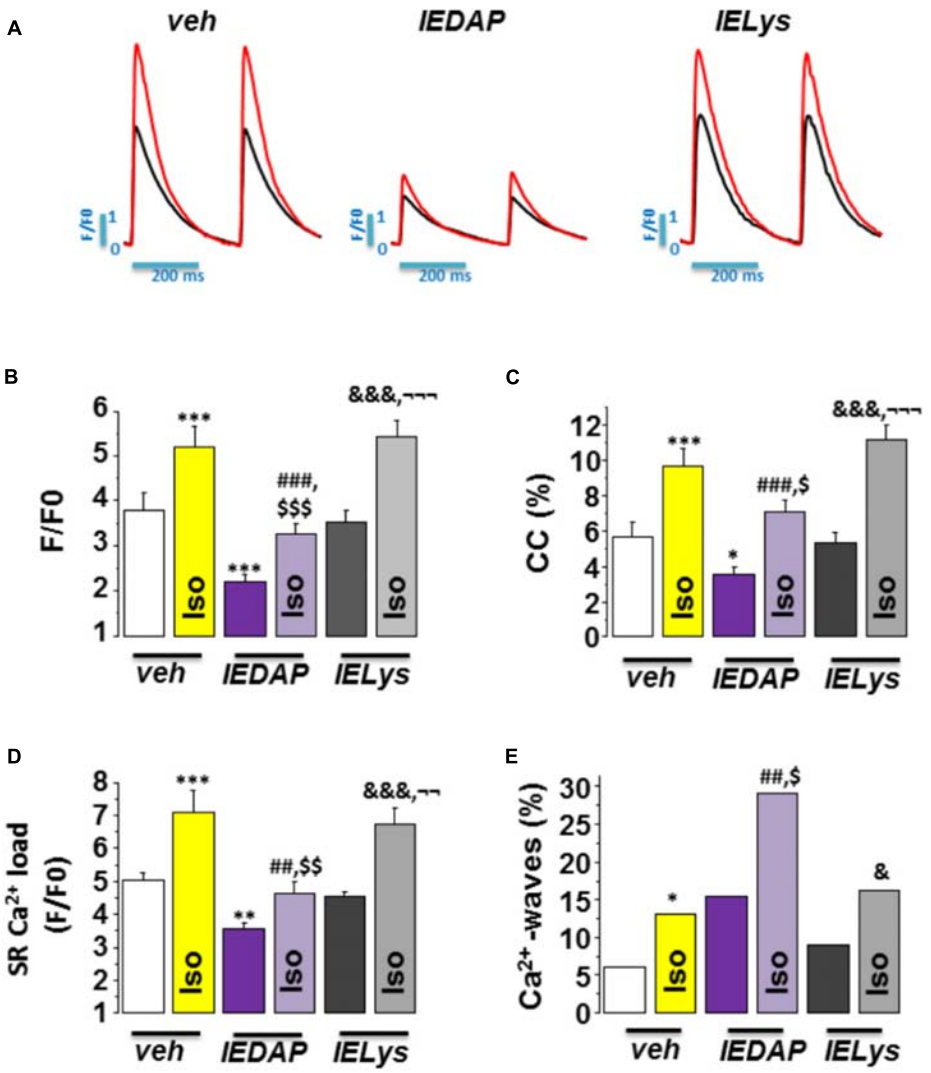

FIGURE 5 | Effect of Isoproterenol on $[Ca^{2+}]_i$ transients, SR-Ca^{2+} load, and diastolic Ca^{2+} release in wild-type cardiomyocytes treated with C12-iE-DAP. **(A)** Representative $[Ca^{2+}]_i$ transients recorded in cardiomyocytes treated with vehicle (left), C12-iEDAP (20 μg/mL IEDAP, middle), and iE-LYS (20 μg/mL IELYS, right), with (red) or without (black) Iso. Mean values of **(B)** peak fluorescence $[Ca^{2+}]_i$ transients, **(C)** cell contraction, **(D)** caffeine-evoked $[Ca^{2+}]_i$ transients amplitude (SR-Ca^{2+} load), and **(E)** Ca^{2+} wave occurrence in cardiomyocytes treated with vehicle (veh; n = 15 cells/7 mice), C12-iE-DAP (IEDAP n = 16 cells/6 mice), or with iE-Lys (IELYS, n = 14 cells/5 mice) in the absence or the presence of Iso. Histograms represent the mean ± SEM: $^{*}P < 0.05$, $^{**}P < 0.01$, $^{***}P < 0.001$ vs veh; $^{\#\#}P < 0.01$, $^{\#\#\#}P < 0.001$ vs IEDAP; $^{\&}P < 0.05$, $^{\&\&\&}P < 0.001$ vs IELYS; $^{\$}P < 0.05$, $^{\$\$}P < 0.01$, $^{\$\$\$}P < 0.001$ vs veh plus Iso; and $^{\neg\neg}P < 0.01$, $^{\neg\neg\neg}P < 0.001$ vs IEDAP
plus Iso.

isoproterenol perfusion was very similar to that found in WT-PMI cardiomyocytes under the same conditions (34.07% in WT-PMI cells and 29.20% in cells treated with iE-DAP; compare **Figures 3C**, **5E**). Supporting these data, iE-DAP administration failed to increase the percentage of Ca^{2+}-wave-positive $Nod1^{-/-}$ cardiomyocytes (data not shown).

Overall, these results indicate that NOD1 activation limits the β-adrenergic regulation of Ca^{2+} handling due to impairment of systolic Ca^{2+} release ($[Ca^{2+}]_i$ transients) and SR-Ca^{2+} load, which are highly conditioned by the increased diastolic Ca^{2+} leak.

DISCUSSION

Over the last decade, a large number of studies have shown that compensatory upregulation of the adrenergic nervous system response is a key factor in disease progression in chronic failing hearts. During the early stages of HF, there is a steady activation of the sympathetic nervous system to maintain cardiac output (Lymperopoulos, 2013), whereas in later stages, continuous adrenergic stimulation triggers negative feedback regulation of β-receptor activity, causing a downregulation in the number of receptors and also functional impairment, a process termed

receptor desensitization (Böhm et al., 1990; Madamanchi, 2007), ultimately contributing to toxicity and worsening of cardiac outcomes.

Some innate immune mediators, such as NLRs, play an important role in the host response to cardiac damage. Among them, NOD1 is expressed and functional in the heart (Fernández-Velasco et al., 2012; Delgado et al., 2015) and is upregulated in failing hearts both in a mouse HF model and in failing human myocardium (Val-Blasco et al., 2017a). Genetic deletion of NOD1 prevents HF-related cardiac dysfunction through modulation of EC coupling, chiefly by improving systolic Ca^{2+} release and by maintaining Ca^{2+} SR load, which are both compromised in HF (Val-Blasco et al., 2017a).

Our present results show that deficiency of NOD1 does not affect the regulation of Ca^{2+} handling by β-adrenergic stimulation under physiological conditions, as systolic Ca^{2+} release and SR-Ca^{2+} load were similar between WT and *Nod1*$^{-/-}$ cardiomyocytes. In the failing heart, however, deficiency of NOD1 prevents the depression of $[Ca^{2+}]_i$ transients and cell contractility due to maintained SR Ca^{2+} load. Accordingly, during β-adrenergic stimulation, deficiency of NOD1 leads to a significant improvement in systolic Ca^{2+} release, cell contraction parameters, and SR Ca^{2+} load in PMI cardiomyocytes, with levels mirroring those found in isoproterenol-stimulated WT and healthy *Nod1*$^{-/-}$cells. These results are interesting given that the decreased β-adrenergic function in HF plays a key role in the compromised cardiac contraction.

Several groups have shown that other pro-inflammatory mediators including TNFα, CXR4 or IL-1β impair the β-adrenergic response and reduce cardiac contractility (Gulick et al., 1989; Finkel et al., 1992; Schulz et al., 1995; Murray and Freeman, 1996; Pyo et al., 2006), and short-term treatment of rat cardiomyocytes with the pro-inflammatory cytokines IL-1α and TNFα blocks isoproterenol-induced increases in cell contractility (Bick et al., 1997). These findings are in agreement with an early report implicating IL-1β in uncoupling β-adrenergic responses in cardiomyocytes (Gulick et al., 1989). Consistent with these data, our study shows that a selective NOD1 agonist induces a minor but significant effect on cell contractility in isoproterenol-treated cardiomyocytes. NOD1 activation also reduced the β-adrenergic modulation of systolic Ca^{2+} release due to reduced SR-Ca^{2+} load, and by increasing the diastolic Ca^{2+} leak. These results can be explained by the fact that NOD1 activation in cardiomyocytes induces the over-phosphorylation of RyR2, promoting the open state of the receptor and inducing Ca^{2+} release from the SR to the cytoplasm, increasing the diastolic Ca^{2+} leak (waves), and compromising the SR-Ca^{2+} load (Delgado et al., 2015; Val-Blasco et al., 2017a).

In many cases, increased diastolic Ca^{2+} release is the cause of depressed SR-Ca^{2+} load in HF. Our data show that during β-adrenergic stimulation, diastolic Ca^{2+} release is significantly increased in failing WT cells, whereas deficiency of NOD1 prevents the increase in the HF-related diastolic Ca^{2+} waves. These data go some way to explain the improvement in the SR-Ca^{2+} load and the resulting improved systolic Ca^{2+} release and cell contractility in *Nod1*$^{-/-}$-PMI cells under isoproterenol stimulation.

Nod1$^{-/-}$-PMI hearts showed physiological levels of phospho-RyR2 (Val-Blasco et al., 2017a), thus contributing to block Ca^{2+} diastolic leak in *Nod1*$^{-/-}$-PMI cardiomyocytes. Aberrant diastolic Ca^{2+} leak in many cases such as HF leads to arrhythmogenesis and cardiac dysfunction (Reiken et al., 2003; Ai et al., 2005; van Oort et al., 2010; Marks, 2013; Terentyev et al., 2014). RyR-derived Ca^{2+} leak can cause arrhythmias by Ca^{2+} waves that trigger delays after depolarizations (Lehnart et al., 2006). Pro-arrhythmogenic events are common in failing patients, particularly under β-adrenergic stimulation, and around 30–50% of these individuals die from sudden cardiac death, mostly associated with ventricular arrhythmias. Our data suggest that blocking NOD1 can be a new tool to prevent ventricular arrhythmias and cardiac dysfunction resulting from Ca^{2+} mishandling in HF.

In line with our results, elevated levels of the inflammatory cytokines TNFα and IL-1β have been reported in both tissue and plasma from HF patients with arrhythmias (Levine et al., 1990; Testa et al., 1996; Aukrust et al., 2004). Moreover, other inflammatory mediators such as Toll-like receptors (TLRs) have been implicated in the generation of ventricular and atrial arrhythmias (Katoh et al., 2014; Monnerat-Cahli et al., 2014; Gurses et al., 2016). Importantly, TLRs seem to play a role in the regulation of the β-adrenergic response. Accordingly, Kizaki et al. (2008) demonstrated that TLR4 stimulation induces a down-regulation of β2 receptors in macrophages (Wang et al., 2009). In this regard, our results demonstrate that hearts from *Nod1*$^{-/-}$-PMI mice have higher mRNA levels of β1 and β2 adrenergic receptors than WT-PMI hearts, suggesting a possible mechanism for the larger systolic Ca^{2+} release and SR Ca^{2+} reuptake in by *Nod1*$^{-/-}$-PMI mice. β-adrenergic receptors are activated through heterotrimeric G proteins and subsequent activation of the adenylyl cyclase, which modulates the activity of several proteins essential for EC Ca^{2+} coupling, such as I_{CaL}, RyR_2, and phospholamban (Mayourian et al., 2018). Therefore, the elevated β-adrenergic receptor levels in *Nod1*$^{-/-}$-PMI cells may increase the efficiency of cardiac EC coupling through the augmented function of I_{CaL}, RyR, and SERCA, improving both systolic Ca^{2+} release and SR Ca^{2+} loading in failing hearts.

One of the most common treatments to manage β-adrenergic impairment in HF patients is the use of β-blockers. It has been demonstrated that β-blocker treatment reduces the detrimental effects of catecholamine stimulation, such as toxicity, pathological elevated heart rate, and adverse remodeling and arrhythmia development in failing patients. Improving β-adrenergic regulation of Ca^{2+} handling by blocking NOD1 can be a new tool to improve the cardiac function in failing hearts.

CONCLUSION

Our study demonstrates that deficiency of NOD1 improves the β-adrenergic modulation of Ca^{2+} handling in isolated cells from failing mice. Therefore, NOD1 emerges as a

new potential target in the treatment of cardiac dysfunction and ventricular arrhythmias associated with HF.

AUTHOR CONTRIBUTIONS

MF-V conceived, designed, and discussed the experiments and wrote the paper. AV-B, JN-G, MT, PP, CZ, MP, LR-R, and MG-F performed the experiments. MF-V, AV-B, JN-G, CD, GR-H, and PP analyzed the data. MF-V, LB, GR-H, and CD contributed reagents, materials, and analysis tools.

FUNDING

MF-V is Miguel Servet II researcher of ISCIII (MSII16/00047 Carlos III Health Institute). This work was supported by grants PI14/01078, CP15/00129, PI17/01093, and PI17/01344 from ISCIII, Fondo Europeo de Desarrollo Regional (FEDER), Ministerio de Economía y Competitividad of Spain (SAF2014-57190-R; SAF2017-84777-R), FSE, and CIBER-CV, a network funded by ISCIII.

ACKNOWLEDGMENTS

We acknowledge the technical assistance of L. Martin, V. Terrón, D. Navarro, and L. Sánchez. We would like to thank Dr. Gabriel Núñez (University of Michigan, United States) for kindly providing *Nod1*$^{-/-}$ mice and Dr. Kenneth McCreath for editorial support.

SUPPLEMENTARY MATERIAL

The Supplementary Material for this article can be found online at: https://www.frontiersin.org/articles/10.3389/fphys.2018.00702/full#supplementary-material

REFERENCES

Ai, X., Curran, J. W., Shannon, T. R., Bers, D. M., and Pogwizd, S. M. (2005). Ca2+/calmodulin-dependent protein kinase modulates cardiac ryanodine receptor phosphorylation and sarcoplasmic reticulum Ca2+ leak in heart failure. *Circ. Res.* 97, 1314–1322. doi: 10.1161/01.RES.0000194329.41863.89

Aukrust, P., Yndestad, A., Damås, J. K., and Gullestad, L. (2004). Inflammation and chronic heart failure-potential therapeutic role of intravenous immunoglobulin. *Autoimmun. Rev.* 3, 221–227. doi: 10.1016/S1568-9972(03)00103-4

Bers, D. M. (2002). Cardiac excitation-contraction coupling. *Nature* 415, 198–205. doi: 10.1038/415198a

Bick, R. J., Liao, J. P., King, T. W., LeMaistre, A., McMillin, J. B., and Buja, L. M. (1997). Temporal effects of cytokines on neonatal cardiac myocyte Ca^{2+} transients and adenylate cyclase activity. *Am. J. Physiol.* 272, H1937–H1944. doi: 10.1152/ajpheart.1997.272.4.H1937

Böhm, M., Ungerer, M., and Erdmann, E. (1990). Beta adrenoceptors and m-cholinoceptors in myocardium of hearts with coronary artery disease or idiopathic dilated cardiomyopathy removed at cardiac transplantation. *Am. J. Cardiol.* 66, 880–882. doi: 10.1016/0002-9149(90)90376-C

Brum, P. C., Hurt, C. M., Shcherbakova, O. G., Kobilka, B., and Angelotti, T. (2006). Differential targeting and function of alpha2A and alpha2C adrenergic receptor subtypes in cultured sympathetic neurons. *Neuropharmacology* 51, 397–413. doi: 10.1016/j.neuropharm.2006.03.032

Bullón, P., Alcocer-Gómez, E., Carrión, A. M., Marín-Aguilar, F., Garrido-Maraver, J., Román-Malo, L., et al. (2016). AMPK phosphorylation modulates pain by activation of NLRP3 Inflammasome. *Antioxid. Redox Signal.* 24, 157–170. doi: 10.1089/ars.2014.6120

Caruso, R., Warner, N., Inohara, N., and Núñez, G. (2014). NOD1 and NOD2: signaling, host defense, and inflammatory disease. *Immunity* 41, 898–908. doi: 10.1016/j.immuni.2014.12.010

Chamaillard, M., Hashimoto, M., Horie, Y., Masumoto, J., Qiu, S., Saab, L., et al. (2003). An essential role for NOD1 in host recognition of bacterial peptidoglycan containing diaminopimelic acid. *Nat. Immunol.* 4, 702–707. doi: 10.1038/ni945

Cross, H. R., Murphy, E., and Steenbergen, C. (2002). Ca(2+) loading and adrenergic stimulation reveal male/female differences in susceptibility to ischemia-reperfusion injury. *Am. J. Physiol. Heart Circ. Physiol.* 283, H481–H489. doi: 10.1152/ajpheart.00790.2001

Delgado, C., Ruiz-Hurtado, G., Gómez-Hurtado, N., González-Ramos, S., Rueda, A., Benito, G., et al. (2015). NOD1, a new player in cardiac function and calcium handling. *Cardiovasc. Res.* 106, 375–386. doi: 10.1093/cvr/cvv118

Feldman, D. S., Carnes, C. A., Abraham, W. T., and Bristow, M. R. (2005). Mechanisms of disease: beta-adrenergic receptors-alterations in signal transduction and pharmacogenomics in heart failure. *Nat. Clin. Pract. Cardiovasc. Med.* 2, 475–483. doi: 10.1038/ncpcardio0309

Fernández-Velasco, M., Prieto, P., Terrón, V., Benito, G., Flores, J. M., Delgado, C., et al. (2012). NOD1 activation induces cardiac dysfunction and modulates cardiac fibrosis and cardiomyocyte apoptosis. *PLoS One* 7:e45260. doi: 10.1371/journal.pone.0045260

Finkel, M. S., Oddis, C. V., Jacob, T. D., Watkins, S. C., Hattler, B. G., and Simmons, R. L. (1992). Negative inotropic effects of cytokines on the heart mediated by nitric oxide. *Science* 257, 387–389. doi: 10.1126/science.1631560

Gómez, A. M., Valdivia, H. H., Cheng, H., Lederer, M. R., Santana, L. F., Cannell, M. B., et al. (1997). Defective excitation-contraction coupling in experimental cardiac hypertrophy and heart failure. *Science* 276, 800–806. doi: 10.1126/science.276.5313.800

Gordan, R., Gwathmey, J. K., and Xie, L. H. (2015). Autonomic and endocrine control of cardiovascular function. *World J. Cardiol.* 7, 204–214. doi: 10.4330/wjc.v7.i4.204

Gulick, T., Chung, M. K., Pieper, S. J., Lange, L. G., and Schreiner, G. F. (1989). Interleukin 1 and tumor necrosis factor inhibit cardiac myocyte beta-adrenergic responsiveness. *Proc. Natl. Acad. Sci. U.S.A.* 86, 6753–6757. doi: 10.1073/pnas.86.17.6753

Gurses, K. M., Kocyigit, D., Yalcin, M. U., Canpinar, H., Yorgun, H., Sahiner, M. L., et al. (2016). Monocyte toll-like receptor expression in patients with atrial fibrillation. *Am. J. Cardiol.* 117, 1463–1467. doi: 10.1016/j.amjcard.2016.02.014

Heinzel, F. R., MacQuaide, N., Biesmans, L., and Sipido, K. (2011). Dyssynchrony of Ca^{2+} release from the sarcoplasmic reticulum as subcellular mechanism of cardiac contractile dysfunction. *J. Mol. Cell. Cardiol.* 50, 390–400. doi: 10.1016/j.yjmcc.2010.11.008

Kanno, S., Nishio, H., Tanaka, T., Motomura, Y., Murata, K., Ihara, K., et al. (2015). Activation of an innate immune receptor, Nod1, accelerates atherogenesis in Apoe-/- mice. *J. Immunol.* 194, 773–780. doi: 10.4049/jimmunol.1302841

Katoh, S., Honda, S., Watanabe, T., Suzuki, S., Ishino, M., Kitahara, T., et al. (2014). Atrial endothelial impairment through Toll-like receptor 4 signaling causes atrial thrombogenesis. *Heart Vessels* 29, 263–272. doi: 10.1007/s00380-013-0369-3

Keestra-Gounder, A. M., Byndloss, M. X., Seyffert, N., Young, B. M., Chávez-Arroyo, A., Tsai, A. Y., et al. (2016). NOD1 and NOD2 signalling links ER stress with inflammation. *Nature* 532, 394–397. doi: 10.1038/nature17631

Kizaki, T., Izawa, T., Sakurai, T., Haga, S., Taniguchi, N., Tajiri, H., et al. (2008). Beta2-adrenergic receptor regulates Toll-like receptor-4-induced nuclear factor-kappaB activation through beta-arrestin 2. *Immunology* 124, 348–356. doi: 10.1111/j.1365-2567.2007.02781.x

Lehnart, S. E., Terrenoire, C., Reiken, S., Wehrens, X. H., Song, L. S., Tillman, E. J., et al. (2006). Stabilization of cardiac ryanodine receptor prevents intracellular

calcium leak and arrhythmias. *Proc. Natl. Acad. Sci. U.S.A.* 103, 7906–7910. doi: 10.1073/pnas.0602133103

Levine, B., Kalman, J., Mayer, L., Fillit, H. M., and Packer, M. (1990). Elevated circulating levels of tumor necrosis factor in severe chronic heart failure. *N. Engl. J. Med.* 323, 236–241. doi: 10.1056/NEJM199007263230405

Lin, L., and Knowlton, A. A. (2014). Innate immunity and cardiomyocytes in ischemic heart disease. *Life Sci.* 100, 1–8. doi: 10.1016/j.lfs.2014.01.062

Lymperopoulos, A. (2013). Physiology and pharmacology of the cardiovascular adrenergic system. *Front. Physiol.* 4:240. doi: 10.3389/fphys.2013.00240

Madamanchi, A. (2007). Beta-adrenergic receptor signaling in cardiac function and heart failure. *Mcgill J. Med.* 10, 99–104.

Mann, D. L. (2015). Innate immunity and the failing heart: the cytokine hypothesis revisited. *Circ. Res.* 116, 1254–1268. doi: 10.1161/CIRCRESAHA.116.302317

Marks, A. R. (2013). Calcium cycling proteins and heart failure: mechanisms and therapeutics. *J. Clin. Invest.* 123, 46–52. doi: 10.1172/JCI62834

Mayourian, J., Ceholski, D. K., Gonzalez, D. M., Cashman, T. J., Sahoo, S., Hajjar, R. J., et al. (2018). Physiologic, pathologic, and therapeutic paracrine modulation of cardiac excitation-contraction coupling. *Circ. Res.* 122, 167–183. doi: 10.1161/CIRCRESAHA.117.311589

Monnerat, G., Alarcón, M. L., Vasconcellos, L. R., Hochman-Mendez, C., Brasil, G., Bassani, R. A., et al. (2016). Macrophage-dependent IL-1beta production induces cardiac arrhythmias in diabetic mice. *Nat. Commun.* 7:13344. doi: 10.1038/ncomms13344

Monnerat-Cahli, G., Alonso, H., Gallego, M., Alarcón, M. L., Bassani, R. A., Casis, O., et al. (2014). Toll-like receptor 4 activation promotes cardiac arrhythmias by decreasing the transient outward potassium current (Ito) through an IRF3-dependent and MyD88-independent pathway. *J. Mol. Cell. Cardiol.* 76, 116–125. doi: 10.1016/j.yjmcc.2014.08.012

Murray, D. R., and Freeman, G. L. (1996). Tumor necrosis factor-alpha induces a biphasic effect on myocardial contractility in conscious dogs. *Circ. Res.* 78, 154–160. doi: 10.1161/01.RES.78.1.154

Park, J. H., Kim, Y. G., McDonald, C., Kanneganti, T. D., Hasegawa, M., Body-Malapel, M., et al. (2007). RICK/RIP2 mediates innate immune responses induced through Nod1 and Nod2 but not TLRs. *J. Immunol.* 178, 2380–2386. doi: 10.4049/jimmunol.178.4.2380

Prieto, P., Vallejo-Cremades, M. T., Benito, G., González-Peramato, P., Francés, D., Agra, N., et al. (2014). NOD1 receptor is up-regulated in diabetic human and murine myocardium. *Clin. Sci.* 127, 665–677. doi: 10.1042/CS20140180

Pyo, R. T., Sui, J., Dhume, A., Palomeque, J., Blaxall, B. C., Diaz, G., et al. (2006). CXCR4 modulates contractility in adult cardiac myocytes. *J. Mol. Cell. Cardiol.* 41, 834–844. doi: 10.1016/j.yjmcc.2006.08.008

Reiken, S., Gaburjakova, M., Guatimosim, S., Gomez, A. M., D'Armiento, J., Burkhoff, D., et al. (2003). Protein kinase A phosphorylation of the cardiac calcium release channel (ryanodine receptor) in normal and failing hearts. Role of phosphatases and response to isoproterenol. *J. Biol. Chem.* 278, 444–453. doi: 10.1074/jbc.M207028200

Ruiz-Hurtado, G., Li, L., Fernández-Velasco, M., Rueda, A., Lefebvre, F., Wang, Y., et al. (2015). Reconciling depressed Ca^{2+} sparks occurrence with enhanced RyR2 activity in failing mice cardiomyocytes. *J. Gen. Physiol.* 146, 295–306. doi: 10.1085/jgp.201511366

Schulz, R., Panas, D. L., Catena, R., Moncada, S., Olley, P. M., and Lopaschuk, G. D. (1995). The role of nitric oxide in cardiac depression induced by interleukin-1 beta and tumour necrosis factor-alpha. *Br. J. Pharmacol.* 114, 27–34. doi: 10.1111/j.1476-5381.1995.tb14901.x

Terentyev, D., Rees, C. M., Li, W., Cooper, L. L., Jindal, H. K., Peng, X., et al. (2014). Hyperphosphorylation of RyRs underlies triggered activity in transgenic rabbit model of LQT2 syndrome. *Circ. Res.* 115, 919–928. doi: 10.1161/CIRCRESAHA.115.305146

Testa, M., Yeh, M., Lee, P., Fanelli, R., Loperfido, F., Berman, J. W., et al. (1996). Circulating levels of cytokines and their endogenous modulators in patients with mild to severe congestive heart failure due to coronary artery disease or hypertension. *J. Am. Coll. Cardiol.* 28, 964–971. doi: 10.1016/S0735-1097(96)00268-9

Val-Blasco, A., Piedras, M. J., Ruiz-Hurtado, G., Suarez, N., Prieto, P., Gonzalez-Ramos, S., et al. (2017a). Role of NOD1 in heart failure progression via regulation of Ca^{2+} handling. *J. Am. Coll. Cardiol.* 69, 423–433. doi: 10.1016/j.jacc.2016.10.073

Val-Blasco, A., Prieto, P., Gonzalez-Ramos, S., Benito, G., Vallejo-Cremades, M. T., Pacheco, I., et al. (2017b). NOD1 activation in cardiac fibroblasts induces myocardial fibrosis in a murine model of type 2 diabetes. *Biochem. J.* 474, 399–410. doi: 10.1042/BCJ20160556

van Oort, R. J., McCauley, M. D., Dixit, S. S., Pereira, L., Yang, Y., Respress, J. L., et al. (2010). Ryanodine receptor phosphorylation by calcium/calmodulin-dependent protein kinase II promotes life-threatening ventricular arrhythmias in mice with heart failure. *Circulation* 122, 2669–2679. doi: 10.1161/CIRCULATIONAHA.110.982298

Venetucci, L. A., Trafford, A. W., O'Neill, S. C., and Eisner, D. A. (2008). The sarcoplasmic reticulum and arrhythmogenic calcium release. *Cardiovasc. Res.* 77, 285–292. doi: 10.1093/cvr/cvm009

Wang, W., Xu, M., Zhang, Y. Y., and He, B. (2009). Fenoterol, a beta(2)-adrenoceptor agonist, inhibits LPS-induced membrane-bound CD14, TLR4/CD14 complex, and inflammatory cytokines production through beta-arrestin-2 in THP-1 cell line. *Acta Pharmacol. Sin.* 30, 1522–1528. doi: 10.1038/aps.2009.153

Conflict of Interest Statement: The authors declare that the research was conducted in the absence of any commercial or financial relationships that could be construed as a potential conflict of interest.

frontiers in Physiology

REVIEW
published: 06 December 2018
doi: 10.3389/fphys.2018.01775

Redox Dependent Modifications of Ryanodine Receptor: Basic Mechanisms and Implications in Heart Diseases

*Roman Nikolaienko, Elisa Bovo and Aleksey V. Zima**

Department of Cell and Molecular Physiology, Loyola University Chicago, Maywood, IL, United States

Heart contraction vitally depends on tightly controlled intracellular Ca regulation. Because contraction is mainly driven by Ca released from the sarcoplasmic reticulum (SR), this organelle plays a particularly important role in Ca regulation. The type two ryanodine receptor (RyR2) is the major SR Ca release channel in ventricular myocytes. Several cardiac pathologies, including myocardial infarction and heart failure, are associated with increased RyR2 activity and diastolic SR Ca leak. It has been suggested that the increased RyR2 activity plays an important role in arrhythmias and contractile dysfunction. Several studies have linked increased SR Ca leak during myocardial infarction and heart failure to the activation of RyR2 in response to oxidative stress. This activation might include direct oxidation of RyR2 as well as indirect activation via phosphorylation or altered interactions with regulatory proteins. Out of ninety cysteine residues per RyR2 subunit, twenty one were reported to be in reduced state that could be potential targets for redox modifications that include S-nitrosylation, S-glutathionylation, and disulfide cross-linking. Despite its clinical significance, molecular mechanisms of RyR dysfunction during oxidative stress are not fully understood. Herein we review the most recent insights into redox-dependent modulation of RyR2 during oxidative stress and heart diseases.

Keywords: heart, Ca signaling, ryanodine receptor, sarcoplasmic reticulum, oxidative stress

OPEN ACCESS

Edited by:
Laetitia Pereira, Institut National de la Santé et de la Recherche Médicale (INSERM), France

Reviewed by:
Juan Antonio Rosado Dionisio, Universidad de Extremadura, Spain
Geoffrey Woodard, Harvard University, United States

***Correspondence:**
Aleksey V. Zima
azima@luc.edu

Specialty section:
This article was submitted to Membrane Physiology and Membrane Biophysics, a section of the journal Frontiers in Physiology

Received: *27 September 2018*
Accepted: *23 November 2018*
Published: *06 December 2018*

Citation:
Nikolaienko R, Bovo E and Zima AV (2018) Redox Dependent Modifications of Ryanodine Receptor: Basic Mechanisms and Implications in Heart Diseases. Front. Physiol. 9:1775. doi: 10.3389/fphys.2018.01775

EXCITATION-CONTRACTION COUPLING

Regular heart contraction critically depends on precisely-controlled cytosolic Ca regulation during each cardiac cycle. The sarcoplasmic reticulum (SR) Ca release plays a particularly important role in activation of myocyte contraction (Zima et al., 2014). During systole, Ca release from the SR is a result of activation of specialized Ca channels – ryanodine receptors (RyR). These channels are activated by an inward Ca current via L-type Ca channels (LTCCs) during an action potential (AP) (**Figure 1A**). The mechanism of RyR activation by cytosolic Ca is known as Ca-induced Ca release (CICR) (Fabiato, 1983). In ventricular myocytes, CICR occurs at specialized microdomains where a T-tubule of the sarcolemma closely approaches a junction of the SR forming the dyad. The junctional SR membrane contains clusters of RyRs (Franzini-Armstrong et al., 1999; Hayashi et al., 2009). The activation of a single RyR cluster generates a local increase in cytosolic Ca ($[Ca]_i$) called Ca spark (Cheng et al., 1993; **Figure 1B**). The spatio-temporal summation of thousands of

Ca sparks produces the global Ca transient that initiates contraction. During diastole, cytosolic Ca is pumped back into the SR by the Ca-ATPase (SERCA) and extruded from the cell by the Na-Ca exchanger (NCX) (Bers, 2002). The rate at which SERCA and NCX remove Ca from the cytosol determines how quickly cardiac muscle relaxes to allow the heart to fill with blood.

RYANODINE RECEPTOR COMPLEX

Three isoforms of RyR have been identified. The RyR1 isoform is dominant in skeletal muscles, whereas the RyR2 represents the cardiac RyRs isoform. The RyR3 isoform is found only at low expression levels in certain skeletal muscle types and brain (Lanner et al., 2010; Meissner, 2017). RyR forms a homo tetrameric assembly comprised of four 560 kDa subunits yielding a total molecular weight of 2,300 kDa (Van Petegem, 2015). The RyR2 is not only an ion channel but also a giant scaffolding protein on which several regulatory proteins and enzymes can be assembled (Fill and Copello, 2002; Bers, 2004; **Figure 1C**). RyR2 forms a multimolecular complex with FK506 binding protein 12.6 (FKBP12.6) and calmodulin (CaM) at the cytosolic side. FKBP12.6 binds to each subunit of RyR2 with high affinity and stabilizes the channel in closed conformation (Brillantes et al., 1994; Timerman et al., 1994; Wehrens et al., 2004). Another small regulatory protein CaM binds RyR with nanomolar affinity, at 1:4 ratio in the absence and presence of Ca (apoCaM and Ca-CaM) (Meissner, 2017). The effect of CaM on RyR activity is isoform specific. At free [Ca] $> 1\ \mu M$ CaM inhibits all three isoforms of RyR, whereas at submicromolar free [Ca] CaM activates RyR1 and RyR3, and inhibits RyR2 (Balshaw et al., 2001; Meissner, 2004). At the luminal side, RyR2 is associated with the complex consisting of triadin-1, junctin and calsequestrin that act together as a luminal Ca sensor (Györke et al., 2004). Other reports suggest RyR2 interactions with junctophilin, homer-1, sorcin and S100A1 (Song D.W. et al., 2011). Additionally, the RyR2 complex comprises enzymes that regulate the channel activity through the interplay of phosphorylation and dephosphorylation by protein kinases and protein phosphatases. Protein kinase A (PKA) phosphorylates RyR2 at serines 2030 and 2808, whereas Ca-CaM dependent protein kinase II (CaMKII) phosphorylates the channel at serine 2814 (Marx et al., 2000; Wehrens, 2004; Xiao et al., 2006). Phosphorylation can be reversed by associated with the RyR2 complex protein phosphatases 1 and 2A (PP1 and PP2A) (Marx et al., 2000).

RYR2-MEDIATED SR Ca LEAK

The majority of SR Ca release occurs during systole via the mechanism of CICR. During diastole, however, spontaneous openings of RyR2s can produce SR Ca leak (Shannon et al., 2003; Zima et al., 2014). At normal physiological conditions, a large fraction of SR Ca leak occurs as uncoordinated openings of individual RyR2s or spark-independent Ca leak. This leak component can serve as an important protective mechanism against SR Ca overload. (Zima et al., 2010). However, in pathological conditions associated with increased RyR2 activity, the majority of SR Ca leak occur in a form of Ca sparks and Ca waves. By activating the electrogenic NCX, spontaneous Ca waves can generate delayed afterdepolarizations (DADs), an effective trigger of cardiac arrhythmias (Pogwizd and Bers, 2004). Increased diastolic SR Ca leak through RyR2s channel has been also implicated in the development of several cardiac pathologies, including heart failure (HF) (Shannon et al., 2003; Kubalova et al., 2005; Belevych et al., 2007; Bers, 2014). It has been suggested that SR Ca leak contributes to the depressed Ca transients and the reduced SR Ca load in HF. The increased RyR2-mediated Ca leak has been also implicated in the progression of arrhythmogenesis in failing hearts (Blayney and Lai, 2009). It has been suggested that oxidative post-translational modifications in RyR2 may play an important role in the abnormal channel activity and the increased SR Ca leak in many cardiac pathologies (Mochizuki et al., 2007; Terentyev et al., 2008; Belevych et al., 2009, 2011, 2012; Bovo et al., 2018a,b). The functional effect of these redox modifications, including disulfide oxidation, mixed disulfide formation (S-glutathionylation) and S-nitrosylation, will be further discussed in this review.

ROS PRODUCTION IN CARDIAC MUSCLE

Cardiac muscle contraction strongly depends on ATP synthesis by the mitochondrial electron transport chain (ETC). In addition to energy production, the ETC activity can lead to generation of reactive oxygen species (ROS). During the reduction of molecular oxygen to water some redox centers, in particular complex I and III, in the ETC may leak electrons to oxygen producing superoxide anion ($O_2^{-}\bullet$) (Turrens, 2003). $O_2^{-}\bullet$ is further converted into hydrogen peroxide ($H_2O_2\bullet$) by superoxide dismutase (SOD) enzymes. Transitional metals can react with H_2O_2 with a formation of even stronger oxidant – hydroxyl radical ($OH\bullet$) (Madamanchi and Runge, 2013). ROS can be also generated by cytochrome P450-based enzymes, xanthine (XO) and NADPH oxidases (NOX) (Zima and Blatter, 2006; Santos et al., 2016). Additionally, cardiomyocytes express two isoforms of nitric oxide ($NO\bullet$) synthase – endothelial and neuronal NOS (NOS1 and NOS3, respectively) that play an important role in the intracellular signaling (Santos et al., 2011). Besides generation of $NO\bullet$, NOSs are also responsible for the production of reactive nitrogen species (RNS). Uncoupled NOSs can generate $O_2^{-}\bullet$, which can be combined with $NO\bullet$ to produce the powerful oxidant peroxinitrite ($ONOO^{-}\bullet$).

Deleterious effects of increased ROS production include lipid peroxidation, protein oxidation, DNA mutagenesis and DNA-protein cross-linking. Therefore, amounts of ROS inside the cell must be tightly controlled by enzymatic and non-enzymatic antioxidant defense mechanisms (Madamanchi and Runge, 2013). These mechanisms comprise catalase, SOD, glutathione peroxidase and vitamins A, C and E (Zima and Blatter, 2006; Santos et al., 2016). $O_2^{-}\bullet$ produced in mitochondria is converted to H_2O_2 by SOD, which is further reduced to water by glutathione peroxidase, catalase, peroxiredoxin

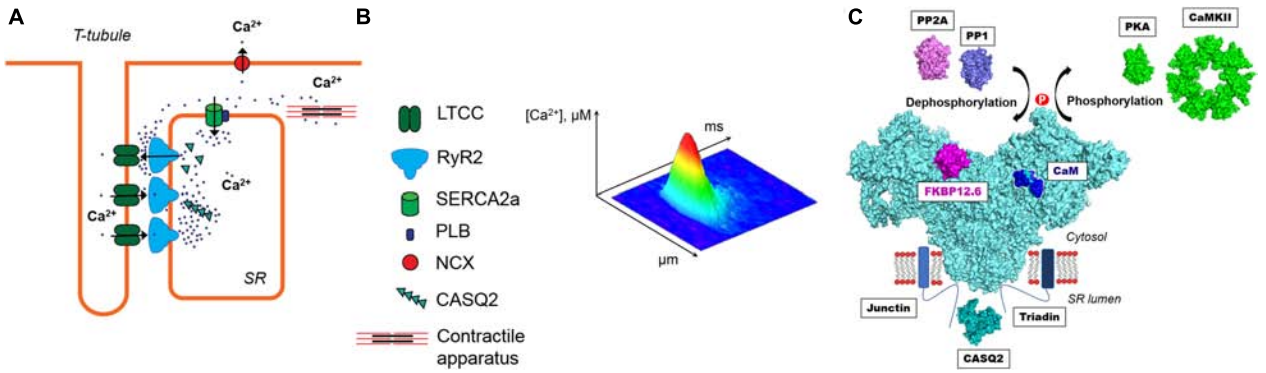

FIGURE 1 | (A) The main components of intracellular Ca regulation in ventricular myocytes. A Ca release unit is formed by a cluster of ryanodine receptors (RyR2) in the junctional sarcoplasmic reticulum (SR) and L-type Ca channels (LTCC) in the sarcolemma. During systole, inward Ca current through the LTCC activates RyR2 by the mechanism called Ca-induced Ca release (CICR). A global Ca transient causes activation of the contractile apparatus and thus myocyte contraction. During diastole, cytosolic Ca is pumped back into the SR by the Ca-ATPase (SERCA) and extruded from the cell by the Na-Ca exchanger (NCX). **(B)** A confocal image of diastolic Ca spark. **(C)** The multimolecular RyR2 complex. On the cytosolic side, RyR2 interacts with calmodulin (CaM) and FK-506 binding protein 12.6 (FKBP12.6). The activity of RyR2 is also regulated by two major protein kinases (PKA and CaMKII) and two phosphatases (PP1 and PP2A). At the luminal side, RyR2 is associated with the Ca-sensing complex formed by triadin, junctin and calsequestrin (CASQ2). The molecular representation of the illustrated proteins was created from Protein Data Bank entries (www.rcsb.com, PDB_IDs: 5L1D, 1CPK, 2W2C, 2BCX, 1UP5, 4MOV, 2IAE, 2VAF, 4IQ2).

and thioredoxin systems (Foster et al., 2009). Non-enzymatic defense mechanisms rely on small antioxidant molecules, primarily on the intracellular pool of reduced glutathione (GSH). It has been shown that GSH can directly acts as ROS scavenger. Upon its reaction with ROS, GSH is oxidized into GSSG that can be reduced back to GSH by glutathione reductase (Schafer and Buettner, 2001). Glutathione reductase plays a key role in maintaining the intracellular GSH/GSSG ratio in a proper physiological range (30:1–100:1). GSH also contributes to the maintenance of the cellular redox state by acting as a substrate for glutathione peroxidase (Foster et al., 2009). When the amount of ROS production overwhelms the intracellular anti-oxidant defense, oxygen free-radicals cause damage of DNA, lipids and proteins. These uncontrolled conditions are also known as oxidative stress (Giordano, 2005).

At physiological conditions, however, low levels of ROS and RNS are involved in the cell signaling by inducing discrete, reversible and site-specific protein modification (Heymes et al., 2003; Giordano, 2005; Foster et al., 2009). The redox signaling is based on the ability of ROS/RNS to modulate protein cysteines, leading to S-nitrosylation, S-glutathionylation, and disulfide bond formation. Such redox modifications would affect activity of the proteins involved in different signaling cascades. For example, in cardiac muscle NOX activity and ROS production can be stimulated by growth factors and cytokines, such as angiotensin II, PDGF and TNF-α (Giordano, 2005). In these pathways, ROS act as important second messengers related to inflammatory and stress response. Redox modifications of signaling proteins can be reversed by specific enzymes. Disulfide bridges and mixed disulfides (S-glutathionylation) can be reduced by both thioredoxin and glutaredoxin systems. Additionally, thioredoxin system can reduce S-nitrosothiols. Both glutaredoxin and thioredoxin system utilize the reducing power of NADPH for reduction of their key enzymes – glutathione and thioredoxin reductases (Paulina Donoso and Gina Sánchez, 2013).

In the heart, increased ROS production during oxidative stress has been associated with different cardiac pathologies, including myocardial infarction (MI) and HF. During MI, the re-oxygenation of ischemic region is vital for heart survival. However, re-oxygenation also causes significant myocardium damage which has been linked to the toxic effects of ROS (Zweier and Talukder, 2006). Significant increase in ROS production during ischemia/reperfusion (I/R) arises from the uncoupled mitochondrial ETC as well us upregulation of NOX, NOS and XO resulting in increased generation of $O_2^{\bullet-}$ and decreased GSH/GSSH ratio (Zima and Mazurek, 2016). Oxidative stress during cardiac pathologies is commonly associated with increased SR Ca leak through the hyperactive RyR2. Moreover, ROS can activate hypertrophic and pro-apoptotic signaling pathways, leading to myocardial remodeling (Sawyer et al., 2002; Santos et al., 2016). HF is frequently viewed as a condition of chronic oxidative stress (Mak and Newton, 2001). The unbalanced metabolism has been suggested to play an important role in development of HF (Mak and Newton, 2001; Ventura-Clapier et al., 2004; Santos et al., 2011). As the disease progresses, oxidative stress worsens due to the increasing energy demand and workload of the failing heart, thus perpetuating a deleterious cycle (Seddon et al., 2007). Although HF is associated with a large number of complex intracellular changes, the focus of this review is directed at understanding the role of oxidative stress in SR Ca regulation and RyR2 function. To date, RyR2 dysfunction has been characterized by increased phosphorylation and oxidation levels. While functionally important phosphorylation sites on RyR2 have been characterized (Marx et al., 2000; Wehrens, 2004; Xiao et al., 2006), the specific mechanisms of oxidative modifications of RyR2 and their contribution to defective SR Ca cycling remain incomplete.

REDOX REGULATION OF RYR2

Historically, oxidative stress has been linked to an increase of SR Ca release (Trimm et al., 1986). It has been proposed that oxidation of cysteines in RyR2 causes significant changes in the channel gating (Abramson and Salama, 1989). Out of 90 cysteine residues in the single subunit of RyR2, about 21 are in the free thiol state and available for redox-modifications (Xu, 1998; Donoso et al., 2011). Therefore, it is no surprise that RyR2 has been characterized as the highly redox sensitive ion channel. During oxidative stress, sulfhydryl groups of cysteine residues on RyR2 can be oxidized by ROS producing sulfenic, sulfinic and sulfonic acids (Giles and Jacob, 2002). While there is no evidence for the functional significance of sulfinic and sulfonic acids, sulfenic acid can react with sulfhydryl groups, RNS and GSH, yielding disulfide bridges, S-nitrosylation, S-glutathionylation, respectively (Paulina Donoso and Gina Sánchez, 2013). In general, oxidation of cysteine residues has been suggested to cause RyR2 activation (Suzuki and Ford, 1999; Zima and Blatter, 2006). However, multiple studies have shown that effects of oxidative agents on RyR2 largely depend on experimental conditions (Mi et al., 2015). It has been demonstrated that low concentrations of oxidizing agents activate RyR2, whereas prolonged exposure or high concentrations of oxidants lead to irreversible RyR2 inhibition (Dulhunty et al., 2000). Different cysteine residues have been suggested to play a role in activation or inhibition of RyR2 by oxidative stress.

The role of RyR2 redox modifications in cardiac pathologies has been investigated in numerous studies. It has been shown that the non-selective beta-blocker with antioxidant properties carvedilol is more effective in a treatment of HF than other beta-blockers. In the pacing-induced HF model, carvedilol was able to preserve the cardiac function by stabilizing RyR2 structure. It has been suggested that some of the beneficial effects of carvedilol can be attributed to its ability to prevent oxidation of RyR2. In experiments with administration of the $NO^{-}\bullet$/$ONOO^{-}\bullet$ donor SIN-1, carvedilol was able to prevent thiol oxidation in RyR2, presumably by acting as a scavenger of $ONOO^{-}\bullet$ (Mochizuki et al., 2007). In the canine model of chronic HF, the increased SR Ca leak has been attributed to redox modification of RyR2 by ROS. Interestingly, reducing agents that target S-nitrosylation and S-glutathionylation failed to reverse SR Ca leak in HF. At the same time, the application of DTT (an agent that can reverse disulfide formation, S-nitrosylation and S-glutathionylation) decreased RyR2-mediated Ca leak, suggesting a central role of disulfide bond formation in this process (Terentyev et al., 2008). Studies of the canine post-MI model with ventricular fibrillation (VF) has also shown increased diastolic SR Ca leak and decreased SR Ca content. Similarly to HF studies, cardiomyocytes isolated from the canine post-MI model were characterized by increased levels of ROS production and RyR2 oxidation (Belevych et al., 2009). Another study of the rabbit I/R model has shown a critical role of RyR2 oxidation in the transition from the positive inotropic to arrhythmogenic effect during β-adrenergic receptor stimulation (Bovo et al., 2018a). Taken together, these data suggest that SR Ca leak due to RyR2 oxidation can be a common mechanism of SR Ca mishandling during different cardiac pathologies. Therefore, reactive cysteines on RyR2 may represent an important target in the development of new therapeutic strategies.

IDENTIFICATION OF RYR2 REDOX-MODIFICATION SITES

Given the functional significance of redox modifications of RyR, several structural studies were performed in order to allocate and characterize sites of these modifications. In the skeletal isoform RyR1, cysteine 3635 located in the CaM-binding site has been shown to undergo functionally significant S-nitrosylation (Sun et al., 2001). Mass spectroscopy study has identified nine cysteine residues (including cysteine 3635) in RyR1 that were S-alkylated by low doses of the maleamide derivative CPM, suggesting their high-sensitivity to redox modifications (Voss et al., 2004). Other studies have proposed that cysteine 3635 can undergo S-glutathionylation and could be also involved in RyR disulfide cross-linking (Aracena-Parks et al., 2006). Twelve RyR1 cysteine residues, including cysteine 3635, have been proposed to be either S-nitrosylated, S-glutathionylated or to form disulfide bridges. Of those twelve cysteines, nine were shown to be endogenously redox-modified. It has been suggested that cysteine 3635 can form a disulfide bond with cysteine residues in the region 1–2401 of RyR1 (possibly with either cysteine 36, 2326, or 2363). However, the functional significance of these redox-modifications remains unclear yet.

While skeletal RyR1 hyper-reactive cysteines have been characterized, little is known about corresponding redox modifications in the cardiac RyR2. A functional role of RyR2 cysteine 3602 (which corresponds to the hyper-reactive cysteine 3635 in RyR1) in Ca overload-induced Ca release has been studied in HEK293 cells expressing recombinant RyR2. It has been shown that the mutation of RyR2 cysteine 3602 to alanine (C3602A) significantly increased SR Ca fractional release by decreasing termination and increasing activation threshold for CICR. Interestingly, the ability of N-ethylmaleamide (NEM) to increase the activation threshold for CICR for the RyR2 was lost for the C3602A mutant, suggesting functional significance of cysteine 3602 alkylation. However, no difference was observed in the effect of cysteine oxidants on WT and C3602A RyR2 (Mi et al., 2015). Despite ∼70% homology between RyR1 and RyR2, these channels appear to exhibit important structural and functional differences, particularly with respect to redox regulation.

S-GLUTATHIONYLATION OF RYR2

High pKa (>8.0) of a sulfhydryl group means that the majority of free thiols is protonated under physiological pH (7.0–7.4) and cannot be oxidized. As a result, protein redox modifications require an initial conversion of a sulfhydryl group to a thiolate anion. Proton dissociation from a thiol group is highly dependent on the local microenvironment and can be facilitated by closely located basic amino-acids (Grek et al., 2013). During oxidative

stress, spontaneous protein S-glutathionylation may occur via multiple pathways that include thiol-disulfide exchange between a protein thiol and GSSG, a reaction between sulfenic acid or thiyl radical (-S•) and GSH, as well as S-glutathionylation induced by RNS. In addition to spontaneous reactions, the rate and efficiency of S-glutathionylation can be enhanced by enzymatic activity of glutathione-S-transferases (GSTs) (Zhang et al., 2018). Because of the ability of glutaredoxin and thioredoxin systems to reverse S-glutathionylation, this redox modification can prevent irreversible oxidation of protein thiol groups into sulfonic acids (Townsend, 2007). However, the addition of large and negatively charged glutathione group may also significantly alter structural and functional properties of a protein. Moreover, two adjacent S-glutathionilated thiols can displace GSH groups with a formation of disulfide bond within the protein (Beer et al., 2004).

Several studies have provided evidence for the functional role of RyR2 S-glutathionylation during oxidative stress (**Figure 2**). It has been reported that preconditioning tachycardia increased NOX activity in the SR microsomes isolated from the canine ventricle. The increased NOX activity led to increased RyR S-glutathionylation and elevated systolic SR Ca release (Sánchez et al., 2005). The same effect was described for the SR microsomes isolated from animals preconditioned with exercises. It has been suggested that NOX activation and RyR2 S-glutathionylation during preconditioning may have a protective effect by increasing systolic SR Ca release while limiting diastolic SR Ca leak (Sánchez et al., 2008). In our recent study, we described the effects of oxidized glutathione (GSSG) on SR Ca leak in rabbit ventricular myocytes. We found that an application of GSSG to permeabilized myocytes increased diastolic SR Ca leak and induced RyR2 disulfide cross-linking (Mazurek et al., 2014). HF myocytes were also characterized by elevated GSSG level, RyR2 cross-linking and increased SR Ca leak. Blocking RyR2 cross-linking with the alkylating agent NEM decreased SR Ca leak and prevented depletion of SR Ca load. Based on these results, we suggested that oxidative stress in the failing heart promotes abnormal inter-subunit interactions within the RyR2 complex that increase channel opening leading to the increased SR Ca leak (Bovo et al., 2018a).

Interestingly, some studies suggest an interaction between RyR and GSTs, enzymes that catalyze S-glutathionylation. The members of GST family CLIC-2, GSTO1-1, and GSTM2-2 were identified as endogenous RyR modulators that exert a strong inhibitory effect on RyR2 and weak excitatory effect on RyR1. The isoform-specific effect of GSTM2-2 has been explained by its binding to the RyR2 divergent region 3, not present in RyR1 (Liu et al., 2012) The C-terminal non-catalytic region of the muscle specific GSTM2-2 has been shown to bind to RyR2 independently from N-terminal glutathione transferase activity (Dulhunty et al., 2011). However, it remains unclear whether GSTM2-2 may be involved in RyR2 S-glutathionylation *in vivo*.

S-NITROSYLATION OF RYR2

NO• plays an important role in cardiovascular signaling through its involvement in the cGMP-dependent vasodilation pathway. NO• binds to guanylate cyclase (GC) increasing the production of cGMP that activates several cGMP-dependent enzymes, including cAMP phosphodiesterase (PDE). The PDE activation would decrease cAMP level and PKA activity. This, in turn, would cause a decrease in PKA phosphorylation of several proteins, including RyR2, LTCC and phospholamban (PLB). cGMP can also activate cGMP-dependent kinase (PKG). It has been reported that PKG can phosphorylate RyR2 at the CaMKII site (Takasago et al., 1991). However, the functional significance of PKG-mediated RyR2 phosphorylation remains elusive. NO•-based signaling reactions can also occur through the NO•-dependent redox-modification, known as S-nitrosylation (Lima et al., 2010; **Figure 2**). The reaction of S-nitrosylation involves a transfer of NO• group to a nucleophilic thiol group yielding S-nitrosothiol (Sun and Murphy, 2010). To initiate S-nitrosylation, thiol groups have to be oxidized (Donoso et al., 2011). It has been shown that intracellular proteins can be effectively nitrosylated by endogenously produced NO• as well by exogenous NO• donors (Hess et al., 2005).

The majority of functional studies of RyR S-nitrosylation have been conducted in lipid bilayer experiments with skeletal and cardiac SR vesicles. It has been shown that NO• donors S-nitrosoglutathione and S-nitrosocysteine can induce S-nitrosylation on each RyR2 subunit at three different sites. S-nitrosylation of RyR2 was associated with an increase of the channel open probability. Interestingly, a comparable RyR2 oxidation of 5-6 thiols per subunit showed no significant effect on the RyR2 function, suggesting a different role of thiol S-nitrosylation and oxidation in the channel activity (Xu, 1998). In another study, S-nitrosothiol reagents increased Ca release from skeletal and cardiac muscle SR vesicles, confirming that RyR S-nitrosylation activates RyR (Stoyanovsky et al., 1997). In both reports, the NO•/$ONOO^-$• donor SIN-1 produced a significant RyR activation that could not be reversed by reducing agents, suggesting irreversible thiol oxidation. The effect of NO• donor SNAP on RyR1 activity in lipid bilayers was complex and dependent on several factors including, concentration, membrane potential and presence of agonists. Low concentrations of NO• donor SNAP increased RyR1 activity, whereas high concentrations (∼1 mM) caused channel inhibition (Hart and Dulhunty, 2000). In another study, a pretreatment of RyR1 with low concentrations of NO• donors prevented disulfide cross-linking induced by diamide. At the same time, NO• donors had no significant effect on the channel open probability. Higher doses of NO• donors, however, were able to increase RyR1 activity and induced disulfide cross-liking (Aghdasi et al., 1997). This type of complex regulation suggests the presence of several groups of functional thiol residues that differently modulate the RyR activity by RNS. Moreover, it has been shown that direct activation of RyR1 by submicromolar concentrations of NO• donors can only occur at physiological pO_2 ∼10 mmHg (in contrast to ambient pO_2 150 mmHg). This suggests that RyR1 thiol residues have to be in the reduced state to be nitrosylated by NO• (Eu et al., 2000). However, these results could not be reproduced by another group. It was reported that NO• donors NOC-12 and GSNO activate RyR1 independently from pO_2 (Cheong et al., 2005). Furthermore, the effect of NO• donors

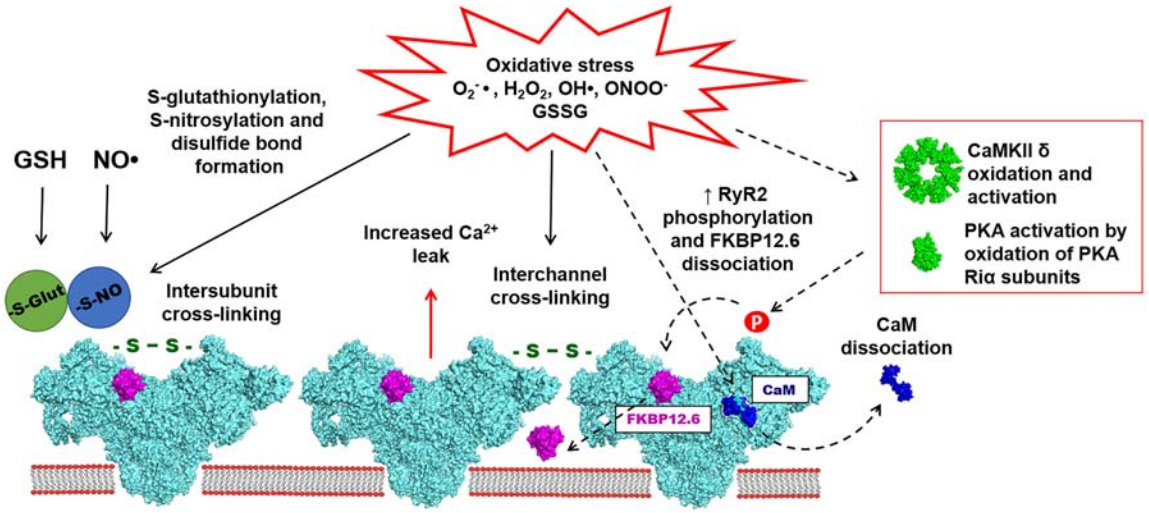

FIGURE 2 | Oxidative stress is associated with the increased accumulation of reactive oxygen and nitrogen species (ROS/RNS), such as O2−•, H_2O_2, OH•, and ONOO−•. ROS and RNS have been implicated in redox-dependent post-translational modifications of cardiac RyR2, including S-glutathionylation, S-nitrosylation and disulfide bond formation (marked with solid arrows). Disulfide bond formation also leads to RyR2 cross-linking, which presumably may take place between subunits within one channel or between subunits of different channels. Oxidative stress may also indirectly modulate the activity of RyR2 (marked dashed arrows). Accumulation of ROS/RNS leads to calmodulin (CaM) dissociation from RyR2, potentially caused by the oxidation of RyR2 and/or CaM. Oxidative stress can also activate PKA and CaMKII leading to an increase of RyR2 phosphorylation on Serine 2808 and Serine 2814 sites. It has been also suggested that the PKA-dependent phosphorylation may lead to increased FKBP12.6 dissociation from RyR2. The effects of oxidative stress on RyR2 mostly lead to the increased diastolic SR Ca leak resulting in arrhythmias and contractile dysfunction in variety of cardiac pathologies.

on RyR1 involved the CaM dissociation and S-nitrosylation at cysteine 3635 (Sun et al., 2003). In contrast to RyR1, RyR2 can be activated only by GSNO, but not NOC-12. S-nitrosylation of cysteine 3602 (corresponding to cysteine 3635 in RyR1) was not required for RyR2 activation by GSNO (Sun et al., 2008).

In cardiomyocytes, NOS1 and NOS3 can induce S-nitrosylation of different substrates, depending on their subcellular localization (Lima et al., 2010). NOS3 is localized within the caveolae together with β-adrenergic receptors and LTCCs. NOS1 resides to the SR, where it modulates the activity of RyR2 (Barouch et al., 2002). Study of RyR2 S-nitrosylation in $NOS1^{-/-}$ mice has shown decreased S-nitrosylation, but increased oxidation of RyR2. Myocytes isolated from $NOS1^{-/-}$ mice were characterized by increased SR Ca leak, decreased SR Ca load and higher propensity of spontaneous Ca waves (Gonzalez et al., 2007). It has been also shown that NOS1 inhibition leads to the development of ventricular arrhythmias under condition of elevated cytosolic [Ca]. The molecular mechanism of arrhythmias has been attributed to the combination of decreased RyR2 S-nitrosylation and increased RyR2 oxidation. Under condition of NOS1 inhibition, the XO inhibitor allopurinol or the NO• donor GSNO could prevent ventricular arrhythmias. Interestingly, NOS1 inhibition was associated with decreased RyR2 phosphorylation at the CaMKII site. Moreover, the combination of NOS1 inhibition and oxidative stress had an additive effect, producing severe arrhythmical phenotype (Cutler et al., 2012). In another study of $NOS1^{-/-}$ myocytes, however, the decreased level of RyR2 S-nitrosylation was associated with decreased SR Ca release. NOS1 knockout or NOS inhibition reduced Ca spark frequency and SR Ca leak. Also, single channel recording revealed decreased open probability of RyR2 in the $NOS1^{-/-}$ mice. The NO• donor SNAP was capable to reverse the observed effects of NOS1 inhibition (Wang et al., 2010). The discrepancy between these two studies may be explained by the complex interplay between S-nitrosylation and oxidation in the regulation of RyR2 activity. It seems that physiological levels of RyR2 S-nitrosylation can be necessary for maintaining the proper channel activity in the healthy heart. Under conditions of oxidative stress, however, S-nitrosylation may function as a protective mechanism against irreversible thiol oxidation and RyR2 dysfunction. Thus, de-nitrosylation of RyR2 would inhibit the channel activity in control conditions and activate it during oxidative stress.

RYR INTERSUBUNIT DISULFIDE CROSS-LINKING

The idea of intersubunit cross-linking has been first introduced for RyR1 (Abramson and Salama, 1989) and then further confirmed for RyR2 (Mazurek et al., 2014). It has been suggested that intersubunit disulfide bond formation leads to structural rearrangements of the channel that cause SR Ca leak (**Figure 2**). Structural aspects of disulfide cross-linking in RyR1 have been extensively characterized in several studies (Moore et al., 1999; Zhang et al., 2003; Aracena-Parks et al., 2006). A cryo-EM analysis of RyR1 oxidation by H_2O_2 revealed a disulfide cross-linking together with significant changes in the channel morphology (Han et al., 2006). These data also revealed that

disulfide bonds can be formed between subunits within the RyR1 complex rather than between different RyR1 tetramers. Multiple studies of RyR1 have suggested that cysteine 3635 can be involved in the disulfide cross-linking and the CaM binding. However, recent Cryo-EM analysis of RyR1 and RyR2 did not provide a structural basis for the possible disulfide formation in this region (Yan et al., 2015; des Georges et al., 2016; Wei et al., 2016; Dhindwal et al., 2017). It has been suggested that disulfide bond formation may take place between N-terminal regions of RyR2 subunits (Zissimopoulos et al., 2013). Alternatively, RyR cross-linking may occur not only between subunits within one channel, but also between subunits of different RyR channels. It is well-known that skeletal and cardiac muscle RyRs are arranged as large clusters (Franzini-Armstrong et al., 1999; Cabra et al., 2016). Given the tight packing of RyRs in the cluster, there is a possibility of disulfide cross-linking between subunits of two neighboring channels (**Figure 2**). However, there are no direct data demonstrating this mechanism.

Because the intersubunit interactions within the RyR2 complex dictate the channel gating (Orlova et al., 1996; Serysheva et al., 2008; Tung et al., 2010), any post-translational modifications that affect an interaction between RyR2 subunits should have a significant impact on the RyR2 function. We found a positive correlation between RyR2 cross-linking and SR Ca leak, suggesting that the post-translational modification is a strong regulator of RyR2. We have also reported that RyR2 oxidation and the intersubunit cross-linking play an important role in activation of SR Ca leak during oxidative stress (Mazurek et al., 2014) and generation of pro-arrhythmogenic Ca waves during excessive adrenergic activation (Bovo et al., 2015). Furthermore, a significant level of RyR2 cross-linking was observed in ventricular myocytes isolated from the rabbit HF model (Bovo et al., 2018a). This RyR2 modification contributed to an increase of SR Ca leak and the blunted force-frequency response of the failing heart.

CALMODULIN DISSOCIATION DURING OXIDATIVE STRESS

CaM acts as an important regulatory protein of RyR2 that inhibits channel activity under both low and high [Ca] (Balshaw et al., 2001). During oxidative stress, increased levels of GSSG can decrease the binding affinity of apo-CaM and Ca-CaM to RyR2 (**Figure 2**). This would relieve the inhibitory effect of CaM on the RyR2 activity (Balshaw et al., 2001). Experiments in permeabilized ventricular myocytes have shown that RyR2 oxidation by H_2O_2 caused an alteration of the channel structure toward its arrhythmogenic unzipped conformation. This abnormal RyR2 conformation decreased the binding affinity to CaM, which can be restored by the RyR antagonist dantrolene (Oda et al., 2015). At the same time, oxidation caused no effect on the FKBP12.6 binding to RyR2. Dissociation of CaM from RyR2 due to the defective inter-domain interaction (or unzipping) has been linked to the increased SR Ca leak in HF (Ono et al., 2010). It has been shown that CaM isoforms with increased binding affinity to RyR2 have a potential to rescue the aberrant SR Ca release in HF (Hino et al., 2012). Furthermore, a recombinant CaM with decreased rate of dissociation from its binding domain on RyR2 unveiled anti-arrhythmogenic properties. In vivo gene delivery of this recombinant CaM into the heart partially restored RyR2 refractoriness and decrease a chance of arrhythmias in the catecholaminergic polymorphic ventricular tachycardia (CPVT) model caused by calsequestrin mutation (Liu et al., 2018).

RYR2 PHOSPHORYLATION AND OXIDATIVE STRESS

At least three functionally important phosphorylation sites have been identified in RyR2, including two PKA specific sites (serine 2030 and 2808) and one CaMKII site (serine 2814) (Marx et al., 2000; Xiao et al., 2006; Marx and Marks, 2013). RyR2 phosphorylation by PKA occurs in response to β-adrenergic receptor activation. Epinephrine and norepinephrine binding to β-adrenergic receptors increases adenylyl cyclase activity and cAMP production, following by PKA activation (El-Armouche and Eschenhagen, 2009). It has been shown that RyR2 phosphorylation at serine 2808 increased RyR2 open probability and caused FKBP12.6 dissociation from the channel (Marx et al., 2000; **Figure 2**). However, studies from different laboratories have yielded conflicting results regarding the role of RyR2 phosphorylation by PKA in HF (Benkusky et al., 2007; Shan et al., 2010a,b; Zhang et al., 2012). Interestingly, increased levels of RyR2 oxidation and S-nitrosylation have been reported in transgenic mice with the RyR2 mutation mimicking the constitutively phosphorylated serine 2808 (S2808D). While RyR2 activity in the S2808D mutant was normal at young age, in older animals the RyR2 displayed increased SR Ca leak caused by its oxidation and S-nitrosylation together with depletion of FKBP12.6 and other regulatory proteins (Shan et al., 2010a). These results were in line with another study in which mutation of one of two RyR2 phosphorylation sites (serine 2808 or 2814) reduced both oxidative stress and SR Ca leak in the mouse model of Duchenne muscular dystrophy (DMD) (Wang et al., 2015). Earlier studies have shown that DMD patients can develop ventricular arrhythmias associated with leaky RyR2 due to S-nitrosylated and FKBP12.6 depletion (Fauconnier et al., 2010).

While the functional significance of RyR2 phosphorylation has been debated, it is important to highlight that both CaMKII and PKA are sensitive to the intracellular redox state (Johnston et al., 2015; **Figure 2**). In contrast to the cAMP-dependent PKA activation, PKA activation by oxidative stress is associated with the disulfide bond formation between two regulatory PKA RIα subunits. In the proposed model, the disulfide cross-linking of two RIα subunits leads to the increased affinity of PKA to AKAP, that promotes subcellular targeting of the kinase catalytic subunit to the corresponding substrate (Brennan et al., 2006). Similarly to PKA, CaMKII can be also activated by oxidative stress (Erickson

et al., 2008). The mechanism of ROS-dependent CaMKII activation required an initial activation by Ca-CaM followed by oxidation of methionine 281 and 282 yielding a persistent activation even after Ca-CaM dissociation. The mechanism of CaMKII activation by ROS was independent from the previously described activation by autophosphorylation. In *in vivo* experiments, NOX activation by angiotensin II (AngII) led to CaMKII oxidation. This activation was not observed in the $p47^{-/-}$ transgenic mice lacking NOX activity (Erickson et al., 2008).

Since HF is commonly associated with oxidative stress (Mak and Newton, 2001), CaMKII activity is expected to be upregulated during this pathology. Once activated by ROS, CaMKII can contribute to arrhythmogenesis in HF by activating late sodium current (Wagner et al., 2011). In another study, a short-termed exposure of myocytes to H_2O_2 has resulted in the prolonged activation of CaMKII and long-termed facilitation of LTCC through mechanisms of CaMKII autophosphorylation and oxidation (Song Y.H. et al., 2011). Consistent with these findings, it has been shown that the pharmacological inhibition of CaMKII prevents arrhythmias induced by oxidative stress (Xie et al., 2009). The upregulation of CaMKII has been associated with the development of atrial fibrillation (AF). It has been shown that RyR2 phosphorylation at the CaMKII site was increased in AF patients, whereas RyR2 expression level was decreased. Cardiomyocytes from AF patients were characterized by increased SR Ca leak, which can be normalized by the CaMKII inhibitor KN93 (Neef et al., 2010). Moreover, it has been shown that NOX activation with AngII caused increased ROS production and CaMKII oxidation followed by an increase in Ca spark frequency. At the same time, the transgenic mice lacking the CaMKII phosphorylation site on RyR2 (S2814A) were protected from AF induced by AngII (Purohit et al., 2013). It has been shown that I/R-mediated arrhythmias were associated with CaMKII-dependent phosphorylation of RyR2 (Said et al., 2011). I/R also increased levels of RyR2 reversible redox modifications: S-glutathionylation and S-nitrosylation (Becerra et al., 2016). Arrhythmogenic effect of cardiac glucosides has been also attributed to the increased ROS production and RyR2 oxidation (Ho et al., 2011). It has been shown later that cardiac glucosides activate NOX2-mediated ROS production that causes CaMKII activation, RyR2 phosphorylation and Ca waves (Ho et al., 2014).

FKBP DISSOCIATION DURING OXIDATIVE STRESS

While there is no evidence that RyR2 oxidation directly causes FKBP12.6 dissociation from the channel, oxidative stress still may affect the RyR2-FKBP12.6 interaction through the mechanism of RyR2 phosphorylation (**Figure 2**). RyR2 hyper-phosphorylation at the PKA site has been shown to promote FKBP12.6 dissociation from RyR2 resulting in the increased channel activity during HF. It was suggested that the RyR2 hyper-phosphorylation was a result of PP1 dissociation from the RyR2 macromolecular complex (Marx et al., 2000). The interplay between RyR2 oxidation and FKBP12.6 dissociation has been studied in WT and the transgenic mice lacking the PKA phosphorylation site in RyR2 (the S2808A mice). In the WT mice excessive β-adrenergic stimulation caused increased FKBP12.6 dissociation from RyR2 in WT mice, but not in the S2808A mice. At the same time, the levels of RyR2 oxidation were increased in both WT and S2808A mice. To study the effects of oxidative stress and phosphorylation on the RyR2-FKBP12.6 interaction, SR vesicles were treated either with H_2O_2 or with H_2O_2 combined with CaMKII or PKA. Both H_2O_2 alone or in combination with CaMKII showed no significant effect on the FKBP12.6 dissociation from RyR2. However, RyR2 oxidation together with PKA caused almost complete FKBP12.6 dissociation. Chronic treatment of WT mice with isoproterenol increased levels of PKA-RyR2 phosphorylation, FKBP12.6 depletion and RyR2 oxidation, whereas in the S2808A mice these effects of adrenergic stimulation were partially abolished (Shan et al., 2010b).

CONCLUSION

The vast body of evidence demonstrates a direct link between oxidative stress, RyR2 oxidation and increased SR Ca leak in several cardiac pathologies, including HF and MI. Molecular mechanisms of the impaired SR Ca handling can include structural and functional changes in the RyR2 complex due to thiol redox-modifications. However, effects of oxidative stress on RyR2 may go beyond the direct redox-modification of the channel and can involve dissociation of regulatory proteins and increased phosphorylation by PKA and CaMKII. It appears that phosphorylation and redox modifications may have an additive effect on RyR2 function. The experiments in the non-ischemic canine HF model have shown that RyR2 phosphorylation and thiol oxidation contribute to the different stages of HF: RyR2 phosphorylation by CaMKII manifests on the early stages of HF with following RyR2 oxidation during later stages (Belevych et al., 2011). In another HF study, the increased SR Ca leak was associated with RyR2 hyper-phosphorylation on both PKA and CaMKII sites together with thiol oxidation (Walweel et al., 2017), suggesting a combined effect of multiple factors on RyR2 dysfunction in HF. Despite abundant amount of experimental data pointing on the importance of oxidative stress, many of clinical trials that used antioxidant for treatment of HF did not yield promising results (Mak and Newton, 2001; Giordano, 2005; Thomson et al., 2007). However, trials with the beta-blocker with antioxidant properties carvedilol have shown some superiority over conventional beta-blockers, which can be attributed to its antioxidant effect (Packer et al., 2001). At the same time, it has been shown that carvedilol may also modulate the function of RyR2 independently from its beta-blocking function or antioxidant activity, but through the direct action on RyR2 activity (Zhou et al., 2011). Nevertheless, strategies focused on restoring the RyR2 structural integrity during oxidative stress may have a high therapeutic potential. Thus, further insights into molecular basis of RyR2 redox regulation are essential for the development of specific and effective therapeutic strategies.

AUTHOR CONTRIBUTIONS

All authors (RN, EB, and AZ) contributed to studying of literature and writing of the manuscript. All authors have approved the version to be published.

FUNDING

This work was supported by the National Heart, Lung, and Blood Institute of the National Institutes of Health under Award No. R01HL130231 (to AZ).

REFERENCES

Abramson, J. J., and Salama, G. (1989). Critical sulfhydryls regulate calcium release from sarcoplasmic reticulum. *J. Bioenerg. Biomembr.* 21, 283–294. doi: 10.1007/BF00812073

Aghdasi, B., Reid, M. B., and Hamilton, S. L. (1997). Nitric oxide protects the skeletal muscle Ca^{2+} release channel from oxidation induced activation. *J. Biol. Chem.* 272, 25462–25467. doi: 10.1074/jbc.272.41.25462

Aracena-Parks, P., Goonasekera, S. A., Gilman, C. P., Dirksen, R. T., Hidalgo, C., and Hamilton, S. L. (2006). Identification of cysteines involved in S-nitrosylation, S-glutathionylation, and oxidation to disulfides in ryanodine receptor type 1. *J. Biol. Chem.* 281, 40354–40368. doi: 10.1074/jbc.M600876200

Balshaw, D. M., Xu, L., Yamaguchi, N., Pasek, D. A., and Meissner, G. (2001). Calmodulin binding and inhibition of cardiac muscle calcium release channel (Ryanodine Receptor). *J. Biol. Chem.* 276, 20144–20153. doi: 10.1074/jbc.M010771200

Barouch, A., Harrisson, R. W., Skaf, M. W., Rosas, G. O., Cappola, T. P., Kobelssi, Z. A., et al. (2002). Nitric oxide regulates the heart by spatial confinement of nitric oxide synthase isoforms. *Nature* 416, 337–340. doi: 10.1038/416337a

Becerra, R., Román, B., Di Carlo, M. N., Mariangelo, J. I., Salas, M., Sanchez, G., et al. (2016). Reversible redox modifications of ryanodine receptor ameliorate ventricular arrhythmias in the ischemic-reperfused heart. *Am. J. Physiol. Hear Circ. Physiol.* 311, H713–H724. doi: 10.1152/ajpheart.00142.2016

Beer, S. M., Taylor, E. R., Brown, S. E., Dahm, C. C., Costa, N. J., Runswick, M. J., et al. (2004). Glutaredoxin 2 catalyzes the reversible oxidation and glutathionylation of mitochondrial membrane thiol proteins: implications for mitochondrial redox regulation and antioxidant defense. *J. Biol. Chem.* 279, 47939–47951. doi: 10.1074/jbc.M408011200

Belevych, A., Kubalova, Z., Terentyev, D., Hamlin, R. L., Carnes, C. A., and Györke, S. (2007). Enhanced ryanodine receptor-mediated calcium leak determines reduced sarcoplasmic reticulum calcium content in chronic canine heart failure. *Biophys. J.* 93, 4083–4092. doi: 10.1529/biophysj.107.114546

Belevych, A. E., Terentyev, D., Terentyeva, R., Ho, H. T., Gyorke, I., Bonilla, I. M., et al. (2012). Shortened Ca^{2+} signaling refractoriness underlies cellular arrhythmogenesis in a postinfarction model of sudden cardiac death. *Circ. Res.* 110, 569–577. doi: 10.1161/CIRCRESAHA.111.260455

Belevych, A. E., Terentyev, D., Terentyeva, R., Nishijima, Y., Sridhar, A., Hamlin, R. L., et al. (2011). The relationship between arrhythmogenesis and impaired contractility in heart failure: role of altered ryanodine receptor function. *Cardiovasc. Res.* 90, 493–502. doi: 10.1093/cvr/cvr025

Belevych, A. E., Terentyev, D., Viatchenko-Karpinski, S., Terentyeva, R., Sridhar, A., Nishijima, Y., et al. (2009). Redox modification of ryanodine receptors underlies calcium alternans in a canine model of sudden cardiac death. *Cardiovasc. Res.* 84, 387–395. doi: 10.1093/cvr/cvp246

Benkusky, N. A., Weber, C. S., Scherman, J. A., Farrell, E. F., Hacker, T. A., John, M. C., et al. (2007). Intact β-adrenergic response and unmodified progression toward heart failure in mice with genetic ablation of a major protein kinase A phosphorylation site in the cardiac ryanodine receptor. *Circ. Res.* 101, 819–829. doi: 10.1161/CIRCRESAHA.107.153007

Bers, D. M. (2002). Cardiac excitation-contraction coupling. *Nature* 415, 198–205. doi: 10.1038/415198a

Bers, D. M. (2004). Macromolecular complexes regulating cardiac ryanodine receptor function. *J. Mol. Cell. Cardiol.* 37, 417–429. doi: 10.1016/j.yjmcc.2004.05.026

Bers, D. M. (2014). Cardiac sarcoplasmic reticulum calcium leak: basis and roles in cardiac dysfunction. *Annu. Rev. Physiol.* 76, 107–127. doi: 10.1146/annurev-physiol-020911-153308

Blayney, L. M., and Lai, F. A. (2009). Ryanodine receptor-mediated arrhythmias and sudden cardiac death. *Pharmacol. Ther.* 123, 151–177. doi: 10.1016/j.pharmthera.2009.03.006

Bovo, E., Mazurek, S. R., Fill, M., and Zima, A. V. (2015). Cytosolic Ca^{2+} buffering determines the intra-SR Ca^{2+} concentration at which cardiac Ca^{2+} sparks terminate. *Cell Calcium* 58, 246–253. doi: 10.1016/j.ceca.2015.06.002

Bovo, E., Mazurek, S. R., and Zima, A. V. (2018a). Oxidation of ryanodine receptor following ischemia/reperfusion increases propensity of Ca^{2+} waves during β-adrenergic receptor stimulation. *Am. J. Physiol. Heart Circ. Physiol* 315, H1032–H1040. doi: 10.1152/ajpheart.00334.2018

Bovo, E., Mazurek, S. R., and Zima, A. V. (2018b). The role of RyR2 oxidation in the blunted frequency-dependent facilitation of Ca^{2+} transient amplitude in rabbit failing myocytes. *Pflugers Arch.* 470, 959–968. doi: 10.1007/s00424-018-2122-3

Brennan, J. P., Bardswell, S. C., Burgoyne, J. R., Fuller, W., Schröder, E., Wait, R., et al. (2006). Oxidant-induced activation of type I protein kinase A is mediated by RI subunit interprotein disulfide bond formation. *J. Biol. Chem.* 281, 21827–21836. doi: 10.1074/jbc.M603952200

Brillantes, A.-M. B., Ondrias, K., Scott, A., Kobrinsky, E., Ondriašová, E., Moschella, M. C., et al. (1994). Stabilization of calcium release channel (ryanodine receptor) function by FK506-binding protein. *Cell* 77, 513–523. doi: 10.1016/0092-8674(94)90214-3

Cabra, V., Murayama, T., and Samsó, M. (2016). Ultrastructural analysis of self-associated RyR2s. *Biophys. J.* 110, 2651–2662. doi: 10.1016/j.bpj.2016.05.013

Cheng, H., Lederer, W. J., and Cannell, M. B. (1993). Calcium sparks: elementary events underlying excitation-contraction coupling in heart muscle. *Science* 262, 740–744. doi: 10.1126/science.8235594

Cheong, E., Tumbev, V., Stoyanovsky, D., and Salama, G. (2005). Effects of pO2on the activation of skeletal muscle ryanodine receptors by NO: a cautionary note. *Cell Calcium* 38, 481–488. doi: 10.1016/j.ceca.2005.07.001

Cutler, M. J., Plummer, B. N., Wan, X., Sun, Q.-A., Hess, D., Liu, H., et al. (2012). Aberrant S-nitrosylation mediates calcium-triggered ventricular arrhythmia in the intact heart. *Proc. Natl. Acad. Sci. U.S.A.* 109, 18186–18191. doi: 10.1073/pnas.1210565109

des Georges, A., Clarke, O. B., Zalk, R., Yuan, Q., Condon, K. J., Grassucci, R. A., et al. (2016). Structural basis for gating and activation of RyR1. *Cell* 167, 145.e–157.e. doi: 10.1016/j.cell.2016.08.075

Dhindwal, S., Lobo, J., Cabra, V., Santiago, D. J., Nayak, A. R., Dryden, K., et al. (2017). A cryo-EM–based model of phosphorylation-and FKBP12.6-mediated allosterism of the cardiac ryanodine receptor. *Sci. Signal.* 10:eaai8842. doi: 10.1126/scisignal.aai8842

Donoso, P., Sánchez, G., Bull, R., and Hidalgo, C. (2011). Modulation of cardiac ryanodine receptor activity by ROS and RNS. *Front. Biosci.* 16, 553–567. doi: 10.2741/3705

Dulhunty, A., Haarmann, C., Green, D., Hart, J., and Al, D. E. T. (2000). Forum minireview how many cysteine residues regulate ryanodine receptor channel activity?? *Antioxid. Redox Signal.* 2, 1–27. doi: 10.1089/ars.2000.2.1-27

Dulhunty, A. F., Hewawasam, R., Liu, D., Casarotto, M. G., and Board, P. G. (2011). Regulation of the cardiac muscle ryanodine receptor by glutathione transferases. *Drug Metab. Rev.* 43, 236–252. doi: 10.3109/03602532.2010.549134

El-Armouche, A., and Eschenhagen, T. (2009). β-Adrenergic stimulation and myocardial function in the failing heart. *Heart Fail. Rev.* 14, 225–241. doi: 10.1007/s10741-008-9132-8

Erickson, J. R., Joiner, M., Ling, A., Guan, X., Kutschke, W., Yang, J., et al. (2008). A dynamic pathway for calcium-independent activation of CaMKII by methionine oxidation. *Cell* 133, 462–474. doi: 10.1016/j.cell.2008.02.048

Eu, J. P., Sun, J., Xu, L., Stamler, J. S., Meissner, G., Abramson, J., et al. (2000). The skeletal muscle calcium release channel: coupled O_2 sensor and NO signaling functions. *Cell* 102, 499–509. doi: 10.1016/s0092-8674(00)00054-4

Fabiato, A. (1983). Calcium-induced release of calcium from the cardiac sarcoplasmic reticulum. *Am. J. Physiol.* 245, C1–C14. doi: 10.1152/ajpcell.1983.245.1.C1

Fauconnier, J., Thireau, J., Reiken, S., Cassan, C., Richard, S., Matecki, S., et al. (2010). Leaky RyR2 trigger ventricular arrhythmias in Duchenne muscular

dystrophy. *Proc. Natl. Acad. Sci. U.S.A.* 107, 1559–1564. doi: 10.1073/pnas.0908540107

Fill, M., and Copello, J. A. (2002). Ryanodine receptor calcium release channels. *Physiol. Rev.* 82, 893–922. doi: 10.1152/physrev.00013.2002

Foster, D. B., Van Eyk, J. E., Marbán, E., and O'Rourke, B. (2009). Redox signaling and protein phosphorylation in mitochondria: progress and prospects. *J. Bioenerg. Biomembr.* 41, 159–168. doi: 10.1007/s10863-009-9217-7

Franzini-Armstrong, C., Protasi, F., and Ramesh, V. (1999). Shape, size, and distribution of Ca^{2+} release units and couplons in skeletal and cardiac muscles. *Biophys. J.* 77, 1528–1539. doi: 10.1016/S0006-3495(99)77000-1

Giles, G. I., and Jacob, C. (2002). Reactive sulfur species: an emerging concept in oxidative stress. *Biol. Chem.* 383, 375–388. doi: 10.1515/BC.2002.042

Giordano, F. J. (2005). Oxygen, oxidative stress, hypoxia, and heart failure. *J. Clin. Invest.* 115, 500–508. doi: 10.1172/JCI200524408

Gonzalez, D. R., Beigi, F., Treuer, A. V., and Hare, J. M. (2007). Deficient ryanodine receptor S-nitrosylation increases sarcoplasmic reticulum calcium leak and arrhythmogenesis in cardiomyocytes. *Proc. Natl. Acad. Sci. U.S.A.* 104, 20612–20617. doi: 10.1073/pnas.0706796104

Grek, C. L., Zhang, J., Manevich, Y., Townsend, D. M., and Tew, K. D. (2013). Causes and consequences of cysteine s-glutathionylation. *J. Biol. Chem.* 288, 26497–26504. doi: 10.1074/jbc.R113.461368

Györke, I., Hester, N., Jones, L. R., and Györke, S. (2004). The role of calsequestrin, triadin, and junctin in conferring cardiac ryanodine receptor responsiveness to luminal calcium. *Biophys. J.* 86, 2121–2128. doi: 10.1016/S0006-3495(04)74271-X

Han, H. M., Wei, R. S., Lai, A. F., and Yin, C. C. (2006). Molecular nature of sulfhydryl modification by hydrogen peroxide on type 1 ryanodine receptor. *Acta Pharmacol. Sin.* 27, 888–894. doi: 10.1111/j.1745-7254.2006.00386.x

Hart, J. D. E., and Dulhunty, A. F. (2000). Nitric oxide activates or inhibits skeletal muscle ryanodine receptors depending on its concentration, membrane potential and ligand binding. *J. Membr. Biol.* 173, 227–236. doi: 10.1007/s002320001022

Hayashi, T., Martone, M. E., Yu, Z., Thor, A., Doi, M., Holst, M. J., et al. (2009). Three-dimensional electron microscopy reveals new details of membrane systems for Ca^{2+} signaling in the heart. *J. Cell Sci.* 122(Pt 7), 1005–1013. doi: 10.1242/jcs.028175

Hess, D. T., Matsumoto, A., Kim, S. O., Marshall, H. E., and Stamler, J. S. (2005). Protein S-nitrosylation: purview and parameters. *Nat. Rev. Mol. Cell Biol.* 6, 150–166. doi: 10.1038/nrm1569

Heymes, C., Bendall, J. K., Ratajczak, P., Cave, A. C., Samuel, J. L., Hasenfuss, G., et al. (2003). Increased myocardial NADPH oxidase activity in human heart failure. *J. Am. Coll. Cardiol.* 41, 2164–2171. doi: 10.1016/S0735-1097(03)00471-6

Hino, A., Yano, M., Kato, T., Fukuda, M., Suetomi, T., Ono, M., et al. (2012). Enhanced binding of calmodulin to the ryanodine receptor corrects contractile dysfunction in failing hearts. *Cardiovasc. Res.* 96, 433–443. doi: 10.1093/cvr/cvs271

Ho, H. T., Liu, B., Snyder, J. S., Lou, Q., Brundage, E. A., Velez-Cortes, F., et al. (2014). Ryanodine receptor phosphorylation by oxidized CaMKII contributes to the cardiotoxic effects of cardiac glycosides. *Cardiovasc. Res.* 101, 165–174. doi: 10.1093/cvr/cvt233

Ho, H. T., Stevens, S. C. W., Terentyeva, R., Carnes, C. A., Terentyev, D., and Györke, S. (2011). Arrhythmogenic adverse effects of cardiac glycosides are mediated by redox modification of ryanodine receptors. *J. Physiol.* 589, 4697–4708. doi: 10.1113/jphysiol.2011.210005

Johnston, A. S., Lehnart, S. E., and Burgoyne, J. R. (2015). Ca^{2+}signaling in the myocardium by (redox) regulation of PKA/CaMKII. *Front. Pharmacol.* 6:166. doi: 10.3389/fphar.2015.00166

Kubalova, Z., Terentyev, D., Viatchenko-Karpinski, S., Nishijima, Y., Gyorke, I., Terentyeva, R., et al. (2005). Abnormal intrastore calcium signaling in chronic heart failure. *Proc. Natl. Acad. Sci. U.S.A.* 102, 14104–14109. doi: 10.1073/pnas.0504298102

Lanner, J. T., Georgiou, D. K., Joshi, A. D., and Hamilton, S. L. (2010). Ryanodine receptors: structure, expression, molecular details, and function in calcium release. *Cold Spring Harb. Perspect. Biol.* 2:a003996. doi: 10.1101/cshperspect.a003996

Lima, B., Forrester, M. T., Hess, D. T., and Stamler, J. S. (2010). S-nitrosylation in cardiovascular signaling. *Circ. Res.* 106, 633–646. doi: 10.1161/CIRCRESAHA.109.207381

Liu, B., Walton, S. D., Ho, H., Belevych, A. E., Tikunova, S. B., Bonilla, I., et al. (2018). Gene transfer of engineered calmodulin alleviates ventricular arrhythmias in a calsequestrin-associated mouse model of catecholaminergic polymorphic ventricular tachycardia. *J. Am. Heart Assoc.* 7:e008155. doi: 10.1161/JAHA.117.008155

Liu, D., Hewawasam, R., Karunasekara, Y., Casarotto, M. G., Dulhunty, A. F., and Board, P. G. (2012). The inhibitory glutathione transferase M2-2 binding site is located in divergent region 3 of the cardiac ryanodine receptor. *Biochem. Pharmacol.* 83, 1523–1529. doi: 10.1016/j.bcp.2012.02.020

Madamanchi, N. R., and Runge, M. S. (2013). Redox signaling in cardiovascular health and disease. *Free Radic. Biol. Med.* 61, 473–501. doi: 10.1016/j.freeradbiomed.2013.04.001

Mak, S., and Newton, G. E. (2001). The oxidative stress hypothesis of congestive heart failure: radical thoughts. *Chest* 120, 2035–2046. doi: 10.1378/chest.120.6.2035

Marx, S. O., and Marks, A. R. (2013). Dysfunctional ryanodine receptors in the heart: new insights into complex cardiovascular diseases. *J. Mol. Cell. Cardiol.* 58, 225–231. doi: 10.1016/j.yjmcc.2013.03.005

Marx, S. O., Reiken, S., Hisamatsu, Y., Jayaraman, T., Burkhoff, D., Rosemblit, N., et al. (2000). PKA phosphorylation dissociates FKBP12.6 from the calcium release channel (Ryanodine Receptor). *Cell* 101, 365–376. doi: 10.1016/S0092-8674(00)80847-8

Mazurek, S. R., Bovo, E., and Zima, A. V. (2014). Regulation of sarcoplasmic reticulum Ca^{2+} release by cytosolic glutathione in rabbit ventricular myocytes. *Free Radic. Biol. Med.* 68, 159–167. doi: 10.1016/j.freeradbiomed.2013.12.003

Meissner, G. (2004). Molecular regulation of cardiac ryanodine receptor ion channel. *Cell Calcium* 35, 621–628. doi: 10.1016/j.ceca.2004.01.015

Meissner, G. (2017). The structural basis of ryanodine receptor ion channel function. *J. Gen. Physiol.* 149, 1065–1089. doi: 10.1085/jgp.201711878

Mi, T., Xiao, Z., Guo, W., Tang, Y., Hiess, F., Xiao, J., et al. (2015). Role of Cys 3602 in the function and regulation of the cardiac ryanodine receptor. *Biochem. J.* 467, 177–190. doi: 10.1042/BJ20141263

Mochizuki, M., Yano, M., Oda, T., Tateishi, H., Kobayashi, S., Yamamoto, T., et al. (2007). Scavenging free radicals by low-dose carvedilol prevents redox-dependent Ca^{2+} leak via stabilization of ryanodine receptor in heart failure. *J. Am. Coll. Cardiol.* 49, 1722–1732. doi: 10.1016/j.jacc.2007.01.064

Moore, C. P., Zhang, J. Z., and Hamilton, S. L. (1999). A role for cysteine 3635 of RYR1 in redox modulation and calmodulin binding. *J. Biol. Chem.* 274, 36831–36834. doi: 10.1074/jbc.274.52.36831

Neef, S., Dybkova, N., Sossalla, S., Ort, K. R., Fluschnik, N., Neumann, K., et al. (2010). CaMKII-dependent diastolic SR Ca^{2+} leak and elevated diastolic Ca^{2+} levels in right atrial myocardium of patients with atrial fibrillation. *Circ. Res.* 106, 1134–1144. doi: 10.1161/CIRCRESAHA.109.203836

Oda, T., Yang, Y., Uchinoumi, H., Thomas, D. D., Chen-Izu, Y., Kato, T., et al. (2015). Oxidation of ryanodine receptor (RyR) and calmodulin enhance Ca release and pathologically alter, RyR structure and calmodulin affinity. *J. Mol. Cell. Cardiol.* 85, 240–248. doi: 10.1016/j.yjmcc.2015.06.009

Ono, M., Yano, M., Hino, A., Suetomi, T., Xu, X., Susa, T., et al. (2010). Dissociation of calmodulin from cardiac ryanodine receptor causes aberrant Ca^{2+} release in heart failure. *Cardiovasc. Res.* 87, 609–617. doi: 10.1093/cvr/cvq108

Orlova, E. V., Serysheva, I. I., Van Heel, M., Hamilton, S. L., and Chiu, W. (1996). Two structural configurations of the skeletal muscle calcium release channel. *Nat. Struct. Biol.* 3, 547–552. doi: 10.1038/nsb0696-547

Packer, M., Coats, A. J. S., Fowler, M. B., Katus, H. A., Krum, H., Mohacsi, P., et al. (2001). Effect of carvedilol on survival in severe chronic heart failure. *N. Engl. J. Med.* 344, 1651–1658. doi: 10.1056/NEJM200105313442201

Paulina Donoso and Gina Sánchez (2013). Redox regulation of sarcoplasmic reticulum Calcium cycling in the heart. *Physiol. MiniRev.* 6, 38–47.

Pogwizd, S. M., and Bers, D. M. (2004). Cellular basis of triggered arrhythmias in heart failure. *Trends Cardiovasc. Med.* 14, 61–66. doi: 10.1016/j.tcm.2003.12.002

Purohit, A., Rokita, A. G., Guan, X., Chen, B., Koval, O. M., Voigt, N., et al. (2013). Oxidized Ca^{2+}/calmodulin-dependent protein kinase II triggers atrial fibrillation. *Circulation* 128, 1748–1757. doi: 10.1161/CIRCULATIONAHA.113.003313

Said, M., Becerra, R., Valverde, C. A., Kaetzel, M. A., Dedman, J. R., Mundiña-Weilenmann, C., et al. (2011). Calcium-calmodulin dependent protein kinase II (CaMKII): a main signal responsible for early reperfusion arrhythmias. *J. Mol. Cell. Cardiol.* 51, 936–944. doi: 10.1016/j.yjmcc.2011.08.010

Sánchez, G., Escobar, M., Pedrozo, Z., Macho, P., Domenech, R., Härtel, S., et al. (2008). Exercise and tachycardia increase NADPH oxidase and ryanodine receptor-2 activity: possible role in cardioprotection. *Cardiovasc. Res.* 77, 380–386. doi: 10.1093/cvr/cvm011

Sánchez, G., Pedrozo, Z., Domenech, R. J., Hidalgo, C., and Donoso, P. (2005). Tachycardia increases NADPH oxidase activity and RyR2 S-glutathionylation in ventricular muscle. *J. Mol. Cell. Cardiol.* 39, 982–991. doi: 10.1016/j.yjmcc.2005.08.010

Santos, C. X. C., Anilkumar, N., Zhang, M., Brewer, A. C., and Shah, A. M. (2011). Redox signaling in cardiac myocytes. *Free Radic. Biol. Med.* 50, 777–793. doi: 10.1016/j.freeradbiomed.2011.01.003

Santos, C. X. C., Raza, S., and Shah, A. M. (2016). Redox signaling in the cardiomyocyte: from physiology to failure. *Int. J. Biochem. Cell Biol.* 74, 145–151. doi: 10.1016/j.biocel.2016.03.002

Sawyer, D. B., Siwik, D. A., Xiao, L., Pimentel, D. R., Singh, K., and Colucci, W. S. (2002). Role of oxidative stress in myocardial hypertrophy and failure. *J. Mol. Cell. Cardiol.* 34, 379–388. doi: 10.1006/jmcc.2002.1526

Schafer, F. Q., and Buettner, G. R. (2001). Redox environment of the cell as viewed through the redox state of the glutathione disulfide/glutathione couple. *Free Radic. Biol. Med.* 30, 1191–1212. doi: 10.1016/S0891-5849(01)00480-4

Seddon, M., Looi, Y. H., and Shah, A. M. (2007). Oxidative stress and redox signalling in cardiac hypertrophy and heart failure. *Heart* 93, 903–907. doi: 10.1136/hrt.2005.068270

Serysheva, I. I., Ludtke, S. J., Baker, M. L., Cong, Y., Topf, M., Eramian, D., et al. (2008). Subnanometer-resolution electron cryomicroscopy-based domain models for the cytoplasmic region of skeletal muscle RyR channel. *Proc. Natl. Acad. Sci. U.S.A.* 105, 9610–9615. doi: 10.1073/pnas.0803189105

Shan, J., Betzenhauser, M. J., Kushnir, A., Reiken, S., Meli, A. C., Wronska, A., et al. (2010a). Role of chronic ryanodine receptor phosphorylation in heart failure and β-adrenergic receptor blockade in mice. *J. Clin. Invest.* 120, 4375–4387. doi: 10.1172/JCI37649.Na

Shan, J., Kushnir, A., Betzenhauser, M. J., Reiken, S., Li, J., Lehnart, S. E., et al. (2010b). Phosphorylation of the ryanodine receptor mediates the cardiac fight or flight response in mice. *J. Clin. Invest.* 120, 4388–4398. doi: 10.1172/JCI32726

Shannon, T. R., Pogwizd, S. M., and Bers, D. M. (2003). Elevated sarcoplasmic reticulum Ca^{2+} leak in intact ventricular myocytes from rabbits in heart failure. *Circ. Res.* 93, 592–594. doi: 10.1161/01.RES.0000093399.11734.B3

Song, D. W., Lee, J.-G., Youn, H.-S., Eom, S. H., and Kim, D. H. (2011). Ryanodine receptor assembly: a novel systems biology approach to 3D mapping. *Prog. Biophys. Mol. Biol.* 105, 145–161. doi: 10.1016/j.pbiomolbio.2010.09.021

Song, Y. H., Choi, E., Park, S. H., Lee, S. H., Cho, H., Ho, W. K., et al. (2011). Sustained CaMKII activity mediates transient oxidative stress-induced long-term facilitation of L-type Ca^{2+}current in cardiomyocytes. *Free Radic. Biol. Med.* 51, 1708–1716. doi: 10.1016/j.freeradbiomed.2011.07.022

Stoyanovsky, D., Murphy, T., Anno, P. R., Kim, Y. M., and Salama, G. (1997). Nitric oxide activates skeletal and cardiac ryanodine receptors. *Cell Calcium* 21, 19–29. doi: 10.1016/S0143-4160(97)90093-2

Sun, J., and Murphy, E. (2010). Protein S-nitrosylation and cardioprotection. *Circ. Res.* 106, 285–296. doi: 10.1161/CIRCRESAHA.109.209452

Sun, J., Xin, C., Eu, J. P., Stamler, J. S., and Meissner, G. (2001). Cysteine-3635 is responsible for skeletal muscle ryanodine receptor modulation by NO. *Proc. Natl. Acad. Sci. U.S.A.* 98, 11158–11162. doi: 10.1073/pnas.201289098

Sun, J., Xu, L., Eu, J. P., Stamler, J. S., and Meissner, G. (2003). Nitric oxide, NOC-12, and S-nitrosoglutathione modulate the skeletal muscle calcium release channel/ryanodine receptor by different mechanisms: an allosteric function for O2 in S-nitrosylation of the channel. *J. Biol. Chem.* 278, 8184–8189. doi: 10.1074/jbc.M211940200

Sun, J., Yamaguchi, N., Xu, L., Eu, J. P., Stamler, J. S., and Meissner, G. (2008). Regulation of the cardiac muscle ryanodine receptor by O_2 tension and S-nitrosoglutathione. *Biochemistry* 47, 13985–13990. doi: 10.1021/bi8012627

Suzuki, Y. J., and Ford, G. D. (1999). Redox regulation of signal transduction in cardiac and smooth muscle. *J. Mol. Cell. Cardiol.* 31, 345–353. doi: 10.1006/jmcc.1998.0872

Takasago, T., Imagawa, T., Furukawa, K. I., Ogurusu, T., and Shigekawa, M. (1991). Regulation of the cardiac ryanodine receptor by protein kinase- dependent phosphorylation. *J. Biochem.* 109, 163–170. doi: 10.1093/oxfordjournals.jbchem.a123339

Terentyev, D., Györke, I., Belevych, A. E., Terentyeva, R., Sridhar, A., Nishijima, Y., et al. (2008). Redox modification of ryanodine receptors contributes to sarcoplasmic reticulum Ca^{2+} leak in chronic heart failure. *Circ. Res.* 103, 1466–1472. doi: 10.1161/CIRCRESAHA.108.184457

Thomson, M. J., Puntmann, V., and Kaski, J. C. (2007). Atherosclerosis and oxidant stress: the end of the road for antioxidant vitamin treatment? *Cardiovasc. Drugs Ther.* 21, 195–210. doi: 10.1007/s10557-007-6027-1

Timerman, A. P., Jayaraman, T., Wiederrecht, G., Onoue, H., Marks, A. R., and Fleischer, S. (1994). The ryanodine receptor from canine heart sarcoplasmic reticulum is associated with a novel FK-506 binding protein. *Biochem. Biophys. Res. Commun.* 198, 701–706. doi: 10.1006/bbrc.1994.1101

Townsend, D. M. (2007). S-glutathionylation: indicator of cell stress and regulator of the unfolded protein response. *Mol. Interv.* 7, 313–324. doi: 10.1124/mi.7.6.7

Trimm, J. L., Salama, G., and Abramson, J. J. (1986). Sulfhydryl oxidation induces rapid calcium release from sarcoplasmic reticulum vesicles. *J. Biol. Chem.* 261, 16092–16098.

Tung, C.-C., Lobo, P. A., Kimlicka, L., and Van Petegem, F. (2010). The amino-terminal disease hotspot of ryanodine receptors forms a cytoplasmic vestibule. *Nature* 468, 585–588. doi: 10.1038/nature09471

Turrens, J. F. (2003). Mitochondrial formation of reactive oxygen species. *J. Physiol.* 552, 335–344. doi: 10.1113/jphysiol.2003.049478

Van Petegem, F. (2015). Ryanodine receptors: allosteric ion channel giants. *J. Mol. Biol.* 427, 31–53. doi: 10.1016/j.jmb.2014.08.004

Ventura-Clapier, R., Garnier, A., and Veksler, V. (2004). Energy metabolism in heart failure. *J. Physiol.* 555, 1–13. doi: 10.1113/jphysiol.2003.055095

Voss, A. A., Lango, J., Ernst-Russell, M., Morin, D., and Pessah, I. N. (2004). Identification of hyperreactive cysteines within ryanodine receptor type 1 by mass spectrometry. *J. Biol. Chem.* 279, 34514–34520. doi: 10.1074/jbc.M404290200

Wagner, S., Ruff, H. M., Weber, S. L., Bellmann, S., Sowa, T., Schulte, T., et al. (2011). Reactive oxygen species-activated Ca/calmodulin kinase IIδ is required for late I(Na) augmentation leading to cellular Na and Ca overload. *Circ. Res.* 108, 555–565. doi: 10.1161/CIRCRESAHA.110.221911

Walweel, K., Molenaar, P., Imtiaz, M. S., Denniss, A., dos Remedios, C., van Helden, D. F., et al. (2017). Ryanodine receptor modification and regulation by intracellular Ca^{2+} and Mg^{2+} in healthy and failing human hearts. *J. Mol. Cell. Cardiol.* 104, 53–62. doi: 10.1016/j.yjmcc.2017.01.016

Wang, H., Viatchenko-Karpinski, S., Sun, J., Györke, I., Benkusky, N. A., Kohr, M. J., et al. (2010). Regulation of myocyte contraction via neuronal nitric oxide synthase: role of ryanodine receptor S-nitrosylation. *J. Physiol.* 588, 2905–2917. doi: 10.1113/jphysiol.2010.192617

Wang, Q., Wang, W., Wang, G., Rodney, G. G., and Wehrens, X. H. T. (2015). Crosstalk between RyR2 oxidation and phosphorylation contributes to cardiac dysfunction in mice with Duchenne muscular dystrophy. *J. Mol. Cell. Cardiol.* 89, 177–184. doi: 10.1016/j.yjmcc.2015.11.009

Wehrens, X. H. T. (2004). Ca^{2+}/calmodulin-dependent protein kinase II phosphorylation regulates the cardiac ryanodine receptor. *Circ. Res.* 94, e61–e70. doi: 10.1161/01.RES.0000125626.33738.E2

Wehrens, X. H. T., Lehnart, S. E., Reiken, S. R., Deng, S.-X., Vest, J. A., Cervantes, D., et al. (2004). Protection from cardiac arrhythmia through ryanodine receptor-stabilizing protein calstabin2. *Science* 304, 292–296. doi: 10.1126/science.1094301

Wei, R., Wang, X., Zhang, Y., Mukherjee, S., Zhang, L., Chen, Q., et al. (2016). Structural insights into Ca^{2+}-activated long-range allosteric channel gating of RyR1. *Cell Res.* 26, 977–994. doi: 10.1038/cr.2016.99

Xiao, B., Zhong, G., Obayashi, M., Yang, D., Chen, K., Walsh, M. P., et al. (2006). Ser-2030, but not Ser-2808, is the major phosphorylation site in cardiac ryanodine receptors responding to protein kinase A activation upon β-adrenergic stimulation in normal and failing hearts. *Biochem. J.* 396, 7–16. doi: 10.1042/BJ20060116

Xie, L. H., Chen, F., Karagueuzian, H. S., and Weiss, J. N. (2009). Oxidative stress-induced afterdepolarizations and calmodulin kinase II signaling. *Circ. Res.* 104, 79–86. doi: 10.1161/CIRCRESAHA.108.183475

Xu, L. (1998). Activation of the cardiac calcium release channel (Ryanodine Receptor) by poly-S-nitrosylation. *Science* 279, 234–237. doi: 10.1126/science.279.5348.234

Yan, Z., Bai, X., Yan, C., Wu, J., Li, Z., Xie, T., et al. (2015). Structure of the rabbit ryanodine receptor RyR1 at near-atomic resolution. *Nature* 517, 50–55. doi: 10.1038/nature14063

Zhang, H., Makarewich, C. A., Kubo, H., Wang, W., Duran, J. M., Li, Y., et al. (2012). Hyperphosphorylation of the cardiac ryanodine receptor at serine 2808 is not involved in cardiac dysfunction after myocardial infarction. *Circ. Res.* 110, 831–840. doi: 10.1161/CIRCRESAHA.111.255158

Zhang, H., Zhang, J. Z., Danila, C. I., and Hamilton, S. L. (2003). A noncontiguous, intersubunit binding site for calmodulin on the skeletal muscle Ca^{2+} release channel. *J. Biol. Chem.* 278, 8348–8355. doi: 10.1074/jbc.M209565200

Zhang, J., Ye, Z. W., Singh, S., Townsend, D. M., and Tew, K. D. (2018). An evolving understanding of the S-glutathionylation cycle in pathways of redox regulation. *Free Radic. Biol. Med.* 120, 204–216. doi: 10.1016/j.freeradbiomed.2018.03.038

Zhou, Q., Xiao, J., Jiang, D., Wang, R., Vembaiyan, K., Wang, A., et al. (2011). Carvedilol and its new analogs suppress arrhythmogenic store overload-induced Ca^{2+} release. *Nat. Med.* 17, 1003–1009. doi: 10.1038/nm.2406

Zima, A. V., and Blatter, L. A. (2006). Redox regulation of cardiac calcium channels and transporters. *Cardiovasc. Res.* 71, 310–321. doi: 10.1016/j.cardiores.2006.02.019

Zima, A. V., Bovo, E., Bers, D. M., and Blatter, L. A. (2010). Ca^{2+} spark-dependent and -independent sarcoplasmic reticulum Ca^{2+} leak in normal and failing rabbit ventricular myocytes. *J. Physiol.* 588, 4743–4757. doi: 10.1113/jphysiol.2010.197913

Zima, A. V., Bovo, E., Mazurek, S. R., Rochira, J. A., Li, W., and Terentyev, D. (2014). Ca handling during excitation–contraction coupling in heart failure. *Pflügers Arch.* 466, 1129–1137. doi: 10.1007/s00424-014-1469-3

Zima, A. V., and Mazurek, S. R. (2016). Functional impact of ryanodine receptor oxidation on intracellular calcium regulation in the heart. *Rev. Physiol. Biochem. Pharmacol.* 171, 39–62. doi: 10.1007/112_2016_2

Zissimopoulos, S., Viero, C., Seidel, M., Cumbes, B., White, J., Cheung, I., et al. (2013). N-terminus oligomerization regulates the function of cardiac ryanodine receptors. *J. Cell Sci.* 126, 5042–5051. doi: 10.1242/jcs.133538

Zweier, J. L., and Talukder, M. A. H. (2006). The role of oxidants and free radicals in reperfusion injury. *Cardiovasc. Res.* 70, 181–190. doi: 10.1016/j.cardiores.2006.02.025

Conflict of Interest Statement: The authors declare that the research was conducted in the absence of any commercial or financial relationships that could be construed as a potential conflict of interest.

frontiers in Physiology

ORIGINAL RESEARCH
published: 13 December 2018
doi: 10.3389/fphys.2018.01801

Long-Term Regulation of Excitation–Contraction Coupling and Oxidative Stress in Cardiac Myocytes by Pirfenidone

*Adrián Monsalvo-Villegas, Diana Stephanie Osornio-Garduño and Guillermo Avila**

Department of Biochemistry, Cinvestav-IPN, Mexico City, Mexico

Pirfenidone (PFD) is used to treat human pulmonary fibrosis. Its administration to animals with distinct forms of cardiovascular disease results in striking improvement in cardiac performance. Here, its functional impact on cardiac myocytes was investigated. Cells were kept 1–2 days under either control culture conditions or the presence of PFD (1 mM). Subsequently, they were subjected to electrical stimulation to assess the levels of contractility and intracellular Ca^{2+}. The PFD treatment promoted an increase in both peak contraction and kinetics of shortening and relaxation. Moreover, the amplitude and kinetics of Ca^{2+} transients were enhanced as well. Excitation–contraction coupling (ECC) was also investigated, under whole-cell patch-clamp conditions. In keeping with a previous report, PFD increased twofold the density of Ca^{2+} current (I_{Ca}). Notably, a similar increase in the magnitude of Ca^{2+} transients was also observed. Thus, the gain of ECC was unaltered. Likewise, PFD did not alter the peak amplitude of caffeine-induced Ca^{2+} release, indicating stimulation of Ca^{2+}-induced–Ca^{2+}-release (CICR) at constant sarcoplasmic reticulum Ca^{2+} load. A phase-plane analysis indicated that PFD promotes myofilament Ca^{2+} desensitization, which is being compensated by higher levels of Ca^{2+} to promote contraction. Interestingly, although the expression of the Na^{+}/Ca^{2+} exchanger (NCX) was unaffected, the decay of Ca^{2+} signal in the presence of caffeine was 50% slower in PFD-treated cells (compared with controls), suggesting that PFD downregulates the activity of the exchanger. PFD also inhibited the production of reactive oxygen species, under both, basal conditions and the presence of oxidative insults (acetaldehyde and peroxide hydrogen). Conversely, the production of nitric oxide was either increased (in atrial myocytes) or remained unchanged (in ventricular myocytes). Protein levels of endothelial and neuronal nitric oxide synthases (eNOS and nNOS) were also investigated. eNOS values did not exhibit significant changes. By contrast, a dual regulation was observed for nNOS, which consisted of inhibition and stimulation, in ventricular and atrial myocytes, respectively. In the latter cells, therefore, an up-regulation of nNOS was sufficient to stimulate the synthesis of NO. These findings improve our knowledge of molecular mechanisms of PFD action and may also help in explaining the corresponding cardioprotective effects.

Keywords: intracellular Ca^{2+}, Ca^{2+} channel, contractility, CICR, Ca^{2+}-induced Ca^{2+} release, cardiomyocyte

OPEN ACCESS

Edited by:
Maria Fernandez-Velasco, Hospital Universitario La Paz, Spain

Reviewed by:
Dmitry Terentyev, Brown University, United States
Julieta Palomeque, Universidad Nacional de La Plata, Argentina

****Correspondence:***
Guillermo Avila
gavila@cinvestav.mx

Specialty section:
This article was submitted to Membrane Physiology and Membrane Biophysics, a section of the journal Frontiers in Physiology

Received: *24 September 2018*
Accepted: *29 November 2018*
Published: *13 December 2018*

Citation:
Monsalvo-Villegas A, Osornio-Garduño DS and Avila G (2018) Long-Term Regulation of Excitation–Contraction Coupling and Oxidative Stress in Cardiac Myocytes by Pirfenidone. Front. Physiol. 9:1801. doi: 10.3389/fphys.2018.01801

INTRODUCTION

Excitation–contraction coupling (ECC) is of pivotal relevance for cardiac contractility. ECC relies, in turn, on a critical phenomenon known as Ca^{2+}-induced–Ca^{2+}-release (CICR). An action potential (AP) activates voltage-gated Ca^{2+} channels of the plasma membrane ($Ca_V1.2$), allowing entry of extracellular Ca^{2+} (I_{Ca}) that activates ryanodine receptors (RyR2) and a consequent release of Ca^{2+} from the sarcoplasmic reticulum (SR). The resulting increase in cytosolic Ca^{2+} (Ca^{2+} transient) activates the contractile machinery, and relaxation occurs as the levels of Ca^{2+} decay thanks to the activity of both the sarco/endoplasmic reticulum Ca^{2+} ATPase (SERCA) and the Na^+/Ca^{2+} exchanger (NCX; for reviews see Bers, 2002; Eisner et al., 2017; Landstrom et al., 2017).

A small synthetic compound termed pirfenidone (PFD, 185 g/mol) is used to treat human pulmonary fibrosis. Many studies have reported that PFD also improves cardiac performance in animal models of: atrial fibrillation (AF, Lee et al., 2006), myocardial infarction (Nguyen et al., 2010; Li et al., 2017; Adamo et al., 2018), Duchenne muscular dystrophy (Van Erp et al., 2006), pressure overload (Mirkovic et al., 2002; Wang et al., 2013; Yamagami et al., 2015), hypertrophy (Yamazaki et al., 2012), diabetic cardiomyopathy (Miric et al., 2001), and diphtheritic myocarditis (Adamo et al., 2018).

In marked contrast, little is known about the corresponding molecular mechanisms. A reduction in tissue fibrosis and stiffness, attributed to low expression levels of a profibrogenic cytokine (transforming growth factor-beta 1, or TGF-β1) is thought to be involved (Avila et al., 2014; Lopez-de la Mora et al., 2015; Graziani et al., 2018). Nevertheless, some effects do not require lowering levels of TGF-β1 or fibrosis. For example, although PFD improves cardiac contractility in dystrophin-deficient (mdx) mice, this action occurs in the absence of changes in tissue fibrosis or stiffness (Van Erp et al., 2006). In addition, treating cardiac myocytes with PFD (1–2 days) induces a substantial increase in the activity of $Ca_V1.2$, by a TGF-β1 independent mechanism (Ramos-Mondragón et al., 2012).

Here, we have investigated whether PFD regulates the function of cardiac myocytes. Our present results show that, indeed, in both atrial and ventricular myocytes, PFD improves the magnitude and kinetics of contractility. This can be explained by a concomitant stimulus on both $Ca_V1.2$ and CICR. PFD also elicited a marked decrease in NCX activity and promoted changes in the synthesis rate of cytosolic free radicals [reactive oxygen species (ROS) and nitric oxide (NO)]. Interestingly, the compound also regulated the expression of neuronal NO synthase (nNOS), but not of that corresponding to NCX or eNOS. These findings may be essential to explaining how PFD exerts its cardioprotective effects.

MATERIALS AND METHODS

Isolation of Cardiac Myocytes

Atrial and ventricular myocytes were obtained as described elsewhere (Ramos-Mondragón et al., 2012; Santamaria-Herrera et al., 2016). The procedure was approved by the *Institutional Animal Care and Use Committee* (IACUC—CINVESTAV, 0199-16), complies with the Mexican Official Norm NOM-062-ZOO-1999 and is in accordance with the Guide for the Care and Use of Laboratory Animals published by the US National Institutes of Health (NIH Publication, 8th Edition, 2011).

In brief, male Wistar rats of approximately 240 g were deeply anesthetized, using a mixture of Ketamine and Xylazine (100:10 mg/Kg, i.p.). The heart was then quickly removed by thoracotomy, cannulated (via aorta) and mounted into a homemade Langendorff system. A warm (37°C) digestion buffer containing a mixture of collagenase type II and protease was retrogradely perfused, and the tissue (either ventricles or right atrium) was excised as soon as became softened. Subsequently, samples were carefully triturated, centrifuged and the resulting myocytes were plated into laminin-coated coverslips, which in turn were lying into 35 mm Petri dishes. The cells were transferred to a CO_2 incubator, kept at 37°C and maintained in the presence of standard culture medium [control (CN)] or culture medium supplemented with PFD (1 mM). Unless otherwise specified, experiments were performed 1–2 days after of have initiated the PFD treatment. This protocol was chosen based on previous determinations of the maximal effect of PFD on $Ca_V1.2$ (Ramos-Mondragón et al., 2012).

Voltage-Clamp Experiments

Ca^{2+} transients and I_{Ca} were investigated simultaneously using a combination of the voltage-clamp technique and epifluorescence (for a more comprehensive description, see Vega et al., 2011). Briefly, either atrial or ventricular myocytes were subjected to voltage-clamp, using the whole-cell patch-clamp technique. The patch-clamp electrodes were filled with an intracellular solution containing a Ca^{2+}-sensitive dye (Fluo-4) and exhibited an electrical resistance of approximately 4 MΩ. The cell capacitance (C_m) was estimated from linear capacitative currents, which were acquired under both cell-attached and whole-cell conditions. Leak currents were eliminated on-line, using a p/N leak subtraction procedure. For each cell, the peak value of I_{Ca} was normalized by C_m and plotted as a function of V_m. The resulting I–V curves were fitted according to the following Boltzmann equation:

$$I_{Ca} = G_{max}(V_m - V_{rev})/\{1 + exp[(V_{1/2} - V_m)/k]\} \quad (1)$$

where G_{max} represents the maximal Ca^{2+} conductance, $V_{1/2}$ is the potential for half-maximal activation of G_{max}, k is a slope factor, and V_{rev} is the apparent reversal potential of I_{Ca}.

Levels of free cytosolic Ca^{2+} were assessed using Fluo-4. The dye was excited using a 100 W mercury arc lamp (at 470–490 nm), and the emitted fluorescence was collected at 515–550 nm using a photomultiplier tube. The magnitude of Ca^{2+} transients was estimated as the maximum fluorescence value during test pulses (F), divided by the basal fluorescence observed before the pulse (F_b), according to: $\Delta F/F = (F - F_b)/F_b$. The gain of EC coupling (ECC Gain) was calculated by normalizing maximal $\Delta F/F$ values to its respective peak value of I_{Ca}. The increase in Ca^{2+} signal

induced by caffeine (30 mM) was used to estimate the amount of releasable SR Ca^{2+} content. Caffeine was applied via a local, rapid perfusion system (Warner Instruments Corporation), first in the absence and then in the presence of extracellular Na^{+} (see *Recording solutions*). For each cell, the NCX function was examined at the holding potential (−50 mV, atrium; and −40 mV, ventricle) by analyzing Ca^{2+} signals remaining at the end of caffeine applications (25 s).

Measurements of Contractility and Intracellular Ca^{2+}

Ca^{2+} transients and mechanical properties were recorded simultaneously in intact (non-patch clamped) myocytes, with the aid of an IonOptix system (as described elsewhere, Santamaria-Herrera et al., 2016). In short, the cells were loaded with Fura-2 AM (6 μM, 15 min) and then transferred to a stimulation chamber that contained Tyrode's solution. Subsequently, the chamber was mounted on an inverted microscope equipped with epifluorescence, and electrical stimuli (20 V, 20 ms) were delivery at 0.2 Hz. A particular myocyte was observed on a PC monitor, using a digital video camera. The fluorescence emission ratio of Fura-2 was recorded (F_{360}/F_{380}), and changes in myocyte length during shortening and re-lengthening were measured at both ends of the cell. In ventricular myocytes, the average sarcomere length was also investigated. Briefly, an area of well-defined striations was selected, and then the average periodicity of Z-line densities was determined (based on a fast Fourier transform algorithm). The sampling frequencies for recordings of contractions and intracellular Ca^{2+} were 0.25 and 1.0 kHz, respectively.

Intracellular Production of ROS and NO

Production of ROS and NO was estimated using fluorescence sensors for these molecules (CM-H_2DCF DA and DAF-FM DA; Ríos-Pérez et al., 2016). Either atrial or ventricular myocytes were incubated (15 min at room temperature) with Tyrode's solution supplemented with a 1:1 mixture of Fura-2 AM and the appropriated sensor (3 μM each). Fura-2 was excited at 360 nm (its isosbestic or Ca^{2+}-insensitive point), and its fluorescence was used to normalize signals corresponding to CM-H_2DCF DA and DAF-FM DA (to prevent for potential differences in loading capacity). Both sensors were excited at 470–490 nm and examined at 515–550 nm.

Western-Blot Analysis

Protein levels of NCX, nNOS and eNOS, were investigated by western-blot analysis (García-Castañeda et al., 2017). The cells were washed with ice-cold PBS and incubated 15 min in lysis buffer (containing inhibitors of proteases and phosphatases). The total protein concentration was determined by Bradford assay, and protein samples (25–50 μg) were separated by electrophoresis in Laemmli buffer before being electrotransferred to PVDF membranes. The membranes were then blocked with 3% BSA, washed and subjected to immunoblotting with primary antibodies for the protein of interest (at 4°C, overnight). Subsequently, the membranes were incubated with a horseradish peroxidase-conjugated secondary antibody (at 37°C for 60 min). Immunoreactivity was revealed by chemiluminescence, and bands were quantified using Image J (NIH, Bethesda, MD, United States). Each particular membrane was also probed for β-tubulin, to account for potential variability in the amount of protein loaded. The following antibodies were used. *Primary*: anti-NCX (R3F1, Swant, 1:1,000), anti-eNOS (610296, BD Bioscience, 1:800), anti-nNOS (610308, BD Bioscience, 1:800), and anti-β-tubulin (32-2600, Invitrogen, 1:4000). *Secondary*: goat anti-mouse IgG (G-21040, Invitrogen, 1:10,000).

Recording Solutions

The Tyrode's solution contained (in mM): NaCl 130, HEPES 25, Glucose 22, KCl 5.4, $CaCl_2$ 2, $MgCl_2$ 0.5, NaH_2PO_4 0.3, lactic acid 1.1, and pyruvic acid 3 (pH = 7.4).

In atrial myocytes, Ca^{2+} transients and I_{Ca} were recorded in the presence of the following solutions. *External* (in mM): methanesulfonic acid 145, TEA-OH 115, HEPES 10, $CaCl_2$ 5, $MgSO_4$ 2, 4-aminopyridine 5, 9-anthracene carboxilic acid 1, glucose 10 and 2-3-butanedione monoxime 2. *Internal* (in mM): Cs-Asp 100, CsCl 10, HEPES 10, Cs-EGTA 1, $CaCl_2$ 0.2, glucose 10, TEA-HCl 20, ATP-Mg 5, GTP-tris 0.05 and Fluo-4 K_5 0.15.

In ventricular myocytes, I_{Ca} and Ca^{2+} transients were recorded in the presence of slightly different solutions (compared with those used for atrial myocytes). *External* (in mM): methanesulfonic acid 125, TEA-OH 115, HEPES 10, $CaCl_2$ 10, $MgSO_4$ 8, 4-aminopyridine 5, 9-anthracene carboxilic acid 1, 2-aminoethyl diphenylborinate 0.01, Creatine 25, glucose 10 and 2-3-butanedione monoxime 2. *Internal* (in mM): Cs-Asp 160, CsCl 10, HEPES 10, Cs-EGTA 6, $CaCl_2$ 1, glucose 10, ATP-Mg 5, TEA-HCl 25, $MgCl_2$ 0.5, GTP-tris 0.05 and Fluo-4 K_5 0.05.

The NCX activity was investigated by comparing intracellular Ca^{2+} responses triggered by caffeine (30 mM), which was applied using the above-cited *external* solutions (supplemented or not with 140 mM Na^{+}. EGTA (0.5 mM) was added as well, to chelate any contaminating Ca^{2+}. When required, TEA was omitted to balance the osmolarity.

In all patch-clamp solutions, the pH was adjusted to 7.3.

Data Analysis

All data were analyzed using the following software packages: SigmaPlot (Systat Software, Inc., San Jose, CA, United States), IonWizard (IonOptix, Westwood, MA, United States), and pCLAMP (Molecular Devices, Sunnyvale, CA, United States). Experimental results are shown as means ± SEM from the indicated number of experiments (n). Two groups were compared by Student's *t*-test, and ANOVA was used for multiple statistical comparisons.

All experiments were performed at room temperature (∼24°C).

RESULTS

Our previous work has shown that the density of I_{Ca} is larger in PFD-treated myocytes than in controls (Ramos-Mondragón et al., 2012). Thus, we first reexamined this aspect, using

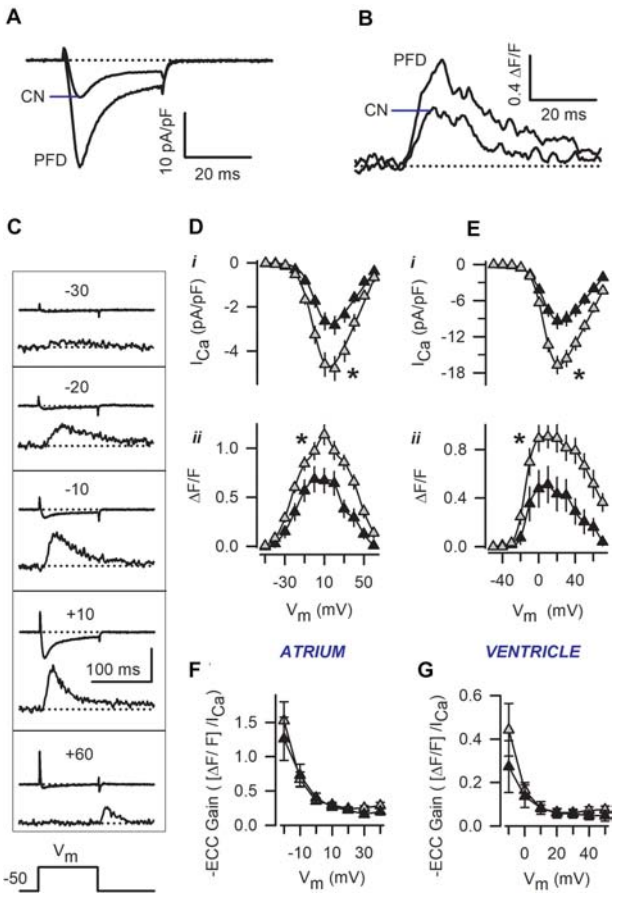

FIGURE 1 | Patch-clamp experiments reveal a pirfenidone (PFD)-induced increase in the magnitude of both I_{Ca} and Ca^{2+} transients. Representative traces of I_{Ca} and Ca^{2+} transients that were recorded simultaneously in either ventricular **(A,B)** or atrial myocytes **(C)**. In **(A,B)**, recordings obtained from control (CN) and PFD-treated (PFD) myocytes were superimposed, and the membrane was depolarized to +10 mV. In contrast, **(C)** illustrates traces obtained at different membrane potentials (V_m, in a control cell; the vertical calibration bar indicates 100 pA and 1.0 ΔF/F). **(D,E)** Average peak values of I_{Ca} (***i***) and Ca^{2+} transients (***ii***) that were obtained as in **(C)**, for both atrial **(D),** and ventricular **(E)** myocytes. Results are from a total of 28 atrial (11 CN, 17 PFD) and 32 ventricular (17 CN, 15 PFD) myocytes. **(F,G)** Voltage-dependence of ECC gain, estimated from data shown in **(D,E)**. Closed and gray symbols denote control and PFD-treated cells, respectively. $^*p < 0.05$, ANOVA.

ventricular myocytes. At the same time, a possible effect on SR Ca^{2+} release was investigated as well. Remarkably, PFD induced a twofold increase in the magnitude of both I_{Ca} and Ca^{2+} transients. More specifically, the following values of I_{Ca} and Ca^{2+} transients were obtained, for control (n = 14) and PFD-treated (n = 16) myocytes: −9.3 ± 2.0 and −20.9 ± 2.7 pA/pF ($p < 0.003$), and 0.34 ± 0.08 and 0.57 ± 0.06 ΔF/F ($p < 0.05$). Some examples of these determinations are show in **Figures 1A,B**.

In subsequent experiments, the voltage-dependence of I_{Ca} and Ca^{2+} transients was investigated (see the representative traces of **Figure 1C**). Interestingly, the PFD effect on both I_{Ca} and Ca^{2+} transients could be observed at different membrane potentials (**Figures 1D,E**). Fitting I–V curves to a Boltzmann function (Eq. 1) led to the conclusion that PFD causes a 65% increase in the maximal Ca^{2+} conductance (G_{max}), in accord with our previous work (Ramos-Mondragón et al., 2012). Specifically, the G_{max} values that were estimated from control and PFD-treated myocytes were: 62 ± 8 and 105 ± 10 nS/pF ($p < 0.01$, *atrium*); and 184 ± 24 and 297 ± 25 nS/pF ($p < 0.003$, *ventricle*). No significant differences were found in the voltage-dependent parameters of G_{Ca} (mid-point and slope factor), between control and PFD-treated myocytes.

The gain of ECC was also investigated, and it was found identical in control and PFD-treated myocytes (**Figures 1F,G**). This result suggests that PFD induces an I_{Ca} that is not redundant for ECC. In other words, the extra I_{Ca} elicits the same degree of Ca^{2+} release as its respective control. The activity of SERCA was examined next, as illustrated in **Figure 2A**. More specifically, the decaying phase of the Ca^{2+} transient was fitted to a simple exponential equation. The resulting average values of τ are shown in **Figures 2B,C**. It can be appreciated that PDF did not alter this parameter in a wide range of membrane potentials, indicating that PFD does not alter the activity of SERCA.

To assess the amount of releasable SR Ca^{2+}, caffeine was applied under both absence and presence of extracellular Na^+ (see the representative traces shown in **Figures 2D,E**). Interestingly no significant differences were found in the peak values of caffeine response (F_{Peak}), between control and PFD-treated myocytes (in either the absence or presence of Na^+, **Figures 2F,H**). These data indicate that the effect of PFD on Ca^{2+} transients (**Figure 1**) is not due to changes in the load of SR Ca^{2+}.

Two different concentrations of extracellular Na^+ were used in **Figures 2D–I**, because this approach allows investigating both the function of the NCX and Na^+-independent transporters responsible for Ca^{2+} extrusion. In particular, we examined ΔF/F signals remaining at the end of 25 s of caffeine exposure, in the absence and presence of 140 mM Na (termed F_0 and F_{Na}, see **Figures 2D,E**). In the absence of Na^+, the rate of Ca^{2+} signal decay seems to be slower in PFD-treated cells (**Figures 2D,E**, *0 Na*$^+$). To quantify this observation, for each cell, F_0 was normalized to its corresponding peak caffeine response (F_{Peak}). The resulting average values were: 0.59 ± 0.04 and 0.78 ± 0.04 (p = 0.001), for control (n = 30) and PFD-treated cells (n = 31). This analysis suggests that PFD inhibits Na^+-independent Ca^{2+} extrusion systems.

The contribution of Na^+ to decreasing [Ca^{2+}] was next estimated, from F_{Na}/F_0 ratios (1.0 means no contribution). Surprisingly, in PFD-treated cells, the NCX activity was not detected (**Figures 2G,I**, *gray bars*), whereas in control myocytes the exchanger contributed by 45% (**Figures 2G,I**, *closed bars*). The NCX function was also more directly compared between control and PFD-treated cells (using the F_{Na}/F_0 values of **Figures 2G,I**). On average, the F_{Na}/F_0 values were: 0.60 ± 0.06 and 0.88 ± 0.06 (p = 0.012), for control (n = 21) and PFD-tread cells (n = 29). These data suggest that PFD inhibits the NCX activity by 30%.

Then we wonder if the effects observed in ECC (under non-physiological conditions; i.e., patch-clamp, **Figure 1**), would have functional consequences. Thus, we investigated the contractility

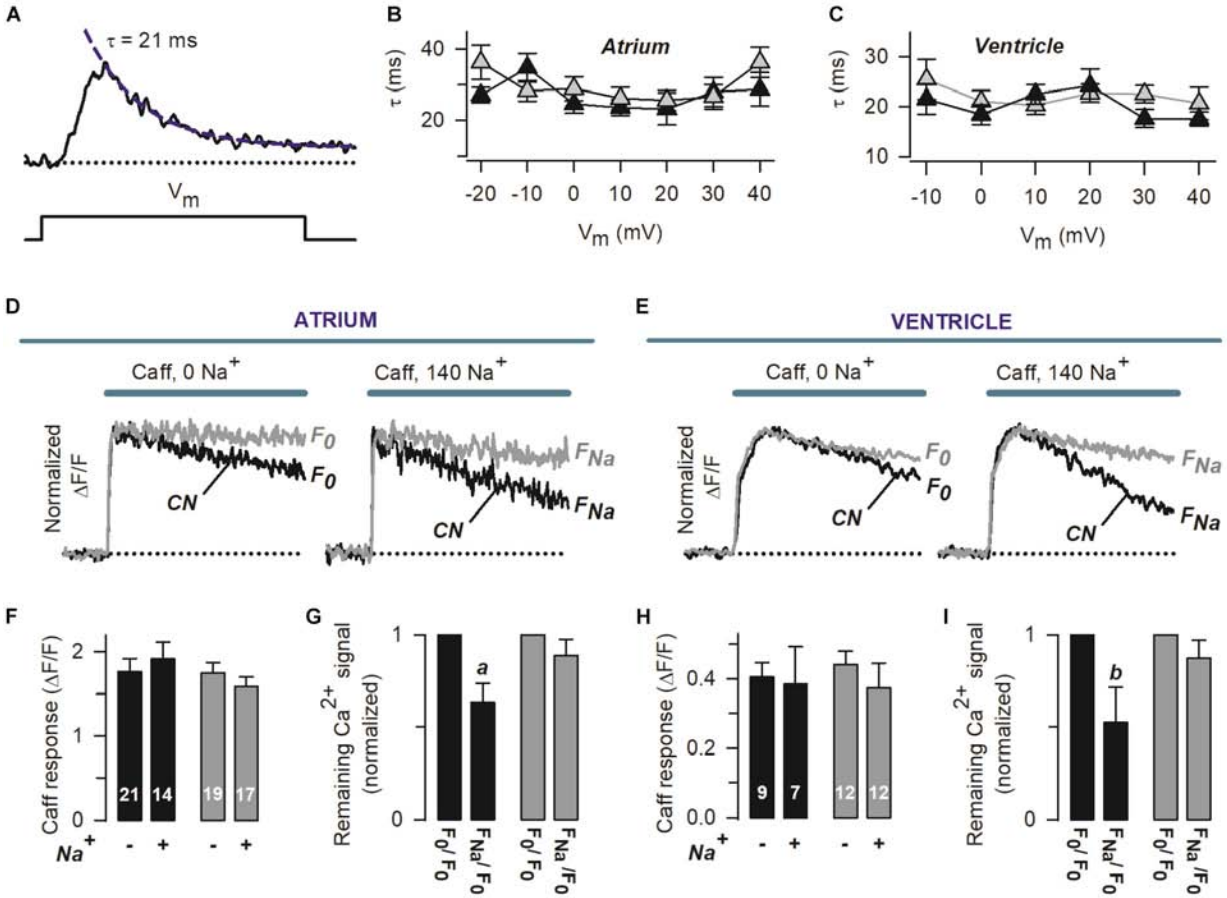

FIGURE 2 | Pirfenidone regulates the rate of Ca^{2+} extrusion via the NCX, but not SERCA activity. **(A)** The panel shows a Ca^{2+} transient recorded as in **Figure 1**, along with an exponential function (dashed line) describing the decaying phase. The corresponding time constant (τ) is also indicated. **(B,C)** Average values of τ that were obtained as in **(A)**, as a function of V_m. **(D,E)** Representative Ca^{2+} transients that were induced by a double pulse of caffeine (Caff), initially in the absence (0 Na^+) and then in the presence of 140 mM extracellular Na^+ (140 Na^+). Recordings were obtained from four different myocytes (two atrial–*D* and two ventricular–*E*). F_0 and F_{Na} stand for the Ca^{2+} signal remaining at the end of caffeine applications, in the absence and presence of Na. The traces are shown normalized to peak caffeine response (F_{Peak}), to emphasize kinetic differences. **(F,H)** Absolute average values of F_{Peak} (*Caff response*) and number of investigated cells. **(G,I)** For each particular cell, F_0 and F_{Na} (see **D,E**) were normalized with respect to F_0, and the resulting values were pooled and averaged. In all panels, black and gray symbols/traces denote control (CN) and PFD-treated cells, respectively. $^a p < 0.005$, $^b p < 0.05$; compared with the matching F_0/F_0 condition (paired *t*-test).

of both sarcomere and cardiomyocytes. Remarkably, PFD increased not only the percent of cell and sarcomere contraction (by 50%) but also the corresponding kinetics of contraction and relaxation (by 30–70%; **Figure 3** and **Supplementary Figure 1**). These PFD effects should lead to improving cardiac blood flow, which is in keeping with results of Nguyen et al. (2010).

In **Figure 3**, contractility was recorded in parallel with Ca^{2+} transients. An analysis of the corresponding Ca^{2+} signal indicated that, in atrial myocytes, PFD promotes not only Ca^{2+} transients of higher magnitude but also lower values of diastolic Ca^{2+} (compared with controls, **Figure 4**, *atrium*). With regard to ventricular myocytes, PFD did not alter the amplitude of the Ca^{2+} transient but increased the average values of systolic Ca^{2+} (**Figure 4**, *ventricle*). Additionally, PFD increased both maximum rate of Ca^{2+} output (in atrium, 21.1 ± 1.6 ΔRatio/s versus 27.5 ± 1.5 ΔRatio/s; $p < 0.05$) and lag time between electrical stimulus and initiation of Ca^{2+} transient decay (in ventricle, 84 ± 4 ms versus 95 ± 4 ms; $p < 0.05$). As a consequence of these changes, the PFD treatment resulted in an increased integral of the initial phase of the Ca^{2+} transient (**Supplementary Figure 2**). Thus, in intact cardiomyocytes, PFD stimulates CICR and thereby also enhances contractility (**Figure 3** and **Supplementary Figure 1**).

We also build phase-plane diagrams, to analyze myofilament Ca^{2+} sensitivity (**Figure 5A**). The corresponding results indicate that, in the ventricle, PFD not only increases the amplitude of shortening (**Figure 3** and **Supplementary Figure 1**) but also shifts the phase-plane trajectories to the right (**Figures 5A,B**). Although in atrium a similar shift to the right was absent (**Figures 5A,B**), an increase in the slope of relaxation was found (**Figure 5C**). This increase was also present in the ventricle (**Figure 5C**) and suggests that PFD promotes myofilament Ca^{2+} desensitization (Spurgeon et al., 1992), which is being compensated by higher levels of $[Ca^{2+}]_i$ to promote contraction (see above).

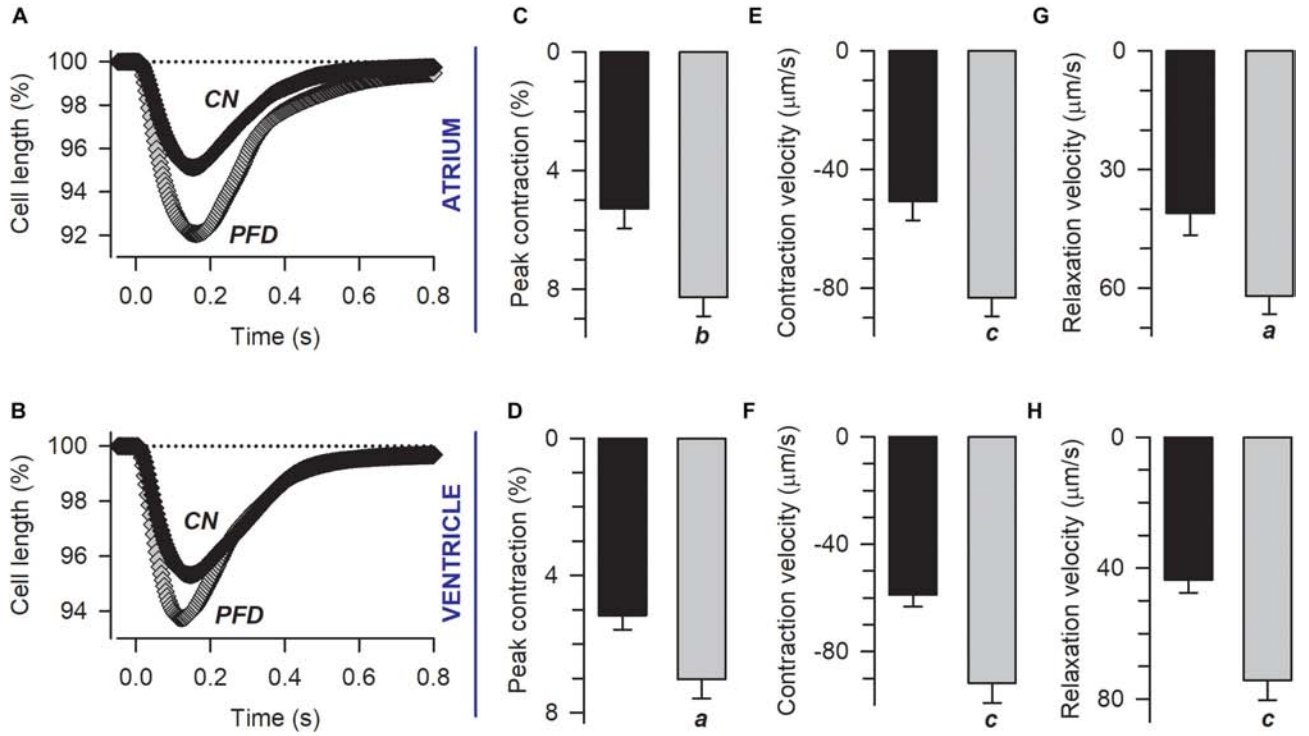

FIGURE 3 | Pirfenidone improves the contractility of cardiac myocytes. **(A,B)** Electrically evoked contractions from atrial **(A)** and ventricular **(B)** myocytes previously kept in culture under either control (CN) or PFD conditions (PFD). Plotted are mean values that were estimated from a total of 56 atrial (30 CN, 26 PFD) and 110 ventricular (59 CN, 51 PFD) myocytes. The corresponding average values (mean ± SEM) of peak cell shortening **(C,D)** and the maximum speed of contraction **(E,F)** and relaxation **(G,H)** are also shown. Black and gray symbols/bars indicate control and PFD-treated cells. $^{a}p < 0.01$, $^{b}p < 0.005$, $^{c}p < 0.001$.

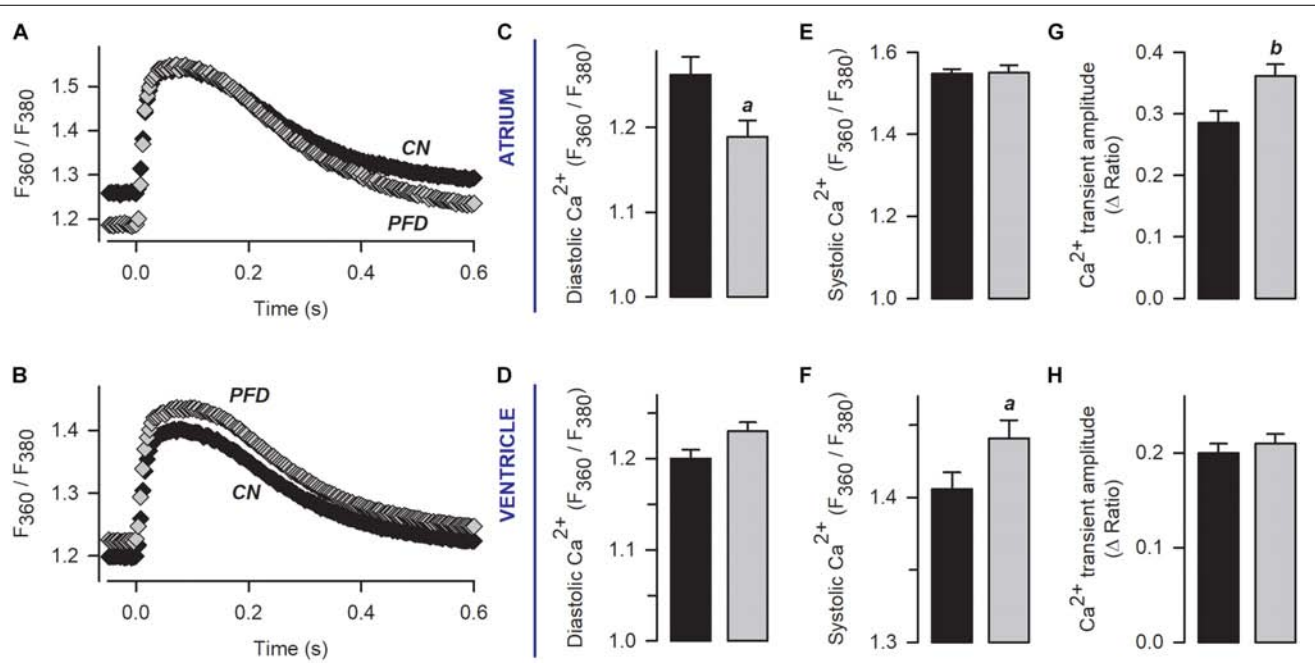

FIGURE 4 | Pirfenidone enhances CICR in intact (non-patch clamped) myocytes. **(A,B)** Mean values of Ca^{2+} transients that were obtained from electrically stimulated atrial (*A*; 42 CN, 37 PFD) and ventricular (*E*; 81 CN, 80 PFD) myocytes. Average values (mean ± SEM) of diastolic **(C,D)** and systolic **(E,F)** Ca^{2+} are also shown, along with the maximum amplitude of the Ca^{2+} transient **(G,H)**. Black and gray symbols/bars indicate control and PFD-treated cells. $^{a}p < 0.05$, $^{b}p < 0.01$.

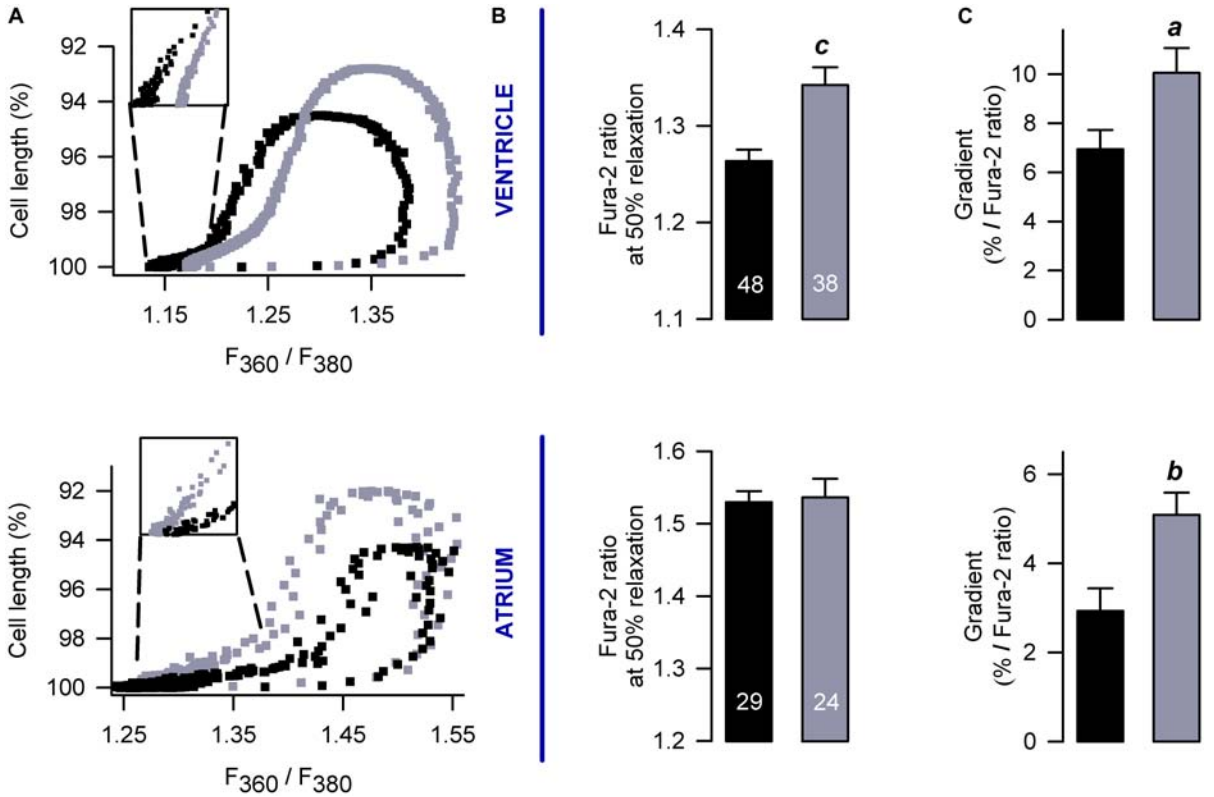

FIGURE 5 | Effects on myofilament Ca^{2+} sensitivity. **(A)** Examples of phase plane diagrams of cell length versus ratio of fluorescence of Fura-2 that were used to analyze myofilament Ca^{2+} sensitivity. Inserts illustrate regions used to estimate the slope of relaxation (or re-lengthening), which were fixed at 90–95% of relaxation. **(B,C)** Average values of Ca^{2+} levels required for 50% of relaxation **(B)** and gradients obtained after fitting endpoint relaxation regions to a straight line (**A**, inserts). The number of investigated cells is shown in **(B)**. $^{a}p < 0.05$, $^{b}p < 0.005$, $^{c}p < 0.001$.

The cAMP-dependent protein kinase (PKA) phosphorylates key elements of ECC, and thus we investigated whether this protein might be involved in the stimulus of contractility. Ventricular myocytes were exposed 30 min to PKI (a cell-permeable PKA inhibitor), which failed in reverting PFD effects (**Supplementary Figure 3**). Although in this experiment Ca^{2+} transients were not investigated, the finding that PKI does not interfere with the magnitude or kinetics of cell shortening (**Supplementary Figure 3**) suggests that myofilament desensitization (**Figure 5**) is not due to PKA-dependent phosphorylation of cTnI (Cheng and Regnier, 2016).

Elevated levels of free radicals production are involved in several cardiovascular disorders (for reviews see Zhang et al., 2004; Korantzopoulos et al., 2007; Köhler et al., 2014). Thus, the possibility that PFD regulates the generation of ROS was also investigated. The corresponding results indicate that PFD causes a significant reduction in the signal of a ROS-sensitive fluorescent compound (CM-H_2DCFDA), revealing a 15–30% inhibition of ROS production (**Figure 6A**). Conversely, a 1.3-fold upregulation of NO synthesis was also observed, particularly in atrial myocytes (**Figure 6B**). A minimum of 8 h of PFD-treatment was needed to observe a significant effect on NO and ROS (**Supplementary Figure 4**), suggesting that changes in protein expression might be involved.

An acute oxidative stress challenge was also investigated, in ventricular myocytes. Specifically, the production of ROS was assessed in cells exposed 30 min to either acetaldehyde (ACA) or hydrogen peroxide (H_2O_2). As predicted from results shown in **Figure 6A**, ROS production was again lower in PFD-treated cells, compared with CN (**Figure 6C**, *PFD* vs. *CN*). Additionally, in both CN (**Figure 6C**, *white bars*) and PFD-treated cells (**Figure 6C**, *gray bars*) the oxidative insults caused a significant increase in ROS production. The production of ROS, however, proved to be identical in the following three experimental conditions: CN, PFD + ACA, and PDF + H_2O_2 (**Figure 6C**). Thus, the results of **Figures 6A,C** demonstrate that PFD attenuates oxidative stress, not only under basal conditions but also in the presence of pro-oxidants.

The regulatory actions on both NCX activity (**Figure 2**) and NO generation (**Figure 6B**) can potentially be explained by parallel changes in steady-state expression levels of related proteins. This point was next investigated, by western-blot analysis. PFD did not alter the expression of NCX (**Figure 7**), suggesting that in PFD-treated cells the disrupted ability of Na^+ to extrude Ca^{2+} (**Figure 2**) reflects the lower activity of a fixed number of exchangers.

Pirfenidone also did not alter the expression of eNOS ($p > 0.3$, **Figure 7**). However, a dual regulation of nNOS was found.

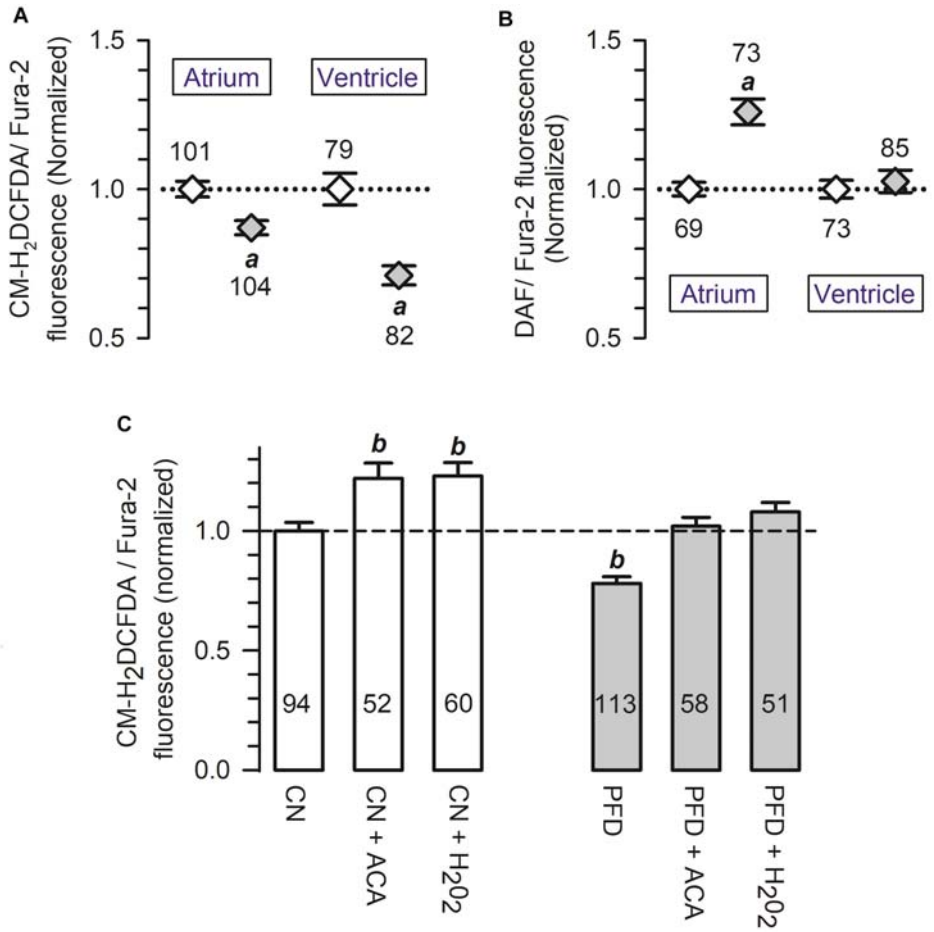

FIGURE 6 | Pirfenidone regulates the production of both ROS and NO. **(A,B)** Cardiomyocytes were loaded with a 1:1 mixture of Fura-2 and a fluorescence sensor for either ROS **(A)** or NO **(B)**. For each cell, the fluorescent signal of the sensor was divided by that of Fura-2 (used as a loading control), and then the resulting ratio was normalized to the respective mean value of control cells. **(C)** Average ROS production measured as in **(A)** (CN, PFD), except that some determinations were performed in the presence of either acetaldehyde (ACA) or H_2O_2 (200 μM, 30 min). Open and gray symbols/bars indicate control and PFD-treated treated cells, respectively. $^{a}p < 0.001$, compared with the corresponding control. $^{b}p < 0.005$, compared with CN.

The expression level of this enzyme was increased by 60% in atrial myocytes and decreased by 55% in ventricular myocytes (**Figure 7**). These data suggest that an elevation in expression levels of nNOS (Figure. 7, *atrium*) is sufficient to increase the synthesis of NO (**Figure 6B**, *atrium*). Conversely, a reduction in these levels (**Figure 7**, *ventricle*) is not sufficient for changing the production of NO (**Figure 6B**, *ventricle*).

DISCUSSION

Cardiac myocytes are of paramount relevance for blood pumping, and its function is compromised in a number of cardiac conditions. On the other hand, many studies show that PFD-treated animals are less prone to develop cardiac dysfunction (Miric et al., 2001; Mirkovic et al., 2002; Lee et al., 2006; Van Erp et al., 2006; Nguyen et al., 2010; Yamazaki et al., 2012; Wang et al., 2013; Yamagami et al., 2015; Li et al., 2017; Adamo et al., 2018). However, no study has systematically investigated the impact of PFD on the function of cardiac myocytes. Consequently, here we have evaluated the influence of PFD on I_{Ca}, Ca^{2+} transients, ECC gain, SR Ca^{2+} content, contractility, ROS, NO, and expression levels of some related proteins (NCX, eNOS, and nNOS). Our results demonstrate, for the first time, that PFD upregulates not only $Ca_V1.2$ but also CICR and ECC. Remarkably, PFD also: enhances the degree and kinetics of contractility, inhibits Ca^{2+} extrusion via NCX (and other secondary pathways), and lowers oxidative stress.

Below we discuss molecular mechanisms that may underlie our findings, along with the corresponding implications for the *in vivo* condition.

Molecular Mechanisms of PFD Action

Investigating contractility under physiological-like situations (i.e., in intact myocytes) is essential because the corresponding results are more likely to be significant for *in vivo* conditions. Unfortunately, however, deciphering the underlying mechanisms

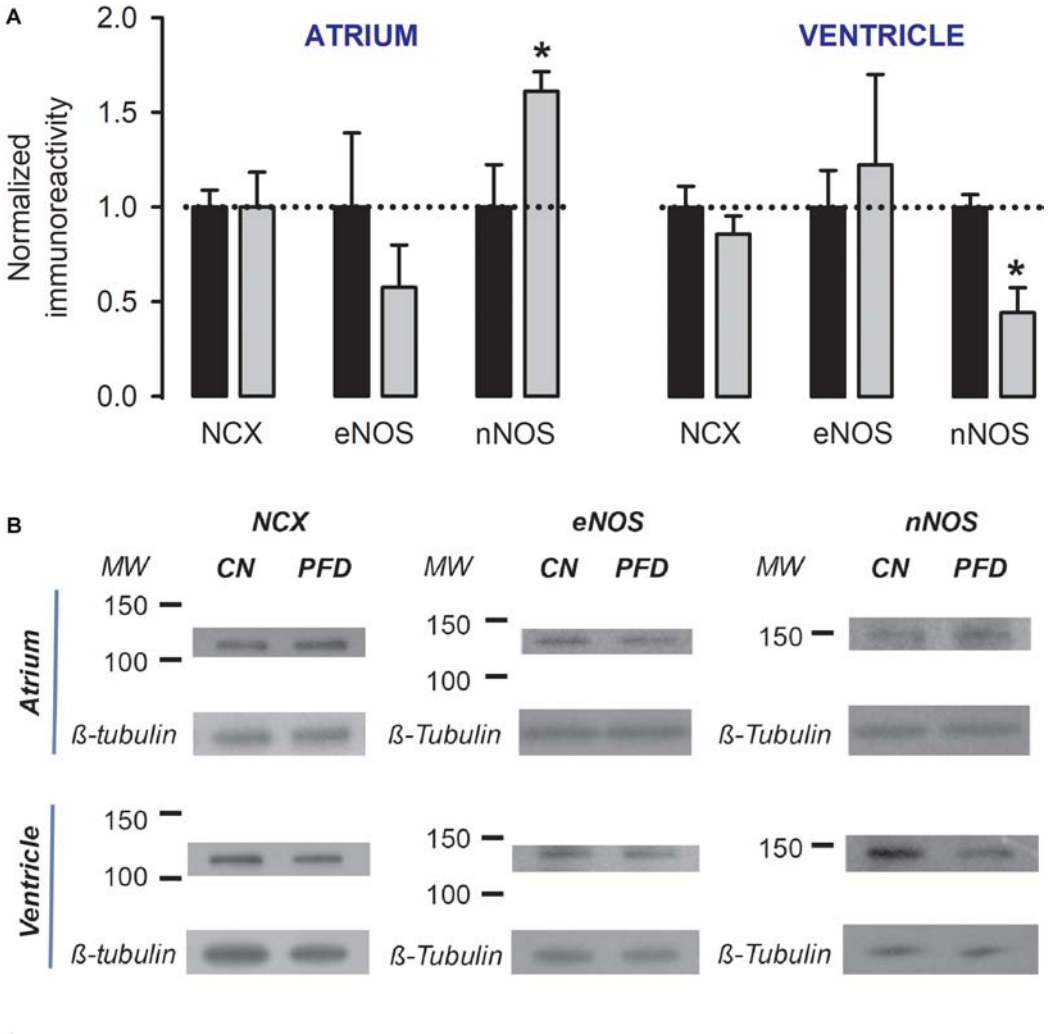

FIGURE 7 | Dual regulation of nNOS expression by PFD. **(A)** Normalized immunoreactivity that was detected in myocytes exposed to primary antibodies against NCX, eNOS, and nNOS (β-tubulin was the loading control). Bars represent the average values from a total of three to four independent experiments. $*p < 0.05$. **(B)** Examples of western blots that were analyzed to generate data shown in **(A)**.

is complicated because they may comprise several interrelated variables and processes —such as resting membrane potential, the fraction of inactivated channels, the affinity of myofilaments for Ca^{2+}, and cytosolic ionic composition (Bers, 2001). On the contrary, interpreting results from voltage-clamp experiments (e.g., under whole-cell patch-clamp) is more straightforward, because many variables either remain constant or are measured (e.g., I_{Ca}, C_m, V_m, intracellular Ca^{2+}, recording solutions). Here we have combined these approaches and obtained evidence suggesting that, by enhancing I_{Ca} and SR Ca^{2+} release, PFD stimulates the contractility of both the sarcomere and cardiomyocytes. We cannot discard, however, a potential contribution of other mechanisms.

Our previous work demonstrated that PDF increases the number of functional $Ca_V1.2$ channels (Ramos-Mondragón et al., 2012). This finding, combined with the present observations that the magnitude of Ca^{2+} transients is also enhanced at constant SR load (**Figures 1**, **2**), suggests that PFD prompts the recruitment of Ca^{2+} release units. Atrial and ventricular myocytes are functional and structurally different (Bootman et al., 2011), and thus it will be of interest to investigate the molecular and ultrastructural basis for the recruitment of otherwise "silent" Ca^{2+} release units. This potential mechanism relies on the assumption that, in control cells, Ca^{2+} release units are not saturated by cytosolic Ca^{2+} (even at voltages where I_{Ca} reaches its maximum). Evidence exists indicating that in rat atrial myocytes this happens, even under basal conditions. This is because Ca^{2+} transients elicited by I_{Ca} cannot recruit RyRs located in central regions of the cell, due to the absence of t-tubules. Besides, the mitochondria act as a buffer of Ca^{2+} that complicates free diffusion of the ion, thereby preventing the activation of this "reserve" of RyRs (Mackenzie et al., 2004). The reserve, however, can be recruited under exceptional conditions. For example, during β-adrenergic stimulation and probably also in response to PFD. The following

supports this view ***(i)*** PFD inhibits the Ca^{2+} uptake by Na^{+}-independent slow systems, which likely include mitochondrial transport; and ***(ii)*** PFD-treated cells must present higher $[Ca^{2+}]_i$ in microdomains of the cell periphery, due to exacerbated I_{Ca}.

A similar model can be proposed for the ventricle. Gómez et al. (1997) reported that hypertrophied ventricular myocytes (derived from hypertensive rats) present a poor ability of I_{Ca} to trigger Ca^{2+} release, in the face of an intact SR Ca^{2+} load. β-adrenergic stimulation reverses this "defective EC coupling," which likely involves a change of the microarchitecture of the dyad (Gómez et al., 1997). In support of this view, it has been reported that the t-tubular system (and other structures) is altered in hypertrophied hearts (Page and McCallister, 1973). Moreover, biophysical evidence exists supporting the notion that in the hypertrophied myocytes the DHPR may be further from the RyR. More specifically, in these cells, the time course of I_{Ca} inactivation is slowed (Gómez et al., 1997). In our experiments, CN myocytes also likely develop a certain degree of defective EC coupling in culture, which PFD may have prevented. The following supports this hypothesis. Although rat ventricular myocytes retain ultrastructural properties like those of healthy, intact cardiac tissue, for at least during 3 days of culture, subtle structural changes began to appear earlier. For example, within 24 h, intercalated disks became internalized (Mitcheson et al., 1998). Moreover, we found evidence that PFD promotes accelerated kinetics of I_{Ca} inactivation, which represents biophysical evidence of enhanced DHPR/RyR functional interaction (**Supplementary Figure 5**).

Regarding ventricular myocytes, an apparent inconsistency exists between the results of **Figure 1** (whole-cell, patch-clamp) and **Figure 4** (intact cells). In particular, PFD increased the magnitude of the Ca^{2+} transient in the former (**Figures 1B,E**) but not in the latter (**Figures 4B,H**). Conceivably, different rates of $Ca_V1.2$ activation and Ca^{2+} diffusion could have led to obtaining distinct results. These processes are likely more rapid under patch-clamp, because: ***(i)*** in these conditions, membrane depolarization is more expedite than in an AP, and ***(ii)*** the recording solution does not contain Ca^{2+}-binding biomolecules (as opposed to the cytosol). Thus, in patch-clamp experiments, PFD probably improved the DHPR/RyR functional interaction more efficiently (see above), because of both enhanced activation kinetics of I_{Ca} and optimized diffusion of the ion. These differences could also account for the observation that in intact ventricular myocytes PFD did not alter the rate of Ca^{2+} output, but instead increased the latency for reaching the peak of the Ca^{2+} transient as well as the corresponding integral (see **Figure 4**, **Supplementary Figure 2** and the corresponding description).

In response to PFD, the diastolic $[Ca^{2+}]$ was decreased in atrial myocytes (**Figures 4A,C**); however, it showed a tendency to be increased in ventricular myocytes ($p = 0.08$; **Figures 4B,D**). The reasons for these opposite effects are currently unknown. Additional data combined with a precise mathematical model may eventually help to explain how the fluxes of Ca^{2+} are being balanced. In this respect, our results suggest that PFD-treated cells efficiently compensate for the higher flux of Ca^{2+} into the cytoplasm: ***(i)*** PFD accelerates Ca^{2+}-dependent inactivation of $Ca_V1.2$. As can be seen in **Supplementary Figure 5**, PFD promotes a 1.3-fold increase in the percentage of I_{Ca} inactivation. Thus, while the influx of Ca^{2+} via $Ca_V1.2$ is higher during the first ∼10 ms, a subsequent accelerated kinetics of inactivation imposes a drastic reduction of Ca^{2+} influx (from at least 30 to 100 ms, **Supplementary Figure 5**). ***(ii)*** PFD increases the absolute level of SR Ca^{2+} uptake, in proportion to its effects on Ca^{2+} transients. The observation that large and small Ca^{2+} transients return both to basal values with similar time constants (τ) means that the activity of SERCA is unchanged (**Figures 2A–C**). Nevertheless, it also implies that absolute levels of SR Ca^{2+} uptake are necessarily higher in the former. In other words, our conclusion that PFD does not alter τ (**Figures 2A–C**) does not mean that SERCA is unable to detect the twofold change in intracellular Ca^{2+} transient amplitude. On the contrary, it can be demonstrated that SERCA detects this change and thereby also accelerates the

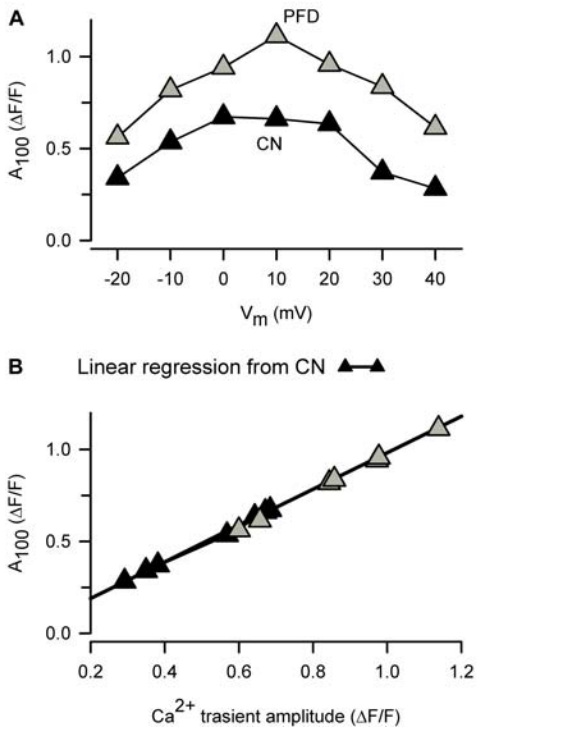

FIGURE 8 | The amount of Ca^{2+} uptake by the SR is higher in PFD-treated cells, compared with controls. **(A)** This plot was built using average values of both τ (**Figure 2**) and Ca^{2+} transients (**Figure 1**), according to: $A_{100} = A\,[1-(\exp - (t_{100}/\tau)]$; where A is the peak Ca^{2+} transient amplitude, t_{100} represents 100 ms, and A_{100} means the estimated drop in **A** in 100 ms. **(B)** Same data as in a (A_{100}) but plotted as a function of peak Ca^{2+} transient amplitude (as opposed to V_m). Data from exclusively control cells (closed symbols) were fitted according to a linear equation, and the resulting parameters were used to create a theoretical function (solid line; the correlation coefficient, r, was 0.999). Of note, this function describes data from both control and PFD-treated cells (gray symbols), indicating that PFD does not alter SERCA activity but instead feeds the system with the substrate (Ca^{2+}).

SR Ca^{2+} uptake. The demonstration consists of estimating the decay of Ca^{2+} transients —in absolute ΔF/F values—, for a fixed period. For example, the decay in ΔF/F per 100 ms is larger in PFD-treated cells than controls (**Figure 8A**, A_{100}). Accordingly, if one displays A_{100} values as a function of the peak Ca^{2+} transient amplitude, it becomes clear that PFD increases the velocity of Ca^{2+} uptake as a consequence of enhancing the magnitude of Ca^{2+} transients (**Figure 8B**).

Pirfenidone has been the subject of numerous studies regarding long-term *in vivo* effects. Its actions can be grouped as anti-inflammatory, antioxidant and antifibrotic. Changes in expression levels of proteins controlling the development of fibrosis (e.g., TGF-β1), inflammation (e.g., interleukins) and oxidative stress (e.g., catalase) are involved. To date, however, the molecular targets responsible for these changes remain unknown (Avila et al., 2014; Lopez-de la Mora et al., 2015; Graziani et al., 2018). Free radicals are the only PFD-binding molecules identified thus far. In particular, PFD scavenges hydroxyl and superoxide radicals (Giri et al., 1999; Misra and Rabideau, 2000; Mitani et al., 2008). Nevertheless, it is unknown whether this ROS scavenging activity mediates chronic effects.

The present study was designed to characterize long-lasting and persistent modifications of cardiomyocyte function (as opposed to rapid and readily reversible). Hence, cells were exposed to PFD for a minimum of 4 h (at 37°C, in culture medium) and experiments were performed 15–50 min after finishing the treatment (i.e., using extracellular solutions devoid of PFD). Therefore, the changes we have observed persist long after PFD removal. Moreover, at least for the case of ROS and NO production, it took a minimum of 8 h of PFD treatment to detect a significant effect (**Supplementary Figure 4**).

Thus, most likely in our experiments PFD initially regulated protein expression (e.g., oxidative stress-related proteins and nNOS), and this, in turn, influenced free radicals production and cell function.

Nevertheless, the precise sequence of PFD effects on cardiomyocytes has yet to be firmly stablished, and it is likely that some of them be interrelated. For example, in atrial myocytes, the inhibition of ROS production (**Figure 6A** and **Supplementary Figure 4**) could have increased the expression of nNOS (**Figure 7**), and thereby PFD also induced higher levels of NO synthesis (**Figure 6B**). The time-course of PFD effects indirectly support these thoughts (**Supplementary Figure 4**). Specifically, ROS production starts to be regulated after 8 h of PFD-treatment (**Supplementary Figure 4B**; *atrium*), whereas the stimulation of NO generation requires 24 h to become evident (**Supplementary Figure 4D**; *atrium*). Moreover, these findings are also in line with results of Kar and collaborators, showing that prolonged exposure of HL-1 atrial myocytes to H_2O_2 results in low expression levels of nNOS (Kar et al., 2015). Thus, in atrial myocytes, both the expression of nNOS and NO synthesis seem to be under control of chronic ROS production.

Additionally, it is well-known that ROS stimulates NCX activity (e.g., Goldhaber, 1996; Santacruz-Toloza et al., 2000; Kuster et al., 2010). Remarkably, this effect has been associated with redox modification of the exchanger, which likely interferes with Na^+-dependent inactivation (Santacruz-Toloza et al., 2000). Thus, in our present control conditions, NCX activity is likely sustained by ROS, and possible removal of redox modification might represent the basis for PFD inhibiting the exchanger. On the other hand, ROS do not appear to be involved in the regulation by PFD of $Ca_V1.2$, because in atrial myocytes several classical antioxidants—such as DMSO, glutathione, and *N*-acetylcysteine (NAC)— do not reproduce the PFD effect on I_{Ca} (Ramos-Mondragón et al., 2012). Thus, in addition to ROS (Giri et al., 1999; Misra and Rabideau, 2000; Mitani et al., 2008), PFD also likely acts through other molecular targets (for review see Avila et al., 2014).

In our experiments, PFD inhibited the NCX function, which was estimated 25 s after caffeine stimulation. Thus, it remains unknown whether this effect has an impact on triggered electrical activity. Investigating the NCX by other methods would not only help to solve this question but also to reinforce our conclusions.

We previously speculated that PFD might decrease the production of NO in cardiomyocytes, based (at least partially) on evidence derived from hepatocytes (Nakanishi et al., 2004; Tsuchiya et al., 2004). However, the present study indicates that, in ventricular myocytes, PFD does not alter the NO production rate (despite causing a significant reduction in expression levels of nNOS). Furthermore, in atrial myocytes, the compound increases the production of NO (which is likely associated with the observed increase in nNOS amount). The NO signaling is both relevant and complex (for review, see Simon et al., 2014). This complexity originates, at least partially, in nNOS and eNOS presenting distinct subcellular distribution. Accordingly, it has been proposed that the former primarily modulate RyR and SERCA because of its closer proximity to the SR. Conversely, eNOS is thought to predominantly regulate Ca^{2+} handling proteins near the sarcolemma, such as NCX, sarcolemma Ca^{2+} pump and $Ca_V1.2$ (Jian et al., 2014). Additionally, a complex interplay exists between nNOS and ROS. As explained above, nNOS expression and NO levels, both depend on chronic ROS production, whereas nNOS activates, in turn, the ROS-NADPH oxidase 2 (Nox2) signaling (Girouard et al., 2009). Moreover, signaling downstream of NO is divided into two main pathways. One of them involves direct S-nitrosylation (of target proteins), whereas another is characterized by modulation of guanylate cyclase (GC) which in turn regulates cGMP- and cAMP-dependent protein kinases (PKG and PKA). Thus, a systematic study concerning nNOS regulation by PFD (**Figure 7A**) could begin by using selective modulators of NOS isoforms and protein kinases, combined with measurements of not only global levels of Ca^{2+} and contractility, but also local production/changes of ROS, NO, and Ca^{2+}. With regard to PKA, our preliminary results suggest that this kinase might not be involved in up-regulation of contractility (**Supplementary Figure 3**).

Potential Pathophysiological Relevance

Regardless of the precise molecular mechanisms involved, the present results are likely to have pathophysiological implications. *In vivo*, PFD decreases the susceptibility to develop arrhythmias

(AF and ventricular tachycardia), and these effects are thought to depend on a concomitant inhibition of fibrosis (Lee et al., 2006; Nguyen et al., 2010). Nevertheless, it is possible that functional changes in cardiomyocytes also contribute. The enhanced activity of $Ca_V1.2$ could increase the effective refractory period, and thereby decrease propensity toward electrical reentry (Ramos-Mondragón et al., 2012; Avila et al., 2014). Besides, the lower activity of the NCX may be decreasing the likelihood of delayed afterdepolarizations (DADs; Voigt et al., 2012), and hence PFD could also inhibit electrical instability and arrhythmia.

Stimulation of CICR, ECC, and contractility, on the other hand, may be of critical relevance to explaining why PFD improves: (***i)*** ventricular developed pressure in mdx mice (both positive and negative dP/dt; Van Erp et al., 2006) and (***ii)*** left ventricular ejection fraction in rats subjected to myocardial infarction (Nguyen et al., 2010).

The inhibition of ROS production by PFD could be relevant in more general terms, because these free radicals are involved in several cardiac conditions, including arrhythmias, myocardial infarct, hypertrophy, alcoholic cardiomyopathy, and heart failure (for reviews see Zhang et al., 2004; Korantzopoulos et al., 2007; Köhler et al., 2014). Thus, shielding myocytes from oxidant damage is likely essential for PFD in preventing cardiac dysfunction.

CONCLUSION

Pirfenidone has been long acknowledged to be of therapeutic potential for a number of heart symptoms. *In vivo*, the underlying mechanisms are likely numerous and interrelated. Here, its effects on isolated myocytes were investigated, limiting influences from additional tissues and cells. Our results show for the first time that PFD stimulates the function of cardiac myocytes. Other *in vivo* effects may be regarded as "auxiliary" because the compound acts on essential components of the cardiac muscle-pump. In particular, it stimulates CICR, ECC, and contractility. Moreover, it also decreases ROS production, suggesting that its effects on myocytes are cytoprotective.

AUTHOR CONTRIBUTIONS

DO-G performed experiments and analyzed data. AM-V and GA performed experiments, analyzed data, and wrote the paper.

FUNDING

This work was financed by Conacyt (Grant No. #253009).

SUPPLEMENTARY MATERIAL

The Supplementary Material for this article can be found online at: https://www.frontiersin.org/articles/10.3389/fphys.2018.01801/full#supplementary-material

REFERENCES

Adamo, L., Staloch, L. J., Rocha-Resende, C., Matkovich, S. J., Jiang, W., Bajpai, G., et al. (2018). Modulation of subsets of cardiac B lymphocytes improves cardiac function after acute injury. *JCI Insight* 3:120137. doi: 10.1172/jci.insight.120137

Avila, G., Osornio-Garduño, D. S., Ríos-Pérez, E. B., and Ramos-Mondragón, R. (2014). Functional and structural impact of pirfenidone on the alterations of cardiac disease and diabetes mellitus. *Cell Calcium* 56, 428–435. doi: 10.1016/j.ceca.2014.07.008

Bers, D. M. (2001). *Excitation-Contraction Coupling and Cardiac Contractile Force*. Berlin: Springer. doi: 10.1007/978-94-010-0658-3

Bers, D. M. (2002). Cardiac excitation-contraction coupling. *Nature* 415, 198–205. doi: 10.1038/415198a

Bootman, M. D., Smyrnias, I., Thul, R., Coombes, S., and Roderick, H. L. (2011). Atrial cardiomyocyte calcium signalling. *Biochim. Biophys. Acta* 1813, 922–934. doi: 10.1016/j.bbamcr.2011.01.030

Cheng, Y., and Regnier, M. (2016). Cardiac troponin structure-function and the influence of hypertrophic cardiomyopathy associated mutations on modulation of contractility. *Arch. Biochem. Biophys.* 601, 11–21. doi: 10.1016/j.abb.2016.02.004

Eisner, D. A., Caldwell, J. L., Kistamás, K., and Trafford, A. W. (2017). Calcium and excitation-contraction coupling in the heart. *Circ. Res.* 121, 181–195. doi: 10.1161/CIRCRESAHA.117.310230

García-Castañeda, M., Vega, A. V., Rodríguez, R., Montiel-Jaen, M. G., Cisneros, B., Zarain-Herzberg, A., et al. (2017). Functional impact of an oculopharyngeal muscular dystrophy mutation in PABPN1. *J. Physiol.* 595, 4167–4187. doi: 10.1113/JP273948

Giri, S. N., Leonard, S., Shi, X., Margolin, S. B., and Vallyathan, V. (1999). Effects of pirfenidone on the generation of reactive oxygen species in vitro. *J. Environ. Pathol. Toxicol. Oncol.* 18, 169–177.

Girouard, H., Wang, G., Gallo, E. F., Anrather, J., Zhou, P., Pickel, V. M., et al. (2009). NMDA receptor activation increases free radical production through nitric oxide and NOX2. *J. Neurosci.* 29, 2545–2552. doi: 10.1523/JNEUROSCI.0133-09.2009

Goldhaber, J. I. (1996). Free radicals enhance Na+/Ca2+ exchange in ventricular myocytes. *Am. J. Physiol.* 271, H823–H833. doi: 10.1152/ajpheart.1996.271.3.H823

Gómez, A. M., Valdivia, H. H., Cheng, H., Lederer, M. R., Santana, L. F., Cannell, M. B., et al. (1997). Defective excitation-contraction coupling in experimental cardiac hypertrophy and heart failure. *Science* 276, 800–806. doi: 10.1126/science.276.5313.800

Graziani, F., Varone, F., Crea, F., and Richeldi, L. (2018). Treating heart failure with preserved ejection fraction: learning from pulmonary fibrosis. *Eur. J. Heart Fail.* 20, 1385–1391. doi: 10.1002/ejhf.1286

Jian, Z., Han, H., Zhang, T., Puglisi, J., Izu, L. T., Shaw, J. A., et al. (2014). Mechanochemotransduction during cardiomyocyte contraction is mediated by localized nitric oxide signaling. *Sci. Signal.* 7:ra27. doi: 10.1126/scisignal.2005046

Kar, R., Kellogg, D. L., and Roman, L. J. (2015). Oxidative stress induces phosphorylation of neuronal NOS in cardiomyocytes through AMP-activated protein kinase (AMPK). *Biochem. Biophys. Res. Commun.* 459, 393–397. doi: 10.1016/j.bbrc.2015.02.113

Köhler, A. C., Sag, C. M., and Maier, L. S. (2014). Reactive oxygen species and excitation-contraction coupling in the context of cardiac pathology. *J. Mol. Cell. Cardiol.* 73, 92–102. doi: 10.1016/j.yjmcc.2014.03.001

Korantzopoulos, P., Kolettis, T. M., Galaris, D., and Goudevenos, J. A. (2007). The role of oxidative stress in the pathogenesis and perpetuation of atrial fibrillation. *Int. J. Cardiol.* 115, 135–143. doi: 10.1016/j.ijcard.2006.04.026

Kuster, G. M., Lancel, S., Zhang, J., Communal, C., Trucillo, M. P., Lim, C. C., et al. (2010). Redox-mediated reciprocal regulation of SERCA and Na+-Ca2+

exchanger contributes to sarcoplasmic reticulum Ca2+ depletion in cardiac myocytes. *Free Radic. Biol. Med.* 48, 1182–1187. doi: 10.1016/j.freeradbiomed.2010.01.038

Landstrom, A. P., Dobrev, D., and Wehrens, X. H. T. (2017). Calcium signaling and cardiac arrhythmias. *Circ. Res.* 120, 1969–1993. doi: 10.1161/CIRCRESAHA.117.310083

Lee, K. W., Everett, T. H., Rahmutula, D., Guerra, J. M., Wilson, E., Ding, C., et al. (2006). Pirfenidone prevents the development of a vulnerable substrate for atrial fibrillation in a canine model of heart failure. *Circulation* 114, 1703–1712. doi: 10.1161/CIRCULATIONAHA.106.624320

Li, C., Han, R., Kang, L., Wang, J., Gao, Y., Li, Y., et al. (2017). Pirfenidone controls the feedback loop of the AT1R/p38 MAPK/renin-angiotensin system axis by regulating liver X receptor-α in myocardial infarction-induced cardiac fibrosis. *Sci. Rep.* 7:40523. doi: 10.1038/srep40523

Lopez-de la Mora, D. A., Sanchez-Roque, C., Montoya-Buelna, M., Sanchez-Enriquez, S., Lucano-Landeros, S., Macias-Barragan, J., et al. (2015). Role and new insights of pirfenidone in fibrotic diseases. *Int. J. Med. Sci.* 12, 840–847. doi: 10.7150/ijms.11579

Mackenzie, L., Roderick, H. L., Berridge, M. J., Conway, S. J., and Bootman, M. D. (2004). The spatial pattern of atrial cardiomyocyte calcium signalling modulates contraction. *J. Cell. Sci.* 117, 6327–6337. doi: 10.1242/jcs.01559

Miric, G., Dallemagne, C., Endre, Z., Margolin, S., Taylor, S. M., and Brown, L. (2001). Reversal of cardiac and renal fibrosis by pirfenidone and spironolactone in streptozotocin-diabetic rats. *Br. J. Pharmacol.* 133, 687–694. doi: 10.1038/sj.bjp.0704131

Mirkovic, S., Seymour, A.-M. L., Fenning, A., Strachan, A., Margolin, S. B., Taylor, S. M., et al. (2002). Attenuation of cardiac fibrosis by pirfenidone and amiloride in DOCA-salt hypertensive rats. *Br. J. Pharmacol.* 135, 961–968. doi: 10.1038/sj.bjp.0704539

Misra, H. P., and Rabideau, C. (2000). Pirfenidone inhibits NADPH-dependent microsomal lipid peroxidation and scavenges hydroxyl radicals. *Mol. Cell. Biochem.* 204, 119–126. doi: 10.1023/A:1007023532508

Mitani, Y., Sato, K., Muramoto, Y., Karakawa, T., Kitamado, M., Iwanaga, T., et al. (2008). Superoxide scavenging activity of pirfenidone-iron complex. *Biochem. Biophys. Res. Commun.* 372, 19–23. doi: 10.1016/j.bbrc.2008.04.093

Mitcheson, J. S., Hancox, J. C., and Levi, A. J. (1998). Cultured adult cardiac myocytes: future applications, culture methods, morphological and electrophysiological properties. *Cardiovasc. Res.* 39, 280–300. doi: 10.1016/S0008-6363(98)00128-X

Nakanishi, H., Kaibori, M., Teshima, S., Yoshida, H., Kwon, A.-H., Kamiyama, Y., et al. (2004). Pirfenidone inhibits the induction of iNOS stimulated by interleukin-1beta at a step of NF-kappaB DNA binding in hepatocytes. *J. Hepatol.* 41, 730–736. doi: 10.1016/j.jhep.2004.07.007

Nguyen, D. T., Ding, C., Wilson, E., Marcus, G. M., and Olgin, J. E. (2010). Pirfenidone mitigates left ventricular fibrosis and dysfunction after myocardial infarction and reduces arrhythmias. *Heart Rhythm* 7, 1438–1445. doi: 10.1016/j.hrthm.2010.04.030

Page, E., and McCallister, L. P. (1973). Quantitative electron microscopic description of heart muscle cells. Application to normal, hypertrophied and thyroxin-stimulated hearts. *Am. J. Cardiol.* 31, 172–181. doi: 10.1016/0002-9149(73)91030-8

Ramos-Mondragón, R., Galindo, C. A., García-Castañeda, M., Sánchez-Vargas, J. L., Vega, A. V., Gómez-Viquez, N. L., et al. (2012). Chronic potentiation of cardiac L-type Ca(2+) channels by pirfenidone. *Cardiovasc. Res.* 96, 244–254. doi: 10.1093/cvr/cvs248

Ríos-Pérez, E. B., García-Castañeda, M., Monsalvo-Villegas, A., and Avila, G. (2016). Chronic atrial ionic remodeling by aldosterone: potentiation of L-type Ca2+ channels and its arrhythmogenic significance. *Pflugers Arch.* 468, 1823–1835. doi: 10.1007/s00424-016-1876-8

Santacruz-Toloza, L., Ottolia, M., Nicoll, D. A., and Philipson, K. D. (2000). Functional analysis of a disulfide bond in the cardiac Na(+)-Ca(2+) exchanger. *J. Biol. Chem.* 275, 182–188. doi: 10.1074/jbc.275.1.182

Santamaria-Herrera, M. A., Ríos-Pérez, E. B., de la Rosa, J. A. M., García-Castañeda, M., Osornio-Garduño, D. S., Ramos-Mondragón, R., et al. (2016). MDIMP, a novel cardiac Ca(2+) channel blocker with atrial selectivity. *Eur. J. Pharmacol.* 781, 218–228. doi: 10.1016/j.ejphar.2016.04.027

Simon, J. N., Duglan, D., Casadei, B., and Carnicer, R. (2014). Nitric oxide synthase regulation of cardiac excitation-contraction coupling in health and disease. *J. Mol. Cell. Cardiol.* 73, 80–91. doi: 10.1016/j.yjmcc.2014.03.004

Spurgeon, H. A., duBell, W. H., Stern, M. D., Sollott, S. J., Ziman, B. D., Silverman, H. S., et al. (1992). Cytosolic calcium and myofilaments in single rat cardiac myocytes achieve a dynamic equilibrium during twitch relaxation. *J. Physiol.* 447, 83–102. doi: 10.1113/jphysiol.1992.sp018992

Tsuchiya, H., Kaibori, M., Yanagida, H., Yokoigawa, N., Kwon, A.-H., Okumura, T., et al. (2004). Pirfenidone prevents endotoxin-induced liver injury after partial hepatectomy in rats. *J. Hepatol.* 40, 94–101. doi: 10.1016/j.jhep.2003.09.023

Van Erp, C., Irwin, N. G., and Hoey, A. J. (2006). Long-term administration of pirfenidone improves cardiac function in mdx mice. *Muscle Nerve* 34, 327–334. doi: 10.1002/mus.20590

Vega, A. V., Ramos-Mondragón, R., Calderón-Rivera, A., Zarain-Herzberg, A., and Avila, G. (2011). Calcitonin gene-related peptide restores disrupted excitation-contraction coupling in myotubes expressing central core disease mutations in RyR1. *J. Physiol.* 589, 4649–4669. doi: 10.1113/jphysiol.2011.210765

Voigt, N., Li, N., Wang, Q., Wang, W., Trafford, A. W., Abu-Taha, I., et al. (2012). Enhanced sarcoplasmic reticulum Ca2+ leak and increased Na+-Ca2+ exchanger function underlie delayed afterdepolarizations in patients with chronic atrial fibrillation. *Circulation* 125, 2059–2070. doi: 10.1161/CIRCULATIONAHA.111.067306

Wang, Y., Wu, Y., Chen, J., Zhao, S., and Li, H. (2013). Pirfenidone attenuates cardiac fibrosis in a mouse model of TAC-induced left ventricular remodeling by suppressing NLRP3 inflammasome formation. *Cardiology* 126, 1–11. doi: 10.1159/000351179

Yamagami, K., Oka, T., Wang, Q., Ishizu, T., Lee, J.-K., Miwa, K., et al. (2015). Pirfenidone exhibits cardioprotective effects by regulating myocardial fibrosis and vascular permeability in pressure-overloaded hearts. *Am. J. Physiol. Heart Circ. Physiol.* 309, H512–H522. doi: 10.1152/ajpheart.00137.2015

Yamazaki, T., Yamashita, N., Izumi, Y., Nakamura, Y., Shiota, M., Hanatani, A., et al. (2012). The antifibrotic agent pirfenidone inhibits angiotensin II-induced cardiac hypertrophy in mice. *Hypertens. Res.* 35, 34–40. doi: 10.1038/hr.2011.139

Zhang, X., Li, S.-Y., Brown, R. A., and Ren, J. (2004). Ethanol and acetaldehyde in alcoholic cardiomyopathy: from bad to ugly en route to oxidative stress. *Alcohol* 32, 175–186. doi: 10.1016/j.alcohol.2004.01.005

Conflict of Interest Statement: The authors declare that the research was conducted in the absence of any commercial or financial relationships that could be construed as a potential conflict of interest.

frontiers in Physiology

ORIGINAL RESEARCH
published: 21 December 2018
doi: 10.3389/fphys.2018.01831

Pharmacological Modulation of Mitochondrial Ca^{2+} Content Regulates Sarcoplasmic Reticulum Ca^{2+} Release via Oxidation of the Ryanodine Receptor by Mitochondria-Derived Reactive Oxygen Species

*Shanna Hamilton[1], Radmila Terentyeva[1], Tae Yun Kim[1], Peter Bronk[1], Richard T. Clements[2,3], Jin O-Uchi[4], György Csordás[5], Bum-Rak Choi[1] and Dmitry Terentyev[1]**

[1] Department of Medicine, The Warren Alpert Medical School of Brown University, Rhode Island Hospital, Cardiovascular Research Center, Providence, RI, United States, [2] Department of Surgery, The Warren Alpert Medical School of Brown University, Rhode Island Hospital, Cardiovascular Research Center, Providence, RI, United States, [3] Vascular Research Laboratory, Providence Veterans Affairs Medical Center, Providence, RI, United States, [4] Lillehei Heart Institute University of Minnesota, Cancer and Cardiovascular Research Building, Minneapolis, MN, United States, [5] Department of Pathology, Anatomy and Cell Biology, Thomas Jefferson University, Philadelphia, PA, United States

OPEN ACCESS

Edited by:
Angélica Rueda,
Centro de Investigación y de Estudios Avanzados (CINVESTAV), Mexico

Reviewed by:
Diego De Stefani,
Università degli Studi di Padova, Italy
José Javier López Barba,
Universidad de Extremadura, Spain

***Correspondence:**
Dmitry Terentyev
dmitry_terentyev@brown.edu

Specialty section:
This article was submitted to Membrane Physiology and Membrane Biophysics, a section of the journal Frontiers in Physiology

Received: 21 September 2018
Accepted: 06 December 2018
Published: 21 December 2018

Citation:
Hamilton S, Terentyeva R, Kim TY, Bronk P, Clements RT, O-Uchi J, Csordás G, Choi B-R and Terentyev D (2018) Pharmacological Modulation of Mitochondrial Ca^{2+} Content Regulates Sarcoplasmic Reticulum Ca^{2+} Release via Oxidation of the Ryanodine Receptor by Mitochondria-Derived Reactive Oxygen Species. Front. Physiol. 9:1831. doi: 10.3389/fphys.2018.01831

In a physiological setting, mitochondria increase oxidative phosphorylation during periods of stress to meet increased metabolic demand. This in part is mediated via enhanced mitochondrial Ca^{2+} uptake, an important regulator of cellular ATP homeostasis. In a pathophysiological setting pharmacological modulation of mitochondrial Ca^{2+} uptake or retention has been suggested as a therapeutic strategy to improve metabolic homeostasis or attenuate Ca^{2+}-dependent arrhythmias in cardiac disease states. To explore the consequences of mitochondrial Ca^{2+} accumulation, we tested the effects of kaempferol, an activator of mitochondrial Ca^{2+} uniporter (MCU), CGP-37157, an inhibitor of mitochondrial Na^{+}/Ca^{2+} exchanger, and MCU inhibitor Ru360 in rat ventricular myocytes (VMs) from control rats and rats with hypertrophy induced by thoracic aortic banding (TAB). In periodically paced VMs under β-adrenergic stimulation, treatment with kaempferol (10 μmol/L) or CGP-37157 (1 μmol/L) enhanced mitochondrial Ca^{2+} accumulation monitored by mitochondrial-targeted Ca^{2+} biosensor mtRCamp1h. Experiments with mitochondrial membrane potential-sensitive dye TMRM revealed this was accompanied by depolarization of the mitochondrial matrix. Using redox-sensitive OMM-HyPer and ERroGFP_iE biosensors, we found treatment with kaempferol or CGP-37157 increased the levels of reactive oxygen species (ROS) in mitochondria and the sarcoplasmic reticulum (SR), respectively. Confocal Ca^{2+} imaging showed that accelerated Ca^{2+} accumulation reduced Ca^{2+}

transient amplitude and promoted generation of spontaneous Ca^{2+} waves in VMs paced under ISO, suggestive of abnormally high activity of the SR Ca^{2+} release channel ryanodine receptor (RyR). Western blot analyses showed increased RyR oxidation after treatment with kaempferol or CGP-37157 vs. controls. Furthermore, in freshly isolated TAB VMs, confocal Ca^{2+} imaging demonstrated that enhancement of mitochondrial Ca^{2+} accumulation further perturbed global Ca^{2+} handling, increasing the number of cells exhibiting spontaneous Ca^{2+} waves, shortening RyR refractoriness and decreasing SR Ca^{2+} content. In *ex vivo* optically mapped TAB hearts, kaempferol exacerbated proarrhythmic phenotype. On the contrary, incubation of cells with MCU inhibitor Ru360 (2 μmol/L, 30 min) normalized RyR oxidation state, improved intracellular Ca^{2+} homeostasis and reduced triggered activity in *ex vivo* TAB hearts. These findings suggest facilitation of mitochondrial Ca^{2+} uptake in cardiac disease can exacerbate proarrhythmic disturbances in Ca^{2+} homeostasis via ROS and enhanced activity of oxidized RyRs, while strategies to reduce mitochondrial Ca^{2+} accumulation can be protective.

Keywords: mitochondria, reactive oxygen species, ryanodine receptor, hypertrophy, ventricular arrhythmia, Ca^{2+}-induced Ca^{2+} release

INTRODUCTION

Sudden cardiac death remains the leading global cause of mortality, and over half of patients with heart failure (HF) die suddenly due to the development of ventricular arrhythmia (Benjamin et al., 2018). Arrhythmogenesis in the failing heart is often linked to enhanced Ca^{2+}-dependent triggered activity, in the form of early and delayed afterdepolarizations (Landstrom et al., 2017). These abnormal electrical activities arise in part as a consequence of untimely and dysregulated Ca^{2+} release from the sarcoplasmic reticulum (SR), through SR Ca^{2+} release channel, the ryanodine receptor (RyR). Abnormal activity of RyR leads to increased Ca^{2+} leak and promotes the generation of spontaneous Ca^{2+} waves (SCWs), that can subsequently propagate to trigger organ-wide arrhythmia (Bers, 2002).

Mitochondria play an essential role in cardiac Ca^{2+} homeostasis in physiological conditions (Kwong et al., 2015; Luongo et al., 2017). Excitation-contraction coupling consumes large amounts of ATP and mitochondria increase oxidative phosphorylation to meet increased metabolic demand. Influx of Ca^{2+} into the mitochondria is critical for the availability of ATP as major enzymes in the tricarboxylic acid cycle are activated by Ca^{2+}. Mitochondria are in close spatial proximity to the SR (Dorn and Scorrano, 2010; Eisner et al., 2013; Lu et al., 2013; Seidlmayer et al., 2016; Lopez-Crisosto et al., 2017; Csordás et al., 2018), and it is well established that during higher workload, there is an elevation of cystolic Ca^{2+} concentration in ventricular myocytes (VMs) that transpires to a small and slow rise in mitochondrial Ca^{2+} concentration ($[Ca^{2+}]_m$), leading to enhanced energy production (Brandes and Bers, 1997; Luongo et al., 2015). Influx of Ca^{2+} through the mitochondrial Ca^{2+} uniporter (MCU) channel complex is driven largely by the negative membrane potential across the inner mitochondrial membrane (Kirichok et al., 2004; Baughman et al., 2011; De Stefani et al., 2011). Conversely, mitochondrial efflux mainly occurs via the mitochondrial $Na/Ca^{2+}/Li^{+}$-exchanger (NCLX) (Palty et al., 2010; Boyman et al., 2013; Luongo et al., 2017).

Mitochondria are a major source of reactive oxygen species (ROS) in the myocyte, and while an increase in oxidative stress is a prerequisite for many cellular stress responses, excessive ROS production in cardiac disease contributes to ventricular arrhythmogenesis by altering the function of multiple ion channels and transporters (Zima and Blatter, 2006; Niggli et al., 2013; Wagner et al., 2013). RyRs are highly sensitive to ROS, and contain multiple redox-sensitive cysteine residues (Zima and Blatter, 2006). Cysteine thiol oxidation of RyR increases channel activity, and many groups including ours have previously established that increased RyR oxidation in VMs from diseased hearts promotes proarrhythmic spontaneous SR Ca^{2+} release in the form of propagating Ca^{2+} waves that underlie increased triggered activity (Terentyev et al., 2008; Belevych et al., 2009; Cooper et al., 2013; Kyrychenko et al., 2013; Bovo et al., 2018). Scavenging of mitochondrial ROS was shown to improve Ca^{2+} homeostasis and attenuate arrhythmic potential in multiple models of cardiac disease including HF, hypertrophy, diabetic cardiomyopathy or aging (Mochizuki et al., 2007; Terentyev et al., 2008; Belevych et al., 2012; Cooper et al., 2013; Luo et al., 2013; Joseph et al., 2016; Kim et al., 2017).

Given the contribution of mitochondrial dysfunction to multiple cardiac disease states, maintaining mitochondrial Ca^{2+} homeostasis remains an attractive therapeutic target (Dietl and Maack, 2017). In conditions with defective intracellular Ca^{2+} and Na^{2+} homeostasis such as in models of HF, increasing $[Ca^{2+}]_m$ above a specific threshold was suggested to improve metabolism and substrate utilization, as well as reduce oxidative stress and ROS overload in the myocyte (Liu and O'Rourke, 2008; Kolhaas et al., 2010; Liu et al., 2014). More recently, Schweitzer

et al. (2017) suggested that pharmacological enhancement of $[Ca^{2+}]_m$ suppressed arrhythmia in a model of catecholaminergic polymorphic ventricular tachycardia (CPVT), a condition characterized by mutations in the RyR macromolecular complex that renders channels hyperactive. Given mitochondria are in close proximity to SR Ca^{2+} release sites, it has been proposed that increasing mitochondrial Ca^{2+} uptake may improve buffering capacity (Seguchi et al., 2005; Drago et al., 2012; Zhao et al., 2013), thereby limiting local Ca^{2+} release events, Ca^{2+} sparks, which would result in a decrease in generation and propagation velocity of proarrhythmic SCWs. Conversely, a reduction of mitochondrial Ca^{2+} uptake may serve as an anti-arrhythmic strategy. In models of HF and ischemia-reperfusion, pathological mitochondrial dysfunction and mitochondria Ca^{2+} overload contribute to oxidative stress and cell death (Santulli et al., 2015). Pharmacological inhibition (García-Rivas Gde et al., 2006; Xie et al., 2018) or genetic ablation (Kwong et al., 2015; Luongo et al., 2015) of MCU, as well as conditional NCLX overexpression (Luongo et al., 2017) has been shown to protect against ischemia-induced myocyte injury, the development Ca^{2+}-dependent arrhythmia and the progression of HF.

In the present study, we aimed to determine the effects of pharmacological facilitation of $[Ca^{2+}]_m$ accumulation and inhibition of mitochondrial Ca^{2+} uptake on intracellular Ca^{2+} homeostasis and arrhythmic potential using rat model of cardiac hypertrophy induced by thoracic aortic banding (TAB). To achieve this goal, we utilized whole heart optical mapping, genetically encoded ROS and mitochondrial Ca^{2+} biosensors, confocal microscopy and biochemistry to dissect the influence of MCU enhancer kaempferol and NCLX inhibitor CGP-37157 on intracellular Ca^{2+} cycling, in both healthy and hypertrophic VMs. Our results suggest that enhancement of mitochondrial Ca^{2+} accumulation in either setting elevates mitochondrial ROS emission, increasing oxidation of RyR and aberrant spontaneous Ca^{2+} release. Attenuating mitochondrial Ca^{2+} uptake serves as an anti-arrhythmic treatment in hypertrophic hearts, whereby triggered activity was reduced by pharmacological inhibition of MCU with Ru360.

MATERIALS AND METHODS

Ethics Statement

Procedures involving animals were approved by The Rhode Island Hospital Institutional Animal Care and Use Committee and followed the Guide for the Care and Use of Laboratory Animals published by the US National Institutes of Health (NIH Publication No. 85-23, revised 2011).

Generation of Adenoviral Constructs

The mitochondrial targeting sequence cytochrome C oxidase subunit IV was fused as the N-terminal of the coding sequence of plasmid RCamp1h (Akerboom et al., 2013) to create a probe to monitor intra-mitochondrial Ca^{2+}. pC1-HyPer-3 was a gift from Vsevolod Belousov (Addgene plasmid # 42131). The mitochondrial localization sequence of mAKAP1 followed by a linker was fused as the N-terminus of the coding sequence of pC1-HyPer-3 (Burns-Hamuro et al., 2003; DiPilato et al., 2004; Bilan et al., 2013). This enables anchoring of the probe to the outer mitochondrial membrane (OMM) to measure H_2O_2 at the mitochondrial surface, and the subsequent viral construct is thus referred to as OMM-HyPer. ERroGFP_iE_pCDNA3 was a gift from David Ron (Addgene plasmid # 47954). The ERroGFP_iE probe is targeted to the endoplasmic reticulum (ER) by the cleavable signal peptide and C-terminal KDEL ER retrieval signal (Avezov et al., 2013). Adenovirus carrying plasmid constructs were generated utilizing the ViraPower Gateway expression system (Thermo Fisher Scientific, Waltham, MA, United States). Briefly, coding regions were cloned into the pENTR^{TM} 1A entry vector, and recombined into pAd/CMV/V5-DEST^{TM} destination vector by LR recombinase reaction. Once sequence-verified, destination vector plasmids were digested with restriction enzyme *PacI* and transfected into HEK293A cells using Lipofectamine^{TM} 2000 (Thermo Fisher Scientific). Adenoviral stock titer was determined using the Adeno-X qPCR Titration Kit (Takara Bio USA, Inc., Mountain View, CA, United States).

Myocyte Isolation and Primary Culture

Myocytes were isolated from male 9- to 12-week-old Sprague-Dawley rats (controls) from Harlan Laboratories (Indianapolis, IN, United States). Male Sprague-Dawley rats with TAB surgery were purchased from Charles River Laboratories (Wilmington, MA, United States). Animals were shipped 5–7 days after surgery and acclimatized for 3–4 weeks in the Rhode Island Hospital animal facility. Experiments were performed 4–5 weeks after aortic banding procedure.

Bilateral thoracotomy was performed on euthanized rats and the heart plunged into ice cold Tyrode's solution. The hearts were mounted on a Langendorff apparatus and retrogradely perfused with Tyrode solution (Terentyev et al., 2009) containing collagenase II (Worthington Biochemical Corp., Lakewood, NJ, United States) at 37°C for 16–17 min. Ventricles were minced and placed in a 37°C water bath shaker in collagenase solution. Isolated VMs were plated onto laminin-coated glass coverslips in 24-well plates.

For experiments with cultured control and TAB rats VMs, myocytes were cultured in serum-free medium 199 (Thermo Fisher Scientific), supplemented with 25 mmol/L $NaHCO_3$, 10 mmol/L HEPES, 5 mmol/L creatine, 5 mmol/L taurine, 10 μ/mL penicillin, 10 μg/mL streptomycin and 10 μg/mL gentamycin (pH 7.3). Unattached cells were removed after 1 h and remaining VMs were cultured for 48 h. Cultured VMs were infected with adenoviruses at multiplicity of infection (MOI) of 10 for all described constructs. Myocytes were cultured at 37°C in 95% air, 5% CO_2 for 36–48 h before analysis.

Pharmacological Modifiers of Mitochondrial Ca^{2+} Uptake, Mitochondrial ROS, and RyR Activity

Kaempferol directly activates MCU (Montero et al., 2004; Vay et al., 2007), and was obtained from Millipore Sigma (Burlington, MA, United States), used at 10 μmol/L. CGP-37571 inhibits

NCLX (Liu and O'Rourke, 2008; Kolhaas et al., 2010; Liu et al., 2010), and was obtained from Millipore Sigma, used at 1 μmol/L. SB 202190 is an inhibitor of p38 mitogen-activated protein (MAP) kinase, has also been shown to activate MCU (Montero et al., 2004), and was obtained from Millipore Sigma, used at 30 μmol/L. Ru360 specifically inhibits mitochondrial Ca^{2+} uptake through MCU (Matlib et al., 1998; García-Rivas Gde et al., 2006), and was obtained from Millipore Sigma, used at 2 μmol/L. MitoTEMPO, a specific scavenger of mitochondrial superoxide was obtained from Millipore Sigma, used at 20 μmol/L. Dantrolene, an RyR antagonist (Kobayashi et al., 2009; Maxwell et al., 2012) was obtained from Millipore Sigma and used at 2 μmol/L.

Confocal Imaging

Confocal imaging was performed using a Leica SP5 II confocal microscope equipped with 63 × 1.4 numerical aperture oil objective in linescan and x–y mode. All confocal imaging experiments were performed under β-adrenergic stimulation with 50 nmol/L isoproterenol (ISO, Millipore Sigma). Control VMs were paced via field stimulation at 2 Hz, while TAB VMs were paced at 0.5 Hz using extracellular platinum electrodes. Myocytes were studied in Tyrode's solution (Terentyev et al., 2009). Confocal imaging data were analyzed using Leica Software, Origin 8.0 (OriginLab, Northampton, MA, United States) and ImageJ (National Institutes of Health, Bethesda, MA, United States).

Intact VMs were loaded with Rhod-2 AM (Thermo Fisher Scientific) at room temperature for 12 min, followed by a 10 min wash. Rhod-2 was excited using 543 nm line of HeNe laser and fluorescence emission was collected at 560–660 nm wavelengths in linescan mode at 200 Hz sampling rate. Calcium transients were recorded at room temperature. To test for the propensity of triggered activity, VMs were paced for 20 s and latency between the last pacing stimulus and the subsequent SCW was calculated. To assess SR Ca^{2+} load, 10 mmol/L caffeine was applied at the end of experiments. The data is presented as $\Delta F/F_0$, where F_0 is basal fluorescence and $\Delta F = F - F_0$.

Biosensor mtRCamp1h was excited using 543 nm line of HeNe laser and fluorescence emission was collected at 560–660 nm wavelengths. For permeabilized VM experiments, myocytes were saponin-permeabilized (0.001%) and equilibrated with a solution containing thapsigargin (10 μmol/L), cytochalasin D (10 μmol/L), FCCP (20 μmol/L), and ionomycin (5 μmol/L). Tyrode's solution containing Ca^{2+} buffer EGTA (2 mmol/L) was applied to obtain minimum mtRCamp1h fluorescence. Maximum fluorescence was achieved by application of Ca^{2+} (100 μmol/L). The data is presented as as $\Delta F/F_0$, where F_0 is basal fluorescence and $\Delta F = F - F_0$. Biosensors ERroGFP_iE and OMM-HyPer were excited using 488 nm line of Argon laser and fluorescence emission was collected at 500–550 nm wavelengths, measured in x–y mode. Maximum fluorescence (Fmax) was obtained by application 200 μmol/L DTDP and minimum fluorescence was obtained by application ROS scavenger DTT (5 mmol/L). Data is presented as a percentage of $\Delta F/\Delta F$max where $\Delta F = F - F$min, and ΔFmax = Fmax−Fmin. Mitochondrial membrane potential was monitored with the voltage-sensitive fluorescent indicator, tetramethylrhodamine, methyl ester (TMRM; Thermo Fisher Scientific). Isolated VMs were loaded with 20 μmol/L for 1 min and washed thoroughly prior to imaging. TMRM was excited using 543 nm line of HeNe laser and fluorescence emission was collected at 560–660 nm wavelengths, measured in x–y mode. Fluorescence of TMRM was normalized to the minimum fluorescence signal obtained by application of mitochondrial uncoupler, carbonyl *p*-(trifluoromethoxy) phenylhydrazone (FCCP, 50 μmol/L). For experiments with mitoTEMPO, isolated VMs were pretreated with mitoTEMPO (20 μmol/L, 30 min), before loading with TMRM as described.

The emission of ROS was measured in isolated VMs in Tyrode solution using MitoSOX Red mitochondrial superoxide indicator (Thermo Fisher Scientific; 20 μmol/L, 30 min loading). The indicator was excited with 514 nm line of an argon laser and emission was collected at 560–660 nm, measured in x–y mode. Fluorescence of MitoSOX was normalized to the maximum fluorescence signal obtained by application of peroxide H_2O_2 (10 mmol/L).

Oxidation of RyR and Western Blotting

Freshly isolated control or TAB rat VMs were treated with ISO (50 nmol/L, 5 min total), kaempferol (10 μmol/L, 5 min total) or CGP (1 μmol/L, 10 min total) and paced for 1 min at 2 Hz at room temperature before immediate lysis in lysis buffer from Cell Signaling (Danvers, MA, United States, Cat#9803S), supplemented with phosphatase (Calbiochem, San Diego, CA, United States, Cat#524625) and protease inhibitor cocktails (Millipore Sigma, Cat#P8340) as described previously (Terentyev et al., 2014). For co-immunoprecipitation, Pierce Co-immunoprecipitation Kit (Thermo Fisher Scientific, Cat#26149) was used. Lysate (500 μl) was pre-cleared with Control Agarose Resin for 30 min at 4°C, centrifuged at 1,000 × *g* for 1 min. Flow-through was incubated with antibody-coupled resin (anti-RyR2, Thermo Fisher Scientific, Cat#MA3-916 and negative control antibody, normal mouse IgG, Santa Cruz Biotechnology, Cat#sc-2025) for 2 h at 4°C. Columns were washed three times. Protein complexes were eluted with elution buffer provided in the kit. To determine oxidation of RyR, the Oxidized Protein Western Blot Kit (Abcam, Cambridge, MA, United States, Cat#ab178020) was used, whereby carbonyl groups of immunoprecipitated RyR2 were derivatized to 2,4 dinitrophenylhydrazone (DNP) by reaction with 2,4 dinitrophenylhydrazine. For control we used Derivatization Control Solution, provided in the kit. The DNP-RyR2 protein samples were separated on 4–20% Mini-PROTEAN TGX gels (Bio-Rad Laboratories, Hercules, CA, United States, Cat#456-1094) and DNP-associated signal assessed by the kit-provided anti-DNP primary antibody and anti-RyR2 (Thermo Fisher Scientific, Cat#MA3-916), followed by HRP-conjugated secondary antibody and anti-mouse lgG(H+L) HRP secondary antibody (Promega, Madison, WI, United States, Cat#W4021). Abcam antibodies (Cat#ab57602 and Cat#ab101055) were used to assess expression levels of mitofusin 1 and mitofusin 2. Anti-glyceraldehyde 3-phosphate dehydrogenase (GAPDH) antibodies were used for loading control (Abcam, Cat#ab8245). Blots were developed with ECL

(Bio-Rad Laboratories) and quantified using ImageJ and Origin 8 software.

Ex vivo Optical Mapping

Beating hearts were harvested from anesthetized TAB rats via thoracotomy and were retrogradely perfused through the aorta in a Langendorff perfusion system (Radnoti Glass Technology, Monrovia, CA, United States) with (in mmol/L): 130 NaCl, 24 $NaHCO_3$, 1.0 $MgCl_2$, 5.0 KCl, 1.2 NaH_2PO_4, 5 dextrose, and 1 $CaCl_2$, at pH 7.4, gassed with 95% O_2 and 5% CO_2. Constant flow perfusion was set to 10 mL/min with a peristaltic pump. Hearts were placed in a water-heated chamber to maintain temperature at 37 ± 0.2°C, and 5 μmol/L blebbistatin was added to perfusate to reduce movement artifact. Hearts were loaded with Ca^{2+} indicator Rhod-2 AM (Thermo Fisher Scientific), using 25 μL of stock solution (1 mg/mL of DMSO) delivered through a bubble trap, above the aortic cannula. The ECGs were continuously monitored with a Powerlab system (AD Instrument, Colorado Springs, CO, United States). The optical apparatus has been described previously (Kim et al., 2015). Fluorescence images of Rhod-2 signal were recorded from the anterior surface of the heart using a CMOS camera (100 × 100 pixels, 2000 frames/sec, 1.5 cm × 1.5 cm field of view, Ultima-L, SciMedia, Japan). Drugs (kaempferol and Ru360) were perfused for 20–30 min and ISO (50 nmol/L) was added to investigate the effect of drugs on VT/VF induction in TAB hearts. The fluorescence (F) from Rhod-2 was normalized with ΔF/F. Hearts were stimulated with 150 ms cycle length followed by premature stimulation of 10 beats of S2 until refractoriness or VT induction. Propagation and duration of Ca^{2+} transients were mapped using $(dF/dt)_{max}$ and 75% recovery, respectively, as previously described (Kim et al., 2015).

Statistics

Statistical analysis of Ca^{2+} imaging and biochemical data was performed using Origin 8 (OriginLab). Data are presented as mean ± standard error (SEM) for single cell and ± standard deviation (SD) for intact heart optical mapping. Uppercase n (N) = number of animals, lowercase n = number of VMs. Statistical significance between groups were performed using Student's t-test (paired and unpaired), Fisher's exact test and one-way ANOVA with Bonferroni *post hoc* test where appropriate. For all analyses, a p-value of less than 0.05 was considered significant.

RESULTS

Mitochondrial Ca^{2+} Accumulation Exacerbates the Proarrhythmic Phenotype of TAB Hearts *ex vivo*

We have previously reported that the rat model hypertrophy induced by TAB is highly arrhythmogenic, with incidences of non-sustained ventricular tachycardia and fibrillation (VT/VF) occurring in 100% of TAB hearts exposed to 50 nmol/L ISO (Kim et al., 2017). We investigated whether the MCU activator, kaempferol (Montero et al., 2004; Vay et al., 2007), increases mitochondrial Ca^{2+} accumulation to reduce cytosolic Ca^{2+} and suppress ventricular arrhythmias in this model. Hearts were isolated and perfused retrogradely as described in "Materials and Methods" and echocardiograms (ECGs) were monitored to investigate arrhythmogenesis under kaempferol and Ru360. ISO induced frequent premature ventricular contractions (PVCs) leading to VFs in TAB rat hearts (**Figure 1A** ECG traces under **TAB+ISO**). Pretreatment with MCU activator, kaempferol (10 μmol/L), did not prevent PVCs and VF induction. ECG traces in **Figure 1A** (**TAB+KAEM+ISO** panel) shows frequent PVCs (red stars) that led to VFs (blue bar) under kaempferol. However, MCU blocker Ru360 (2 μmol/L) suppressed number of PVCs and prevented VFs in TAB rat hearts (**Figure 1A**, **TAB+Ru360+ISO** panel).

We investigated the effect of kaempferol on Ca^{2+} handling and arrhythmogenesis using optical mapping. Kaempferol reduces the Ca^{2+} transient amplitude by 53% (**Figure 1B**, $^*p = 0.002$) but despite smaller Ca^{2+} transients, kaempferol induced transient VTs in two of four TAB hearts, even without ISO. Addition of ISO caused frequent PVCs (**Figure 1D**) and long-lasting VFs (**Figure 1E**) in three of four hearts. Activation maps of PVCs (**Figure 1D**) and VFs (**Figure 1E**) suggest that focal activity play a major role in the initiation and maintenance of VFs. The frequencies of VF were significantly higher with kaempferol (17.6 ± 2.1 Hz, $n = 3$, in kaempferol vs. 14 ± 1.8 Hz, $n = 7$, control TAB with ISO, $^*p = 0.042$, **Figure 1C**). In contrast, MCU inhibitor, Ru360 (Matlib et al., 1998; García-Rivas Gde et al., 2006), suppressed spontaneous VT/VFs in the presence of ISO in four of four hearts. S1S2 pacing induced reentry and VFs in two of four hearts in the presence of Ru360 (**Figure 1F**), suggesting that conduction block, not focal activity, underlies VF induction during S1S2 pacing in Ru360 group. These intact heart optical mapping data suggest that enhancement of mitochondrial Ca^{2+} accumulation may exacerbate ventricular arrhythmias in TAB rat hearts through increasing focal activity.

Pharmacological Enhancers of Mitochondrial Ca^{2+} Accumulation Modulate Time Course, Not Amplitude During Periodic Pacing

To gain mechanistic insights as to how increasing mitochondrial Ca^{2+} accumulation affects global Ca^{2+} handling in VMs, we used a genetically encoded fluorescent Ca^{2+} biosensor, mtRCamp1h. The RCamp1h indicator, with a $Kd \sim 1.3$ μM (Akerboom et al., 2013), was fused with an N-terminal cytochrome C oxidase subunit IV tag for targeting to the mitochondrial matrix. We generated adenovirus encoding the sensor, and VMs isolated from control rat hearts were infected with adenovirus at a MOI of 10 and cultured for 48 h prior to experimentation. Rat myocytes are thought to preserve electrical properties and structure including T-tubule organization for the first 48 h of culture (Banyasz et al., 2008).

The correct cellular localization of mtRCamp1h was confirmed with co-expression of mitochondrial matrix-targeted GFP, as shown in **Figure 2A**. As shown in **Figure 2B**, basal mtRCamp1h fluorescence appears well within the dynamic range

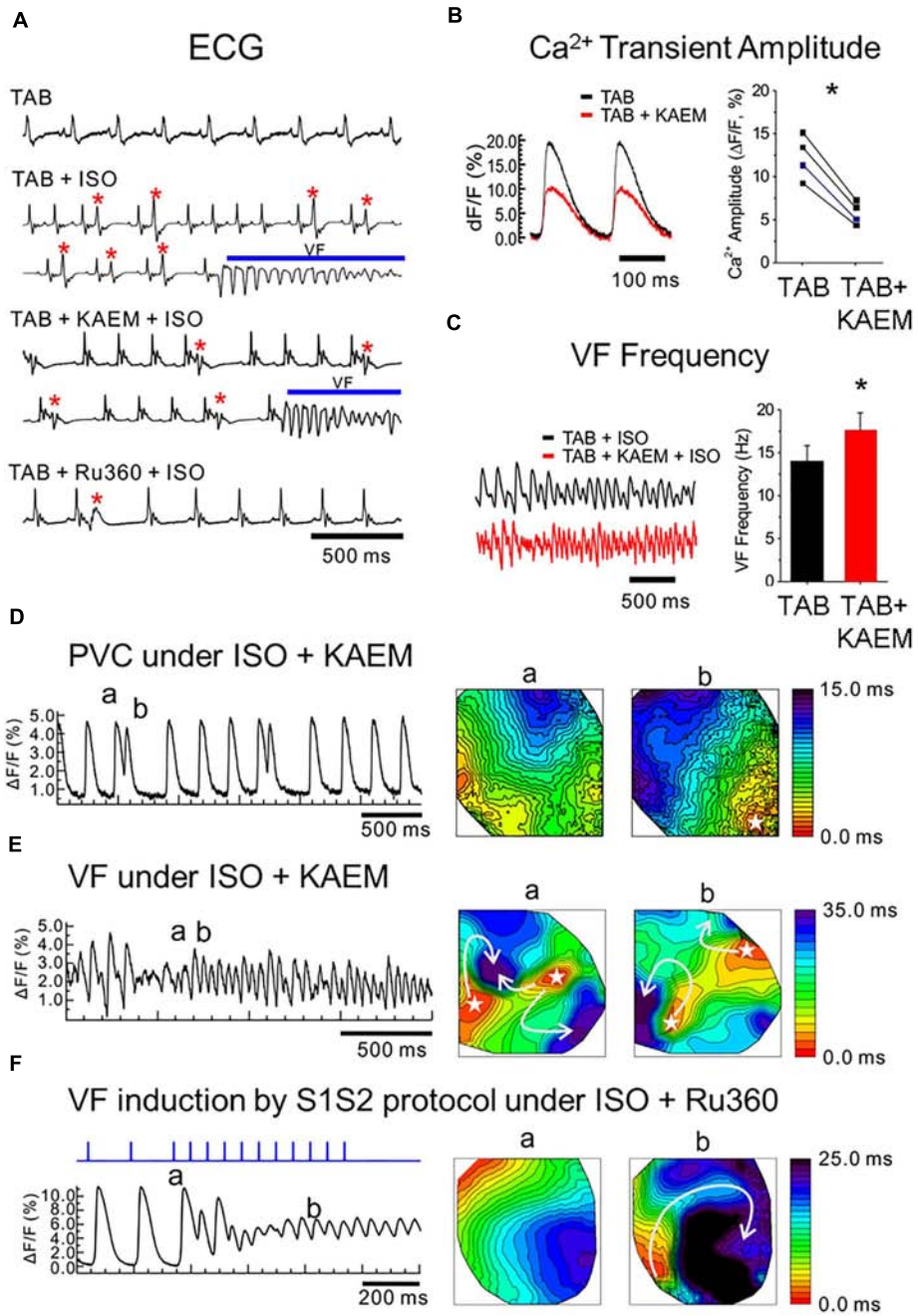

FIGURE 1 | MCU enhancer kaempferol exacerbates ventricular arrhythmias in TAB rat hearts. **(A)** ECG recordings from *ex vivo* intact hearts. *TAB*: ECGs under normal condition. *TAB+ISO*: ISO (50 nmol/L) perfusion frequently induces PVCs (red stars) and VT/VF in TAB rat hearts. *TAB+KAEM+ISO*: Pretreatment of kaempferol (KAEM, 1 μmol/L) failed to prevent PVCs and VT/VF induction. *TAB+RU360+ISO*: Ru360 pretreatment (2 μmol/L) reduced PVC events (red star) and prevented VT/VF induction under ISO in TAB rat hearts. **(B)** KAEM reduced Ca^{2+} transient amplitude (12.3 ± 2.6 $\Delta F/F$ before KAEM vs. 5.8 ± 1.3 $\Delta F/F$ after KAEM, $^*p = 0.0018$, paired Student's *t*-test, $N = 4$). **(C)** KAEM increases VF frequency (14.1 ± 1.8 Hz before KAEM vs. 17.6 ± 2.1 Hz after KAEM). **(D,E)** Frequent PVCs before VF induction and focal activity in the presence of KAEM. Activation maps are shown in the right panel. **(F)** Conduction block and reentry formation by S1S2 pacing protocol in the presence of Ru360 ($N = 4$).

of the probe when adenovirally expressed in VMs. Furthermore, as seen in **Figure 2B**, we can indeed observe measurable changes in mitochondrial Ca^{2+} concentration, as indicated by an increase in mtRCamp1h fluorescence, when cultured control VMs are paced at 2 Hz for 1 min under β-adrenergic stimulation with ISO (pacing indicated by red bar). We did not observe significant loading of mitochondria with Ca^{2+} under baseline conditions with no ISO stimulation (data not

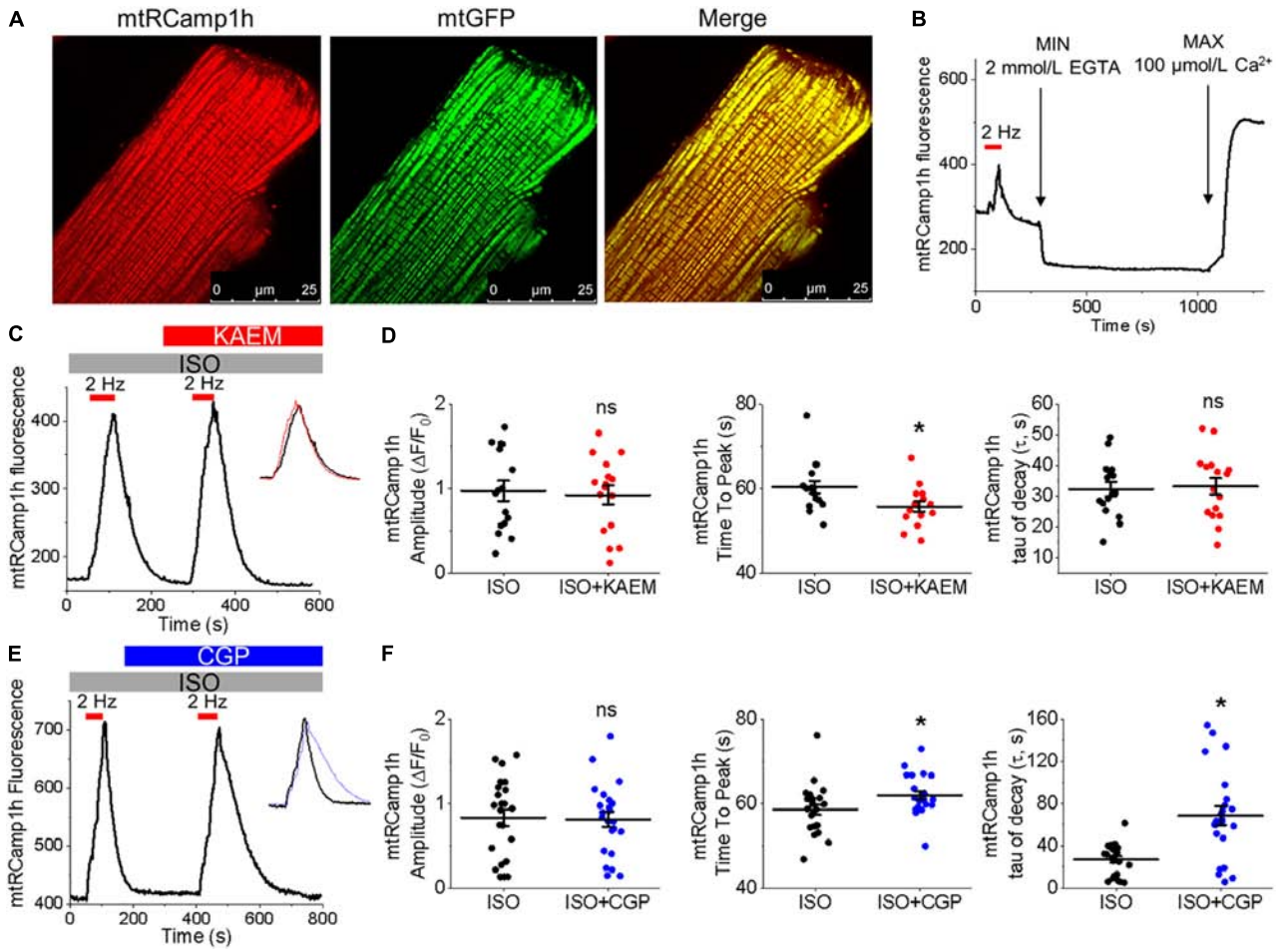

FIGURE 2 | Expression of biosensor mtRCamp1h in cultured control rat VMs reveals mitochondrial Ca^{2+} accumulation is modified by kaempferol and CGP-37157. **(A)** Representative images of a cultured VM 48 h after adenoviral infection with mtRCamp1h (left, red, MOI of 10) and mitochondrial-targeted GFP (center, green, MOI of 10). A merged image is indicated on the right. **(B)** Recording of a permeabilized VM infected with mtRCamp1h. *F*max and *F*min were assessed by addition of EGTA (2 mmol/L) and Ca^{2+} (100 µmol/L), respectively. **(C)** Representative trace from cultured VM expressing mtRCamp1h. VMs were treated with ISO (50 nmol/L) and paced at 2 Hz for 60 s intervals (red bars), then treated with kaempferol (KAEM, 10 µmol/L) and paced again peaks are overlaid in the inset for visualization, with ISO in black, ISO+KAEM in red. Graphs in **(D)** depict mean data ± SEM of mtRCamp1h transient amplitude, time to transient peak and tau of decay (n = 16 per group, N = 5, $^*p < 0.05$, paired Student's t-test). **(E)** Representative trace from VM expressing mtRCamp1h. VMs were treated with ISO and paced at 2 Hz for 60 s intervals (red bars), then treated with CGP-37157 (CGP, 1 µmol/L) and paced again. Peaks are overlaid in the inset for visualization, with ISO in black, ISO+CGP in blue. Graphs in **(F)** depict mean data ± SEM from mtRCamp1h transient amplitude, time to transient peak and tau of decay (n = 23, N = 4, $^*p < 0.05$, paired Student's t-test).

shown). To determine *F*min and *F*max for mtRCamp1h, VMs were saponin-permeabilized (0.001%) and equilibrated with a solution containing thapsigargin (10 µmol/L) to deplete SR Ca^{2+}, cytochalasin D (10 µmol/L) to reduce cell contraction, as well as FCCP (20 µmol/L) and ionomycin (5 µmol/L) to dissipate mitochondrial membrane potential ($\Delta\psi m$). Solution containing Ca^{2+} buffer EGTA at high concentration (2 mmol/L) was applied to obtain minimum mtRCamp1h fluorescence, while maximum fluorescence was achieved by application of Ca^{2+} (100 µmol/L), as illustrated in **Figure 2B**.

Measurement of peak mtRCamp1h signal indicated accumulation of $[Ca^{2+}]_m$ during workload, but after treatment with MCU enhancer kaempferol (10 µmol/L; **Figure 2C**) or NCLX blocker CGP-37157 (1 µmol/L; **Figure 2E**), no significant change in transient amplitude (an increase in $[Ca^{2+}]_m$) was observed (**Figures 2D,F**, respectively). However, accumulation of mitochondrial Ca^{2+} during pacing was significantly faster after treatment with kaempferol (**Figure 2D**, time to peak 59.31 ± 1.01 s. ISO vs. 55.84 ± 1.24 s. ISO and kaempferol, $^*p$ = 0.03), while the time constant of transient decay, τ, was significantly increased after application of CGP-37157 (**Figure 2F**, τ = 27.16 ± 3.10 ISO vs. 68.70 ± 8.81 ISO and CGP-37157, $^*p < 0.001$). The time to peak of transient after application of CGP-37157 was also increased (58.59 ± 1.23 s. ISO vs. 62.01 ± 0.98 s. ISO and CGP-37157, $^*p$ = 0.01). This indicates that while pharmacological enhancers of $[Ca^{2+}]_m$ do not increase overall mitochondrial Ca^{2+} loading in cultured control VMs during workload of 1 min pacing, they modify the

time course for which those VMs accumulate or retain Ca^{2+}. The finding that the rate of mitochondrial Ca^{2+} uptake in intact myocytes is only modestly accelerated with kaempferol and even slowed down with CGP-37157 suggest the existence of overriding feedback mechanisms to prevent mitochondrial Ca^{2+} overload that can cause cell death (Broekemeier et al., 1998; Hüser and Blatter, 1999; Elrod et al., 2010).

Enhanced Mitochondrial Ca^{2+} Accumulation Dissipates $\Delta\psi m$

It was established that the excessive mitochondrial Ca^{2+} uptake can be effectively limited by a reduction in $\Delta\psi m$ at least in part via activation of mitochondrial Ca^{2+}-dependent K^+ channels (O'Rourke et al., 2005; Stowe et al., 2006). While irreversible mPTP opening collapses $\Delta\psi m$, brief openings of the pore may also provide a protective efflux mechanism against mitochondrial Ca^{2+} overload (Broekemeier et al., 1998; Elrod et al., 2010). We used isolated control rat VMs stained with voltage sensitive dye TMRM (20 μmol/L for 1 min) to determine if enhancement of mitochondrial Ca^{2+} accumulation modifies $\Delta\psi m$ (**Figure 3**). As in **Figure 2**, VMs under β-adrenergic stimulation with ISO were paced at 2 Hz for 1 min, as indicated by red bars. Representative images **Figure 3A** shows VMs before and after the application of kaempferol. A representative trace is shown in **Figure 3B**, whereby signal was normalized to minimum fluorescence obtained by the application of FCCP (50 μmol/L). Application of kaempferol significantly reduced TMRM fluorescence (**Figure 3C**, 88.31 ± 1.73% ISO vs. 53.17 ± 4.69% ISO and kaempferol, $^*p < 0.001$). Application of CGP-37157 had similar effects (**Figures 3D–F**, 86.49 ± 1.95% ISO vs. 71.15 ± 3.38% ISO and CGP-37157, $^*p < 0.001$, respectively). The decrease in driving force due to the drop in $\Delta\psi m$ may explain why kaempferol or CGP-37157 are not able to increase the amplitude of $[Ca^{2+}]_m$ effectively limiting mitochondrial Ca^{2+} uptake, as measured with mtRCamp1h in **Figure 2**.

Facilitation of Mitochondrial Ca^{2+} Accumulation Promotes Proarrhythmic SCWs in VMs

Having demonstrated the effects of kaempferol and CGP-37157 on mitochondrial Ca^{2+} and $\Delta\psi m$, we next sought to establish the effects of modulating mitochondrial Ca^{2+} on cytosolic Ca^{2+} handling in VMs, as illustrated in **Figure 4**. Cultured control VMs were loaded with the fluorescent Ca^{2+} indicator Rhod-2 and we

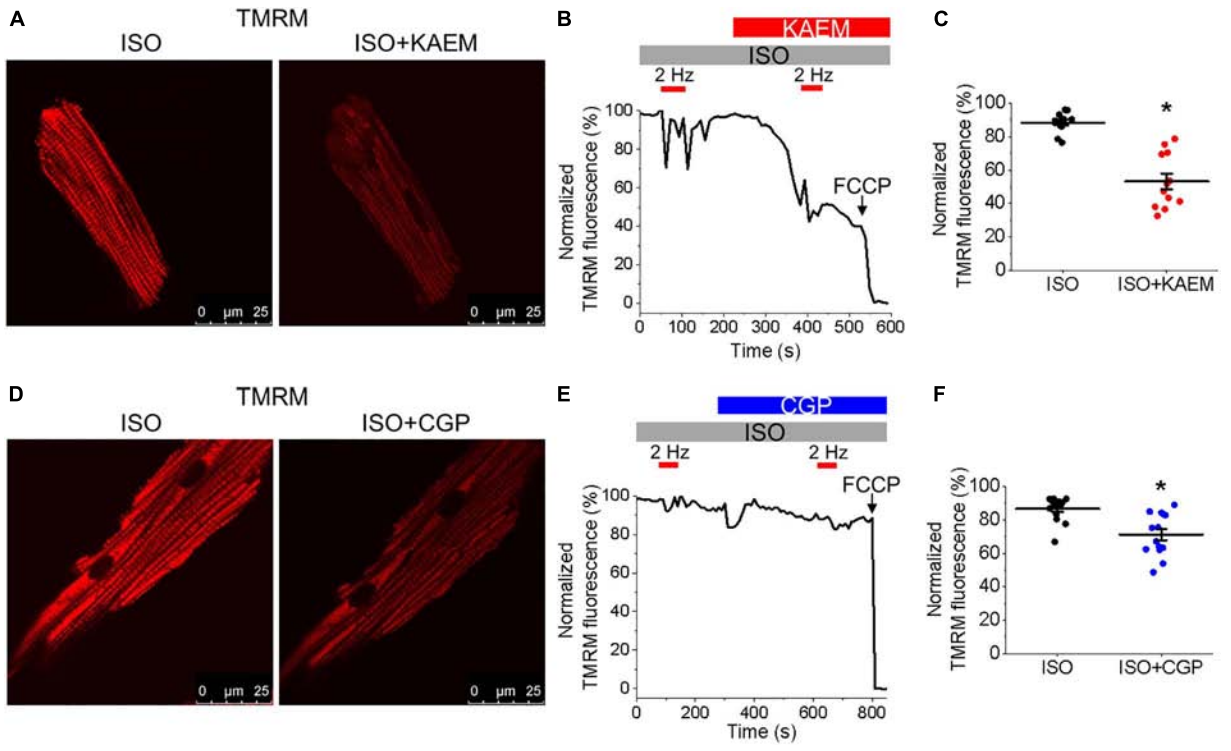

FIGURE 3 | Pharmacological enhancers of mitochondrial Ca^{2+} accumulation modulate $\Delta\psi m$ in cultured control rat VMs. **(A)** Representative images of a VM treated with ISO (50 nmol/L) before and after application of kaempferol (KAEM, 10 μmol/L). $\Delta\psi m$ of VMs was monitored by TMRM fluorescence (20 μmol/L). **(B)** Representative recording of changes in $\Delta\psi m$ in response to application of ISO and pacing at 2 Hz (red bars) for 60 s, followed by application of KAEM. TMRM signal was normalized to minimum fluorescence obtained by application of FCCP (50 μmol/L) and represented as percentage of baseline. Graph in **(C)** depicts pooled data for minimum fluorescence after pacing and application of ISO or KAEM ($n = 12$, $N = 4$, $^*p < 0.05$, paired Student's t-test). **(D)** Representative images of a VM treated with ISO before and after application of CGP-37157 (CGP, 1 μmol/L). $\Delta\psi m$ of VMs was monitored by TMRM fluorescence. **(E)** Representative recordings of changes in $\Delta\psi m$ in response to application of ISO and pacing at 2 Hz for 60 s, followed by application of CGP. Graph in **(F)** depicts pooled mean data ± SEM for minimum fluorescence after pacing and application of ISO or KAEM ($n = 14$, $N = 3$, $^*p < 0.05$, paired Student's t-test).

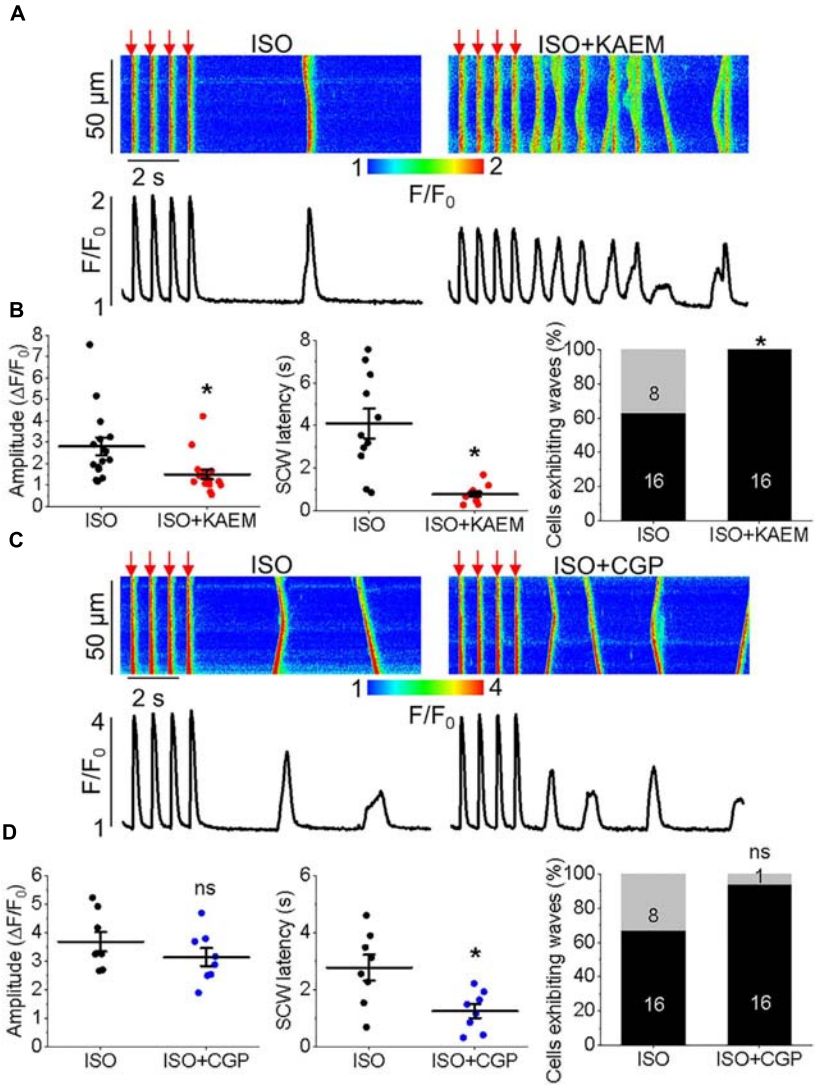

FIGURE 4 | Enhanced mitochondrial Ca^{2+} accumulation promotes proarrhythmic spontaneous Ca^{2+} waves in control cultured rat VMs. **(A)** Representative confocal line scan images of Ca^{2+} transients and Rhod-2 fluorescence (F/F_0) profiles ISO treated (50 nmol/L) rat VM undergoing 2 Hz pace-pause protocol (red arrows) to induce SCW, before and after application of kaempferol (KAEM, 10 µmol/L). Graphs in **(B)** depict mean data ± SEM from Ca^{2+} transient amplitude (n = 15, N = 5, $^*p < 0.05$, paired Student's t-test), SCW latency (n = 11, N = 5, paired Student's t-test) and the percentage of cells exhibiting waves (N = 5, $^*p < 0.05$, Fisher's exact test). **(C)** Representative confocal line scan images of Ca^{2+} transients and Rhod-2 fluorescence (F/F_0) profiles of ISO treated rat VM undergoing 2 Hz pace-pause protocol before and after application of CGP-37157 (CGP, 1 µmol/L). Graphs in **(D)** depict mean data ± SEM from Ca^{2+} transient amplitude (n = 7, N = 4, ns is not significant, paired Student's t-test), SCW latency (n = 8, N = 4, $^*p < 0.05$, paired Student's t-test) and the percentage of cells exhibiting waves (N = 4, ns is not significant, Fisher's exact test).

recorded cytosolic Ca^{2+} in the presence of β-adrenergic receptor agonist ISO (50 nmol/L), subjected to a burst-pace pause protocol (2 Hz, 20 s). We assessed Ca^{2+} transient amplitude and SCW latency as an indication of the propensity for arrhythmogenic Ca^{2+} release. As shown in **Figures 4A,B**, VMs treated with ISO and kaempferol have a significantly lower Ca^{2+} transient amplitude in comparison to ISO alone (2.77 ± 0.44 $\Delta F/F_0$ ISO vs. 1.57 ± 0.23 $\Delta F/F_0$ ISO and kaempferol, $^*p = 0.006$). We observed a fivefold shortening in SCW latency after treatment with kaempferol ($^*p < 0.001$), as well a significant increase in the percentage of VMs exhibiting SCWs (63% ISO vs. 100% ISO and kaempferol, $^*p < 0.001$). A similar pattern was obtained in VMs treated with CGP-37157 (**Figures 4C,D**), whereby the SCW latency was shortened approximately twofold ($^*p = 0.002$). Changes in Ca^{2+} transient amplitude and the percentage of cells exhibiting waves were not significant on treatment with CGP-37157.

To provide additional evidence that facilitation of mitochondrial Ca^{2+} accumulation exerts strong deleterious effects on intracellular Ca^{2+} handling we performed experiments using another MCU enhancer SB 202190 (Montero et al., 2004) (**Figure 5**). As seen from experiments in ISO-treated VMs

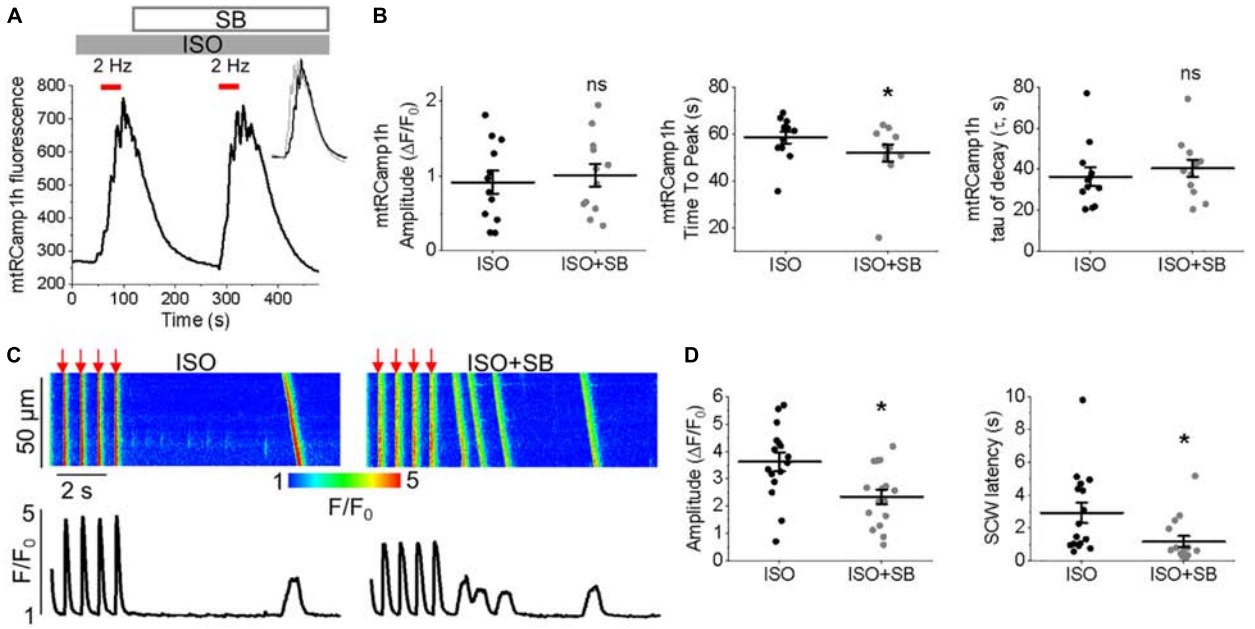

FIGURE 5 | MCU enhancer SB 202190 has similar effects to kaempferol in cultured control rat VMs. **(A)** Representative trace from cultured VM expressing mtRCamp1h. VMs were treated with ISO (50 nmol/L) and paced at 2 Hz for 60 s intervals (red bars), then treated with SB 202190 (SB) and paced again. Peaks are overlaid in the inset for visualization, with ISO in black, ISO+SB in gray. Graphs in **(B)** depict mean data ± SEM of mtRCamp1h transient amplitude, time to transient peak and tau of decay (n = 12 per group, N = 3, $^*p < 0.05$, paired Student's t-test). **(C)** Representative confocal line scan images of Ca^{2+} transients and Rhod-2 fluorescence (F/F_0) profiles ISO treated (50 nmol/L) rat VM undergoing 2 Hz pace-pause protocol (red arrows) to induce SCW, before and after application of SB 202190 (SB, 30 µmol/L). Graphs in **(D)** depict mean data ± SEM from Ca^{2+} transient amplitude (n = 16, N = 3, $^*p < 0.05$, paired Student's t-test) and SCW latency (n = 16, N = 3, $^*p < 0.05$, paired Student's t-test).

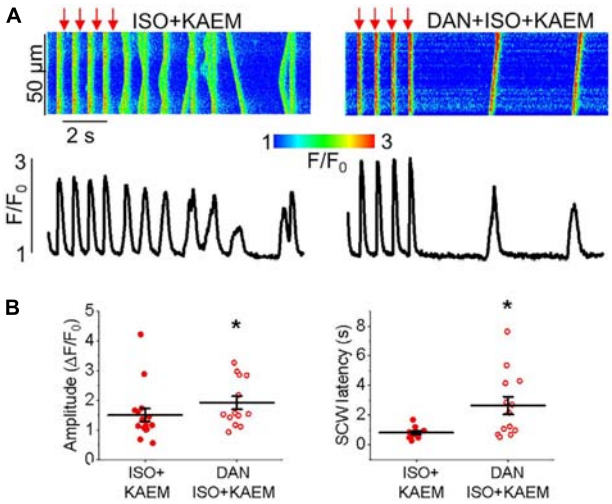

FIGURE 6 | Inhibition of RyR with dantrolene reduces proarrhythmic effects of kaempferol on Ca^{2+} handling in cultured control rat VMs. **(A)** Representative confocal line scan images of Ca^{2+} transients and Rhod-2 fluorescence (F/F_0) profiles of TAB rat VMs undergoing 2 Hz pace-pause protocol (red arrows) to induce SCWs. VMs were treated with isoproterenol (ISO, 50 nmol/L) and kaempferol (KAEM, 10 µmol/L), or were pretreated for 5 min with dantrolene (DAN, 2 µmol/L) before ISO and KAEM treatment. Graphs in **(B)** depict mean data ± SEM from Ca^{2+} transient amplitude (n = 13–15, N = 3–4, $^*p < 0.05$, Student's t-test) and SCW latency (n = 11–13, N = 3–4, $^*p < 0.05$, Student's t-test).

expressing mtRCamp1h, application of SB 202190 (30 µmol/L) moderately but significantly accelerated rate of mitochondrial Ca^{2+} uptake while failed to increase overall amplitude of mitochondrial Ca^{2+} transients (**Figures 5A,B**), in line with the effects of kaempferol (**Figure 2C**). Importantly, similar to kaempferol, incubation with SB reduced amplitude of Ca^{2+} transients and shortened and latency of SCWs in periodically paced ISO-treated cells (**Figures 5C,D**).

Enhanced propensity to generate SCWs is often attributed to abnormally high activity of SR Ca^{2+} release channels, RyRs (Bers, 2002). To test whether stabilization of RyRs can attenuate kaempferol–mediated effects on Ca^{2+} handling, we treated VMs with dantrolene (2 µmol/L, 5 min), a specific inhibitor of RyR. **Figure 6** shows that dantrolene restores Ca^{2+} transient amplitude and significantly reduces kaempferol-mediated shortening of SCW latency in ISO-treated VMs (SCW latency 3.34 ± 0.73 s ISO and kaempferol vs. 2.64 ± 0.60 s ISO, kaempferol and dantrolene, $^*p < 0.001$).

Taken together, these data suggest that facilitation of mitochondrial Ca^{2+} accumulation promotes generation of proarrhythmic SCWs by enhancement of activity of RyRs.

Kaempferol and CGP-37157 Increase ROS and Oxidation of RyRs

RyR is well established as a ROS sensor, with increased oxidation and thus RyR activity associated with enhanced propensity for spontaneous SR Ca^{2+} release and proarrhythmic SCWs.

Mitochondria is a major intracellular source of ROS and excessive RyR oxidation by mitochondria-derived ROS has been demonstrated in many models of HF and aging (Zima and Blatter, 2006). Facilitation of mitochondrial Ca^{2+} uptake may accelerate the rate of emission of ROS by stimulating electron transport (Bertero and Maack, 2018). Therefore, to test the possible effects of kaempferol on mitochondrial redox state, control VMs were infected (MOI of 10) with adenovirus construct carrying sequence encoding the novel H_2O_2 probe OMM-HyPer, and cultured for 48 h prior to imaging. As shown in **Figure 7**, application of kaempferol significantly increases the signal of mitochondrial-targeted peroxide-sensitive indicator (normalized fluorescence 16.29 ± 2.11% ISO vs. 54.23 ± 5.31% ISO and kaempferol, $^*p < 0.001$), confirming that facilitation of mitochondrial Ca^{2+} accumulation induces mitochondrial ROS release.

Considering the close proximity of mitochondria and SR, we next sought to determine whether facilitation of mitochondrial Ca^{2+} accumulation leads to an increase in local ROS levels in the vicinity of RyR in cultured control VMs, measured using the ER-tuned redox-sensitive biosensor ERroGFP_iE (Avezov et al., 2013). The GFP sensor contains engineered cysteine residues that enable formation of di-thiol in response to oxidant stress (Cannon and Remington, 2009). After we generated adenovirus encoding the sensor, VMs were infected at a MOI of 10 and cultured for 48 h prior to imaging. As shown in **Figure 8A**, ERroGFP_iE-infected VMs exhibit a striated pattern indicative of SR targeting of the probe.

Figures 8B,D show representative recordings where signal of ERroGFP_iE was normalized to minimal fluorescence obtained by application of reducing agent dithiothreitol (DTT, 5 mmol/L) and maximal fluorescence obtained by application of oxidizing agent 2,2'-dithiodipyridine (DTDP, 200 μmol/L). At baseline under β-adrenergic stimulation with ISO, little change in oxidation in the form of increased fluorescence and di-thiol formation is observed. However, treatment with kaempferol or CGP-37157 still leads to a measurable and significant increase in ERroGFP_iE signal (8.19 ± 0.83% ISO vs. 22.20 ± 2.49% ISO and kaempferol, $^*p < 0.001$ and 11.21 ± 2.03% ISO vs. 16.26 ± 2.32 ISO and CGP-37157, $^*p = 0.006$, respectively), indicative of increased oxidation and ROS emission in close proximity of RyR (**Figures 8C,E**, respectively).

To directly test the hypothesis that pharmacological enhancement of $[Ca^{2+}]_m$ accumulation results in increased RyR oxidation, the free thiol content of immunoprecipitated RyRs was measured using DNP-antibody. **Figure 8F** demonstrates that

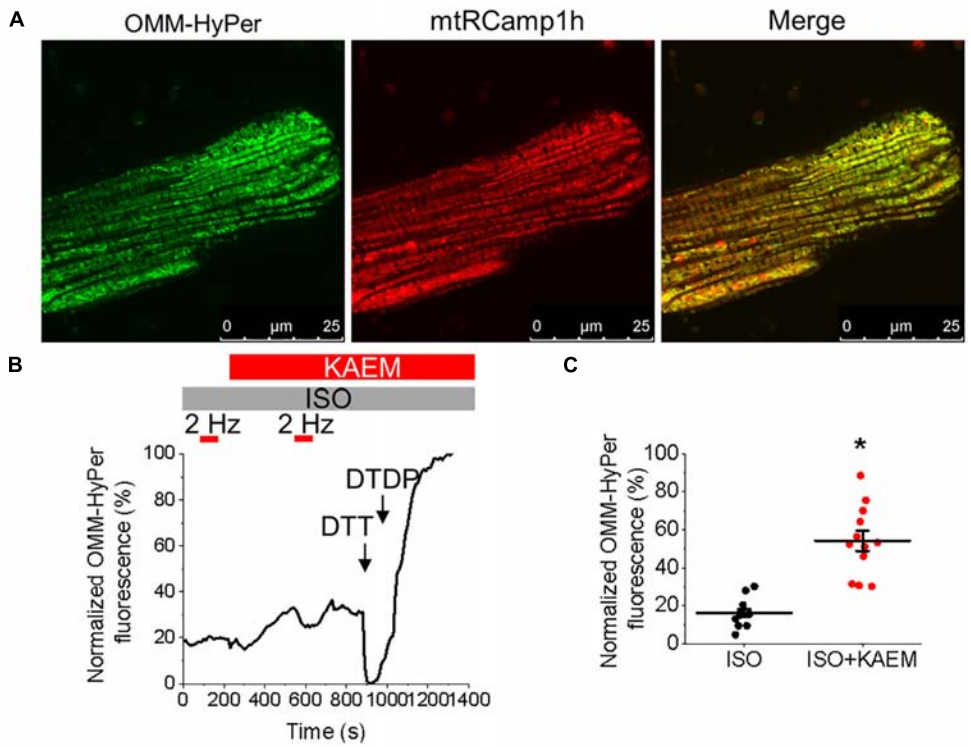

FIGURE 7 | Pharmacological enhancement of mitochondrial Ca^{2+} accumulation increases mitochondrial ROS in cultured control rat VMs. **(A)** Representative image of a cultured control VM 48 h after adenoviral infection with biosensor OMM-HyPer (left, green, MOI of 10) and mtRCamp1h (center, red, MOI of 10). A merged image is indicated on the right. **(B)** Representative trace of OMM-HyPer fluorescence from a VM treated with ISO (50 nmol/L), paced at 2 Hz (red bars) and subsequently treated with kaempferol (KAEM, 10 μmol/L) before further pacing. OMM-HyPer signal was normalized to minimum fluorescence obtained by application of dithiothreitol (DTT, 5 mmol/L) and maximum fluorescence obtained by application of deoxythymidine diphosphate (DTDP, 200 μmol/L). Graph in **(C)** depicts mean data ± SEM for maximum normalized fluorescence after pacing and application of ISO and KAEM ($n = 12$, $N = 4$, $^*p < 0.05$, paired Student's t-test).

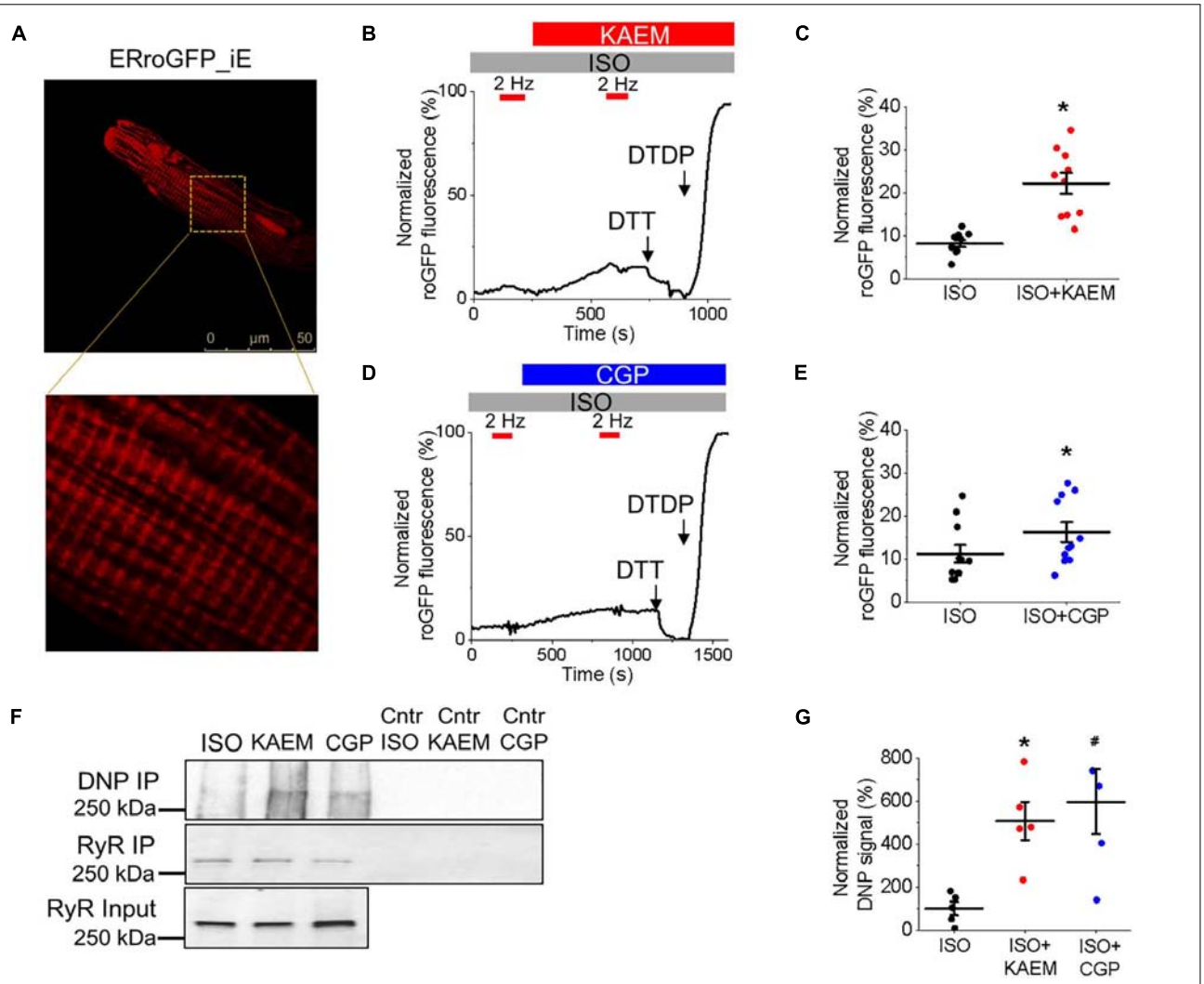

FIGURE 8 | Pharmacological enhancement of mitochondrial Ca^{2+} accumulation increases ROS in the vicinity of RyR in cultured control rat VMs. **(A)** Representative image of a cultured control VM 48 h after adenoviral infection with biosensor ERroGFP_iE (MOI of 10). **(B)** Representative trace of ERroGFP_iE fluorescence from a VM treated with ISO (50 nmol/L), paced at 2 Hz (red bars) and subsequently treated with kaempferol (KAEM, 10 µmol/L) before further pacing. ERroGFP_iE signal was normalized to minimum fluorescence obtained by application of dithiothreitol (DTT, 5 mmol/L) and maximum fluorescence obtained by application of deoxythymidine diphosphate (DTDP, 200 µmol/L). Graph in **(C)** depicts mean data ± SEM for maximum normalized fluorescence after pacing and application of ISO and KAEM (n = 10, N = 3, $^*p < 0.05$, paired Student's t-test). **(D)** Representative trace of ERroGFP_iE fluorescence from a VM treated with ISO, paced at 2 Hz and subsequently treated with CGP-37157 (CGP, 1 µmol/L) before further pacing. ERroGFP_iE signal was normalized to minimum fluorescence obtained by application of DTT and maximum fluorescence obtained by application of DTDP. Graph in **(E)** depicts mean data ± SEM for maximum fluorescence after pacing and application of ISO and CGP (n = 11, N = 3, $^*p < 0.05$, paired Student's t-test). **(F)** RyR in freshly isolated control VMs was immunoprecipitated (IP) and immunoblotted for oxidation using DNP antibody. Representative images of DNP IP, RyR IP and RyR input signal from VMs treated with ISO, ISO and KAEM, or ISO and CGP, with controls (Cntr). **(G)** Quantification of normalized DNP signal (%, N = 5, $^*p$ and $^\#p < 0.05$ vs. ISO, one-way ANOVA with Bonferroni *post hoc* test).

treatment with kaempferol or CGP-37157 (for 5 and 10 min, respectively) significantly increases oxidation of RyR fivefold and sixfold, respectively (**Figure 8G**, $^*p = 0.047$ and $^\#p = 0.015$), shown by increased DNP signal. These data demonstrate that in control VMs, enhanced mitochondrial Ca^{2+} accumulation leads to increased ROS in the closely situated SR. Subsequent increased RyR oxidation is likely the responsible mechanism for the shortened latency for proarrhythmic RyR-mediated SCWs in VMs with pharmacologically enhanced mitochondrial Ca^{2+} accumulation.

The Effects of Pharmacological Modulators on Mitochondrial Ca^{2+} Accumulation in TAB VMs

Kaempferol and CGP-37157 modulate mitochondrial Ca^{2+} accumulation, membrane potential and ROS emission in cultured VMs from control rat hearts, as well as intracellular Ca^{2+} cycling and SCW generation. However, in the diseased heart, redox balance is altered and both intracellular and mitochondrial Ca^{2+} handling can be compromised already (Kim et al., 2017).

To test whether tethering of mitochondria to the SR is altered in TABs rat VMs, we performed western blot analysis of expression levels of mitofusin 1 and mitofusin 2; proteins that scaffold these two organelles (de Brito and Scorrano, 2008; Chen et al., 2012; Filadi et al., 2015). We did not find changes in expression levels of both these proteins in VMs of TABs vs. those of controls (**Figure 9**). Next, isolated TAB VMs were infected with adenoviruses to express mitochondrial Ca^{2+} indicator mtRCamp1h. **Figures 10A–D** demonstrate that the effects of kaempferol and CGP-37157 on mitochondrial Ca^{2+} accumulation are qualitatively similar to those in control VMs. As in controls, kaempferol accelerates Ca^{2+} accumulation (time to peak 72.43 ± 3.75 s ISO vs. 56.14 ± 4.47 s ISO and kaempferol, $^*p < 0.001$) but the amplitude does not change significantly, while CGP-37157 impedes mitochondrial Ca^{2+} transient decay (tau of decay 32.08 ± 7.49 s ISO vs. 72.38 ± 14.99 s ISO and CGP-37157, $^*p = 0.006$). In addition, we tested the effects of MCU inhibitor Ru360. **Figures 10E,F** show representative traces and respective pooled data for mitochondrial Ca^{2+} transients in ISO-treated control VMs under basal conditions and after 30 min incubation with 2 μmol/L Ru360. **Figures 10G,H** demonstrates that Ru360 reduces mitochondrial Ca^{2+} accumulation in TABs (0.29 ± 0.07 $\Delta F/F_0$ ISO vs. 0.14 ± 0.03 $\Delta F/F_0$ ISO and Ru360, $^*p < 0.001$). Notably, the amplitude of pacing-induced mitochondrial Ca^{2+} transients in ISO-treated TAB VMs is significantly smaller that in controls (amplitude 1.15 ± 0.09 $\Delta F/F_0$ ISO Control vs. 0.30 ± 0.07 $\Delta F/F_0$ ISO TAB, $^*p < 0.001$, Student's *t*-test). Given this difference, we next performed experiments using freshly isolated VMs from hypertrophic TAB rat hearts, to test whether kaempferol and CGP-37157 have deleterious effects in a disease setting, or on the contrary could be protective.

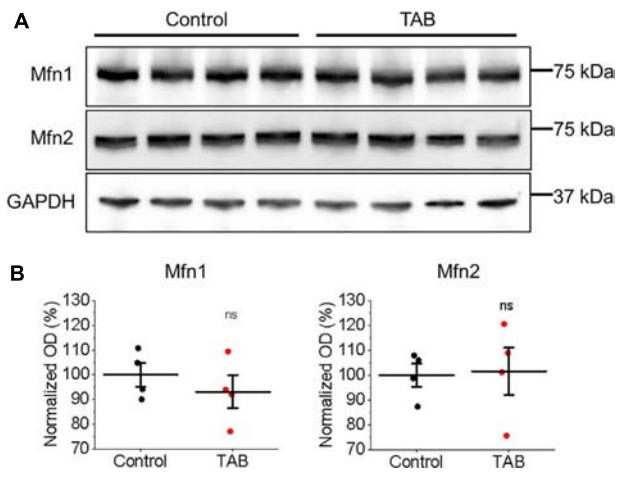

FIGURE 9 | Expression of mitochondrial associated membrane proteins Mfn1 and Mfn2 is not altered in hypertrophic rat VMs. **(A)** Representative images of control and TAB VMs immunoblotted for expression of mitofusin 1 (Mfn1) and mitofusin 2 (Mfn2). GAPDH was used as a loading control. **(B)** Quantification of normalized optical densities ($N = 4$ per group, Student's *t*-test).

Enhanced Mitochondrial Ca^{2+} Accumulation Further Perturbs Intracellular Ca^{2+} Cycling in TAB VMs

We studied the effects of enhancing mitochondrial Ca^{2+} accumulation in TAB VMs on cytosolic Ca^{2+} cycling using Rhod-2, as illustrated in **Figure 11**. As with control VMs, the burst pacing-pause protocol was used to assess the propensity of arrhythmogenic Ca^{2+} release (**Figure 11A**). After treatment with kaempferol, TAB VMs has a significantly reduced Ca^{2+} transient amplitude (5.59 ± 0.71 $\Delta F/F_0$ ISO vs. 3.08 ± 0.42 $\Delta F/F_0$ ISO and kaempferol, $^*p = 0.002$), as well as a approximately twofold in decrease in SCW latency (**Figure 11C**, $^*p = 0.001$). The percentage of cells exhibiting SCWs was also significantly increased after kaempferol application (71% ISO vs. 100% ISO and kaempferol, $^*p = 0.01$). These changes were accompanied by a significant decrease in SR Ca^{2+} content assessed by application of 10 mmol/L caffeine (**Figure 11B**, 5.46 ± 0.77 $\Delta F_{caf}F/F_0$ ISO vs. 3.19 ± 0.30 $\Delta F_{caf}F/F_0$ ISO and kaempferol, $^*p = 0.01$). Decreased Ca^{2+} transient amplitude and reduced SR Ca^{2+} load is indicative of increased Ca^{2+} leak via hyperactive RyRs (Belevych et al., 2007; Terentyev et al., 2008).

Excessive ROS production is a hallmark of hypertrophy and we have previously established that in TAB VMs, there is increased mitochondrial ROS production in comparison to healthy controls which results in oxidation and thereby abnormally high activity of RyRs (Kim et al., 2017). In the present study, parallel experiments using the mitochondria-specific ROS indicator MitoSOX demonstrated that enhancement of mitochondrial Ca^{2+} accumulation with kaempferol further increased ROS emission in diseased VMs (**Figures 11D,E**). Signal was normalized to maximal fluorescence obtained upon application of 10 mmol/L H_2O_2.

Similar effects on cytosolic Ca^{2+} transients were obtained when enhancing mitochondrial Ca^{2+} accumulation in TAB VMs with block of NCLX via CGP-37157 (**Figures 12A,B**). There was a significant reduction in SCW latency (**Figure 12C**, 4.79 ± 0.38 s. ISO vs. 1.99 ± 0.45 s. ISO and CGP-37157, $^*p < 0.001$), although no significant change in the SR Ca^{2+} content assessed by caffeine application was observed (**Figures 12B,C**).

Inhibition of Mitochondrial Ca^{2+} Uptake With Ru360 Reduces ROS Emission and Increases Latency for Proarrhythmic SCWs

Given that application of MCU-inhibitor Ru360 attenuated triggered activity and arrhythmogenesis in TAB hearts *ex vivo* (**Figure 1**), we next assessed intracellular Ca^{2+} handling of VMs preincubated with 2 μmol/L Ru360 for 30 min. There were no significant differences in the Ca^{2+} transient amplitude and the percentage of cells exhibiting waves or the caffeine-sensitive SR Ca^{2+} content (**Figures 13A–C**). However, there was a significant increase in SCW latency, (**Figures 13A,C**, 1.42 ± 0.19 s. ISO vs. 1.96 ± 0.19 s. ISO and Ru360, $^*p < 0.001$), indicative of stabilization of RyR-mediated Ca^{2+} release. Myocytes from TAB hearts displayed a decrease in MitoSOX fluorescence after

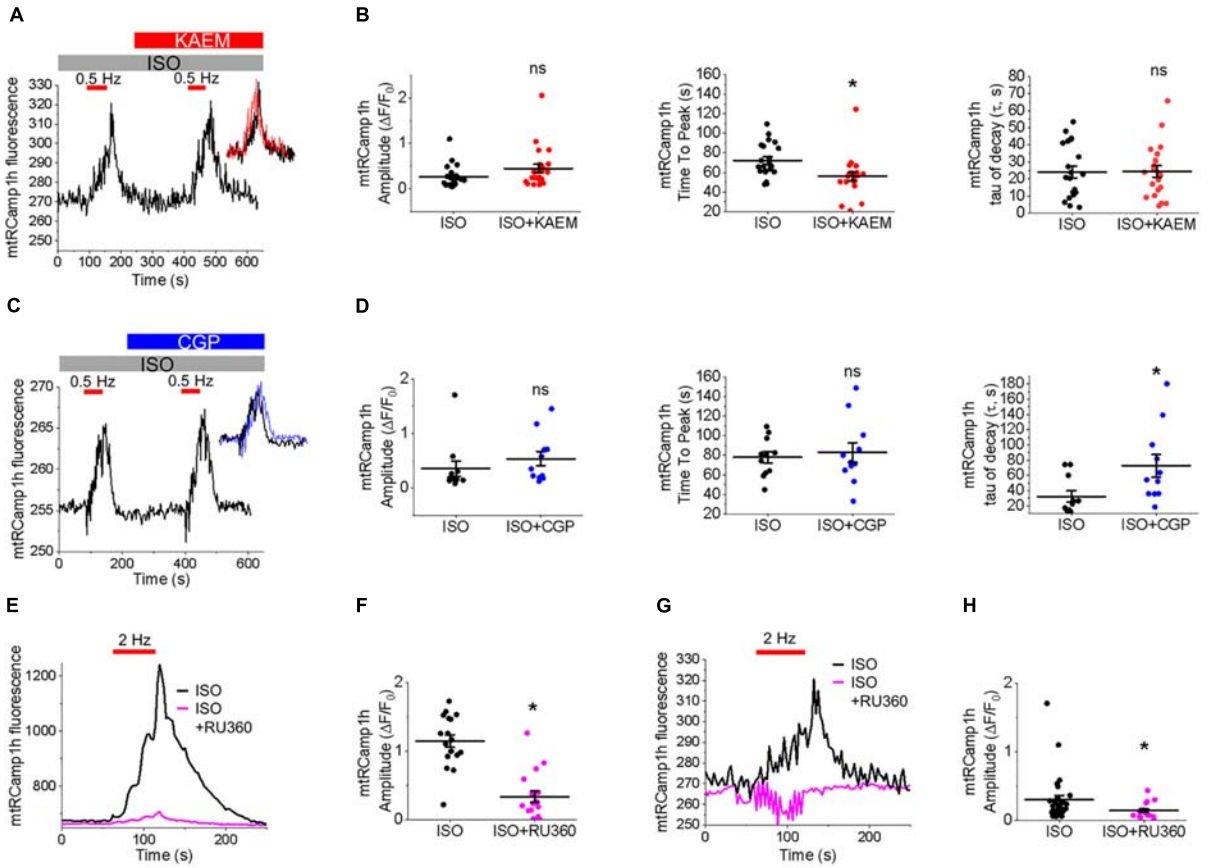

FIGURE 10 | Pharmacological modulators of mitochondrial Ca^{2+} in TAB VMs exert similar effects to those on controls, despite hypertrophy-related impairment in mitochondrial Ca^{2+} homeostasis. **(A)** Representative trace from cultured TAB VM expressing mtRCamp1h. TAB VMs were treated with ISO (50 nmol/L) and paced at 0.5 Hz for 60 s intervals (red bars), before treatment with kaempferol (KAEM, 10 μmol/L) and further pacing. Peaks are overlaid in the inset for visualization, with ISO in black, ISO+KAEM in red. Graphs in **(B)** depict mean data ± SEM of mtRCamp1h transient amplitude, time to transient peak and tau of decay (n = 22 per group, N = 4, $^*p < 0.05$, paired Student's t-test). **(C)** Representative trace from cultured TAB VM expressing mtRCamp1h. VMs were treated with ISO and paced at 0.5 Hz for 60 s intervals (red bars), before treatment with CGP-37157 (CGP, 1 μmol/L) and further pacing. Peaks are overlaid in the inset for visualization, with ISO in black, ISO+CGP in blue. Graphs in **(D)** depict mean data ± SEM from mtRCamp1h transient amplitude, time to transient peak and tau of decay (n = 11, N = 3, $^*p < 0.05$, paired Student's t-test). **(E)** Representative trace from a cultured control VM expressing mtRCamp1h. Myocytes were treated with ISO (black line) and paced at 2 Hz for 60 s (red bar), or pretreated with Ru360 (2 μmol/L) for 30 min before treatment with ISO and pacing at 2 Hz (pink line). Graph in **(F)** depicts mean data ± SEM from mtRCamp1h transient amplitude (n = 17–18, N = 3, $^*p < 0.05$, Student's t-test). **(G)** Representative trace from a cultured TAB VM expressing mtRCamp1h. Myocytes were treated with ISO (black line) and paced at 2 Hz for 60 s (red bar), or pretreated with Ru360 (2 μmol/L) for 30 min before treatment with ISO and pacing at 0.5 Hz (pink line). Graph in **(H)** depicts mean data ± SEM from mtRCamp1h transient amplitude (n = 17, N = 4, $^*p < 0.05$, Student's t-test).

preincubation with Ru360 (**Figures 13D,E** 15.46 ± 1.91% ISO vs. 14.93 ± 2.15% ISO and Ru360, $^*p < 0.001$). There was also a significant reduction in oxidation of immunoprecipitated RyRs after treatment with Ru360 assessed using anti-DNP antibodies (**Figures 13F,G**). These data suggest that stabilization of SR Ca^{2+} release stems from attenuation of ROS emission by mitochondria and normalization of RyR redox state.

Modifiers of Mitochondrial Ca^{2+} Uptake and Retention Do Not Alter the Velocity of SCWs

Regenerative SCWs propagate via the 'fire-diffuse-fire' mechanism (Keizer and Smith, 1998; Maxwell and Blatter, 2012), whereby Ca^{2+} released from one cluster of RyR channels activates Ca^{2+} release from another. Increasing Ca^{2+} buffering can intercept Ca^{2+} diffusing from cluster to cluster and modulate SCW velocity (Ramay et al., 2010; Eisner et al., 2017), as was shown with SR Ca^{2+}-ATPase (SERCa) enhancers (Fernandez-Tenorio and Niggli, 2018). It could be suggested that slower SCW wave propagation after enhancement of mitochondrial Ca^{2+} accumulation indicates a Ca^{2+} buffering capacity of mitochondria, serving as a sink for cytosolic Ca^{2+}. However, neither the enhancement (with kaempferol or CGP-37157) nor attenuation (with Ru360) of mitochondrial Ca^{2+} accumulation altered the velocity of SCWs in either cultured control VMs (**Figure 14A**) or hypertrophic TAB VMs (**Figure 14B**). These data suggest that buffering capacity of mitochondria is insufficient to interrupt or slow SCWs, possibly due to concomitant changes in $\Delta\psi$m and local ROS.

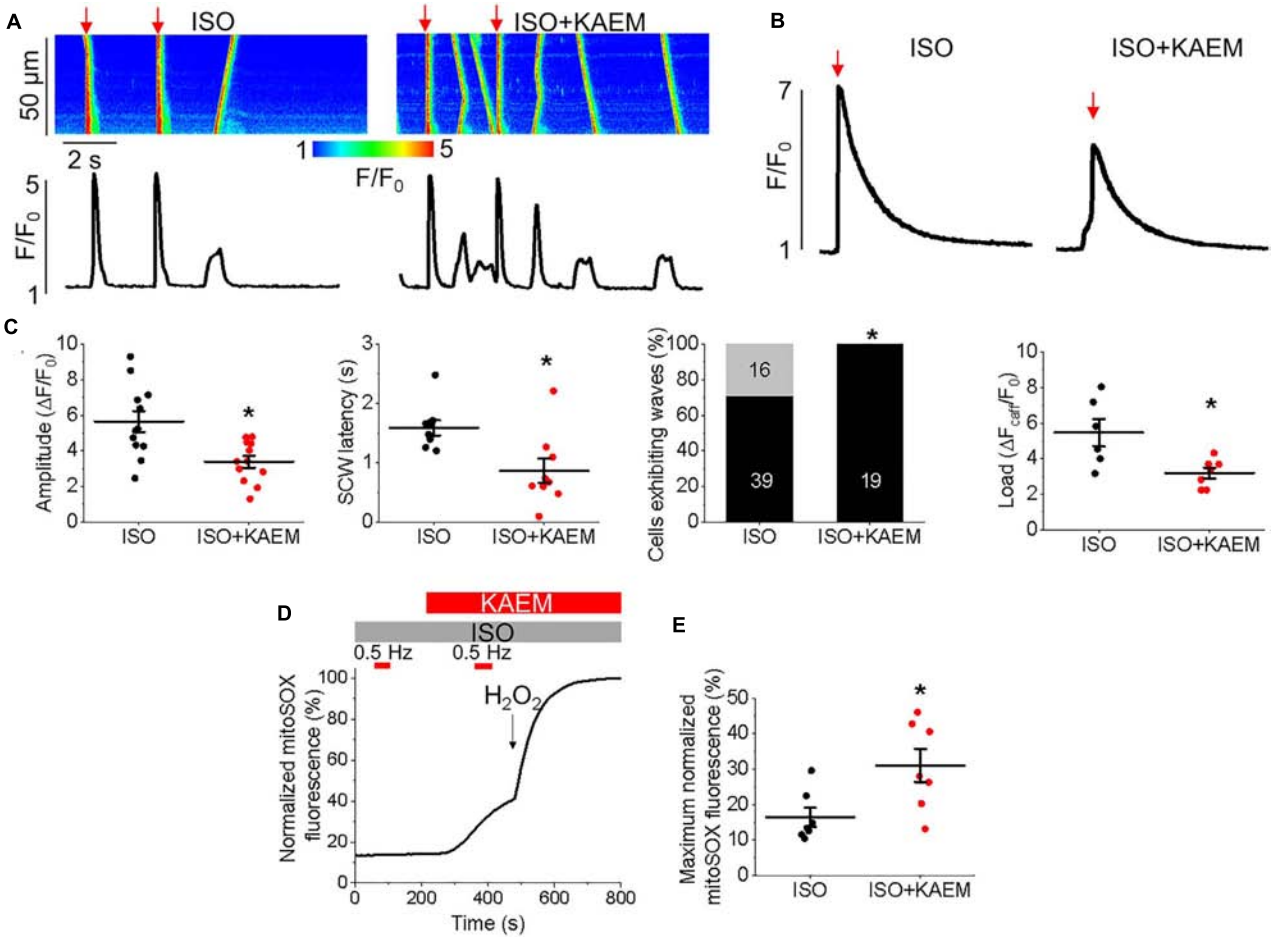

FIGURE 11 | Enhanced mitochondrial Ca^{2+} accumulation by kaempferol promotes proarrhythmic SCWs in TAB rat VMs. **(A)** Representative confocal line scan images of Ca^{2+} transients and Rhod-2 fluorescence (F/F_0) profiles of ISO treated (50 nmol/L) TAB rat VMs undergoing 0.5 Hz pace-pause protocol (red arrows) to induce SCWs, before and after application of kaempferol (KAEM, 10 µmol/L). **(B)** Representative traces of caffeine-induced Ca^{2+} transients (10 mmol/L). Graphs in **C** depict mean data ± SEM from Ca^{2+} transient amplitude ($n = 12$, $N = 4$, $^*p < 0.05$, paired Student's t-test), SCW latency ($n = 9$, $N = 4$, $^*p < 0.05$, paired Student's t-test), the percentage of cells exhibiting waves ($^*p < 0.05$, $N = 4$, Fisher's exact test) and the caffeine-sensitive Ca^{2+} store load ($n = 6$ per group, $^*p < 0.05$, Student's t-test). **(D)** Representative recording of ROS production measured with MitoSOX in VMs. Signal was normalized to maximum fluorescence obtained on application of 10 mmol/L H_2O_2. VMs were treated with ISO and kaempferol and paced at 2 Hz (red bars) for 60 s. Graph in **(E)** depicts mean data ± SEM of normalized MitoSOX fluorescence ($n = 7$, $N = 3$, $^*p < 0.05$, paired Student's t-test).

DISCUSSION

The contribution of mitochondrial Ca^{2+} flux to myocyte excitation-contraction remains the subject of intense research, with both enhancement or reduction of $[Ca^{2+}]_m$ posited as therapeutic strategies to improve cardiac function and prevent arrhythmia in cardiac disease (Liu and O'Rourke, 2008; Kolhaas et al., 2010; Liu et al., 2014; Dietl and Maack, 2017; Schweitzer et al., 2017; Xie et al., 2018). Our present study provides evidence that enhanced mitochondrial Ca^{2+} accumulation dissipates $\Delta\psi m$ and drives increased ROS in the mitochondria-SR microdomain. Subsequently, increased modification of RyR by ROS enhances channel activity and increases the propensity for proarrhythmic spontaneous SR Ca^{2+} release in the form of SCWs. This mechanism further exacerbates proarrhythmic triggered activity in hypertrophic hearts. Conversely, inhibition of MCU is protective against arrhythmogenesis, attenuating oxidative stress and reducing aberrant activity of RyR.

Modulation of Mitochondrial Ca^{2+} and the Effects on Mitochondrial Function

The physical and functional coupling of the SR and mitochondria is critical for matching myocyte workload to mitochondrial ATP generation (Dorn and Maack, 2013; Lopez-Crisosto et al., 2017). The close association facilitates mitochondrial Ca^{2+} influx upon SR Ca^{2+} release (Sharma et al., 2000; Szalai et al., 2000; Csordás et al., 2001). To maintain Ca^{2+} flux balance in the steady state, uptake of mitochondrial Ca^{2+} is well matched to extrusion, so net $[Ca^{2+}]_m$ does not significantly change. We assessed mitochondrial Ca^{2+} uptake in cultured control and TAB VMs with the genetically encoded Ca^{2+} probe mtRCamp1h.

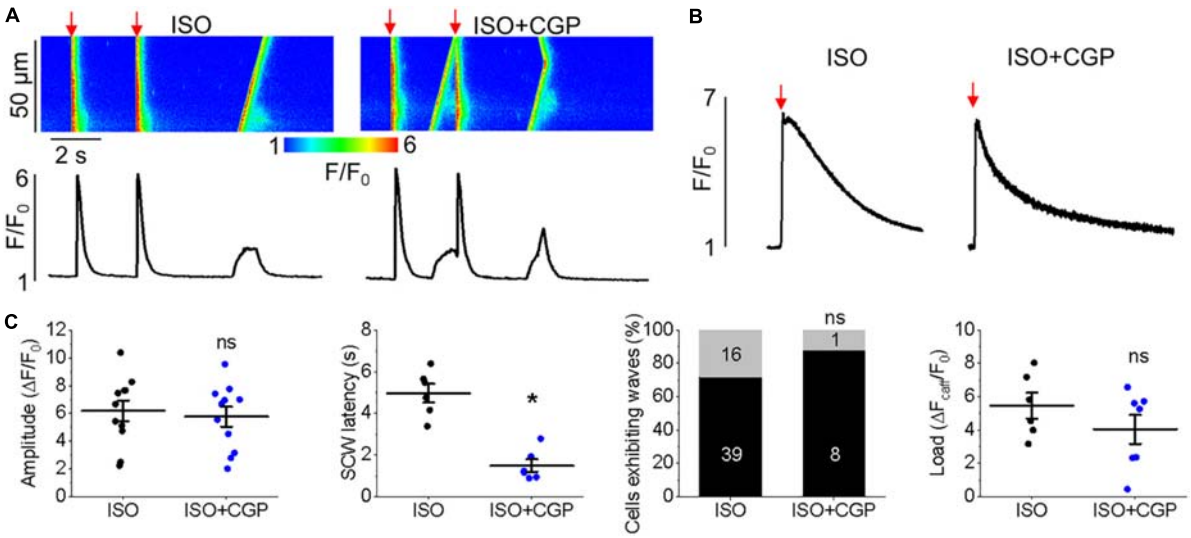

FIGURE 12 | Enhanced mitochondrial Ca^{2+} accumulation by CGP-37157 promotes proarrhythmic SCWs in TAB rat VMs. **(A)** Representative confocal line scan images of Ca^{2+} transients and Rhod-2 fluorescence (F/F_0) profiles of ISO treated (50 nmol/L) rat VMs undergoing 0.5 Hz pace-pause protocol before and after application of CGP-37157 (CGP, 1 µmol/L). **(B)** Representative traces of caffeine-induced Ca^{2+} transients (10 mmol/L). Graphs in **(C)** depict mean data ± SEM from Ca^{2+} transient amplitude (n = 11, N = 5, ns is not significant, paired Student's t-test), SCW latency (n = 6, N = 5, $^*p < 0.05$, paired Student's t-test), the percentage of cells exhibiting waves (n = 18–55, N = 5, ns is not significant, Fisher's exact test), and the caffeine-sensitive Ca^{2+} store load (n = 6, N = 5, ns is not significant, Student's t-test).

In comparison to baseline, under β-adrenergic stimulation with ISO we observed an increase in $[Ca^{2+}]_m$ during periodic pacing (**Figures 2B,E**, **10A,C**), likely to match the increased demand for ATP.

To modulate mitochondrial Ca^{2+} influx in cultured control VMs, we applied kaempferol or SB 202190 to directly enhance uptake through MCU, or CGP-37157 to inhibit NCLX thus attenuating Ca^{2+} efflux. Interestingly, application of these pharmacological agents did not increase $[Ca^{2+}]_m$, but instead altered the dynamics of Ca^{2+} accumulation or retention (**Figures 2D,F**). Similar effects were observed in TAB VMs treated with kaempferol and CGP-37157 (**Figures 10B,D**). The inability to significantly increase total $[Ca^{2+}]_m$ under these conditions points to the existence of limiting factors, preventing excessive mitochondrial Ca^{2+} loading in VMs.

There are three established mechanisms to prevent mitochondrial Ca^{2+} overload. Activation of mitochondrial Ca^{2+}-activated K^+ channels limits depolarization of the mitochondria, reducing the electrochemical inward driving force for Ca^{2+} (O'Rourke et al., 2005; Clements et al., 2015). Acidification of the mitochondrial matrix by an increased H^+ flow through ATP-synthase has been shown to inhibit MCU (Moreau and Parekh, 2009). Additionally, increased matrix Ca^{2+} also promotes the opening of mPTP, dissipating $\Delta\psi m$ and limiting $[Ca^{2+}]_m$ accumulation (Broekemeier et al., 1998; Hüser and Blatter, 1999; Elrod et al., 2010). This is evident in **Figure 3**, whereby application of kaempferol or CGP-37157 to cultured control VMs significantly depolarized $\Delta\psi m$. Interestingly, preincubation of VMs with mitoTEMPO, a specific mitochondria ROS scavenger (20 µmol/L, 30 min), did not prevent dissipation of $\Delta\psi m$ by kaempferol (normalized TMRM fluorescence 89.7 ± 2.16% mitoTEMPO and ISO vs. 39.17 ± 3.59% mitoTEMPO, ISO and kaempferol, $^*p < 0.001$, paired Student's t-test, n = 19, N = 3), suggesting that this process is not ROS-dependent.

Modulation of SR Ca^{2+} Release by $[Ca^{2+}]_m$ Is Mediated by Mitochondrial ROS

The RyR-mediated release of Ca^{2+} from the SR is critical to contractile activation. Termination of SR Ca^{2+} release allows for Ca^{2+} released into the cytosol to be resequestered and maintains the refractoriness of Ca^{2+} signaling during diastole (Terentyev et al., 2002; Szentesi et al., 2004; Sobie et al., 2005). Shortened Ca^{2+} signaling refractoriness due to hyperactive RyR increases the rate of SCWs in diseased myocytes (Belevych et al., 2012; Brunello et al., 2013), contributing to the pathogenesis of triggered arrhythmias (Pogwizd and Bers, 2004).

We assessed the effects of $[Ca^{2+}]_m$ modulation on Ca^{2+} handling and initiation of triggered activity at the whole organ level, using hearts from rats with TAB-induced hypertrophy, as illustrated in **Figure 1**. Application of MCU activator kaempferol reduced Ca^{2+} transient amplitude and exacerbated the proarrhythmic phenotype, with incidences of PVCs and spontaneous VT/VFs with higher VF frequencies. The focal activity and/or transmural outbreak-like activation patterns were frequently seen during PVCs and VFs, suggesting enhanced triggered activity may underlie exacerbated ventricular arrhythmias by kaempferol. In contrast the MCU blocker, Ru360, suppressed spontaneous VT/VFs. The activation maps of pacing induced VFs showed that rapid pacing caused conduction

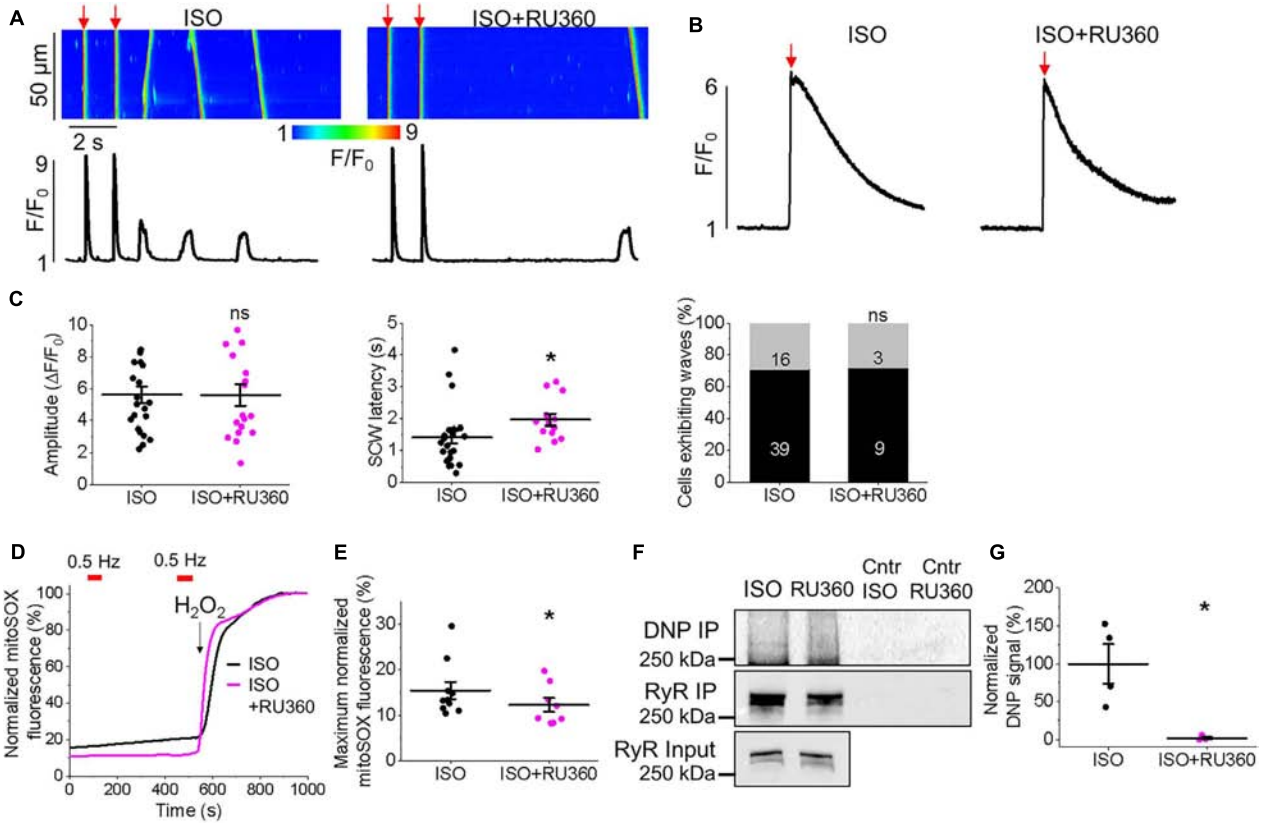

FIGURE 13 | Block of mitochondrial Ca^{2+} uptake through MCU stabilizes RyRs in TAB rat VMs. **(A)** Representative confocal line scan images of Ca^{2+} transients and Rhod-2 fluorescence (F/F_0) profiles of ISO-treated (50 nmol/L) TAB VM undergoing 0.5 Hz pace-pause protocol to induce spontaneous Ca^{2+} waves (SCWs), after 30 min. preincubation with Ru360 (2 µmol/L). **(B)** Representative traces of caffeine-induced Ca^{2+} transients (10 mmol/L). Graphs in **(C)** depict mean data ± SEM from Ca^{2+} transient amplitude (n = 19–22, N = 4, ns is not significant, Student's t-test), SCW latency (n = 13–24, N = 4, ns is non-significant, $^*p < 0.05$, Student's t-test), the percentage of cells exhibiting waves ($^*p < 0.05$, Fisher's exact test) and the caffeine-sensitive Ca^{2+} store load (calculated by application of 10 mmol/L caffeine, n = 6, n = 4, $^*p < 0.05$, Student's t-test). N = 4. **(D)** Representative recording of mitochondrial ROS production measured with MitoSOX in VMs. Signal was normalized to maximum fluorescence obtained on application of H_2O_2 (10 mmol/L). Myocytes were treated with ISO (black line) or ISO and Ru360 (pink line) and paced at 2 Hz (red bars). Graph in **(E)** depicts mean data ± SEM of normalized MitoSOX fluorescence (n = 7–10, N = 3, $^*p < 0.05$, Student's t-test). **(F)** RyR in freshly isolated control and TAB VMs was immunoprecipitated (IP) and immunoblotted for oxidation using DNP antibody. Representative images of DNP IP, RyR IP and RyR input signal from VMs treated with ISO or ISO and Ru360, with controls (Cntr). **(G)** Quantification of normalized DNP signal (%, N = 4 per group, $^*p < 0.05$ vs. ISO, Student's t-test).

block and reentry formation, suggesting that the protective effect of Ru360 is most likely through suppressing triggered activity. In recordings of intracellular Ca^{2+} transients, it was evident that kaempferol and NCLX inhibitor CGP-37157 had detrimental effects on both cultured control VMs (**Figure 4**) and TAB VMs (**Figures 11**, **12**), shortening SCW latency and increasing the propensity for spontaneous Ca^{2+} release, indicative of increased activity of RyR in both cultured control and hypertrophic TAB VMs. The experiments with RyR inhibitor dantrolene demonstrating attenuation of kaempferol-induced disturbances in Ca^{2+} cycling (**Figure 6**) further confirm the central role of dysregulated RyR-mediated Ca^{2+} release in this process.

Hyperactivity of RyR in cardiac disease is often attributed to posttranslational modifications, including phosphorylation of PKA- and CaMKII-specific sites, and oxidation of many reactive cysteines within the protein (Györke and Carnes, 2008; Niggli et al., 2013; Zima et al., 2014). Mitochondria are a major source of ROS in the myocyte and excessive ROS production is a hallmark of HF, hypertrophy and aging (Zima and Blatter, 2006), in parallel with perturbed Ca^{2+} homeostasis (Terentyev et al., 2008; Cooper et al., 2013; Kim et al., 2017). Mitochondrial-ROS signaling has also been suggested to directly modulate Ca^{2+} spark activity (Yan et al., 2008; Zhou et al., 2011). Our experiments using mitochondria-targeted ROS biosensor OMM-HyPer3 show that kaempferol induces surge in mito-ROS production (**Figure 7**). Furthermore, in the present study, **Figure 8** clearly demonstrates increased local ROS in the vicinity of RyR and RyR oxidation in myocytes treated with kaempferol and CGP-37157. Importantly, while oxidative stress is already significant in hypertrophic myocytes, application of kaempferol further increased mitochondrial ROS emission in TAB VMs (**Figure 11D**), exacerbating Ca^{2+} mishandling.

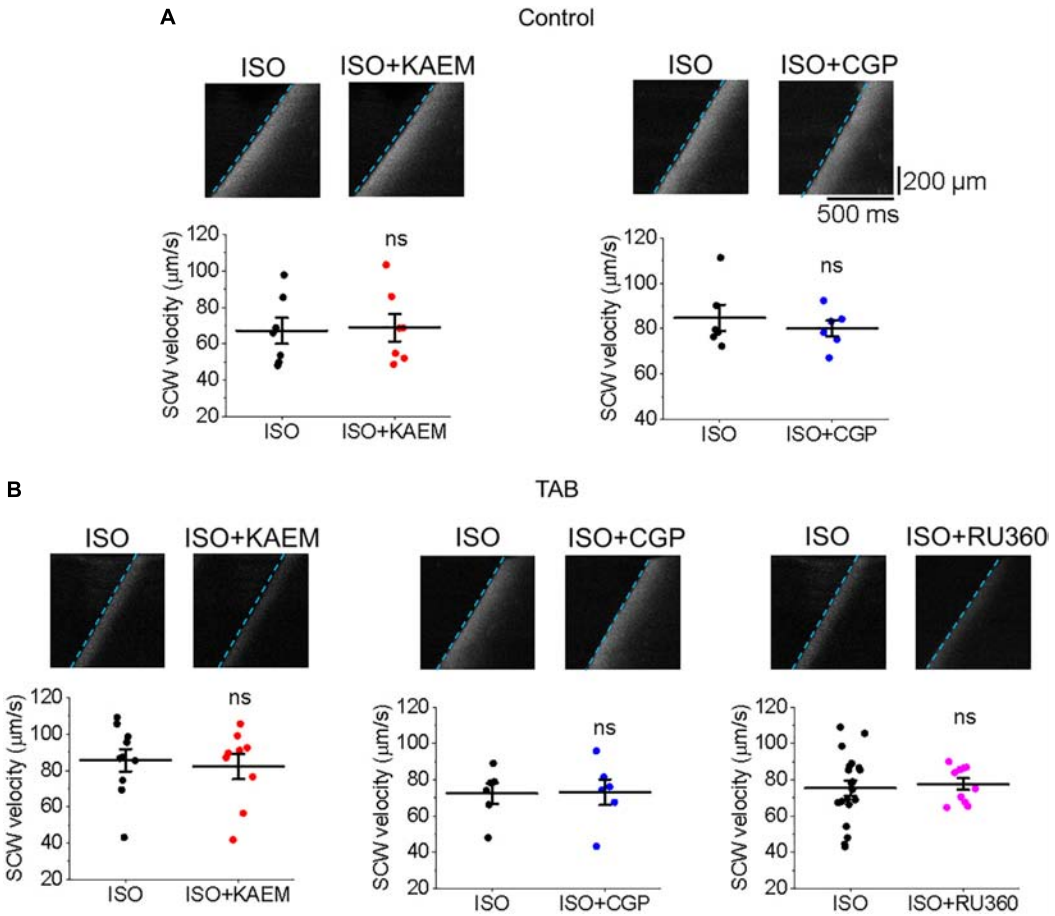

FIGURE 14 | Enhancement or inhibition of mitochondrial Ca^{2+} accumulation does not modulate SCW propagation. **(A)** Velocity of SCWs in cultured control VMs. Graphs depict mean ± SEM (n = 6–9, N = 4–5, ns is non-significant, paired Student's t-test). **(B)** Velocity of spontaneous Ca^{2+} waves (SCWs) in TAB VMs. Graphs depict mean ± SEM (n = 10–20, N = 4–5, ns is non-significant, Student's t-test and paired Student's t-test where appropriate).

Scavenging of mitochondrial ROS has been sufficient to alleviate the arrhythmogenic phenotype in multiple disease states (Mochizuki et al., 2007; Belevych et al., 2012; Cooper et al., 2013; Luo et al., 2013; Joseph et al., 2016) and normalize the redox state of RyR in TAB-induced hypertrophy (Kim et al., 2017). Importantly, inhibition of mitochondrial Ca^{2+} uptake with Ru360 was sufficient to attenuate Ca^{2+}-dependent arrhythmia in *ex vivo* TAB hearts (**Figure 1**) and normalize Ca^{2+} homeostasis in isolated TAB VMs, stabilizing RyR-mediated Ca^{2+} release and attenuating proarrhythmic SCWs (**Figures 13A–C**). Furthermore, Ru360 reduced mitochondrial ROS emission assessed using mitochondria-specific ROS indicator mitoSOX (**Figures 13D,E**). This indicates that block of mitochondrial Ca^{2+} influx reduces mitochondrial ROS signaling in TAB VMs resulting in reduction of oxidation levels of RyR (**Figures 13F,G**). Our data suggest that increased mitochondrial Ca^{2+} accumulation facilitates increased mitochondrial ROS emission and the oxidation of RyR. This underlies enhanced RyR activity, increased spontaneous Ca^{2+} release in the form of arrhythmogenic SCWs, and a vicious cycle of Ca^{2+}/ROS-induced myocyte dysfunction.

Inhibition of NCLX-Mediated Mitochondrial Ca^{2+} Efflux Exacerbates Ca^{2+} Mishandling

During pathological mitochondrial Ca^{2+} overload, opening of mPTP offers an additional Ca^{2+} efflux pathway (Broekemeier et al., 1998; Hüser and Blatter, 1999; Elrod et al., 2010). Pharmacological inhibition of mPTP with cyclosporine A or genetic ablation of mPTP component cyclophilin D (that reduces opening) has shown to be protective against HF or ischemia-reperfusion injury (Griffiths and Halestrap, 1993; Hausenloy et al., 2010; Yarana et al., 2012; Gordan et al., 2016). However, there is ongoing controversy as to whether inhibition of NCLX can be protective in cardiac disease. In a guinea pig HF model, chronic inhibition of NCLX with CGP-37157 restored diminished $[Ca^{2+}]_m$, thereby improving redox homeostasis and protecting against arrhythmogenesis (Liu et al., 2014). In agreement with these findings, we recorded diminished mitochondrial Ca^{2+} transients in VMs from diseased hearts in comparison to controls (**Figure 2** vs. **Figure 10**). However, incubation with CGP-37157 did not

change significantly mitochondrial Ca^{2+} transient amplitude despite slowing down transient decay in TABs. It also did not improve but even worsened aberrant intracellular Ca^{2+} handling (**Figure 12**). Xie et al. (2018) reported an increased mitochondrial Ca^{2+} influx during diastolic period in mice with non-ischemic HF and posited that increased mitochondrial Ca^{2+} efflux drives activation of the sarcolemmal NCX and initiates EADs. In this work, inhibition of both influx and efflux were reported to have anti-arrhythmic effects. In direct contrast, the present study clearly demonstrates that inhibition of NCLX in both control and TAB VMs promotes proarrhythmic spontaneous SR Ca^{2+} release (**Figures 4**, **12**). Importantly, knockdown of NCLX in a conditional loss-of-function mouse model caused severe myocardial dysfunction, HF and sudden cardiac death (Luongo et al., 2017). This was attributed to substantially increased ROS generation due to mitochondrial Ca^{2+} overload. Our results are in line with the latter and inhibition of NCLX with CGP-37157 significantly increased ROS emission in cultured control VMs (**Figures 7**, **8**), resulting in defective SR Ca^{2+} handling in both cultured control (**Figure 4**) and TAB (**Figure 12**) VMs.

Modification of Mitochondrial Ca^{2+} Influx and Efflux Does Not Affect SCW Propagation

While mitochondrial Ca^{2+} flux is closely associated with ATP generation and ROS emission, it has also been suggested that mitochondria may act as buffers that can shape global Ca^{2+} transients during EC coupling (Maack et al., 2006; Yan et al., 2008; Walsh et al., 2009; Drago et al., 2012; Zhao et al., 2013). Although the low affinity of MCU for Ca^{2+} ($Kd \sim 10$–$20\ \mu mol/L$ Ca^{2+}; Bernardi, 1999) would limit uptake during diastole and normal Ca^{2+} transients, mitochondrial Ca^{2+} uptake could occur at high local $[Ca^{2+}]$ near SR Ca^{2+} release sites (Andrienko et al., 2009). One end of the mitochondria is in close proximity to these sites (∼37–270 nm; Sharma et al., 2000), and is physically tethered to the SR (García-Pérez et al., 2011; Chen et al., 2012) with strategic positioning of MCU near RyR (De La Fuente et al., 2016). This facilitates crosstalk between the organelles and tunneling of Ca^{2+} between the two has been reported in striated muscle (Shkryl and Shirokova, 2006). In cardiac disease, mitochondria-SR interfaces and therefore Ca^{2+} transport may be altered due to changes in expression levels of scaffolding proteins including Mfn1 and 2 (Dorn et al., 2015). We tested whether this occurs in our model of hypertrophy and did not find changes in expression levels of these proteins (**Figure 9**). Mitochondria may act as a buffer, serving as a sink of local Ca^{2+}. Indeed, in a mouse model of CPVT, enhancement of mitochondrial Ca^{2+} influx reduced frequency of arrhythmogenic Ca^{2+} waves and incidences of VT/VF (Schweitzer et al., 2017). Also, Zhao et al. (2013) saw a reduction in the frequency of SCWs in myocytes treated with kaempferol after an FCCP-induced reduction in $\Delta\psi m$, while Ru360 increased SCW frequency.

Although SR Ca^{2+} release events are an important driver of $[Ca^{2+}]_m$, as the total mitochondria Ca^{2+} flux is small, the overall ability of mitochondria to shape intracellular Ca^{2+} dynamics remains debated (Dedkova and Blatter, 2008, 2013; O'Rourke and Blatter, 2009; Hohendanner et al., 2013; Williams et al., 2013; Eisner et al., 2017). Troponin I and SERCa are significant Ca^{2+} buffers in the myocyte, and enhancement or increased expression of SERCa has been shown to significantly improve Ca^{2+} buffering capacity and attenuate arrhythmogenic spontaneous Ca^{2+} release (Lyon et al., 2011; Briston et al., 2014). In recent work of Fernandez-Tenorio and Niggli (2018), specific enhancers of SERCa activity reduced the frequency and velocity of SCWs in mouse VMs. In the present study, enhancement of mitochondrial Ca^{2+} influx significantly increases the propensity for SCW in both cultured control and TAB VMs (**Figures 4**, **5**, **11**, **12**), while neither enhancement or inhibition of $[Ca^{2+}]_m$ modulated the velocity and propagation of SCWs (**Figure 14**). Importantly, we do not find any differences in the rate of propagation of SCWs between control and TAB VMs where impairment of mitochondria to sequester Ca^{2+} leads to profound approximately fourfold decrease in the amplitude of pacing-induced mitochondrial Ca^{2+} transient (**Figures 2**, **10**). These data are in line with previous studies that suggest while Ca^{2+} modulates mitochondrial function, mitochondria do not serve as a significant buffer of intracellular cytosolic Ca^{2+} (Bers et al., 1993; Negretti et al., 1993; Lu et al., 2013; Williams et al., 2013). The effects of increased ROS emission on intracellular Ca^{2+} homeostasis are likely overwhelming and cannot be compensated for by an increase in local Ca^{2+} buffering capacity by mitochondria.

CONCLUSION

In conclusion, our data suggest that pharmacological enhancement of mitochondrial Ca^{2+} accumulation produces deleterious effects on Ca^{2+} homeostasis under β-adrenergic stimulation. It promotes excessive ROS that enhances RyR activity thereby proarrhythmic spontaneous Ca^{2+} release. In cardiac hypertrophy, where ROS defenses are weakened, it exacerbates the proarrhythmic alterations in Ca^{2+} handling. Inhibition of mitochondria Ca^{2+} uptake is protective because it reduces emission of ROS by mitochondria.

AUTHOR CONTRIBUTIONS

SH, B-RC, JO-U, GC, and DT participated in the study design. SH wrote first draft of manuscript. SH, RT, TYK, PB, RC, JO-U performed the experiments. SH, RT, TYK, B-RC, DT conducted data interpretation and analyses. SH, RT, TYK, PB, RC, JO-U, GC, B-RC and DT reviewed the manuscript submitted for publication. All authors revised and approved the final version of the manuscript.

FUNDING

This work was supported by American Heart Association Grant #18POST33960456 to SH, National Heart, Lung, and Blood Institute at the National Institutes of Health (NIH) RO1HL135236 to RC, NIH 7R01HL136757 to JO-U, NIH 1R01HL142864 to GC, NIH R01HL096669 to B-RC, American Heart Association Grant in Aid 15GRNT25650002 and NIH R01HL121796 to DT.

REFERENCES

Akerboom, J., Carreras Calderón, N., Tian, L., Wabnig, S., Prigge, M., Tolö, J., et al. (2013). Genetically encoded calcium indicators for multi-color neural activity imaging and combination with optogenetics. *Front. Mol. Neurosci.* 4:2. doi: 10.3389/fnmol.2013.00002

Andrienko, T. N., Picht, E., and Bers, D. M. (2009). Mitochondrial free calcium regulation during sarcoplasmic reticulum calcium release in rat cardiac myocytes. *J. Mol. Cell Cardiol.* 46, 1027–1036. doi: 10.1016/j.yjmcc.2009.03.015

Avezov, E., Cross, B. C., Kaminski Schierle, G. S., Winters, M., Harding, H. P., Melo, E. P., et al. (2013). Lifetime imaging of a fluorescent protein sensor reveals surprising stability of ER thiol redox. *J. Cell Biol.* 201, 337–349. doi: 10.1083/jcb.201211155

Banyasz, T., Lozinskiy, I., Payne, C. E., Edelmann, S., Norton, B., Chen, B., et al. (2008). Transformation of adult rat cardiac myocytes in primary culture. *Exp. Physiol.* 93, 370–382. doi: 10.1113/expphysiol.2007.040659

Baughman, J. M., Perocchi, F., Girgis, H. S., Plovanich, M., Belcher-Timme, C. A., Sancak, Y., et al. (2011). Integrative genomics identifies MCU as an essential component of the mitochondrial calcium uniporter. *Nature* 476, 341–345. doi: 10.1038/nature10234

Belevych, A., Kubalova, Z., Terentyev, D., Hamlin, R. L., Carnes, C. A., and Györke, S. (2007). Enhanced ryanodine receptor-mediated calcium leak determines reduced sarcoplasmic reticulum calcium content in chronic canine heart failure. *Biophys. J.* 93, 4083–4092. doi: 10.1529/biophysj.107.114546

Belevych, A. E., Terentyev, D., Terentyeva, R., Ho, H. T., Gyorke, I., Bonilla, I. M., et al. (2012). Shortened Ca2+ signaling refractoriness underlies cellular arrhythmogenesis in a postinfarction model of sudden cardiac death. *Circ. Res.* 110, 569–577. doi: 10.1161/CIRCRESAHA.111.260455

Belevych, A. E., Terentyev, D., Viatchenko-Karpinski, S., Terentyeva, R., Sridhar, A., Nishijima, Y., et al. (2009). Redox modification of ryanodine receptors underlies calcium alternans in a canine model of sudden cardiac death. *Cardiovasc. Res.* 84, 387–395. doi: 10.1093/cvr/cvp246

Benjamin, E. J., Virani, S. S., Callaway, C. W., Chamberlain, A. M., Chang, A. R., Cheng, S., et al. (2018). Heart disease and stroke statistics-2018 update: a report from the american heart association. *Circulation* 137, e67–e492. doi: 10.1161/CIR.0000000000000558

Bernardi, P. (1999). Mitochondrial transport of cations: channels, exchangers, and permeability transition. *Physiol. Rev.* 79, 1127–1155. doi: 10.1152/physrev.1999.79.4.1127

Bers, D. M. (2002). Cardiac excitation-contraction coupling. *Nature* 10, 198–205. doi: 10.1038/415198a

Bers, D. M., Bassani, J. W., and Bassani, R. A. (1993). Competition and redistribution among calcium transport systems in rabbit cardiac myocytes. *Cardiovasc. Res.* 27, 1772–1777. doi: 10.1093/cvr/27.10.1772

Bertero, E., and Maack, C. (2018). Calcium signaling and reactive oxygen species in mitochondria. *Circ. Res.* 122, 1460–1478. doi: 10.1161/CIRCRESAHA.118.310082

Bilan, D. S., Pase, L., Joosen, L., Gorokhovatsky, A. Y., Ermakova, Y. G., Gadella, T. W., et al. (2013). HyPer-3: a genetically encoded H(2)O(2) probe with improved performance for ratiometric and fluorescence lifetime imaging. *ACS Chem. Biol.* 8, 535–542. doi: 10.1021/cb300625g

Bovo, E., Mazurek, S. R., and Zima, A. V. (2018). Oxidation of ryanodine receptor following ischemia/reperfusion increases propensity of Ca2+ waves during β-adrenergic receptor stimulation. *Am. J. Physiol. Heart Circ. Physiol.* 315, H1032–H1040. doi: 10.1152/ajpheart.00334.2018

Boyman, L., Williams, G. S., Khananshvili, D., Sekler, I., and Lederer, W. J. (2013). NCLX: the mitochondrial sodium calcium exchanger. *J. Mol. Cell. Cardiol.* 59, 205–213. doi: 10.1016/j.yjmcc.2013.03.012

Brandes, R., and Bers, D. M. (1997). Intracellular Ca2+ increases the mitochondrial NADH concentration during elevated work in intact cardiac muscle. *Circ. Res.* 80, 82–87. doi: 10.1161/01.RES.80.1.82

Briston, S. J., Dibb, K. M., Solaro, R. J., Eisner, D. A., and Trafford, A. W. (2014). Balanced changes in Ca buffering by SERCA and troponin contribute to Ca handling during β-adrenergic stimulation in cardiac myocytes. *Cardiovasc. Res.* 104, 347–354. doi: 10.1093/cvr/cvu201

Broekemeier, K. M., Klocek, C. K., and Pfeiffer, D. R. (1998). Proton selective substate of the mitochondrial permeability transition pore: regulation by the redox state of the electron transport chain. *Biochemistry* 22, 13059–13065. doi: 10.1021/bi980820c

Brunello, L., Slabaugh, J. L., Radwanski, P. B., Ho, H. T., Belevych, A. E., Lou, Q., et al. (2013). Decreased RyR2 refractoriness determines myocardial synchronization of aberrant Ca2+ release in a genetic model of arrhythmia. *Proc. Natl. Acad. Sci. U.S.A.* 110, 10312–10317. doi: 10.1073/pnas.1300052110

Burns-Hamuro, L. L., Ma, Y., Kammerer, S., Reineke, U., Self, C., Cook, C., et al. (2003). Designing isoform-specific peptide disruptors of protein kinase a localization. *Proc. Natl. Acad. Sci. U.S.A.* 100, 4072–4077. doi: 10.1073/pnas.2628038100

Cannon, M. B., and Remington, S. J. (2009). Redox-sensitive green fluorescent protein: probes for dynamic intracellular redox responses. A review. *Methods Mol. Biol.* 476, 50–64. doi: 10.1007/978-1-59745-129-1_4

Chen, Y., Csordás, G., Jowdy, C., Schneider, T. G., Csordás, N., Wang, W., et al. (2012). Mitofusin 2-containing mitochondrial-reticular microdomains direct rapid cardiomyocyte bioenergetic responses via interorganelle Ca(2+) crosstalk. *Circ. Res.* 111, 863–875. doi: 10.1161/CIRCRESAHA.112.266585

Clements, R. T., Terentyev, D., and Sellke, F. W. (2015). Ca(2+)-activated K(+) channels as therapeutic targets for myocardial and vascular protection. *Circ. J.* 79, 455–462. doi: 10.1253/circj.CJ-15-0015

Cooper, L. L., Li, W., Lu, Y., Centracchio, J., Terentyeva, R., Koren, G., et al. (2013). Redox modification of ryanodine receptors by mitochondria-derived reactive oxygen species contributes to aberrant Ca2+ handling in ageing rabbit hearts. *J. Physiol.* 591(Pt 23), 5895–5911. doi: 10.1113/jphysiol.2013.260521

Csordás, G., Thomas, A. P., and Hajnóczky, G. (2001). Calcium signal transmission between ryanodine receptors and mitochondria in cardiac muscle. *Trends Cardiovasc. Med.* 11, 269–275. doi: 10.1016/S1050-1738(01)00123-2

Csordás, G., Weaver, D., and Hajnóczky, G. (2018). Endoplasmic reticulum-mitochondrial contactology: structure and signaling functions. *Trends Cell Biol.* 28, 523–540. doi: 10.1016/j.tcb.2018.02.009

de Brito, O. M., and Scorrano, L. (2008). Mitofusin 2 tethers endoplasmic reticulum to mitochondria. *Nature* 456, 605–610. doi: 10.1038/nature07534

De La Fuente, S., Fernandez-Sanz, C., Vail, C., Agra, E. J., Holmstrom, K., Sun, J., et al. (2016). Strategic positioning and biased activity of the mitochondrial calcium uniporter in cardiac muscle. *J. Biol. Chem.* 28, 23343–23362. doi: 10.1074/jbc.M116.755496

De Stefani, D., Raffaello, A., Teardo, E., Szabò, I., and Rizzuto, R. (2011). A forty-kilodalton protein of the inner membrane is the mitochondrial calcium uniporter. *Nature* 476, 336–340. doi: 10.1038/nature10230

Dedkova, E. N., and Blatter, L. A. (2008). Mitochondrial Ca2+ and the heart. *Cell Calcium* 44, 77–91. doi: 10.1016/j.ceca.2007.11.002

Dedkova, E. N., and Blatter, L. A. (2013). Calcium signaling in cardiac mitochondria. *J. Mol. Cell. Cardiol.* 58, 125–133. doi: 10.1016/j.yjmcc.2012.12.021

Dietl, A., and Maack, C. (2017). Targeting mitochondrial calcium handling and reactive oxygen species in heart failure. *Curr. Heart Fail. Rep.* 14, 338–349. doi: 10.1007/s11897-017-0347-7

DiPilato, L. M., Cheng, X., and Zhang, J. (2004). Fluorescent indicators of cAMP and Epac activation reveal differential dynamics of cAMP signaling within discrete subcellular compartments. *Proc. Natl. Acad. Sci. U.S.A.* 23, 16513–16518. doi: 10.1073/pnas.0405973101

Dorn, G. W., and Maack, C. (2013). SR and mitochondria: calcium cross-talk between kissing cousins. *J. Mol. Cell. Cardiol.* 55, 42–49. doi: 10.1016/j.yjmcc.2012.07.015

Dorn, G. W., and Scorrano, L. (2010). Two close, too close: sarcoplasmic reticulum-mitochondrial crosstalk and cardiomyocyte fate. *Circ. Res.* 107, 689–699. doi: 10.1161/CIRCRESAHA.110.225714

Dorn, G. W., Song, M., and Walsh, K. (2015). Functional implications of mitofusin 2-mediated mitochondrial-SR tethering. *J. Mol. Cell. Cardiol.* 78, 123–128. doi: 10.1016/j.yjmcc.2014.09.015

Drago, I., De Stefani, D., Rizzuto, R., and Pozzan, T. (2012). Mitochondrial Ca2+ uptake contributes to buffering cytoplasmic Ca2+ peaks in cardiomyocytes. *Proc. Natl. Acad. Sci. U.S.A.* 109, 12986–12991. doi: 10.1073/pnas.1210718109

Eisner, D. A., Caldwell, J. L., Kistamás, K., and Trafford, A. W. (2017). Calcium and excitation- contraction coupling in the heart. *Circ. Res.* 121, 181–195. doi: 10.1161/CIRCRESAHA.117.310230

Eisner, V., Csordás, G., and Hajnóczky, G. (2013). Interactions between sarco-endoplasmic reticulum and mitochondria in cardiac and skeletal muscle -

pivotal roles in Ca^{2}+ and reactive oxygen species signaling. *J. Cell Sci.* 126(Pt 14), 2965–2978. doi: 10.1242/jcs.093609

Elrod, J. W., Wong, R., Mishra, S., Vagnozzi, R. J., Sakthievel, B., Goonasekera, S. A., et al. (2010). Cyclophilin D controls mitochondrial pore-dependent Ca(2+) exchange, metabolic flexibility, and propensity for heart failure in mice. *J. Clin. Invest.* 120, 3680–3687. doi: 10.1172/JCI43171

Fernandez-Tenorio, M., and Niggli, E. (2018). Stabilization of Ca2+ signaling in cardiac muscle by stimulation of SERCA. *J. Mol. Cell Cardiol.* 119, 87–95. doi: 10.1016/j.yjmcc.2018.04.015

Filadi, R., Greotti, E., Turacchio, G., Luini, A., Pozzan, T., and Pizzo, P. (2015). Mitofusin 2 ablation increases endoplasmic reticulum-mitochondria coupling. *Proc. Natl. Acad. Sci. U.S.A.* 112, E2174–E2181. doi: 10.1073/pnas.1504880112

García-Pérez, C., Schneider, T. G., Hajnóczky, G., and Csordás, G. (2011). Alignment of sarcoplasmic reticulum-mitochondrial junctions with mitochondrial contact points. *Am. J. Physiol. Heart Circ. Physiol.* 301, H1907–H1915. doi: 10.1152/ajpheart.00397.2011

García-Rivas Gde, J., Carvajal, K., Correa, F., and Zazueta, C. (2006). Ru360, a specific mitochondrial calcium uptake inhibitor, improves cardiac post-ischaemic functional recovery in rats in vivo. *Br. J. Pharmacol.* 149, 829–837. doi: 10.1038/sj.bjp.0706932

Gordan, R., Fefelova, N., Gwathmey, J. K., and Xie, L. H. (2016). Involvement of mitochondrial permeability transition pore (mPTP) in cardiac arrhythmias: evidence from cyclophilin D knockout mice. *Cell Calcium* 60, 363–372. doi: 10.1016/j.ceca.2016.09.001

Griffiths, E. J., and Halestrap, A. P. (1993). Protection by cyclosporin a of ischemia/reperfusion- induced damage in isolated rat hearts. *J. Mol. Cell Cardiol.* 25, 1461–1469. doi: 10.1006/jmcc.1993.1162

Györke, S., and Carnes, C. (2008). Dysregulated sarcoplasmic reticulum calcium release: potential pharmacological target in cardiac disease. *Pharmacol. Ther.* 119, 340–354. doi: 10.1016/j.pharmthera.2008.06.002

Hausenloy, D. J., Lim, S. Y., Ong, S. G., Davidson, S. M., and Yellon, D. M. (2010). Mitochondrial cyclophilin-D as a critical mediator of ischaemic preconditioning. *Cardiovasc. Res.* 88, 67–74. doi: 10.1093/cvr/cvq113

Hohendanner, F., Ljubojević, S., MacQuaide, N., Sacherer, M., Sedej, S., Biesmans, L., et al. (2013). Intracellular dyssynchrony of diastolic cytosolic [Ca^{2+}] decay in ventricular cardiomyocytes in cardiac remodeling and human heart failure. *Circ. Res.* 113, 527–538. doi: 10.1161/CIRCRESAHA.113.300895

Hüser, J., and Blatter, L. A. (1999). Fluctuations in mitochondrial membrane potential caused by repetitive gating of the permeability transition pore. *Biochem. J.* 343(Pt 2), 311–317. doi: 10.1042/bj3430311

Joseph, L. C., Subramanyam, P., Radlicz, C., Trent, C. M., Iyer, V., Colecraft, H. M., et al. (2016). Mitochondrial oxidative stress during cardiac lipid overload causes intracellular calcium leak and arrhythmia. *Heart Rhythm.* 13, 1699–1706. doi: 10.1016/j.hrthm.2016.05.002

Keizer, J., and Smith, G. D. (1998). Spark-to-wave transition: saltatory transmission of calcium waves in cardiac myocytes. *Biophys. Chem.* 5, 87–100. doi: 10.1016/S0301-4622(98)00125-2

Kim, T. Y., Kunitomo, Y., Pfeiffer, Z., Patel, D., Hwang, J., Harrison, K., et al. (2015). Complex excitation dynamics underlie polymorphic ventricular tachycardia in a transgenic rabbit model of long QT syndrome type 1. *Heart Rhythm.* 12, 220–228. doi: 10.1016/j.hrthm.2014.10.003

Kim, T. Y., Terentyeva, R., Roder, K. H., Li, W., Liu, M., Greener, I., et al. (2017). SK channel enhancers attenuate Ca2+-dependent arrhythmia in hypertrophic hearts by regulating mito-ROS-dependent oxidation and activity of RyR. *Cardiovasc. Res.* 113, 343–353. doi: 10.1093/cvr/cvx005

Kirichok, Y., Krapivinsky, G., and Clapham, D. E. (2004). The mitochondrial calcium uniporter is a highly selective ion channel. *Nature* 22, 360–364. doi: 10.1038/nature02246

Kobayashi, S., Yano, M., Suetomi, T., Ono, M., Tateishi, H., Mochizuki, M., et al. (2009). Dantrolene, a therapeutic agent for malignant hyperthermia, markedly improves the function of failing cardiomyocytes by stabilizing interdomain interactions within the ryanodine receptor. *J. Am. Coll. Cardiol.* 53, 1993–2005. doi: 10.1016/j.jacc.2009.01.065

Kolhaas, M., Liu, T., Knopp, A., Zeller, T., Ong, M. F., Böhm, M., et al. (2010). Elevated cytosolic Na+ increases mitochondrial formation of reactive oxygen species in failing cardiac myocytes. *Circulation* 121, 1606–1613. doi: 10.1161/CIRCULATIONAHA.109.914911

Kwong, J. Q., Lu, X., Correll, R. N., Schwanekamp, J. A., Vagnozzi, R. J., Sargent, M. A., et al. (2015). The mitochondrial calcium uniporter selectively matches metabolic output to acute contractile stress in the heart. *Cell Rep.* 12, 15–22. doi: 10.1016/j.celrep.2015.06.002

Kyrychenko, S., Poláková, E., Kang, C., Pocsai, K., Ullrich, N. D., Niggli, E., et al. (2013). Hierarchical accumulation of RyR post-translational modifications drives disease progression in dystrophic cardiomyopathy. *Cardiovasc. Res.* 97, 666–675. doi: 10.1093/cvr/cvs425

Landstrom, A. P., Dobrev, D., and Wehrens, X. H. T. (2017). Calcium signaling and cardiac arrhythmias. *Circ. Res.* 120, 1969–1993. doi: 10.1161/CIRCRESAHA.117.310083

Liu, T., Brown, D. A., and O'Rourke, B. (2010). Role of mitochondrial dysfunction in cardiac glycoside toxicity. *J. Mol. Cell Cardiol.* 49, 728–736. doi: 10.1016/j.yjmcc.2010.06.012

Liu, T., and O'Rourke, B. (2008). Enhancing mitochondrial Ca2+ uptake in myocytes from failing hearts restores energy supply and demand matching. *Circ. Res.* 103, 279–288. doi: 10.1161/CIRCRESAHA.108.175919

Liu, T., Takimoto, E., Dimaano, V. L., DeMazumder, D., Kettlewell, S., Smith, G., et al. (2014). Inhibiting mitochondrial Na+/Ca2+ exchange prevents sudden death in a Guinea pig model of heart failure. *Circ. Res.* 115, 44–54. doi: 10.1161/CIRCRESAHA.115.303062

Lopez-Crisosto, C., Pennanen, C., Vasquez-Trincado, C., Morales, P. E., Bravo-Sagua, R., Quest, A. F. G., et al. (2017). Sarcoplasmic reticulum-mitochondria communication in cardiovascular pathophysiology. *Nat. Rev. Cardiol.* 14, 342–360. doi: 10.1038/nrcardio.2017.23

Lu, X., Ginsburg, K. S., Kettlewell, S., Bossuyt, J., Smith, G. L., and Bers, D. M. (2013). Measuring local gradients of intramitochondrial [Ca(2+)] in cardiac myocytes during sarcoplasmic reticulum Ca(2+) release. *Circ. Res.* 112, 424–431. doi: 10.1161/CIRCRESAHA.111.300501

Luo, M., Guan, X., Luczak, E. D., Lang, D., Kutschke, W., Gao, Z., et al. (2013). Diabetes increases mortality after myocardial infarction by oxidizing CaMKII. *J. Clin. Invest.* 123, 1262–1274. doi: 10.1172/JCI65268

Luongo, T. S., Lambert, J. P., Gross, P., Nwokedi, M., Lombardi, A. A., Shanmughapriya, S., et al. (2017). The mitochondrial Na+/Ca2+ exchanger is essential for Ca2+ homeostasis and viability. *Nature* 545, 93–97. doi: 10.1038/nature22082

Luongo, T. S., Lambert, J. P., Yuan, A., Zhang, X., Gross, P., Song, J., et al. (2015). The mitochondrial calcium uniporter matches energetic supply with cardiac workload during stress and modulates permeability transition. *Cell Rep.* 12, 23–34. doi: 10.1016/j.celrep.2015.06.017

Lyon, A. R., Bannister, M. L., Collins, T., Pearce, E., Sepehripour, A. H., Dubb, S. S., et al. (2011). SERCA2a gene transfer decreases sarcoplasmic reticulum calcium leak and reduces ventricular arrhythmias in a model of chronic heart failure. *Circ. Arrhythm. Electrophysiol.* 4, 362–372. doi: 10.1161/CIRCEP.110.961615

Maack, C., Cortassa, S., Aon, M. A., Ganesan, A. N., Liu, T., and O'Rourke, B. (2006). Elevated cytosolic Na+ decreases mitochondrial Ca2+ uptake during excitation-contraction coupling and impairs energetic adaptation in cardiac myocytes. *Circ. Res.* 21, 172–182. doi: 10.1161/01.RES.0000232546.92777.05

Matlib, M. A., Zhou, Z., Knight, S., Ahmed, S., Choi, K. M., Krause-Bauer, J., et al. (1998). Ru360 specifically inhibits Ca2+ uptake into mitochondria in vitro and in situ in cardiac myocytes. *J. Biol. Chem.* 24, 10223–10231. doi: 10.1074/jbc.273.17.10223

Maxwell, J. T., and Blatter, L. A. (2012). Facilitation of cytosolic calcium wave propagation by local calcium uptake into the sarcoplasmic reticulum in cardiac myocytes. *J. Physiol.* 590, 6037–6045. doi: 10.1113/jphysiol.2012.239434

Maxwell, J. T., Domeier, T. L., and Blatter, L. A. (2012). Dantrolene prevents arrhythmogenic Ca2+ release in heart failure. *Am. J. Physiol. Heart Circ. Physiol.* 302, H953–H963. doi: 10.1152/ajpheart.00936.2011

Mochizuki, M., Yano, M., Oda, T., Tateishi, H., Kobayashi, S., Yamamoto, T., et al. (2007). Scavenging free radicals by low-dose carvedilol prevents redox-dependent Ca2+ leak via stabilization of ryanodine receptor in heart failure. *J. Am. Coll. Cardiol.* 24, 1722–1732. doi: 10.1016/j.jacc.2007.01.064

Montero, M., Lobatón, C. D., Hernández-Sanmiguel, E., Santodomingo, J., Vay, L., Moreno, A., et al. (2004). Direct activation of the mitochondrial calcium uniporter by natural plant flavonoids. *Biochem. J.* 384(Pt 1), 19–24. doi: 10.1042/BJ20040990

Moreau, B., and Parekh, A. B. (2009). Ca2+ -dependent inactivation of the mitochondrial Ca2+ uniporter involves proton flux through the ATP synthase. *Curr. Biol.* 18, 855–859. doi: 10.1016/j.cub.2008.05.026

Negretti, N., O'Neill, S. C., and Eisner, D. A. (1993). The relative contributions of different intracellular and sarcolemmal systems to relaxation in rat ventricular myocytes. *Cardiovasc. Res.* 27, 1826–1830. doi: 10.1093/cvr/27.10.1826

Niggli, E., Ullrich, N. D., Gutierrez, D., Kyrychenko, S., Poláková, E., and Shirokova, N. (2013). Posttranslational modifications of cardiac ryanodine receptors: Ca(2+) signaling and EC- coupling. *Biochim. Biophys. Acta* 1833, 866–875. doi: 10.1016/j.bbamcr.2012.08.016

O'Rourke, B., and Blatter, L. A. (2009). Mitochondrial Ca2+ uptake: tortoise or hare? *J. Mol. Cell. Cardiol.* 46, 767–774. doi: 10.1016/j.yjmcc.2008.12.011

O'Rourke, B., Cortassa, S., and Aon, M. (2005). Mitochondrial ion channels: gatekeepers of life and death. *Physiology* 20, 303–315. doi: 10.1152/physiol.00020.2005

Palty, R., Silverman, W. F., Hershfinkel, M., Caporale, T., Sensi, S. L., Parnis, J., et al. (2010). NCLX is an essential component of mitochondrial Na+/Ca2+ exchange. *Proc. Natl. Acad. Sci. U.S.A.* 107, 436–441. doi: 10.1073/pnas.0908099107

Pogwizd, S. M., and Bers, D. M. (2004). Cellular basis of triggered arrhythmias in heart failure. *Trends Cardiovasc. Med.* 14, 61–66. doi: 10.1016/j.tcm.2003.12.002

Ramay, H. R., Jafri, M. S., Lederer, W. J., and Sobie, E. A. (2010). Predicting local SR Ca(2+) dynamics during Ca(2+) wave propagation in ventricular myocytes. *Biophys. J.* 98, 2515–2523. doi: 10.1016/j.bpj.2010.02.038

Santulli, G., Xie, W., Reiken, S. R., and Marks, A. R. (2015). Mitochondrial calcium overload is a key determinant in heart failure. *Proc. Natl. Acad. Sci. U.SA.* 112, 11389–11394. doi: 10.1073/pnas.1513047112

Schweitzer, M. K., Wilting, F., Sedej, S., Dreizehnter, L., Dupper, N. J., Tian, Q., et al. (2017). Suppression of arrhythmia by enhancing mitochondrial Ca2+ uptake in catecholaminergic ventricular tachycardia models. *JACC Basic Transl. Sci.* 2, 737–747. doi: 10.1016/j.jacbts.2017.06.008

Seguchi, H., Ritter, M., Shizukuishi, M., Ishida, H., Chokoh, G., Nakazawa, H., et al. (2005). Propagation of Ca2+ release in cardiac myocytes: role of mitochondria. *Cell Calcium* 38, 1–9. doi: 10.1016/j.ceca.2005.03.004

Seidlmayer, L. K., Kuhn, J., Berbner, A., Arias-Loza, P. A., Williams, T., Kaspar, M., et al. (2016). Inositol 1,4,5-trisphosphate-mediated sarcoplasmic reticulum-mitochondrial crosstalk influences adenosine triphosphate production via mitochondrial Ca2+ uptake through the mitochondrial ryanodine receptor in cardiac myocytes. *Cardiovasc. Res.* 112, 491–501. doi: 10.1093/cvr/cvw185

Sharma, V. K., Ramesh, V., Franzini-Armstrong, C., and Sheu, S. S. (2000). Transport of Ca2+ from sarcoplasmic reticulum to mitochondria in rat ventricular myocytes. *J. Bioenerg. Biomembr.* 32, 97–104. doi: 10.1023/A:1005520714221

Shkryl, V. M., and Shirokova, N. (2006). Transfer and tunneling of Ca2+ from sarcoplasmic reticulum to mitochondria in skeletal muscle. *J. Biol. Chem.* 20, 1547–1554. doi: 10.1074/jbc.M505024200

Sobie, E. A., Song, L. S., and Lederer, W. J. (2005). Local recovery of Ca2+ release in rat ventricular myocytes. *J. Physiol.* 565(Pt 2), 441–447. doi: 10.1113/jphysiol.2005.086496

Stowe, D. F., Aldakkak, M., Camara, A. K., Riess, M. L., Heinen, A., Varadarajan, S. G., et al. (2006). Cardiac mitochondrial preconditioning by Big Ca2+-sensitive K+ channel opening requires superoxide radical generation. *Am. J. Physiol. Heart Circ. Physiol.* 290, H434–H440. doi: 10.1152/ajpheart.00763.2005

Szalai, G., Csordás, G., Hantash, B. M., Thomas, A. P., and Hajnóczky, G. (2000). Calcium signal transmission between ryanodine receptors and mitochondria. *J. Biol. Chem.* 19, 15305–15313. doi: 10.1074/jbc.275.20.15305

Szentesi, P., Pignier, C., Egger, M., Kranias, E. G., and Niggli, E. (2004). Sarcoplasmic reticulum Ca2+ refilling controls recovery from Ca2+-induced Ca2+ release refractoriness in heart muscle. *Circ. Res.* 15, 807–813. doi: 10.1161/01.RES.0000146029.80463.7d

Terentyev, D., Belevych, A. E., Terentyeva, R., Martin, M. M., Malana, G. E., Kuhn, D. E., et al. (2009). miR-1 overexpression enhances Ca(2+) release and promotes cardiac arrhythmogenesis by targeting PP2A regulatory subunit B56alpha and causing CaMKII- dependent hyperphosphorylation of RyR2. *Circ. Res.* 104, 514–521. doi: 10.1161/CIRCRESAHA.108.181651

Terentyev, D., Györke, I., Belevych, A. E., Terentyeva, R., Sridhar, A., Nishijima, Y., et al. (2008). Redox modification of ryanodine receptors contributes to sarcoplasmic reticulum Ca2+ leak in chronic heart failure. *Circ. Res.* 103, 1466–1472. doi: 10.1161/CIRCRESAHA.108.184457

Terentyev, D., Rochira, J. A., Terentyeva, R., Roder, K., Koren, G., and Li, W. (2014). Sarcoplasmic reticulum Ca^{2+} release is both necessary and sufficient for SK channel activation in ventricular myocytes. *Am. J. Physiol. Heart. Circ. Physiol.* 306, H738-H746. doi: 10.1152/ajpheart.00621.2013

Terentyev, D., Viatchenko-Karpinski, S., Valdivia, H. H., Escobar, A. L., and Györke, S. (2002). Luminal Ca2+ controls termination and refractory behavior of Ca2+-induced Ca2+ release in cardiac myocytes. *Circ. Res.* 6, 414–420. doi: 10.1161/01.RES.0000032490.04207.BD

Vay, L., Hernández-SanMiguel, E., Santo-Domingo, J., Lobatón, C. D., Moreno, A., Montero, M., et al. (2007). Modulation of Ca^{2+} release and Ca^{2+} oscillations in HeLa cells and fibroblasts by mitochondrial Ca^{2+} uniporter stimulation. *J. Physiol.* 580, 39–49. doi: 10.1113/jphysiol.2006.126391

Wagner, S., Rokita, A. G., Anderson, M. E., and Maier, L. S. (2013). Redox regulation of sodium and calcium handling. *Antioxid. Redox Signal.* 18, 1063–1077. doi: 10.1089/ars.2012.4818

Walsh, C., Barrow, S., Voronina, S., Chvanov, M., Petersen, O. H., and Tepikin, A. (2009). Modulation of calcium signalling by mitochondria. *Biochim. Biophys. Acta* 1787, 1374–1382. doi: 10.1016/j.bbabio.2009.01.007

Williams, G. S., Boyman, L., Chikando, A. C., Khairallah, R. J., and Lederer, W. J. (2013). Mitochondrial calcium uptake. *Proc. Natl. Acad. Sci. U.S.A.* 110, 10479–10486. doi: 10.1073/pnas.1300410110

Xie, A., Song, Z., Liu, H., Zhou, A., Shi, G., Wang, Q., et al. (2018). Mitochondrial Ca2+ influx contributes to arrhythmic risk in nonischemic cardiomyopathy. *J. Am. Heart Assoc.* 7:e007805. doi: 10.1161/JAHA.117.007805

Yan, Y., Liu, J., Wei, C., Li, K., Xie, W., Wang, Y., et al. (2008). Bidirectional regulation of Ca2+ sparks by mitochondria-derived reactive oxygen species in cardiac myocytes. *Cardiovasc. Res.* 15, 432–441. doi: 10.1093/cvr/cvm047

Yarana, C., Sripetchwandee, J., Sanit, J., Chattipakorn, S., and Chattipakorn, N. (2012). Calcium- induced cardiac mitochondrial dysfunction is predominantly mediated by cyclosporine A- dependent mitochondrial permeability transition pore. *Arch. Med. Res.* 43, 333–338. doi: 10.1016/j.arcmed.2012.06.010

Zhao, Z., Gordan, R., Wen, H., Fefelova, N., Zang, W. J., and Xie, L. H. (2013). Modulation of intracellular calcium waves and triggered activities by mitochondrial ca flux in mouse cardiomyocytes. *PLoS One* 8:e80574. doi: 10.1371/journal.pone.0080574

Zhou, L., Aon, M. A., Liu, T., and O'Rourke, B. (2011). Dynamic modulation of Ca2+ sparks by mitochondrial oscillations in isolated guinea pig cardiomyocytes under oxidative stress. *J. Mol. Cell. Cardiol.* 51, 632–639. doi: 10.1016/j.yjmcc.2011.05.007

Zima, A. V., and Blatter, L. A. (2006). Redox regulation of cardiac calcium channels and transporters. *Cardiovasc. Res.* 71, 310–321. doi: 10.1016/j.cardiores.2006.02.019

Zima, A. V., Bovo, E., Mazurek, S. R., Rochira, J. A., Li, W., and Terentyev, D. (2014). Ca handling during excitation-contraction coupling in heart failure. *Pflugers Arch.* 466, 1129–1137. doi: 10.1007/s00424-014-1469-3

Conflict of Interest Statement: The authors declare that the research was conducted in the absence of any commercial or financial relationships that could be construed as a potential conflict of interest.

frontiers in Physiology

ORIGINAL RESEARCH
published: 06 February 2019
doi: 10.3389/fphys.2019.00055

Role of Phosphatidylinositol 3-Kinase (PI3K), Mitogen-Activated Protein Kinase (MAPK), and Protein Kinase C (PKC) in Calcium Signaling Pathways Linked to the α_1-Adrenoceptor in Resistance Arteries

*Alejandro Gutiérrez, Cristina Contreras, Ana Sánchez and Dolores Prieto**

Departamento de Fisiología, Facultad de Farmacia, Universidad Complutense de Madrid, Madrid, Spain

OPEN ACCESS

Edited by:
Maria Fernandez-Velasco,
Hospital Universitario La Paz, Spain

Reviewed by:
Peter S. Reinach,
Wenzhou Medical University, China
Marta Gil-Ortega,
CEU San Pablo University, Spain

****Correspondence:***
Dolores Prieto
dprieto@ucm.es

Specialty section:
This article was submitted to Membrane Physiology and Membrane Biophysics, a section of the journal Frontiers in Physiology

Received: *17 September 2018*
Accepted: *17 January 2019*
Published: *06 February 2019*

Citation:
Gutiérrez A, Contreras C, Sánchez A and Prieto D (2019) Role of Phosphatidylinositol 3-Kinase (PI3K), Mitogen-Activated Protein Kinase (MAPK), and Protein Kinase C (PKC) in Calcium Signaling Pathways Linked to the α_1-Adrenoceptor in Resistance Arteries. Front. Physiol. 10:55. doi: 10.3389/fphys.2019.00055

Insulin resistance plays a key role in the pathogenesis of type 2 diabetes and is also related to other health problems like obesity, hypertension, and metabolic syndrome. Imbalance between insulin vascular actions via the phosphatidylinositol 3-Kinase (PI3K) and the mitogen activated protein kinase (MAPK) signaling pathways during insulin resistant states results in impaired endothelial PI3K/eNOS- and augmented MAPK/endothelin 1 pathways leading to endothelial dysfunction and abnormal vasoconstriction. The role of PI3K, MAPK, and protein kinase C (PKC) in Ca^{2+} handling of resistance arteries involved in blood pressure regulation is poorly understood. Therefore, we assessed here whether PI3K, MAPK, and PKC play a role in the Ca^{2+} signaling pathways linked to adrenergic vasoconstriction in resistance arteries. Simultaneous measurements of intracellular calcium concentration ($[Ca^{2+}]_i$) in vascular smooth muscle (VSM) and tension were performed in endothelium-denuded branches of mesenteric arteries from Wistar rats mounted in a microvascular myographs. Responses to $CaCl_2$ were assessed in arteries activated with phenylephrine (PE) and kept in Ca^{2+}-free solution, in the absence and presence of the selective antagonist of L-type Ca^{2+} channels nifedipine, cyclopiazonic acid (CPA) to block sarcoplasmic reticulum (SR) intracellular Ca^{2+} release or specific inhibitors of PI3K, ERK-MAPK, or PKC. Activation of α_1-adrenoceptors with PE stimulated both intracellular Ca^{2+} mobilization and Ca^{2+} entry along with contraction in resistance arteries. Both $[Ca^{2+}]_i$ and contractile responses were inhibited by nifedipine while CPA abolished intracellular Ca^{2+} mobilization and modestly reduced Ca^{2+} entry suggesting that α_1-adrenergic vasoconstriction is largely dependent Ca^{2+} influx through L-type Ca^{2+} channel and to a lesser extent through store-operated Ca^{2+} channels. Inhibition of ERK-MAPK did not alter intracellular Ca^{2+} mobilization but largely reduced L-type Ca^{2+} entry elicited by PE without altering vasoconstriction. The PI3K blocker LY-294002 moderately reduced intracellular Ca^{2+} release, Ca^{2+} entry and contraction induced by the α_1-adrenoceptor agonist, while PKC inhibition decreased PE-elicited Ca^{2+} entry and to a lesser extent contraction without affecting intracellular Ca^{2+} mobilization. Under

conditions of ryanodine receptor (RyR) blockade to inhibit Ca^{2+}-induced Ca^{2+}-release (CICR), inhibitors of PI3K, ERK-MAPK, or PKC significantly reduced $[Ca^{2+}]_i$ increases but not contraction elicited by high K^+ depolarization suggesting an activation of L-type Ca^{2+} entry in VSM independent of RyR. In summary, our results demonstrate that PI3K, ERK-MAPK, and PKC regulate Ca^{2+} handling coupled to the α_1-adrenoceptor in VSM of resistance arteries and related to both contractile and non-contractile functions. These kinases represent potential pharmacological targets in pathologies associated to vascular dysfunction and abnormal Ca^{2+} handling such as obesity, hypertension and diabetes mellitus, in which these signaling pathways are profoundly impaired.

Keywords: ERK-MAPK, PI3K, PKC, L-type Ca^{2+} channel, RyR, intracellular Ca^{2+} mobilization, α_1-adrenergic vasoconstriction, resistance arteries

INTRODUCTION

Insulin resistance plays a key role in the pathogenesis of type 2 diabetes and is also associated to other metabolic and cardiovascular abnormalities such as obesity, dyslipidemia and hypertension, jointly referred as to metabolic syndrome (Ford, 2005). Imbalance between insulin vascular actions via the phosphatidylinositol 3-Kinase (PI3K) and the mitogen activated protein kinase (MAPK) signaling pathways in insulin resistant states results in impaired endothelial vasodilator PI3K/eNOS/NO and augmented vasoconstrictor MAPK/endothelin 1 (ET1) pathways leading to endothelial dysfunction and exacerbated vasoconstriction (Kim et al., 2006; Prieto et al., 2013). However, altered Ca^{2+} homeostasis in the arterial wall usually underlies abnormal vasoconstriction and the vascular complications associated to metabolic disease, such as hypertension and coronary artery disease (Okon et al., 2005; Ford et al., 2010; Villalba et al., 2011).

Vascular smooth muscle (VSM) contraction is triggered by the elevation of free intracellular Ca^{2+} concentration $[Ca^{2+}]_i$ due to extracellular Ca^{2+} influx and/or Ca^{2+} release from intracellular stores in the sarcoplasmic reticulum (SR), followed by Ca^{2+}-calmodulin-dependent activation of myosin light chain (MLC) kinase (MLCK), MLC phosphorylation and actin/myosin crossbridges formation (Liu and Khalil, 2018). However, increases in force development at a given cytosolic Ca^{2+} concentration can also occur and hence a dissociation between $[Ca^{2+}]_i$, MLC phosphorylation and vasoconstriction mediated by Ca^{2+} sensitization mechanisms (Somlyo and Somlyo, 2003; Villalba et al., 2007). Ca^{2+} release from SR intracellular stores, Ca^{2+} entry through plasma membrane channels and Ca^{2+} sensitization mechanisms can differentially contribute to VSM contraction depending on the vasoconstrictor agonist and/or vessel size (Nobe and Paul, 2001; Villalba et al., 2007; Kitazawa and Kitazawa, 2012). Furthermore, relative contribution of protein kinases to Ca^{2+} handling coupled to receptor-mediated arterial vasoconstriction has also been reported to be size-dependent and thus, involvement of PKC and Rho kinase (RhoK) increase and decrease, respectively, with decreasing arterial size (Kitazawa and Kitazawa, 2012; Martinsen et al., 2012). Although kinases such as PKC and RhoK have traditionally been associated to Ca^{2+} sensitization mechanisms involved in smooth muscle contraction (Nobe and Paul, 2001; Somlyo and Somlyo, 2003; Villalba et al., 2007), increasing experimental evidence supports a role for protein kinase-mediated regulation of intracellular Ca^{2+} mobilization and Ca^{2+} entry mechanisms in VSM and cardiac myocytes (Ghisdal et al., 2003; Villalba et al., 2008; Smani et al., 2010), and differences between large/conductance and small/resistance arteries concerning the role of various kinases in Ca^{2+} handling have also been demonstrated (Kitazawa and Kitazawa, 2012; Martinsen et al., 2012).

Peripheral small arteries or resistance arteries, whose vasoconstrictor activity is under the sympathetic nervous control, play a key role in blood pressure regulation, hypertension being a common vascular complication in metabolic syndrome and insulin resistant states (Ford, 2005). Both impairment of the signaling pathways including MAPK, PI3K, and PKC in endothelial cells and altered Ca^{2+} handling in VSM have been reported to underlie abnormal vasoconstriction in metabolic disease (Okon et al., 2005; Kim et al., 2006; Villalba et al., 2011; Prieto et al., 2013). Since the role of MAPK, PI3K, and PKC in Ca^{2+} handling of resistance arteries is poorly understood, we assessed here whether these kinases are involved in Ca^{2+} signaling pathways linked to adrenergic vasoconstriction in resistance arteries.

MATERIALS AND METHODS

Animal Model

Animal care and experimental protocols conformed to the European Directive for the Protection of Animals Used for Scientific Purposes (European Union Directive 2010/63/EU) and were also supervised by the Animal Care and Use Committee Complutense University of Madrid. Male Wistar rats were housed at the Pharmacy School animal care facility under controlled suitable environmental conditions of temperature (24°C), lighting (12 h light/12 h dark cycle) and humidity (50–60%), and maintained on standard chow and water *ad libitum*. They were anesthetized with sodium pentobarbital (50 mg/kg, i.p.) and euthanized by decapitation and exsanguination at 12-weeks age.

Dissection and Mounting of Mesenteric Resistance Arteries

After animals were euthanized, the mesentery was quickly removed and placed on cold physiological saline solution (PSS) of the following composition (mM): NaCl 119, $NaHCO_3$ 25, KCl 4.7, KH_2PO_4 1.17, $MgSO_4$ 1.18, $CaCl_2$ 1.5, ethylenediaminetetraacetic acid 0.027 and glucose 11, continuously gassed with a mixture of 5% CO_2 /95% O_2 to maintain pH at 7.4. Mesenteric resistance arteries, third order branches of the superior mesenteric artery, were carefully dissected by removing the surrounding connective and fat tissue. Arterial segments were mounted in parallel in double microvascular myographs (Danish Myo Technology, DMT-Denmark) by inserting two 40 μm tungsten wires and equilibrated for 30 min in PSS at 37°C. The relationship between passive wall tension and internal circumference was determined for each individual artery. The arteries were set to an internal circumference (L_1) equal to 90% of that given by a transmural pressure of 100 mmHg for a relaxed vessel *in situ*, L_{100} ($L_1 = 0.9 \times L_{100}$) at which tension development is maximal (Mulvany and Halpern, 1977). At the beginning of each experiment, arteries were stimulated twice with (KPSS), similar to PSS except that NaCl was substituted for KCl on an equimolar basis, in order to test vessel viability. The endothelium was mechanically removed by inserting a human hair in the vessel lumen and guiding it back and forwards several times. The absence of functional endothelium was confirmed by lack of the relaxation to acetylcholine (10 μM). Arteries were chemically denervated by incubation with guanethidine (10 μM) for 45 min to inhibit adrenergic nerve endings.

Simultaneous Measurements of Intracellular Ca^{2+} ($[Ca^{2+}]_i$) and Tension

Simultaneous measurements of the intracellular calcium concentration ($[Ca^{2+}]_i$) and tension were performed by FURA-2 AM fluorescence in mesenteric resistance arteries as previously reported (Villalba et al., 2007). Arteries were incubated in the dark with 8 μM Fura-2 AM in PSS for 2 h at 37°C. The myograph chamber was mounted on a Zeiss inverted microscope equipped for dual excitation wavelength fluorimetry (Deltascan, Photon Technology). After loading, arteries were illuminated with alternating 340 and 380 nm light using a monochromator-based system (Deltascan, Photon Technology). Fluorescence emission was detected at 510 nm wavelength. The Ratio (R) F340/F380 was taken as a measure of $[Ca^{2+}]_i$. At the end of each experiment fluorescence not related to Ca^{2+} was measured by bathing the artery in PSS containing 25 mM $MnCl_2$ plus ionomycin (10 μM) to quench Ca^{2+}-insensitive signals and the values obtained were subtracted from those obtained throughout the experiment.

Experimental Procedures for the Functional Experiments

The role of ERK-MAPK, PI3K, and PKC kinases in Ca^{2+} handling of resistance arteries was assessed in endothelium-denuded arteries kept in Ca^{2+}-free medium. Arteries were exposed for 5 min to Ca^{2+}-free PSS (0 mM Ca^{2+}, 0.1 mM EGTA) to remove all extracellular Ca^{2+} available for contraction. The myograph solution was then replaced by "nominally Ca^{2+}-free PSS" (0 mM Ca^{2+}, 0 mM EGTA) and concentration-response curves (CRCs) for $CaCl_2$ (10 μM-3 mM) were performed in arteries activated with phenylephrine (PE, 10 μM), in the absence (controls) and presence of the selective blocker of L-type Ca^{2+} channels nifedipine (0.3 μM), the inhibitor of the Orai1—mediated Ca^{2+} entry Pyr6 (3 μM) or the specific inhibitors of ERK-MAPK (PD-98059, 3 μM), p38MAPK (SB-203580, 0.3 μM), PI3K (LY-294002, 3 μM) or PKC (GF-109203X, 0.1 μM). The effect of SR Ca^{2+} store depletion on Ca^{2+} entry and contraction stimulated by PE was assessed in arteries kept in nominally Ca^{2+}-free medium stimulated with 10 μM PE and then activated with a single Ca^{2+} concentration (1 mM), before and after SR Ca^{2+}ATPase (SERCA) inhibition with cyclopiazonic acid (CPA, 10 μM), and then treatment with CPA plus nifedipine. The combined effect of SR Ca^{2+} store depletion with CPA (10 μM) and inhibition of Orai1-mediated Ca^{2+} entry channels with Pyr6 (3 μM) was also examined on Ca^{2+} entry and vasoconstriction of mesenteric arteries stimulated with PE (10 μM).

The inhibitory effect of PD-98059 (3 μM), LY-294002 (3 μM), or GF-109203X (0.1 μM) on Ca^{2+} entry was also assessed in KPSS-depolarized arteries. After a first stimulation with KPSS, arteries were incubated with the inhibitors for at least 30 min before a second stimulation with KPSS was repeated. To evaluate the potential relationship between the PI3K, MAPK, and PKC pathways and the ryanodine receptor (RyR)-mediated Ca^{2+}-induced Ca^{2+}-release (CICR) mechanism in resistance arteries (Sánchez et al., 2018), RyR was blocked by incubation with 10 μM ryanodine for 25 min and then 1.5 mM $CaCl_2$ was added to arteries depolarized with Ca^{2+}-free high K^+ solution ($KPSS^0{}_0$). The effect of the selective inhibitors of ERK-MAPK, PI3K, or PKC was further assessed in arteries under conditions of RyR blockade.

Solutions and Drugs

Ca^{2+}-free PSS and Ca^{2+}-free KPSS solutions were similar to PSS and KPSS, respectively, except that $CaCl_2$ was replaced by 100 μM of EGTA, which was omitted when $CaCl_2$ was administered *("nominally Ca^{2+}-free solution,"* 0 mM Ca^{2+}, 0 mM EGTA). Acetylcholine, guanethidine, and phenylephrine were obtained from Sigma-Aldrich (Spain). All of them were dissolved in distilled water. Nifedipine, CPA, Pyr6 and kinase inhibitors (PD-98059, LY-294002, GF-109203X, and SB-203580) were obtained from Tocris Cookson (Bristol, United Kingdom). Stock solutions of Pyr6, PD-98059 and LY-294002 were made in distilled water, and those of CPA Pyr6, ryanodine, SB-203580, and GF-109203X in DMSO and further diluted in water. Nifedipine was initially dissolved in ethanol and further dilutions were made in distilled water.

Statistical Analysis

Results are expressed as either absolute values (units of R F340/F380 or Nm^{-1} of active tension) or as a percentage of the response to KPSS in each artery, as means ± SEM of 6–10 arteries (one artery from each animal). Arterial sensitivity to

agonists was expressed in terms of pEC_{50}, that was the negative value of log EC_{50}, EC_{50} being the concentration of agonist giving 50% of the maximal response or effect (Emax). Statistically significant differences between means were analyzed by using paired or unpaired Student's *t*-test where appropriate, or one-way ANOVA followed by Bonferroni's *post hoc* test for comparisons involving more than two groups. Probability levels lower than 5% ($P < 0.05$) were considered statistically significant. Calculations were made using a standard software package (GraphPad Prism 5.0, GraphPad Software, Inc., San Diego, CA, United States).

RESULTS

Ca^{2+} Signaling Mechanisms Coupled to the α_1-Adrenoceptor in Resistance Arteries

In order to assess the involvement of intracellular Ca^{2+} mobilization and Ca^{2+} entry mechanisms coupled to the α_1-adrenoceptor in resistance arteries, endothelium-denuded mesenteric arteries were kept in a nominally Ca^{2+}-free medium, stimulated with PE and further activated with increasing Ca^{2+} concentrations (**Figure 1A**). PE induced an initial rapid increase in VSM $[Ca^{2+}]_i$ and a simultaneous phasic contraction showing intracellular Ca^{2+} mobilization (**Figures 1A,C**), and a further sustained elevation of $[Ca^{2+}]_i$ along with vasoconstriction upon Ca^{2+} re-addition, indicative of VSM Ca^{2+} entry (**Figures 1A,B**). While there were no significant differences in the initial PE-induced $[Ca^{2+}]_i$ increases and contraction corresponding to intracellular Ca^{2+} mobilization (**Figure 1C**), PE-induced vasoconstriction upon Ca^{2+} re-addition was larger than the simultaneous sustained $[Ca^{2+}]_i$ increases (**Figure 1C**). Involvement of Ca^{2+} sensitization in the α_1-adrenoceptor-mediated vasoconstriction was further depicted by the steep slope of the $[Ca^{2+}]_i$ -tension relationship for PE, showing that large contractions are developed without parallel increases in $[Ca^{2+}]_i$ levels (**Figure 1D**).

Treatment with the blocker of L-type voltage-dependent Ca^{2+} channels nifedipine largely inhibited the $CaCl_2$ CCR in arteries stimulated with PE (**Figure 2A**), while the inhibitor of the Orai1—mediated Ca^{2+} entry Pyr6 only induced a moderate decrease of these responses (**Figure 2B**). Combined treatment with the SERCA inhibitor CPA to deplete SR Ca^{2+} stores plus the inhibitor of store-operated Ca^{2+} channels Pyr6 caused a larger inhibition of PE-induced vasoconstriction (**Figure 2B**). The effect of SR store depletion by treatment with CPA was further assessed on changes in $[Ca^{2+}]_i$ and contraction elicited by PE, in arteries kept in nominally Ca^{2+}-free medium and further stimulated with 1 mM Ca^{2+} (**Figures 2C,D**). CPA inhibited PE-induced intracellular Ca^{2+} mobilization and phasic contraction and reduced the sustained Ca^{2+} entry and vasoconstriction elicited by the α_1-adrenoceptor PE. The latter were abolished by combined treatment with CPA plus the blocker of the L-type voltage-dependent channels nifedipine (**Figures 2C,D**). These data demonstrate that α_1-adrenergic vasoconstriction is largely due to Ca^{2+} influx through L-type voltage-dependent Ca^{2+} channels and to lesser extent to Ca^{2+}release from the SR and store-operated Ca^{2+} entry.

PI3K Inhibition Decreased Intracellular Ca^{2+} Mobilization and Ca^{2+} Entry Induced by PE

Treatment with the PI3K inhibitor LY-294002 was used to evaluate whether PI3K is involved in Ca^{2+} entry, Ca^{2+} mobilization and/or Ca^{2+} sensitization coupled to the α_1-adrenoceptor in resistance arteries. This blocker moderately reduced both Ca^{2+} entry and vasoconstriction induced by PE (**Figures 3A,B** and **Table 1**), without affecting $[Ca^{2+}]_i$-contraction relationships for this agonist which suggests no changes in Ca^{2+} sensitization (**Figure 3C**). Interestingly, PI3K inhibition also reduced PE-induced intracellular Ca^{2+} mobilization and the associated phasic contraction (**Figures 3D,E**).

ERK-MAPK Inhibition Reduced Ca^{2+} Entry but Not Vasoconstriction Coupled to the α_1-Adrenoceptor

The effects of the inhibitor of ERK-MAPK PD-98059 on changes in VSM $[Ca^{2+}]_i$ and contraction in mesenteric resistance arteries kept in nominally Ca^{2+}-free medium and activated by PE (10 μM) before increasing $CaCl_2$ concentrations were added are shown in **Figure 4**. Treatment with PD-98059 largely reduced increases in $[Ca^{2+}]_i$ elicited by PE upon Ca^{2+} re-addition (**Figure 4A** and **Table 1**) without altering vasoconstriction (**Figure 4B** and **Table 1**). PE-induced contractions were not altered either by treatment with the p38MAPK inhibitor SB-203580 (0.3 μM) (**Supplementary Figure S1**). The relationship $[Ca^{2+}]_i$-contraction for PE was left-shifted upon ERK-MAPK kinase blockade in resistance arteries (**Figure 4C**), indicating decreased Ca^{2+} sensitization under conditions of ERK-MAPK blockade and suggesting Ca^{2+} entry through L-type channels not coupled to vasoconstriction and linked to ERK-MAPK kinase cascade in mesenteric resistance arteries. However, PD-98059 treatment did not affect PE-induced intracellular Ca^{2+} mobilization and contraction associated to the α_1-adrenergic stimulation (**Figures 4D,E**).

PKC Inhibition Reduced Ca^{2+} Entry and Contraction Elicited by PE

The PKC inhibitor GF-109203X was used to assess the involvement of PKC in Ca^{2+} handling coupled to the α_1-adrenoceptor in mesenteric resistance arteries. Treatment with GF-109203X reduced the increases in $[Ca^{2+}]_i$ and to a minor extent vasoconstriction induced by Ca^{2+} re-addition in arteries stimulated by PE kept in a nominally Ca^{2+}-free medium (**Figures 5A,B** and **Table 1**). Both Ca^{2+} sensitization (**Figure 5C**) and PE-induced intracellular Ca^{2+}mobilization and phasic contraction (**Figures 5D,E**) remained unaffected by PKC inhibition.

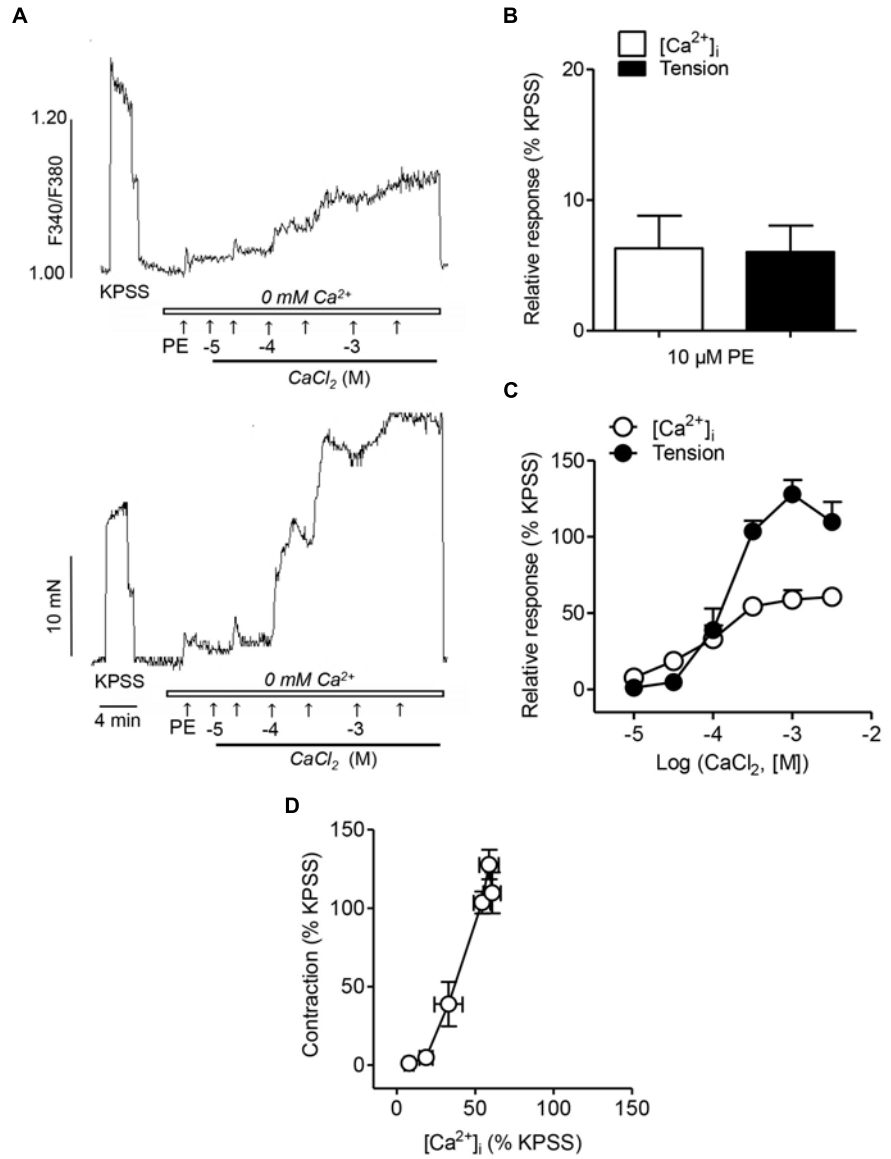

FIGURE 1 | α_1-Adrenoceptor activation involves intracelular Ca^{2+} mobilization, Ca^{2+} entry and Ca^{2+} sensitization associated to contraction **(A)** Representative traces illustrating the changes in both $[Ca^{2+}]_i$ mobilization (top) and vasoconstriction (bottom) induced by activation of α_1-adrenoceptors by a single dose of Phenylephrine (PE) (10 μM) and further cumulative addition of $CaCl_2$ (closed bar) in endothelium-denuded mesenteric arteries kept in nominally Ca^{2+}-free medium (0 mM Ca^{2+}, open bar). **(B,C)** Summarized data showing changes in $[Ca^{2+}]_i$ and vasoconstrictor responses stimulated by 10 μM PE addition in arteries kept in nominally Ca^{2+}-free medium **(B)** and further cumulative re-addition of $CaCl_2$ **(C)**. **(D)** Relationship between $[Ca^{2+}]_i$-contraction in response to cumulative addition of Ca^{2+} in arteries kept in Ca^{2+} free medium and stimulated with 10 μM PE. Responses are expressed as absolute values of either $[Ca^{2+}]_i$ ($\Delta F_{340}/F_{380}$) or tension (Nm^{-1}) **(A)** or relative to those elicited by KPSS **(B–D)**. Values are means ± SEM of $n = 7$ arteries (one from each animal).

Inhibition of ERK-MAPK, PI3K, and PKC Pathways Reduced L-Type Ca^{2+} Channel-Mediated $[Ca^{2+}]_i$ Increases Independently of RyR

Since $[Ca^{2+}]_i$ changes coupled to the α_1-adrenoceptor in resistance arteries are largely due to Ca^{2+} entry through L-type Ca^{2+} channels, the effects of PD-98059, LY-294002, and GF-109203X were tested on the increase in $[Ca^{2+}]_i$ elicited by high K^+ depolarization in order to assess whether the modulatory effect of ERK-MAPK, PI3K, and PKC on Ca^{2+} entry elicited by PE is exerted through L-type Ca^{2+} channels. Treatment with PD-98059, LY-294002, or GF-109203X reduced Ca^{2+} entry stimulated by KPSS (**Supplementary Figures S2A–C**) suggesting that these kinases regulate L-type Ca^{2+} channel entry in resistance arteries.

RyR-mediated Ca^{2+}-induced Ca^{2+}-release (CICR) upon L-type channel activation has recently been shown in VSM of mesenteric resistance arteries (Sánchez et al., 2018), and therefore we further assessed the potential relationship

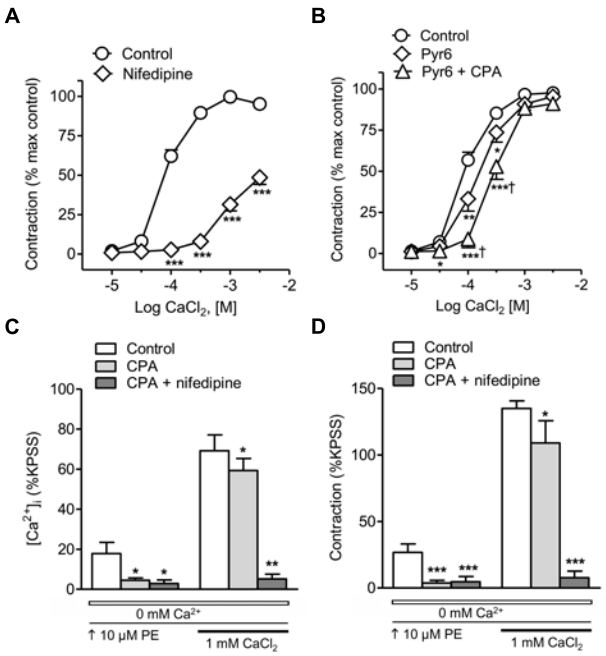

FIGURE 2 | α_1-Adrenoceptor-elicited vasoconstriction in resistance arteries is mostly due to Ca^{2+} entry through voltage-dependent L-type channels. **(A,B)** Average inhibitory effects of the selective L-type Ca^{2+} channel blocker nifedipine (0.3 μM) **(A)** or the inhibitor of the Orai1–mediated Ca^{2+} entry Pyr6 (3 μM) alone or in combination with the SERCA inhibitor CPA (10 μM) **(B)** on the $CaCl_2$ concentration-response curves (CRCs) in endothelium-denuded mesenteric resistance arteries kept in nominally Ca^{2+}-free medium and stimulated with 10 μM PE. **(C,D)** Summarized data showing the effects of SR Ca^{2+} store depletion by SERCA inhibition with CPA (10 μM) alone or CPA plus nifedipine (0.3 μM) on the changes in $[Ca^{2+}]_i$ **(C)** and contraction **(D)** in response to 10 μM PE in resistance arteries kept in a nominally Ca^{2+}-free medium (0 mM Ca^{2+}, open bar) after Ca^{2+} readmission (1 mM $CaCl_2$, closed bar). Results are expressed as a percentage of control maximal responses **(A,B)** or the KPSS responses **(C,D)**. Values are means ± SEM of $n = 6$ arteries (one from each animal). $^*P < 0.05$, $^{**}P < 0.01$, $^{***}P < 0.001$ vs. control. $^{\dagger}P < 0.05$ vs. Pyr6-treated.

between PI3K, PKC, and MAPK pathways and RyR-mediated CICR mechanism. Treatment with ryanodine (10 μM) to selectively block the RyR (Meissner, 2017) and the subsequent SR Ca^{2+} mobilization and amplification of Ca^{2+} entry through L-type channels, reduced nifedipine-sensitive increases in $[Ca^{2+}]_i$ and contraction elicited by Ca^{2+} readdition in high K^+-depolarized endothelium-denuded arteries (**Figures 6A,B**), thus confirming CICR upon L-type channel activation. On the other hand, in ryanodine-treated arteries to block CICR, selective inhibition of MAPK with PD-98059 (**Figures 6C,D**), PI3K with LY-294002 (**Figure 6E**) or PKC with GF-109203X (**Figure 6F**) resulted in a further significant reduction of the increases in $[Ca^{2+}]_i$ but not contraction elicited by Ca^{2+} re-addition in high K^+-depolarized arteries, thus demonstrating a direct stimulatory effect of MAPK, PI3K, and PKC on L-type Ca^{2+} entry independent of RyR mechanisms.

DISCUSSION

An increasing body of experimental evidence during the last decade gives support to a key role for protein kinase-mediated regulation of Ca^{2+} handling in arterial and cardiac myocytes, through phosphorylation of channels involved in either Ca^{2+} entry through plasma membrane or Ca^{2+} release from SR intracellular stores. The present study provides new insights into the modulation of Ca^{2+} handling by PI3K, MAPK, and PKC signaling pathways coupled to the α_1–adrenoceptor in resistance arteries and linked to both contractile and non-contractile functions. A graphical summary of our findings is depicted in **Figure 7**.

Hypertension and augmented vasoconstriction associated to metabolic disease have traditionally been ascribed to protein kinase-mediated Ca^{2+} sensitization of the VSM contractile machinery leading to increased vascular tone and systemic vascular resistance (Martínez et al., 2000; Naik et al., 2006; Villalba et al., 2007, 2011; Crestani et al., 2017). However, Ca^{2+} signaling mechanisms and the relative contribution of Ca^{2+} sensitization and Ca^{2+} mobilization mechanisms to arterial contraction are size-dependent. Thus, sensitivity of vasoconstriction and $[Ca^{2+}]_i$ changes induced by α_1-adrenoceptor activation to pharmacological inhibitors of voltage-dependent L-type Ca^{2+} entry is higher in resistance arteries compared to large conductance arteries (Prieto et al., 1991; Kitazawa and Kitazawa, 2012; Martinsen et al., 2012). Moreover, contractions of large arteries have been reported to involve kinases such as RhoK and PKC to varying degrees, while vasoconstriction of resistance arteries seem to be mediated exclusively by PKC (Budzyn et al., 2006; Kitazawa and Kitazawa, 2012). The present results confirm early studies demonstrating the involvement of Ca^{2+} sensitization mechanisms in the noradrenergic vasoconstriction of small mesenteric arteries (Buus et al., 1998; Kitazawa and Kitazawa, 2012), but further demonstrate that PI3K, MAPK, and PKC are involved in the regulation of Ca^{2+} entry and intracellular Ca^{2+} mobilization coupled to α_1-adrenoceptor activation in resistance arteries.

The PI3K/Akt signaling pathway is stimulated upon activation of the insulin receptor in the vascular endothelium and coupled to eNOS phosphorylation, NO production and vasodilatation. This pathway is impaired and associated to endothelial dysfunction in insulin resistant states (Kim et al., 2006; Contreras et al., 2010). However, PI3Ks play also a main role in the Ca^{2+} signaling of neurons and cardiac and vascular myocytes (Viard et al., 2004; Ghigo et al., 2017). In VSM, PI3Ks have been involved in the regulation of L-type Ca^{2+} entry in response to vasoconstrictors and growth factors (Macrez et al., 2001; Le Blanc et al., 2004) but also in the Ca^{2+}-dependent Rho-mediated negative control of MLCP linked to Ca^{2+} sensitization and contraction (Wang et al., 2006). In the present study, pharmacological inhibition of PI3K moderately reduced both Ca^{2+} entry and vasoconstriction elicited by PE in resistance arteries, without affecting the relationship Ca^{2+}-tension for the α_1-adrenergic agonist indicative of changes in Ca^{2+} sensitization. These findings are consistent with earlier studies

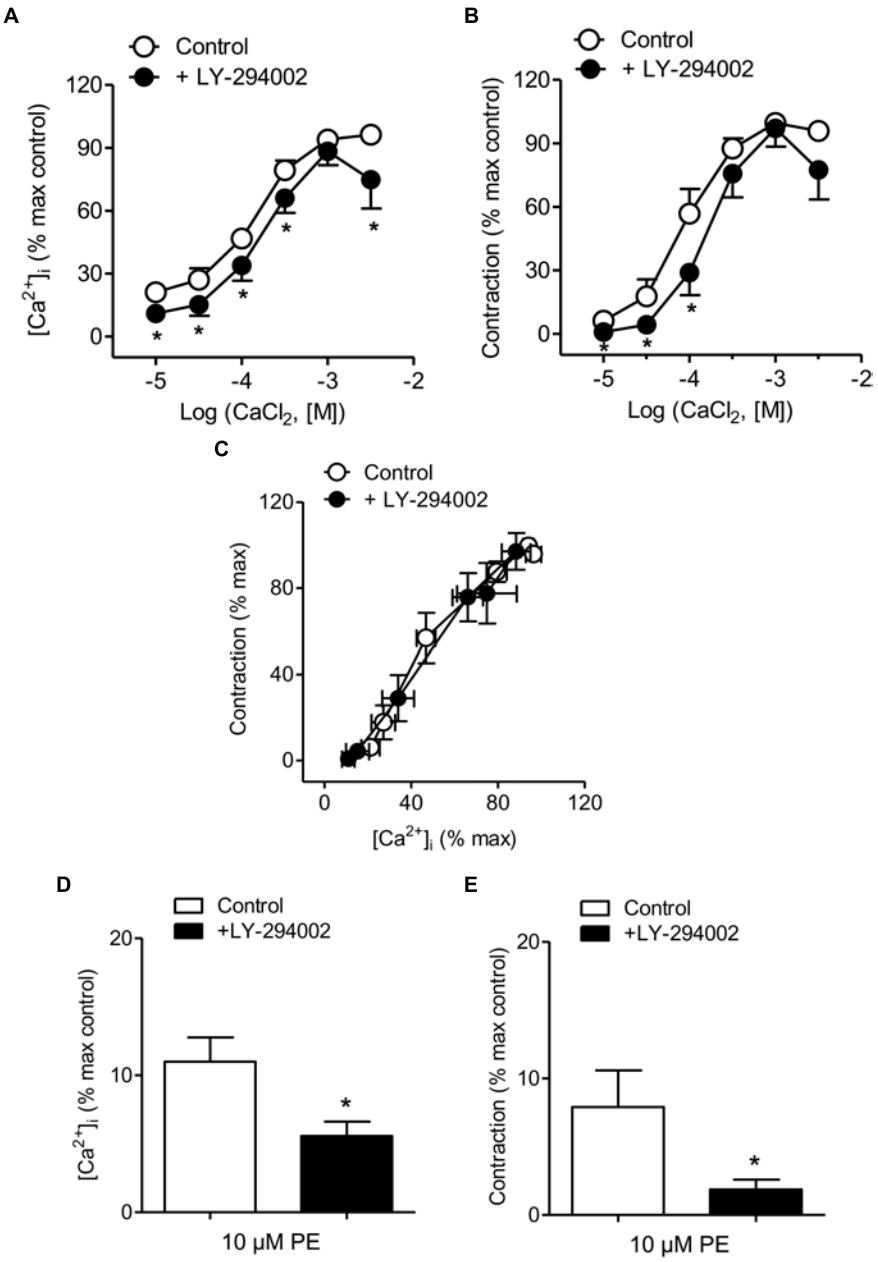

FIGURE 3 | PI3K inhibition reduced Ca^{2+} entry, vasoconstriction and intracellular Ca^{2+} mobilization in response to α_1-adrenoceptor activation. **(A,B)** Summarized data showing the effects of the PI3K inhibitor LY-294002 (3 μM) on the increases in $[Ca^{2+}]_i$ **(A)** and contraction **(B)** elicited by cumulative addition of $CaCl_2$ in endothelium-denuded arteries kept in a nominally Ca^{2+}-free medium and stimulated by 10 μM PE. **(C)** Effect of LY-294002 on the $[Ca^{2+}]_i$-contraction relationship for 10 μM PE in mesenteric resistance arteries and **(D,E)** the increases in $[Ca^{2+}]_i$ and contraction elicited by 10 μM PE in nominally Ca^{2+}-free PSS. Results are expressed as a percentage of control maximal responses. Values are means ± SEM of n = 8 arteries (one from each animal). *$P < 0.05$ vs. control.

involving PI3K activation in the transduction pathways for the angiotensin II (AII)-induced Ca^{2+} responses and contraction in VSM (Le Blanc et al., 2004; Rakotoarisoa et al., 2006). In vascular myocytes, PI3Kγ isoform was initially shown to mediate AII-induced activation of L-type voltage-dependent Ca^{2+} currents, to increase $[Ca^{2+}]_i$ and elicit contraction (Quignard et al., 2001; Le Blanc et al., 2004; Rakotoarisoa et al., 2006). This is confirmed in the endothelium-denuded intact resistance arteries of the present study by the inhibitory effect of the PI3K blocker LY294002 on L-type Ca^{2+} entry elicited by high K^+ depolarization. PI3Kγ/Akt phosphorylates $Ca_v\beta_2$ and induces $Ca_v\alpha_1C$ translocation thus increasing L-type Ca^{2+} currents in arterial myocytes, and pharmacological inhibition PI3Kγ has vasodilator effects and reduces arterial blood pressure (Carnevale and Lembo, 2012). However, our results further demonstrate that PI3K inhibition markedly reduced intracellular Ca^{2+} release and

TABLE 1 | Effects of the inhibitors of PI3K LY-294002 (3 μM), ERK-MAPK kinase PD-98059 (3 μM) and PKC GF-109203X (0.1 μM) on the sensitivity and maximal responses of the $CaCl_2$ concentration-response curves in mesenteric arteries stimulated by PE (10 μM) in a Ca^{2+}-free medium.

	$[Ca^{2+}]_i$ (F_{340}/F_{380})			Tension (Nm^{-1})		
	pEC_{50}	E_{max}	*n*	pEC_{50}	Emax	*n*
Control	3.77 ± 0.06	0.34 ± 0.04	7	4.12 ± 0.09	4.73 ± 0.47	7
+ LY-294002	3.86 ± 0.04	0.25 ± 0.03*	7	3.79 ± 0.09**	4.81 ± 0.61	7
Control	3.85 ± 0.08	0.42 ± 0.06	7	3.78 ± 0.06	4.36 ± 0.33	7
+ PD-98059	3.71 ± 0.17	0.23 ± 0.06***	7	3.73 ± 0.24	4.24 ± 0.32	7
Control	3.96 ± 0.10	0.33 ± 0.04	8	3.91 ± 0.12	5.97 ± 0.63	8
+ GF-109203X	3.90 ± 0.13	0.25 ± 0.04*	8	3.93 ± 0.14	4.81 ± 0.69**	8

*Data are means ± SEM; "n" number of arteries (one per animal) from Wistar rats. Results are expressed as absolute values, as the increases in the intracellular Ca^{2+} concentration $[Ca^{2+}]_i$ (ratio F_{340}/F_{380}) and tension (Nm^{-1}) elicited by PE or $CaCl_2$. pEC_{50} is – log(EC_{50}), EC_{50} being the concentration of agonist giving 50% of the maximum effect (E_{max}). Significant differences were analyzed by paired Student's t-test. *P < 0.05; **P < 0.01; ***P < 0.001 vs. control.*

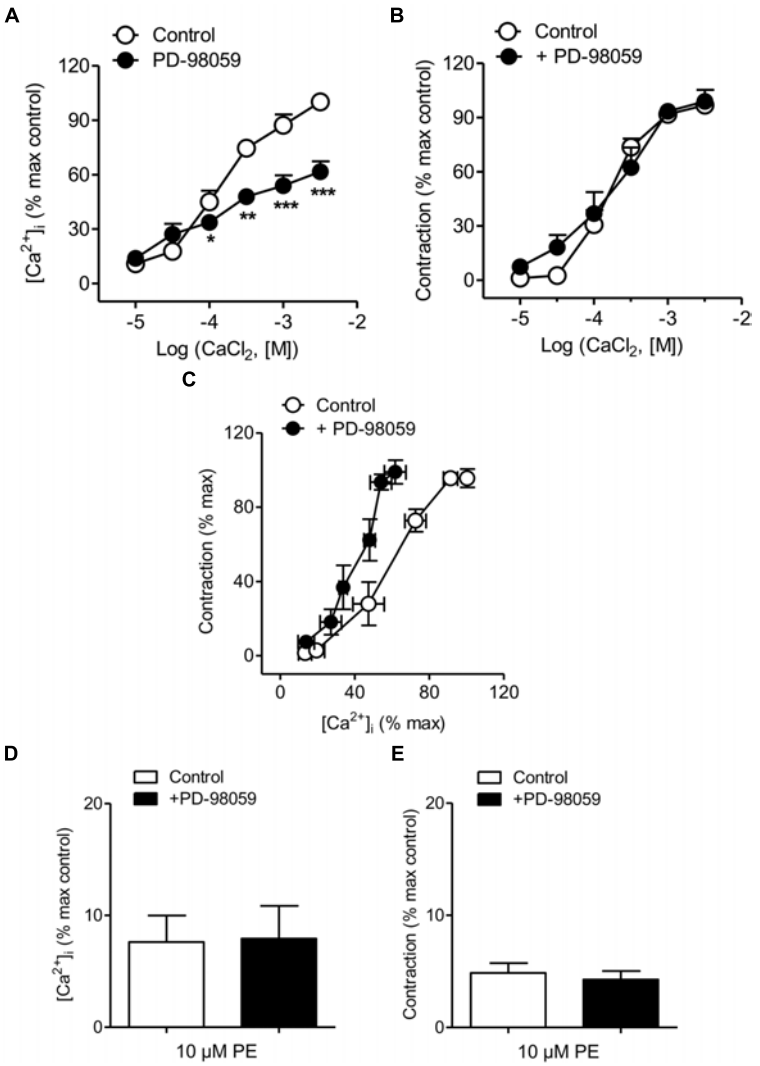

FIGURE 4 | ERK-MAPK inhibition reduced Ca^{2+} entry but not vasoconstriction and increased Ca^{2+} sensitization elicited by α_1-adrenoceptor activation. **(A,B)** Average effects of the ERK-MAPK inhibitor PD-98059 (3 μM) on the increases in $[Ca^{2+}]_i$ **(A)** and contraction **(B)** elicited by cumulative addition of $CaCl_2$ in endothelium-denuded arteries kept in a nominally Ca^{2+}-free medium and stimulated by 10 μM PE. **(C)** Effect of PD-98059 on the $[Ca^{2+}]_i$-contraction relationship for 10 μM PE in mesenteric resistance arteries and **(D,E)** on the increases in $[Ca^{2+}]_i$ and contraction elicited by 10 μM PE in Ca^{2+}-free PSS. Results are expressed as a percentage of control maximal responses. Values are means ± SEM of *n* = 7 arteries (one from each animal). **P* < 0.05, ***P* < 0.01, ****P* < 0.001 vs. control.

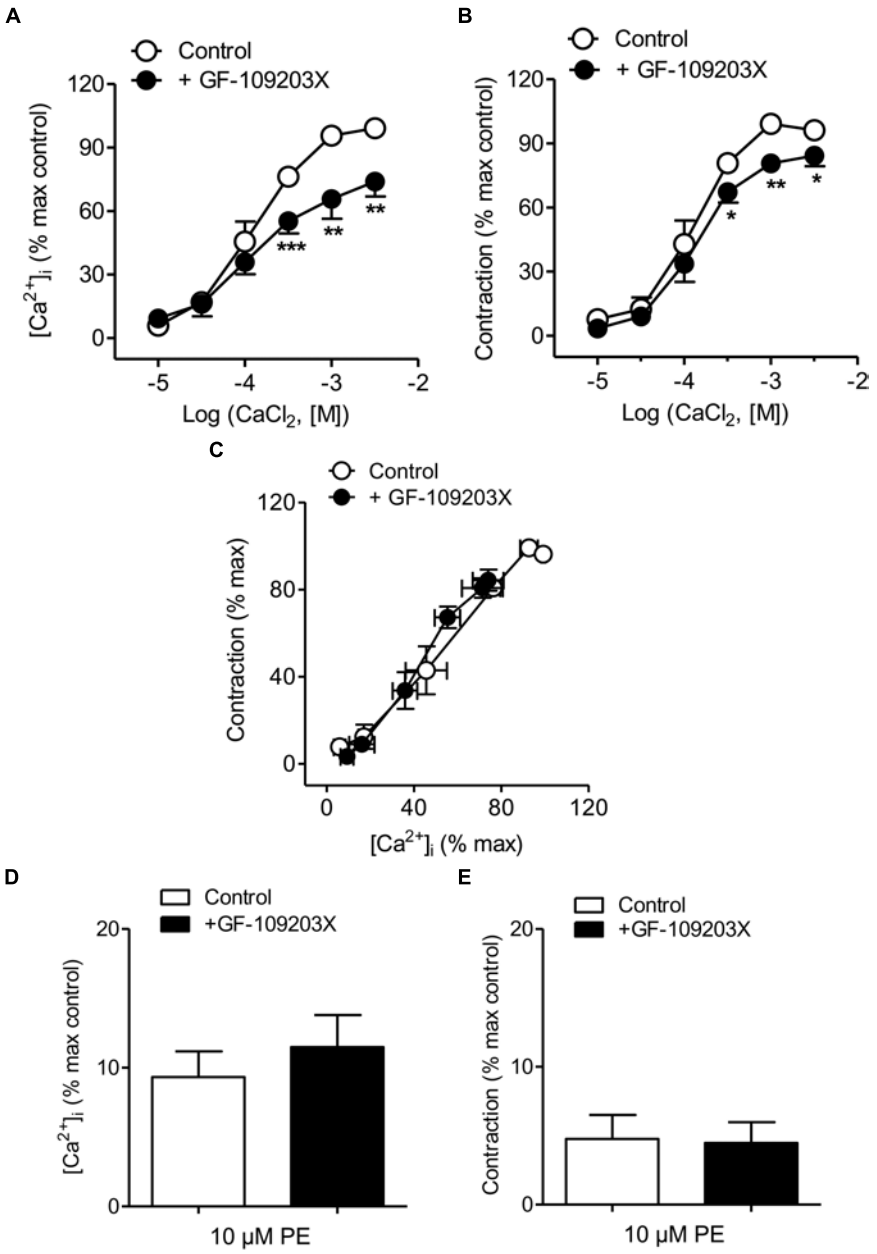

FIGURE 5 | PKC inhibition reduced Ca^{2+} entry and vasoconstriction without changing Ca^{2+} sensitization elicited by α_1-adrenoceptor activation. **(A,B)** Average effects of the PKC inhibitor GF-109203X (0.1 μM) on the increases in $[Ca^{2+}]_i$ **(A)** and contraction **(B)** elicited by cumulative addition of $CaCl_2$ in endothelium-denuded arteries kept in a Ca^{2+}-free medium and stimulated by 10 μM PE. **(C)** Effect of GF-109203X on the $[Ca^{2+}]_i$-contraction relationships for PE in mesenteric resistance arteries and **(D,E)** on the increases in $[Ca^{2+}]_i$ and contraction elicited by 10 μM PE in in Ca^{2+}-free PSS. Results are expressed as a percentage of control maximal responses. Values are means ± SEM of $n = 7$ arteries (one from each animal). $^*P < 0.05$, $^{**}P < 0.01$, $^{***}P < 0.001$ vs. control.

phasic contraction induced by PE in resistance arteries, which suggests that PI3K might also activate voltage-independent store-operated Ca^{2+} entry through stimulation of intracellular Ca^{2+} release. This pathway is linked to the α_1-adrenoceptor in resistance arteries, as depicted by the inhibitory effect on Ca^{2+} entry and contraction induced by SR depletion by blockade of SERCA with CPA, or by treatment with the store-operated Ca^{2+} entry blocker Pyr6 (Santiago et al., 2015).

α_1-Adrenoceptor stimulation causes intracellular Ca^{2+} mobilization via IP_3 receptor-mediated Ca^{2+} release from SR stores (Liu and Khalil, 2018). Therefore, it seems likely that the reduction of PE-induced intracellular Ca^{2+} mobilization by the PI3K blocker LY294002 to be due to the inhibition of PI3K-stimulated IP_3-dependent intracellular Ca^{2+} release, as earlier reported for the IGF-1 receptor linked to a G protein-PI3K-phospholipase C signaling pathway in cardiac myocytes

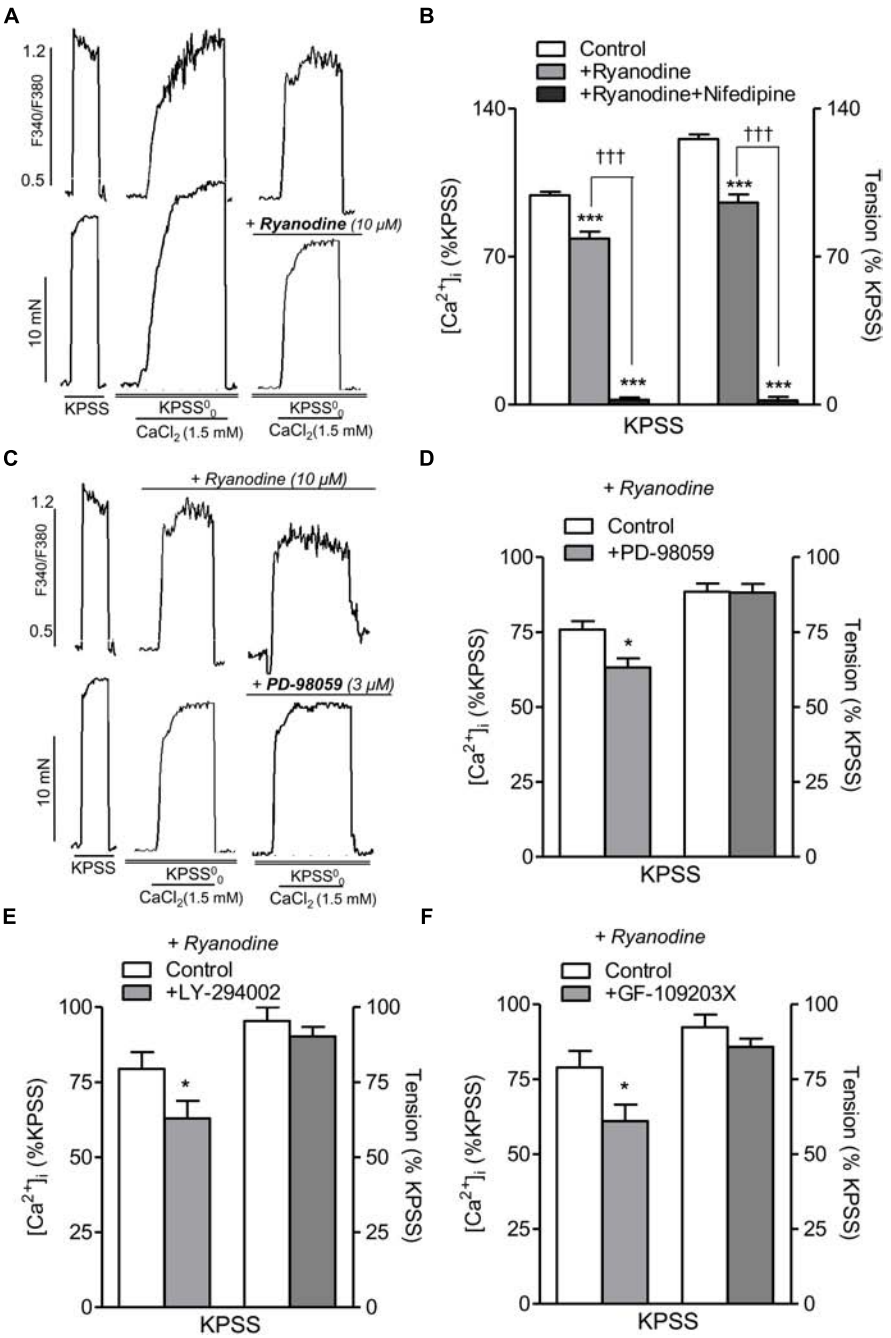

FIGURE 6 | Inhibition of ERK-MAPK, PI3K, or PKC kinase reduces intracelular Ca^{2+} mobilization elicited by voltage-dependent L-type Ca^{2+}channel activation independently of RyR-mediated Ca^{2+} release. **(A)** Representative traces showing the effects of ryanodine (10 μM) treatment on changes in both $[Ca^{2+}]_i$ (top) and vasoconstriction (bottom) induced by $CaCl_2$ (1.5 mM) re-addition in endothelium-denuded mesenteric arteries depolarized with high K^+ in Ca^{2+} free medium ($KPSS^0{}_0$). **(B)** Summarized data showing the average effects of ryanodine (10 μM) on changes in $[Ca^{2+}]_i$ and contraction elicited by $CaCl_2$ (1.5 mM) re-addition in arteries depolarized with a high K^+ solution. **(C)** Representative traces showing the effects of inhibition of MAPK with PD-98059 (3 μM) on changes in both $[Ca^{2+}]_i$ (top) and vasoconstriction (bottom) induced by $CaCl_2$ (1.5 mM) re-addition in endothelium-denuded mesenteric arteries depolarized with high K^+ ($KPSS^0{}_0$) and treated with ryanodine (30 μM) to block RyR. **(D)** Summarized data showing the average effects of PD-98059 (3 μM) on changes in $[Ca^{2+}]_i$ and vasoconstriction elicited by $CaCl_2$ (1.5 mM) re-addition in arteries depolarized with a high K^+ solution under conditions of RyR blockade with ryanodine. Average effects of the PI3K inhibitor LY-294002 (3 μM) **(E)** or the PKC inhibitor GF-109203X (0.1 μM) **(F)** on changes in $[Ca^{2+}]_i$ and vasoconstriction elicited by $CaCl_2$ (1.5 mM) re-addition in arteries depolarized with a high K^+ solution under conditions of RyR blockade. Responses are expressed as absolute values of either $[Ca^{2+}]_i$ ($\Delta F_{340}/F_{380}$) or tension (Nm^{-1}) **(A,C)** or relative to those elicited by KPSS **(B,D–F)**. Values are means ± SEM of $n = 5$ arteries (one from each animal). Significant differences were analyzed by paired Student's *t*-test or one-way ANOVA. $^*P < 0.05$ vs. control. $^{***}P < 0.001$ vs. control. $^{†††}P < 0.001$ vs. ryanodine-treated.

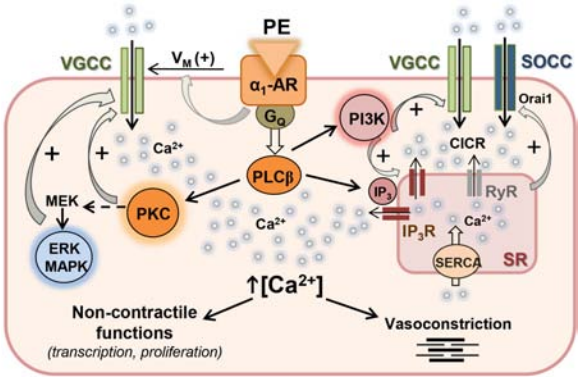

FIGURE 7 | Proposed mechanism for the regulation of Ca^{2+} handling by PI3K, MAPK, and PKC in resistance arteries VSM. Activation of α_1-adrenoceptor (α_1-AR) with phenylephrine (PE) is coupled to membrane depolarization (+Vm), stimulation of Ca^{2+} influx through L-type voltage-gated Ca^{2+} channels (VGCC) and vasoconstriction. α_1-AR is also coupled to PLCβ activation which stimulates Ca^{2+} release from sarcoplasmic reticulum (RS) Ca^{2+} store through IP_3 receptors (IP_3R), and also stimulates PKC which in turn activates the MEK-ERK MAPK intracellular signaling cascade. Both PKC and ERK MAPK can directly act on L-type VGCC and reinforce Ca^{2+} influx mostly related to non-contractile functions. α_1-AR is also coupled to PI3K activation and stimulation of both IP_3R-mediated Ca^{2+} release and Ca^{2+} entry through VGCC. Ca^{2+} influx through VGCC amplifies Ca^{2+} signal through the ryanodine receptor (RyR)-mediated Ca^{2+}-induced Ca^{2+} release (CICR). Emptying of the SR Ca^{2+} store leads to store-operated Ca^{2+} channel (SOCC) entry to refill empty store.

(Ibarra et al., 2004). However, we have recently demonstrated RyR-mediated CICR upon activation of L-type channels as a potent amplifying mechanism of Ca^{2+} entry and contraction in mesenteric resistance arteries (Sánchez et al., 2018). Since RyR1 and RyR2 can be phosphorylated by kinases such as PKA leading to SR Ca^{2+} leak (Bovo et al., 2017; Meissner, 2017), we further investigated whether PI3K may regulate RyR-mediated CICR stimulated by L-type Ca^{2+} channel activation. Under conditions of RyR blockade with ryanodine, selective PI3K inhibition with LY294002 significantly reduced increases $[Ca^{2+}]_i$ but not contraction elicited by high K^+ depolarization. Although RyR phosphorylation cannot be ruled out, the present finding suggest that PI3K activation mainly stimulates Ca^{2+} entry through direct regulation of L-type Ca^{2+} channels in resistance arteries, as discussed above and reported for isolated vascular myocytes (Le Blanc et al., 2004).

Enhanced activity of PI3K and up-regulation of PI3Kδ have been found to be associated to augmented L-type Ca^{2+} entry in arterial myocytes from rat models of type I diabetes (Pinho et al., 2010) and insulin resistance (Sánchez et al., 2018). While in the former PI3K contributed to enhanced vasoconstriction, in the latter PI3K-mediated increased Ca^{2+} entry compensated for SR Ca^{2+} store dysfunction. In the heart, PI3Kα/Akt signaling is involved in insulin inotropic actions and activates Ca^{2+} currents in microdomains containing L-type Ca^{2+} channels (Lu et al., 2009). This pathway and the corresponding L-type Ca^{2+} entry is defective in insulin-deficient and resistant states which might contribute to the cardiac contractile dysfunction in diabetic cardiomyopathy (Lu et al., 2007; Ghigo et al., 2017).

On the other hand, ERK1/2 MAPK pathway is involved in insulin mitogenic actions but has also been associated to insulin-mediated enhanced vasoconstriction in insulin resistant states (Kim et al., 2006; Contreras et al., 2010; Prieto et al., 2013). In the present study, the selective inhibitor of ERK-MAPK PD98059 did not alter the initial rapid Ca^{2+} increase in response to PE corresponding to intracellular Ca^{2+} mobilization, but caused a profound inhibition of the sustained Ca^{2+} entry stimulated by PE without altering the associated contraction in resistance arteries. These findings differ from earlier studies involving ERK-MAPK in both Ca^{2+}-dependent vasoconstriction coupled to the AII receptor in human resistance arteries (Touyz et al., 1999), and in Ca^{2+} sensitization-mediated contraction of coronary artery myocytes linked to the ET1 receptor (Cain et al., 2002). Moreover, the present results differ from reports involving the p38 and JNK limbs of the MAPK pathway in nifedipine-sensitive vasoconstriction linked to α-adrenoceptors in VSM of large arteries (Ok et al., 2011). In contrast, our results suggest a major role of MAPK in the regulation of L-type Ca^{2+} entry coupled to the α_1-adrenergic adrenoceptor in resistance arteries, supported by the marked reduction elicited by PD98059 on the high K^+ depolarization-induced Ca^{2+} entry under conditions of RyR receptor blockade. These findings are in agreement with reports showing that ERK MAPK phosphorylates $Ca_v1.2$ channels and enhances L-type currents in cardiac myocytes in response to growth factors involved in cardiac hypertrophy (Takahashi et al., 2004). Differences in the involvement of the ERK-MAPK in Ca^{2+} handling and contraction in vascular myocytes may be ascribed to the differential activation of this pathway by various receptors. Our results suggest that ERK-MAPK-mediated modulation of Ca^{2+} handling might be related to VSM non-contractile proliferative pathways coupled to the α_1-adrenoceptor in resistance arteries (Kudryavtseva et al., 2013). Further studies are needed to elucidate the role of receptor-coupled MAPK pathways as modulators of both L-type and non-L-type Ca^{2+} influx involved in cell proliferation.

In cardiac myocytes, ERK MAPK phosphorylation of $Ca_v1.2$ channels and increased L-type currents are activated upstream by PKC linked to activation of G protein-coupled receptors (Smani et al., 2010). The role of PKC in arterial Ca^{2+} handling and vasoconstriction is well-documented, although this kinase has mostly been involved in Ca^{2+} sensitization mechanisms coupled to the α_1-adrenoceptor in resistance arteries (Buus et al., 1998; Villalba et al., 2007; Kitazawa and Kitazawa, 2012). PKC phosphorylates the phosphoprotein CPI-17, a potent inhibitor of MLCP, rendering it inactive and therefore promoting increased vascular tone (Somlyo and Somlyo, 2003). However, in our study, the PKC inhibitor GF-109203X did not alter the initial Ca^{2+} rise but markedly reduced the sustained $[Ca^{2+}]_i$ increase in response to PE, and to a lesser extent the simultaneous vasoconstriction of mesenteric resistance arteries, which suggests a major role for PKC in the regulation of Ca^{2+} entry rather than in the enhancement of myofilament Ca^{2+} sensitivity of arterial myocytes, as also supported by the unchanged Ca^{2+}-tension relationship for the α_1-adrenergic agonist in presence of the

PKC inhibitor. Involvement of PKC in Ca^{2+} entry in resistance arteries partially agrees with that recently reported by Kitazawa and Kitazawa (2012). However, these authors showed that GF-109203X induced a small reduction of PE-induced Ca^{2+} entry, while it abolished vasoconstriction and reduced phosphorylation of MLC, CPI-17 and MYPT1, supporting a major involvement of PKC in Ca^{2+} sensitization. The discrepancies between our data showing a minor inhibitory effect of GF-109203X on Ca^{2+} sensitization coupled to PE vasoconstriction and those in the study by Kitazawa and Kitazawa (2012) might be ascribed to the fact that different PKC isoforms mediate Ca^{2+} sensitization and Ca^{2+} entry pathways in arterial smooth muscle (Liu and Khalil, 2018). Thus, the conventional Ca^{2+}-dependent PKC isoforms (α, -β1, -β2, and -γ) are activated by cytosolic Ca^{2+} and diacylglycerol, and in turn phosphorylate a wide array of substrates implicated in the regulation of Ca^{2+} fluxes; specifically, PKCα has been involved in the regulation of L-type Ca^{2+} entry in both vascular and cardiac myocytes (Yang et al., 2009; Gulia et al., 2013). In contrast, the novel PKC isoforms appear to mediate vasoconstriction coupled to Ca^{2+} sensitizing pathways (Liu and Khalil, 2018). GF-109203X is selective for the conventional PKCα and β1 isoforms but it may also inhibit the novel δ and ε PKC isoforms at the higher micromolar range used in the study of Kitazawa and Kitazawa (2012) and Liu and Khalil (2018).

In the present study, involvement of PKC in the sustained Ca^{2+} entry induced by PE and sensitive to L-type Ca^{2+} channel blockade is further supported by the marked inhibitory effect found for GF-109203X on the L-type channel-mediated Ca^{2+} entry elicited by high K^+ depolarization, thus suggesting that PKC modulates voltage-dependent L-type Ca^{2+} entry coupled to the α_1-adrenergic vasoconstriction in resistance arteries, and supporting that PKC-mediated modulation of L-type channels in arterial myocytes (Gulia et al., 2013) contributes not only to myogenic tone but also to agonist-induced vasoconstriction (Cobine et al., 2007; Potts et al., 2012). Activity of both conventional and novel PKC isoforms is chronically enhanced by hyperglycemia, lipotoxicity and oxidative stress, which has been associated to the cardiovascular complications in the insulin resistant states (Geraldes and King, 2010; Turban and Hajduch, 2011). Abnormal PKC activity contributes to the augmented arterial L-type Ca^{2+} entry and enhanced vasoconstriction in diabetic arteries (Ungvari et al., 1999) and arteries from genetically obese rats (Sánchez et al., 2018), and in the latter compensates for SR Ca^{2+} store dysfunction.

CONCLUSION

The present findings demonstrate that PI3K, MAPK, and PKC are involved in the regulation of Ca^{2+} entry and intracellular Ca^{2+} mobilization coupled to α_1-adrenoceptor activation in resistance arteries and mostly associated to non-contractile functions of VSM. Under conditions of vascular disease, vascular myocytes change from a contractile to a synthetic phenotype that is able to proliferate and migrate. The present results showing a protein kinase-mediated regulation of Ca^{2+} handling linked to the α_1-adrenoceptor in resistance arteries suggest that changes in PI3K, MAPK, and PKC signaling pathways involving enhanced Ca^{2+} mobilization not coupled to contraction, might participate in the changes toward a VSM proliferative phenotype and be involved in vascular remodeling in hypertension and other insulin resistant states. Further studies are needed to elucidate this issue.

AUTHOR CONTRIBUTIONS

DP conceived, designed, and discussed the experiments. AG and AS performed the experiments and analyzed the data. AG, AS, and DP wrote the manuscript. AG, CC, and AS contributed to discussion, and edited the manuscript.

FUNDING

This work was supported by grants SAF2012-31631 and SAF2016-77526R from MINECO (Spain) cofounded by the FEDER Program of EU.

ACKNOWLEDGMENTS

Manuel Perales and Francisco Puente are thanked for expert technical assistance.

SUPPLEMENTARY MATERIAL

The Supplementary Material for this article can be found online at: https://www.frontiersin.org/articles/10.3389/fphys.2019.00055/full#supplementary-material

FIGURE S1 | p38MAPK inhibition does not alter PE-induced vasososntriction. Average effects of the p38MAPK inhibitor SB-203580 (0.3 μM) on the contractions elicited by cumulative addition of $CaCl_2$ in endothelium-denuded arteries kept in a nominally Ca^{2+}-free medium and stimulated by 10 μM PE. Results are expressed as a percentage of control maximal responses. Values means ± SEM of $n = 6$ arteries (two from each animal).

FIGURE S2 | ERK-MAPK, PI3K, or PKC kinase inhibitors reduce Ca^{2+} entry through voltage-dependent L-type channels. Average inhibitory effects ERK-MAPK inhibitor PD-98059 (3 μM) **(A)**, the PI3K inhibitor LY-294002 (3 μM) **(B)** or the PKC inhibitor GF-109203X (0.1 μM) **(C)**, on the increases in $[Ca^{2+}]_i$ elicited by depolarization high K^+ (KPSS). Results are expressed as absolute values of $[Ca^{2+}]_i$ ($\Delta F_{340}/F_{380}$). Values are means ± SEM of five arteries (one from each animal). Significant differences were analyzed by paired Student's *t*-test; $^*P < 0.05$ vs. control.

REFERENCES

Bovo, E., Huke, S., Blatter, L. A., and Zima, A. V. (2017). The effect of PKA-mediated phosphorylation of ryanodine receptor on SR Ca2+ leak in ventricular myocytes. *J. Mol. Cell. Cardiol.* 104, 9–16. doi: 10.1016/j.yjmcc.2017.01.015

Budzyn, K., Paull, M., Marley, P. D., and Sobey, C. G. (2006). Segmental differences in the roles of rho-kinase and protein kinase C in mediating

vasoconstriction. *J. Pharmacol. Exp. Ther.* 317, 791–796. doi: 10.1124/jpet.105.100040

Buus, C. L., Aalkjaer, C., Nilsson, H., Juul, B., Moller, J. V., and Mulvany, M. J. (1998). Mechanisms of Ca2+ sensitization of force production by noradrenaline in rat mesenteric small arteries. *J. Physiol.* 510, 577–590. doi: 10.1111/j.1469-7793.1998.577bk.x

Cain, A. E., Tanner, D. M., and Khalil, R. A. (2002). Endothelin-1–induced enhancement of coronary smooth muscle contraction via MAPK-dependent and MAPK-independent [Ca(2+)](i) sensitization pathways. *Hypertension* 39, 543–549. doi: 10.1161/hy0202.103129

Carnevale, D., and Lembo, G. (2012). PI3Kγ in hypertension: a novel therapeutic target controlling vascular myogenic tone and target organ damage. *Cardiovasc. Res.* 95, 403–408. doi: 10.1093/cvr/cvs166

Cobine, C. A., Callaghan, B. P., and Keef, K. D. (2007). Role of L-type calcium channels and PKC in active tone development in rabbit coronary artery. *Am. J. Physiol. Heart Circ. Physiol.* 292, H3079–H3088. doi: 10.1152/ajpheart.01261.2006

Contreras, C., Sánchez, A., Martínez, P., Raposo, R., Climent, B., García-Sacristán, A., et al. (2010). Insulin resistance in penile arteries from a rat model of metabolic syndrome. *Br. J. Pharmacol.* 161, 350–364. doi: 10.1111/j.1476-5381.2010.00825.x

Crestani, S., Webb, R. C., and da Silva-Santos, J. E. (2017). High-salt intake augments the activity of the RhoA/rock pathway and reduces intracellular calcium in arteries from rats. *Am. J. Hypertens* 30, 389–399. doi: 10.1093/ajh/hpw201

Ford, E. S. (2005). Risks for all-cause mortality, cardiovascular disease, and diabetes associated with the metabolic syndrome: a summary of the evidence. *Diabetes Care* 28, 1769–1778. doi: 10.2337/diacare.28.7.1769

Ford, E. S., Zhao, G., and Li, C. (2010). Pre-diabetes and the risk for cardiovascular disease: a systematic review of the evidence. *J. Am. Cell. Cardiol.* 55, 1310–1317. doi: 10.1016/j.jacc.2009.10.060

Geraldes, P., and King, G. L. (2010). Activation of protein kinase C isoforms and its impact on diabetic complications. *Circ. Res.* 106, 1319–1331. doi: 10.1161/CIRCRESAHA.110.217117

Ghigo, A., Laffargue, M., Li, M., and Hirsch, E. (2017). PI3K and calcium signaling in cardiovascular disease. *Circ. Res.* 121, 282–292. doi: 10.1161/CIRCRESAHA.117.310183

Ghisdal, P., Vandenberg, G., and Morel, N. (2003). Rho-dependent kinase is involved in agonist-activated calcium entry in rat arteries. *J. Physiol.* 551, 855–867. doi: 10.1113/jphysiol.2003.047050

Gulia, J., Navedo, M. F., Gui, P., Chao, J. T., Mercado, J. L., Santana, L. F., et al. (2013). Regulation of L-type calcium channel sparklet activity by c-Src and PKC-α. *Am. J. Physiol. Cell. Physiol.* 305, C568–C577. doi: 10.1152/ajpcell.00381.2011

Ibarra, C., Estrada, M., Carrasco, L., Chiong, M., Liberona, J. L., Cardenas, C., et al. (2004). Insulin-like growth factor-1 induces an inositol 1,4,5-trisphosphate-dependent increase in nuclear and cytosolic calcium in cultured rat cardiac myocytes. *J. Biol. Chem.* 27, 7554–7565. doi: 10.1074/jbc.M311604200

Kim, J. A., Montagnani, M., Koh, K. K., and Kuon, M. J. (2006). Reciprocal relationships between insulin resistance and endothelial dysfunction: molecular and pathophysiological mechanisms. *Circulation* 113, 1888–1904. doi: 10.1161/CIRCULATIONAHA.105.563213

Kitazawa, T., and Kitazawa, K. (2012). Size-dependent heterogeneity of contractile Ca2+ sensitization in rat arterial smooth muscle. *J. Physiol.* 590, 5401–5423. doi: 10.1113/jphysiol.2012.241315

Kudryavtseva, O., Aalkjaer, C., and Matchkov, V. V. (2013). Vascular smooth muscle cell phenotype is defined by Ca2+-dependent transcription factors. *FEBS J.* 280, 5488–5499. doi: 10.1111/febs.12414

Le Blanc, C., Mironneau, C., Barbot, C., Henaff, M., Bondeva, T., Wetzker, R., et al. (2004). Regulation of vascular L-type Ca2+ channels by phosphatidylinositol 3,4,5-trisphosphate. *Circ. Res.* 95, 300–307. doi: 10.1161/01.RES.0000138017.76125.8b

Liu, Z., and Khalil, R. A. (2018). Evolving mechanisms of vascular smooth muscle contraction highlight key targets in vascular disease. *Biochem. Pharmacol.* 153, 91–122. doi: 10.1016/j.bcp.2018.02.012

Lu, Z., Jiang, Y. P., Wang, W., Xu, X. H., Mathias, R. T., Entcheva, E., et al. (2009). Loss of cardiac phosphoinositide 3-kinase p110 alpha results in contractile dysfunction. *Circulation* 120, 318–325. doi: 10.1161/CIRCULATIONAHA.109.873380

Lu, Z., Jiang, Y. P., Xu, X. H., Ballou, L. M., Cohen, I. S., and Lin, R. Z. (2007). Decreased L-type Ca2+ current in cardiac myocytes of type 1 diabetic akita mice due to reduced phosphatidylinositol 3-kinase signaling. *Diabetes* 56, 2780–2789. doi: 10.2337/db06-1629

Macrez, N., Mironneau, C., Carricaburu, V., Quignard, J. F., Babich, A., Czupalla, C., et al. (2001). Phosphoinositide 3-kinase isoforms selectively couple receptors to vascular L-type Ca(2+) channels. *Circ. Res.* 89, 692–699. doi: 10.1161/hh2001.097864

Martínez, M. C., Randriamboavonjy, V., Ohlmann, P., Komas, N., Duarte, J., Schneider, F., et al. (2000). Involvement of protein kinase C, tyrosine kinases, and Rho kinase in Ca2+ handling of human small arteries. *Am. J. Physiol. Heart Circ. Physiol.* 279, H1228–H1238. doi: 10.1152/ajpheart.2000.279.3.H1228

Martinsen, A., Yerna, X., Rath, G., Gomez, E. L., Dessy, C., and Morel, N. (2012). Different effect of Rho kinase inhibition on calcium signaling in rat isolated large and small arteries. *J. Vasc. Res.* 49, 522–533. doi: 10.1159/000341230

Meissner, G. (2017). The structural basis of ryanodine receptor ion channel function. *J. Gen. Physiol.* 149, 1065–1089. doi: 10.1085/jgp.201711878

Mulvany, M. J., and Halpern, W. (1977). Contractile properties of small arterial resistance vessels in spontaneously hypertensive and normotensive rats. *Circ. Res.* 41, 19–26. doi: 10.1161/01.RES.41.1.19

Naik, J. S., Xiang, L., and Hester, R. L. (2006). Enhanced role for RhoA-associated kinase in adrenergic-mediated vasoconstriction in gracilis arteries from obese Zucker rats. *Am. J. Physiol. Regul. Integr. Comp. Physiol.* 290, R154–R161. doi: 10.1152/ajpregu.00245.2005

Nobe, K., and Paul, R. J. (2001). Distinct pathways of Ca(2+) sensitization in porcine coronary artery: effects of Rho-related kinase and protein kinase C inhibition on force and intracellular Ca(2+). *Circ. Res.* 88, 1283–1290. doi: 10.1161/hh1201.092035

Ok, S. H., Jeong, Y. S., Kim, J. G., Lee, S. M., Sung, H. J., Kim, H. J., et al. (2011). c-Jun NH2-terminal kinase contributes to dexmedetomidine-induced contraction in isolated rat aortic smooth muscle. *Yonsei. Med. J.* 52, 420–428. doi: 10.3349/ymj.2011.52.3.420

Okon, E. B., Chung, A. W., Rauniyar, P., Padilla, E., Tejerina, T., McManus, B. M., et al. (2005). Compromised arterial function in human type 2 diabetic patient. *Diabetes* 54, 2415–2423. doi: 10.2337/diabetes.54.8.2415

Pinho, J. F., Medeiros, M. A., Capettini, L. S., Rezende, B. A., Campos, P. P., Andrade, S. P., et al. (2010). Phosphatidylinositol 3-kinase-δ up-regulates L-type Ca2+ currents and increases vascular contractility in a mouse model of type 1 diabetes. *Br. J. Pharmacol.* 161, 1458–1471. doi: 10.1111/j.1476-5381.2010.00955.x

Potts, L. B., Ren, Y., Lu, G., Kuo, E., Ngo, E., Kuo, L., et al. (2012). Constriction of retinal arterioles to endothelin-1: requisite role of rho kinase independent of protein kinase C and L-type calcium channels. *Invest. Ophthalmol. Visc. Sci.* 53, 2904–2912. doi: 10.1167/iovs.12-9542

Prieto, D., Contreras, C., and Sánchez, A. (2013). Endothelial dysfunction, obesity and insulin resistance. *Curr. Vasc. Pharmacol.* 11, 412–426.

Prieto, D., Mulvany, M. J., and Nyborg, N. C. (1991). (+)-S-12967 and (-)-S-12968: 1,4-dihydropyridine stereoisomers with calcium channel agonistic and antagonistic properties in rat resistance arteries. *Br. J. Pharmacol.* 103, 1703–1708. doi: 10.1111/j.1476-5381.1991.tb09850.x

Quignard, J. F., Mironneau, J., Carricaburu, V., Fournier, B., Babich, A., Nurnberg, B., et al. (2001). Phosphoinositide 3-kinase gamma mediates angiotensin II-induced stimulation of L-type calcium channels in vascular myocytes. *J. Biol. Chem.* 276, 32545–32551. doi: 10.1074/jbc.M102582200

Rakotoarisoa, L., Carricaburu, V., Leblanc, C., Mironneau, C., Mironneau, J., and Macrez, N. (2006). Angiotensin II-induced delayed stimulation of phospholipase C gamma1 requires activation of both phosphatidylinositol 3-kinase gamma and tyrosine kinase in vascular myocytes. *J. Cell. Mol. Med.* 10, 734–748.

Sánchez, A., Contreras, C., Climent, B., Gutiérrez, A., Muñoz, M., García-Sacristán, A., et al. (2018). Impaired Ca2+ handling in resistance arteries from genetically obese zucker rats: role of the PI3K, ERK1/2 and PKC signaling pathways. *Biochem. Pharmacol.* 152, 114–128. doi: 10.1016/j.bcp.2018.03.020

Santiago, E., Climent, B., Muñoz, M., García-Sacristán, A., Rivera, L., and Prieto, D. (2015). Hydrogen peroxide activates store-operated Ca(2+) entry in coronary arteries. *Br. J. Pharmacol.* 172, 5318–5332. doi: 10.1111/bph.13322

Smani, T., Calderón-Sanchez, E., Gómez-Hurtado, N., Fernández-Velasco, M., Cachofeiro, V., Lahera, V., et al. (2010). Mechanisms underlying the activation of L-type calcium channels by urocortin in rat ventricular myocytes. *Cardiovasc Res.* 87, 459–466. doi: 10.1093/cvr/cvq063

Somlyo, A. P., and Somlyo, A. V. (2003). Ca2+ sensitivity of smooth muscle and nonmuscle myosin II: modulated by G proteins, kinases, and myosin phosphatase. *Physiol. Rev.* 83, 1325–1358. doi: 10.1152/physrev.00023.2003

Takahashi, E., Fukuda, K., Miyoshi, S., Murata, M., Kato, T., Ita, M., et al. (2004). Leukemia inhibitory factor activates cardiac L-Type Ca2+ Channels via Phosphorylation of Serine 1829 in the rabbit cav1.2 Subunit. *Circ. Res.* 94, 1242–1248. doi: 10.1161/01.RES.0000126405.38858.BC

Touyz, R. M., El Mabrouk, M., He, G., Wu, X. H., and Schiffrin, E. L. (1999). Mitogen-activated protein/extracellular signal-regulated kinase inhibition attenuates angiotensin II-mediated signaling and contraction in spontaneously hypertensive rat vascular smooth muscle cells. *Circ. Res.* 84, 505–515. doi: 10.1161/01.RES.84.5.505

Turban, S., and Hajduch, E. (2011). Protein kinase C isoforms: mediators of reactive lipid metabolites in the development of insulin resistance. *FEBS Lett.* 585, 269–274. doi: 10.1016/j.febslet.2010.12.022

Ungvari, Z., Pacher, P., Kecskemeti, V., Papp, G., Szollár, L., and Koller, A. (1999). Increased myogenic tone in skeletal muscle arterioles of diabetic rats. Possible role of increased activity of smooth muscle Ca2+ channels and protein kinase, C. *Cardiovasc. Res.* 43, 1018–1028. doi: 10.1016/S0008-6363(99)00106-6

Viard, P., Butcher, A. J., Halet, G., Davies, A., Nürnberg, B., Heblich, F., et al. (2004). PI3K promotes voltage-dependent calcium channel trafficking to the plasma membrane. *Nat. Neurosci.* 7, 939–946. doi: 10.1038/nn1300

Villalba, N., Contreras, C., Hernández, M., García-Sacristán, A., and Prieto, D. (2011). Impaired Ca2+ handling in penile arteries from prediabetic zucker rats: involvement of rho kinase. *Am. J. Physiol. Heart Circ. Physiol.* 300, H2044–H2053. doi: 10.1152/ajpheart.01204.2010

Villalba, N., Stankevicius, E., Garcia-Sacristán, A., Simonsen, U., and Prieto, D. (2007). Contribution of both Ca2+ entry and Ca2+ sensitization to the alpha1-adrenergic vasoconstriction of rat penile small arteries. *Am. J. Physiol. Heart Circ. Physiol.* 292, H1157–H1169. doi: 10.1152/ajpheart.01034.2006

Villalba, N., Stankevicius, E., Simonsen, U., and Prieto, D. (2008). Rho kinase is involved in Ca2+ entry of rat penile small arteries. *Am. J. Physiol. Heart Circ. Physiol.* 294, H1923–H1932. doi: 10.1152/ajpheart.01221.2007

Wang, Y., Yoshioka, K., Azam, M. A., Takuwa, N., Sakurada, S., Kayaba, Y., et al. (2006). Class II phosphoinositide 3-kinase alpha-isoform regulates Rho, myosin phosphatase and contraction in vascular smooth muscle. *Biochem. J.* 394, 581–592. doi: 10.1042/BJ20051471

Yang, L., Doshi, D., Morrow, J., Katchman, A., Chen, X., and Marx, S. O. (2009). Protein kinase C isoforms differentially phosphorylate Ca(v)1.2 *alpha(*1c). *Biochemistry.* 48, 6674–6683. doi: 10.1021/bi900322a

Conflict of Interest Statement: The authors declare that the research was conducted in the absence of any commercial or financial relationships that could be construed as a potential conflict of interest.

frontiers in Physiology

ORIGINAL RESEARCH
published: 07 February 2019
doi: 10.3389/fphys.2019.00040

Gender-Dependent Alteration of Ca^{2+} and TNFα Signaling in *db/db* Mice, an Obesity-Linked Type 2 Diabetic Model

Carmen Delgado[1], Ana-Maria Gomez[2]*, Magali Samia El Hayek[2], Gema Ruiz-Hurtado[3†] and Laetitia Pereira[2†]*

[1]Instituto de Investigaciones Biomédicas "Alberto Sols" (CSIC-UAM)/CIBER-CV, Madrid, Spain, [2]INSERM UMR-S 1180, University of Paris-Sud, University of Paris-Saclay, Châtenay-Malabry, France, [3]Cardiorenal Translational Laboratory, Institute of Research i+12, Hospital Universitario 12 de Octubre/CIBER-CV, Madrid, Spain

OPEN ACCESS

Edited by:
José Antonio Pariente, Universidad de Extremadura, Spain

Reviewed by:
Juan Martinez-Pinna, University of Alicante, Spain
Gines M. Salido, Universidad de Extremadura, Spain
Belma Turan, Ankara University, Turkey

***Correspondence:**
Carmen Delgado
cdelgado@iib.uam.es
Ana-Maria Gomez
ana-maria.gomez@inserm.fr

†These authors have contributed equally to this work

Specialty section:
This article was submitted to Membrane Physiology and Membrane Biophysics, a section of the journal Frontiers in Physiology

Received: *04 November 2018*
Accepted: *14 January 2019*
Published: *07 February 2019*

Citation:
Delgado C, Gomez A-M, Samia El Hayek M, Ruiz-Hurtado G and Pereira L (2019) Gender-Dependent Alteration of Ca^{2+} and TNFα Signaling in db/db Mice, an Obesity-Linked Type 2 Diabetic Model. Front. Physiol. 10:40. doi: 10.3389/fphys.2019.00040

Cardiovascular complications are the primary death cause in type 2 diabetes, where inflammation can play a role. We, and others, have previously shown that, in diabetic cardiomyopathy, cardiac dysfunction is associated with Ca^{2+} mishandling. It is possible that diabetic cardiomyopathy differently affects men and women, as the latter present higher risk to develop heart failure and a higher plasmatic level of the pro-inflammatory cytokine, tumor necrosis factor alpha (TNFα), than men. However, the gender-dependent regulation of Ca^{2+} signaling in diabetes and its relationship with TNFα signaling are still unclear. Here, we analyzed TNFα signaling pathway and its role in Ca^{2+} signaling dysfunction in male and female rodent models of type 2 diabetes linked to obesity (*db/db* mice) using confocal microscopy in freshly isolated cardiomyocytes. TNFα increased $[Ca^{2+}]_i$ transient amplitude and accelerated its decay without affecting SR Ca^{2+} load or Ca^{2+} spark frequency in cells from control mice. All TNFα effects on Ca^{2+} handling were prevented by the inhibition of the ceramidase and the phospholipase A2 (PLA2). While the plasmatic level of TNFα was similar in male and female *db/db* mice, only male *db/db* hearts over-expressed both TNFα converting enzyme (TACE) and the protective TNFα receptors 2 (TNF-R2). TNFα receptor 1 (TNF-R1) expression, involved in negative inotropic response of TNFα, was unchanged in both male and female *db/db* mice compared to controls. We found that male *db/db* mice cardiomyocytes presented a decrease in $[Ca^{2+}]_i$ transient amplitude associated to a drop of sarcoplasmic reticulum Ca^{2+} load, not seen in female *db/db* mice. Interestingly, sustained incubation with TNFα did not restored Ca^{2+} signaling alteration observed in male *db/db* mice but still induces an increase in Ca^{2+} spark frequency as seen in control littermates. In cardiomyocytes from female *db/db* mice, TNFα had no visible effects on Ca^{2+} handling. In conclusion, our study shows that the alteration of Ca^{2+} signaling and TNFα, seen in *db/db* mice, is gender specific presenting an increase in TNFα cardio-protective pathway in male mice.

Keywords: diabetic cardiomyopathy, TNFα, calcium, gender difference, *db/db* mice

INTRODUCTION

Cardiovascular complications, such as coronary artery diseases, hypertension, and heart failure, are a leading cause of death in type 2 diabetes (Laakso, 1999; Bauters et al., 2003; Bell, 2007). Preclinical studies have shown that diabetic cardiac dysfunction, with depressed contraction and relaxation, results from dysregulation of metabolism, mitochondrial function, oxidative stress, and Ca^{2+} handling (Bugger and Abel, 2014). These knowledge result almost exclusively from male animal studies. However, in the clinical setting, the risk for developing cardiac diseases in diabetes is known to be gender specific (Galderisi et al., 1991; Rutter et al., 2003; Toedebusch et al., 2018). Indeed, the Framingham Heart Study showed that diabetic women present a 5.1-fold increased risk to develop heart failure than non-diabetic patients, whereas in diabetic men, this risk is only multiplied by 2.4 (Galderisi et al., 1991; Rutter et al., 2003). In addition, the hospital admission rate for cardiovascular diseases is higher in diabetic women compared to diabetic men. Yet, the gender differences in the alterations of cardiac cellular function in diabetes are unclear, notably regarding Ca^{2+} mishandling.

Ca^{2+} regulates contraction through the excitation-contraction coupling in cardiomyocytes. For each heartbeat, sarcolemmal L type Ca^{2+} channels open during the action potential, leading to Ca^{2+} influx that activates Ca^{2+} release from the ryanodine receptors (RyR) located at the sarcoplasmic reticulum (SR). This release of Ca^{2+} by the RyR (visualized as a $[Ca^{2+}]_i$ transient) activates contractile myofibrils to generate cardiomyocyte contraction. After the contraction, the Ca^{2+} is re-uptaken into the SR by the SERCA pump and extruded outside the cardiomyocytes mainly by the Na^+/Ca^{2+} exchanger, resulting in cardiomyocyte relaxation. We and others have shown that, in animal models of type 2 diabetes linked to obesity, contractile dysfunction is associated with a decrease in the Ca^{2+} transient amplitude. This lower Ca^{2+} transient amplitude is associated to reduced L-type Ca^{2+} current density combined with downregulation of RyR expression (Belke et al., 2004; Pereira et al., 2006b, 2014). We found that these alterations may be different in male and female *db*/*db* mice (Pereira et al., 2014); however, the mechanisms remain unclear.

Clinical and preclinical studies pointed out an increase in plasmatic level of TNFα, in type 2 diabetes, notably in women (Yamakawa et al., 1995; Pereira et al., 2006a; Preciado-Puga et al., 2014). TNFα is an inflammatory cytokine commonly associated to infectious and non-infectious cardiomyopathy, such as viral myocarditis, congestive heart failure, and myocardial infarction. The level of TNFα seems correlated to the development of cardiac dysfunction (Feldman et al., 2000; Blum and Miller, 2001), and its over-expression leads to cardiac hypertrophy, fibrosis, arrhythmia, and dysfunction (Kubota et al., 1997; Kadokami et al., 2000; London et al., 2003). Yet, whether TNFα is a cause or a consequence of cardiac dysfunction is still under debate. The biological response of TNFα is mediated through two receptors, the TNFα receptor 1 (TNF-R1) and TNFα receptor 2 (TNF-R2). TNF-R1 activation is responsible for a cardiac negative inotropic response, whereas TNF-R2 mediates cardiac positive inotropic response (Meldrum, 1998). At the cellular level, TNFα regulates contraction either by direct regulation of Ca^{2+} signaling in acute condition or *via* iNOS activation in sustained conditions (Fernandez-Velasco et al., 2007). Still, whether TNFα activation positively or negatively alters the Ca^{2+} transient is quite controversial, and studies found either a decrease, an increase, or no effect on Ca^{2+} transient. Those discrepancies seem to depend on the animal model, the concentration of TNFα used, and the incubation time (Yokoyama et al., 1993; Goldhaber et al., 1996; Bick et al., 1997; Sugishita et al., 1999; Li et al., 2003; Zhang et al., 2005; Duncan et al., 2010; Greensmith and Nirmalan, 2013). In addition, whether the regulation of TNFα signaling in type 2 diabetic cardiomyopathy linked to obesity is gender specific remains unknown.

Considering all these controversial findings surrounding TNFα regulation of Ca^{2+} handling, we first studied the effect of TNFα on Ca^{2+} signaling in WT mice. Then, using the *db*/*db* mice, an animal model of type 2 diabetes with insulin resistance linked to obesity, we found that both Ca^{2+} and TNFα signaling underwent distinct alterations in male compared to female. Here, we found that male *db*/*db* mice presented a depressed Ca^{2+} transient associated with a lower SR Ca^{2+} load, not seen in female *db*/*db* mice. More interestingly, in male *db*/*db*, cardiomyocytes seem to put in place a protective mechanism to counteract those alterations by increasing the expression of cardio-protective TNF-R2 signaling pathway.

MATERIALS AND METHODS

Cell Isolation

Experiments were carried out according to the ethical principles of the French Ministry of Agriculture and the European Parliament on the protection of animals. Ventricular adult cardiomyocytes were isolated from 8 weeks old male C56Bl6 mice, male and female 15 weeks old *db*/*db* (Janvier), and their control littermates (*db*/+). Mice were euthanized by intraperitoneal injection of sodium pentobarbital (100 mg/kg). Cardiac ventricular myocyte isolation was performed by standard enzymatic methods (collagenase type II, Worthington) using the Langendorff perfusion as previously described (Pereira et al., 2006b, 2007, 2012; Leroy et al., 2011; Ruiz-Hurtado et al., 2015). After isolation, cells were kept in 1 mM $[Ca^{2+}]$ for an hour prior experiments. Only rod-shaped cells and quiescent cells when unstimulated and excitable were used for the Ca^{2+} experiments.

Abbreviations: ATK, arachidonyl trifluoromethyl ketone; TNFα, tumor necrosis factor alpha; TNF-R1, TNFα receptor 1; TNF-R2, TNFα receptor 2; KO, knock-out; NO, nitric oxide; NOE, n-oleoylethanolamine; o.i., oil immersion; PKA, protein kinase A; PLA2, phospholipase A2; RyR, cardiac ryanodine receptor; SR, sarcoplasmic reticulum; SERCA, sarco/endoplasmic reticulum Ca^{2+}-ATPase; TACE, TNFα converting enzyme.

Measurements of Plasmatic TNFα

TNFα determination by ELISA Soluble TNFα concentration was determined in plasma samples from mice using commercial ELISA test (BIOTRAK, Amersham Life Science, Sweden).

Confocal Microscopy

Ca^{2+} handling was recorded in freshly isolated ventricular adult cardiomyocytes loaded with the fluorescent Ca^{2+} dye, the Fluo-3 acetoxymethyl ester (Fluo-3 AM, Molecular Probes) at 5 μM diluted in a mixture of DMSO-pluronic acid 20%. A line scan across the longitudinal axis of the myocyte was performed to measure cardiomyocyte shortening. Cardiomyocyte shortening corresponds to the difference between cardiomyocyte length at rest and cardiomyocyte length during contraction (during electrical stimulation), as previously described (Fernandez-Velasco et al., 2009). Ca^{2+} transient, Ca^{2+} sparks, and SR Ca^{2+} load were recorded using confocal microscopy (Meta Zeiss LSM 510, objective w.i. 63×, n.a. 1.2) in line scan mode (1.54 ms) along the longitudinal axis of the cell. Ca^{2+} transients were evoked by field stimulation (1 Hz) applied through two parallel platinum electrodes. Spontaneous Ca^{2+} sparks were recorded in quiescent cells after Ca^{2+} transient recording. Ca^{2+} transient decay time corresponds to the kinetic of the relaxation phase due to the re-uptake of Ca^{2+} into the SR by the SERCA pump as well as the extrusion of Ca^{2+} by the Na^{2+}/Ca^{2+} exchanger. Ca^{2+} transient decay time is calculated using a mono-exponential function to fit the Ca^{2+} transient decline phase. SR Ca^{2+} load was assessed by rapid caffeine application (10 mM) after 1 min pacing to reach the steady state. Parameters were studied with or without TNFα (1 h to 1 h 30 min) supplemented or not with a ceramidase inhibitor n-oleoylethanolamine (NOE, 5 μM) and a phospholipase A2 (PLA2) inhibitor (ATK, 10 μM) (Sigma-Aldrich). Fluo-3 AM was excited with an Argon laser (λ_{ex} = 488 nm), and emission was collected at wavelengths >505 nm. Image analysis was performed using homemade routines in interactive data language (IDL).

Western-Blot Analysis

Adult ventricular homogenates were quickly frozen in liquid nitrogen and then placed in Tris solution (50 mmol/L, pH = 7.4) containing proteases and phosphatase inhibitors (10 μg/ml leupeptin, 10 μg/ml trypsin inhibitor, 2 μg/ml aprotinin, and 5 μM okadaic acid). Homogenization was performed on ice using a Politron. Homogenate was centrifuged at 18,925 g for 10 min at 4°C. Proteins were resuspended in Laemmli (5%) sample buffer, boiled (90°C for 5–10 min), and separated by sodium dodecyl sulfate polyacrylamide gel electrophoresis (SDS-PAGE) using 10% polyacrylamide gels. After separation, proteins were transferred to polyvinylidene fluoride membranes (Amersham Biosciences), and non-specific binding sites were blocked overnight at 4°C in 5% dried milk and Tris-buffer saline (TBS, pH = 7.4) and 0.01% Tween 20. Membranes were incubated overnight (at 4°C) for the rabbit polyclonal anti-TACE (1:300; Proscience) and the rabbit polyclonal anti-TNFR2 (H-202) (1:250; Santa Cruz), at room temperature for 1 h 30 min for the rabbit polyclonal anti-TNFR1 (H-271) (1:500; Santa Cruz). A secondary horseradish peroxidase-conjugated goat anti-rabbit IgG (Amersham Biosciences) was used in combination with an enhanced chemiluminescence detection system (SuperSignal West Pico Chemiluminescent Substrate, Pierce) to visualize the primary antibodies. Band densities were determined with a laser-scanning densitometer (HP-3970) and Quantity One software (BioRad SA). Protein loading was controlled by probing all Western blots with anti-GADPH antibody (1:4,000) (Ambion).

Statistical Analysis

Results were expressed as mean ± SEM. Significance between two groups was determined using unpaired Student's *t* test or non-parametric Mann-Whitney test. Data involving more than two groups were analyzed using either one-way ANOVA or two-way ANOVA as appropriate. We used GraphPad Prism 7 (GraphPad) for statistical comparison. Differences with values of $p < 0.05$ were considered significant.

RESULTS

Sustained TNFα Exposure Increases Ca^{2+}-Induced Ca^{2+} Release

TNFα-mediated Ca^{2+} signaling regulation is quite controversial, which is probably due to protocol differences. Therefore, we first studied, in our experimental settings, the effect of sustained activation (1–1 h 30 min) of TNFα on Ca^{2+} handling parameters such as Ca^{2+} transient, Ca^{2+} spark frequency, and SR Ca^{2+} load (**Figure 1**). In our hands, 10 and 50 ng/ml TNFα treatment significantly increased Ca^{2+} transient amplitude (F/F_0 of 3.1 ± 0.3 for 10 ng/ml, 3.5 ± 0.3 for 50 ng/ml vs. 2.5 ± 0.14 for baseline, $p < 0.05$). Moreover, TNFα significantly accelerated the Ca^{2+} re-uptake into the SR as shown by the faster SR Ca^{2+} transient decay time (**Figures 1A,B**) (~29% faster for 10 ng/ml and ~25% for 50 ng/ml, $p < 0.01$). This acceleration of Ca^{2+} re-uptake did not modified SR Ca^{2+} load (**Figure 1D**) and did not affect Ca^{2+} spark frequency (**Figures 1E,F**) at any concentration studied. However, 100 ng/ml of TNFα had no effects on either Ca^{2+} transient amplitude, Ca^{2+} spark frequency, or SR Ca^{2+} load. However, 100 ng/ml of TNFα still accelerated the Ca^{2+} transient decay (**Figure 1C**). These results clearly show that sustained TNFα activation mediates an increase in systolic Ca^{2+} release. Altogether, our results lean toward the idea of a positive inotropic effect.

PLA2 and Ceramidase Mediate TNFα Regulation of Ca^{2+} Signaling

Previous work has suggested that TNFα response is mediated by the sphingosine signaling pathway (Hofmann et al., 2003). To investigate the signaling pathway involved in TNFα regulation of Ca^{2+} signaling, we used a ceramidase inhibitor

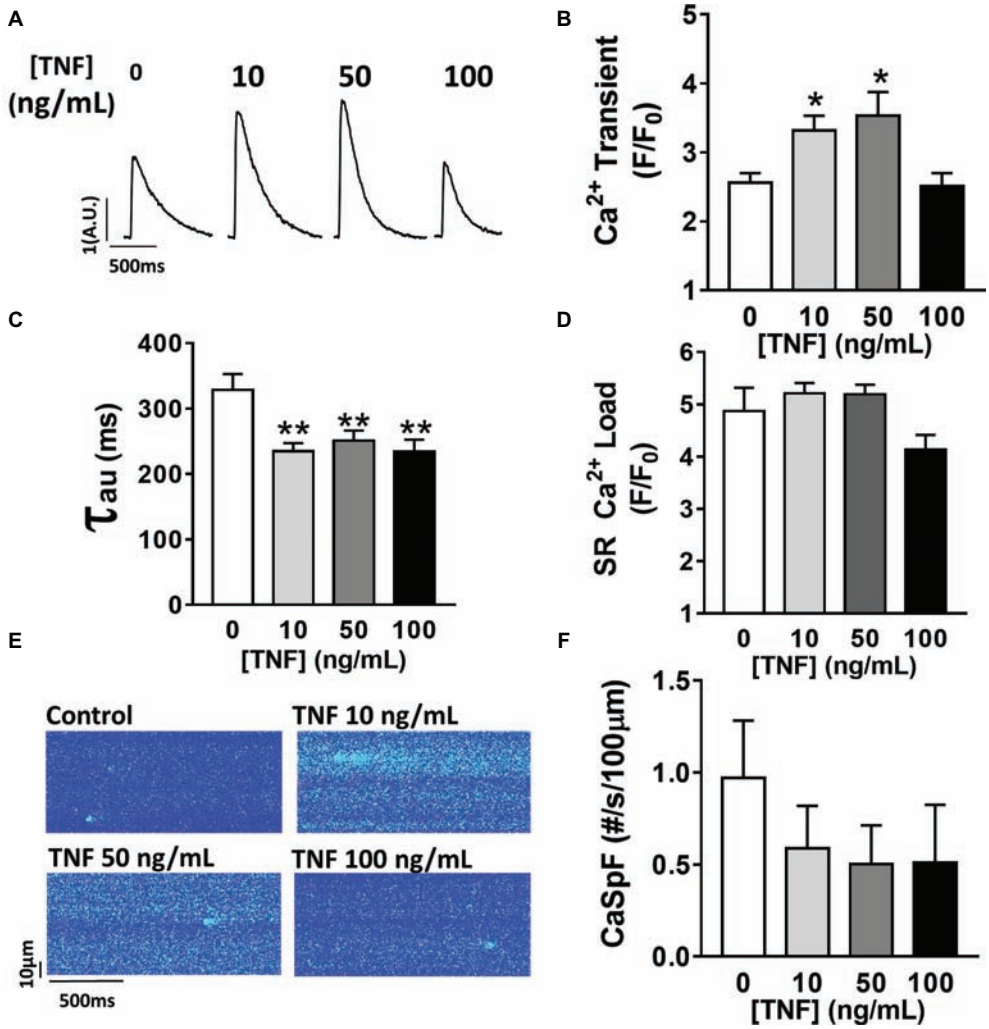

FIGURE 1 | Positive inotropic effect of TNFα incubation. **(A)** Examples of Ca^{2+} transient recordings in freshly isolated cardiomyocytes (5 μM Fluo-3 AM) at baseline, at 10 ng/ml TNFα and 100 ng/ml TNFα. **(B)** Mean Ca^{2+} transient amplitude from cardiomyocytes at baseline (n = 22) and with incremental TNFα treatment (n = 21 for 10 ng/ml, n = 15 for 50 ng/ml, n = 10 for 100 ng/ml). **(C)** Ca^{2+} transient decay time (in ms) at baseline (n = 20) and with incremental TNFα treatments (n = 20 for 10 ng/ml, n = 15 for 50 ng/ml, n = 9 for 100 ng/ml). **(D)** Mean of sarcoplasmic reticulum (SR) Ca^{2+} load obtained by caffeine application after 1 min field stimulation in same conditions (respectively, n = 10, n = 11, n = 11, and n = 7). **(E)** Examples Ca^{2+} spark frequency (CaSpF) recording in freshly isolated cardiomyocytes at baseline, at 10 ng/ml TNFα and 100 ng/ml TNFα. **(F)** Mean of CaSpF (number of sparks (#) per second per 100 μm) obtained in same groups as in **(A)** (respectively, n = 19, n = 20, n = 15, and n = 7). $^*p < 0.05$, $^{**}p < 0.01$.

(5 μM NOE) and a PLA2 inhibitor (10 μM ATK). NOE fully prevented the increase of Ca^{2+} transient amplitude (**Figures 2A,B**) and the faster Ca^{2+} transient decay time induced by 10 ng/ml of TNFα (**Figure 2C**). NOE had no significant effects on neither the Ca^{2+} spark frequency nor the SR Ca^{2+} load (**Figures 2D–F**). Similarly, the phospholipase A2 inhibitor blunted all TNFα-mediated effects on the Ca^{2+} transient and the Ca^{2+} transient decay time (**Figures 2B,C**). As for NOE, ATK had no effect on SR Ca^{2+} load (**Figure 2D**). However, ATK, contrarily to NOE, did significantly reduce basal Ca^{2+} spark frequency. Altogether, those results suggest that TNFα alters Ca^{2+} signaling *via* the activation of the ceramidase and phospholipase A2 signaling pathway.

Gender Differences in Upstream TNFα Signaling Pathway in Obesity-Linked Type 2 Diabetic Mice (*db/db*)

Since plasmatic TNFα level is significantly elevated in type 2 diabetic patients, we first measured the plasmatic level of TNFα in male and female *db*/*db* mice. At 15 weeks old, *db*/*db* mice develop a type 2 diabetes linked to obesity with associated cardiomyopathy (Pereira et al., 2006b). Surprisingly, neither male nor female *db*/*db* mice presented an increase in their plasmatic level of TNFα compared to control (**Figure 3A**). Then, we measured the expression of key proteins involved in the TNFα signaling pathway, such as type 1 and type 2 TNFα receptors and the TNFα conversion enzyme TACE in both male and female *db*/*db*

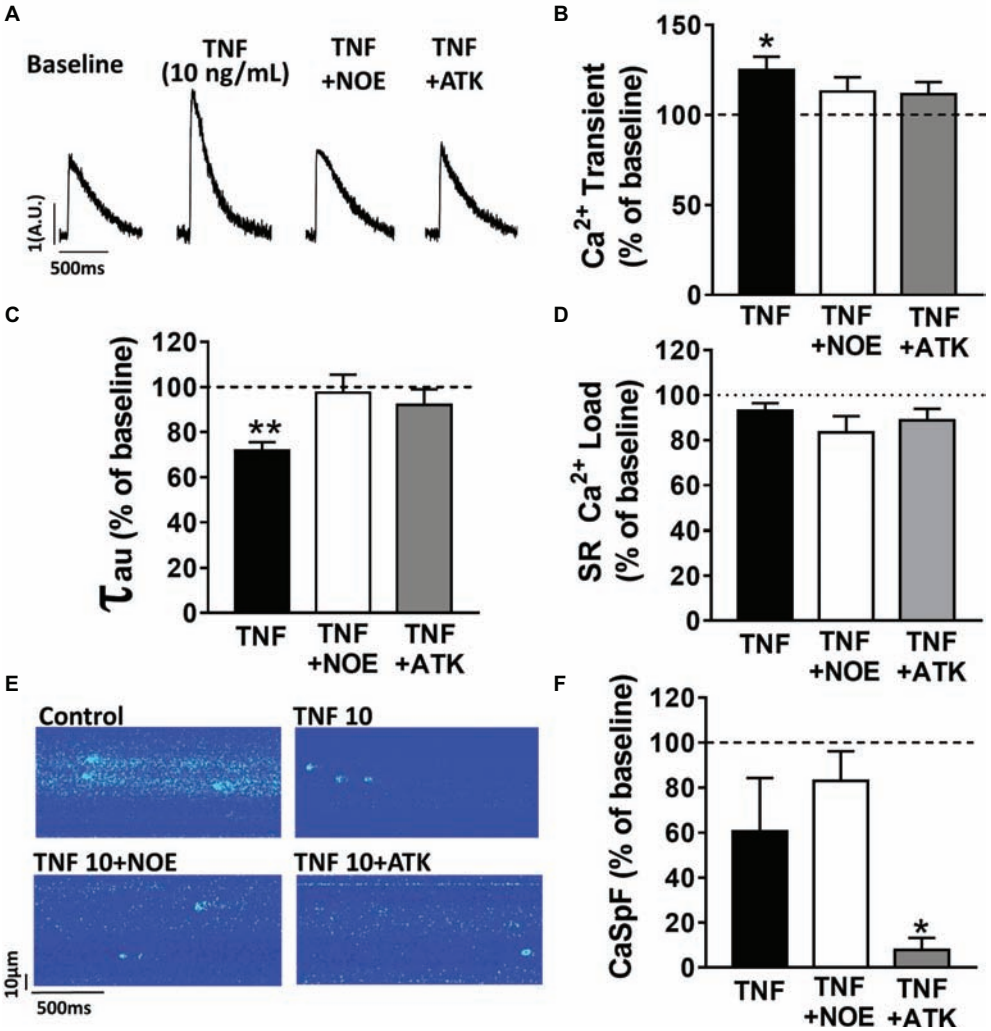

FIGURE 2 | TNFα regulates Ca^{2+} signaling *via* the sphingosine pathway. **(A)** Representative Ca^{2+} transient examples obtained at baseline, at 10 ng/ml TNFα ± ceramide inhibitor (NOE) or phospholipase A2 inhibitor (ATK). **(B)** Percentage of effect on Ca^{2+} transient amplitude of TNFα treatment ±NOE or ATK (n = 20 for 10 ng/ml TNFα, n = 10 for TNFα+NOE, and n = 10 for TNFα+ATK). **(C)** Ca^{2+} transient decay time (in ms) in same groups (respectively, n = 19, n = 10, and n = 10). **(D)** Mean of SR Ca^{2+} load in the same groups (respectively, n = 11, n = 10, and n = 9). **(E)** Examples Ca^{2+} spark frequency recording in freshly isolated cardiomyocytes at baseline, at TNFα ± NOE or ATK. **(F)** Mean of CaSpF obtained in conditions (respectively, n = 20, n = 10, and n = 10). *$p < 0.05$, **$p < 0.01$.

mice. Interestingly, TACE expression was significantly higher in male *db*/*db* mice compared to controls, whereas no change was detectable in the female group (**Figure 3B**). Moreover, while TNF-R1 receptor expression was unchanged in both *db*/*db* groups (**Figure 3C**), TNF-R2 in the *db*/*db* male group was significantly increased (**Figure 3D**). These results clearly suggest that in male *db*/*db* mice hearts, the TNF-R2, known to mediate a cardio-protective pathway, is over-expressed, probably to protect the heart from diabetic-induced stress.

Gender Differences in Obesity-Linked Type 2 Diabetic (*db*/*db*) Ca^{2+} Mishandling

In *db*/*db* mice, cardiac dysfunction has been associated with a decrease in SR Ca^{2+} transient amplitude and SR Ca^{2+} load (Belke et al., 2004; Pereira et al., 2006b, 2014). Here, we confirmed, in isolated cardiac myocytes from male *db*/*db* mice, that Ca^{2+} transient amplitude is significantly decreased (**Figures 4A,B**). This drop in Ca^{2+} transient amplitude (~51% lower than control, $p < 0.01$) is correlated with a drop in SR Ca^{2+} load (**Figure 4D**) (~51% lower than control, $p < 0.01$), which could explain the smaller (although not significant) cardiac cell shortening (**Figure 4C**). In our experimental conditions, Ca^{2+} spark frequency does not seem to be altered in *db*/*db* compared to control (*db*/+) (p = N.S.) (**Figures 4E,F**). In female *db*/*db* mice, the Ca^{2+} handling was similar in *db*/*db* compared to their control littermates (**Figure 5**). Indeed, all parameters such as Ca^{2+} transient amplitude (**Figure 5A**), Ca^{2+} spark frequency (**Figure 5C**), SR Ca^{2+} load (**Figure 5D**), and cell shortening (**Figure 5B**) were not significantly modified in freshly isolated cardiomyocytes in female *db*/*db* compared to control. In

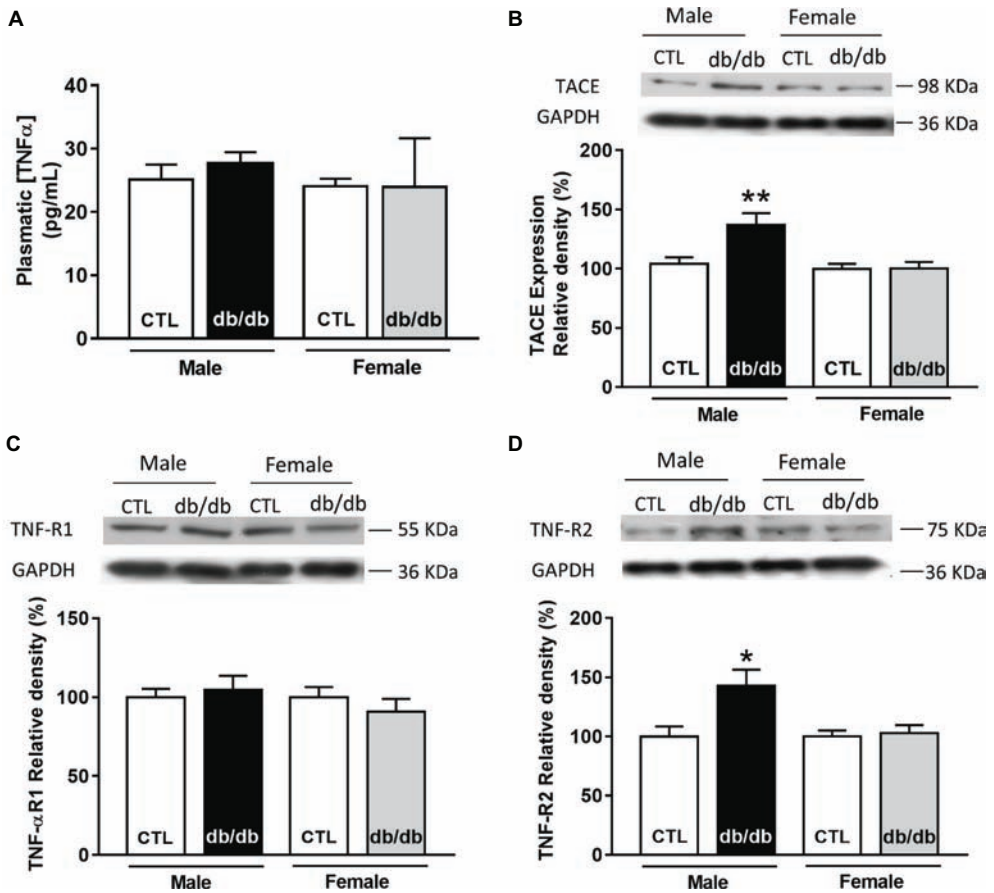

FIGURE 3 | Gender-dependent alteration of the TNFα signaling pathway in type 2 diabetic mice (*db/db*). **(A)** Plasmatic level of TNFα obtained in male and female control and *db/db* heart tissue homogenates (male control: $n = 5$, male *db/db*: $n = 7$; female control and *db/db*: $n = 8$). **(B)** Representative Western-blot example of TACE (98 kDa) and the percent of relative density normalized by GAPDH signal from male and female control ($n = 15$, $n = 17$) and *db/db* ($n = 14$, $n = 17$) heart tissue homogenates. **(C)** Representative Western-blot example of TNF-R1 (55 kDa) expression and percentage of relative density normalized by GAPDH signal in male and female control ($n = 16$, $n = 18$) and *db/db* ($n = 16$, $n = 18$) heart tissue homogenates. **(D)** Representative Western-blot example of TNF-R2 (75 kDa) expression and percentage of relative density normalized by GAPDH signal in male and female control ($n = 13$, $n = 13$) and *db/db* ($n = 13$, $n = 15$) heart tissue homogenates. *$p < 0.05$.

conclusion, we found a gender-specific alteration of Ca^{2+} handling in *db*/*db* mice, with lower SR Ca^{2+} release associated to a drop in SR Ca^{2+} load in male, not seen in female.

Gender Differences of TNFα-Mediated Effect in Type 2 Diabetic (*db/db*)

Next, we compared TNFα regulation of Ca^{2+} signaling between male and female *db*/*db* mice. In male *db*/*db* mice, 10 ng/ml TNFα did not alter Ca^{2+} transient amplitude, cell shortening, nor SR Ca^{2+} load (**Figures 4A–C,F**). However, 10 ng/ml of TNFα similarly increased Ca^{2+} spark frequency in both control (~3.29 fold, $p < 0.05$) and *db*/*db* (1.5 fold, $p = 0.06$) (**Figure 4D**). In female control, the higher Ca^{2+} transient amplitude and cell shortening did not reach significance. Both female *db*/*db* and control had unchanged Ca^{2+} spark frequency. Those results suggest that, in 15 weeks old female *db*/*db*, the excitation-contraction coupling is unchanged compared to female control. Moreover, TNFα fails to show the effects found in male *db*/*db* (**Figure 4D**). Therefore, there are gender differences in Ca^{2+} mishandling and the underlying mechanisms in type 2 diabetes.

DISCUSSION

We have previously shown that cardiac dysfunction in type 2 diabetes is associated with cardiomyocyte Ca^{2+} mishandling, resulting from a decrease in the Ca^{2+} channels involved in the Ca^{2+}-induced Ca^{2+} release process (RyR and L-Type Ca^{2+} channels) (Belke et al., 2004; Pereira et al., 2006b). Although TNFα is elevated in diabetic patient and animal model of diabetes (Yamakawa et al., 1995; Pereira et al., 2006a; Preciado-Puga et al., 2014), little was known about its role in cellular alteration, notably regarding the Ca^{2+} signaling pathway and gender specificity in animal model of diabetes linked to obesity. Here, we found a gender-specific alteration of Ca^{2+} and TNFα signaling in *db*/*db* mice, a common model of type 2 diabetes linked to obesity. Indeed, we found that male *db*/*db* mice, not

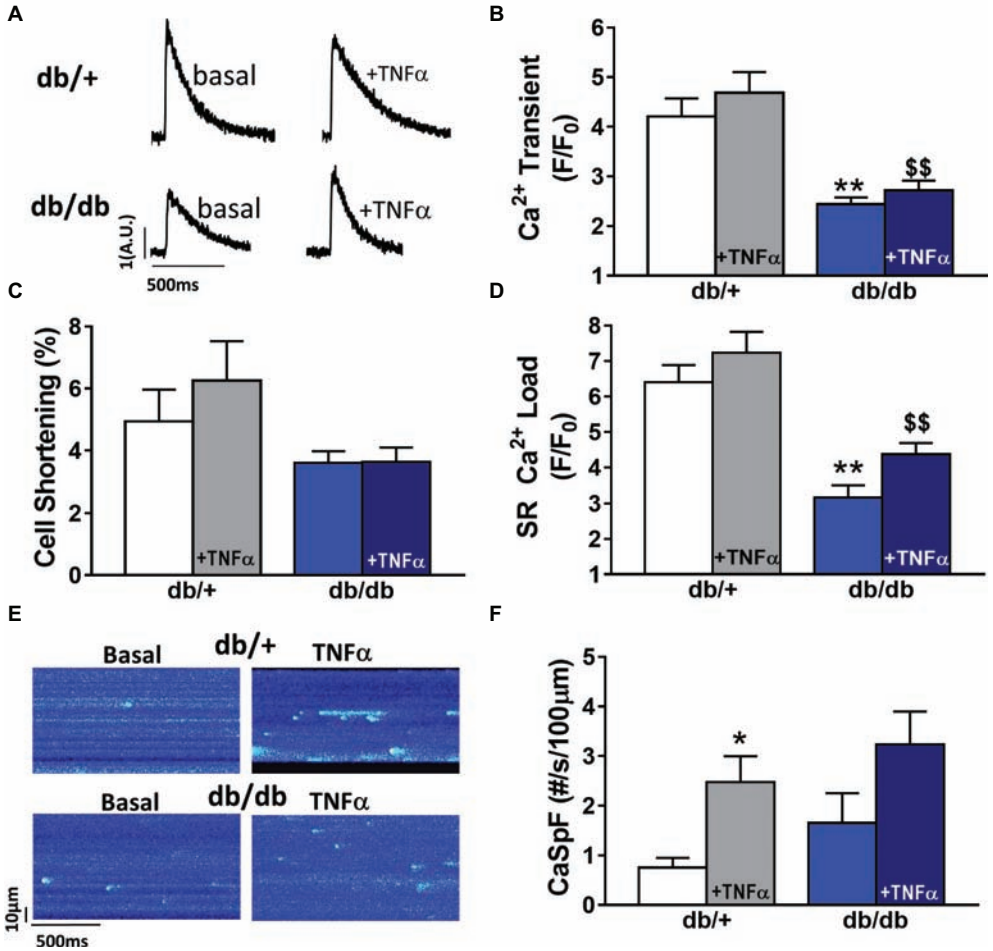

FIGURE 4 | Ca^{2+} signaling is impaired in male type 2 diabetic mice. **(A)** Line scan images of Ca^{2+} transient recorded in male cardiomyocytes from *db*/+, *db*/*db* ± TNFα (10 ng/ml). **(B)** Mean of Ca^{2+} transient amplitude from *db*/*db* ± TNFα (n = 21 and n = 19) cardiomyocytes and their control littermates (*db*/+, n = 14 and n = 20). **(C)** Cell shortening measured in intact *db*/*db* ± TNFα (n = 13 and n = 15) and *db*/+ cardiomyocytes (n = 10 and n = 13) stimulated at 1 Hz. **(D)** Mean of SR Ca^{2+} load in intact *db*/*db* ± TNFα (n = 6 and n = 11) and *db*/+ cardiomyocytes (n = 10 and 11). **(E)** Examples Ca^{2+} spark frequency recording in freshly isolated cardiomyocytes at in *db*/+ and *db*/*db* with or without TNFα **(F)** Ca^{2+} spark frequency in the same groups (for *db*/*db*: n = 12 and 17, for *db*/+: n = 12 and n = 18) $^{**}p < 0.01$ compared to *db*/+ and $^{\$\$}p < 0.05$ compared to *db*/*db* without TNFα treatment.

female, presented the previously described Ca^{2+} mishandling with lower systolic Ca^{2+} release and SR Ca^{2+} load. More interestingly, we found that male and female *db*/*db* mice expressed differently TNF-R2, with an increased expression in male *db*/*db* mice that might reflect the activation of the TNFα cardio-protective TNF-R2-dependent pathway, not seen in female *db*/*db*.

Cardiac Positive Inotropic Effect of TNFα

Discrepancies regarding the TNFα regulation of Ca^{2+} signaling are quite important in the literature with reported positive or negative ionotropic effect. For instance, in cat cardiomyocytes, short time exposure of TNFα reduced Ca^{2+} transient amplitude in response to a disruption of Ca^{2+} influx *via* L type Ca^{2+} channels leading to cellular shortening, supporting, then, a negative ionotropic effect of TNFα (Yokoyama et al., 1993). This negative inotropic effect of TNFα has been also described, in rabbit and guinea pigs, with TNFα-induced impaired cellular shortening cardiomyocytes mediated by NO dependent but Ca^{2+} independent (Goldhaber et al., 1996; Sugishita et al., 1999). However, various studies performed in rodents have shown that TNFα can lead to inotropic positive effects (Bick et al., 1997; Greensmith and Nirmalan, 2013). Here, we found that TNFα treatments (10 and 50 ng/ml) induced a time and concentration-dependent effect leading to a significant increase in Ca^{2+} transient amplitude between 1 h and 1 h 30 min suggesting a positive inotropic effect. Our results are in concordance with Bick et al. study (Bick et al., 1997), who have found that TNFα incubation increases Ca^{2+} transient and cellular contraction in neo-natal cardiomyocytes. In adult rat cardiomyocytes treated with 50 ng/ml of TNFα (Greensmith and Nirmalan, 2013), Ca^{2+} transient amplitude and cellular shortening were also increased (Greensmith and Nirmalan, 2013). The absence of effect observed under 100 ng/ml of TNFα might be explained by its bimodal effect, as previously described in cardiomyocytes, depending on exposure time or dose (Amadou et al., 2002; Shanmugam et al., 2016). Then, 100 ng/ml TNFα

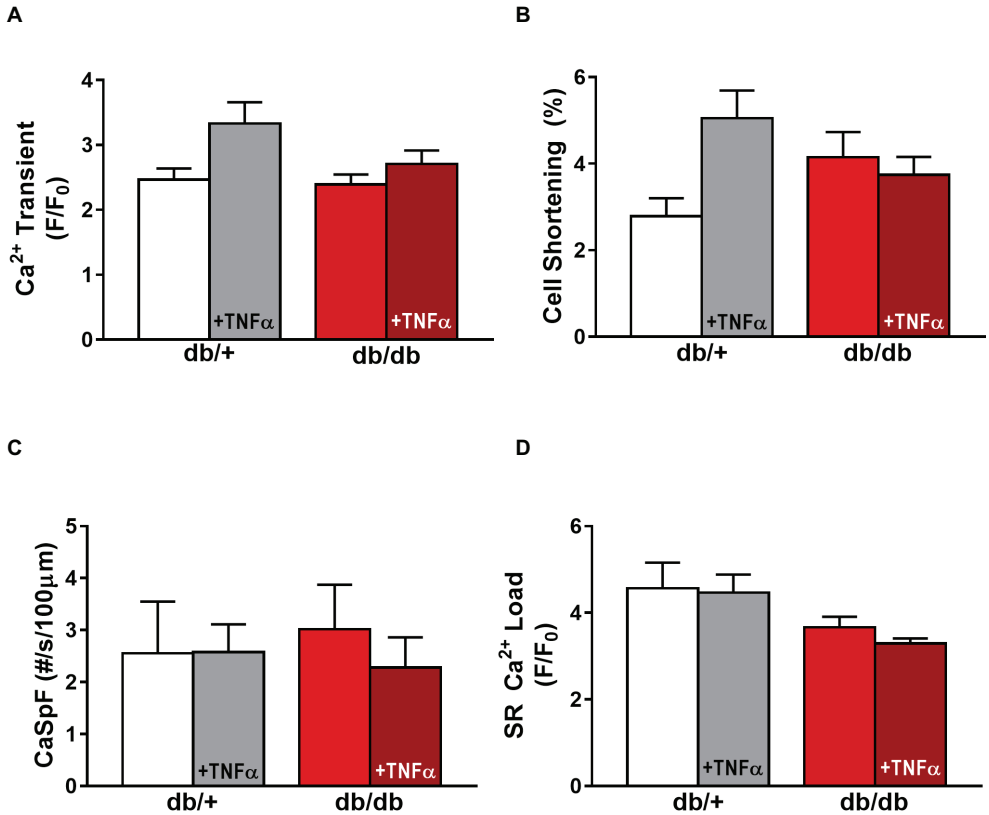

FIGURE 5 | EC coupling is unchanged in type 2 diabetic female mice. **(A)** Mean Ca^{2+} transient amplitude from *db/db* ± TNFα (n = 27 and n = 23) cardiomyocytes and their control littermates (*db/+*, n = 11 and n = 18). **(B)** Cell shortening measured in intact *db/db* ± TNFα (n = 12 and n = 9) and *db/+* cardiomyocytes (n = 8 and n = 14). **(C)** Ca^{2+} spark frequency in the same groups (for *db/db*: n = 9 and n = 12, for *db/+*: n = 10 and n = 17). **(D)** Mean of SR Ca^{2+} load in intact *db/db* ± TNFα (n = 17 and n = 18) and *db/+* cardiomyocytes (n = 9 and n = 14). p = N.S.

or higher doses, and with prolonged exposure, is expected to induce negative inotropic effects on Ca^{2+} handling.

In Mice Cardiomyocytes, TNFα Regulates Ca^{2+} Signaling *via* the Sphingosine and PLA2 Pathways

Previous studies have shown that TNFα produces myocardial effects (negative or positive inotropic effect) through different mechanisms such as PLA2 or sphingosine signaling pathway (Murray and Freeman, 1996; Oral et al., 1997; Liu and McHowat, 1998). Here, we found that exposure of TNFα (1 h to 1 h 30 min) mediates Ca^{2+} transient increase *via* the activation of both ceramidase (sphingosine precursor) and PLA2 (for arachidonic acid production). Sphingosine is commonly associated to short-term (within minutes) negative inotropic effect of TNFα (Oral et al., 1997). However, other studies have shown that ceramide enhanced SR Ca^{2+} release and SR Ca^{2+} re-uptake in adult ventricular myocytes (Liu and Kennedy, 2003). Those results are in line with our prevention of TNFα-mediated elevation of systolic Ca^{2+} release and Ca^{2+} transient decay time in cardiomyocytes treated with the ceramidase inhibitor NOE (**Figures 2B,C**). Moreover, inhibition of the PLA2 prevented TNFα-mediated increase in Ca^{2+} transient amplitude and SR Ca^{2+} transient decay time, suggesting that TNFα induces Ca^{2+} mishandling *via* PLA2-mediated phosphorylation of RyR. Indeed, 10 ng/ml of TNFα has been shown to increase Ca^{2+} transient amplitude as a result of PLA-2 mediated RyR PKA phosphorylation at serine 2,808 in wild-type mice of RASSF1A knock out (Mohamed et al., 2014). This PKA-dependent mediated effect of PLA-2/arachidonic acid on the RyR phosphorylation state perfectly explains why we observed a dramatic drop of Ca^{2+} spark frequency under the inhibition of the PLA-2 (**Figure 2F**). In addition, TNFα also accelerates SR Ca^{2+} re-uptake reflecting an increase in SERCA pump activity as seen under PKA phosphorylation of phospholamban supporting the TNFα/PLA-2/PKA pathway. This mechanism is confirmed by the restoration of the TNFα-mediated acceleration Ca^{2+} transient decay time under ATK, the PLA-2 inhibitor (**Figures 2B,C**).

Gender-Dependent Ca^{2+} Mishandling in *db/db* Mice, an Obesity-Linked Type 2 Diabetic Model

Type 2 diabetes is the most common form of diabetes. In western countries, 80% of type 2 diabetic patients have developed a diabetes linked to obesity resulting in severe glucose intolerance

compared to lean type 2 diabetic patients (Schaffer and Mozaffari, 1996). Our study was performed in *db*/*db* mice, a model that recapitulates, in that sense, the human pathology. Indeed, the leptin receptor mutation of *db*/*db* mice impairs the satiety feeling and leads to obesity around 4–5 weeks of age, which is followed by diabetic state with hyperglycemia and insulin resistance (Coleman, 1978). In type 2 diabetes linked to obesity, cardiac dysfunction has been associated to Ca^{2+} mishandling and structural remodeling (Belke et al., 2004; Pereira et al., 2006b; Falcao-Pires and Leite-Moreira, 2012). Indeed, overall, animal models of type 2 diabetes present a reduced Na^+/Ca^{2+} exchanger activity, and depressed Ca^{2+} transient linked to downregulation of Ca^{2+} channels, RyRs, and reduced SERCA activity (Netticadan et al., 2001; Zhong et al., 2001; Abe et al., 2002; Belke et al., 2004; Pereira et al., 2006b; Boudina and Abel, 2010). Here, our results show that those effects are recapitulated in male *db*/*db* mice (**Figure 4**), but not in female *db*/*db* mice. However, the gender-specific regulation in Ca^{2+} handling and/or β-adrenergic response has been previously described (Parks et al., 2014). Supporting this idea, we found that basal Ca^{2+} transient amplitude is lower in female control compared to male control cardiomyocytes. Although Parks et al. (2014) have shown that Ca^{2+} current, diastolic Ca^{2+}, and SR Ca^{2+} load were similar between control male and female, basal cAMP level was lower in control female compared to control male due to higher PDE4B expression in female. These results are in line with our previous work showing that *db*/*db* female mice have reduced phosphorylation of the RyR, which reduce Ca^{2+} spark frequency and could explain the preserve SR Ca^{2+} load and Ca^{2+} transient seen in female *db*/*db* compared to *db*/*db* male. Our results are paradoxical compared to the higher risk to develop heart failure for type 2 diabetic women compared to diabetic men. This discrepancy could be explain as follow: the decrease in $[Ca^{2+}]_i$ transient in male *db*/*db* mice could be protective at long term, maybe by preventing Ca^{2+} toxic effects such as apoptosis or preserve ATP content by limiting the ATP expense in pumping Ca^{2+} (Javorkova et al., 2010; Parks et al., 2014). Future studies will be needed to confirm this hypothesis.

Gender Dependent Alteration of Molecular TNFα Signaling Pathway in *db*/*db*

To our knowledge, plasmatic TNFα level parallels the degree of cardiac dysfunction in diabetic patients. In the *db*/*db* mice, we did not observe any changes in the plasmatic level of TNFα compared to control. Even though circulating TNFα is unchanged, male *db*/*db* mice present an increase in TACE expression suggesting a paracrine elevation of TNFα in the heart. Surprisingly, despite cardiomyocyte treatment with 10 ng/ml of TNFα, a concentration within the *in vivo* range measured under stress and injury (Bitterman et al., 1991), TNFα did not induce an increase in Ca^{2+} transient amplitude or decay time in *db*/*db*, as seen in C57Bl6 mice (**Figures 4B,C**). One explanation could be that in *db*/*db* control littermate strain background (C57BKS/J strain), TNFα is not as effective as in C57Bl6 strain. Indeed, genetic background, such as between C57BL6/J and C57BL6/N, has been shown to influence cardiac phenotype and propensity to develop cardiomyopathies (Tian et al., 2011; Simon et al., 2013). This could also explain the ineffective response of TNFα in female control and *db*/*db* mice (**Figure 5**). Although TNFα activation has been linked with oxidative stress, no gender-specific difference in cardiomyocytes redox state at baseline or during pathology has been observed (Ren, 2007; Bell et al., 2015). Another possibility could be that in male *db*/*db*, the dramatically reduced SR Ca^{2+} load would prevent the high Ca^{2+} systolic release induced by TNFα probably due to the phosphorylation of the RyR *via* the activation of PLA2. Indeed, we found in the presence of TNFα an increase in Ca^{2+} spark frequency in both *db*/+ and *db*/*db* mice reflecting an elevated diastolic RyR opening resulting from RyR phosphorylation by PKA previously described in male *db*/*db* (Pereira et al., 2014). Interestingly, in male *db*/*db* mice, the TNF-R2 was overexpressed, which is known to exert cardio-protective effects *via* the activation of NF-κB (Burchfield et al., 2010). Indeed, in liver, TNFα inhibits PDE3 expression elevating cAMP level and PKA activation (Ke et al., 2015). This activation of PKA could explain, in cardiomyocytes, the elevation of Ca^{2+} spark frequency in male *db*/+ cardiomyocytes treated with TNFα (**Figure 4F**). Moreover, TNF-R2 is known to be involved in positive cardiac inotropic effect (Defer et al., 2007). As a result, $[Ca^{2+}]$ overload was prevented and Ca^{2+} transient increased leading to an increase in inotropic response. The over-expressed TNF-R2 in a male *db*/*db* appears as an attempt to counteract the already present Ca^{2+} mishandling to protect from cardiac dysfunction. Indeed, prolonged activation of the TNF-R2 pathway in the *db*/*db* male cardiomyocytes could then activate phosphorylation of excitation-contraction coupling key proteins, such as phospholamban, to restore Ca^{2+} transient and cardiomyocytes contraction.

In conclusion, we found for the first time that both Ca^{2+} and TNFα signaling are altered only in male type 2 diabetic mice, whereas female does not seem to be affected. Although this study has several limitations in the interpretation such as non-comparable hormonal state between female *db*/*db* mice and diabetic women, lower effect of TNFα in *db*/+ than C57BL6 control, we still clearly show that male *db*/*db* mice develop Ca^{2+} mishandling leading to impaired contraction already at a young age, while woman seemed to be protected. Moreover, we found that male *db*/*db* mice put into place a protective mechanism to counteract those negative effects by over-expressing TNF-R2 cardio-protective signaling pathway.

DATA AVAILABILITY

The datasets generated for this study are available on request to the corresponding author.

ETHICS STATEMENT

The study was carried out in accordance to the ethical principles of the French Ministry of Agriculture and the European Parliament on the protection of animals. The protocol was

approved by the French Ministry of Agriculture and Bioethical Committee of the CSIC following recommendation of the Spanish Animal Care and the European Parliament on the protection of animals.

AUTHOR CONTRIBUTIONS

CD and AG conceived and designed the project, supervised the data acquisition and participated in analysis. LP and GR performed most of the experiments and analyses. LP interpreted the data and wrote the first draft of the manuscript. MS participated in the figure preparation. All authors have edited the manuscript.

FUNDING

This work has been funded by Acuerdos Bilaterales España-Francia (CSIC-INSERM) grant no. 2005FR0020 and partially by SAF2017-84777R from the Spanish Ministerio de Industria, Economia y Competitividad (to CD) and partially by CP15/00129 and PI17/01093 (to GR), and the ANR-11-1DEX-0003-02 to LP as members of the Laboratory of Excellence LERMIT.

REFERENCES

Abe, T., Ohga, Y., Tabayashi, N., Kobayashi, S., Sakata, S., Misawa, H., et al. (2002). Left ventricular diastolic dysfunction in type 2 diabetes mellitus model rats. *Am. J. Physiol. Heart Circ. Physiol.* 282, H138–H148. doi: 10.1152/ajpheart.2002.282.1.H138

Amadou, A., Nawrocki, A., Best-Belpomme, M., Pavoine, C., and Pecker, F. (2002). Arachidonic acid mediates dual effect of TNF-alpha on Ca^{2+} transients and contraction of adult rat cardiomyocytes. *Am. J. Phys. Cell Physiol.* 282, C1339–C1347. doi: 10.1152/ajpcell.00471.2001

Bauters, C., Lamblin, N., Mc Fadden, E. P., Van Belle, E., Millaire, A., and de Groote, P. (2003). Influence of diabetes mellitus on heart failure risk and outcome. *Cardiovasc. Diabetol.* 2:1. doi: 10.1186/1475-2840-2-1

Belke, D. D., Swanson, E. A., and Dillmann, W. H. (2004). Decreased sarcoplasmic reticulum activity and contractility in diabetic db/db mouse heart. *Diabetes* 53, 3201–3208. doi: 10.2337/diabetes.53.12.3201

Bell, D. S. (2007). Heart failure in the diabetic patient. *Cardiol. Clin.* 25, 523–538; vi. doi: 10.1016/j.ccl.2007.08.003

Bell, J. R., Raaijmakers, A. J., Curl, C. L., Reichelt, M. E., Harding, T. W., Bei, A., et al. (2015). Cardiac CaMKIIdelta splice variants exhibit target signaling specificity and confer sex-selective arrhythmogenic actions in the ischemic-reperfused heart. *Int. J. Cardiol.* 181, 288–296. doi: 10.1016/j.ijcard.2014.11.159

Bick, R. J., Liao, J. P., King, T. W., LeMaistre, A., McMillin, J. B., and Buja, L. M. (1997). Temporal effects of cytokines on neonatal cardiac myocyte Ca^{2+} transients and adenylate cyclase activity. *Am. J. Phys.* 272, H1937–H1944. doi: 10.1152/ajpheart.1997.272.4.H1937

Bitterman, H., Kinarty, A., Lazarovich, H., and Lahat, N. (1991). Acute release of cytokines is proportional to tissue injury induced by surgical trauma and shock in rats. *J. Clin. Immunol.* 11, 184–192. doi: 10.1007/BF00917424

Blum, A., and Miller, H. (2001). Pathophysiological role of cytokines in congestive heart failure. *Annu. Rev. Med.* 52, 15–27. doi: 10.1146/annurev.med.52.1.15

Boudina, S., and Abel, E. D. (2010). Diabetic cardiomyopathy, causes and effects. *Rev. Endocr. Metab. Disord.* 11, 31–39. doi: 10.1007/s11154-010-9131-7

Bugger, H., and Abel, E. D. (2014). Molecular mechanisms of diabetic cardiomyopathy. *Diabetologia* 57, 660–671. doi: 10.1007/s00125-014-3171-6

Burchfield, J. S., Dong, J. W., Sakata, Y., Gao, F., Tzeng, H. P., Topkara, V. K., et al. (2010). The cytoprotective effects of tumor necrosis factor are conveyed through tumor necrosis factor receptor-associated factor 2 in the heart. *Circ. Heart Fail.* 3, 157–164. doi: 10.1161/CIRCHEARTFAILURE.109.899732

Coleman, D. L. (1978). Obese and diabetes: two mutant genes causing diabetes-obesity syndromes in mice. *Diabetologia* 14, 141–148. doi: 10.1007/BF00429772

Defer, N., Azroyan, A., Pecker, F., and Pavoine, C. (2007). TNFR1 and TNFR2 signaling interplay in cardiac myocytes. *J. Biol. Chem.* 282, 35564–35573. doi: 10.1074/jbc.M704003200

Duncan, D. J., Yang, Z., Hopkins, P. M., Steele, D. S., and Harrison, S. M. (2010). TNF-alpha and IL-1beta increase Ca^{2+} leak from the sarcoplasmic reticulum and susceptibility to arrhythmia in rat ventricular myocytes. *Cell Calcium* 47, 378–386. doi: 10.1016/j.ceca.2010.02.002

Falcao-Pires, I., and Leite-Moreira, A. F. (2012). Diabetic cardiomyopathy: understanding the molecular and cellular basis to progress in diagnosis and treatment. *Heart Fail. Rev.* 17, 325–344. doi: 10.1007/s10741-011-9257-z

Feldman, A. M., Combes, A., Wagner, D., Kadakomi, T., Kubota, T., Li, Y. Y., et al. (2000). The role of tumor necrosis factor in the pathophysiology of heart failure. *J. Am. Coll. Cardiol.* 35, 537–544.

Fernandez-Velasco, M., Rueda, A., Rizzi, N., Benitah, J. P., Colombi, B., Napolitano, C., et al. (2009). Increased Ca^{2+} sensitivity of the ryanodine receptor mutant RyR2R4496C underlies catecholaminergic polymorphic ventricular tachycardia. *Circ. Res.* 104, 201–209, 212p following 209. doi: 10.1161/CIRCRESAHA.108.177493

Fernandez-Velasco, M., Ruiz-Hurtado, G., Hurtado, O., Moro, M. A., and Delgado, C. (2007). TNF-alpha downregulates transient outward potassium current in rat ventricular myocytes through iNOS overexpression and oxidant species generation. *Am. J. Physiol. Heart Circ. Physiol.* 293, H238–H245. doi: 10.1152/ajpheart.01122.2006

Galderisi, M., Anderson, K. M., Wilson, P. W., and Levy, D. (1991). Echocardiographic evidence for the existence of a distinct diabetic cardiomyopathy (the Framingham Heart Study). *Am. J. Cardiol.* 68, 85–89. doi: 10.1016/0002-9149(91)90716-X

Goldhaber, J. I., Kim, K. H., Natterson, P. D., Lawrence, T., Yang, P., and Weiss, J. N. (1996). Effects of TNF-alpha on $[Ca^{2+}]i$ and contractility in isolated adult rabbit ventricular myocytes. *Am. J. Phys.* 271, H1449–H1455. doi: 10.1152/ajpheart.1996.271.4.H1449

Greensmith, D. J., and Nirmalan, M. (2013). The effects of tumor necrosis factor-alpha on systolic and diastolic function in rat ventricular myocytes. *Phys. Rep.* 1:e00093. doi: 10.1002/phy2.93

Hofmann, U., Domeier, E., Frantz, S., Laser, M., Weckler, B., Kuhlencordt, P., et al. (2003). Increased myocardial oxygen consumption by TNF-alpha is mediated by a sphingosine signaling pathway. *Am. J. Physiol. Heart Circ. Physiol.* 284, H2100–H2105. doi: 10.1152/ajpheart.00888.2002

Javorkova, V., Mezesova, L., Vlkovicova, J., and Vrbjar, N. (2010). Influence of sub-chronic diabetes mellitus on functional properties of renal Na(+),K(+)-ATPase in both genders of rats. *Gen. Physiol. Biophys.* 29, 266–274. doi: 10.4149/gpb_2010_03_266

Kadokami, T., McTiernan, C. F., Kubota, T., Frye, C. S., and Feldman, A. M. (2000). Sex-related survival differences in murine cardiomyopathy are associated with differences in TNF-receptor expression. *J. Clin. Invest.* 106, 589–597. doi: 10.1172/JCI9307

Ke, B., Zhao, Z., Ye, X., Gao, Z., Manganiello, V., Wu, B., et al. (2015). Inactivation of NF-kappaB p65 (RelA) in liver improves insulin sensitivity and inhibits cAMP/PKA pathway. *Diabetes* 64, 3355–3362. doi: 10.2337/db15-0242

Kubota, T., McTiernan, C. F., Frye, C. S., Slawson, S. E., Lemster, B. H., Koretsky, A. P., et al. (1997). Dilated cardiomyopathy in transgenic mice with cardiac-specific overexpression of tumor necrosis factor-alpha. *Circ. Res.* 81, 627–635. doi: 10.1161/01.RES.81.4.627

Laakso, M. (1999). Hyperglycemia and cardiovascular disease in type 2 diabetes. *Diabetes* 48, 937–942. doi: 10.2337/diabetes.48.5.937

Leroy, J., Richter, W., Mika, D., Castro, L. R., Abi-Gerges, A., Xie, M., et al. (2011). Phosphodiesterase 4B in the cardiac L-type Ca(2)(+) channel complex regulates Ca(2)(+) current and protects against ventricular arrhythmias in mice. *J. Clin. Invest.* 121, 2651–2661. doi: 10.1172/JCI44747

Li, X. Q., Zhao, M. G., Mei, Q. B., Zhang, Y. F., Guo, W., Wang, H. F., et al. (2003). Effects of tumor necrosis factor-alpha on calcium movement in rat ventricular myocytes. *Acta Pharmacol. Sin.* 24, 1224–1230.

Liu, S. J., and Kennedy, R. H. (2003). Positive inotropic effect of ceramide in adult ventricular myocytes: mechanisms dissociated from its reduction in Ca^{2+} influx. *Am. J. Physiol. Heart Circ. Physiol.* 285, H735–H744. doi: 10.1152/ajpheart.01098.2002

Liu, S. J., and McHowat, J. (1998). Stimulation of different phospholipase A2 isoforms by TNF-alpha and IL-1beta in adult rat ventricular myocytes. *Am. J. Phys.* 275, H1462–H1472.

London, B., Baker, L. C., Lee, J. S., Shusterman, V., Choi, B. R., Kubota, T., et al. (2003). Calcium-dependent arrhythmias in transgenic mice with heart failure. *Am. J. Physiol. Heart Circ. Physiol.* 284, H431–H441. doi: 10.1152/ajpheart.00431.2002

Meldrum, D. R. (1998). Tumor necrosis factor in the heart. *Am. J. Phys.* 274, R577–R595.

Mohamed, T. M., Zi, M., Prehar, S., Maqsood, A., Abou-Leisa, R., Nguyen, L., et al. (2014). The tumour suppressor Ras-association domain family protein 1A (RASSF1A) regulates TNF-alpha signalling in cardiomyocytes. *Cardiovasc. Res.* 103, 47–59. doi: 10.1093/cvr/cvu111

Murray, D. R., and Freeman, G. L. (1996). Tumor necrosis factor-alpha induces a biphasic effect on myocardial contractility in conscious dogs. *Circ. Res.* 78, 154–160. doi: 10.1161/01.RES.78.1.154

Netticadan, T., Temsah, R. M., Kent, A., Elimban, V., and Dhalla, N. S. (2001). Depressed levels of Ca^{2+}-cycling proteins may underlie sarcoplasmic reticulum dysfunction in the diabetic heart. *Diabetes* 50, 2133–2138. doi: 10.2337/diabetes.50.9.2133

Oral, H., Dorn, G. W., 2nd, and Mann, D. L. (1997). Sphingosine mediates the immediate negative inotropic effects of tumor necrosis factor-alpha in the adult mammalian cardiac myocyte. *J. Biol. Chem.* 272, 4836–4842. doi: 10.1074/jbc.272.8.4836

Parks, R. J., Ray, G., Bienvenu, L. A., Rose, R. A., and Howlett, S. E. (2014). Sex differences in SR Ca(2+) release in murine ventricular myocytes are regulated by the cAMP/PKA pathway. *J. Mol. Cell. Cardiol.* 75, 162–173. doi: 10.1016/j.yjmcc.2014.07.006

Pereira, F. O., Frode, T. S., and Medeiros, Y. S. (2006a). Evaluation of tumour necrosis factor alpha, interleukin-2 soluble receptor, nitric oxide metabolites, and lipids as inflammatory markers in type 2 diabetes mellitus. *Mediat. Inflamm.* 2006:39062. doi: 10.1155/MI/2006/39062

Pereira, L., Matthes, J., Schuster, I., Valdivia, H. H., Herzig, S., Richard, S., et al. (2006b). Mechanisms of [Ca2+]i transient decrease in cardiomyopathy of db/db type 2 diabetic mice. *Diabetes* 55, 608–615. doi: 10.2337/diabetes.55.03.06.db05-1284

Pereira, L., Metrich, M., Fernandez-Velasco, M., Lucas, A., Leroy, J., Perrier, R., et al. (2007). The cAMP binding protein Epac modulates Ca^{2+} sparks by a Ca^{2+}/calmodulin kinase signalling pathway in rat cardiac myocytes. *J. Physiol.* 583, 685–694. doi: 10.1113/jphysiol.2007.133066

Pereira, L., Ruiz-Hurtado, G., Morel, E., Laurent, A. C., Metrich, M., Dominguez-Rodriguez, A., et al. (2012). Epac enhances excitation-transcription coupling in cardiac myocytes. *J. Mol. Cell. Cardiol.* 52, 283–291. doi: 10.1016/j.yjmcc.2011.10.016

Pereira, L., Ruiz-Hurtado, G., Rueda, A., Mercadier, J. J., Benitah, J. P., and Gomez, A. M. (2014). Calcium signaling in diabetic cardiomyocytes. *Cell Calcium* 56, 372–380. doi: 10.1016/j.ceca.2014.08.004

Preciado-Puga, M. C., Malacara, J. M., Fajardo-Araujo, M. E., Wrobel, K., Wrobel, K., Kornhauser-Araujo, C., et al. (2014). Markers of the progression of complications in patients with type 2 diabetes: a one-year longitudinal study. *Exp. Clin. Endocrinol. Diabetes* 122, 484–490. doi: 10.1055/s-0034-1372594

Ren, J. (2007). Influence of gender on oxidative stress, lipid peroxidation, protein damage and apoptosis in hearts and brains from spontaneously hypertensive rats. *Clin. Exp. Pharmacol. Physiol.* 34, 432–438. doi: 10.1111/j.1440-1681.2007.04591.x

Ruiz-Hurtado, G., Li, L., Fernandez-Velasco, M., Rueda, A., Lefebvre, F., Wang, Y., et al. (2015). Reconciling depressed Ca^{2+} sparks occurrence with enhanced RyR2 activity in failing mice cardiomyocytes. *J. Gen. Physiol.* 146, 295–306. doi: 10.1085/jgp.201511366

Rutter, M. K., Parise, H., Benjamin, E. J., Levy, D., Larson, M. G., Meigs, J. B., et al. (2003). Impact of glucose intolerance and insulin resistance on cardiac structure and function: sex-related differences in the Framingham Heart Study. *Circulation* 107, 448–454. doi: 10.1161/01.CIR.0000045671.62860.98

Schaffer, S. W., and Mozaffari, M. (1996). Abnormal mechanical function in diabetes: relation to myocardial calcium handling. *Coron. Artery Dis.* 7, 109–115. doi: 10.1097/00019501-199602000-00003

Shanmugam, G., Narasimhan, M., Sakthivel, R., Kumar, R. R., Davidson, C., Palaniappan, S., et al. (2016). A biphasic effect of TNF-alpha in regulation of the Keap1/Nrf2 pathway in cardiomyocytes. *Redox Biol.* 9, 77–89. doi: 10.1016/j.redox.2016.06.004

Simon, M. M., Greenaway, S., White, J. K., Fuchs, H., Gailus-Durner, V., Wells, S., et al. (2013). A comparative phenotypic and genomic analysis of C57BL/6J and C57BL/6N mouse strains. *Genome Biol.* 14:R82. doi: 10.1186/gb-2013-14-7-r82

Sugishita, K., Kinugawa, K., Shimizu, T., Harada, K., Matsui, H., Takahashi, T., et al. (1999). Cellular basis for the acute inhibitory effects of IL-6 and TNF- alpha on excitation-contraction coupling. *J. Mol. Cell. Cardiol.* 31, 1457–1467. doi: 10.1006/jmcc.1999.0989

Tian, C., Shao, C. H., Moore, C. J., Kutty, S., Walseth, T., DeSouza, C., et al. (2011). Gain of function of cardiac ryanodine receptor in a rat model of type 1 diabetes. *Cardiovasc. Res.* 91, 300–309. doi: 10.1093/cvr/cvr076

Toedebusch, R., Belenchia, A., and Pulakat, L. (2018). Diabetic cardiomyopathy: impact of biological sex on disease development and molecular signatures. *Front. Physiol.* 9:453. doi: 10.3389/fphys.2018.00453

Yamakawa, T., Tanaka, S., Yamakawa, Y., Kiuchi, Y., Isoda, F., Kawamoto, S., et al. (1995). Augmented production of tumor necrosis factor-alpha in obese mice. *Clin. Immunol. Immunopathol.* 75, 51–56. doi: 10.1006/clin.1995.1052

Yokoyama, T., Vaca, L., Rossen, R. D., Durante, W., Hazarika, P., and Mann, D. L. (1993). Cellular basis for the negative inotropic effects of tumor necrosis factor-alpha in the adult mammalian heart. *J. Clin. Invest.* 92, 2303–2312. doi: 10.1172/JCI116834

Zhang, M., Xu, Y. J., Saini, H. K., Turan, B., Liu, P. P., and Dhalla, N. S. (2005). TNF-alpha as a potential mediator of cardiac dysfunction due to intracellular Ca^{2+}-overload. *Biochem. Biophys. Res. Commun.* 327, 57–63. doi: 10.1016/j.bbrc.2004.11.131

Zhong, Y., Ahmed, S., Grupp, I. L., and Matlib, M. A. (2001). Altered SR protein expression associated with contractile dysfunction in diabetic rat hearts. *Am. J. Physiol. Heart Circ. Physiol.* 281, H1137–H1147. doi: 10.1152/ajpheart.2001.281.3.H1137

Conflict of Interest Statement: The authors declare that the research was conducted in the absence of any commercial or financial relationships that could be construed as a potential conflict of interest.

frontiers in Physiology

REVIEW
published: 01 March 2019
doi: 10.3389/fphys.2019.00159

TRP Channels: Current Perspectives in the Adverse Cardiac Remodeling

Debora Falcón[1†], Isabel Galeano-Otero[1†], Eva Calderón-Sánchez[1,2†], Raquel Del Toro[1,2], Marta Martín-Bórnez[1], Juan A. Rosado[3], Abdelkrim Hmadcha[4,5] and Tarik Smani[1,2]*

[1]Department of Medical Physiology and Biophysics, Institute of Biomedicine of Seville, University of Seville, Sevilla, Spain, [2]CIBERCV, Madrid, Spain, [3]Department of Physiology (Cell Physiology Research Group), University of Extremadura, Cáceres, Spain, [4]Department of Generation and Cell Therapy, Andalusian Center for Molecular Biology and Regenerative Medicine (CABIMER), University of Pablo de Olavide-University of Seville-CSIC, Sevilla, Spain, [5]CIBERDEM, Madrid, Spain

Calcium is an important second messenger required not only for the excitation-contraction coupling of the heart but also critical for the activation of cell signaling pathways involved in the adverse cardiac remodeling and consequently for the heart failure. Sustained neurohumoral activation, pressure-overload, or myocardial injury can cause pathologic hypertrophic growth of the heart followed by interstitial fibrosis. The consequent heart's structural and molecular adaptation might elevate the risk of developing heart failure and malignant arrhythmia. Compelling evidences have demonstrated that Ca^{2+} entry through TRP channels might play pivotal roles in cardiac function and pathology. TRP proteins are classified into six subfamilies: TRPC (canonical), TRPV (vanilloid), TRPM (melastatin), TRPA (ankyrin), TRPML (mucolipin), and TRPP (polycystin), which are activated by numerous physical and/or chemical stimuli. TRP channels participate to the handling of the intracellular Ca^{2+} concentration in cardiac myocytes and are mediators of different cardiovascular alterations. This review provides an overview of the current knowledge of TRP proteins implication in the pathologic process of some frequent cardiac diseases associated with the adverse cardiac remodeling such as cardiac hypertrophy, fibrosis, and conduction alteration.

Keywords: calcium, TRP channels, cardiac remodeling, hypertrophy, fibrosis, conduction disorders

OPEN ACCESS

Edited by:
Maria Fernandez-Velasco, University Hospital La Paz, Spain

Reviewed by:
Antonio Ferrer-Montiel, Universidad Miguel Hernández de Elche, Spain
Karel Talavera, KU Leuven, Belgium

***Correspondence:**
Tarik Smani
tasmani@us.es

[†]These authors have contributed equally to this work

Specialty section:
This article was submitted to Membrane Physiology and Membrane Biophysics, a section of the journal Frontiers in Physiology

Received: *18 November 2018*
Accepted: *08 February 2019*
Published: *01 March 2019*

Citation:
Falcón D, Galeano-Otero I, Calderón-Sánchez E, Del Toro R, Martín-Bórnez M, Rosado JA, Hmadcha A and Smani T (2019) TRP Channels: Current Perspectives in the Adverse Cardiac Remodeling. Front. Physiol. 10:159. doi: 10.3389/fphys.2019.00159

INTRODUCTION

Calcium (Ca^{2+}) is an important second messenger necessary for the excitation-contraction (EC) coupling process in cardiac myocytes (Berridge, 2002; Bers, 2002; Eisner et al., 2017), which occurs as a consequence of Ca^{2+} entry to the cytosol due to L-type Ca^{2+} channels that provoke Ca^{2+} release from sarcoplasmic reticulum causing cardiac myocyte contraction. Cardiac relaxation starts when intracellular Ca^{2+} concentration ($[Ca^{2+}]_i$) decreases as a result of the activity of sarco/endoplasmic reticulum Ca^{2+} ATPase (SERCA) responsible for the Ca^{2+} reuptake into the sarcoplasmic reticulum and the Na^+/Ca^{2+} exchanger responsible of the Ca^{2+} extrusion out of cardiomyocytes (Bers, 2002; Eder, 2017). Ca^{2+} is also required for the activation of signaling pathway that plays minor roles in the healthy heart, for example, those involved in the cardiac remodeling and heart failure (Yue et al., 2015; Eder, 2017; Freichel et al., 2017; Avila-Medina et al., 2018; Domínguez-Rodríguez et al., 2018).

Among the wide Ca^{2+}-permeable channels known in the heart, transient receptor potential (TRP) channels contribute to the Ca^{2+} influx induced by a wide spectrum of physico-chemical stimuli from cellular microenvironments, such as thermal, mechanical stresses, and neurohormonal (Freichel et al., 2017). Likewise, a wide variety of vasoactive agent, including endothelin-1, thrombin, ATP, angiotensin-II, or bradykinin, also stimulates TRP (Suzuki et al., 2011; Albarrán et al., 2013; Gerhold and Schwartz, 2016; Sawamura et al., 2017). TRP channels comprise a large Ca^{2+}-permeable cation channel superfamily showing a common architecture. They contain six transmembrane domains (TM1–TM6) and the cation-permeable pore region formed by a loop between TM5 and TM6 (Gaudet, 2007). They are divided into six major subgroups based on their specific function and sequence analogies (Nilius and Droogmans, 2001; Owsianik et al., 2006; Peng et al., 2015): the canonical channel (TRPC), the vanilloid-related channel (TRPV), and the melastatin-related channel (TRPM) formed by 7, 6, and 8 different channel proteins, respectively (Montell et al., 2002; Venkatachalam and Montell, 2007; Yu et al., 2010); the ankyrin-related channel (TRPA) subfamily containing only one protein; the mucolipin-related channel (TRPML) formed by three proteins; and polycystin-related channel (TRPP) constituted by three members also known as polycystic kidney disease protein (PKD2) (Montell et al., 2002; Venkatachalam and Montell, 2007).

TRP channels display diverse cation selectivity and activation mechanisms (Venkatachalam and Montell, 2007). Most of them are nonselective for cation and are permeable to monovalent and divalent cations, more permeability for Ca^{2+} than Na^{+} (ratio P_{Ca}/P_{Na}) that ranges from channels selective for monovalent cations, such as TRPM4 and TRPM5 with a ratio $P_{Ca}/P_{Na} < 0.05$, to highly Ca^{2+} selective channels, as TRPV5 and TRPV6, which exhibit a ratio P_{Ca}/P_{Na} close to 100 (Yue et al., 2015). TRPM6 and TRPM7 are also permeable to Mg^{2+}, Ca^{2+}, Na^{+}, Zn^{2+}, and other metals [for an extensive review see Freichel et al. (2017)]. Most of TRP channels lack the typical voltage sensor; therefore, they are not gated by voltage (Ramsey et al., 2006; Alonso-Carbajo et al., 2017; Jardín et al., 2017) but they can be modulated by a different chemical and physical stimuli, including temperature fluctuations and mechanical stretch (Islas, 2017; Nazıroğlu and Braidy, 2017; Yamaguchi et al., 2017), extracellular and intracellular ions (including H^{+}, Ca^{2+}, and Mg^{2+}) (Launay et al., 2002; Jiang et al., 2005; Li et al., 2007), intracellular ligands [as diacylglycerol (Palazzo et al., 2013), phosphoinositide-4,5-bisphosphate (PIP2) (Ong and Ambudkar, 2017)], and various exogenous natural and synthetic ligands (Vetter and Lewis, 2011; Holzer and Izzo, 2014).

TRP channels have been suggested as regulators of local micro domains signaling pathway related with changes in the $[Ca^{2+}]_i$ or by the interplay with Ca^{2+}-dependent regulatory proteins. Actually, they contribute to Ca^{2+} homeostasis by directly conducting Ca^{2+} or indirectly *via* membrane depolarization and modulation of voltage-gated Ca^{2+} channels (Nilius and Droogmans, 2001; Owsianik et al., 2006; Freichel et al., 2014; Pires et al., 2017). Hence, during the last two decades, TRPs have been suggested as intermediaries of diverse physiological and pathophysiological cardiovascular processes (Inoue et al., 2006, 2018; Egginton, 2009; Smani et al., 2015; Yue et al., 2015).

EXPRESSION OF TRP CHANNELS IN CARDIAC CELLS

RT-PCR, western blot, immunostaining, and functional current recordings demonstrated that TRPs are expressed ubiquitously in cardiac myocytes and fibroblasts of different species (Sabourin et al., 2011; Yue et al., 2015). In the case of TRPC channel, the seven members TRPC1–7 are expressed in the majority of the cell types in heart (Eder, 2017; Freichel et al., 2017). Consistently, all TRPCs, except TRPC5, were detected in the sinoatrial node (Ju et al., 2007). Interestingly, significant overexpression of TRPC1/C3/C4/C5 or TRPC6 was detected in patients with heart failure as compared to nonfailing heart (Bush et al., 2006; Morine et al., 2016). Interestingly, these TRPC channels show distinct profiles of expression in the ventricles of patients with heart failure as it happens in murine models of univentricular pressure overload (Morine et al., 2016). As in other cell types, TRPC channels are implicated in signal transduction in cardiac myocytes (Flockerzi and Nilius, 2014; Eder, 2017; Freichel et al., 2017). TRPC family requires the phospholipase C (PLC) pathway for activation. TRPC3, TRPC6, and TRPC7 interact directly with diacylglycerol (Yamaguchi et al., 2018), while TRPC1, TRPC4, and TRPC5 are activated indirectly through a still unidentified mechanism (Sabourin et al., 2011; Zhang and Trebak, 2014; He et al., 2017). Some TRPC channels are activated by intracellular Ca^{2+} store depletion, which stimulates the store-operated Ca^{2+} entry (SOCE) required for diverse cardiac physiopathological process (Ong et al., 2016; Eder, 2017). It has been proposed that TRPC1 associates with TRPC4 or TRPC5, thereby forming the store-operated Ca^{2+} channel, while TRPC3, TRPC6, and TRP7 are suggested to form the receptor-operated channel (Ju and Allen, 2007; Saleh et al., 2008; Sabourin et al., 2012). Others studies demonstrated that long-term stimulation of cardiac myocytes with angiotensin II, phenylephrine, endothelin-1, or aldosterone evoked an exacerbated SOCE elicited by thapsigargin, correlating with an increment in the expression or activation of TRPC1, TRPC4, and/or TRPC5 (Watanabe et al., 2008; Makarewich et al., 2014; Camacho Londoño et al., 2015; Sabourin et al., 2016). The use of dominant negative mutants confirmed that TRPC4 is sensitive to passive Ca^{2+} store depletion, while TRPC3 and TRPC6 respond to the diacylglycerol stimulus, regardless of store depletion (Makarewich et al., 2014). Furthermore, upregulation of TRPC3/C4 in adult ventricular cardiomyocytes correlated with the enhanced SOCE and pro-arrhythmic

Abbreviations: AF, Atrial Fibrillation; $[Ca^{2+}]i$, concentration of intracellular Ca^{2+}; ROS, reactive oxygen species; SOCE, store-operated Ca^{2+} entry; TRP, transient receptor potential; TRPC, transient receptor potential-canonical; TRPV, transient receptor potential-vanilloid; TRPM, transient receptor potential-melastatin; TRPA, transient receptor potential-ankyrin; TRPML, transient receptor potential-mucolipin; TRPP, transient receptor potential-polycystin.

spontaneous Ca^{2+} waves (Domínguez-Rodríguez et al., 2015). Importantly, transient occlusion of coronary artery in rats also enhanced the expression of TRPC1/C3/C4/C5 and TRPC6 either in risk or in remote zone of the infarcted heart (Domínguez-Rodríguez et al., 2018). Finally, TRPC7 activation was proposed to initiate angiotensin-II activation to myocardial apoptosis (Satoh et al., 2007).

TRPV channels were also detected in mammalian hearts, especially TRPV1, TRPV2, and TRPV4 (Yue et al., 2015). Most of TRPV channels are sensitive to temperature and ligands, and they participate in sensation of hot temperature and in chemoreception (Vriens et al., 2007; Islas, 2017). TRPV1 was identified principally in sensory nerves in the cardiovascular system but also in the myocardium (Zahner et al., 2003; Gao et al., 2015; Randhawa and Jaggi, 2017). Bradykinin evoked a TRPV1-dependent $[Ca^{2+}]_i$ increase in cardiac neurons, indicating that TRPV1 activation was responsible for stimulation/sensitization by bradykinin of cardiac nociceptors (Wu and Pan, 2007). An early study demonstrated that after *trpv1* gene deletion, an exacerbated inflammation and cardiac remodeling occurred due to impaired post-ischemic recovery in isolated perfused infarcted heart (Wang and Wang, 2005). More recently, the overexpression of TRPV2 after myocardial infarction was observed in cardiac tissue of rats (Entin-Meer et al., 2014), and TRPV2 downregulation in knockout mice was related to a better recovery after myocardial infarction (Entin-Meer et al., 2017), probably because of an attenuated pro-inflammatory response in these mice. Another study also suggested that TRPV2 may play a critical role in stretch-activated Ca^{2+} influx pathway in dystrophic cardiomyopathy, contributing to $[Ca^{2+}]_i$ mishandling (Lorin et al., 2015). In the case of TRPV4, it is also highly expressed in the heart and is activated during myocardial ischemia and reperfusion, which induced Ca^{2+} influx with subsequent reactive oxygen species (ROS) release (Wu et al., 2017). Recently, TRPV4 upregulation in cardiomyocytes was also linked with aging in mice (Jones et al., 2018). Indeed, pharmacological inhibition of TRPV4 with HC067047 prevented stress-induced cardiomyocyte death and ischemia and reperfusion-induced cardiac damage in aged mice. These findings might have potential implications in the treatment of elderly populations at increased risk of myocardial infarction.

Regarding the expression of TRPM channels in hearts, it is known that eight isoforms are present in different parts of the heart, and TRPM2/4/7 is expressed specifically in cardiac myocytes (Yue et al., 2015). The analysis of mRNA and/or protein levels showed that levels of TRPM2, TRPM3 and TRPM8 were reduced in left and right ventricle of patients with failing heart (Morine et al., 2016), meanwhile increased expression of TRPM7 was observed in the left ventricle of patients with ventricular tachycardia (Parajuli et al., 2015). TRPM2 seems essential for cardiac myocyte bioenergetics maintenance (Hoffman et al., 2015). Its activation protected the heart from ischemia and reperfusion injury by improving mitochondrial dysfunction and reducing ROS levels (Miller et al., 2014). TRPM4 is thought to interfere in cardiac myocyte contraction by its activation of voltage-gated Ca^{2+} channel (Alonso-Carbajo et al., 2017). Actually, the exacerbated activity of TRPM4, which is activated by physiological range of Ca^{2+} concentration, was related with arrhythmic changes (Hu et al., 2017). Also, TRPM7 is believed indispensable during the myocardial proliferation in early stages of cardiogenesis, since the deletion of *trpm7* gene, before embryonic day 9 of mice, provoked heart failure and embryonic death (Sah et al., 2013). Nevertheless, the mechanism by which TRPM7 regulates cardiac cell proliferation remains unknown (Chubanov et al., 2017).

In relation to the expression and function of other TRP channels in heart, TRPA1 was detected in cardiac endothelial cells, vascular smooth muscle, and in cardiac myocytes (Yue et al., 2015), where its activation seems relevant to attenuate ischemia and reperfusion injury (Lu et al., 2016). Furthermore, the presence of TRPP2 has been proven in knockout mice who died before birth as a result of cardiac malformations (Pennekamp et al., 2002). Recently, a study confirmed that TRPP2 was able to regulate autophagy through Ca^{2+} homeostasis in cardiac myocytes (Criollo et al., 2018). However, there are only few studies which looked on the role of these channels in the function of cardiac cells.

ROLE OF TRP CHANNELS IN THE ADVERSE CARDIAC REMODELING

Ca^{2+} plays critical role in the adaptation of the heart to environmental demands, leading to cardiac remodeling (Eder, 2017; Avila-Medina et al., 2018). Physical exercise or pregnancy are reversible stimuli that induce physiologic cardiac hypertrophy to adapt the increase in consumption of nutrients and oxygen, whereas sustained neurohumoral activation, hypertension, or myocardial injury can lead to pathological heart hypertrophy followed by interstitial fibrosis (Pfeffer and Braunwald, 1990; Klug et al., 1993; Hill and Olson, 2008). These events might cause left ventricular dilation and dysfunction, what is known as the adverse cardiac remodeling, which increases the risk of heart failure and malignant arrhythmia (Hill and Olson, 2008; van der Bruggen et al., 2017).

Initial attentions have been given to describe the role of TRP channels in the appearance of cardiac remodeling using different experimental procedures *in vitro* and *in vivo* in animal models (Guinamard and Bois, 2007; Eder and Molkentin, 2011; Yue et al., 2015). Here, we will focus on the role of TRPCs, TRPVs, and TRPMs role in the adverse cardiac remodeling, since little is known regarding the other subfamilies and their participation in these processes.

TRPs and Cardiac Hypertrophy

Compelling evidence confirmed that the activity and expression of several TRP channels are upregulated in pathological hypertrophy and heart failure as reviewed elsewhere (Watanabe et al., 2008; Yue et al., 2015; Freichel et al., 2017), and as summarized in **Figure 1**. Special attention has been given to TRPC's role in cardiac hypertrophy, but the implication of TRPV1, TRPV2, and TRPM4 has been also demonstrated.

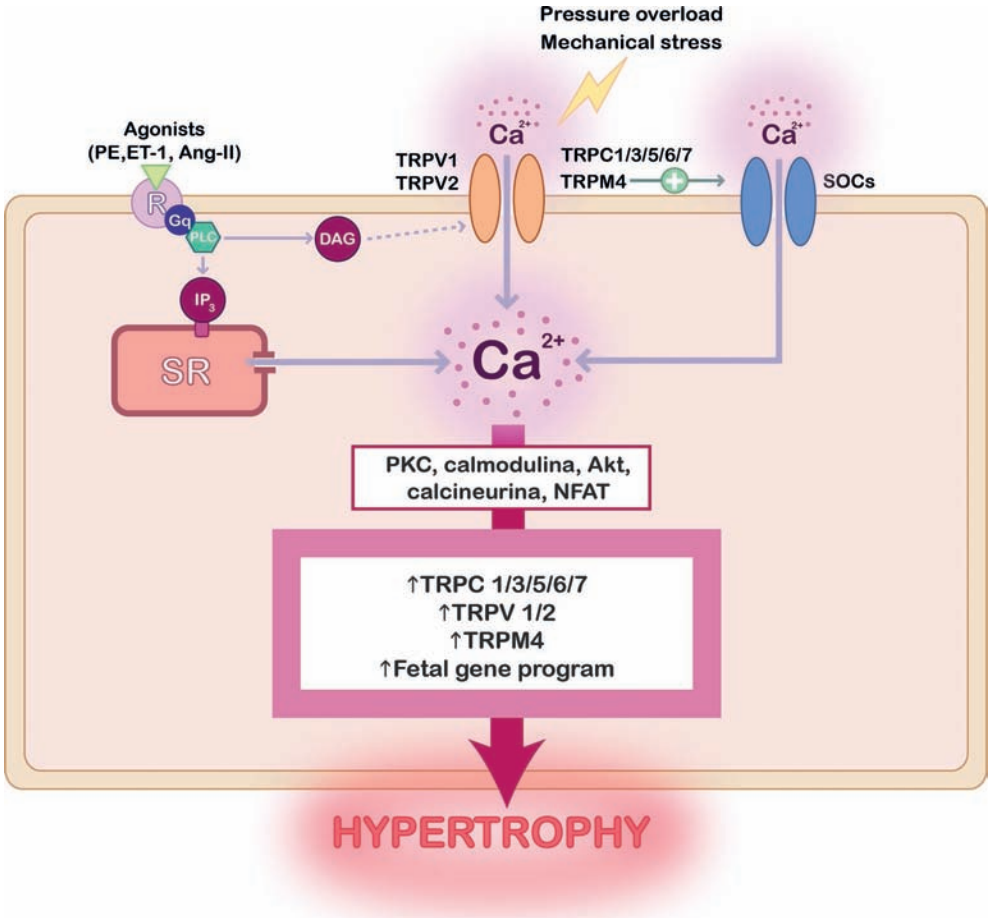

FIGURE 1 | Scheme summarizing the role of TRP channels in cardiac hypertrophy. Activation of TRP channels can be preceded by stimulation of G-coupled receptors with hypertrophic agonists, by mechanical stress, or pressure overload. The consequent increase of the intracellular Ca^{2+} concentration stimulates different signaling protein, such as PKC, AKT, calcineurin, and NFAT, whose activation promotes TRP channels overexpression and the activation of fetal genes reprograming leading to cardiac hypertrophy.

TRPCs and Hypertrophy

The role of TRPCs in the pathological cardiac hypertrophy has been extensively studied in isolated neonatal and adult cardiac myocytes and in different animal model of cardiac hypertrophy (Nishida and Kurose, 2008; Watanabe et al., 2008; Eder and Molkentin, 2011; Xiao et al., 2017). Ca^{2+} entry through TRPCs is considered essential to activate signaling pathways involving PKC, calmodulin-kinase, and calcineurin/NFAT, which promotes cardiac hypertrophy by the re-expression of the fetal gene program (Heineke and Molkentin, 2006; Nakayama et al., 2006; Eder and Molkentin, 2011). Independent reports demonstrated that stimulation of neonatal rat cardiac myocytes with hypertrophic agonists such as ATP, endothelin-1, phenylephrine, or angiotensin-II, increased cells size, correlating with the upregulation and activation of TRPC1 (Ohba et al., 2007), TRPC3 (Brenner and Dolmetsch, 2007), TRPC5 (Sunggip et al., 2018), and TRPC7 (Satoh et al., 2007). Using animal models of pressure overload-induced heart hypertrophy, different studies demonstrated that TRPC1 (Ohba et al., 2007), TRPC3 (Bush et al., 2006; Brenner and Dolmetsch, 2007), and TRPC6 (Kuwahara et al., 2006) are upregulated in heart. Conversely, the overexpression of TRPC3 in transgenic mice increased cardiac hypertrophy through calcineurin/NFAT activation when mice were subjected to angiotensin-II and phenylephrine treatment or pressure overload (Nakayama et al., 2006). Similarly, the overexpression of TRPC6 in transgenic mice leaded to the development of cardiac hypertrophy and heart failure (Kuwahara et al., 2006). In contrast, the use of cardiomyocyte-specific dominant-negative mutants in transgenic mice for TRPC3 and TRPC6 or for TRPC4 reduced cardiac hypertrophic responses following either the infusion of neuroendocrine agonists or pressure overload stimulation through calcineurin/NFAT (Wu et al., 2010). Moreover, *trpc1* gene deletion in mice attenuated pressure overload-induced hypertrophy by the alteration of calcineurin/NFAT and Akt signaling pathway (Seth et al., 2009). Intriguingly and in contrast to other studies mentioned here, a previous study reported that TRPC3/TRPC6 double knockout mice did not develop pressure-overload induced hypertrophy; however, *trpc3* or *trpc6* gene's deletion did not protect the heart from hypertrophy or dysfunction due to pressure overload, suggesting the need of both channels to promote the deleterious

hypertrophic response (Seo et al., 2014). This finding worth further investigation and confirmation in other model of pathological cardiac hypertrophy.

TRPVs and Hypertrophy

Most studies focused on TRPV1 and TRPV2 role in hypertrophy and the adverse cardiac remodeling. An early study revealed that TRPV1 knockout mice showed a reduced increase in heart's weight as compared to wild-type mice, and they were partially protected from pressure-overload induced cardiac hypertrophy (Buckley and Stokes, 2011). A recent study demonstrated that TRPV1's expression is increased in hypertrophied heart of mice evoked by transverse aorta constriction (TAC) (Chen et al., 2016). However, *Trpv1* gene's deletion was associated with excessive inflammation, exaggerated cardiac hypertrophy, and abnormal cardiac function after TAC, suggesting a protective role of TRPV1 (Zhong et al., 2018a). This study proposed that TRPV1, highly expressed in sensory nerves, might be involved in the regulation of cardiovascular function due to its anti-inflammatory effects *via* calcitonin gene-related peptide. Conversely, a previous study revealed that pharmacological activation of TRPV1 with SA13353 prevents the increase of cardiomyocyte size evoked by endothelin-1 (Zhang et al., 2012b). SA13353 also attenuated and reduced cold stress-induced hypertrophy and decreased the fractional shortening among others functional cardiac and cellular parameters (Zhang et al., 2012b). In contrast, another study showed that TRPV1 activation with capsaicin can antagonize high-salt diet-mediated cardiac hypertrophy, by ameliorating the mitochondrial complex I oxidative phosphorylation and suggesting that TRPV1-mediated amendment of mitochondrial dysfunction may represent a novel target for the management of early cardiac dysfunction (Lang et al., 2015). Therefore, the role of TRPV1 in the molecular mechanism underlying pathological cardiac hypertrophy still remains unclear.

TRPV2 is also significantly upregulated in wild-type mice subjected to TAC, whereas the absence of functional TRPV2 reduces significantly the left ventricular hypertrophy after TAC, suggesting a role of TRPV2 in the development of cardiomyocyte hypertrophy because of an increased afterload (Koch et al., 2017). In this way, the overexpression of TRPV2 was also associated with enlarged hearts in patients with dilated cardiomyopathy (Iwata et al., 2013). TRPV3 is also overexpressed in angiotensin-II-induced cardiomyocyte hypertrophy, which aggravated cardiac hypertrophy through calcineurin/NFATc3 signaling pathway activation (Zhang et al., 2018).

TRPMs and Hypertrophy

In the case of TRPMs, different studies focused especially on TRPM4 role in hypertrophy, while little is known regarding other TRPM channels. TRPM4 is thought to fine-tune the amount of Ca^{2+} influx into cardiomyocytes via store-operated Ca^{2+} channels after chronic angiotensin-II stimulation, through a mechanism involving calcineurin–NFAT activation (Kecskés et al., 2015). TRPM4 upregulation was observed in hypertrophied ventricular cardiomyocytes freshly isolated from well-established genetic model of spontaneously hypertensive rats when compared to control, the Wistar Kyoto rats (Guinamard et al., 2006). Interestingly, selective removal of TRPM4 from the heart resulted in an increased hypertrophic growth after chronic mice treatment with angiotensin-II as compared to wild type mice (Kecskés et al., 2015), suggesting a protective role of TRPM4. Recently, a study confirmed the beneficial role of TRPM4 in hard training-induced physiological hypertrophy because TRPM4 knockout mice developed a pathological cardiac hypertrophy when they were subjected to endurance training (Demion et al., 2014). The deletion of the *Trpm4* gene in 12-week-old mice was linked with moderate cardiac hypertrophy as well as ventricular dilation, increased cellular density, and reduced left ventricular cardiomyocytes size, suggesting that TRPM4 might act as a negative regulator of cardiomyocytes proliferation during prenatal development (Demion et al., 2014).

Role of TRPs in Interstitial Fibrosis

Cardiac fibroblasts represent ∼75% of all cardiac cells, although they represent about ∼10–15% of total cardiac cell volume due to their small size. However, the activation of cardiac fibroblasts plays a crucial role in cardiac pathology. Cardiac fibrosis is caused by an excessive extracellular matrix proteins produced by myofibroblasts, the differentiated phenotype of fibroblasts under stress situations (Yue et al., 2013), where the Ca^{2+} signaling is essential for transcriptional control regulation and myocardial fibrosis (Ramires et al., 1998), as illustrated in **Figure 2**. The role of TRP channels in cardiac fibroblasts activation, proliferation, and differentiation has been extensively investigated (Du et al., 2010; Yue et al., 2013; Certal et al., 2017). However, unlike in cardiac myocytes, TRPs-activated Ca^{2+} signaling mechanisms are not fully understood in fibroblasts.

TRPCs and Fibrosis

TRPC1, TRPC3, and TRPC6 are considered the main TRPCs implicated in cardiac fibrosis, but most studies focused on TRPC3's role in cardiac fibrosis, as reviewed recently (Numaga-Tomita et al., 2017). A role of background Ca^{2+} entry through TRPC1 and TRPC4 was associated with fibrosis in double knockout mice subjected to pressure overload (Camacho Londoño et al., 2015). In mechanically stressed hearts, TRPC3 activation triggered an aberrant increase of ROS production, leading to RhoA activation in both cardiac myocytes and fibroblasts, resulting in interstitial fibrosis (Kitajima et al., 2016). Actually, *trpc*3 gene deletion suppressed cardiac fibrosis in response to pressure overload or to angiotensin-II infusion (Domes et al., 2015; Kitajima et al., 2016; Numaga-Tomita et al., 2016). TRPC3 blockade with Pyr3 also inhibited angiotensin-II-induced Ca^{2+} entry, proliferation, and differentiation of fibroblasts isolated from left atrial of electrically maintained atrial fibrillation in a dog model (Harada et al., 2012). Recently, chronic treatment of rat models of pressure overload with GSK503A, proposed to inhibit both TRPC3 and TRPC6, showed no interstitial cardiac fibrosis (Seo et al., 2014), suggesting that TRPC3 and TRPC6 are needed for the fibrosis appearance. TRPC6 has been supposed as a regulator of myofibroblast differentiation, since its silencing in human cardiac fibroblasts attenuated the upregulation of α-SMA, a marker of myofibroblast transformation, induced by TGF-β1, a pro-fibrotic agonist (Kapur et al., 2014). Conversely, the loss of TRPC6 in knockout mice prevented TGF-β1-mediated

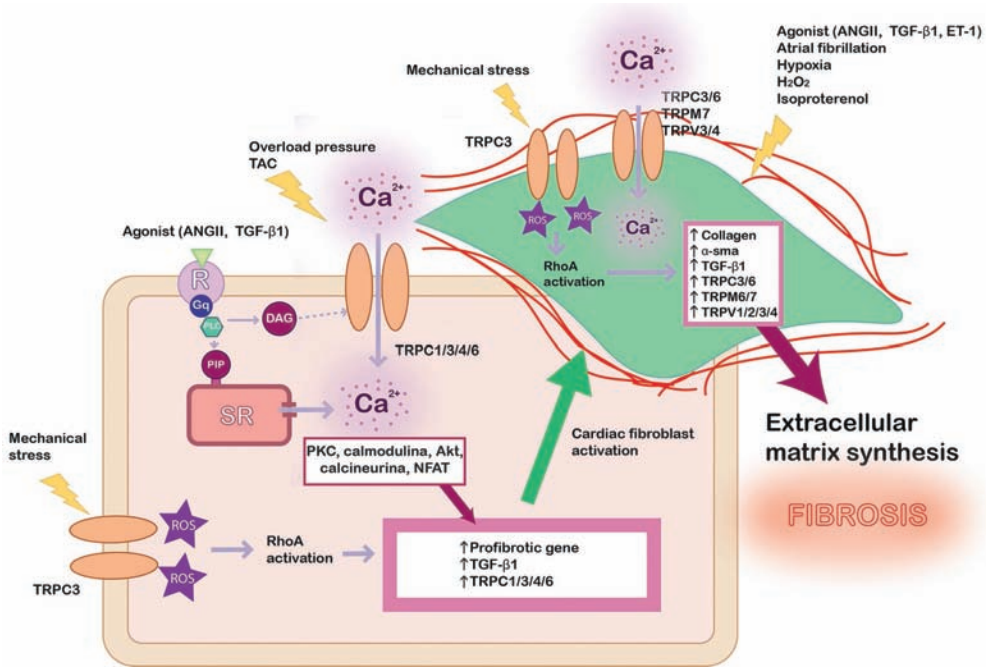

FIGURE 2 | Scheme summarizing the role of TRP channels in cardiac fibrosis. In pathological conditions, different kind of stress stimulates Ca^{2+} entry in cardiac myocyte through TRP channels and other signaling pathway as RhoA dependent on reactive oxygen species (ROS) production, which lead to profibrotic gene's expression. Profibrotic agonists and other stimuli activate cardiac fibroblast (green) leading to their proliferation and differentiation. The intracellular Ca^{2+} concentration increase through TRP channels promotes the expression of pro-fibrotic agonist (TGF-β1), α-SMA, collagen, and different isoforms of TRP channels, leading to exacerbated extracellular matrix synthesis and fibrosis.

myofibroblast transformation. In addition, TRPC6 overexpression using adenovirus promoted fibroblast conversion to myofibroblast, a hallmark of fibrosis (Davis et al., 2012). In contrast to this finding, an early report proposed that silencing of TRPC6 enhanced myofibroblast formation (Nishida et al., 2007), which questions whether TRPC6 is relevant for cardiac fibrosis.

TRPVs and Fibrosis

TRPV channels seem also critical for cardiac fibroblast differentiation to myofibroblasts. It was shown that the ablation of TRPV1 markedly enhanced the fibrosis due to myocardial infarction, by the stimulation of the TGF-β1 and Smad2 signaling pathway (Huang et al., 2010). In contrast, the administration of a TRPV1 antagonist in TAC mice protected the heart from the fibrotic process (Horton et al., 2013). Conversely, in a pressure-overload mice model, it demonstrated a reduction of hypertrophy and fibrosis-mediated TRPV1 channel activation by capsaicin (Wang et al., 2014). Capsaicin blunted pressure overload–induced upregulation of TGF-β1 and Smad2/3 phosphorylation. It also reduced angiotensin-II-induced proliferation of cardiac fibroblast isolated from wild-type but not from TRPV1-knockout mice (Wang et al., 2014). Recently, the overexpression of TRPV1 in transgenic mice-attenuated isoproterenol-induced myocardial fibrosis *in vitro* and *in vivo* in primary cultured cardiac fibroblasts (Wang et al., 2016).

Other reports suggested that TRPV2, TRPV3, and TRPV4 channels also participate in cardiac fibrosis. TRPV2 functional deletion was associated with a decreased development of fibrosis associated with aging (Jones et al., 2017), while TRPV2 upregulation was associated with enlarged hearts, increased fibrosis, and myocardial structural defects in patients with dilated cardiomyopathy (Iwata et al., 2013). Furthermore, TRPV3 activation intensified cardiac fibrosis, stimulating cardiac fibroblast proliferation in the pressure-overloaded rat hearts (Liu et al., 2018). TRPV4 seems also necessary for cardiac fibroblasts differentiation to myofibroblasts, since AB159908, a TRPV4 antagonist, as well as TRPV4 siRNA inhibited TGF-β1-induced fibroblasts differentiation (Adapala et al., 2013). Actually, TRPV4-knockout mice presented decreased fibrosis after myocardial infarction (Adapala et al., 2018).

TRPMs and Fibrosis

Several reports made special attention to the abnormal expression of TRPM7 and the development of cardiac fibrosis; however, little is known regarding other TRPM channels (Xu et al., 2015). Recently, higher amount of mRNA and protein levels of TRPM6 in addition to significant increase in markers of myocardial fibrosis as TGF-β1, collagen I and III, were detected in atrial fibrillation patients, suggesting possible contribution of TRPM6 to atrial fibrosis (Zhang et al., 2015).

Experimental strategies treating human or animal cardiac fibroblasts with pro-fibrotic agonists or with hormones as angiotensin-II increased significantly the expression of TRPM7. In fact, TGF-β1 addition to human atrial fibroblasts upregulated

the expression of TRPM7; meanwhile, TRPM7 silencing inhibited fibroblasts proliferation, differentiation, and collagen production induced by TGF-β1 (Du et al., 2010). Angiotensin-II also stimulated TRPM7 resulting in an increased expression of α-SMA and fibronectin protein (Yu et al., 2014). Moreover, rat cardiac fibroblasts incubated with angiotensin-II increased levels of protein expression of TRPM7, collagens I and III, which promoted fibrosis (Zhou et al., 2015). In contrast, the downregulation of TRPM7 decreased its related current density and inhibited angiotensin-II mediated cardiac fibroblasts proliferation, differentiation, and collagen synthesis (Li et al., 2017). Moreover, in rats with sick sinus syndrome, TRPM7 regulated angiotensin II-induced cardiac fibroblasts proliferation and collagen synthesis of sinoatrial node, involving Smad signaling pathway (Zhong et al., 2018b). Recently, a role of TRPM7 was reported in miRNA-135a inhibition of isoproterenol-induced cardiac fibrosis (Wu et al., 2018) and in fibrosis evoked by H_2O_2 and hypoxia (Guo et al., 2014; Lu et al., 2017). Therefore, TRPM7 stand out as an interesting possible target to attenuate pathological cardiac fibrosis.

TRPs and Conduction Disorders

Atrial fibrillation (AF) is the most sustained clinical arrhythmia, which occurs due to structural remodeling, involving prominent fibrotic changes (Yue et al., 2011). TRP channels do not influence the excitability of heart's pacemaker but apparently their upregulation mediate the arrhythmogenesis and the progression of electrical remodeling of the diseased heart (Yue et al., 2015). Special advances have been made by studying the role of TRPM4, TRPC3, and TRPM7 in conduction disorders in the heart.

TRPM4 contribution to cardiac conduction as well as the development of arrhythmias has been demonstrated using different approaches, such as channel inhibition with 9-phenantrol, a blocker for TRPM4 (Grand et al., 2008), using TRPM4-deficient mouse models, and by the identification of TRPM4 mutants detected in a variety of inherited human cardiac arrhythmias (Freichel et al., 2017). A pro-arrhythmic role of TRPM4 and its participation in membrane potential depolarization likely explain the triggering of spontaneous beating and the increase of action potential duration described in the hypertrophied heart (Demion et al., 2014). *In vitro* experiments showed that 9-phenanthrol decreased Ca^{2+} oscillations in atrial HL-1 mouse cardiac myocytes, thought to play a critical role in arrhythmias (Burt et al., 2013). TRPM4 inhibition with 9-phenanthrol also mimicked the reduction of action potential duration evoked by TRPM4 deletion in atrial cells (Simard et al., 2013) and reverted the early after-depolarization involved in cardiac arrhythmias observed after a process of hypoxia and re-oxygenation (Simard et al., 2012). Recently, it was shown that physiological range of $[Ca^{2+}]_i$ could activate TRPM4, and its upregulation altered action potential characteristics in HL-1 cells treated with angiotensin-II, which increased the arrhythmic propensity of cardiac tissue in pathological situation (Hu et al., 2017). Interestingly, *trpm4* gene mutations were linked to progressive familial heart block type 1 (Kruse et al., 2009; Daumy et al., 2016), isolated cardiac conduction disease (Liu et al., 2010), atrio-ventricular block (Stallmeyer et al., 2012; Syam et al., 2016), right bundle branch block (Stallmeyer et al., 2012), Brugada syndrome (Liu et al., 2013; Gualandi et al., 2017), and recently to either complete heart block or idiopathic ventricular fibrillation (Bianchi et al., 2018).

Additional indications suggested that TRPM7 and TRPC3 might also mediate the pathogenesis of AF. In atrial fibroblasts from AF patients, TRPM7 is notably upregulated (Du et al., 2010; Zhang et al., 2012a) and was suggested to play a pivotal role in AF due to fibrogenesis in the atrium since fibrosis is the main factor for AF. TRPM7 knockdown suppressed endogenous TRPM7 currents, decreased Ca^{2+} influx in atrial fibroblasts, and inhibited TGF-β1-induced fibroblast proliferation, differentiation, and collagen production (Du et al., 2010). TRPC3 is also significantly upregulated in the atria of AF patients (Zhao et al., 2013). In fibroblasts freshly isolated from left atrial of dogs undergoing AF, by sustained atrial tachypacing, it was observed a significantly increase in TRPC3 protein expression, currents, ERK phosphorylation, and extracellular matrix gene expression (Harada et al., 2012). Further evidence for a role of TRPC3 has been demonstrated in experiments using TRPC3 knockout mice, in which the effect of angiotensin-II addition to pacing-induced AF mice was significantly reduced compared to wild-type mice (Ju et al., 2015). Interestingly, a recent study examined the expression of different TRPs in leukocytes of patients with nonvalvular AF (Düzen et al., 2017). They observed marked increase in gene expression of TRPC1-C7, TRPV1-V6, TRPM1-M8, TRPML1-ML3, TRPA1, and TRPP2. A possible correlation between these leukocytes genes' expression and those examined from the atrium will be of major interest. Therefore, further investigations are undoubtedly needed for understanding the role of all these TRP channels in AF.

CONCLUSIONS AND PERSPECTIVES

A growing body of evidence has demonstrated that, by controlling Ca^{2+} homeostasis, different TRP isoforms are critically involved in pathological cardiac remodeling and heart failure. However, molecular mechanisms which trigger the transition of the heart from adaptation to maladaptation by these channels are still unknown. In the last two decades, the use of genetically modified animal and mice models of cardiac disease provided valuable information about TRPs implication in cardiac remodeling. Nevertheless, substantial work is still required to understand why many TRPs from different subfamilies are activated by similar pro-hypertrophic or pro-fibrotic stimuli, and whether they associate or interact between them to activate signaling pathway involved in hypertrophy, fibrosis, or conduction disorders. Unfortunately, the wide range of agonists and antagonists used to modulate TRPs failed to determine which TRPs might be the right target(s) to characterize and consider as therapeutic tools. More specific inhibitors/activators of TRPs are eagerly awaited to shed a light on the complex mechanism of cardiac diseases associated with remodeling. Of hope, the increasing amount of available information related to TRP-drug

interaction sites and gating processes of TRP channels is expected to facilitate the development of novel therapeutic concepts by pharmaceutical companies. Overall, and in the light of the reported studies, TRP channels are still considered promising therapeutic targets to regulate pathological cardiac plasticity.

AUTHOR CONTRIBUTIONS

TS conceived the concept of the review. TS, IG-O, DF, RT, MM-B, and EC-S wrote the review. IG-O, DF, AH and JR designed and formatted the figures. TS, IG-O, RT, DF, AH, and JR read and edited the review manuscript.

FUNDING

This work was supported by Spanish Ministry of Economy and Competitiveness [BFU2016–74932-C2]; Institute of Carlos III [PI15/00203; PI16/00259; CB16/11/00431]; the Andalusia Government [PI-0313-2016]. This study was co-financed by FEDER Funds.

REFERENCES

Adapala, R. K., Thoppil, R. J., Luther, D. J., Paruchuri, S., Meszaros, J. G., Chilian, W. M., et al. (2013). TRPV4 channels mediate cardiac fibroblast differentiation by integrating mechanical and soluble signals. *J. Mol. Cell. Cardiol.* 54, 45–52. doi: 10.1016/j.yjmcc.2012.10.016

Adapala, R., Minasyan, A., Kanugula, A. K., Cappelli, H. C., Paruchuri, S., Meszaros, G. J., et al. (2018). Targeting TRPV4 channels protects heart from pathological remodeling following myocardial infarction. *Circulation.* 136:A24061.

Albarrán, L., Lopez, J. J., Dionisio, N., Smani, T., Salido, G. M., and Rosado, J. A. (2013). Transient receptor potential ankyrin-1 (TRPA1) modulates store-operated Ca(2+) entry by regulation of STIM1-Orai1 association. *Biochim. Biophys. Acta* 1833, 3025–3034. doi: 10.1016/j.bbamcr.2013.08.014

Alonso-Carbajo, L., Kecskes, M., Jacobs, G., Pironet, A., Syam, N., Talavera, K., et al. (2017). Muscling in on TRP channels in vascular smooth muscle cells and cardiomyocytes. *Cell Calcium* 66, 48–61. doi: 10.1016/j.ceca.2017.06.004

Avila-Medina, J., Mayoral-Gonzalez, I., Dominguez-Rodriguez, A., Gallardo-Castillo, I., Ribas, J., Ordoñez, A., et al. (2018). The complex role of store operated calcium entry pathways and related proteins in the function of cardiac, skeletal and vascular smooth muscle cells. *Front. Physiol.* 9:257. doi: 10.3389/fphys.2018.00257

Berridge, M. J. (2002). The endoplasmic reticulum: a multifunctional signaling organelle. *Cell Calcium* 32, 235–249. doi: 10.1016/S0143416002001823

Bers, D. M. (2002). Cardiac excitation-contraction coupling. *Nature* 415, 198–205. doi: 10.1038/415198a

Bianchi, B., Ozhathil, L. C., Medeiros-Domingo, A., Gollob, M. H., and Abriel, H. (2018). Four TRPM4 cation channel mutations found in cardiac conduction diseases lead to altered protein stability. *Front. Physiol.* 9:177. doi: 10.3389/fphys.2018.00177

Brenner, J. S., and Dolmetsch, R. E. (2007). TrpC3 regulates hypertrophy-associated gene expression without affecting myocyte beating or cell size. *PLoS One* 2:e802. doi: 10.1371/journal.pone.0000802

Buckley, C. L., and Stokes, A. J. (2011). Mice lacking functional TRPV1 are protected from pressure overload cardiac hypertrophy. *Channels* 5, 367–374. doi: 10.4161/chan.5.4.17083

Burt, R., Graves, B. M., Gao, M., Li, C., Williams, D. L., Fregoso, S. P., et al. (2013). 9-Phenanthrol and flufenamic acid inhibit calcium oscillations in HL-1 mouse cardiomyocytes. *Cell Calcium* 54, 193–201. doi: 10.1016/j.ceca.2013.06.003

Bush, E. W., Hood, D. B., Papst, P. J., Chapo, J. A., Minobe, W., Bristow, M. R., et al. (2006). Canonical transient receptor potential channels promote cardiomyocyte hypertrophy through activation of calcineurin signaling. *J. Biol. Chem.* 281, 33487–33496. doi: 10.1074/jbc.M605536200

Camacho Londoño, J. E., Tian, Q., Hammer, K., Schröder, L., Camacho Londoño, J., Reil, J. C., et al. (2015). A background Ca^{2+} entry pathway mediated by TRPC1/TRPC4 is critical for development of pathological cardiac remodelling. *Eur. Heart J.* 36, 2257–2266. doi: 10.1093/eurheartj/ehv250

Certal, M., Vinhas, A., Barros-Barbosa, A., Ferreirinha, F., Costa, M. A., and Correia-de-Sá, P. (2017). ADP-induced Ca2+signaling and proliferation of rat ventricular myofibroblasts depend on phospholipase C-linked TRP channels activation within lipid rafts. *J. Cell. Physiol.* 232, 1511–1526. doi: 10.1002/jcp.25656

Chen, M., Xin, J., Liu, B., Luo, L., Li, J., Yin, W., et al. (2016). Mitogen-activated protein kinase and intracellular polyamine signaling is involved in TRPV1 activation–induced cardiac hypertrophy. *J. Am. Heart Assoc.* 5. doi: 10.1161/JAHA.116.003718

Chubanov, V., Ferioli, S., and Gudermann, T. (2017). Assessment of TRPM7 functions by drug-like small molecules. *Cell Calcium* 67, 166–173. doi: 10.1016/j.ceca.2017.03.004

Criollo, A., Altamirano, F., Pedrozo, Z., Schiattarella, G. G., Li, D. L., Rivera-Mejías, P., et al. (2018). Polycystin-2-dependent control of cardiomyocyte autophagy. *J. Mol. Cell. Cardiol.* 118, 110–121. doi: 10.1016/j.yjmcc.2018.03.002

Daumy, X., Amarouch, M. -Y., Lindenbaum, P., Bonnaud, S., Charpentier, E., Bianchi, B., et al. (2016). Targeted resequencing identifies TRPM4 as a major gene predisposing to progressive familial heart block type I. *Int. J. Cardiol.* 207, 349–358. doi: 10.1016/j.ijcard.2016.01.052

Davis, J., Burr, A. R., Davis, G. F., Birnbaumer, L., and Molkentin, J. D. (2012). A TRPC6-dependent pathway for myofibroblast transdifferentiation and wound healing in vivo. *Dev. Cell* 23, 705–715. doi: 10.1016/j.devcel.2012.08.017

Demion, M., Thireau, J., Gueffier, M., Finan, A., Khoueiry, Z., Cassan, C., et al. (2014). Trpm4 gene invalidation leads to cardiac hypertrophy and electrophysiological alterations. *PLoS One* 9:e115256. doi: 10.1371/journal.pone.0115256

Domes, K., Patrucco, E., Loga, F., Dietrich, A., Birnbaumer, L., Wegener, J. W., et al. (2015). Murine cardiac growth, TRPC channels, and cGMP kinase I. *Pflügers Arch.—Eur. J. Physiol.* 467, 2229–2234. doi: 10.1007/s00424-014-1682-0

Domínguez-Rodríguez, A., Mayoral-Gonzalez, I., Avila-Medina, J., de Rojas-de Pedro, E. S., Calderón-Sánchez, E., Díaz, I., et al. (2018). Urocortin-2 prevents dysregulation of ca^{2+} homeostasis and improves early cardiac remodeling after ischemia and reperfusion. *Front. Physiol.* 9:813. doi: 10.3389/fphys.2018.00813

Domínguez-Rodríguez, A., Ruiz-Hurtado, G., Sabourin, J., Gómez, A. M., Alvarez, J. L., and Benitah, J. -P. (2015). Proarrhythmic effect of sustained EPAC activation on TRPC3/4 in rat ventricular cardiomyocytes. *J. Mol. Cell. Cardiol.* 87, 74–78. doi: 10.1016/j.yjmcc.2015.07.002

Du, J., Xie, J., Zhang, Z., Tsujikawa, H., Fusco, D., Silverman, D., et al. (2010). TRPM7-mediated Ca^{2+} signals confer fibrogenesis in human atrial fibrillation. *Circ. Res.* 106, 992–1003. doi: 10.1161/CIRCRESAHA.109.206771

Düzen, I. V, Yavuz, F., Vuruskan, E., Saracoglu, E., Poyraz, F., Göksülük, H., et al. (2017). Leukocyte TRP channel gene expressions in patients with non-valvular atrial fibrillation. *Sci. Rep.* 7:9272. doi: 10.1038/s41598-017-10039-0

Eder, P. (2017). "Cardiac remodeling and disease: SOCE and TRPC signaling in cardiac pathology" in *Advances in experimental medicine and biology*, (Springer Nature) 505–521. doi: 10.1007/978-3-319-57732-6_25

Eder, P., and Molkentin, J. D. (2011). TRPC Channels As Effectors of Cardiac Hypertrophy. *Circ. Res.* 108, 265–272. doi: 10.1161/CIRCRESAHA.110.225888

Egginton, S. (2009). Invited review: activity-induced angiogenesis. *Pflugers Arch. Eur. J. Physiol.* 457, 963–977. doi: 10.1007/s00424-008-0563-9

Eisner, D. A., Caldwell, J. L., Kistamás, K., and Trafford, A. W. (2017). Calcium and excitation-contraction coupling in the heart. *Circ. Res.* 121, 181–195. doi: 10.1161/CIRCRESAHA.117.310230

Entin-Meer, M., Cohen, L., Hertzberg-Bigelman, E., Levy, R., Ben-Shoshan, J., and Keren, G. (2017). TRPV2 knockout mice demonstrate an improved cardiac performance following myocardial infarction due to attenuated activity of peri-infarct macrophages. *PLoS One* 12:e0177132. doi: 10.1371/journal.pone.0177132

Entin-Meer, M., Levy, R., Goryainov, P., Landa, N., Barshack, I., Avivi, C., et al. (2014). The transient receptor potential vanilloid 2 cation channel is abundant in macrophages accumulating at the peri-infarct zone and may enhance their migration capacity towards injured cardiomyocytes following myocardial infarction. *PLoS One* 9:e105055. doi: 10.1371/journal.pone.0105055

Flockerzi, V., and Nilius, B. (2014). "TRPs: Truly Remarkable Proteins" in *Handbook of experimental pharmacology*, ed. J. E. Barrett (Springer Nature), 1–12. doi: 10.1007/978-3-642-54215-2_1

Freichel, M., Berlin, M., Schürger, A., Mathar, I., Bacmeister, L., Medert, R., et al. (2017). "TRP channels in the heart" in *Neurobilogy of TRP Channels*, ed. T. L. R. Emir (Boca Raton (FL): CRC Press/Taylor & Francis. Chapter 9).

Freichel, M., Tsvilovskyy, V., and Camacho-Londoño, J. E. (2014). "TRPC4- and TRPC4-Containing Channels" in *Handbook of experimental pharmacology*. ed. J. E. Barrett (Springer Nature), 85–128. doi: 10.1007/978-3-642-54215-2_5

Gao, Y., Song, J., Chen, H., Cao, C., and Lee, C. (2015). TRPV1 activation is involved in the cardioprotection of remote limb ischemic postconditioning in ischemia-reperfusion injury rats. *Biochem. Biophys. Res. Commun.* 463, 1034–1039. doi: 10.1016/j.bbrc.2015.06.054

Gaudet, R. (2007). "Structural insights into the function of TRP channels" in *TRP Ion Channel Function in Sensory Transduction and Cellular Signaling Cascades* (Boca Raton (FL) CRC Press/Taylor & Francis. Chapter 25).

Gerhold, K. A., and Schwartz, M. A. (2016). Ion channels in endothelial responses to fluid shear stress. *Physiology* 31, 359–369. doi: 10.1152/physiol.00007.2016

Grand, T., Demion, M., Norez, C., Mettey, Y., Launay, P., Becq, F., et al. (2008). 9-phenanthrol inhibits human TRPM4 but not TRPM5 cationic channels. *Br. J. Pharmacol.* 153, 1697–1705. doi: 10.1038/bjp.2008.38

Gualandi, F., Zaraket, F., Malagù, M., Parmeggiani, G., Trabanelli, C., Fini, S., et al. (2017). Mutation load of multiple ion channel gene mutations in brugada syndrome. *Cardiology* 137, 256–260. doi: 10.1159/000471792

Guinamard, R., and Bois, P. (2007). Involvement of transient receptor potential proteins in cardiac hypertrophy. *Biochim. Biophys. Acta - Mol. Basis Dis.* 1772, 885–894. doi: 10.1016/j.bbadis.2007.02.007

Guinamard, R., Demion, M., Magaud, C., Potreau, D., and Bois, P. (2006). Functional expression of the TRPM4 cationic current in ventricular cardiomyocytes from spontaneously hypertensive rats. *Hypertension* 48, 587–594. doi: 10.1161/01.HYP.0000237864.65019.a5

Guo, J. -L., Yu, Y., Jia, Y. -Y., Ma, Y. -Z., Zhang, B. -Y., Liu, P. -Q., et al. (2014). Transient receptor potential melastatin 7 (TRPM7) contributes to H_2O_2-induced cardiac fibrosis via mediating Ca(2+) influx and extracellular signal-regulated kinase 1/2 (ERK1/2) activation in cardiac fibroblasts. *J. Pharmacol. Sci.* 125, 184–192. doi: 10.1254/jphs.13224FP

Harada, M., Luo, X., Qi, X. Y., Tadevosyan, A., Maguy, A., Ordog, B., et al. (2012). Transient receptor potential canonical-3 channel-dependent fibroblast regulation in atrial fibrillation. *Circulation* 126, 2051–2064. doi: 10.1161/CIRCULATIONAHA.112.121830

He, X., Li, S., Liu, B., Susperreguy, S., Formoso, K., Yao, J., et al. (2017). Major contribution of the 3/6/7 class of TRPC channels to myocardial ischemia/reperfusion and cellular hypoxia/reoxygenation injuries. *Proc. Natl. Acad. Sci.* 114, E4582–E4591. doi: 10.1073/pnas.1621384114

Heineke, J., and Molkentin, J. D. (2006). Regulation of cardiac hypertrophy by intracellular signalling pathways. *Nat. Rev. Mol. Cell Biol.* 7, 589–600. doi: 10.1038/nrm1983

Hill, J. A., and Olson, E. N. (2008). Cardiac plasticity. *N. Engl. J. Med.* 358, 1370–1380. doi: 10.1056/NEJMra072139

Hoffman, N. E., Miller, B. A., Wang, J., Elrod, J. W., Rajan, S., Gao, E., et al. (2015). Ca^{2+} entry via Trpm2 is essential for cardiac myocyte bioenergetics maintenance. *Am. J. Physiol. Circ. Physiol.* 308, H637–H650. doi: 10.1152/ajpheart.00720.2014

Holzer, P., and Izzo, A. A. (2014). The pharmacology of TRP channels. *Br. J. Pharmacol.* 171, 2469–2473. doi: 10.1111/bph.12723

Horton, J. S., Buckley, C. L., and Stokes, A. J. (2013). Successful TRPV1 antagonist treatment for cardiac hypertrophy and heart failure in mice. *Channels (Austin)* 7, 17–22. doi: 10.4161/chan.23006

Hu, Y., Duan, Y., Takeuchi, A., Hai-Kurahara, L., Ichikawa, J., Hiraishi, K., et al. (2017). Uncovering the arrhythmogenic potential of TRPM4 activation in atrial-derived HL-1 cells using novel recording and numerical approaches. *Cardiovasc. Res.* 113, 1243–1255. doi: 10.1093/cvr/cvx117

Huang, W., Rubinstein, J., Prieto, A. R., and Wang, D. H. (2010). Enhanced postmyocardial infarction fibrosis via stimulation of the transforming growth factor-beta-Smad2 signaling pathway: role of transient receptor potential vanilloid type 1 channels. *J. Hypertens.* 28, 367–376. doi: 10.1097/HJH.0b013e328333af48

Inoue, R., Jensen, L. J., Shi, J., Morita, H., Nishida, M., Honda, A., et al. (2006). Transient receptor potential channels in cardiovascular function and disease. *Circ. Res.* 99, 119–131. doi: 10.1161/01.RES.0000233356.10630.8a

Inoue, R., Kurahara, L. -H., and Hiraishi, K. (2018). TRP channels in cardiac and intestinal fibrosis. *Semin. Cell Dev. Biol.* pii: S1084-9521(18)30045-4. doi: 10.1016/J.SEMCDB.2018.11.002

Islas, L. D. (2017). "Molecular Mechanisms of Temperature Gating in TRP Channels" in *Neurobilogy of TRP Channles*. ed. T. L. R. Emir (Boca Raton (FL): CRC Press/Taylor & Francis. Chapter 2).

Iwata, Y., Ohtake, H., Suzuki, O., Matsuda, J., Komamura, K., and Wakabayashi, S. (2013). Blockade of sarcolemmal TRPV2 accumulation inhibits progression of dilated cardiomyopathy. *Cardiovasc. Res.* 99, 760–768. doi: 10.1093/cvr/cvt163

Jardín, I., López, J. J., Diez, R., Sánchez-Collado, J., Cantonero, C., Albarrán, L., et al. (2017). TRPs in pain sensation. *Front. Physiol.* 8:392. doi: 10.3389/fphys.2017.00392

Jiang, J., Li, M., and Yue, L. (2005). Potentiation of TRPM7 inward currents by protons. *J. Gen. Physiol.* 126, 137–150. doi: 10.1085/jgp.200409185

Jones, J. L., Peana, D., Veteto, A. B., Lambert, M. D., Nourian, Z., Karasseva, N. G., et al. (2018). TRPV4 increases cardiomyocyte calcium cycling and contractility yet contributes to damage in the aged heart following hypoosmotic stress. *Cardiovasc. Res.* 115, 46–56. doi: 10.1093/cvr/cvy156

Jones, S., Mann, A., Worley, M. C., Fulford, L., Hall, D., Karani, R., et al. (2017). The role of transient receptor potential vanilloid 2 channel in cardiac aging. *Aging Clin. Exp. Res.* 29, 863–873. doi: 10.1007/s40520-016-0663-x

Ju, Y. -K., Chu, Y., Chaulet, H., Lai, D., Gervasio, O. L., Graham, R. M., et al. (2007). Store-operated Ca2+ influx and expression of TRPC genes in mouse sinoatrial node. *Circ. Res.* 100, 1605–1614. doi: 10.1161/CIRCRESAHA.107.152181

Ju, Y. -K., Lee, B. H., Trajanovska, S., Hao, G., Allen, D. G., Lei, M., et al. (2015). The involvement of TRPC3 channels in sinoatrial arrhythmias. *Front. Physiol.* 6:86. doi: 10.3389/fphys.2015.00086

Ju, Y., and Allen, D. G. (2007). Store-operated Ca2+ entry and TRPC expression; possible roles in cardiac pacemaker tissue. *Heart. Lung Circ.* 16, 349–355. doi: 10.1016/j.hlc.2007.07.004

Kapur, N. K., Qiao, X., Paruchuri, V., Mackey, E. E., Daly, G. H., Ughreja, K., et al. (2014). Reducing endoglin activity limits calcineurin and TRPC-6 expression and improves survival in a mouse model of right ventricular pressure overload. *J. Am. Heart Assoc.* 3. doi: 10.1161/JAHA.114.000965

Kecskés, M., Jacobs, G., Kerselaers, S., Syam, N., Menigoz, A., Vangheluwe, P., et al. (2015). The Ca(2+)-activated cation channel TRPM4 is a negative regulator of angiotensin II-induced cardiac hypertrophy. *Basic Res. Cardiol.* 110:43. doi: 10.1007/s00395-015-0501-x

Kitajima, N., Numaga-Tomita, T., Watanabe, M., Kuroda, T., Nishimura, A., Miyano, K., et al. (2016). TRPC3 positively regulates reactive oxygen species driving maladaptive cardiac remodeling. *Sci. Rep.* 6, 37001. doi: 10.1038/srep37001

Klug, D., Robert, V., and Swynghedauw, B. (1993). Role of mechanical and hormonal factors in cardiac remodeling and the biologic limits of myocardial adaptation. *Am. J. Cardiol.* 71, 46A–54A.

Koch, S. E., Mann, A., Jones, S., Robbins, N., Alkhattabi, A., Worley, M. C., et al. (2017). Transient receptor potential vanilloid 2 function regulates cardiac hypertrophy via stretch-induced activation. *J. Hypertens.* 35, 602–611. doi: 10.1097/HJH.0000000000001213

Kruse, M., Schulze-Bahr, E., Corfield, V., Beckmann, A., Stallmeyer, B., Kurtbay, G., et al. (2009). Impaired endocytosis of the ion channel TRPM4 is associated with human progressive familial heart block type I. *J. Clin. Invest.* 119, 2737–2744. doi: 10.1172/JCI38292

Kuwahara, K., Wang, Y., McAnally, J., Richardson, J. A., Bassel-Duby, R., Hill, J. A., et al. (2006). TRPC6 fulfills a calcineurin signaling circuit during pathologic cardiac remodeling. *J. Clin. Invest.* 116, 3114–3126. doi: 10.1172/JCI27702

Lang, H., Li, Q., Yu, H., Li, P., Lu, Z., Xiong, S., et al. (2015). Activation of TRPV1 attenuates high salt-induced cardiac hypertrophy through improvement of mitochondrial function. *Br. J. Pharmacol.* 172, 5548–5558. doi: 10.1111/bph.12987

Launay, P., Fleig, A., Perraud, A. L., Scharenberg, A. M., Penner, R., and Kinet, J. P. (2002). TRPM4 is a Ca^{2+}−activated nonselective cation channel mediating cell membrane depolarization. *Cell* 109, 397–407. doi: 10.1016/S0092-8674(02)00719-5

Li, M., Du, J., Jiang, J., Ratzan, W., Su, L. -T., Runnels, L. W., et al. (2007). Molecular determinants of Mg^{2+} and Ca^{2+} permeability and pH sensitivity in TRPM6 and TRPM7. *J. Biol. Chem.* 282, 25817–25830. doi: 10.1074/jbc.M608972200

Li, S., Li, M., Yi, X., Guo, F., Zhou, Y., Chen, S., et al. (2017). TRPM7 channels mediate the functional changes in cardiac fibroblasts induced by angiotensin II. *Int. J. Mol. Med.* 39, 1291–1298. doi: 10.3892/ijmm.2017.2943

Liu, H., Chatel, S., Simard, C., Syam, N., Salle, L., Probst, V., et al. (2013). Molecular genetics and functional anomalies in a series of 248 Brugada cases with 11 mutations in the TRPM4 channel. *PLoS One* 8:e54131. doi: 10.1371/journal.pone.0054131

Liu, H., El Zein, L., Kruse, M., Guinamard, R., Beckmann, A., Bozio, A., et al. (2010). Gain-of-function mutations in TRPM4 cause autosomal dominant isolated cardiac conduction disease. *Circ. Cardiovasc. Genet.* 3, 374–385. doi: 10.1161/CIRCGENETICS.109.930867

Liu, Y., Qi, H., E., M., Shi, P., Zhang, Q., Li, S., et al. (2018). Transient receptor potential vanilloid-3 (TRPV3) activation plays a central role in cardiac fibrosis induced by pressure overload in rats via TGF-β1 pathway. *Naunyn. Schmiedebergs. Arch. Pharmacol.* 391, 131–143. doi: 10.1007/s00210-017-1443-7

Lorin, C., Vögeli, I., and Niggli, E. (2015). Dystrophic cardiomyopathy: role of TRPV2 channels in stretch-induced cell damage. *Cardiovasc. Res.* 106, 153–162. doi: 10.1093/cvr/cvv021

Lu, J., Wang, Q. -Y., Zhou, Y., Lu, X. -C., Liu, Y. -H., Wu, Y., et al. (2017). AstragalosideIV against cardiac fibrosis by inhibiting TRPM7 channel. *Phytomedicine* 30, 10–17. doi: 10.1016/j.phymed.2017.04.002

Lu, Y., Piplani, H., McAllister, S. L., Hurt, C. M., and Gross, E. R. (2016). Transient receptor potential ankyrin 1 activation within the cardiac myocyte limits ischemia–reperfusion injury in rodents. *Anesthesiology* 125, 1171–1180. doi: 10.1097/ALN.0000000000001377

Makarewich, C. A., Zhang, H., Davis, J., Correll, R. N., Trappanese, D. M., Hoffman, N. E., et al. (2014). Transient receptor potential channels contribute to pathological structural and functional remodeling after myocardial infarction. *Circ. Res.* 115, 567–580. doi: 10.1161/CIRCRESAHA.115.303831

Miller, B. A., Hoffman, N. E., Merali, S., Zhang, X. -Q., Wang, J., Rajan, S., et al. (2014). TRPM2 channels protect against cardiac ischemia-reperfusion injury. *J. Biol. Chem.* 289, 7615–7629. doi: 10.1074/jbc.M113.533851

Montell, C., Birnbaumer, L., Flockerzi, V., Bindels, R. J., Bruford, E. A., Caterina, M. J., et al. (2002). A unified nomenclature for the superfamily of TRP cation channels. *Mol. Cell.* 9, 229–231. doi: 10.1016/S1097-2765(02)00448-3

Morine, K. J., Paruchuri, V., Qiao, X., Aronovitz, M., Huggins, G. S., DeNofrio, D., et al. (2016). Endoglin selectively modulates transient receptor potential channel expression in left and right heart failure. *Cardiovasc. Pathol.* 25, 478–482. doi: 10.1016/j.carpath.2016.08.004

Nakayama, H., Wilkin, B. J., Bodi, I., and Molkentin, J. D. (2006). Calcineurin-dependent cardiomyopathy is activated by TRPC in the adult mouse heart. *Faseb. J.* 20, 1660–1670. doi: 10.1096/fj.05-5560com

Nazıroğlu, M., and Braidy, N. (2017). Thermo-sensitive TRP channels: novel targets for treating chemotherapy-induced peripheral pain. *Front. Physiol.* 8:1040. doi: 10.3389/fphys.2017.01040

Nilius, B., and Droogmans, G. (2001). Ion channels and their functional role in vascular endothelium. *Physiol. Rev.* 81, 1415–1459. doi: 10.1152/physrev.2001.81.4.1415

Nishida, M., and Kurose, H. (2008). Roles of TRP channels in the development of cardiac hypertrophy. *Naunyn. Schmiedebergs. Arch. Pharmacol.* 378, 395–406. doi: 10.1007/s00210-008-0321-8

Nishida, M., Onohara, N., Sato, Y., Suda, R., Ogushi, M., Tanabe, S., et al. (2007). Galpha12/13-mediated up-regulation of TRPC6 negatively regulates endothelin-1-induced cardiac myofibroblast formation and collagen synthesis through nuclear factor of activated T cells activation. *J. Biol. Chem.* 282, 23117–23128. doi: 10.1074/jbc.M611780200

Numaga-Tomita, T., Kitajima, N., Kuroda, T., Nishimura, A., Miyano, K., Yasuda, S., et al. (2016). TRPC3-GEF-H1 axis mediates pressure overload-induced cardiac fibrosis. *Sci. Rep.* 6:39383. doi: 10.1038/srep39383

Numaga-Tomita, T., Oda, S., Shimauchi, T., Nishimura, A., Mangmool, S., and Nishida, M. (2017). TRPC3 channels in cardiac fibrosis. *Front. Cardiovasc. Med.* 4, 1–11. doi: 10.3389/fcvm.2017.00056

Ohba, T., Watanabe, H., Murakami, M., Takahashi, Y., Iino, K., Kuromitsu, S., et al. (2007). Upregulation of TRPC1 in the development of cardiac hypertrophy. *J. Mol. Cell. Cardiol.* 42, 498–507. doi: 10.1016/J.YJMCC.2006.10.020

Ong, H. L., and Ambudkar, I. S. (2017). "STIM-TRP pathways and microdomain organization: contribution of TRPC1 in store-operated Ca^{2+} entry: impact on Ca^{2+} signaling and cell function" in *Advances in experimental medicine and biology* (Springer Nature), 159–188. doi: 10.1007/978-3-319-57732-6_9

Ong, H. L., de Souza, L. B., and Ambudkar, I. S. (2016). "Role of TRPC channels in store-operated calcium entry" in *Advances in experimental medicine and biology* (Springer Nature), 87–109. doi: 10.1007/978-3-319-26974-0_5

Owsianik, G., D'hoedt, D., Voets, T., and Nilius, B. (2006). Structure-function relationship of the TRP channel superfamily. *Rev. Physiol. Biochem. Pharmacol.* 156, 61–90. doi: 10.1007/s10254-005-0006-3

Palazzo, E., Rossi, F., de Novellis, V., and Maione, S. (2013). Endogenous modulators of TRP channels. *Curr. Top. Med. Chem.* 13, 398–407. doi: 10.2174/1568026611313030014

Parajuli, N., Valtuille, L., Basu, R., Famulski, K. S., Halloran, P. F., Sergi, C., et al. (2015). Determinants of ventricular arrhythmias in human explanted hearts with dilated cardiomyopathy. *Eur. J. Clin. Invest.* 45, 1286–1296. doi: 10.1111/eci.12549

Peng, G., Shi, X., and Kadowaki, T. (2015). Evolution of TRP channels inferred by their classification in diverse animal species. *Mol. Phylogenet. Evol.* 84, 145–157. doi: 10.1016/J.YMPEV.2014.06.016

Pennekamp, P., Karcher, C., Fischer, A., Schweickert, A., Skryabin, B., Horst, J., et al. (2002). The ion channel polycystin-2 is required for left-right axis determination in mice. *Curr. Biol.* 12, 938–943. doi: 10.1016/S0960-9822(02)00869-2

Pfeffer, M. A., and Braunwald, E. (1990). Ventricular remodeling after myocardial infarction. Experimental observations and clinical implications. *Circulation* 81, 1161–1172. doi: 10.1161/01.CIR.81.4.1161

Pires, P. W., Ko, E. -A., Pritchard, H. A. T., Rudokas, M., Yamasaki, E., and Earley, S. (2017). The angiotensin II receptor type 1b is the primary sensor of intraluminal pressure in cerebral artery smooth muscle cells. *J. Physiol.* 595, 4735–4753. doi: 10.1113/JP274310

Ramires, F. J., Sun, Y., and Weber, K. T. (1998). Myocardial fibrosis associated with aldosterone or angiotensin II administration: attenuation by calcium channel blockade. *J. Mol. Cell. Cardiol.* 30, 475–483. doi: 10.1006/jmcc.1997.0612

Ramsey, I. S., Delling, M., and Clapham, D. E. (2006). An introduction to TRP channels. *Annu. Rev. Physiol.* 68, 619–647. doi: 10.1146/annurev.physiol.68.040204.100431

Randhawa, P. K., and Jaggi, A. S. (2017). TRPV 1 channels in cardiovascular system: a double edged sword? *Int. J. Cardiol.* 228, 103–113. doi: 10.1016/j.ijcard.2016.11.205

Sabourin, J., Antigny, F., Robin, E., Frieden, M., and Raddatz, E. (2012). Activation of transient receptor potential canonical 3 (TRPC3)-mediated Ca^{2+} entry by A1 adenosine receptor in cardiomyocytes disturbs atrioventricular conduction. *J. Biol. Chem.* 287, 26688–26701. doi: 10.1074/jbc.M112.378588

Sabourin, J., Bartoli, F., Antigny, F., Gomez, A. M., and Benitah, J. -P. (2016). Transient receptor potential canonical (TRPC)/Orai1-dependent store-operated Ca^{2+} channels: new targets of aldosterone in cardiomyocytes. *J. Biol. Chem.* 291, 13394–13409. doi: 10.1074/jbc.M115.693911

Sabourin, J., Robin, E., and Raddatz, E. (2011). A key role of TRPC channels in the regulation of electromechanical activity of the developing heart. *Cardiovasc. Res.* 92, 226–236. doi: 10.1093/cvr/cvr167

Sah, R., Mesirca, P., Mason, X., Gibson, W., Bates-Withers, C., Van den Boogert, M., et al. (2013). Timing of myocardial TRPM7 deletion during cardiogenesis variably disrupts adult ventricular function, conduction, and repolarization. *Circulation* 128, 101–114. doi: 10.1161/CIRCULATIONAHA.112.000768

Saleh, S. N., Albert, A. P., Peppiatt-Wildman, C. M., and Large, W. A. (2008). Diverse properties of store-operated TRPC channels activated by protein kinase C in vascular myocytes. *J. Physiol.* 586, 2463–2476. doi: 10.1113/jphysiol.2008.152157

Satoh, S., Tanaka, H., Ueda, Y., Oyama, J. I., Sugano, M., Sumimoto, H., et al. (2007). Transient receptor potential (TRP) protein 7 acts as a G protein-activated Ca^{2+} channel mediating angiotensin II-induced myocardial apoptosis. *Mol. Cell. Biochem.* 294, 205–215. doi: 10.1007/s11010-006-9261-0

Sawamura, S., Shirakawa, H., Nakagawa, T., Mori, Y., and Kaneko, S. (2017). *TRP channels in the brain: what are they there for?* CRC Press/Taylor & Francis.

Seo, K., Rainer, P. P., Shalkey Hahn, V., Lee, D. -i., Jo, S. -H., Andersen, A., et al. (2014). Combined TRPC3 and TRPC6 blockade by selective small-molecule or genetic deletion inhibits pathological cardiac hypertrophy. *Proc. Natl. Acad. Sci.* 111, 1551–1556. doi: 10.1073/pnas.1308963111

Seth, M., Zhang, Z. -S., Mao, L., Graham, V., Burch, J., Stiber, J., et al. (2009). TRPC1 channels are critical for hypertrophic signaling in the heart. *Circ. Res.* 105, 1023–1030. doi: 10.1161/CIRCRESAHA.109.206581

Simard, C., Hof, T., Keddache, Z., Launay, P., and Guinamard, R. (2013). The TRPM4 non-selective cation channel contributes to the mammalian atrial action potential. *J. Mol. Cell. Cardiol.* 59, 11–19. doi: 10.1016/j.yjmcc.2013.01.019

Simard, C., Sallé, L., Rouet, R., and Guinamard, R. (2012). Transient receptor potential melastatin 4 inhibitor 9-phenanthrol abolishes arrhythmias induced by hypoxia and re-oxygenation in mouse ventricle. *Br. J. Pharmacol.* 165, 2354–2364. doi: 10.1111/j.1476-5381.2011.01715.x

Smani, T., Shapovalov, G., Skryma, R., Prevarskaya, N., and Rosado, J. A. (2015). Functional and physiopathological implications of TRP channels. *Biochim. Biophys. Acta - Mol. Cell Res.* 1853, 1772–1782. doi: 10.1016/J.BBAMCR.2015.04.016

Stallmeyer, B., Zumhagen, S., Denjoy, I., Duthoit, G., Hébert, J. -L., Ferrer, X., et al. (2012). Mutational spectrum in the Ca(2+)-activated cation channel gene TRPM4 in patients with cardiac conductance disturbances. *Hum. Mutat.* 33, 109–117. doi: 10.1002/humu.21599

Sunggip, C., Shimoda, K., Oda, S., Tanaka, T., Nishiyama, K., Mangmool, S., et al. (2018). TRPC5-eNOS axis negatively regulates atp-induced cardiomyocyte hypertrophy. *Front. Pharmacol.* 9:523. doi: 10.3389/fphar.2018.00523

Suzuki, Y., Kodama, D., Goto, S., and Togari, A. (2011). Involvement of TRP channels in the signal transduction of bradykinin in human osteoblasts. *Biochem. Biophys. Res. Commun.* 410, 317–321. doi: 10.1016/J.BBRC.2011.05.140

Syam, N., Chatel, S., Ozhathil, L. C., Sottas, V., Rougier, J. -S., Baruteau, A., et al. (2016). Variants of transient receptor potential melastatin member 4 in childhood atrioventricular block. *J. Am. Heart Assoc.* 5. doi: 10.1161/JAHA.114.001625

van der Bruggen, C. E. E., Tedford, R. J., Handoko, M. L., van der Velden, J., and de Man, F. S. (2017). RV pressure overload: from hypertrophy to failure. *Cardiovasc. Res.* 113, 1423–1432. doi: 10.1093/cvr/cvx145

Venkatachalam, K., and Montell, C. (2007). TRP channels. *Annu. Rev. Biochem.* 76, 387–417. doi: 10.1146/annurev.biochem.75.103004.142819

Vetter, I., and Lewis, R. J. (2011). "Natural product ligands of TRP channels" in *Advances in experimental medicine and biology* (Springer Nature), 41–85. doi: 10.1007/978-94-007-0265-3_3

Vriens, J., Owsianik, G., Janssens, A., Voets, T., and Nilius, B. (2007). Determinants of 4α-phorbol sensitivity in transmembrane domains 3 and 4 of the cation channel TRPV4. *J. Biol. Chem.* 282, 12796–12803. doi: 10.1074/jbc.M610485200

Wang, L., and Wang, D. H. (2005). TRPV1 gene knockout impairs postischemic recovery in isolated perfused heart in mice. *Circulation* 112, 3617–3623. doi: 10.1161/CIRCULATIONAHA.105.556274

Wang, Q., Ma, S., Li, D., Zhang, Y., Tang, B., Qiu, C., et al. (2014). Dietary capsaicin ameliorates pressure overload-induced cardiac hypertrophy and fibrosis through the transient receptor potential vanilloid type 1. *Am. J. Hypertens.* 27, 1521–1529. doi: 10.1093/ajh/hpu068

Wang, Q., Zhang, Y., Li, D., Zhang, Y., Tang, B., Li, G., et al. (2016). Transgenic overexpression of transient receptor potential vanilloid subtype 1 attenuates isoproterenol-induced myocardial fibrosis in mice. *Int. J. Mol. Med.* 38, 601–609. doi: 10.3892/ijmm.2016.2648

Watanabe, H., Murakami, M., Ohba, T., Takahashi, Y., and Ito, H. (2008). TRP channel and cardiovascular disease. *Pharmacol. Ther.* 118, 337–351. doi: 10.1016/J.PHARMTHERA.2008.03.008

Wu, Q. -F., Qian, C., Zhao, N., Dong, Q., Li, J., Wang, B. -B., et al. (2017). Activation of transient receptor potential vanilloid 4 involves in hypoxia/reoxygenation injury in cardiomyocytes. *Cell Death Dis.* 8:e2828. doi: 10.1038/cddis.2017.227

Wu, X., Eder, P., Chang, B., and Molkentin, J. D. (2010). TRPC channels are necessary mediators of pathologic cardiac hypertrophy. *Proc. Natl. Acad. Sci. USA.* 107, 7000–7005. doi: 10.1073/pnas.1001825107

Wu, Y., Liu, Y., Pan, Y., Lu, C., Xu, H., Wang, X., et al. (2018). MicroRNA-135a inhibits cardiac fibrosis induced by isoproterenol via TRPM7 channel. *Biomed. Pharmacother.* 104, 252–260. doi: 10.1016/j.biopha.2018.04.157

Wu, Z. -Z., and Pan, H. -L. (2007). Role of TRPV1 and intracellular Ca^{2+} in excitation of cardiac sensory neurons by bradykinin. *Am. J. Physiol. Integr. Comp. Physiol.* 293, R276–R283. doi: 10.1152/ajpregu.00094.2007

Xiao, X., Liu, H. -X., Shen, K., Cao, W., and Li, X. -Q. (2017). Canonical transient receptor potential channels and their link with cardio/cerebro-vascular diseases. *Biomol. Ther. (Seoul)* 25, 471–481. doi: 10.4062/biomolther.2016.096

Xu, T., Wu, B. -M., Yao, H. -W., Meng, X. -M., Huang, C., Ni, M. -M., et al. (2015). Novel insights into TRPM7 function in fibrotic diseases: a potential therapeutic target. *J. Cell. Physiol.* 230, 1163–1169. doi: 10.1002/jcp.24801

Yamaguchi, Y., Iribe, G., Kaneko, T., Takahashi, K., Numaga-Tomita, T., Nishida, M., et al. (2018). TRPC3 participates in angiotensin II type 1 receptor-dependent stress-induced slow increase in intracellular Ca^{2+} concentration in mouse cardiomyocytes. *J. Physiol. Sci.* 68, 153–164. doi: 10.1007/s12576-016-0519-3

Yamaguchi, Y., Iribe, G., Nishida, M., and Naruse, K. (2017). Role of TRPC3 and TRPC6 channels in the myocardial response to stretch: Linking physiology and pathophysiology. *Prog. Biophys. Mol. Biol.* 130, 264–272. doi: 10.1016/j.pbiomolbio.2017.06.010

Yu, P., Gu, S., Bu, J., and Du, J. (2010). TRPC1 is essential for in vivo angiogenesis in zebrafish. *Circ. Res.* 106, 1221–1232. doi: 10.1161/CIRCRESAHA.109.207670

Yu, Y., Chen, S., Xiao, C., Jia, Y., Guo, J., Jiang, J., et al. (2014). TRPM7 is involved in angiotensin II induced cardiac fibrosis development by mediating calcium and magnesium influx. *Cell Calcium* 55, 252–260. doi: 10.1016/j.ceca.2014.02.019

Yue, L., Xie, J., and Nattel, S. (2011). Molecular determinants of cardiac fibroblast electrical function and therapeutic implications for atrial fibrillation. *Cardiovasc. Res.* 89, 744–753. doi: 10.1093/cvr/cvq329

Yue, Z., Xie, J., Yu, A. S., Stock, J., Du, J., and Yue, L. (2015). Role of TRP channels in the cardiovascular system. *Am. J. Physiol. Circ. Physiol.* 308, H157–H182. doi: 10.1152/ajpheart.00457.2014

Yue, Z., Zhang, Y., Xie, J., Jiang, J., and Yue, L. (2013). Transient receptor potential (TRP) channels and cardiac fibrosis. *Curr. Top. Med. Chem.* 13, 270–282, doi: 10.2174/1568026611313030005

Zahner, M. R., Li, D. -P., Chen, S. -R., and Pan, H. -L. (2003). Cardiac vanilloid receptor 1-expressing afferent nerves and their role in the cardiogenic sympathetic reflex in rats. *J. Physiol.* 551, 515–523. doi: 10.1113/jphysiol.2003.048207

Zhang, Q., Qi, H., Cao, Y., Shi, P., Song, C., Ba, L., et al. (2018). Activation of transient receptor potential vanilloid 3 channel (TRPV3) aggravated pathological cardiac hypertrophy via calcineurin/NFATc3 pathway in rats. *J. Cell. Mol. Med.* 22, 6055–6067. doi: 10.1111/jcmm.13880

Zhang, X., and Trebak, M. (2014). "Transient receptor potential canonical 7: a diacylglycerol-activated non-selective cation channel" in *Handbook of experimental pharmacology*. ed. J. E. Barrett (Springer Nature), 189–204. doi: 10.1007/978-3-642-54215-2_8

Zhang, Y. -H., Sun, H. -Y., Chen, K.-H., Du, X. -L., Liu, B., Cheng, L. -C., et al. (2012a). Evidence for functional expression of TRPM7 channels in human atrial myocytes. *Basic Res. Cardiol.* 107:282. doi: 10.1007/s00395-012-0282-4

Zhang, Y. -J., Ma, N., Su, F., Liu, H., and Mei, J. (2015). Increased TRPM6 expression in atrial fibrillation patients contribute to atrial fibrosis. *Exp. Mol. Pathol.* 98, 486–490. doi: 10.1016/j.yexmp.2015.03.025

Zhang, Y., Li, L., Hua, Y., Nunn, J. M., Dong, F., Yanagisawa, M., et al. (2012b). Cardiac-specific knockout of ETA receptor mitigates low ambient temperature-induced cardiac hypertrophy and contractile dysfunction. *J. Mol. Cell Biol.* 4, 97–107. doi: 10.1093/jmcb/mjs002

Zhao, J., Wang, X., Hang, P., Yun, F., Zhao, H., Xu, W., et al. (2013). Valsartan inhibits transient receptor potential canonical-3 channel in

canine atrial fibrillation. *Int. J. Cardiol.* 168, 4417–4418. doi: 10.1016/j.ijcard.2013.05.029

Zhong, B., Rubinstein, J., Ma, S., and Wang, D. H. (2018a). Genetic ablation of TRPV1 exacerbates pressure overload-induced cardiac hypertrophy. *Biomed. Pharmacother.* 99, 261–270. doi: 10.1016/j.biopha.2018.01.065

Zhong, H., Wang, T., Lian, G., Xu, C., Wang, H., and Xie, L. (2018b). TRPM7 regulates angiotensin II-induced sinoatrial node fibrosis in sick sinus syndrome rats by mediating Smad signaling. *Heart Vessels* 33, 1094–1105. doi: 10.1007/s00380-018-1146-0

Zhou, Y., Yi, X., Wang, T., and Li, M. (2015). Effects of angiotensin II on transient receptor potential melastatin 7 channel function in cardiac fibroblasts. *Exp. Ther. Med.* 9, 2008–2012. doi: 10.3892/etm.2015.2362

Conflict of Interest Statement: The authors declare that the research was conducted in the absence of any commercial or financial relationships that could be construed as a potential conflict of interest.

frontiers in Physiology

ORIGINAL RESEARCH
published: 13 March 2019
doi: 10.3389/fphys.2019.00172

Calcium Signaling and Contractility in Cardiac Myocyte of Wolframin Deficient Rats

Michal Cagalinec[1,2,3], Alexandra Zahradníková[1,2], Alexandra Zahradníková Jr.[1,2], Dominika Kováčová[4], Ludovit Paulis[4,5], Simona Kureková[2], Matej Hoťka[2,6], Jana Pavelková[1,2], Mario Plaas[3], Marta Novotová[1,2] and Ivan Zahradník[1,2]*

[1] Department of Cellular Cardiology, Institute of Experimental Endocrinology, Biomedical Research Center, University Science Park for Biomedicine, Slovak Academy of Sciences, Bratislava, Slovakia, [2] Institute of Molecular Physiology and Genetics, Centre of Biosciences, Slovak Academy of Sciences, Bratislava, Slovakia, [3] Institute of Biomedicine and Translational Medicine, Faculty of Medicine, University of Tartu, Tartu, Estonia, [4] Institute of Pathophysiology, Faculty of Medicine, Comenius University, Bratislava, Slovakia, [5] Institute of Normal and Pathological Physiology, Centre of Experimental Medicine, Slovak Academy of Sciences, Bratislava, Slovakia, [6] Department of Neurophysiology and Neuropharmacology, Center of Physiology and Pharmacology, Medical University of Vienna, Vienna, Austria

OPEN ACCESS

Edited by:
Gema Ruiz-Hurtado, Instituto de Investigación Hospital 12 de Octubre, Spain

Reviewed by:
Marcela Sorelli Carneiro-Ramos, Federal University of ABC, Brazil
Senka Holzer, Medical University of Graz, Austria

***Correspondence:**
Michal Cagalinec
michal.cagalinec@savba.sk

Specialty section:
This article was submitted to Membrane Physiology and Membrane Biophysics, a section of the journal Frontiers in Physiology

Received: *05 October 2018*
Accepted: *12 February 2019*
Published: *13 March 2019*

Citation:
Cagalinec M, Zahradníková A, Zahradníková A Jr, Kováčová D, Paulis L, Kureková S, Hoťka M, Pavelková J, Plaas M, Novotová M and Zahradník I (2019) Calcium Signaling and Contractility in Cardiac Myocyte of Wolframin Deficient Rats. Front. Physiol. 10:172. doi: 10.3389/fphys.2019.00172

Wolframin (Wfs1) is a membrane protein of the sarco/endoplasmic reticulum. Wfs1 mutations are responsible for the Wolfram syndrome, characterized by diabetic and neurological symptoms. Although Wfs1 is expressed in cardiac muscle, its role in this tissue is not clear. We have characterized the effect of invalidation of Wfs1 on calcium signaling-related processes in isolated ventricular myocytes of exon5-Wfs1 deficient rats ($Wfs1^{-e5/-e5}$) before the onset of overt disease. Calcium transients and contraction were measured in field-stimulated isolated myocytes using confocal microscopy with calcium indicator fluo-3 AM and sarcomere length detection. Calcium currents and their calcium release-dependent inactivation were characterized in whole-cell patch-clamp experiments. At 4 months, $Wfs1^{-e5/-e5}$ animals were euglycemic, and echocardiographic examination revealed fully compensated cardiac function. In field-stimulated isolated ventricular myocytes, both the amplitude and the duration of contraction of $Wfs1^{-e5/-e5}$ animals were elevated relative to control $Wfs1^{+/+}$ littermates. Increased contractility of myocytes resulted largely from prolonged cytosolic calcium transients. Neither the amplitude of calcium currents nor their voltage dependence of activation differed between the two groups. Calcium currents in $Wfs1^{-e5/-e5}$ myocytes showed a larger extent of inactivation by short voltage prepulses applied to selectively induce calcium release-dependent inactivation of calcium current. Neither the calcium content of the sarcoplasmic reticulum, measured by application of 20 mmol/l caffeine, nor the expression of SERCA2, determined from Western blots, differed significantly in myocytes of $Wfs1^{-e5/-e5}$ animals compared to control ones. These experiments point to increased duration of calcium release in ventricular myocytes of $Wfs1^{-e5/-e5}$ animals. We speculate that the lack of functional wolframin might cause changes leading to upregulation of RyR2 channels resulting in prolongation of channel openings and/or a delay in termination of calcium release.

Keywords: calcium current, calcium transient, contractility, cardiac myocyte, Wolfram syndrome, wolframin

INTRODUCTION

Wolfram syndrome (WS; OMIM 222300) is a rare hereditary disorder, first identified as a clinical entity separate from the juvenile type of diabetes mellitus by Wolfram and Wagener (1938). WS is characterized by symptoms including diabetes insipidus (DI), diabetes mellitus (DM), optical atrophy (OA), and deafness (D), and therefore it is termed also DIDMOAD (Barrett et al., 1995). Most WS cases are caused by recessive mutations of the *Wfs1* gene, located on chromosome 4p16.1. The Wfs1 protein is highly expressed in the brain, heart and pancreatic β-cells (Inoue et al., 1998; Yamada et al., 2006); pancreas and brain represent the crucial organs responsible for most of clinical symptoms in WS. Cardiac symptoms of WS were not originally recognized; however, emerging clinical findings include heart malformations as well as sinus tachycardia, atrial or ventricular arrhythmias (Medlej et al., 2004; Fabbri et al., 2005; Ganie et al., 2011; Korkmaz et al., 2016). The high expression of Wfs1 in the heart tissue, and the cardiac symptoms identified until now suggest functional importance of Wfs1 in the heart.

Although the *Wfs1* gene was identified 20 years ago (Inoue et al., 1998), the function of Wfs1 has not been resolved yet, and little is known about its 3D-structure. Wfs1 is composed of 890 amino acids (MW of ≈100 kDa), and was shown to reside on the membrane of endoplasmic reticulum (ER; Takeda et al., 2001). It was proposed to contain at least nine transmembrane helices (Hofmann et al., 2003), and the amino- and carboxy- terminals were shown to be located in the cytoplasm and in the lumen of ER, respectively. Wfs1 seems to exist predominantly as a tetramer (Hofmann et al., 2003), and ion channel activity was observed after reconstitution of microsomes of Wfs1-expressing Xenopus oocytes in lipid bilayers (Osman et al., 2003). However, homology modeling studies (Qian et al., 2015; Safarpour Lima et al., 2016) produced structures that lack clear channel-forming helices.

Wfs1 was suggested to participate in the response of cells to ER stress: In Wfs1-transfected COS7 cells, Wfs1 negatively regulated the activating transcription factor 6α (ATF6α), a key transcription factor involved in ER stress signaling, and stabilized the E3 ubiquitin ligase HRD1 (Fonseca et al., 2010). In line with this, Cagalinec et al. (2016) have shown that overexpression of Wfs1 leads to massive activation of the key factors of ER stress, namely, ATF6, ATF4, and XBP1 in primary cultured rat cortical neurons. Silencing of Wfs1 by specific shRNA in neurons also induced increased expression of these factors but only to a moderate extent. ER stress caused by Wfs1 deficiency was implicated also in the disruption of β-cell function (Morikawa et al., 2017; Ohta et al., 2017). Wfs1 was also suggested to participate in calcium handling: silencing of Wfs1 by specific shRNA in neurons resulted in depression of calcium transients and of Ca^{2+} release from the ER (Cagalinec et al., 2016). Moreover, expression of Wfs1 in HEK293 cells has been shown to positively modulate Ca^{2+} levels in the ER by increasing the rate of Ca^{2+} uptake (Takei et al., 2006). In addition, Wfs1 co-immunoprecipitates with SERCA, the pump transporting Ca^{2+} from cytosol to lumen of the reticular membrane system (Zatyka et al., 2015). Depletion of Wfs1 led to decreased and delayed cytosolic Ca^{2+} elevations in response to glucose stimuli (Ishihara et al., 2004) and to increased expression of SERCA in β-cells and β-cell lines (Zatyka et al., 2015). Wfs1 has been shown as a molecular partner of calmodulin (Yurimoto et al., 2009) and affected the function of the calcium-dependent protease calpain2 (Lu et al., 2014). In addition, it has been demonstrated recently that Wfs1 forms a complex with neuronal calcium sensor 1 (NCS1) and inositol 1,4,5-trisphosphate receptor (IP3R) to promote Ca^{2+} transfer between the ER and mitochondria in WS patient fibroblasts (Angebault et al., 2018). All these facts demonstrate strong involvement of Wfs1 in calcium signaling and ER-stress mediated pathways.

To understand the role of Wfs1 on the cellular, organ and body level, a Wfs1 deficient mouse model (Luuk et al., 2009) and a Wfs1 loss-of-function rat model (exon5-Wfs1 deficient; $Wfs1^{-e5/-e5}$; Plaas et al., 2017) were developed. In the latter, DM develops at the age of 13 months (Plaas et al., 2017).

Since calcium ions are the sole trigger for myocyte contraction and Wfs1 is strongly involved in calcium metabolism, in this work we evaluated calcium transients and contractility of left ventricular myocytes freshly isolated from the exon5-Wfs1 deficient ($Wfs1^{-e5/-e5}$) rats. To assess whether the cardiac complications in this model develop independently from insulin deficiency, in this study we have studied animals at the age of 4 months, i.e., before the development of hyperglycemia.

MATERIALS AND METHODS

Experimental Model

The impact of Wfs1 malfunction on calcium signaling in cardiac myocytes was studied using the Wfs1 loss-of-function (exon5 deficiency, $Wfs1^{-e5/-e5}$) rat model (Plaas et al., 2017). We used animals at the age of 4 months to avoid complications due to involvement of diabetes.

Rats were kept in groups of two to three in polypropylene cages under a standard 12:12 h light/dark regime at a temperature of 22 ± 2°C and 60–70% humidity. A standard balanced pellet diet and tap water were provided *ad libitum*. The genotype of rats in the control group ($Wfs1^{+/+}$; $n = 17$) and the experimental group ($Wfs1^{-e5/-e5}$; $n = 19$) was verified by PCR (see below). The number of animals used in individual experiments is given together with the data. All experiments conformed to the European directive 2010/63/EU and to Act No. 377/2012 of the Government of the Slovak Republic, were carried out in compliance with the guidelines for the care and use of laboratory animals, and were approved by the Ethical committee of the Centre of Biosciences, Slovak Academy of Sciences and by the State Veterinary and Food Administration of the Slovak Republic (approval No. Ro-1007/16-221 and Ro-2498/18-221a). Rats were sacrificed under full anesthesia by exsanguination. Before chest opening, rats were heparinized (5000 U/kg i.p.) and deeply anesthetized with sodium pentobarbital (100 mg/kg i.p.) until cessation of the paw withdrawal reflex and corneal reflex. Excised hearts attached to the cannula were mounted on the Langendorff set-up for isolation of myocytes, or for whole heart fixation.

The genotype of rats was verified using primers from Plaas et al. (2017), namely, rwfs_zf_genoR1 (5′-AAGAGTGGGTATGGTGCTGG-3′) and rwfs_zf_genoF1 (5′-AGAAGTGGCTACCCAGGGAT-3′). The PCR product was separated in 1.5% agarose gel. A single, 333 ($Wfs1^{+/+}$) or 149 bp ($Wfs1^{-e5/-e5}$) long band was detected in every animal.

Echocardiography

Transthoracic echocardiography (Liu and Rigel, 2009) was carried out before cardiotomy and isolation of cardiac myocytes. The examination was performed using a GE Medical Vivid E9 (GE Healthcare, Horten, Norway) using a 10-MHz matrix probe (ML6-15). The rat under sodium pentobarbital anesthesia was placed in supine position on a warming pad (37°C) and the anterior chest was shaved. Left ventricular function and structure were assessed from parasternal short axis views and from the four-chamber apical view. LV end-systolic and end-diastolic diameters and posterior wall thickness during systole and diastole were measured from two-dimensional anatomical M-mode in parasternal short axis view by the leading edge method. LV ejection fraction was calculated by using the Teichholz formula. Aortic outflow was acquired using pulsed wave Doppler. Left ventricular diastolic function was assessed using transmitral flow parameters—the ratio of peak velocity of early (E) and late (A) diastolic filling—from the four-chamber apical view with conventional pulsed wave Doppler. Each measurement was obtained from three consecutive cardiac cycles.

Blood Glucose Measurements

Blood samples were taken from the tail vein on the day of the experiment after induction of anesthesia and before echocardiographic examination. Glycemia was measured by the glucose oxidase method (Beckman, United States) as described previously (Kurdiova et al., 2014).

Solutions

Ripa buffer (in mmol/l): 150 NaCl, 25 Trizma base (pH 7.6), supplemented with 1% deoxycholate, 0.1% SDS, 1% Triton X-100, and 50 μl/ml protease inhibitor cocktail (Roche Diagnostics, Indianapolis).

PBST solution (in mmol/l): 150 NaCl, 3 KCl, 2 KH_2PO_4, 8 Na_2HPO_4, supplemented with 0.1% Tween-20.

1Ca Tyrode solution (in mmol/l): 135 NaCl, 5.4 KCl, 5 $MgCl_2$, 1 $CaCl_2$, 0.33 NaH_2PO_4, 10 HEPES; pH adjusted to 7.25 with 1 mol/l NaOH, osmolarity 300 mosm/l.

0Ca Tyrode solution (in mmol/l): 135 NaCl, 5.4 KCl, 5 $MgCl_2$, 0.003 $CaCl_2$, 0.33 NaH_2PO_4, 10.0 HEPES; pH adjusted to 7.25 with 1 mol/l NaOH, osmolarity 300 mosm/l.

Supplemented 0Ca Tyrode solution was prepared from 0Ca Tyrode solution by adding (in mmol/l): 10 glucose, 10 creatine, 10 taurine; pH adjusted to 7.25 with 1 mol/l NaOH, osmolarity 330 mosm/l.

Low-calcium Tyrode solution was prepared from the Supplemented 0Ca Tyrode solution by adding 50 μmol/l $CaCl_2$.

Enzymatic solution was prepared from the low-calcium Tyrode solution by adding 0.05–0.2 mg/ml Liberase TM (Roche, Cat. No. 05 401 127 001).

External bath solution (in mmol/l): 135 NaCl, 5.4 CsCl, 10 HEPES, 5 $MgCl_2$, 0.33 NaH_2PO_4, 1 $CaCl_2$, 0.01 IBMX, 0.02 TTX.

Internal solution (in mmol/l): 135 $CsCH_3SO_3$, 10 CsCl, 10 HEPES, 3 $MgSO_4$, 3 $ATPNa_2$, 0.05 cAMP, 1 EGTA, and 0.1 Fluo-3.

Perfusion solution was prepared from the *Supplemented 0Ca Tyrode* by adding an aliquot of 1 mol/l $CaCl_2$ stock solution (Merck) to a final concentration of 1.2 mmol/l $CaCl_2$.

Caffeine solution was prepared from *Perfusion solution* by adding caffeine at a final concentration of 20 mmol/l.

Western Blotting

Ventricular cardiomyocytes were lyzed in Ripa buffer. The samples were incubated for 45 min on ice. Total extracts were cleared by centrifugation for 10 min at 4°C at 14,000 × *g* and assayed for protein content by Lowry's method. Aliquots from each cell lysate containing 25 μg of protein were separated by SDS-PAGE on an 8% gel and transferred to nitrocellulose membrane. Membranes were blocked for 2 h with 5% skim milk in PBST solution, and then incubated with the primary antibody (suspended in 5% skim milk-PBST) overnight or 4 h at room temperature. Primary antibodies used were anti-SERCA2 (1:1000, SC-376235, Santa Cruz) and anti-GAPDH (1:1000, MAB374, Merck-Millipore). Membranes were washed with PBST (three times, 10 min each) and incubated with HRP anti-mouse antibody (1:2000, W4021, Promega) for 1.5 h at room temperature. The bands were visualized with a chemiluminescence immunodetection system (Amersham Biosciences, Piscataway, NJ, United States). Images were analyzed with the Origin software (OriginLab, Ver. 9) by subtracting the background, integrating the signal in each band, and normalizing the SERCA signal to the GAPDH signal in each lane.

Electron Microscopy

Samples of left ventricular muscle were prepared for morphological analysis as described previously (Mikusová et al., 2009). In brief, the hearts of experimental animals in deep anesthesia were rapidly excised, mounted on a Langendorff setup, and perfused with 1Ca Tyrode solution for 3 min, with 0Ca Tyrode solution for 3 min, and finally with 2% glutaraldehyde in cacodylate buffer (in mmol/l: 150 Na-cacodylate, 2 $CaCl_2$, pH 7.3) for 5 min. Three samples of left ventricular muscle per animal (five animals per group) were dissected, exposed to 2% glutaraldehyde in cacodylate buffer for 45 min, postfixed by 1% osmium tetroxide in cacodylate buffer for 30 min, and contrasted with 1% aqueous solution of uranyl acetate. After dehydration in graded ethanol series and propylene oxide, the samples were embedded in Durcupan blocks (ACM Fluka, Sweden). Ultrathin (58–60 nm) longitudinal sections were cut from each block at three distant levels using an ultramicrotome (Power-Tome MT-XL, RMC/Sorvall, Tucson, United States) and mounted on formvar-coated copper grids. The sections were contrasted with lead citrate and examined with a JEM 1200 electron microscope (Jeol, Tokyo, Japan) at 80 kV. The images were recorded with a CCD camera (Gatan DualVision 300W). The endomembrane

distribution and ultrastructure were studied at magnification of 2,000–100,000×.

Isolation of Cardiac Myocytes

Left ventricular cardiac myocytes were isolated from 6 $Wfs1^{+/+}$ and 8 $Wfs1^{-e5/-e5}$ male rats at the age of 4 months. The hearts of experimental animals in deep anesthesia were rapidly excised, cannulated, and mounted on a Langendorff perfusion system. The heart was retrogradely perfused first with 1Ca Tyrode solution until the blood was completely washed out. This was then replaced with Supplemented 0Ca Tyrode solution and perfused for further 5 min. After this, the heart was perfused with Enzymatic solution until the tissue became marble red-white (usually 6–8 min). All solutions were oxygenated and equilibrated at 37°C. During perfusion, the heart was positioned inside a heating chamber maintaining the temperature at 37°C. The heart was then taken off from the perfusion system, the atria and the right ventricle were discarded and the left ventricle was cut gently into several small pieces. The tissue was filtered through a nylon mesh (100 μm). The filtrate containing the dissociated myocytes was gently centrifuged at 50 × *g* for 1 min, the supernatant was discarded and replaced with 1.5 ml low-calcium Tyrode solution. The tissue that remained on the filter was further enzymatically digested for further 5 min at 37°C with Enzyme solution, in which collagenase activity was reduced using BSA (1% w./v.). This procedure was repeated four to five times. The batch with the highest yield of viable myocytes was then processed further by increasing the concentration of $CaCl_2$ in low-calcium Tyrode solution to 100, 500, and 1000 μmol/l in three 15-min steps to maintain the myocytes calcium tolerant. All experiments were performed within 8 h after isolation.

Patch Clamp

Myocytes were whole-cell patch clamped using patch-pipettes of 1.6–1.8 MΩ filled with Internal solution and a VE-2 amplifier (Alembic Instruments, Canada), a Digidata 1320A A/D converter, and pClamp software (Ver. 10, all from Axon Instruments, United States). Cell capacitance and series resistance were compensated to 50–85%. Myocytes were kept at a −50 mV holding potential. The myocytes were kept in a phosphorylated state by the use of ATP and cAMP in the Internal solution and of the membrane-permeable phosphodiesterase inhibitor IBMX in the External solution (Zahradnik and Palade, 1993). Calcium currents elicited by voltage pulses applied by specific protocols were filtered at 10 kHz and sampled at 20 kHz. Current–voltage curves were measured by applying a series of 70-ms test pulses to −40 to +50 mV in 10-mV increments once in 30 s. Inactivation of I_{Ca} was assessed by two types of two-pulse protocols (Zahradníková et al., 2004). *Protocol 1* consisted of a series of twin pulses, applied at 30-s intervals, where the prepulses (duration 5 ms, prepulse potential increasing from −50 to +40 mV by 10 mV increments) were followed by a constant 70-ms test pulse to 0 mV delivered 30 ms after the prepulse. This protocol was used to determine the voltage dependence of the voltage-, current-, and calcium release-dependent components of I_{Ca} inactivation. *Protocol 2* consisted of a series of twin pulses, applied at 30-s intervals, where the prepulses (prepulse potential +60 mV, duration increasing from 0 to 4.5 ms by 0.5 ms) were followed by a constant 70-ms test pulse to 0 mV delivered 30 ms after the prepulse. This protocol served for determination of the calcium release-dependent component of I_{Ca} inactivation. In both inactivation protocols, the fraction of non-inactivated calcium current was calculated for each prepulse as the ratio of the peak amplitude of test I_{Ca} to the peak amplitude of the test I_{Ca} in the absence of the prepulse.

Confocal Imaging

Myocytes were loaded with the calcium indicator fluo-3 AM (1 μmol/l) for 15 min at room temperature. Fluo-3-labeled myocytes suspended in the experimental chamber were left to settle on the coverglass for 1 min and then perfused at a rate of 1 ml/min with Perfusion solution and electrically paced to contract at a frequency of 1 Hz using field stimulation (32 mA, 40 ms, DS3 Isolated Current Stimulator, Digitimer Ltd., United Kingdom). The TCS SP-8 STED confocal microscope (Leica Microsystems) was used in the line scan mode (2.5 ms per line, 8000 lines, excitation 500 nm, emission 510–570 nm) to record fluo-3 fluorescence images in parallel with the transmission images. Thus, calcium transients and the corresponding myocyte shortenings could be assessed simultaneously (**Figure 1**). In a subset of experiments, rapid perfusion with Caffeine solution was applied after the series of electrical stimuli to evoke maximal calcium release and to assess the sarcoplasmic reticulum calcium content.

The transmission images were used to determine changes in sarcomere length using the SarConfoCal plugin (Pasqualin et al., 2017) in the Fiji environment (Schindelin et al., 2012) of ImageJ (Schneider et al., 2012). The adjacent averaging filter was set to 17. Only the intracellular regions of the images were analyzed.

The time courses of fluorescence and sarcomere length were normalized to the diastolic values ($\Delta F/F_0$, $\Delta L/L_0$), and imported into the Clampfit software (pClamp 10, Molecular Devices, United States). Here, the response to each stimulus, i.e., the calcium transient and its corresponding sarcomere length transient was analyzed. The following parameters were determined for calcium transient and sarcomere length transient: baseline, amplitude, half-width, rise time (20–80%), and decay time (80–20%). Smoothing window was set to five samples.

Data Processing

Current–voltage data were fitted by the equation

$$I_{Ca}(V) = g_{max}(V - V_r)/(1 + \exp(-(V - V_{1/2a})/V_{Sa}))^4 \quad (1)$$

where I_{Ca} is the peak calcium current amplitude, V is the test pulse voltage, g_{max} is the maximal conductance, V_r is the reversal potential, $V_{1/2a}$ is the potential of half-activation, and V_{Sa} is the slope factor of activation.

Inactivation curves of the two-pulse inactivation protocols were fitted by the respective Boltzmann functions:

$$I_{Ca}(V_p) = -F_{iV}/(1 + \exp((V_p - V_{1/2i})/V_{SiV})) + F_{iV} \quad (2)$$

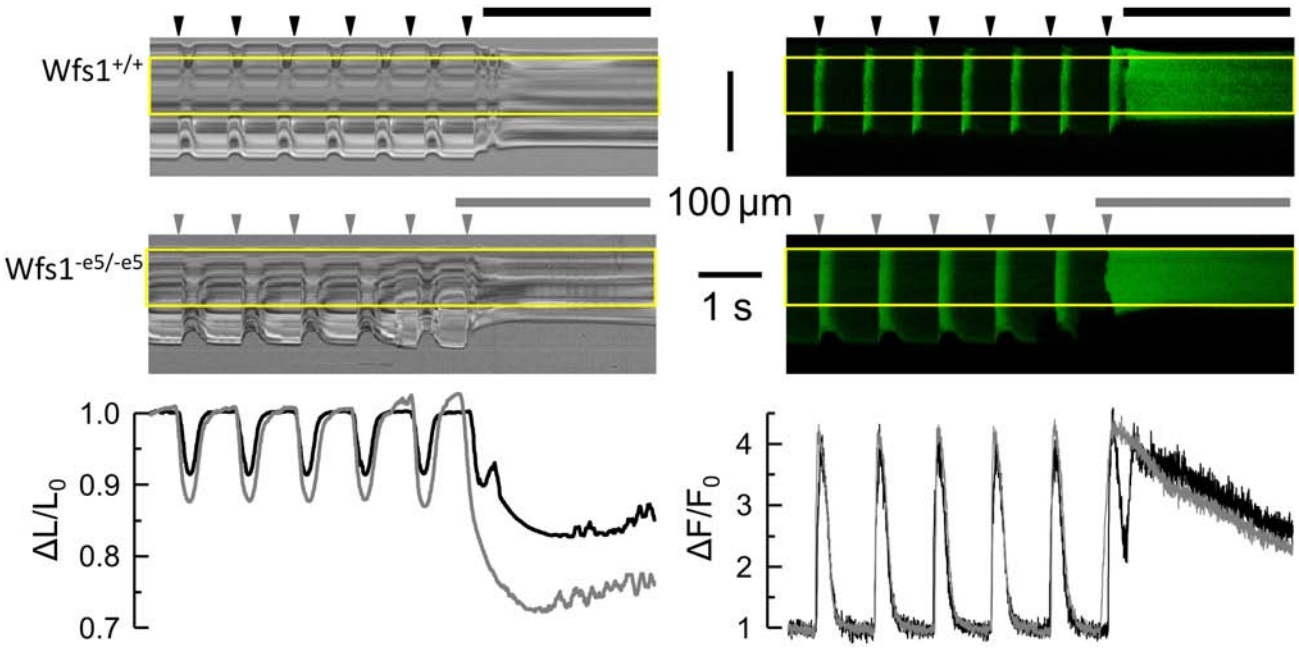

FIGURE 1 | Typical records of sarcomere length and cytosolic Ca^{2+} in response to field stimulation. *Left column* – transmitted light records of line-scans along the myocyte long axis. Deflections correspond to contractions of the myocyte. *Right column* – fluorescence records of calcium signal in confocal line-scans corresponding to the contraction records (left). The yellow rectangles denote the analyzed region. *Top row* – $Wfs1^{+/+}$ myocyte. *Middle row* – $Wfs1^{-e5/-e5}$ myocyte. Arrowheads – the timings of field stimuli. Horizontal lines – applications of caffeine. *Bottom row* – the time course of changes in the relative sarcomere length (left) and cytosolic calcium signals (right) corresponding to the top and middle row records (black – $Wfs1^{+/+}$, gray – $Wfs1^{-e5/-e5}$).

where V_p is the prepulse voltage, F_{iV} is the inactivated fraction of the peak I_{Ca} amplitude at the test pulse, $V_{1/2i}$ is the half-inactivation potential, and V_{SiV} is the slope factor, and

$$I_{Ca}(t_p) = -F_{it}/(1+\exp((t_p - t_{1/2i})/V_{Sit})) + F_{it} \quad (3)$$

where t_p is the prepulse duration, F_{it} is the inactivated fraction of the peak I_{Ca} amplitude at the test pulse, $t_{1/2i}$ is the prepulse duration for half-inactivation, and V_{Sit} is the slope factor.

Statistical analysis was performed in Origin (OriginLab, Ver. 9) using Student's *t*-test. The *P*-values were calculated for two-tailed data distributions.

Data fitting was performed in Origin using the Levenberg–Marquardt method. The fitted parameters of two datasets were considered significantly different if their 95% confidence intervals did not overlap.

RESULTS

Invalidation of Wolframin Does Not Lead to Heart Disease or Diabetes at the Age of 4 Months

The genotype of all experimental animals was verified using PCR. Overall examination of animals and their hearts excised for experiments did not show malformations or differences in comparison with standard rats. The weight of $Wfs1^{-e5/-e5}$ rats taken into experiments was significantly smaller (524 ± 11 g, n = 19, $P < 0.05$) than that of their $Wfs1^{+/+}$ littermates (570 ± 19 g, n = 17). Similar values and differences in the body weight at the age of 4 months were reported by Plaas et al. (2017). Tests for postprandial blood glucose showed slightly but significantly higher glycemia in $Wfs1^{-e5/-e5}$ (7.79 ± 0.47 mmol/l, n = 8) than in $Wfs1^{+/+}$ animals (6.10 ± 0.16, n = 6, P = 0.009) but no hyperglycemia in either group, in agreement with the original study for this age group (Plaas et al., 2017). This confirms that the cohort of experimental animals used in this study was not biased by specific or unspecific side effects related to breeding.

Echocardiographic examination did not reveal myocardial hypertrophy, infarction, or other major changes in the studied hearts. Quantitative evaluation provided similar parameters in both groups (n = 6 for $Wfs1^{+/+}$ and n = 8 for $Wfs1^{-e5/-e5}$, **Table 1**). The posterior wall thicknesses, either diastolic or systolic, were unchanged. Functional parameters showed some small differences between groups. The heart rate was somewhat higher, while the end-diastolic and stroke volumes were somewhat smaller in $Wfs1^{-e5/-e5}$ than in $Wfs1^{+/+}$ animals; these differences did not reach statistical significance. The aortic valve maximal flow velocity was significantly higher in $Wfs1^{-e5/-e5}$ than in $Wfs1^{+/+}$ animals, although its time integral was not different in the two groups. Based on measurements of the ejection fraction, which did not show significant differences between the two groups of animals, systolic function in

TABLE 1 | Echocardiographic parameters.

	Wfs1$^{+/+}$ (*n* = 6)	**Wfs1$^{-e5/-e5}$ (*n* = 8)**	***P***
Heart rate (1/min)	307.4 ± 19.1	340.7 ± 15.9	0.20
PWd (mm)	1.74 ± 0.02	1.75 ± 0.08	0.87
PWs (mm)	2.43 ± 0.09	2.46 ± 0.11	0.84
EDV (cm^3)	1.35 ± 0.09	1.16 ± 0.08	0.14
SV (cm^3)	1.02 ± 0.06	0.90 ± 0.06	0.23
EF (%)	75.8 ± 1.6	77.4 ± 0.7	0.32
AV_{max} (mm/s)	1779 ± 85	2165 ± 141	0.05
AV VTI (mm)	92.4 ± 5.0	100.5 ± 6.7	0.38
MV E/A	1.30 ± 0.12	1.35 ± 0.10	0.74

PWd – posterior wall thickness (diastolic), PWs – posterior wall thickness (systolic), EDV – end diastolic volume, SV – stroke volume, EF – ejection fraction, AV_{max} – aortic valve maximal flow velocity, AV VTI – aortic valve velocity time integral, MV E/A – mitral valve early (E)/late (A) peak velocity ratio, n – the number of animals, P – P-value of the t-test for two-tailed distribution.

TABLE 2 | Parameters of cell shortening.

	Wfs1$^{+/+}$ (*n* = 23)	**Wfs1$^{-e5/-e5}$ (*n* = 30)**	***P***
Sarcomere length (μm)	1.72 ± 0.01	1.73 ± 0.01	0.23
Peak fractional contraction ($\Delta L/L_0$)	0.094 ± 0.006	0.112 ± 0.005	0.03
FDHM (ms)	224 ± 6	256 ± 7.7	0.004
Rise time 20–80% (ms)	75.1 ± 2.1	76.7 ± 1.7	0.54
Decay time 80–20% (ms)	101 ± 4	107 ± 3.5	0.26

n – The number of analyzed cells. Data are given as mean ± SEM. P – P-value of the t-test for two-tailed distribution.

TABLE 3 | Parameters of calcium transients.

Field stimulation	**Wfs1$^{+/+}$ (*n* = 36)**	**Wfs1$^{-e5/-e5}$ (*n* = 55)**	***P***
Peak calcium transient ($\Delta F/F_0$)	3.02 ± 0.13	2.77 ± 0.13	0.20
FDHM (ms)	171 ± 3	188 ± 3	0.0001
Rise time 20–80% (ms)	24.9 ± 1.6	23.0 ± 1.3	0.34
Decay time 80–20% (ms)	129 ± 2	136 ± 3	0.09
Caffeine	**Wfs1$^{+/+}$ (*n* = 7)**	**Wfs1$^{-e5/-e5}$ (*n* = 14)**	
Peak calcium transient ($\Delta F/F_0$)	4.16 ± 0.26	4.29 ± 0.18	0.70

n – The number of analyzed cells. Data are given as mean ± SEM. P – P-value of the t-test for two-tailed distribution.

Wfs1$^{-e5/-e5}$ and Wfs1$^{+/+}$ animals was fully preserved. At the organ level, therefore, the heart function of Wfs1$^{-e5/-e5}$ animals can be considered compensated at this stage of disease development.

Invalidation of Wolframin Leads to Elevated Contraction and Prolonged Calcium Transients

Contractile and calcium transient responses of isolated cardiac myocytes to field or caffeine stimulation (six Wfs1$^{+/+}$ and eight Wfs1$^{-e5/-e5}$ rats) were evaluated by optical methods of transmission and fluorescence microscopy, respectively (**Figure 1**). The resting sarcomere length was the same in both studied groups (**Table 2**); however, the contractile responses were different. The amplitude of peak contraction as well as the duration of contraction at the half-peak amplitude were significantly higher in Wfs1$^{-e5/-e5}$ than in Wfs1$^{+/+}$ myocytes. Since the rise time and the decay time of contraction did not change, prolongation of contraction resulted from prolonged duration of the plateau. Since contractions were recorded in the unloaded isotonic mode, they do not reflect metabolic or energy supply aspects of myocyte function.

In contrast to contractions, the respective peak amplitudes of stimulated calcium transients in Wfs1$^{-e5/-e5}$ myocytes did not differ from those in Wfs1$^{+/+}$ myocytes; however, their duration in Wfs1$^{-e5/-e5}$ myocytes was significantly longer than in Wfs1$^{+/+}$ myocytes (**Table 3**). The prolongation of contractions correlated well with prolongation of calcium transients, resulting in similar increases in FDHM (10 vs. 12%, respectively, **Tables 2**, **3**).

Stimulation of isolated myocytes by caffeine is a useful tool for estimation of calcium content of sarcoplasmic reticulum. Calcium transients in response to caffeine application were not different between groups (**Table 3**), indicating similar calcium content of the sarcoplasmic reticulum. Caffeine-induced

contractures were always of supramaximal amplitude (unloaded cells) and therefore their kinetics were not evaluated.

Invalidation of Wolframin Affects Release-Dependent Inactivation of Calcium Channels

The change in contractility could result from a change of the calcium current (the trigger for calcium release) and/or from a change of calcium release itself. We estimated both calcium signals in isolated cardiac myocytes from 6 $Wfs1^{+/+}$ and 8 $Wfs1^{-e5/-e5}$ rats by means of a voltage-clamp experiment (Zahradníková et al., 2004). The voltage dependence of calcium currents is shown in **Figure 2A** together with the fitted curves according to Eq. 1. No statistically significant differences between parameters of the current–voltage curves of the two myocyte groups were observed. The parameters of the fit are summarized in **Table 4**.

The efficiency of calcium current to induce calcium release was analyzed according to Zahradníková et al. (2004). The extent of calcium release was estimated from the extent of calcium release-dependent inactivation of calcium current. The fraction of inactivated current (F_i) was assessed by two two-pulse protocols. First, inactivation of I_{Ca} was assessed by Protocol 1, in which the potential of the 5-ms prepulse was varied. The dependence of F_{iV} on prepulse potential is shown in **Figure 2B**, and parameters of the curves fitted using Eq. 2 are given in **Table 4**. The voltage parameters of inactivation were not significantly different but the fraction F_{iV} of inactivated calcium current was significantly larger in $Wfs1^{-e5/-e5}$ than in $Wfs1^{+/+}$ myocytes. In the second

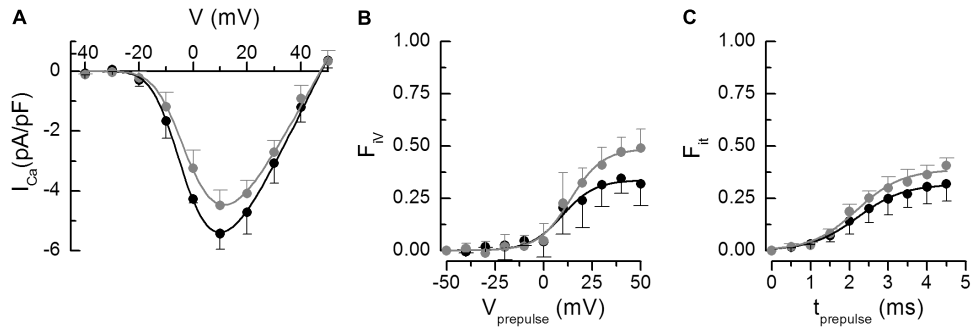

FIGURE 2 | Analysis of calcium currents. The parameters of the fitted curves are in **Table 4**. **(A)** Voltage dependence of the peak calcium current amplitudes. The curves represent the respective fits by Eq. 1. **(B)** Fractional inactivation of the test pulse calcium current amplitude by variable prepulse voltages of 5-ms duration. The curves represent the respective fits by Eq. 2. **(C)** Fractional inactivation of the test pulse calcium current amplitude by prepulses to +60 mV of variable duration. The curves represent the respective fits by Eq. 3. In all panels, black – $Wfs1^{+/+}$, gray – $Wfs1^{-e5/-e5}$. Data are given as mean ± SEM (the number of cells n = 4, 4, and 2 for **A**, **B**, and **C**, respectively).

TABLE 4 | Parameters of calcium currents and the release dependent inactivation depicted in **Figure 2**.

Figure 2A	**$Wfs1^{+/+}$ (n = 40)**	**$Wfs1^{-e5/-e5}$ (n = 40)**
g_{max} (pA/pF/mV)	0.18 ± 0.02	0.17 ± 0.02
V_r (mV)	47.4 ± 1.7	47.0 ± 1.7
$V_{1/2a}$ (mV)	−14.7 ± 1.8	−13.5 ± 2.0
V_{Sa} (mV)	8.9 ± 1.8	9.4 ± 2. 1
Figure 2B	**$Wfs1^{+/+}$ (n = 44)**	**$Wfs1^{-e5/-e5}$ (n = 44)**
F_{iV}	0.34 ± 0.02	0.49 ± 0.02*
$V_{1/2i}$ (mV)	9.6 ± 2.1	13.7 ± 1.3
V_{SiV} (mV)	8.3 ± 1.7	8.3 ± 1.0
Figure 2C	**$Wfs1^{+/+}$ (n = 20)**	**$Wfs1^{-e5/-e5}$ (n = 20)**
F_{it}	0.32 ± 0.01	0.39 ± 0.02*
$t_{1/2i}$ (ms)	2.20 ± 0.05	2.18 ± 0.10
V_{Sit} (ms)	0.60 ± 0.04	0.58 ± 0.08

*For **Figure 2A**: the best fit parameters using Eq. 1: g_{max} – conductance, V_r – reversal potential, $V_{1/2a}$ – potential of half-activation, V_{Sa} – slope factor of the voltage-dependent activation.*

*For **Figure 2B**: the best fit parameters using Eq. 2: F_{iV} – maximum fraction of I_{Ca} inactivated by 5-ms prepulses, $V_{1/2i}$ – prepulse potential for half-inactivation, V_{SiV} – slope factor of the inactivation curve.*

*For **Figure 2C**: the best fit parameters using Eq. 3: F_{it} – maximum fraction of I_{Ca} inactivated by +60-mV prepulses, $t_{1/2i}$ – prepulse duration for half-inactivation, V_{Sit} – slope factor of the inactivation curve.*

*n – The number of fitted data points. *Significantly different from $Wfs1^{+/+}$.*

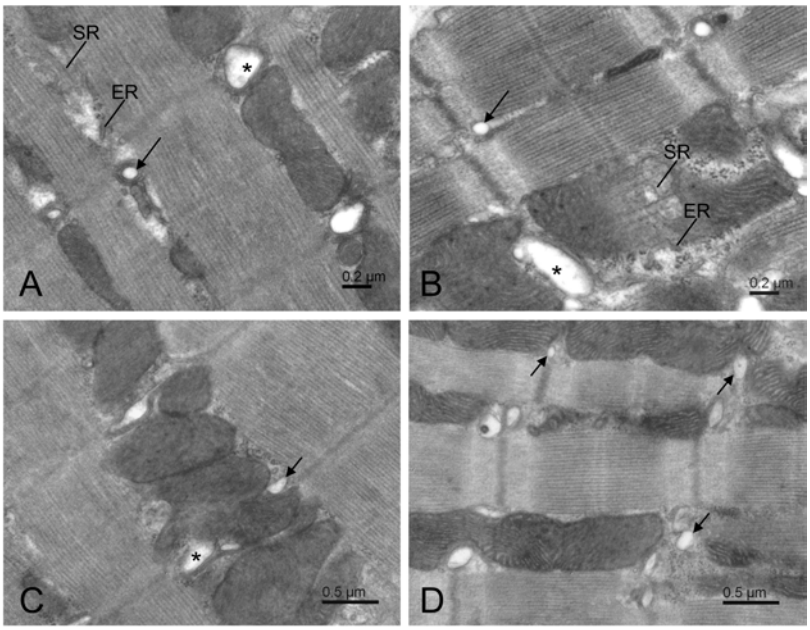

FIGURE 3 | Electron micrographs of typical central area of $Wfs1^{+/+}$ **(A,C)** and $Wfs1^{-e5/-e5}$ **(B,D)** cardiomyocytes. Long arrows and asterisks indicate dyads containing small and large t-tubule profiles, respectively. Short arrows indicate non-dyadic t-tubules, that is, those without apposed terminal cisternae. ER – rough and SR – smooth reticular membranes.

two-pulse protocol experiment, calcium release was triggered by prepulses to +60 mV with variable duration that activated brief tail calcium currents of variable amplitude, known to induce only the calcium release-dependent component of inactivation (Zahradníková et al., 2004). The subsequent test pulse to 0 mV was used to assess the amplitude of calcium current that was not inactivated by calcium release (Protocol 2). The dependence of the fraction of inactivated current, F_{it}, on the prepulse duration is shown in **Figure 2C** and the parameters of the curves fitted using Eq. 3 are shown in **Table 4**. The parameters of inactivation were not significantly different between the two myocyte groups except for the fraction F_{it}, which was again significantly elevated in $Wfs1^{-e5/-e5}$ myocytes.

These data show that the fraction of calcium current inactivated by short prepulses is increased in $Wfs1^{-e5/-e5}$ animals, despite no observed changes in the amplitude or the voltage-dependence of the calcium current itself. Since neither the half-inactivation nor slope factors of prepulse-induced I_{Ca} inactivation were changed, these data suggest that the voltage dependence of I_{Ca} inactivation was not affected by wolframin invalidation. To summarize, these two-pulse experiments revealed an increased effect of calcium release on calcium current inactivation in $Wfs1^{-e5/-e5}$ myocytes relative to $Wfs1^{+/+}$ myocytes. This could be caused only by increased calcium release at individual dyads.

Invalidation of Wolframin Does Not Affect Ultrastructure of Cardiomyocytes

Electron microscopic examination of ultrastructure of cardiomyocytes (five $Wfs1^{+/+}$ and five $Wfs1^{-e5/-e5}$ rats) revealed very similar morphology in both groups of experimental animals (**Figure 3**). The myocytes displayed standard shape, contractile myofibrils were well organized, and mitochondria formed columns between myofibrils. The ribosomes were present in the cytosol between mitochondria and myofibrils. Both the rough and smooth reticular membrane systems occurred in the intermyofibrillar space. Cardiomyocytes of both groups contained dyads near Z-lines. According to visual examination, the diameter of t-tubule profiles in dyads seemed somewhat different between groups, albeit not substantially (**Figures 3A,B**). The two groups seem to differ by higher occurrence of small non-dyadic t-tubules near Z-lines in the $Wfs1^{-e5/-e5}$ rats in comparison to $Wfs1^{+/+}$ (**Figures 3C,D**).

Invalidation of Wolframin Does Not Affect Protein Expression of SERCA

To determine whether invalidation of wolframin affects expression of SERCA, its protein levels in myocytes (six $Wfs1^{+/+}$ and eight $Wfs1^{-e5/-e5}$ rats) were determined by western blots using the housekeeper protein GAPDH as a loading control (**Figure 4**). The analysis yielded values of 0.44 ± 0.07 vs. 0.45 ± 0.06 a.u. for $Wfs1^{+/+}$ and $Wfs1^{-e5/-e5}$, respectively (mean ± SEM, $n = 4$), indicating no difference between protein expression of SERCA of either group.

DISCUSSION

In this work, we studied the effect of invalidation of wolframin on cardiac function using exon5-Wfs1 deficient rats ($Wfs1^{-e5/-e5}$),

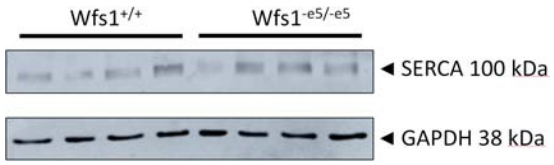

FIGURE 4 | Expression of SERCA2 protein in cardiac myocytes of Wfs1$^{+/+}$ (n = 4) and Wfs1$^{-e5/-e5}$ (n = 4) animals. GAPDH was used as a loading control.

with emphasis on calcium signaling related to contractility of cardiac myocytes. At the level of whole heart, we used echocardiography to assess cardiac functional parameters. At the level of isolated ventricular myocytes, we characterized cell contraction and intracellular calcium transients together with calcium currents. In addition to genotyping and blood glucose level verification, we examined changes in the expression of SERCA2 and in the ultrastructure of the left ventricular myocytes.

This is to our knowledge the first study of the effect of wolframin invalidation on calcium handling in cardiac myocytes. Previous works on wolframin were performed mostly in pancreatic β-cells and neurons or in cell lines. In those studies, the changes in cell function induced by wolframin invalidation or silencing went hand-in-hand with induction of ER stress (Takei et al., 2006; Hara et al., 2014; Zatyka et al., 2015; Cagalinec et al., 2016; Morikawa et al., 2017), with suppression of SERCA activity (Takei et al., 2006; Hara et al., 2014; Morikawa et al., 2017) and mRNA expression (Morikawa et al., 2017). Paradoxically, increase of SERCA protein expression was also observed (Zatyka et al., 2015). It has been proposed that the role of wolframin in pancreatic β-cells is to target SERCA to proteasome-mediated degradation (Zatyka et al., 2015). On the other hand, induction of ER stress by wolframin deficiency was not observed in either cardiac or skeletal muscle cells under conditions, when ER stress was clearly present in pancreatic β-cells (Yamada et al., 2006). It should be noted that in β-cells the role of SERCA is to damp the amplitude of cytosolic calcium oscillations during cell depolarization by sequestration to the ER (Félix-Martínez and Godínez-Fernández, 2014). In cardiac myocytes, SERCA primes calcium stores for stimulated calcium release and it returns calcium back to the store after the stimulus. It is therefore plausible that the role of wolframin in cardiac myocytes differs from that in pancreatic β-cells and neurons.

Ultrasonographic examination showed that the function of Wfs1$^{-e5/-e5}$ hearts was fully compensated at this age of WS development, despite the lower body weight of Wfs1$^{-e5/-e5}$ rats relative to control littermates. Additionally, no overt difference in the ultrastructure of ventricular myocytes or SERCA2 expression was observed between the two groups in our study. These findings comply with previous findings that symptoms of WS develop in Wfs1$^{-e5/-e5}$ rats at the age of 13 months (Plaas et al., 2017). However, we have observed several differences in the function of cardiomyocytes between the two groups. Invalidation of wolframin led to increased release of calcium measured either as fractional inactivation of calcium current, or as prolongation of cytosolic calcium transients and myocyte contraction, or as increased amplitude of cell contraction in response to field stimulation. Interestingly, the amplitudes of calcium transients induced by caffeine were not different, suggesting that the SR content was similar in both myocyte groups. Together with no difference in expression of SERCA2, this indicates no effect of wolframin invalidation on calcium accumulation in the SR of Wfs1$^{-e5/-e5}$ myocytes at the studied age of rats.

Prolonged cytosolic calcium transients at the same maximal intensity and prolonged contraction observed in Wfs1$^{-e5/-e5}$ myocytes can be explained by the local control mechanism of calcium release (Cannell et al., 1994; Zahradníková et al., 2010; Janíček et al., 2012). According to this, the amplitude and the rate of cytosolic calcium increase result from temporal summation of individual release events arising at dyads and the number of dyads recruited from their cellular pool. The resulting contraction convolves with a certain delay the cytosolic calcium increase, the supply of ATP to drive the myosin motors, and sequestration of calcium to SR by SERCA.

It could be that in the field-stimulated isolated myocytes the observed differences occurred in part due to longer action potential duration in Wfs1$^{-e5/-e5}$ myocytes. In this respect, patch-clamp experiments showed similar voltage dependent characteristics of calcium currents in both groups, i.e., no change in function of L-type calcium channels that could cause action potential prolongation. To the contrary, we observed increased calcium current inactivation due to calcium induced calcium release mechanism (Sham, 1997; Zahradníková et al., 2004) that should contribute to faster termination of the action potential. However, we could not exclude changes in potassium currents controlling termination of action potentials.

Our results show that calcium release in Wfs1$^{-e5/-e5}$ is prolonged relative to that of Wfs1$^{+/+}$ myocytes under conditions of identical activating stimuli. We speculate that the longer duration but unchanged intensity of calcium release might arise by a yet unknown mechanism from the regulatory effect of wolframin on RyR2 channel open time and/or termination of calcium release, or on modulation of the calcium signal by mitochondria. All of these pathways are plausible, since wolframin was shown to interact with calmodulin (Yurimoto et al., 2009), a regulator of RyR2 activity with a potential role in RyR refractoriness (Liu et al., 2018), and since wolframin deficiency affected mitochondrial function in cortical neurons (Cagalinec et al., 2016).

CONCLUSION

We have shown that invalidation of Wfs1 results in subtle changes in calcium signaling, present before overt onset of disease. These subtle changes result in significant augmentation of both amplitude and duration of contraction. However, the sensitivity of our methods did not allow

us to find the molecular basis of the observed changes. To resolve this question, further studies are necessary, such as direct measurements of calcium release flux from individual dyads, and/or analysis of expression and function of all proteins involved in calcium cycling. It is tempting to speculate on wolframin regulation of RyR2 gating, e.g., by prolongation of channel openings or by delaying calcium release termination. Moreover, since the structure, density, size, and distribution of dyads was recognized as an important player in proper function of cardiac calcium release, the role of wolframin in their formation is worth further study.

DATA AVAILABILITY

The datasets generated for this study are available on request to the corresponding author.

AUTHOR CONTRIBUTIONS

MC, AZ, and IZ conceived of or designed the study. MC and AZ contributed to measurements of calcium transients and myocyte shortening. AZjr and MH contributed to electrophysiology. MN and IZ contributed to electron microscopy. DK and LP contributed to echocardiography. SK and AZjr contributed to western blotting. MC, JP, AZ, AZjr, and IZ analyzed the data. AZ, IZ, and MC wrote the manuscript. MP provided materials. MC, AZ, AZjr, and IZ edited the manuscript for important intellectual content.

FUNDING

The work was supported by the SASPRO grant no. 0063/01/02, financed by the Slovak Academy of Sciences and by a "Co-financing of regional, national, and international programs (COFUND)," which is part of the Marie Curie Action of the EU 7th Framework Program, under Grant Agreement No. 609427; Slovak Research and Development Agency grant APVV 15-0302; Science Grant Agency grants VEGA 2/0169/16, VEGA 2/0143/17; and by the project "Completing the infrastructure for modern research of lifestyle diseases" (ITMS 26230120006), funded by ERDF.

ACKNOWLEDGMENTS

We thank the Centre of Experimental Medicine SAS – Institute for Heart Research for providing the GE Medical Vivid E9 Echocardiograph. We thank M. Nemec, Laboratory of Diabetes and Metabolic Derangements, IEE BRC SAS, for determination of blood glucose levels. We thank G. Gajdošíková for animal care and assistance with isolation of cardiac myocytes. We also thank L. Novota for technical assistance with electron microscopy.

REFERENCES

Angebault, C., Fauconnier, J., Patergnani, S., Rieusset, J., Danese, A., Affortit, C. A., et al. (2018). ER-mitochondria cross-talk is regulated by the Ca2+ sensor NCS1 and is impaired in Wolfram syndrome. *Sci. Signal.* 11:eaaq1380. doi: 10.1126/scisignal.aaq1380

Barrett, T. G., Bundey, S. E., and Macleod, A. F. (1995). Neurodegeneration and diabetes: UK nationwide study of Wolfram (DIDMOAD) syndrome. *Lancet* 346, 1458–1463. doi: 10.1016/S0140-6736(95)92473-6

Cagalinec, M., Liiv, M., Hodurova, Z., Hickey, M. A., Vaarmann, A., Mandel, M., et al. (2016). Role of mitochondrial dynamics in neuronal development: mechanism for wolfram syndrome. *PLoS Biol.* 14:e1002511. doi: 10.1371/journal.pbio.1002511

Cannell, M. B., Cheng, H., and Lederer, W. J. (1994). Spatial non-uniformities in [Ca2+]i during excitation-contraction coupling in cardiac myocytes. *Biophys. J.* 67, 1942–1956. doi: 10.1016/S0006-3495(94)80677-0

Fabbri, L. P., Nucera, M., Grippo, A., Menicucci, A., De Feo, M. L., Becchi, C., et al. (2005). Wolfram syndrome. How much could knowledge challenge the fate? A case report. *Med. Sci. Monit.* 11, CS40–CS44.

Félix-Martínez, G. J., and Godínez-Fernández, J. R. (2014). Mathematical models of electrical activity of the pancreatic β-cell: a physiological review. *Islets* 6:e949195. doi: 10.4161/19382014.2014.949195

Fonseca, S. G., Ishigaki, S., Oslowski, C. M., Lu, S., Lipson, K. L., Ghosh, R., et al. (2010). Wolfram syndrome 1 gene negatively regulates ER stress signaling in rodent and human cells. *J. Clin. Invest.* 120, 744–755. doi: 10.1172/JCI39678

Ganie, M. A., Laway, B. A., Nisar, S., Wani, M. M., Khurana, M. L., Ahmad, F., et al. (2011). Presentation and clinical course of Wolfram (DIDMOAD) syndrome from North India. *Diabet. Med.* 28, 1337–1342. doi: 10.1111/j.1464-5491.2011.03377.x

Hara, T., Mahadevan, J., Kanekura, K., Hara, M., Lu, S., and Urano, F. (2014). Calcium efflux from the endoplasmic reticulum leads to β-cell death. *Endocrinology* 155, 758–768. doi: 10.1210/en.2013-1519

Hofmann, S., Philbrook, C., Gerbitz, K. D., and Bauer, M. F. (2003). Wolfram syndrome: structural and functional analyses of mutant and wild-type wolframin, the WFS1 gene product. *Hum. Mol. Genet.* 12, 2003–2012. doi: 10.1093/hmg/ddg214

Inoue, H., Tanizawa, Y., Wasson, J., Behn, P., Kalidas, K., Bernal-Mizrachi, E., et al. (1998). A gene encoding a transmembrane protein is mutated in patients with diabetes mellitus and optic atrophy (Wolfram syndrome). *Nat. Genet.* 20, 143–148. doi: 10.1038/2441

Ishihara, H., Takeda, S., Tamura, A., Takahashi, R., Yamaguchi, S., Takei, D., et al. (2004). Disruption of the WFS1 gene in mice causes progressive beta-cell loss and impaired stimulus-secretion coupling in insulin secretion. *Hum. Mol. Genet.* 13, 1159–1170. doi: 10.1093/hmg/ddh125

Janíček, R., Zahradníková, A., Poláková, E., Pavelková, J., Zahradník, I., and Zahradníková, A. (2012). Calcium spike variability in cardiac myocytes results from activation of small cohorts of ryanodine receptor 2 channels. *J. Physiol.* 590, 5091–5106. doi: 10.1113/jphysiol.2012.234823

Korkmaz, H. A., Demir, K., Hazan, F., Yıldız, M., Elmas, ÖN., Özkan, B., et al. (2016). Association of Wolfram syndrome with fallot tetralogy in a girl. *Arch. Argent. Pediatr.* 114, e163–e166. doi: 10.5546/aap.2016.eng.e163

Kurdiova, T., Balaz, M., Vician, M., Maderova, D., Vlcek, M., Valkovic, L., et al. (2014). Effects of obesity, diabetes and exercise on Fndc5 gene expression and irisin release in human skeletal muscle and adipose tissue: in vivo and in vitro studies. *J. Physiol.* 592, 1091–1107. doi: 10.1113/jphysiol.2013.264655

Liu, B., Walton, S. D., Ho, H. T., Belevych, A. E., Tikunova, S. B., Bonilla, I., et al. (2018). Gene transfer of engineered calmodulin alleviates ventricular arrhythmias in a calsequestrin-associated mouse model of catecholaminergic polymorphic ventricular tachycardia. *J. Am. Heart Assoc.* 7:e008155. doi: 10.1161/JAHA.117.008155

Liu, J., and Rigel, D. F. (2009). "Echocardiographic examination in rats and mice," in *Cardiovascular Genomics. Methods in Molecular BiologyTM (Methods and Protocols)*, ed. K. DiPetrillo (Totowa, NJ: Humana Press), 139–155. doi: 10.1007/978-1-60761-247-6_8

Lu, S., Kanekura, K., Hara, T., Mahadevan, J., Spears, L. D., Oslowski, C. M., et al. (2014). A calcium-dependent protease as a potential therapeutic target for Wolfram syndrome. *Proc. Natl. Acad. Sci.* 111, E5292–E5301. doi: 10.1073/pnas.1421055111

Luuk, H., Plaas, M., Raud, S., Innos, J., Sütt, S., Lasner, H., et al. (2009). Wfs1-deficient mice display impaired behavioural adaptation in stressful environment. *Behav. Brain Res.* 198, 334–345. doi: 10.1016/j.bbr.2008.11.007

Medlej, R., Wasson, J., Baz, P., Azar, S., Salti, I., Loiselet, J., et al. (2004). Diabetes mellitus and optic atrophy: a study of Wolfram syndrome in the Lebanese population. *J. Clin. Endocrinol. Metab.* 89, 1656–1661. doi: 10.1210/jc.2002-030015

Mikusová, A., Králová, E., Tylková, L., Novotová, M., and Stankovicová, T. (2009). Myocardial remodelling induced by repeated low doses of isoproterenol. *Can. J. Physiol. Pharmacol.* 87, 641–651. doi: 10.1139/y09-053

Morikawa, S., Tajima, T., Nakamura, A., Ishizu, K., and Ariga, T. (2017). A novel heterozygous mutation of the WFS1 gene leading to constitutive endoplasmic reticulum stress is the cause of Wolfram syndrome. *Pediatr. Diabetes* 18, 934–941. doi: 10.1111/pedi.12513

Ohta, Y., Taguchi, A., Matsumura, T., Nakabayashi, H., Akiyama, M., Yamamoto, K., et al. (2017). Clock gene dysregulation induced by chronic ER stress disrupts β-cell function. *EBioMedicine* 18, 146–156. doi: 10.1016/j.ebiom.2017.03.040

Osman, A. A., Saito, M., Makepeace, C., Permutt, M. A., Schlesinger, P., and Mueckler, M. (2003). Wolframin expression induces novel ion channel activity in endoplasmic reticulum membranes and increases intracellular calcium. *J. Biol. Chem.* 278, 52755–52762. doi: 10.1074/jbc.M31033 1200

Pasqualin, C., Gannier, F., Yu, A., Malécot, C. O., Bredeloux, P., and Maupoil, V. (2017). SarConfoCal: simultaneous sarcomere length and cytoplasmic calcium measurements for laser scanning confocal microscopy images. *Bioinformatics* 33, 789–790. doi: 10.1093/bioinformatics/btw754

Plaas, M., Seppa, K., Reimets, R., Jagomäe, T., Toots, M., Koppel, T., et al. (2017). Wfs1-deficient rats develop primary symptoms of Wolfram syndrome: insulin-dependent diabetes, optic nerve atrophy and medullary degeneration. *Sci. Rep.* 7:10220. doi: 10.1038/s41598-017-09392-x

Qian, X., Qin, L., Xing, G., and Cao, X. (2015). Phenotype prediction of pathogenic nonsynonymous single nucleotide polymorphisms in WFS1. *Sci. Rep.* 5:14731. doi: 10.1038/srep14731

Safarpour Lima, B., Ghaedi, H., Daftarian, N., Ahmadieh, H., Jamshidi, J., Khorrami, M., et al. (2016). C.376G > A mutation in WFS1 gene causes Wolfram syndrome without deafness. *Eur. J. Med. Genet.* 59, 65–69. doi: 10.1016/j.ejmg.2016.01.001

Schindelin, J., Arganda-Carreras, I., Frise, E., Kaynig, V., Longair, M., Pietzsch, T., et al. (2012). Fiji: an open-source platform for biological-image analysis. *Nat. Methods* 9, 676–682. doi: 10.1038/nmeth.2019

Schneider, C. A., Rasband, W. S., and Eliceiri, K. W. (2012). NIH Image to ImageJ: 25 years of image analysis. *Nat. Methods* 9, 671–675. doi: 10.1038/nmeth.2089

Sham, J. S. (1997). Ca2+ release-induced inactivation of Ca2+ current in rat ventricular myocytes: evidence for local Ca2+ signalling. *J. Physiol.* 500, 285–295. doi: 10.1113/jphysiol.1997.sp022020

Takeda, K., Inoue, H., Tanizawa, Y., Matsuzaki, Y., Oba, J., Watanabe, Y., et al. (2001). WFS1 (Wolfram syndrome 1) gene product: predominant subcellular localization to endoplasmic reticulum in cultured cells and neuronal expression in rat brain. *Hum. Mol. Genet.* 10, 477–484. doi: 10.1093/hmg/10.5.477

Takei, D., Ishihara, H., Yamaguchi, S., Yamada, T., Tamura, A., Katagiri, H., et al. (2006). WFS1 protein modulates the free Ca2+concentration in the endoplasmic reticulum. *FEBS Lett.* 580, 5635–5640. doi: 10.1016/j.febslet.2006.09.007

Wolfram, D. J., and Wagener, H. P. (1938). Diabetes mellitus and simple optic atrophy among siblings: report on four cases. *Mayo Clin. Proc.* 1, 715–718.

Yamada, T., Ishihara, H., Tamura, A., Takahashi, R., Yamaguchi, S., Takei, D., et al. (2006). WFS1-deficiency increases endoplasmic reticulum stress, impairs cell cycle progression and triggers the apoptotic pathway specifically in pancreatic β-cells. *Hum. Mol. Genet.* 15, 1600–1609. doi: 10.1093/hmg/ddl081

Yurimoto, S., Hatano, N., Tsuchiya, M., Kato, K., Fujimoto, T., Masaki, T., et al. (2009). Identification and characterization of wolframin, the product of the Wolfram syndrome gene (WFS1), as a novel calmodulin-binding protein. *Biochemistry* 48, 3946–3955. doi: 10.1021/bi900260y

Zahradnik, I., and Palade, P. (1993). Multiple effects of caffeine on calcium current in rat ventricular myocytes. *Pflugers Arch.* 424, 129–136. doi: 10.1007/BF00374603

Zahradníková, A., Kubalová, Z., Pavelková, J., Györke, S., and Zahradník, I. (2004). Activation of calcium release assessed by calcium release-induced inactivation of calcium current in rat cardiac myocytes. *Am. J. Physiol. Cell Physiol.* 286, C330–C341. doi: 10.1152/ajpcell.00272.2003

Zahradníková, A., Valent, I., and Zahradník, I. (2010). Frequency and release flux of calcium sparks in rat cardiac myocytes: a relation to RYR gating. *J. Gen. Physiol.* 136, 101–116. doi: 10.1085/jgp.200910380

Zatyka, M., Da Silva Xavier, G., Bellomo, E. A., Leadbeater, W., Astuti, D., Smith, J., et al. (2015). Sarco(endo)plasmic reticulum atpase is a molecular partner of wolfram syndrome 1 protein, which negatively regulates its expression. *Hum. Mol. Genet.* 24, 814–827. doi: 10.1093/hmg/ddu499

Conflict of Interest Statement: The authors declare that the research was conducted in the absence of any commercial or financial relationships that could be construed as a potential conflict of interest.

frontiers in Physiology

ORIGINAL RESEARCH
published: 30 April 2019
doi: 10.3389/fphys.2019.00520

Impaired Activity of Ryanodine Receptors Contributes to Calcium Mishandling in Cardiomyocytes of Metabolic Syndrome Rats

*Gaudencio Fernández-Miranda†, Tatiana Romero-Garcia†, Tarín P. Barrera-Lechuga†, Martha Mercado-Morales and Angélica Rueda**

Departamento de Bioquímica, Centro de Investigación y de Estudios Avanzados del IPN (CINVESTAV), Mexico City, Mexico

OPEN ACCESS

Edited by:
Tarik Smani,
Universidad de Sevilla, Spain

Reviewed by:
Aleksey V. Zima,
Loyola University Chicago, United States
Alicia Mattiazzi,
Centro de Investigaciones Cardiovasculares, Argentina

***Correspondence:**
Angélica Rueda
arueda@cinvestav.mx

† These authors have contributed equally to this work

Specialty section:
This article was submitted to Membrane Physiology and Membrane Biophysics, a section of the journal Frontiers in Physiology

Received: *14 December 2018*
Accepted: *11 April 2019*
Published: *30 April 2019*

Citation:
Fernández-Miranda G, Romero-Garcia T, Barrera-Lechuga TP, Mercado-Morales M and Rueda A (2019) Impaired Activity of Ryanodine Receptors Contributes to Calcium Mishandling in Cardiomyocytes of Metabolic Syndrome Rats. Front. Physiol. 10:520. doi: 10.3389/fphys.2019.00520

Metabolic syndrome (MetS) has become a global epidemic. MetS is a serious health problem because of its related cardiovascular complications, which include hypertension and delayed heart rate recovery after exercise. The molecular bases of cardiac dysfunction in MetS are still under scrutiny and may be related to anomalies in the activity and expression of key proteins involved in the cardiac excitation–contraction coupling (ECC). The cardiac Ca^{2+} channel/ryanodine receptor (RyR2) participates in releasing Ca^{2+} from internal stores and plays a key role in the modulation of ECC. We examined alterations in expression, phosphorylation status, Ca^{2+} sensitivity, and *in situ* function (by measuring Ca^{2+} sparks and Ca^{2+} transients) of RyR2; alterations in these characteristics could help to explain the Ca^{2+} handling disturbances in MetS cardiomyocytes. MetS was induced in rats by adding commercially refined sugar (30% sucrose) to their drinking water for 24 weeks. Cardiomyocytes of MetS rats displayed decreased Ca^{2+} transient amplitude and cell contractility at all stimulation frequencies. Quiescent MetS cardiomyocytes showed a decrease in Ca^{2+} spark frequency, amplitude, and spark-mediated Ca^{2+} leak. The [^{3}H]-ryanodine binding data showed that functionally active RyRs are significantly diminished in MetS heart microsomes; and exhibited rapid Ca^{2+}-induced inactivation. The phosphorylation of corresponding Ser2814 (a preferential target for CaMKII) of the hRyR2 was significantly diminished. RyR2 protein expression and Ser2808 phosphorylation level were both unchanged. Further, we demonstrated that cardiomyocyte Ca^{2+} mishandling was associated with reduced SERCA pump activity due to decreased Thr17-PLN phosphorylation, suggesting a downregulation of CaMKII in MetS hearts, though the SR Ca^{2+} load remained unchanged. The reduction in the phosphorylation level of RyR2 at Ser2814 decreases RyR2 availability for activation during ECC. In conclusion, the impaired *in situ* activity of RyR2 may also account for the poor overall cardiac outcome reported in MetS patients; hence, the SERCA pump and RyR2 are both attractive potential targets for future therapies.

Keywords: ryanodine receptor, calcium sparks, ryanodine binding, SERCA pump, cardiomyocytes, calcium mishandling, metabolic syndrome

INTRODUCTION

Metabolic syndrome (MetS) is a cluster of biochemical and physiological risk factors for cardiovascular disease and diabetes mellitus type 2 (DM2); it represents a severe public health problem around the world (Alberti et al., 2009). Risk factors for MetS include obesity (particularly central obesity), elevated triglyceride (TG) levels, low high-density lipoprotein cholesterol (HDL-C) levels, high blood pressure, and dysglycemia. Insulin resistance is considered to be the critical factor underlying MetS, though the pathogenesis remains unclear (Alberti et al., 2009). The definition of what clinically constitutes MetS has generated considerable debate; however, it is generally accepted that a combination of at least three or more of the risk factors must exist to diagnose MetS (Nolan et al., 2017; Tune et al., 2017). People diagnosed with MetS exhibit delayed heart rate recovery after exercise and 50–60% higher cardiovascular risk than those without it (Sung et al., 2006; Qiao et al., 2007). Specifically, MetS is associated with a twofold increase in cardiovascular mortality, myocardial infarction, and stroke (Mottillo et al., 2010). MetS-associated alterations in heart function include impaired myocardial contractility and diastolic dysfunction that predisposes to congestive heart failure (HF) (Tune et al., 2017). At the molecular level in cardiac cells, excitation–contraction coupling (ECC) initiates with T-tubule membrane depolarization, which induces L-type Ca^{2+} channel (LTCC) activation. Ca^{2+} entry is not of sufficient magnitude to activate the contractile machinery but triggers a larger Ca^{2+} release from the stores in the sarcoplasmic reticulum (SR) via the activation of the intracellular Ca^{2+} channel/ryanodine receptor (RyR2), thus promoting cell contraction. This process is known as Ca^{2+}-induced Ca^{2+} release (CICR). Relaxation takes place after Ca^{2+} removal, primarily through its recapture into the intracellular Ca^{2+} stores by the sarco/endoplasmic reticulum Ca^{2+} ATPase (SERCA pump) and its extrusion by the action of both the Na^{+}/Ca^{2+} exchanger (NCX1) and the plasma membrane calcium ATPase (PMCA) (Fabiato, 1983; Bers, 2014). ECC defects in MetS cardiomyocytes are chiefly characterized by a slow rate of shortening and relengthening. Moreover, depressed cell shortening and slower cytosolic Ca^{2+} clearing have been documented in cardiomyocytes of the prediabetic sucrose-fed rat model at early stages of MetS development (6–18 weeks of sucrose treatment) (Dutta et al., 2001; Hintz and Ren, 2002; Davidoff et al., 2004; Wold et al., 2005; Vasanji et al., 2006; Balderas-Villalobos et al., 2013; Okatan et al., 2016), but the participation of the RyR2 has not been fully elucidated.

The study of RyR2 dysregulation in cardiovascular diseases—including those of inherited and non-inherited etiology—has gained considerable interest in recent years due to its crucial role in the development of HF and cardiac arrhythmias. In the context of type 2 diabetic cardiomyopathy, depressed RyR2 activity is reportedly linked to a reduction in its protein expression; however, other studies did not observe changes in RyR2 at the protein level (Pereira et al., 2006, 2014). In the context of MetS, the function, expression, and phosphorylation status of cardiac RyR are still under analysis. Moreover, altered RyR phosphorylation status has been linked to the impairment of RyR activity, which leads to diabetic cardiomyopathy (Belke et al., 2004; Pereira et al., 2014). Additionally, intricate effects of both protein kinase A- (PKA) and Ca^{2+}/Calmodulin-dependent protein kinase II- (CaMKII) mediated RyR phosphorylation have been reported in cardiomyocytes from prediabetic rats, resulting in defective RyR2 regulation (Okatan et al., 2016; Sommese et al., 2016).

Alterations in the *in situ* activity, expression, and regulation by phosphorylation of RyR2 have not been thoroughly evaluated in rat experimental models of MetS, particularly after 24-week treatment with 30% sucrose in drinking water, which elicits a condition resembling a chronic state of MetS in humans. Thus, we sought to examine RyR2 performance in the sucrose-induced MetS rat model. We evaluated the *in situ* activity of RyRs in cardiomyocytes by characterizing electrically-stimulated Ca^{2+} transients, Ca^{2+} spark properties, and spark-mediated Ca^{2+} leak. We also used biochemical approaches ([^{3}H]-Ryanodine binding and Western Blots assays) to quantify functional RyR2 and to measure the Ca^{2+} sensitivity, protein expression, and phosphorylation status at Ser2808 and Ser2814 of RyR2 in heart homogenates and SR-enriched membranes.

MATERIALS AND METHODS

Development of the Sucrose-Induced Metabolic Syndrome Model

Male *Wistar* rats, aged 25 days, were divided into two groups and maintained under a dark–light cycle of 12 h and controlled temperature of 22 ± 2°C. The first experimental group (MetS) received 30% sucrose (refined commercial sugar) in their drinking water and commercial rat chow (PicoLab Rodent Diet 20, LabDiet, St. Louis, MO, United States) *ad libitum* for 24 weeks. The second group (control, C) received water and commercial rat chow *ad libitum* during the same 24 weeks. Measurement of systolic blood pressure (SBP) was carried out by the tail-cuff method with a sensor connected to a pressure transducer and a PC equipped with special software (Grass PolyView) for data capture and processing. Recordings were taken in quadruplicate and were compared with those from invasive techniques: no difference has been found, in agreement with previous reports (Perez-Torres et al., 2009; de Alba-Aguayo et al., 2017).

Measurement of Serum Glucose, Triglycerides, Total Cholesterol, and HDL-Cholesterol

After fasting overnight, rats were treated with heparin (1000 units/kg) and anesthetized with sodium pentobarbital (50 mg/kg, i.p.). Anesthetized animals were subjected to a thoracotomy, during which the heart was exposed and excised

rapidly, and blood samples were collected immediately from the sectioned aorta. The serum levels of glucose, triglycerides, total cholesterol, and HDL-cholesterol were measured using glucose and lipid panel strips with the CardioCheck PA analyzer (PTS Diagnostics, Indianapolis, IN, United States).

Cardiomyocyte Isolation

Left ventricle myocytes were enzymatically isolated from MetS and control rat hearts following a previously reported protocol (de Alba-Aguayo et al., 2017). Animals were treated with heparin (1000 units/kg) and anesthetized with sodium pentobarbital (50 mg/kg, i.p.). The heart was excised rapidly via a thoracotomy and placed in ice-cold (0°C) oxygenated Tyrode solution containing (in mM): NaCl 130, KCl 5.4, NaH_2PO_4 0.4, $MgCl_2$ 0.5, glucose 22, Hepes 25 and insulin 10^{-3} (pH 7.4 with NaOH). The aorta was cannulated above the aortic valve and heart was perfused by gravity with warm (37°C) Tyrode solution supplemented with 0.1 mM EGTA for 5 min. Enzyme solution containing 0.8 g/L collagenase Type II (Worthington Biochemical, Corp., Lakewood, NJ, United States) in Tyrode solution supplemented with 0.1 mM $CaCl_2$ was then perfused until the aortic valve was digested (confirmed by the increased outflow of perfusate). The heart was transferred to a Petri dish containing enzyme solution supplemented with 1 mg/mL bovine serum albumin (BSA) and gently shaken for 2–3 min at 37°C to disperse individual myocytes. The resulting cell suspension was centrifuged for 3 min at 170 × *g*. The cell pellet was suspended in Tyrode solution supplemented with 0.5 mM $CaCl_2$ and was centrifuged again at the same speed. Finally, the cell pellet was suspended in storage solution containing Tyrode solution supplemented with 1 mM $CaCl_2$.

Recording of Ca^{2+} Sparks, Ca^{2+} Transients, and Assessment of SR Ca^{2+} Load

Spontaneous Ca^{2+} sparks and field-stimulated Ca^{2+} transients were imaged in Fluo-3 loaded cardiomyocytes as previously reported (de Alba-Aguayo et al., 2017), with some modifications. Cells were superfused with recording solution (in mM: NaCl 130, $CaCl_2$ 1.8, $MgCl_2$ 2.0, KCl 5.4, glucose 10, HEPES 10, insulin 0.01, pH 7.4) and 2D-images were obtained with a confocal microscope (Leica TCS SP5, Leica Microsystems, Wetzlar, Germany) in the line-scan mode (1.9 ms/line). To obtain electrically-stimulated Ca^{2+} transients, cells were paced at different frequencies using a Grass stimulator set at 70 V and pulse length of 20 ms; 5 images of the cell were taken for each stimulation frequency. The Y-axis of the image indicates the length of the cell (in μm) and the X-axis indicates the scan time (in s). Fluo-3 was excited at 488 nm using an argon laser at 2% intensity. The emitted fluorescence of the dye was measured at 510 nm. To determined SR Ca^{2+} load, myocytes were paced at 1 Hz for at least 1 min to restore steady state SR Ca^{2+} load, then confocal laser scanning was initiated and four electrically-evoked Ca^{2+} transients were followed by rapid application of caffeine (10 mM) (Fernández-Velasco et al., 2009; de Alba-Aguayo et al., 2017).

Analysis of Confocal Images

Image analysis was performed using IDL 5.5 software (Research Systems, Inc.) running a custom protocol written by Ana Maria Gómez (Inserm UMR-S 1180, Châtenay-Malabry, France), including baseline fluorescence correction and normalizing fluorescence levels (F) with respect to basal fluorescence (F_0) (de Alba-Aguayo et al., 2017). The fluorescence transient was obtained by averaging the fluorescence values in a 1.4-μm frame over time. Amplitude was measured as the maximum value of F/F_0, where F is the fluorescence signal, and F_0 is the basal fluorescence (measured as the average of the 50 lowest values on the fluorescence transient). Cell shortening was reported in % respect to total cell length. Cells with cell shortening values below 4.5% were not considered in the analysis. Decay Time (in ms) was determined at 50% of recovery of the Ca^{2+} transient peak. Parameters such as amplitude (F/F_0), frequency (events/s*100 μm), full duration at half maximum (FDHM in ms), full width at half maximum (FWHM in μm), time-to-peak (in ms) and decay time constant (in ms), were analyzed for Ca^{2+} sparks (de Alba-Aguayo et al., 2017). The spark-mediated Ca^{2+} leak was calculated according to the method reported by Biesmans and collaborators, in which the spark-mediated Ca^{2+} leak is defined as spark frequency*spark mass; and spark mass is calculated as spark amplitude*duration*width (Biesmans et al., 2011).

Preparation of Heart Homogenates and SR-Enriched Fractions

Heart homogenates and SR-enriched fractions were prepared from left-ventricle tissue pulverized to a fine powder with a mortar and pestle over liquid N_2. Tissue powder was suspended in homogenization buffer (in mM: sucrose 300, NaF 20, HEPES 20, aprotinin 5.2×10^4, benzamidine 0.5, leupeptin, 0.012, PMSF 0.1; pH 7.2 with KOH) and homogenized with a Potter-Elvehjem homogenizer (Cole-Parmer, Vernon Hills, IL, United States) and spun at 2000 × *g* for 10 min; the resulting supernatant (homogenate) was spun at 8000 × *g* for 10 min; SR-enriched fractions (or microsomes) were isolated using the second supernatant by ultracentrifugation at 40000 × *g* for 30 min at 4°C. The resulting pellets were suspended in homogenization buffer and protein concentration was determined using the Lowry method as previously reported (de Alba-Aguayo et al., 2017).

Measurement of SR Ca^{2+} Uptake

Fura-4F acid form (pentapotassium salt, Molecular Probes/Thermo Fisher Scientific, Inc.) was added outside SR-membrane vesicles and used to monitor the SERCA-dependent Ca^{2+} uptake accordingly to a previously described method (de Alba-Aguayo et al., 2017). SR Ca^{2+} uptake was measured in a buffer containing (in mM): KCl 100, $MgCl_2$ 4, MOPS 20, potassium oxalate 10, ATP-Mg 1.25, creatine phosphate 1.5, pH 7.4 with KOH, and 0.3 U/ml creatine phosphokinase. 10 μM Ruthenium Red was added to inhibit Ca^{2+} release through RyRs. Fura-4F was added

to a final concentration of 0.5 μM. 600 μg of protein from SR-enriched vesicles were added to a cuvette with uptake buffer and equilibrated at 37°C during 5 min with stirring. Fluorescence was measured in a QM-8 spectrofluorometer (*PTI*, excitation wavelengths at 340, 360, and 380 nm; emission was collected at 510 nm). The addition of 5 μM $CaCl_2$ initiated Ca^{2+} uptake reactions; the fluorescence was recorded up to 900 s. The experiment was finished by adding Thapsigargin (1 μM). To determine R_{max}, 200 μM $CaCl_2$ was added; to measure R_{min}, 250 μM EGTA was added. Ratio values of fluorescence (F340/F380) were subsequently transformed into Ca^{2+} concentrations using the Grynkiewicz equation (Grynkiewicz et al., 1985). Ca^{2+} uptake speed was calculated as the first derivative of the monoexponential decay equation used to fit the Ca^{2+} uptake curve.

[^{3}H]-Ryanodine Binding Assays

[^{3}H]-ryanodine binding experiments were performed as previously described using SR-enriched fractions (Fernández-Velasco et al., 2009; de Alba-Aguayo et al., 2017). [^{3}H]-ryanodine saturation curves were carried out in medium containing 1 M KCl, 0.1 mM $CaCl_2$, 20 mM HEPES (pH 7.2 with KOH); and [^{3}H]-ryanodine in the range of 0.625 to 20 nM. Equilibrium binding data were fitted to the one-site model (Hill equation), apparent dissociation constant (*Kd*) and total functional RyRs (*Bmax*) were calculated from the fitted curve. The Ca^{2+} dependence of [^{3}H]-ryanodine binding was assessed in incubation medium containing 0.2 mM KCl, 20 HEPES (pH 7.2 with KOH), 50 μg of SR-enriched fractions, 10 nM [^{3}H]-ryanodine, 1 mM EGTA, and $CaCl_2$ necessary to set free Ca^{2+} in the range of 10 nM to 10 mM (total volume 100 μl). Ca^{2+}-EGTA ratios were calculated using the MaxChelator program[1] (Bers et al., 2010). All incubations lasted 90 min at 36°C. Samples were run in duplicate, filtered onto glass fiber filters (Whatman GF/B), and washed three times with 5 ml of cold water using a Brandel M-24R cell harvester. The filters were placed in scintillation vials, 8 ml of liquid scintillation mixture was added, and the retained radioactivity was measured in a Beckman LS-6500 β-counter. The specific binding was defined as the difference between the binding in the absence (total binding) and presence (non-specific binding) of 20 μM unlabeled ryanodine. Data represent the normalized mean ± SEM of the indicated *n* in the respective figure. Fitting of data was accomplished with the computer program OriginPro 8 (OriginLab Corporation, Northampton, MA, United States) to the following equation: $B = B_{max}([Ca^{2+}]^{na}/([Ca^{2+}]^{na}+K_a{}^{na}))(1-[Ca^{2+}]^{ni}/([Ca^{2+}]^{ni}+K_i{}^{ni}))+C$, modified from Meissner's group (Liu et al., 1998), where B is the [^{3}H]-ryanodine binding value at a given $[Ca^{2+}]$, B_{max} is the binding maximum, K_a and K_i are Hill activation and inactivation constants, respectively, n_a and n_i are the respective Hill coefficients, and C is an initial [^{3}H]-ryanodine binding value at very low $[Ca^{2+}]$ (pCa8) (Fernández-Velasco et al., 2009; de Alba-Aguayo et al., 2017).

[1]http://maxchelator.stanford.edu/index.html

SDS-PAGE and Western Blot Analysis

SDS-PAGE and Western Blots were performed as a modification of previously reported protocols (Fernández-Velasco et al., 2009; de Alba-Aguayo et al., 2017). Gradient polyacrylamide gels (4–16%). Gels were loaded with the indicated μg of protein from heart homogenates in Laemmli buffer. Each gel was transferred onto a PVDF membrane for 2 h, 100 V at 4°C in a humid chamber. PVDF membrane was blocked from non-specific binding with 5% non-fat dry milk in PBS-T buffer (composition in mM: KH_2PO_4 2.9, Na_2HPO_4 10.07, $NaCl_2$ 150.58 and Tween 20, 0.1%) for 1 h, before incubation with primary antibody against RyR2 (C3-33 dil: 1:5000, Cat# MA3-916, Thermo Fisher, Inc., Waltham, MA United States), pSer2808RyR2 (dil: 1:5000, Cat# A010-30, Badrilla, Leeds, United Kingdom), pSer2814RyR2 (dil: 1:5,000 Cat# A010-31, Badrilla, Leeds, United Kingdom), SERCA2a (dil: 1,5000 Cat# A010-20, Badrilla, Leeds, United Kingdom), PLN (dil: 1:25,000 Cat# A010-14, Badrilla, Leeds, United Kingdom), pSer16PLN (dil: 1:3,000 Cat# A010-12, Badrilla, Leeds, United Kingdom), pThr17PLN (dil: 1:5,000 Cat# A010-13, Badrilla, Leeds, United Kingdom), CaMKII (dil: 1:2,500 Cat# 4436S, Cell Signaling, Danvers, MA, United States), and GAPDH (dil: 1:100,000 Cat# AM4300, Ambion®, Thermo Fisher Scientific, Waltham, MA, United States) for 2 h at room temperature. After washing, the membranes were incubated with corresponding secondary peroxidase-conjugated antibodies (dil 1:5,000 of goat anti-mouse IgG peroxidase conjugated, Cat. No. 401215, or goat anti-rabbit IgG peroxidase conjugated, Cat. No. 401315; both from Calbiochem® Merck, Co., Kenilworth, NJ, United States) for 1 h. The membranes were washed (3X, 10 min each with PBS-T buffer). Proteins were visualized by chemiluminescent reaction (SuperSignal® West Pico Chemiluminescent Substrate, Thermo Fisher Scientific, Waltham, MA, United States) and the relative amount of protein was determined by densitometric analysis using Kodak MI SE Software (v.5.01.30. Molecular Imaging Software).

Statistical Data Analysis

Data are presented as the mean ± SEM of indicated independent determinations, where "N" was used to designate the number of animals or hearts; and "n" to specify the number of cells, Ca^{2+} release events, or experiments. Statistical significance was evaluated by Student's *t*-test or one-way ANOVA followed by Tukey *post hoc* test, when appropriated (OriginPro 8 software from Origin Lab Corporation, Northampton, MA, United States). Significance was defined at $P < 0.05$.

RESULTS

Characteristics of the Chronic Sucrose-Induced MetS Model

Male rats that received 30% sucrose in the drinking water for 24 weeks developed several of the hallmark characteristics of MetS: for instance, a significant increase in body weight

(32%) and visceral fat accumulation (2.4-fold) compared to the control group (**Table 1**). Additionally, average SBP was significantly higher in MetS rats than controls (**Table 1**). Although the heart weight was slightly augmented in the MetS condition, features such as heart weight-to-body weight ratio, left ventricle weight, and left ventricle-to-heart weight ratio showed no alterations, indicating the lack of severe structural remodeling in the heart (**Table 1**). Serum parameters evidenced the development of hypertriglyceridemia (2.6-fold increase in serum triglycerides levels); and a significant increase in the TG-to-HDL-C ratio, which is indicative of a higher degree of cardio-metabolic risk in the insulin-resistant condition (Salazar et al., 2014). These alterations in both body and serum parameters are strong evidence of the development of MetS in rats as a consequence of the sucrose-rich diet (Wong et al., 2016).

Diminished Ca^{2+} Transient Amplitude in Cardiomyocytes of Metabolic Syndrome Rats

Previous studies have demonstrated depressed cardiac contractile function in sucrose-fed animals, evidenced by the reduction of ejection fraction, left ventricle systolic function, and heart fractional shortening (Vasanji et al., 2006). Moreover, reduced peak tension in papillary muscle strips has been reported in MetS condition (Okatan et al., 2016). Because the intensity of cardiomyocyte contractile response relies on the magnitude and duration of the intracellular Ca^{2+} transient (Spurgeon et al., 1992), we investigated whether MetS affected electrically-evoked Ca^{2+} transients and associated cell shortening in single cardiomyocytes at three different stimulation frequencies. **Figure 1A** shows representative confocal images (acquired in *line scan* mode) of Fluo-3-loaded cardiomyocytes from control (*top*) and MetS (*bottom*) rats at 0.5 Hz, with their corresponding Ca^{2+} transient profiles (F/F_0), cellular shortening (% of resting cell size), and Ca^{2+} transient decay time (ms). Cardiomyocytes of both experimental groups exhibited a rate-dependent fall in the Ca^{2+} transient amplitude; however, in the MetS condition, the magnitude of the Ca^{2+} transient was consistently lower than in control cells (**Figure 1B**). In MetS cells, the amplitude of the Ca^{2+} transient represented 76.6, 62.8, and 61.5%, of corresponding Ca^{2+} transient amplitude in control cells, at 0.5, 1, and 2 Hz, respectively. Interestingly, a rate-dependent decline in cell contraction was found in the MetS group, with a significant reduction of 32.8, 48, and 65.9% in cell shortening of MetS cardiomyocytes at 0.5, 1, and 2 Hz, respectively (**Figure 1C**). We investigated whether alterations in the distance between T-tubules in cardiomyocytes to estimate sarcomere length (SL), could account for these results (see **Supplementary Materials and Methods**), since SL above or below the optimal range is known to contribute to a decrease in cardiomyocyte contractility. However, we found similar T-tubule distances in RyR-immunostained cardiomyocytes from both experimental groups (average T-tubule distance, in μm: 1.67 ± 0.03 in n = 5 control cells, vs. 1.64 ± 0.019 in n = 5 MetS cells, P = 0.535. **Supplementary Figure 1**), ruling out the presence of structural T-tubule remodeling in MetS cardiomyocytes. Analysis of Ca^{2+} transient kinetics revealed that the decay time (at 50% of the peak) was slightly increased in MetS cells at all frequencies (**Figure 1D**), suggesting that the Ca^{2+} clearing mechanisms are slowed. The Ca^{2+} handling abnormalities could be related to a decreased rate of SR Ca^{2+} uptake and/or an increased SR Ca^{2+} leak; we therefore evaluated the Ca^{2+} spark-mediated Ca^{2+} leak.

TABLE 1 | Body characteristics and biochemical parameters of metabolic syndrome and control animals.

Body parameters	Control	Metabolic syndrome
Body weight (g)	545.0 ± 27.9	721.1 ± 33.9**
Visceral fat (g)	9.8 ± 1.1	23.9 ± 1.5**
Systolic pressure (mmHg)	113.8 ± 1.7	143.2 ± 4.9**
Heart weight (g)	1.8 ± 0.1	2.0 ± 0.1*
Hw/Bw ratio × 100	0.34 ± 0.02	0.35 ± 0.03
Left ventricle weight (g)	1.1 ± 0.05	1.1 ± 0.05
LV/Hw ratio	0.63 ± 0.03	0.54 ± 0.05
Biochemical parameters		
Glucose (mg/dL)	71.4 ± 3.6	77.0 ± 4.4
Total cholesterol (mg/dL)	72.9 ± 14.5	65.4 ± 6.9
HDL-C (mg/dL)	41.3 ± 5.5	35.8 ± 3.0
Triglycerides (mg/dL)	84.6 ± 12.0	219.6 ± 20.5**
TG/HDL-C ratio	1.93 ± 0.45	6.13 ± 0.69**

*Data are means ± SEM of N = 14 control rats and N = 12 MetS rats. Bw, body weight; HDL-C, high-density lipoprotein cholesterol; Hw, heart weight; LV, left ventricle; TGs, triglycerides. *P < 0.05 and **P < 0.001 vs. Control group.*

Reduced Diastolic Ca^{2+} Leak in Cardiomyocytes of Metabolic Syndrome Rats

The extent of SR Ca^{2+} leak impacts the SR Ca^{2+} available for release, causing systolic dysfunction. Increased SR Ca^{2+} leak elevates diastolic Ca^{2+} level, contributing to diastolic dysfunction; causes triggered arrhythmias and it is energetically costly (Bers, 2014). Thus, in a first approach, we analyzed the Ca^{2+} -spark mediated Ca^{2+} leak in intact Fluo 3-loaded cardiomyocytes of both experimental groups. **Figure 2A** shows representative confocal images of spontaneous Ca^{2+} sparks taken from control (*top*) and MetS (*bottom*) cardiomyocytes in *line scan* mode. Analyses of Ca^{2+} spark characteristics are summarized in **Figures 2B** through 2H. Ca^{2+} sparks recorded in MetS cells showed significantly reduced frequency (by 34.7%, **Figure 2B**) and amplitude (by 7%, **Figure 2C**) compared to control cells. Ca^{2+} spark mass calculated as the product of Ca^{2+} spark amplitude*duration*width was lower in MetS cell than in controls, resulting in a significant reduction of the Ca^{2+} spark-mediated Ca^{2+} leak (**Figure 2F**). Other Ca^{2+} spark parameters such as duration (**Figure 2D**), size (**Figure 2E**) time-to-peak (**Figure 2G**), and decay time (**Figure 2H**) remained unchanged.

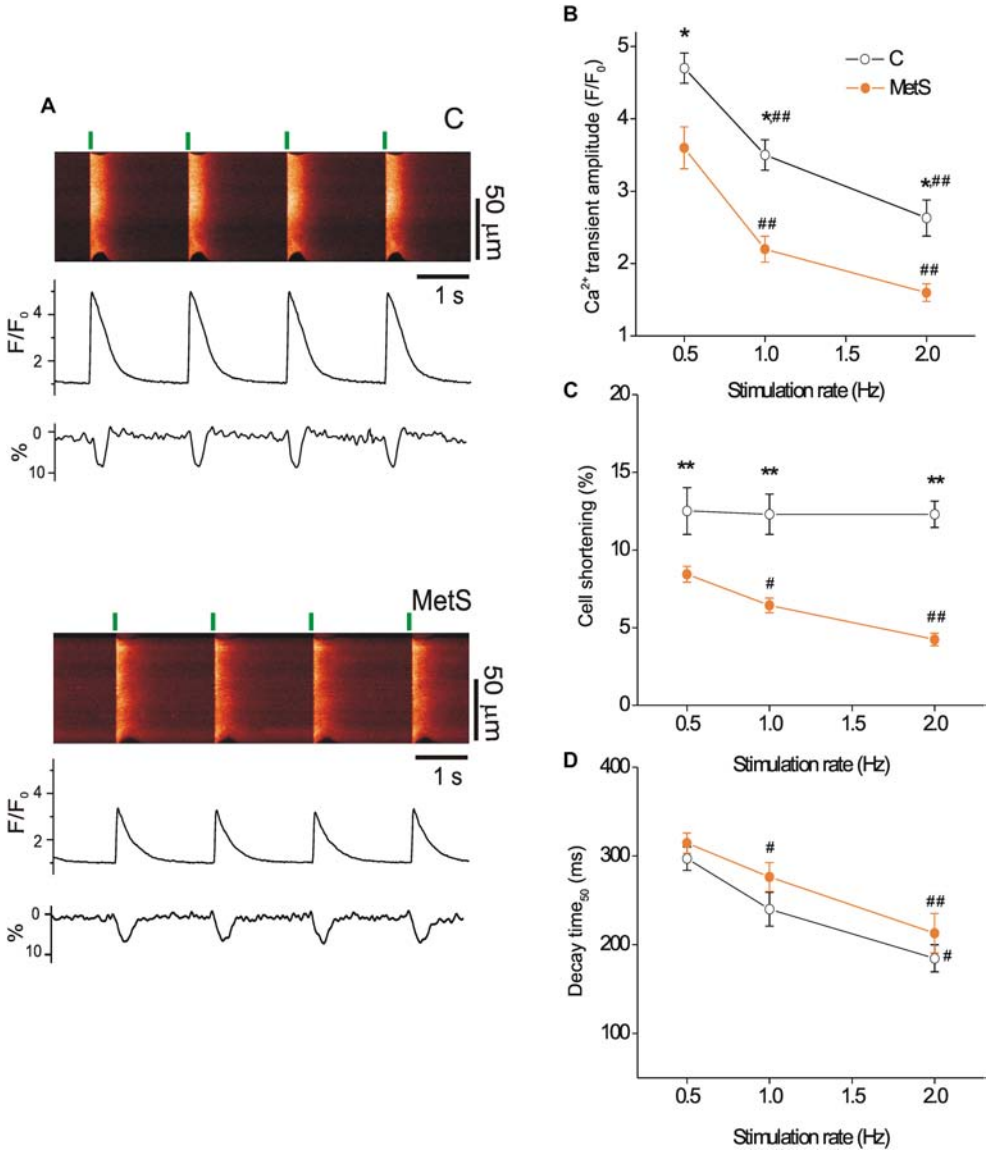

FIGURE 1 | Metabolic syndrome (MetS) cardiomyocytes exhibit a rate-dependent decrease in Ca^{2+} transient amplitude and contraction. Representative line-scan images **(A)** recorded during electric stimulation (0.5 Hz) of Fluo 3-loaded ventricular myocytes isolated from control (C) and MetS rats. Green lines indicate the start of electric stimulation. The corresponding normalized fluorescence traces (F/F_0) and contraction profiles (in %) are shown below. **(B)** Average of Ca^{2+} transient amplitude (expressed as F/F_0, where F is the peak fluorescence signal and F_0 the diastolic fluorescence) of control (*open circles*) and MetS (*orange circles*) cardiomyocytes obtained by field stimulation at 0.5, 1, and 2 Hz. Average cell shortening **(C)**, and decay time at 50% of the normalized Ca^{2+} transient **(D)** at 0.5, 1, and 2 Hz in $n = 17$ control cells vs. $n = 32$ MetS cardiomyocytes. $^{*}P < 0.05$, $^{**}P < 0.001$ respect to control cells. $^{\#}P < 0.05$, $^{\#\#}P < 0.001$ respect to 0.5 Hz in the same condition.

SR Ca^{2+} Load Is Unaffected in MetS Cardiomyocytes

The amount of Ca^{2+} stored inside the SR that is available for release during the cardiomyocyte contraction is primarily determined by the delicate balance between diastolic Ca^{2+} leak and SERCA pump-mediated Ca^{2+} uptake (Zima et al., 2010). Thus, we hypothesized that the decrease in the Ca^{2+} spark-mediated Ca^{2+} leak in MetS cells could be attributable to a significant reduction of the SR Ca^{2+} load. Accordingly, we determined the SR Ca^{2+} load in steady state conditions by measuring the amplitude of the caffeine-induced Ca^{2+} transient in cardiomyocytes previously paced at 1 Hz. **Figure 3A** shows representative line-scan images of caffeine-induced Ca^{2+} transients recorded in Fluo-3 loaded control and MetS cells. Our results show that the development of MetS did not modify the SR Ca^{2+} loading in steady-state conditions because the amplitude of the caffeine-induced Ca^{2+} transient was similar in both groups (**Figure 3B**), in agreement with previous reports in sucrose-fed rats at early stages of MetS development (Wold

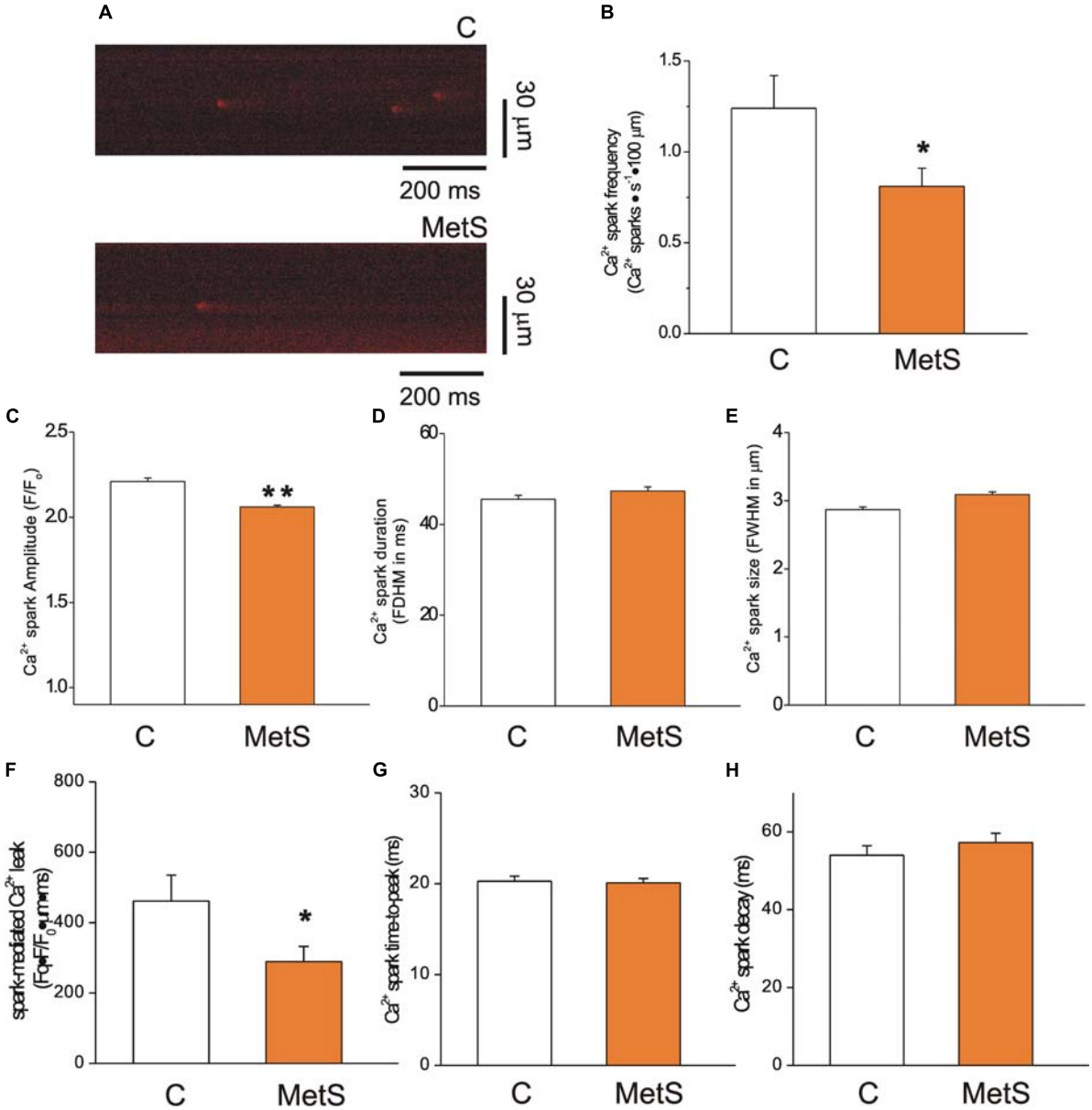

FIGURE 2 | Reduced spark-mediated Ca^{2+} leak in cardiomyocytes of MetS animals. Representative line-scan images (2 ms/line) of spontaneous Ca^{2+} sparks recorded in Fluo 3-loaded cardiomyocytes from control (C) and MetS hearts **(A)**. Bar graphs comparing the average frequency (**B**, events/s·100 μm), amplitude (**C**, F/F_0), duration (**D**, FDHM in ms), size (**E**, FWHM in μm), spark-mediated Ca^{2+} leak (**F**, reported as spark frequency*spark mass), time-to-peak (**G,** in ms), and decay time (**H,** in ms) of Ca^{2+} sparks in control (*white bars*; n = 907 events recorded in 41 cells) and MetS (*orange bars*; n = 1050 events recorded in 50 cells) cardiomyocytes. *$P < 0.05$; **$P < 0.001$ respect to control parameters.

et al., 2005; Balderas-Villalobos et al., 2013). Unchanged SR Ca^{2+} content is incompatible with reduced diastolic Ca^{2+} leak in the MetS cardiomyocytes—unless SERCA pump activity is compromised. Although the decay time of Ca^{2+} transients was found to be slightly increased in MetS cells, this parameter is a combination of several mechanisms, including SR Ca^{2+} uptake, cytoplasmic Ca^{2+} buffering, and plasma membrane Ca^{2+} extrusion, among others (Bode et al., 2011). Therefore, by further analyzing the caffeine-induced Ca^{2+} recordings, we specifically examined SERCA function using a previously reported method (Bode et al., 2011; Delgado et al., 2015). We calculated the SERCA-dependent portion of the rate constant of decay of the Ca^{2+} transient (k SERCA) by subtracting the rate constant of decay of the caffeine-evoked Ca^{2+} transient from that of the systolic Ca^{2+} transients. These calculations demonstrated that k SERCA was significantly reduced in MetS cardiomyocytes (4.23 ± 0.38 s^{-1}, n = 6 in control vs. 3.37 ± 0.12 s^{-1}, n = 8, in MetS group; $P < 0.05$). These data

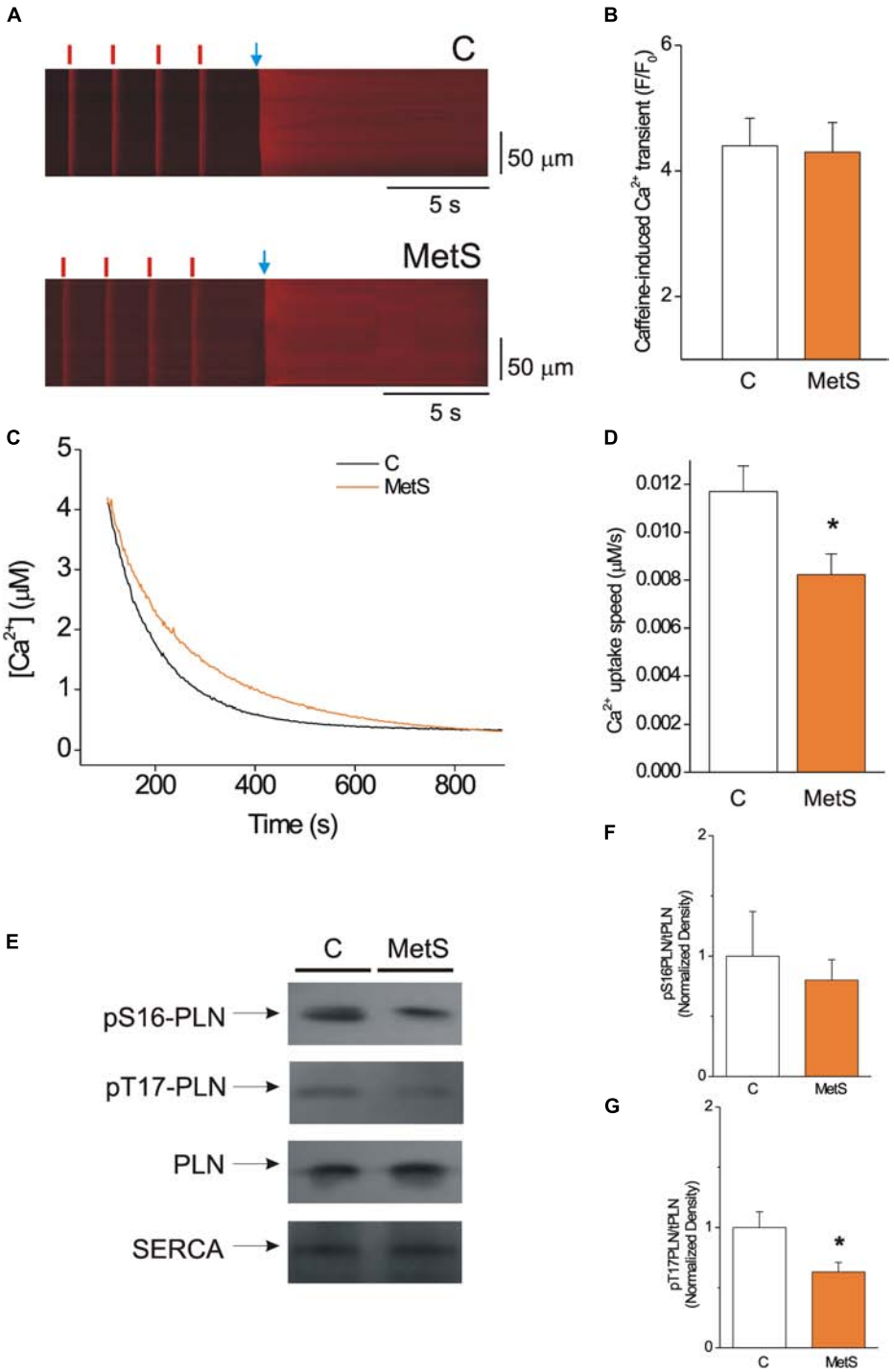

FIGURE 3 | SERCA pump activity is impaired, but this condition does not alter the SR Ca^{2+} load in MetS cardiomyocytes. **(A)** Representative line-scan images of caffeine-induced Ca^{2+} transients recorded in isolated Fluo 3-loaded cardiomyocytes from control (C, *top*) and MetS (*bottom*) rats to determine SR Ca^{2+} loading. Cells were superfused with recording solution and paced at a frequency of 1 Hz (*red lines*) before caffeine challenge (indicated by the *blue arrow*). **(B)** The bar graph represents average values of the caffeine-induced Ca^{2+} transient amplitude (F/F_0) in control (*white bar*, $n = 14$ cells) and MetS (*orange bar*, $n = 22$ cells) cardiomyocytes. **(C)** Representative traces of Ca^{2+} uptake assays in SR-enriched microsomes obtained from control (C, *black trace*) and MetS (*orange trace*) hearts. **(D)** The bar graph compares the average Ca^{2+} uptake speed (in µM/s) in control (*white bar*, $n = 10$), and MetS (*orange bars*, $n = 8$) microsomal preparations. **(E)** Representative Western Blot images of phosphorylated PLN at Ser16, Thr17, total PLN, and SERCA pump in whole heart homogenates of control (C) and MetS rats. Bar graphs of normalized phosphorylation levels of pS16 PLN **(F)** and pT17 PLN **(G)** in whole heart homogenates of control (C, *white bars*) and MetS (*orange bars*) rats. $N = 4$–7 heart preparations for each experimental group. All values in graphs are presented as Mean ± SEM. $^*P < 0.05$ vs. control values.

enabled us to hypothesize impaired SERCA pump function in MetS cardiomyocytes.

We therefore used a more direct approach to investigate SERCA pump enzymatic activity by performing a SERCA pump-mediated Ca^{2+} uptake assay in cardiac SR-enriched membranes (**Figure 3C**). These experiments revealed a 33% decrease in the rate of Ca^{2+} uptake speed in MetS microsomes compared to the control microsomes (**Figure 3D**). SERCA-pump mediated Ca^{2+} uptake was slowed in MetS microsomes, though SERCA pump protein expression was not affected (normalized SERCA pump expression: 1.0 ± 0.11 in $n = 11$ control samples vs. 1.05 ± 0.14 in $n = 11$ MetS samples; $P > 0.05$, N.S.). This result agrees with our finding of unchanged SR Ca^{2+} load despite the reduced diastolic Ca^{2+} leak observed in MetS cardiomyocytes.

Because PLN regulates SERCA-mediated Ca^{2+} uptake, changes in PLN expression level and/or phosphorylation status would be expected modify SERCA activity (Mattiazzi and Kranias, 2014). To gain insight into the molecular mechanisms involved in the observed SERCA pump dysfunction, we analyzed PLN expression and phosphorylation status of phosphosites Ser16 (a PKA site) and Thr17 (a CaMKII site; **Figure 3E**). Total PLN expression and PLN/SERCA pump ratio were similar in both experimental conditions (PLN/SERCA pump, normalized data: 1.0 ± 0.16 in $n = 7$ control samples vs. 1.31 ± 0.18 in $n = 7$ MetS samples, $P < 0.2307$). Western Blot data showed a slight but not significant decrease in the phosphorylation level of Ser16-PLN (**Figure 3F**). However, Thr17-PLN phosphorylation was significantly reduced in MetS heart homogenates (**Figure 3G**), which correlates with the reduction in SERCA activity observed in SR Ca^{2+} uptake assays (**Figures 3C,D**).

Dysfunctional Cardiac RyRs in the Metabolic Syndrome Condition

In our experimental model of MetS, the decrease in both the Ca^{2+} transient amplitude and the Ca^{2+} spark-mediated Ca^{2+} leak in isolated cardiomyocytes cannot be explained by a reduction in the SR Ca^{2+} load; therefore, we explored additional alterations in the RyR that might enable us to understand the changes in its activity. The fact that ryanodine binds only to open RyRs enables estimation of functional RyRs under *in vitro* conditions. **Figure 4A** shows saturation binding curves for [^{3}H]-ryanodine in SR-enriched fractions from MetS and control hearts. SR membranes from MetS hearts bound significantly less [^{3}H]-ryanodine (38.2%) than those from control hearts. Importantly, the *Kd* for [^{3}H]-ryanodine was found in the nanomolar range and remained unchanged (**Table 2**), indicating that the apparent ryanodine affinity of RyRs remains similar in both experimental groups. We also examined whether the Ca^{2+}-dependent activation of [^{3}H]-ryanodine binding might differ between MetS and control microsomes. **Figure 4B** shows bell-shape-like curves for both control and MetS heart microsomes. Both data sets were fitted with the same equation, indicating that RyRs followed a bimodal Ca^{2+} activation/inactivation response as previously reported (Liu et al., 1998; de Alba-Aguayo et al., 2017). The fitted parameters indicate that Ca^{2+} was equally effective in activating RyRs from control and MetS heart microsomes, since the range for *Ka* value remained similar (**Table 3**) and in agreement with previous reports (Liu et al., 1998). However, RyRs from MetS hearts exhibited rapid Ca^{2+}-induced inactivation (**Figure 4B**), and showed a significant decrease (26.3%) in the total amount of RyRs capable of binding [^{3}H]-ryanodine at optimal [Ca^{2+}] (indicated by the *Bmax* value in **Table 3**), with a slight, but not significant, decrease in the initial quantity of active RyR at very low [Ca^{2+}] (indicated by the *C* value in **Table 3**). Thus, our results

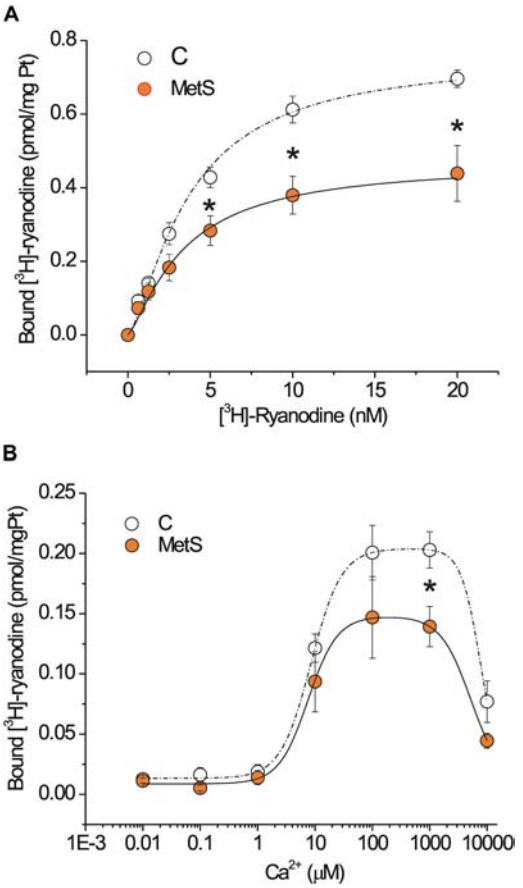

FIGURE 4 | Functional ryanodine receptors are decreased and showed rapid Ca^{2+}-induced inactivation in MetS hearts. Saturation binding curve with [^{3}H]-ryanodine. **(A)** Aliquots of 50 μg of protein from microsomes (SR-enriched fraction) from control ($N = 6$) and MetS ($N = 5$) hearts were incubated with [^{3}H]-ryanodine (concentration range of 0.625–20 nM) in incubation medium (containing in mM: 1000 KCl, 0.1 $CaCl_2$ 20 HEPES, pH 7.2) for 90 min at 37°C. **(B)** Specific Ca^{2+}-dependent [^{3}H]-ryanodine binding curves of SR-enriched fractions from control (*open symbols; N* = 9) and MetS (*orange symbols*; $N = 6$) hearts. Microsomes were incubated with 7 nM [^{3}H]-ryanodine and the indicated $[Ca^{2+}]_i$ at 37°C for 90 min. Values have been normalized and fitted to a modified version of the equation $B = B_{max}([Ca^{2+}]^{na}/([Ca^{2+}]^{na}+K_a{}^{na}))(1-[Ca^{2+}]^{ni}/([Ca^{2+}]^{ni}+K_i{}^{ni}))+C$. Non-specific [^{3}H]-ryanodine binding was determined in the presence of 20 μM ryanodine and subtracted from all reported values. *Open symbols*, control; *orange symbols*, MetS; *dashed line* indicates the fitting curve for control and *dark solid line* the fitting curve for MetS microsomes. *$P < 0.05$ with respect to corresponding control values.

TABLE 2 | Parameters of saturation [^{3}H]-ryanodine binding curves in microsomes of MetS and control hearts.

Experimental group	*Bmax* (pmol [^{3}H]ryanodine/mg Pt)	*Kd* (nM)	Hill coefficient	*N*
Control	0.76 ± 0.06	3.69 ± 0.63	1.4 ± 0.38	6
MetS	0.47 ± 0.08*	3.41 ± 0.43	1.3 ± 0.23	5

*Data are Mean ± SEM of indicated heart preparations for each experimental group. *P < 0.05 vs. control group.*

TABLE 3 | Ca^{2+}-dependence of [^{3}H]-ryanodine binding in microsomes of MetS and controls hearts.

Condition	*Bmax* (pmol [^{3}H]ryanodine/mg Pt)	*Ka* (μM)	*Ki* (mM)	*C* (pmol [^{3}H]ryanodine/mg Pt)	*N*
Control	0.19 ± 0.01	8.48 ± 1.05	7.6 ± 0.6	0.013 ± 0.001	9
MetS	0.14 ± 0.08*	7.57 ± 0.86	5.2 ± 1.0	0.009 ± 0.003	6

*Values are Mean ± SEM of indicated independent determinations for each experimental group. Bmax indicates the maximum number of active RyRs, K_a and K_i are Hill activation and inactivation constants, respectively; and C is an initial [^{3}H]-ryanodine binding value at very low [Ca^{2+}] (pCa8). N indicates the number of hearts. *P < 0.05 vs. control group.*

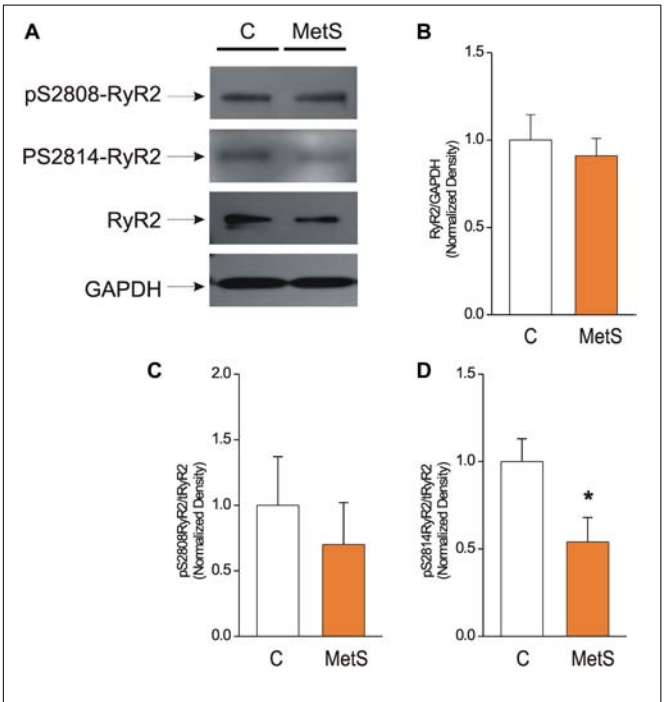

FIGURE 5 | Reduced phosphorylation levels of Cardiac Ryanodine Receptor at Ser-2814 underlie its dysfunctional activity. **(A)** Representative Western Blot images of phosphorylated RyR2 at Ser2808 (pS2808-RyR2), Ser2814 (pS2814-RyR2), and total ryanodine receptor (RyR2) in whole heart homogenates of control (C) and MetS rats. GAPDH signals were used as loading controls. 50 μg of protein from whole heart homogenates of each experimental group (C and MetS) were subjected to 4–16% gradient SDS-PAGE, blotted onto PVDF membranes during 2 h, and probed with the respective primary and secondary antibodies. Bar graphs indicate normalized expression levels of total RyR2 **(B)**, pS2808RyR2/RyR2 total **(C)**, and pS2814RyR2/RyR2 total **(D)** in whole heart homogenates of control (C, *white bars*) and MetS (*orange bars*) rats. *N* = 6–7 heart preparations for each experimental group. All values in graphs are presented as Mean ± SEM. *$P < 0.05$ vs. control values.

show an important reduction of active RyR2 that inactivate faster in MetS microsomes, which could help explain the decrease in both Ca^{2+} transient amplitude and the diastolic Ca^{2+} leak in MetS cardiomyocytes despite the unchanged SR Ca^{2+} load.

Western blot analysis was used to determine the total amount of RyR2 protein expression in control and MetS heart preparations. We also analyzed the phosphorylation levels of the corresponding Ser2808 (a substrate for several kinases, PKA and CaMKII among them) and Ser2814 (a preferential target for CaMKII) in RyR2, in light of the finding that modifications of RyR phosphorylation level account for the dysfunctional activity of cardiac RyRs in insulin-resistance and prediabetes (Dincer, 2012; Okatan et al., 2016; Sommese et al., 2016). **Figure 5A** shows representative immunoblots of pSer-2808-RyR2, pSer-2814-RyR2, and total RyR. The bar graph in **Figure 5B** shows that the total amount of RyR2 was unmodified in MetS heart preparations in comparison with controls (normalized total RyR2 expression: 1.0 ± 0.15 in $N = 6$ control hearts vs. 0.91 ± 0.10 in $N = 7$ MetS hearts; $P > 0.05$, N.S.). Nevertheless, we found a significant reduction (46%) in the phosphorylation status of Ser2814 (Normalized pSer2814RyR2: 1.0 ± 0.13 in $N = 6$ control vs. 0.54 ± 0.14 in $N = 6$ MetS hearts; $^*P < 0.05$. **Figure 5D**), while the phosphorylation level of Ser2808 remained unchanged (normalized pSer2808RyR2: 1.0 ± 0.37 in $N = 6$ control vs. 0.7 ± 0.32 in $N = 6$ MetS hearts; $P > 0.05$, N.S.; **Figure 5C**). The decreased levels of pSer2814-RyR2 and pThr17-PLN, both well-known CaMKII target sites, suggests that CaMKII activity might be compromised in our MetS model. Although CaMKII expression was similar in both experimental groups (total CaMKII expression: 1.0 ± 0.07 in $N = 7$ control hearts vs. 1.01 ± 0.07 in $N = 8$ MetS hearts; $P > 0.05$, N.S.; **Supplementary Figure 2**), we cannot rule out that changes in its activity could account for the Ca^{2+} handling alterations reported in this work. Since CaMKII activity is modulated by a wide range of post-translational modifications, further analysis regarding this issue will be required.

DISCUSSION

In diabetic cardiomyopathy, the mechanisms that regulate intracellular Ca^{2+} handling are altered and the function of

RyR2 is clearly compromised; the latter has been associated with a decrease in RyR2 protein expression and reduced SR Ca^{2+} load (Pereira et al., 2014); however, the data concerning the contribution of RyRs to the Ca^{2+} mishandling in MetS cardiomyocytes has, until now, been lacking.

Thus, the main aim of this study was to more closely examine the *in situ* activity, protein expression, Ca^{2+} sensitivity, and phosphorylation status of the RyR2 in an animal model of MetS. Sucrose administration (30% in drinking water) for 24 weeks successfully generated key features of MetS in rats, characterized by the presence of central obesity, hypertension, hypertriglyceridemia, and increased TG/HDL-C ratio (**Table 1**). Previous reports in experimental models of MetS at early stages of development induced by administration of either fructose or sucrose in the diet have shown differential development of hypertriglyceridemia, hypertension, and increased abdominal fat accumulation, though not necessarily an increase in body weight (Hintz and Ren, 2002; Davidoff et al., 2004; Schwanke et al., 2006; Balderas-Villalobos et al., 2013; Sommese et al., 2016). Under our experimental conditions, the sucrose-fed rats showed a phenotype closely related with MetS patients, in whom a significant increase in blood presure, TG/HDL-C ratio, body weight, and visceral fat accumulation are considered key cardiovascular risk factors (Wilson et al., 2005). In our MetS model, several hallmark metabolic disturbances are strongly established, leading to a condition that more closely resembles chronic prediabetic state in obese humans. We believe that the differences in our model respect to others are mainly attributable to the prolonged administration of sucrose (e.g., 6 months rather than only 4).

Our results demonstrate the detrimental effect of a high carbohydrate diet on the metabolic condition—and specifically in cardiomyocyte performance, which agrees well with previous publications (Cárdenas et al., 2006; Balderas-Villalobos et al., 2013; Okatan et al., 2016).

Alterations in heart contractile activity have been previously reported in sucrose-fed rats; intracellular Ca^{2+} mishandling was proposed as the underlying mechanism (Carvajal and Baños, 2002; Vasanji et al., 2006; Okatan et al., 2016). Indeed, we consistently found a significant reduction in the Ca^{2+} transient amplitude of MetS cardiomyocytes (**Figure 1B**); our data agreed with previous reports (Hintz et al., 2003; Balderas-Villalobos et al., 2013; Okatan et al., 2016). Contrary to what might have been expected, we found no rate-dependent increase in the Ca^{2+} transient peak as previously reported (Bassani et al., 1995). The reason for this discrepancy is not apparent to us. Possible factors influencing this discrepancy are the different age and strain of our rats vs., the ones used by Bassani and cols. With regard to contraction, in the case of rodents (like rats and mice) the force-frequency relationship (FFR) is even or negative at very low *ex vivo* frequencies (Janssen and Periasamy, 2007). In our hands, the contraction-frequency relationship showed a pronounced drop in MetS cells while remaining unchanged in controls (**Figure 1C**). Of note, there is a dissociation between the important decrease in the amplitude of Ca^{2+} transients with increasing frequency and the less important or even lack of decrease in the amount of shortening. This dissociation may reveal an increase in Ca^{2+} myofilament sensitivity with increasing stimulation frequency, which appears as more important in control than in MetS cells. A frequency-dependent 'sensitization' of the myofilaments has been previously suggested (see for instance Gao et al., 1998). In addition, a possible explanation for the impairment of cell contractility in MetS cells might be related to the finding that in male *Wistar* rats under high-sucrose diet, both myosin and actomyosin Ca^{2+}-ATPase are downregulated in the heart (Pierce et al., 1989); this should be addressed in the future.

In light of the fact that *k* SERCA was reduced in MetS cardiomyocytes, the observation that the Ca^{2+} transient decay time was not considerably augmented might seem surprising. However, it should be pointed out that additional Ca^{2+} clearing mechanisms are involved in the Ca^{2+} transient decline (i.e., Ca^{2+} extrusion by the NCX, cytoplasmic Ca^{2+}-buffering proteins, dynamic RyR open time, etc.). Some of these are excluded when *k* SERCA is calculated as reported by Bode et al. (2011), unveiling a depressed SERCA function in MetS cells.

Because local, spontaneous Ca^{2+} release events (Ca^{2+} sparks) constitute the building blocks of Ca^{2+} transients (Cheng and Lederer, 2008), we studied the Ca^{2+} spark properties in MetS and control cells. Our results revealed a significant decrease in Ca^{2+} spark frequency and amplitude, reducing the diastolic Ca^{2+} leak in MetS cells (**Figure 2**); this suggests reduced RyR recruitment or activation (Hoang-Trong et al., 2015). Sucrose-fed rat hearts have a marked diminution of ATP and phosphocreatine content and creatine kinase activity (Carvajal et al., 2003). Because diastolic Ca^{2+} leak is energetically costly, the finding of a significant reduction of this parameter in MetS cardiomyocytes is not surprising, though it is in disagreement with other reports in insulin-resistant rats (Okatan et al., 2016; Sommese et al., 2016). However, when the heart is energetically compromised as in MetS condition, increasing the diastolic Ca^{2+} leak may add additional complications to already established energetic issues; thus, we propose that reducing the amount of Ca^{2+} leakage during diastole could be rather beneficial at rest, but may compromise heart function under high demand (i.e., β-adrenergic stimulus, stress, or exhausting exercise). Although an augmentation in diastolic $[Ca^{2+}]_i$ might participate in the impairment of the relaxation speed in MetS cells, previous reports in related insulin resistant models showed no changes in basal Ca^{2+} in cardiac cells (Dutta et al., 2001; Hintz et al., 2003), which is consistent with the decreased spark-mediated Ca^{2+} leak observed in our MetS model. However, it should be mentioned that increased diastolic Ca^{2+} levels have been also reported in sucrose- and fructose-fed rats (Okatan et al., 2016; Sommese et al., 2016). Moreover, at this moment we cannot rule out alterations in other forms of diastolic Ca^{2+} leak in MetS cardiomyocytes (Bovo et al., 2011).

In physiological conditions, free $[Ca^{2+}]_{SR}$ influences RyR2 activity by establishing the driving force for SR Ca^{2+} release (Györke and Terentyev, 2008). A reduction in the SR Ca^{2+} content induces a decrease in Ca^{2+} spark frequency (Satoh et al., 1997; Bers et al., 2003; Zima et al., 2010). In light of these findings, we analyzed caffeine-induced Ca^{2+} transients to assess whether the diminished diastolic Ca^{2+} leak observed

in MetS cardiomyocytes was due to changes in SR Ca^{2+} load. Our results showed that MetS development does not modify the SR Ca^{2+} loading in cardiomyocytes, which is in agreement with some reports (Wold et al., 2005; Balderas-Villalobos et al., 2013) but not with others (Okatan et al., 2016; Sommese et al., 2016). The discrepancies are related to differences in the diastolic Ca^{2+} leak, which, in two of the abovementioned reports, was increased and explained the reduction in SR Ca^{2+} load (Okatan et al., 2016; Sommese et al., 2016). SERCA pump is one of the most studied proteins in the context of cardiomyopathies associated with diabetes; in the case of prediabetes, it is generally demonstrated that its activity decreases (Wold et al., 2005; Vasanji et al., 2006; Balderas-Villalobos et al., 2013; Okatan et al., 2016). Independently of the unchanged SR Ca^{2+} load, we corroborated the existence of a dysfunctional SERCA pump in MetS hearts, by the use of direct (SR Ca^{2+} uptake assays) and indirect (by calculating *k* SERCA) approaches (**Figure 3**). One conceivable explanation for the decrease in SERCA pump activity despite unchanged protein expression is that the oxidative stress level could be exacerbated in insulin resistant cardiomyocytes (Dutta et al., 2001; Hintz et al., 2003), this would increase the number of oxidized thiols in the SERCA pump, thereby depressing its activity (Balderas-Villalobos et al., 2013). Another explanation relies on the fact of reported reduced phosphorylation levels of PLN. In this work we found that pThr-17 PLN was significantly reduced, in agreement with one study in sucrose-fed rats reporting decreased phosphorylation of PLN at both Ser-16 and Thr-17, which could account for its reduced activity (Vasanji et al., 2006). On the other hand, SERCA pump activity is highly dependent on energy supply; thus, it is not surprising to find its activity depressed in MetS cardiomyocytes (**Figure 3**).

Neither SR Ca^{2+} load nor RyR2 protein expression was modified in MetS condition; therefore, this parameter cannot explain the depressed *in situ* activity of RyR2 in MetS cardiomyocytes. We performed [^{3}H]-ryanodine binding assays to gain more insight into the molecular modifications of RyR2. Our results revealed that in MetS heart, the maximum number of functional RyRs was significantly reduced, though no significant changes (besides *Bmax* value) in Ca^{2+} dependent RyR activation/inactivation curves were revealed. We therefore examined RyR2 phosphorylation status at Serines 2808 and 2814 (in human and mouse nomenclature). These post-translational modifications, induced by kinases such as PKA and CaMKII, have been defined as a critical regulatory mechanism for this intracellular Ca^{2+} channel (Takasago et al., 1989, 1991; Huke and Bers, 2008; Camors and Valdivia, 2014). In our experimental model of MetS, we found a significant reduction in the phosphorylation level of Ser2814, which no doubt contributed to the impaired functional activity of RyRs in MetS hearts.

A seminal study in a dog model of MetS reported dysfunctional cardiac RyRs, characterized by a decreased capacity for [^{3}H]-Ryanodine binding despite higher levels of Ser2808 phosphorylation compared with control hearts (Dincer et al., 2006). In our MetS model, the phosphorylation of Ser2808 remained unchanged. Perplexing a different study reported diminished phosphorylation of Ser2808 in MetS heart preparations, but did not further explore the impact of this variation in RyR functional activity (Paulino et al., 2010). Finally, additional studies have proposed that the "leaky" RyR2 phenotype in MetS cardiomyocytes is associated with augmented RyR phosphorylation at either Ser-2808 (Okatan et al., 2016) or Ser-2814 (Sommese et al., 2016). The only point where most publications—including ours— agree is about the fact that RyR2 protein expression remains unmodified in MetS models (Dincer et al., 2006; Paulino et al., 2010; Okatan et al., 2016; Sommese et al., 2016).

We are aware of the controversial role of Ser2808 phosphorylation in the abnormal activity of RyR2 in the setting of HF. The unsolved controversy is supported by a considerable amount of data that is primarily in favor of phasing out the importance of Ser2808 as the key player in HF (Valdivia, 2012); our data from a completely distinct cardiac disease support this idea. A definitive role for RyR2 phosphorylation has not yet been reached (Camors and Valdivia, 2014). Thus it is plausible that, in the case of MetS cardiomyopathy, a RyR2 that is dephosphorylated at a crucial residue (e.g., Ser2814) could be more difficult to activate. Indeed, the work of Dhindwal et al. (2017) supports the latter. This group proposed that phosphorylation causes RyR2 to adopt a protein conformation that requires less energy for the transition to the open state, using a structural basis to explain activating effects of phosphorylation in RyRs. Thus, we propose that in a metabolic condition such as MetS, the RyR is primarily dephosphorylated at Ser2814, thus impairing its physiological activation.

The downregulation of the CaMKII kinase could account for the reduced RyR phosphorylation, particularly at the Ser2814 site (**Figure 5C**). To test the involvement of this kinase, we evaluated the phosphorylation of PLN at Thr-17, which was significantly reduced in MetS heart preparations. However, CaMKII expression was not significantly changed (**Supplementary Figure 2**). It is important to note that CaMKII activity is regulated through several mechanisms. For example, CaMKII is susceptible to several post-translational modifications, including autophosphorylation, oxidation, S-nitrosylation, and O-GlcNAcylation, all of which are capable of sustaining the kinase's activation (Mollova et al., 2015). Thus, we intend to address this issue in future work. Another mechanism that could be responsible for the apparent CaMKII downregulation could relate to disturbances of the CaM-CaMKII interaction due to the altered CaM oxidation state. However, this has not been demonstrated in the cardiac isoform (Robison et al., 2007).

CONCLUSION

Principal findings of this work are that abnormal Ca^{2+} transient amplitude, contractile dysfunction; and impaired relaxation of MetS cardiomyocytes underlies intrinsic dysfunctional RyR2 and SERCA pump. Abnormal activity of RyRs was evidenced by its decreased ability to bind [^{3}H]-ryanodine. Although the MetS condition does not modify RyR2 protein expression, its phosphorylation at Ser2814 is decreased, which impairs its

capacity for activation during ECC. The dysfunctional RyRs, together with a decreased activity of SERCA pump due to decreased Thr17-PLN phosphorylation suggest a downregulation of CaMKII in MetS hearts, though its expression remained unchanged. Dysfunctional RyR2 and SERCA pump participate in the Ca^{2+} mishandling of MetS cardiomyocytes (i.e., reduced Ca^{2+} transient amplitude, and decreased Ca^{2+} spark-mediated Ca^{2+} leak), may account for the poor overall cardiac outcome reported in MetS patients and could be targeted for future therapies.

ETHICS STATEMENT

This study was carried out in accordance with the ethical guidelines of the Mexican Official Norm (NOM-062-ZOO-1999) and the National Institutes of Health Guide for the Care and Use of Laboratory Animals (NIH publication updated in 2011); and was approved by the Institutional Bioethical Committee for Care and Handling of Laboratory Animals at the CINVESTAV-IPN (approved CICUAL Protocol No. 0105-14).

AUTHOR CONTRIBUTIONS

GF-M, TR-G, and TB-L contributed to the generation and characterization of the experimental model of MetS in rats, isolation of cardiomyocytes, confocal imaging of Ca^{2+} sparks, electrically stimulated Ca^{2+} transients, determination of SR Ca^{2+} load; [^{3}H]-ryanodine bindings, Ca^{2+} uptake assays and data analysis. M-MM contributed towards SDS-PAGE, Western Blots, and densitometric analysis. AR contributed towards the experimental design, data analysis, data interpretation, and manuscript preparation.

FUNDING

This work was supported by the Secretaría de Ciencia y Tecnología of México City (SECITI-CDMX, Grant No. 331/2010) by Conacyt CB Grant 80960 to AR; and by a PRODEP-SEP grant to the Academic Group CINVESTAV-CA-10, ID 28915/2018.

ACKNOWLEDGMENTS

We deeply thank Dr. Agustín Guerrero-Hernández (Department of Biochemistry, CINVESTAV-IPN, Mexico) and Dr. José Antonio Arias-Montaño (Department of Physiology, Biophysics and Neurosciences, CINVESTAV-IPN, Mexico) for providing us with the facilities to perform the microsome Ca^{2+} uptake and [^{3}H]-ryanodine binding experiments, respectively. Anti pSer16-PLN, pSer17-PLN, PLN and CaMKII antibodies were a generous gift from Dr. Héctor H. Valdivia (University of Wisconsin-Madison, Madison, WI, United States). We thank Dr. E. Michelle Frank (The Well-Tempered Word LLC) for critical reading of the manuscript. We also wish to acknowledge the technical assistance of Juan Carlos García Torres; and M.Sc. Iván Galván (Microscopy Unit, LANSE-CINVESTAV-IPN). We also thank Roche S. A. de C. V., for the award of Medical Research Dr. Jorge Rosenkranz in Diabetes field, Young category to AR.

SUPPLEMENTARY MATERIAL

The Supplementary Material for this article can be found online at: https://www.frontiersin.org/articles/10.3389/fphys.2019.00520/full#supplementary-material

REFERENCES

Alberti, K. G., Eckel, R. H., Grundy, S. M., Zimmet, P. Z., Cleeman, J. I., Donato, K. A., et al. (2009). Harmonizing the metabolic syndrome: a joint interim statement of the international diabetes federation task force on epidemiology and prevention; national heart, lung, and blood institute; American heart association; world heart federation; international. *Circulation* 120, 1640–1645. doi: 10.1161/CIRCULATIONAHA.109.192644

Balderas-Villalobos, J., Molina-Muñoz, T., Mailloux-Salinas, P., Bravo, G., Carvajal, K., and Gómez-Viquez, N. L. (2013). Oxidative stress in cardiomyocytes contributes to decreased SERCA2a activity in rats with metabolic syndrome. *Am. J. Physiol. Heart Circ. Physiol.* 305, H1344–H1353. doi: 10.1152/ajpheart.00211.2013

Bassani, R. A., Mattiazzi, A., and Bers, D. M. (1995). CaMKII is responsible for activity-dependent acceleration of relaxation in rat ventricular myocytes. *Am. J. Physiol. Circ. Physiol.* 268, H703–H712.

Belke, D. D., Swanson, E. A., and Dillmann, W. H. (2004). Decreased sarcoplasmic reticulum activity and contractility in diabetic db/db mouse heart. *Diabetes* 53, 3201–3208. doi: 10.2337/diabetes.53.12.3201

Bers, D. M. (2014). Cardiac sarcoplasmic reticulum calcium leak: basis and roles in cardiac dysfunction. *Annu. Rev. Physiol.* 76, 107–127. doi: 10.1146/annurev-physiol-020911-153308

Bers, D. M., Eisner, D. A., and Valdivia, H. H. (2003). Sarcoplasmic reticulum Ca2+ and Heart failure: roles of diastolic leak and ca2+ transport. *Circ. Res.* 93, 487–490. doi: 10.1161/01.res.0000091871.54907.6b

Bers, D. M., Patton, C. W., and Nuccitelli, R. (2010). "A practical guide to the preparation of Ca2+ buffers," in *Methods in Cell Biology*, ed. T. Weimbs (Amsterdam: Elsevier), 1–26. doi: 10.1016/b978-0-12-374841-6.00001-3

Biesmans, L., Macquaide, N., Heinzel, F. R., Bito, V., Smith, G. L., Karin, R., et al. (2011). Subcellular heterogeneity of ryanodine receptor properties in ventricular myocytes with low T-tubule density. *PLoS One* 6:e25100. doi: 10.1371/journal.pone.0025100

Bode, E. F., Briston, S. J., Overend, C. L., O'Neill, S. C., Trafford, A. W., and Eisner, D. A. (2011). Changes of SERCA activity have only modest effects on sarcoplasmic reticulum Ca2+ content in rat ventricular myocytes. *J. Physiol.* 589, 4723–4729. doi: 10.1113/jphysiol.2011.211052

Bovo, E., Mazurek, S. R., Blatter, L. A., and Zima, A. V. (2011). Regulation of sarcoplasmic reticulum Ca2+ leak by cytosolic Ca2+ in rabbit ventricular myocytes. *J. Physiol.* 589, 6039–6050. doi: 10.3389/fphys.2012.00351

Camors, E., and Valdivia, H. H. (2014). CaMKII regulation of cardiac ryanodine receptors and inositol triphosphate receptors. *Front. Pharmacol.* 5:101. doi: 10.3389/fphar.2014.00101

Cárdenas, G., Carlos Torres, J., Zamora, J., Pérez, I., and Baños, G. (2006). Isolated heart function after ischemia and reperfusion in sucrose-fed rats: influence of gender and treatment. *Clin. Exp. Hypertens.* 28, 85–107. doi: 10.1080/10641960500468235

Carvajal, K., and Baños, G. (2002). Myocardial function and effect of serum in isolated heart from hypertriglyceridemic and hypertensive rats. *Clin. Exp. Hypertens.* 24, 235–248. doi: 10.1081/ceh-120004228

Carvajal, K., Baños, G., and Moreno-Sánchez, R. (2003). Impairment of glucose metabolism and energy transfer in the rat heart. *Mol. Cell. Biochem.* 249, 157–165. doi: 10.1007/978-1-4419-9236-9_20

Cheng, H., and Lederer, W. J. (2008). Calcium sparks. *Physiol. Rev.* 88, 1491–1545. doi: 10.1152/physrev.00030.2007

Davidoff, A. J., Mason, M. M., Davidson, M. B., Carmody, M. W., Hintz, K. K., Wold, L. E., et al. (2004). Sucrose-induced cardiomyocyte dysfunction is both preventable and reversible with clinically relevant treatments. *Am. J. Physiol. Endocrinol. Metab.* 286, E718–E724.

de Alba-Aguayo, D. R., Pavón, N., Mercado-Morales, M., Miranda-Saturnino, M., López-Casamichana, M., Guerrero-Hernández, A., et al. (2017). Increased calcium leak associated with reduced calsequestrin expression in hyperthyroid cardiomyocytes. *Cell Calcium* 62, 29–40. doi: 10.1016/j.ceca.2017.01.009

Delgado, C., Ruiz-Hurtado, G., Gómez-Hurtado, N., González-Ramos, S., Rueda, A., Benito, G., et al. (2015). NOD1, a new player in cardiac function and calcium handling. *Cardiovasc. Res.* 106, 375–386. doi: 10.1093/cvr/cvv118

Dhindwal, S., Lobo, J., Cabra, V., Santiago, D. J., Nayak, A. R., Dryden, K., et al. (2017). A cryo-EM-based model of phosphorylation- and FKBP12.6-mediated allosterism of the cardiac ryanodine receptor. *Sci. Signal.* 10, eaai8842. doi: 10.1126/scisignal.aai8842

Dincer, U. D. (2012). Cardiac ryanodine receptor in metabolic syndrome: is JTV519 (K201) future therapy? *Diabetes. Metab. Syndr. Obes.* 5, 89–99. doi: 10.2147/DMSO.S30005

Dincer, U. D., Araiza, A., Knudson, J. D., Shao, C. H., Bidasee, K. R., and Tune, J. D. (2006). Dysfunction of cardiac ryanodine receptors in the metabolic syndrome. *J. Mol. Cell. Cardiol.* 41, 108–114. doi: 10.1016/j.yjmcc.2006.04.018

Dutta, K., Podolin, D. A., Davidson, M. B., and Davidoff, A. J. (2001). Cardiomyocyte dysfunction in sucrose-fed rats is associated with insulin resistance. *Diabetes* 50, 1186–1192. doi: 10.2337/diabetes.50.5.1186

Fabiato, A. (1983). Calcium-induced release of calcium from the cardiac sarcoplasmic reticulum. *Am. J. Physiol.* 245, C1–C14.

Fernández-Velasco, M., Rueda, A., Rizzi, N., Benitah, J.-P., Colombi, B., Napolitano, C., et al. (2009). Increased Ca2+ sensitivity of the ryanodine receptor mutant RyR2R4496C underlies catecholaminergic polymorphic ventricular tachycardia. *Circ. Res.* 104, 201–209. doi: 10.1161/CIRCRESAHA.108.177493

Gao, W. D., Perez, N. G., and Marban, E. (1998). Calcium cycling and contractile activation in intact mouse cardiac muscle. *J. Physiol.* 507(Pt 1), 175–184. doi: 10.1111/j.1469-7793.1998.175bu.x

Grynkiewicz, G., Poenie, M., and Tsien, R. Y. (1985). A new generation of Ca2+ indicators with greatly improved fluorescence properties. *J. Biol. Chem.* 260, 3440–3450.

Györke, S., and Terentyev, D. (2008). Modulation of ryanodine receptor by luminal calcium and accessory proteins in health and cardiac disease. *Cardiovasc. Res.* 77, 245–255. doi: 10.1093/cvr/cvm038

Hintz, K. K., Aberle, N. S., and Ren, J. (2003). Insulin resistance induces hyperleptinemia, cardiac contractile dysfunction but not cardiac leptin resistance in ventricular myocytes. *Int. J. Obes.* 27, 1196–1203. doi: 10.1038/sj.ijo.0802389

Hintz, K. K., and Ren, J. (2002). Prediabetic insulin resistance is not permissive to the development of cardiac resistance to insulin-like growth factor I in ventricular myocytes. *Diabetes Res. Clin. Pract.* 55, 89–98. doi: 10.1016/s0168-8227(01)00323-0

Hoang-Trong, T. M., Ullah, A., and Jafri, M. S. (2015). Calcium sparks in the heart: dynamics and regulation. *Res. Rep. Biol.* 6:203. doi: 10.2147/rrb.s61495

Huke, S., and Bers, D. M. (2008). Ryanodine receptor phosphorylation at Serine 2030, 2808 and 2814 in rat cardiomyocytes. *Biochem. Biophys. Res. Commun.* 376, 80–85. doi: 10.1016/j.bbrc.2008.08.084

Janssen, P. M. L., and Periasamy, M. (2007). Determinants of frequency-dependent contraction and relaxation of mammalian myocardium. *J. Mol. Cell. Cardiol.* 43, 523–531. doi: 10.1016/j.yjmcc.2007.08.012

Liu, W., Pasek, D. A., and Meissner, G. (1998). Modulation of Ca2 + -gated cardiac muscle Ca2 + -release channel (ryanodine receptor) by mono- and divalent ions. *Am. J. Physiol.* 274, C120–C128.

Mattiazzi, A., and Kranias, E. G. (2014). The role of CaMKII regulation of phospholamban activity in heart disease. *Front. Pharmacol.* 5:5. doi: 10.3389/fphar.2014.00005

Mollova, M. Y., Katus, H. A., and Backs, J. (2015). Regulation of CaMKII signaling in cardiovascular disease. *Front. Pharmacol.* 6:178. doi: 10.3389/fphar.2015.00178

Mottillo, S., Filion, K. B., Genest, J., Joseph, L., Pilote, L., Poirier, P., et al. (2010). The metabolic syndrome and cardiovascular risk: a systematic review and meta-analysis. *J. Am. Coll. Cardiol.* 56, 1113–1132. doi: 10.1016/j.jacc.2010.05.034

Nolan, P. B., Carrick-Ranson, G., Stinear, J. W., Reading, S. A., and Dalleck, L. C. (2017). Prevalence of metabolic syndrome and metabolic syndrome components in young adults: a pooled analysis. *Prev. Med. Rep.* 7, 211–215. doi: 10.1016/j.pmedr.2017.07.004

Okatan, E. N., Durak, A. T., and Turan, B. (2016). Electrophysiological basis of metabolic-syndrome-induced cardiac dysfunction. *Can. J. Physiol. Pharmacol.* 94, 1064–1073. doi: 10.1139/cjpp-2015-0531

Paulino, E. C., Ferreira, J. C. B., Bechara, L. R., Tsutsui, J. M., Mathias, W., Lima, F. B., et al. (2010). Exercise training and caloric restriction prevent reduction in cardiac Ca2+-handling protein profile in obese rats. *Hypertension* 56, 629–635. doi: 10.1161/HYPERTENSIONAHA.110.156141

Pereira, L., Matthes, J., Schuster, I., Valdivia, H. H., Herzig, S., Richard, S., et al. (2006). Mechanisms of [Ca2+]i transient decrease in cardiomyopathy of db/db type 2 diabetic mice. *Diabetes* 55, 608–615. doi: 10.2337/diabetes.55.03.06.db05-1284

Pereira, L., Ruiz-Hurtado, G., Rueda, A., Mercadier, J.-J., Benitah, J.-P., and Gómez, A. M. (2014). Calcium signaling in diabetic cardiomyocytes. *Cell Calcium* 56, 372–380. doi: 10.1016/j.ceca.2014.08.004

Perez-Torres, I., Roque, P., El Hafidi, M., Díaz-Díaz, E., Baños, G., Hafidi, M. E. L., et al. (2009). Association of renal damage and oxidative stress in a rat model of metabolic syndrome. Influence of gender. *Free Radic. Res.* 43, 761–771. doi: 10.1080/10715760903045296

Pierce, G. N., Lockwood, M. K., and Eckhert, C. D. (1989). Cardiac contracile protein ATPase activity in a diet induced model of noninsulin dependent diabetes mellitus. *Can. J. Cardiol.* 5, 117–120.

Qiao, Q., Gao, W., Zhang, L., Nyamdorj, R., and Tuomilehto, J. (2007). Metabolic syndrome and cardiovascular disease. *Ann. Clin. Biochem.* 44, 232–263.

Robison, A. J., Winder, D. G., Colbran, R. J., and Bartlett, R. K. (2007). Oxidation of calmodulin alters activation and regulation of CaMKII. *Biochem. Biophys. Res. Commun.* 356, 97–101. doi: 10.1016/j.bbrc.2007.02.087

Salazar, M. R., Carbajal, H. A., Espeche, W. G., Aizpurúa, M., Leiva Sisnieguez, C. E., Leiva Sisnieguez, B. C., et al. (2014). Use of the plasma triglyceride/high-density lipoprotein cholesterol ratio to identify cardiovascular disease in hypertensive subjects. *J. Am. Soc. Hypertens.* 8, 724–731. doi: 10.1016/j.jash.2014.08.002

Satoh, H., Blatter, L. A., and Bers, D. M. (1997). Effects of [Ca2+]i, SR Ca2+ load, and rest on Ca2+ spark frequency in ventricular myocytes. *Am. J. Physiol. Circ. Physiol.* 272, H657–H668.

Schwanke, M. L., Dutta, K., Podolin, D. A., and Davidoff, A. J. (2006). Cardiomyocyte dysfunction in insulin-resistant rats: a female advantage. *Diabetologia* 49, 1097–1105. doi: 10.1007/s00125-006-0184-9

Sommese, L., Valverde, C. A., Blanco, P., Castro, M. C., Rueda, O. V., Kaetzel, M., et al. (2016). Ryanodine receptor phosphorylation by CaMKII promotes spontaneous Ca2+ release events in a rodent model of early stage diabetes: the arrhythmogenic substrate. *Int. J. Cardiol.* 202, 394–406. doi: 10.1016/j.ijcard.2015.09.022

Spurgeon, H. A., duBell, W. H., Stern, M. D., Sollott, S. J., Ziman, B. D., Silverman, H. S., et al. (1992). Cytosolic calcium and myofilaments in single rat cardiac myocytes achieve a dynamic equilibrium during twitch relaxation. *J. Physiol.* 447, 83–102. doi: 10.1113/jphysiol.1992.sp018992

Sung, J., Choi, Y.-H., and Park, J. B. (2006). Metabolic syndrome is associated with delayed heart rate recovery after exercise. *J. Korean Med. Sci.* 21:621. doi: 10.3346/jkms.2006.21.4.621

Takasago, T., Imagawa, T., Furukawa, K., Ogurusu, T., and Shigekawa, M. (1991). Regulation of the cardiac ryanodine receptor by protein kinase-dependent phosphorylation. *J. Biochem.* 109, 163–170. doi: 10.1093/oxfordjournals.jbchem.a123339

Takasago, T., Imagawa, T., and Shigekawa, M. (1989). Phosphorylation of the cardiac ryanodine receptor by cAMP-dependent protein kinase. *J. Biochem.* 106, 872–877. doi: 10.1093/oxfordjournals.jbchem.a122945

Tune, J. D., Goodwill, A. G., Sassoon, D. J., and Mather, K. J. (2017). Cardiovascular consequences of metabolic syndrome. *Transl. Res.* 183, 57–70. doi: 10.1016/j.trsl.2017.01.001

Valdivia, H. H. (2012). Ryanodine receptor phosphorylation and heart failure: phasing out S2808 and "criminalizing" S2814. *Circ. Res.* 110, 1398–1402. doi: 10.1161/circresaha.112.270876

Vasanji, Z., Cantor, E. J. F., Juric, D., Moyen, M., and Netticadan, T. (2006). Alterations in cardiac contractile performance and sarcoplasmic reticulum function in sucrose-fed rats is associated with insulin resistance. *Am. J. Physiol.* 291, 772–780.

Wilson, P. W. F., D'Agostino, R. B., Parise, H., Sullivan, L., and Meigs, J. B. (2005). Metabolic syndrome as a precursor of cardiovascular disease and type 2 diabetes mellitus. *Circulation* 112, 3066–3072. doi: 10.1161/circulationaha.105.539528

Wold, L. E., Dutta, K., Mason, M. M., Ren, J., Cala, S. E., Schwanke, M. L., et al. (2005). Impaired SERCA function contributes to cardiomyocyte dysfunction in insulin resistant rats. *J. Mol. Cell. Cardiol.* 39, 297–307. doi: 10.1016/j.yjmcc.2005.03.014

Wong, S. K., Chin, K.-Y., Suhaimi, F. H., Fairus, A., and Ima-Nirwana, S. (2016). Animal models of metabolic syndrome: a review. *Nutr. Metab.* 13:65.

Zima, A. V., Bovo, E., Bers, D. M., and Blatter, L. A. (2010). Ca2+ spark-dependent and -independent sarcoplasmic reticulum Ca2+ leak in normal and failing rabbit ventricular myocytes. *J. Physiol.* 588, 4743–4757. doi: 10.1113/jphysiol.2010.197913

Conflict of Interest Statement: The authors declare that the research was conducted in the absence of any commercial or financial relationships that could be construed as a potential conflict of interest.

frontiers in Physiology

ORIGINAL RESEARCH
published: 03 July 2019
doi: 10.3389/fphys.2019.00773

Transmural Autonomic Regulation of Cardiac Contractility at the Intact Heart Level

Yuriana Aguilar-Sanchez[1], Ainhoa Rodriguez de Yurre[2], Mariana Argenziano[3], Ariel L. Escobar[4] and Josefina Ramos-Franco[1]**

[1] Department of Physiology and Biophysics, School of Medicine, Rush University Medical Center, Chicago, IL, United States, [2] Laboratorio de Cardio Inmunologia, Instituto de Biofisica Carlos Chagas Filho, Rio de Janeiro, Brazil, [3] Division of Human Genetics, Children's Hospital of Philadelphia, Philadelphia, PA, United States, [4] Department of Bioengineering, School of Engineering, University of California, Merced, Merced, CA, United States

The relationship between cardiac excitability and contractility depends on when Ca^{2+} influx occurs during the ventricular action potential (AP). In mammals, it is accepted that Ca^{2+} influx through the L-type Ca^{2+} channels occurs during AP phase 2. However, in murine models, experimental evidence shows Ca^{2+} influx takes place during phase 1. Interestingly, Ca^{2+} influx that activates contraction is highly regulated by the autonomic nervous system. Indeed, autonomic regulation exerts multiple effects on Ca^{2+} handling and cardiac electrophysiology. In this paper, we explore autonomic regulation in endocardial and epicardial layers of intact beating mice hearts to evaluate their role on cardiac excitability and contractility. We hypothesize that in mouse cardiac ventricles the influx of Ca^{2+} that triggers excitation–contraction coupling (ECC) does not occur during phase 2. Using pulsed local field fluorescence microscopy and loose patch photolysis, we show sympathetic stimulation by isoproterenol increased the amplitude of Ca^{2+} transients in both layers. This increase in contractility was driven by an increase in amplitude and duration of the L-type Ca^{2+} current during phase 1. Interestingly, the β-adrenergic increase of Ca^{2+} influx slowed the repolarization of phase 1, suggesting a competition between Ca^{2+} and K^+ currents during this phase. In addition, cAMP activated L-type Ca^{2+} currents before SR Ca^{2+} release activated the Na^+-Ca^{2+} exchanger currents, indicating $Ca_V1.2$ channels are the initial target of PKA phosphorylation. In contrast, parasympathetic stimulation by carbachol did not have a substantial effect on amplitude and kinetics of endocardial and epicardial Ca^{2+} transients. However, carbachol transiently decreased the duration of the AP late phase 2 repolarization. The carbachol-induced shortening of phase 2 did not have a considerable effect on ventricular pressure and systolic Ca^{2+} dynamics. Interestingly, blockade of muscarinic receptors by atropine prolonged the duration of phase 2 indicating that, in isolated hearts, there is an intrinsic release of acetylcholine. In addition, the acceleration of repolarization induced by carbachol was blocked by the acetylcholine-mediated K^+ current inhibition. Our results reveal the transmural ramifications of autonomic regulation in intact mice hearts and support our hypothesis that Ca^{2+} influx that triggers ECC occurs in AP phase 1 and not in phase 2.

Keywords: mouse ventricle, endocardium, epicardium, adrenergic, cholinergic, whole heart

OPEN ACCESS

Edited by:
Angélica Rueda, Centro de Investigación y de Estudios Avanzados (CINVESTAV), Mexico

Reviewed by:
Nieves Gómez-Hurtado, Autonomous University of Madrid, Spain
Roberto R. M., University of Michigan, United States

****Correspondence:***
Ariel L. Escobar
aescobar4@ucmerced.edu
Josefina Ramos-Franco
jrfranco@rush.edu

Specialty section:
This article was submitted to Integrative Physiology, a section of the journal Frontiers in Physiology

Received: *10 January 2019*
Accepted: *03 June 2019*
Published: *03 July 2019*

Citation:
Aguilar-Sanchez Y, Rodriguez de Yurre A, Argenziano M, Escobar AL and Ramos-Franco J (2019) Transmural Autonomic Regulation of Cardiac Contractility at the Intact Heart Level. Front. Physiol. 10:773. doi: 10.3389/fphys.2019.00773

INTRODUCTION

Cardiac excitability and contractility are tightly controlled by the autonomic nervous system (ANS) (Lee and Shideman, 1959; Katz, 1967; Lindemann and Watanabe, 1985; Cohn, 1989; Henning, 1992). The ANS comprises two antagonistic branches, the sympathetic and parasympathetic nervous systems. The sympathetic nervous system modulates the cardiac function through the local release of norepinephrine and systemic action of epinephrine that alter both, Ca^{2+}dynamics (Lee and Shideman, 1959; Evans, 1986; Marks, 2013) and electrical activity of myocardial cells. At the cellular level, these catecholamines bind to β-adrenergic receptors (β-ARs) leading to the activation of adenylyl cyclase (AC) (Hildebrandt et al., 1983; Brum et al., 1984), through a G_s protein mechanism, to increase cAMP levels (Osterrieder et al., 1982). The cAMP activates PKA (Krebs, 1972; Hayes and Mayer, 1981), inducing the dissociation of the catalytic subunit to subsequently phosphorylate several key Ca^{2+} handling proteins. Some of these key proteins include the L-type Ca^{2+} channel (Collins et al., 1981; Osterrieder et al., 1982), ryanodine receptor (RyR2) (Suko et al., 1993; Valdivia et al., 1995) and phospholamban (PLN) (Mundiña de Weilenmann et al., 1987), a protein that inhibits the sarcoplasmic reticulum Ca^{2+} ATPase (SERCA).

The other branch, the parasympathetic nervous system, acts through the release of acetylcholine (ACh) from postganglionic cholinergic intracardiac neurons. The locally released ACh binds to muscarinic (M2) receptors which in turn inhibit AC through a G_i protein (Krebs, 1972). The AC inhibition favors low levels of cAMP, reducing the fraction of the activated PKA. The reduction of activated PKA will decrease the degree of phosphorylation of Ca^{2+} handling proteins. In atria, SA and AV nodes, the G_i protein-βγ subunits interact with an inward rectifying K^+ channel increasing its open probability to produce an outward hyperpolarizing K^+ current (I_{KACh}) (Breitwieser and Szabo, 1988; Clapham and Kim, 1989; Kurachi et al., 1989; Wickman et al., 1999). Although the role of I_{KACh} in regulating the electrical properties of atria, SA and AV nodes have been extensively studied, the role of I_{KACh} during ventricular excitability is still obscure (Hiltunen et al., 2000; Rysevaite et al., 2011).

The influx of Ca^{2+} in ventricular myocytes is driven by the activation of L-type Ca^{2+} channels during an AP depolarization. In large mammals including humans, the prolongation of the AP plateau phase (phase 2) increases the time L-type Ca^{2+} channels are open leading to a sustained influx of Ca^{2+} into the myocyte. Small mammals like mice have a high metabolic demand. Thus, the heart needs to beat at higher rates to handle their metabolic needs. To cope with a higher heart rate, the mouse heart has developed a short duration ventricular AP. These characteristic kinetics promoted the idea that mouse ventricular AP lacks a plateau phase (phase 2) (Nerbonne and Kass, 2005; Dilly et al., 2006). Recently, our group presented experimental evidence showing that *in situ* mouse ventricular APs display a well-defined phase 2 (Ferreiro et al., 2012; Ramos-Franco et al., 2016). Interestingly, mouse AP phase 2 was more hyperpolarized than in large mammals (Kornyeyev et al., 2010; Valverde et al., 2010; Ferreiro et al., 2012) and it was driven by an influx of Na^+ through the Na^+-Ca^{2+} exchanger (NCX) (Ramos-Franco et al., 2016). However, up to now, it has not been possible to rule out the effect of AP phase 2 kinetics on intracellular Ca^{2+} dynamics in mouse hearts.

As sympathetic and parasympathetic drives impact the kinetics of both phase 1 and phase 2 (Litovsky and Antzelevitch, 1990) mimicking these autonomic regulations could be a physiological way to assess the role of these AP phases on cardiac contractility across the ventricular wall. Consequently, our goal is to test the hypothesis that in mouse cardiac ventricles the influx of Ca^{2+} that triggers excitation–contraction coupling (ECC) does not occur during phase 2. Our results reveal for the first time the transmural effects of autonomic regulation in intact mice hearts and confirm our previous observation that Ca^{2+} influx that triggers ECC occurs in the AP phase 1 and not in phase 2.

MATERIALS AND METHODS

Heart Preparation

Experiments were conducted on 8-week-old, male Balb/c mice (Charles River Labs, Wilmington, MA, United States). Mice were maintained in accordance to the National Institutes of Health Guide for the Care and Use of Laboratory Animals (NIH Publication No. 85–23, Revised 1996) and the Institutional Animal Care and Use Committee guidelines of the University of California, Merced (Protocol # 2008–201). Mice were injected intraperitoneally with sodium heparin 15 min before euthanasia. Hearts were extracted by thoracotomy and perfused in a Langendorff apparatus with tyrode solution containing (in mM): 140 NaCl, 5.4 KCl, 2 $CaCl_2$, 1 $MgCl_2$, 0.33 $NaPO_4H_2$, 10 HEPES, and 10 glucose, pH 7.4 and equilibrated with 100% O_2. Experiments were conducted at physiological temperatures of 35–37°C using a Peltier unit. The myosin ATPase inhibitor, blebbistatin (10 μM) was added to the tyrode solution to inhibit the heart's mechanical activity. Blebbistatin was continuously perfused throughout the whole duration of the experiment to avoid introducing movement artifacts, breaking the glass electrode and photolability. All salts and drugs were obtained from Sigma (St. Louis, MO, United States). Tertiapin was purchased from Tocris (Minneapolis, MN, United States).

Pressure Recordings

A new experimental approach, the micro-hemodynamic analyzer, was developed to measure left ventricular pressure in the whole intact heart (López Alarcón et al., 2019). A common device used to obtain this measurement consists of a small latex or plastic balloon coupled to a cannula that is introduced through the mitral valve. Usually, this balloon-cannula device is sutured to the atrial tissue and may cause damage. To avoid this problem, we introduced a tiny vitrectomy ophthalmic-valved trocar (Alcon, Fort Worth, TX, United States) in the apex of the left ventricle. The ventricular tissue, itself, provided a tight seal around the trocar avoiding any kind of leak from the left ventricular chamber. A 23-gage coupling valve was connected to the trocar, and the pressure at the outlet of the valve was measured with a solid-state integrated differential pressure

transducer (Honeywell, Morris Plains, NJ, United States). The pressure transducer has an expanded dynamic range and can linearly measure pressures up to 200 mmHg. All the pressure measurements were performed under isotonic constant load conditions.

Pulsed Local Field Fluorescence Microscopy

The pulsed local field fluorescence microscopy (PLFFM) technique has been previously used by our group (Mejía-Alvarez et al., 2003; Valverde et al., 2010; Ferreiro et al., 2012; Kornyeyev et al., 2012; Aguilar-Sanchez et al., 2017). Briefly, the PLFFM technique is capable of assessing physiological parameters by exciting exogenous probes present in the tissue and detecting the light emitted by these fluorescent indicators. The excitation (532 nm Yag laser) and emitted light propagate through a multimode fiber optic (200 μm diameter, 0.67 NA) placed on the surface of the intact heart. The emitted light then travels back through the multimode fiber, dichroic mirrors, and filters (610 nm) and is focused on an avalanche photodiode (Perkin Elmer, Waltham, MA, United States) with the aid of a microscope objective. The signal is digitized by an A/D converter (National Instruments) and acquired by a PC. Here, the PLFFM technique was modified to perform a comparative study, between endocardium and epicardium at the intact heart. We included a beam splitter which allowed us to use two fiber optics. This experimental arrangement facilitated the simultaneous recording of fluorescence from two distinct anatomical regions of the heart. For endocardial measurements, a small incision was made on the surface of the ventricular wall to gain access to the endocardial layer as previously described (Aguilar-Sanchez et al., 2017). Rhod-2 AM and Di-8-ANEPPS (Thermo Fisher Scientific, Waltham, MA, United States) were used to record intracellular Ca^{2+} transients and membrane potential, respectively. Rhod-2 AM and Di-8-ANEPPS were prepared with 20% Pluronic (Biotium, Hayward, CA, United States) in tyrode solution as previously described (Ferreiro et al., 2012; Aguilar-Sanchez et al., 2017). All dyes were sonicated for 20 min and then recirculated into the heart for 30 min at room temperature using peristaltic pumps.

Electrical Recordings

Epicardial electrical recordings of the action potentials (APs) were obtained by means of sharp glass microelectrodes filled with 3M KCl that were connected to a high input impedance differential amplifier (WPI, Sarasota, FL, United States). Glass microelectrodes were fabricated with a micropipette puller (Flaming/Brown Micropipette Puller, Sutter Instrument Co., CA, United States) and had a resistance of 10–20 MΩ. All the AP recordings were performed in hearts that were externally paced at 6–7 Hz.

Loose-Patch Photolysis

Our developed LPP technique was used to measure membrane currents during a triggered AP, at the intact heart level (Ramos-Franco et al., 2016). LPP combines three major elements: loose patch recordings, local field optical measurements, and a fiber optic laser-driven flash photolysis. The loose patch was performed using macro patch pipettes with a tip diameter of 250 μm. A fiber optic (200 μm) was placed in the interior to photolyze different drugs locally. This fiber delivered UV pulses to break photosensitive compounds on the membrane patch surface, making it possible to record the immediately resulting currents from 25 to 50 myocytes. Using this procedure, we were able to record membrane currents (capacitive and ionic) during an externally triggered AP before and after a UV flash. To dissect the UV-induced current, these sequential recordings were subtracted using pCLAMP. As we previously reported (Ramos-Franco et al., 2016), the capacitive current was not modified before and after the flash due to the electrotone imposed by the surrounding tissue on the small 200 μm UV flash site. Thus, the only current changing was the ionic current. We used the UV-sensitive compound, nifedipine (10 μM), such that the resulting currents were Ca^{2+}-driven. The LPP was used to measure any changes in the Ca^{2+}-driven currents in the epicardium under either continuous β-adrenergic or cholinergic stimulation. In addition, for transient β-adrenergic stimulation, we used the UV-sensitive caged cAMP (4,5-dimethoxy-2-nitrobenzyl adenosine 3′,5′-cyclic monophosphate).

RNA Analysis

Hearts were perfused with RNAlater (Qiagen) to inhibit the RNAses. Then, left ventricular square pieces of 4 × 4 mm were included in agarose to facilitate slicing. Specimens were sliced in 200 μm sections using a vibratome (Leica VT1000S). For RNA extraction, individual slices were placed in a 1.5 mL Eppendorf containing 0.5 mL of Trizol reagent. Tissue was homogenized with an ultrasonic cell disruptor. The homogenate was incubated for 5 min at room temperature and 0.2 mL of chloroform per mL of Trizol was added. After 2–3 min of incubation, the sample was centrifuged at 12,000 × *g* 15 min 4°C. The clear phase was transferred to a new tube and 500 μL of isopropanol per mL of Trizol was added and centrifuged at 12,000 × g for 10 min at 4°C. The supernatant was removed and 1 mL of 75% ethanol per mL of Trizol was added and centrifuged at 7,500 × *g* for 5 min at 4°C. The dried pellet was dissolved in 30 μL of RNAse free water. For real time PCR, RNA was quantified (NanoDrop 1000 Spectrophotometer) and 2 μg was used for the reverse transcription reaction. The 2 μg of RNA was mixed with 1 μL of random primers (200 ng/μL) and water up to 12.5 μL. 7.5 μL of a MIX solution containing 4 μL of reaction buffer, 0.5 μL of RNAse free water, 2 μL dNTPs mix and 1 μL of RevertAid was added before the thermocycle cycles began. cDNA samples were diluted with water, 6.25 μL of Mix (FastStart Roche), 0.37 μL of forward primers, and 0.37 μL of reverse primers (see **Supplementary Table 1**). The reaction samples were placed in a 96-well plate and real time qPCR cycles were started. Finally, mRNA levels were normalized to GAPDH mRNA and analyzed by the Pfaffl method.

Statistical Analysis

It is important to mention that in whole heart experiments there are two main sources of variance. First, the hearts are not identical between each other and second, although we are

measuring Ca^{2+} transients and APs in the same region (the mid region of the left ventricle), it is impossible to perform the recordings in the same precise location between different hearts. Thus, the data is presented as the measured times with their standard error (SEM) in Tables and then as percentage change in Graphs, where data was normalized to the control values. To assess electrical changes, AP traces were evaluated at certain repolarization times. Specifically, the time it takes for the AP to reach 30%, half of phase 2, or 90% repolarization was assessed and referred to as APD30, APD half phase 2, or APD90, respectively. To evaluate the kinetics of the recorded Ca^{2+} transients, these were normalized between zero (minimum fluorescence) and one (maximum fluorescence). The kinetics parameters of the Ca^{2+} transients evaluated were the rise time (time for the transient to rise between 10% and 90%), time-to-peak (time for the transient to reach a maximum amplitude), half duration (time for half of the Ca^{2+} transient to be complete), and fall time (time taken for the transient to fall between 10% and 90% of the relaxation). Each recorded parameter for AP and Ca^{2+} transient kinetics, control and non-control experiments, were evaluated and normalized to the control values for each heart used. After this normalization, data was compiled and statistical analysis was performed. Data is presented as multiple measurements (n; dot cloud) recorded on different hearts (N) with the mean ± SEM (solid lines). The statistical significance was tested using a two-sample Kolmogorov–Smirnov test (OriginPro 2019). The difference was considered to be significant if the p-value was <0.01.

RESULTS

In the heart, both excitability and contractility are tightly controlled by the ANS. Although there is substantial information about sympathetic and parasympathetic regulation of the electrical and mechanical function, it is not clear how autonomically driven changes in the AP kinetics impact contractility in the mouse heart, which is often used as a model system.

In a beating heart, the classical way to assess the degree of autonomic regulation is to evaluate the developed pressure during the cardiac cycle. Using intact perfused mouse hearts, we measured the effect of catecholamines in the developed pressure during the cardiac cycle. **Figure 1** illustrates the time course of the developed pressure using the micro-hemodynamic analyzer (μHA) (López Alarcón et al., 2019). As was described in the "Materials and Methods" section, this newly developed method does not use an intraventricular balloon. Specifically, an ophthalmic-valved trocar was introduced through the apex of the left ventricle to gain access to the intra chamber pressure. The pressure at the outlet of the electro-valve was then measured with a solid-state integrated pressure transducer. This method permits an easy access to the ventricular chamber with no need of a more intrusive intraventricular balloon. **Figure 1A** illustrates how a sympathetic drive can increase the developed pressure in Langendorff perfused hearts. Indeed, when the hearts were coronary retro-perfused with 500 nM isoproterenol, we were able to record systolic pressures that were significantly larger than in control conditions. **Figure 1B** summarizes the pressure data obtained with our device, before and after the coronary perfusion with isoproterenol. The amplitudes of the developed pressures were normalized to the mean control. Isoproterenol induced a significant increase in the developed pressure (1 ± 0.06 for the control vs. 1.62 ± 0.05 for isoproterenol, $N = 4$ hearts $p < 0.01$), showing that the perfused hearts used here respond to a β-adrenergic drive.

To assess the β-adrenergic regulation in the endocardial and epicardial layers, we examined the properties of Ca^{2+} transients in those particular regions using the PLFFM technique. **Figure 2A** illustrates normalized Ca^{2+} transients recorded simultaneously at the endocardial and epicardial layer. Perfusion of the hearts with 500 nM isoproterenol increased the amplitude of Ca^{2+} transients in both layers (**Figures 2B,C**). A summary

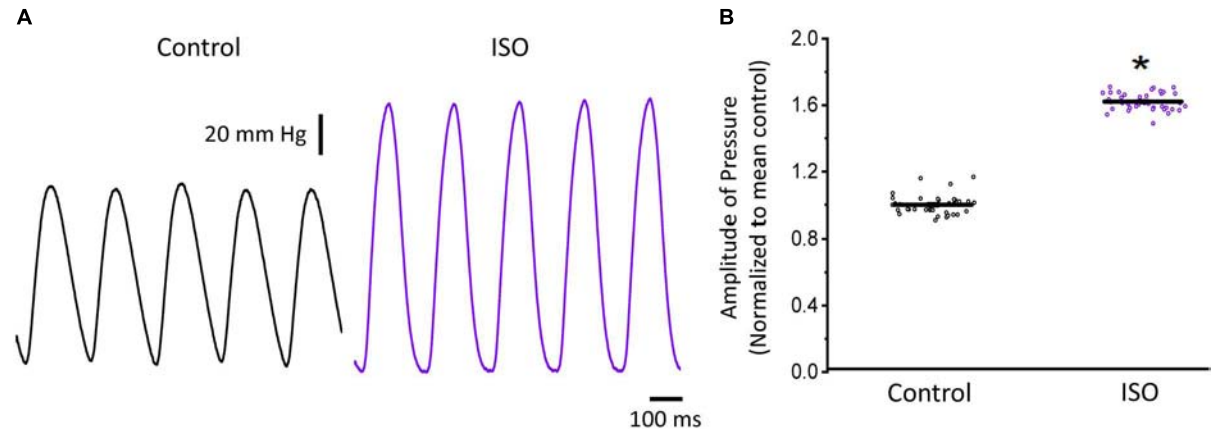

FIGURE 1 | β-Adrenergic stimulation increases the left ventricular developed pressure. **(A)** Representative traces of the left ventricular pressure before (black) and after 500 nM isoproterenol (ISO; purple). **(B)** Data shows the change in the normalized amplitude of the developed pressure before and after isoproterenol. Data is presented as multiple measurements (n; dot cloud) recorded on different hearts ($N = 4$) with mean ± SEM (solid line) $^*p < 0.01$.

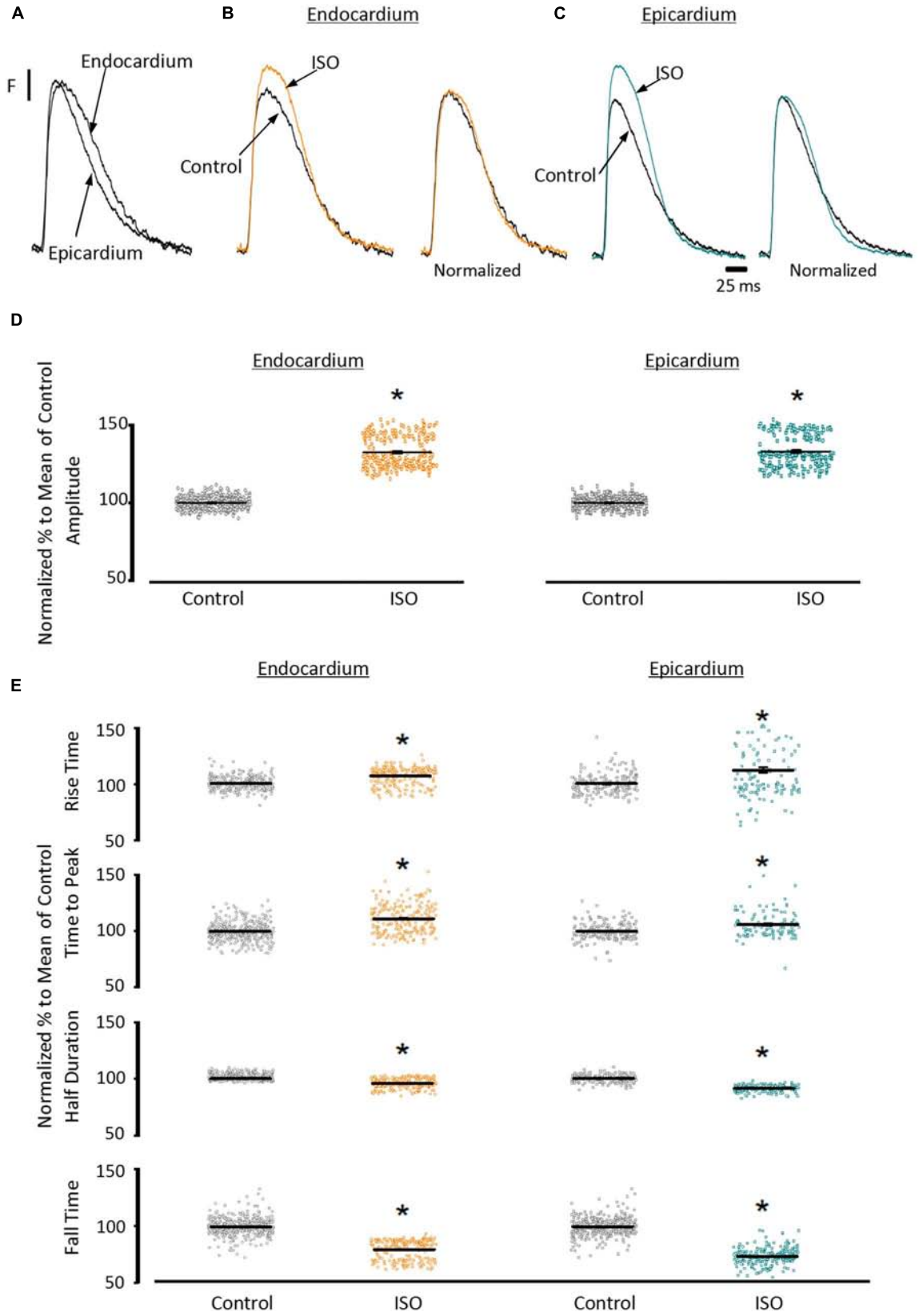

FIGURE 2 | Continued

FIGURE 2 | β-Adrenergic stimulation modulates Ca^{2+} transients in endocardium and epicardium. **(A)** Normalized fluorescent Ca^{2+} transients recorded, simultaneously, from endocardium and epicardium using Rhod-2 and the pulsed local field fluorescence microscopy technique. **(B)** Representative fluorescent traces of the endocardial Ca^{2+} transients before (black) and after 500 nM isoproterenol (ISO; orange). *Right panel*: Ca^{2+} transient traces normalized to their corresponding maximum fluorescence. **(C)** Representative Ca^{2+} transients recorded from the epicardium before (black) and after isoproterenol (cyan). *Right panel*: Ca^{2+} transients normalized to their maximum fluorescence. **(D)** Summary of the normalized amplitude of the Ca^{2+} transient changes, from the endocardium (circles) and epicardium (squares), before and after isoproterenol. **(E)** Data showing the kinetic changes in the normalized Ca^{2+} transients before and after isoproterenol. Means ± SEM are represented as the solid horizontal lines. *$p < 0.01$, $N = 4$ hearts.

TABLE 1 | Isoproterenol effects on Ca^{2+} transient kinetics and AP durations.

Isoproterenol effects on Ca^{2+} transient kinetics				
Condition	**RT (ms)**	**TP (ms)**	**HD (ms)**	**FT (ms)**
Endo Control	7.95 ± 0.05 (*n* = 269)	11.59 ± 0.07 (*n* = 376)	49.93 ± 0.49 (*n* = 390)	65.61 ± 0.40 (*n* = 426)
Endo Iso	7.96 ± 0.08 (*n* = 210)*	12.51 ± 0.08 (*n* = 199)*	49.20 ± 0.61 (*n* = 216)*	52.76 ± 0.70 (*n* = 215)*
Epi Control	6.78 ± 0.05 (*n* = 185)	11.70 ± 0.08 (*n* = 183)	46.83 ± 0.18 (*n* = 335)	69.30 ± 0.39 (*n* = 311)
Epi Iso	7.16 ± 0.13 (*n* = 130)*	12.11 ± 0.90 (*n* = 112)*	43.09 ± 0.31 (*n* = 233)*	49.79 ± 0.44 (*n* = 232)*
Isoproterenol effects on AP durations				
Condition	**APD30 (ms)**	**APD half phase 2 (ms)**	**APD90 (ms)**	
Endo Control	8.26 ± 0.13 (*n* = 143)	58.91 ± 0.27 (*n* = 89)	76.01 ± 0.66 (*n* = 90)	
Endo Iso	10.21 ± 0.16 (*n* = 141)*	54.54 ± 0.18 (*n* = 87)*	67.10 ± 0.33 (*n* = 88)*	
Epi Control	2.93 ± 0.03 (*n* = 236)	62.08 ± 0.30 (*n* = 90)	77.45 ± 0.54 (*n* = 90)	
Epi Iso	3.77 ± 0.04 (*n* = 280)*	54.43 ± 0.18 (*n* = 89)*	69.81 ± 0.45 (*n* = 88)*	

*Endo, endocardium; Epi, epicardium; Iso, isoproterenol; RT, rise time; TP, time to peak; HD, half duration; FT, fall time. APD, AP durations measured at 30, half phase 2, and 90% repolarization. *Kolmogorov–Smirnov test, $p < 0.01$, $N = 4$.*

of the effect of isoproterenol on the amplitude of the Ca^{2+} transients is presented in **Figure 2D** where it is possible to observe that there is a significant increase in both the endocardium (32.2 ± 0.83%) and the epicardium (32.9 ± 0.85%). This result is consistent with the effect of isoproterenol on the developed pressure as shown in **Figure 1**. Isoproterenol not only has an inotropic effect but also a lusitropic action. In **Figures 2B,C** it is possible to observe that the relaxation of the Ca^{2+} transients is faster in the presence of isoproterenol. Different kinetic parameters for endocardial and epicardial Ca^{2+} transients are compiled from 4 different hearts in **Table 1** (measured times) and **Figure 2E** (normalized percentages). Isoproterenol induced significant changes in all the measured parameters of endocardial and epicardial Ca^{2+} transients. The rise time of the Ca^{2+} transients marginally increased (6.5 ± 0.83% for endocardium and 11.6 ± 3.1% for epicardium). As expected, the time to peak of the Ca^{2+} transients follow the same trend (11.1 ± 1.3% for endocardium and 5.9 ± 1.70% for epicardium). Isoproterenol induced a reduction in Ca^{2+} transients' half duration. The half duration is statistically significant shorter in the presence of isoproterenol (5.9 ± 0.42% endocardium and 8.8 ± 0.45% epicardium). However, the changes in the fall time of the relaxation (20.3 ± 0.96% endocardium and 26.3 ± 0.92% epicardium) were larger than those observed in the half durations. The large effect of isoproterenol on the fall time compared to the half duration could be explained by the fact that isoproterenol not only has a positive lusitropic effect but also changes the morphology of the Ca^{2+} transients as shown in **Figures 2B,C**. The changes in fall time for the epicardial were significantly faster ($p < 0.01$) than those in the endocardial layer (**Figure 2E**, bottom panel). It is known that cardiac myocytes from the endocardial, midmyocardial and epicardial layers are characterized by molecular heterogeneities at the level of transcription and expression of proteins. Thus, the faster fall time observed in epicardium can be molecularly defined by a higher expression of SERCA in this layer. Indeed, when we assessed the levels of mRNA transcription by qPCR, there were significant changes in the expression of RyR2, SERCA and Kv4.3, a K^+ channel responsible for I_{to} that consistently shows a higher expression in the ventricular epicardium (**Figure 3**). However, we did not find significant differences in the expression of L-type Ca^{2+} channels, NCX, PKA, M2 muscarinic receptors and β-ARs between both layers. Since the expression of both RyR2 and SERCA is unevenly distributed across the ventricular wall, we expected to have a differential response between endocardium and epicardium.

Another remarkable difference that distinguishes the endocardial and epicardial layers is their electrical properties. One of the main differences is in the phase 1 repolarization of the AP due to the higher expression of Kv4.3 in the epicardial layer (**Figure 3**). Thus, we designed experiments to evaluate the hypothesis that β-adrenergic stimulation will differentially affect the time course of endocardial and epicardial APs. **Figure 4A** compares optically recorded ventricular APs in the endocardium and epicardium, where all phases are distinguished. The APs in both layers have a well-defined phase 2. However, the repolarization rate of phase 1 is faster in epicardium than in endocardium (**Table 1**). The perfusion with

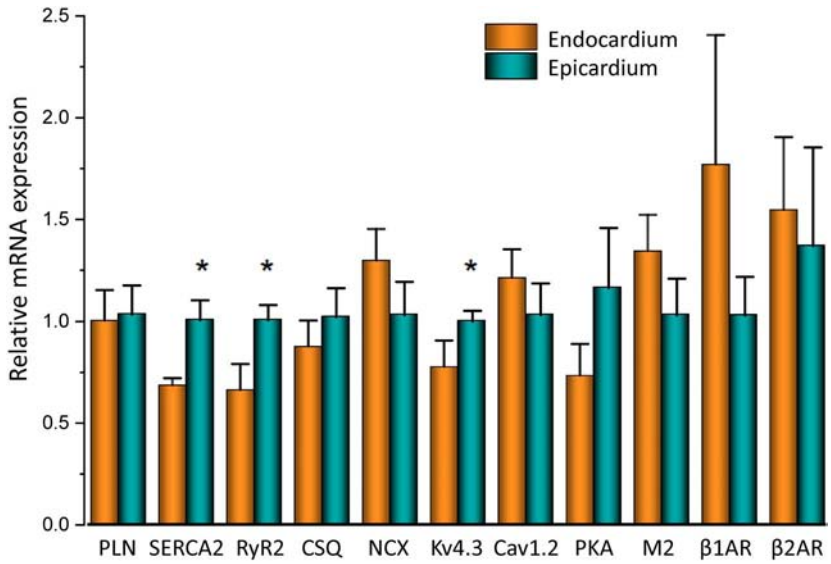

FIGURE 3 | mRNA differences across the ventricular wall. Endocardial and epicardial mRNA quantification of the different proteins involved in Ca^{2+} signaling. mRNA levels (bars) were normalized to the housekeeping gene, GAPDH and expressed as mean ± SEM. $N = 5$. $^*p < 0.05$.

500 nM isoproterenol produced changes in the AP morphology (**Figures 4B,C**). Unexpectedly, isoproterenol decreased the repolarization rate of phase 1, in both the endocardium (**Figure 4B**, inset) and the epicardium (**Figure 4C**, inset). **Table 1** and **Figure 4D** summarizes different endocardial and epicardial AP parameters from four hearts. The most salient features of β-AR activation were an increase in the duration of phase 1 (APD30) and a shortening of the late phases of the AP (APD half phase 2 and APD90). Indeed, isoproterenol induced an increase in APD30 of 21.2 ± 2.40% in endocardium and 27.6 ± 2.18% in epicardium. As in other mammalian species (Litovsky and Antzelevitch, 1990), isoproterenol induced a shortening in APD half phase 2 duration in endocardium and epicardium, 6.9 ± 0.90% and 12.6 ± 0.59%, respectively. Isoproterenol also shortened APD90, 11.5 ± 0.96% in the endocardium and of 9.8 ± 0.73% in epicardium (**Figure 4D**).

The decrease of the repolarization rate of phase 1 with isoproterenol can be attributed to an increase in the amplitude of L-type Ca^{2+} currents. We recently demonstrated that most of the Ca^{2+} influx that triggers Ca^{2+}-induced Ca^{2+}-release (CICR) occurs during phase 1 (Ramos-Franco et al., 2016) and that the influx of Ca^{2+} through L-type Ca^{2+} channels slows down the rate of repolarization during phase 1 (López Alarcón et al., 2019). To directly evaluate any changes in the L-type Ca^{2+} currents during isoproterenol perfusion, we used the novel Loose Patch Photolysis (LPP) technique. We simultaneously acquired Ca^{2+}-driven currents with the corresponding APs before and after isoproterenol. In **Figure 5A**, the AP showed an increase in APD30 (inset) as well as in phase 2. However, due to the presence of nifedipine, this increase in APD30 is smaller than in its absence (**Table 1** and **Figure 4D**). **Figure 5B** shows a typical experiment where Ca^{2+} currents, activated by the photolysis of nifedipine on the membrane patch surface (see "Materials and Methods" section for details), were recorded before and after the heart was perfused with isoproterenol. We observed a clear increase in the amplitude of the Ca^{2+}-driven currents, displayed as an early fast component (i_{early}) and a late slower component (i_{late}). Unfortunately, the simultaneous measurement of Ca^{2+} driven currents in the endocardium and epicardium was not possible due to the size of the patch pipettes. To reach the endocardial layer with the patch pipette would require a large size hole that would result in electrical conduction alterations. **Figure 5C** shows the effect of isoproterenol on the amplitude of i_{early} that increased from 13.9 ± 0.2 nA/nF to 27.6 ± 0.2 nA/nF. In a recent work (Ramos-Franco et al., 2016), we showed that Ca^{2+} released from the sarcoplasmic reticulum (SR), activated the NCX in the forward mode, resulting in i_{late} (Ferreiro et al., 2012; Ramos-Franco et al., 2016). This i_{late} was abolished (**Figure 5D**) when we blocked SR Ca^{2+} release with a combination of ryanodine and thapsigargin. The family of traces correspond to consecutive current recordings, where the Ca^{2+} currents were evoked locally by progressively photolyzing greater fractions of nifedipine by using UV laser pulses of increasing beam energy (fluence). To test the hypothesis that β-adrenergic stimulation directly increases the amplitude of the Ca^{2+} current occurring during phase 1, we performed an identical experiment to the one presented in **Figure 5D** but in the presence of isoproterenol (**Figure 5E**). We observed that isoproterenol dramatically increased the amplitude of i_{early}. The simultaneous recording of the corresponding APs shows that isoproterenol only altered the kinetics of phase 1 (**Figure 5E**, right panel). **Figure 5F** shows the peak values of i_{early} as a function of the fluence, before and after isoproterenol. It is possible to observe that i_{early} saturates at high fluence values (>16 J/cm^2) indicating that most of the nifedipine was photolyzed.

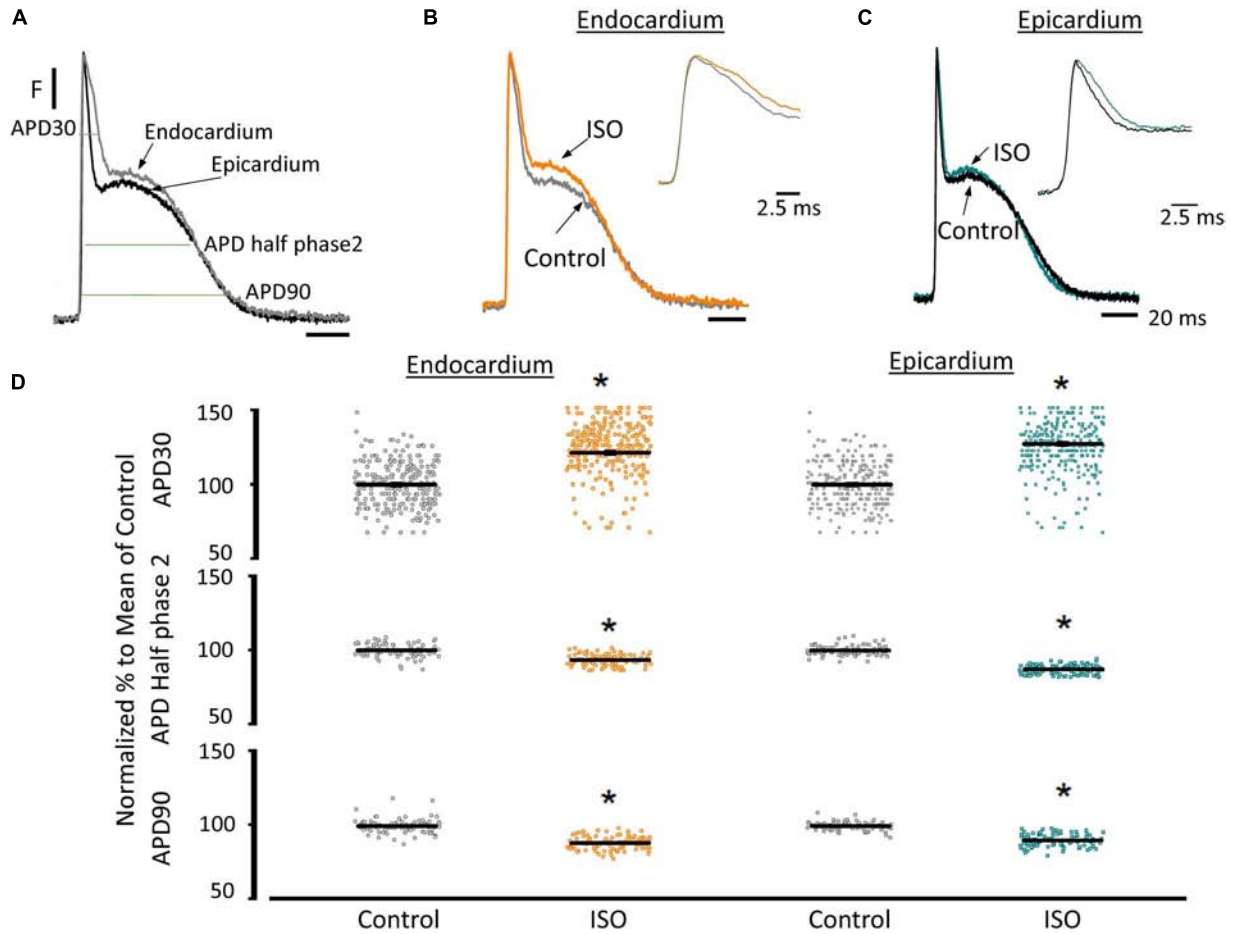

FIGURE 4 | β-Adrenergic stimulation modifies AP morphology in endocardium and epicardium. **(A)** Normalized APs from the endocardium (gray) and epicardium (black) recorded optically using Di-8-ANEPPS and the pulsed local field fluorescence microscopy technique. The evaluated AP parameters are marked. **(B)** Normalized APs from the endocardium before (gray) and after perfusion with 500 nM isoproterenol (ISO; orange). *Inset*: Expanded view of AP phase 0 and 1 to visualize the isoproterenol effects. **(C)** Normalized APs recorded from the epicardium before (black) and after perfusion with 500 nM isoproterenol (cyan). *Inset*: Expanded view of AP phase 0 and 1 to visualize the isoproterenol effect. **(D)** Summary of the normalized APD30, APD half phase 2 and APD90 changes from the endocardium (circles) and epicardium (squares), before and after isoproterenol. Means ± SEM are represented as the solid horizontal lines. $^*p < 0.01$, $N = 4$ hearts.

Figure 5 shows that isoproterenol induced an increase in the amplitude of i_{early}. It is well known that catecholamines activate PKA, which in turn leads to the phosphorylation of multiple targets involved in Ca^{2+} signaling (i.e., the L-type Ca^{2+} channels, RyR2 and PLN). In order to determine which target is phosphorylated first, the effect of catecholamines on the time course of Ca^{2+}-driven currents was evaluated. We performed experiments in which we mimicked a transient β-adrenergic stimulation by photolyzing caged 3′,5′-cyclic adenosine monophosphate (cAMP). A typical response is illustrated in **Figure 6A** where upon immediate photolysis (purple arrow), both components of the Ca^{2+}-driven current, i_{early} and i_{late}, began to increase over time. To better illustrate the changes of i_{early} and i_{late}, in **Figure 6B,** we overlapped the current traces at different time points: before, 1 s and 10 s after the uncaging. Plotting the amplitude peaks of i_{early} and i_{late} as a function of time during consecutive cardiac cycles, highlighted that both currents changed over time, but with a greater effect on i_{early} (**Figure 6C**). When we normalized these currents (**Figure 6D**), it became apparent that i_{early} also responded sooner to the transient β-adrenergic stimulation.

Sympathetic stimulation is highly antagonized by the other branch of the ANS, the parasympathetic nervous system. Parasympathetic stimulation is thought to generally predominate over an existing sympathetic activation. Next, we evaluated the response of endocardium and epicardium to muscarinic cholinergic agonists. **Figure 7A** shows that upon perfusion with 5 μM carbachol, there were no measurable changes in the developed ventricular pressure. Our pressure data (**Figure 7B**) shows there was no significant differences before and after carbachol (0.99 ± 0.15 vs. 0.99 ± 0.07, $N = 3$ hearts). These results suggest that in the absence of a β-adrenergic stimulus, carbachol by itself does not induce a decrease in the developed ventricular pressure during the cardiac cycle.

To assess the cholinergic regulation of contractility, we examined the properties of Ca^{2+} transients across the ventricular

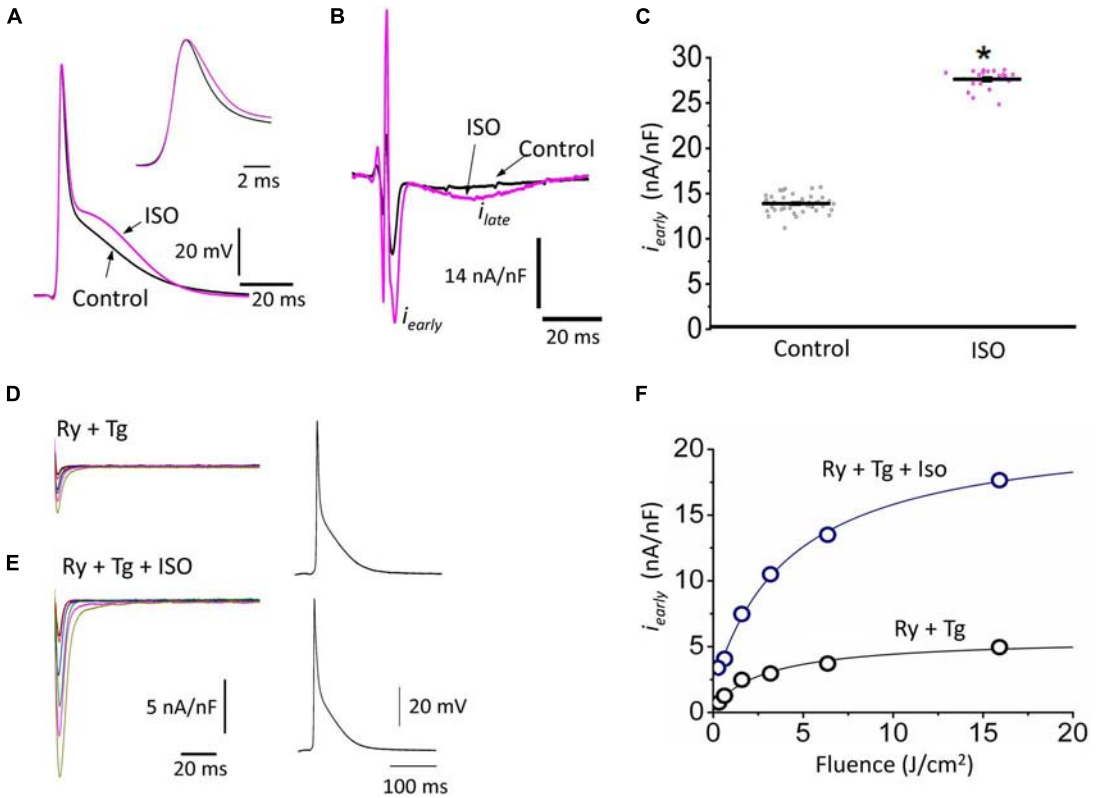

FIGURE 5 | β-Adrenergic stimulation increases Ca^{2+}-driven currents. **(A)** APs recorded from the epicardium using glass microelectrodes before (black) and after 500 nM isoproterenol (ISO; pink). *Inset*: Expanded view of the phase 0 and 1 showing the effects of isoproterenol on APD30. **(B)** Representative traces of Ca^{2+}-driven currents recorded after the local photolysis of nifedipine using the Loose Patch Photolysis technique showing the i_{early} and i_{late} components upon β-adrenergic stimulation. **(C)** Data from the i_{early} component, representing the L-type Ca^{2+} currents, before (gray) and after isoproterenol (pink). The means ± SEM are represented as the solid horizontal lines. $^*p < 0.01$, $N = 4$ hearts. **(D)** Representative traces of Ca^{2+}-driven currents recorded consecutively at increasing UV energies (fluences) in control conditions in the presence of ryanodine (Ry, 10 μM) and thapsigargin (Tg, 2 μM). *Right panel*: Simultaneously recorded AP in the same conditions. **(E)** Ca^{2+}-driven currents recorded consecutively at increasing UV energies (fluences) with isoproterenol in the presence of ryanodine (Ry, 10 μM) and thapsigargin (Tg, 2 μM). *Right panel*: Simultaneously recorded AP in the same conditions. **(F)** Peak values of i_{early} as a function of the fluence, before (black) and after isoproterenol (blue) in the presence of Ry and Tg.

wall in the presence of a cholinergic agonist and antagonist (**Table 2**). **Figure 8** illustrates normalized Ca^{2+} transients recorded simultaneously at both the endocardial (**Figure 8A**) and epicardial (**Figure 8B**) layer with carbachol and carbachol and atropine. Perfusion of the hearts with 5 μM carbachol induced a minor but statistically significant decrease in the amplitude of the Ca^{2+} transients by 3.5 ± 0.35% in the endocardium, and 7.5 ± 0.58% in epicardium (**Figure 8C**). However, this effect was smaller than the increase in the amplitude of Ca^{2+} transients observed when hearts were perfused with isoproterenol. The effects of carbachol on various kinetic parameters of the Ca^{2+} transients are summarized ($N = 5$ hearts) in **Figure 8D**. Although, carbachol did not significantly change the normalized rise time in endocardium or epicardium, the time to peak of the Ca^{2+} transients were significantly increased in endocardium (5.5 ± 1.17%) but not in epicardium (2.5 ± 1.83%). Carbachol induced a significant increase in the half duration (endocardium 1.9 ± 0.3%; epicardium 3.0 ± 0.57%) and fall time of the Ca^{2+} transients (endocardium 3.3 ± 0.69%; epicardium 4.1 ± 1.07%). Although the changes in the fall times are significantly different, they were smaller than the kinetic effects observed with isoproterenol (**Figure 2**). Thus, we conclude that perfusion with carbachol did not have a large impact on the amplitude and the kinetics of endocardial and epicardial Ca^{2+} transients, compared to those observed with the perfusion of isoproterenol. When the hearts were perfused with both agonist and antagonist (5 μM carbachol plus 40 μM atropine) it was possible to observe significant values above the control, for rise time (epicardium 5.3 ± 3.14%), time to peak (endocardium 6.7 ± 1.18%; epicardium 6.5 ± 2.01%), half duration (endocardium 9.4 ± 0.34%; epicardium 10.3 ± 0.64%) and fall time (endocardium 4.2 ± 0.74%; epicardium 6.8 ± 1.29%).

Since the effects induced by carbachol in the contractility were minor, we decided to explore how the activation of a parasympathetic pathway affects the electrophysiological behavior of the endocardial and the epicardial layers. In **Table 2** and **Figure 9** we compared ventricular APs optically recorded in the endocardium (**Figure 9A**) and epicardium (**Figure 9B**). The perfusion with 5 μM carbachol produced significant changes in the AP morphology. **Figure 9C** summarizes different endocardial

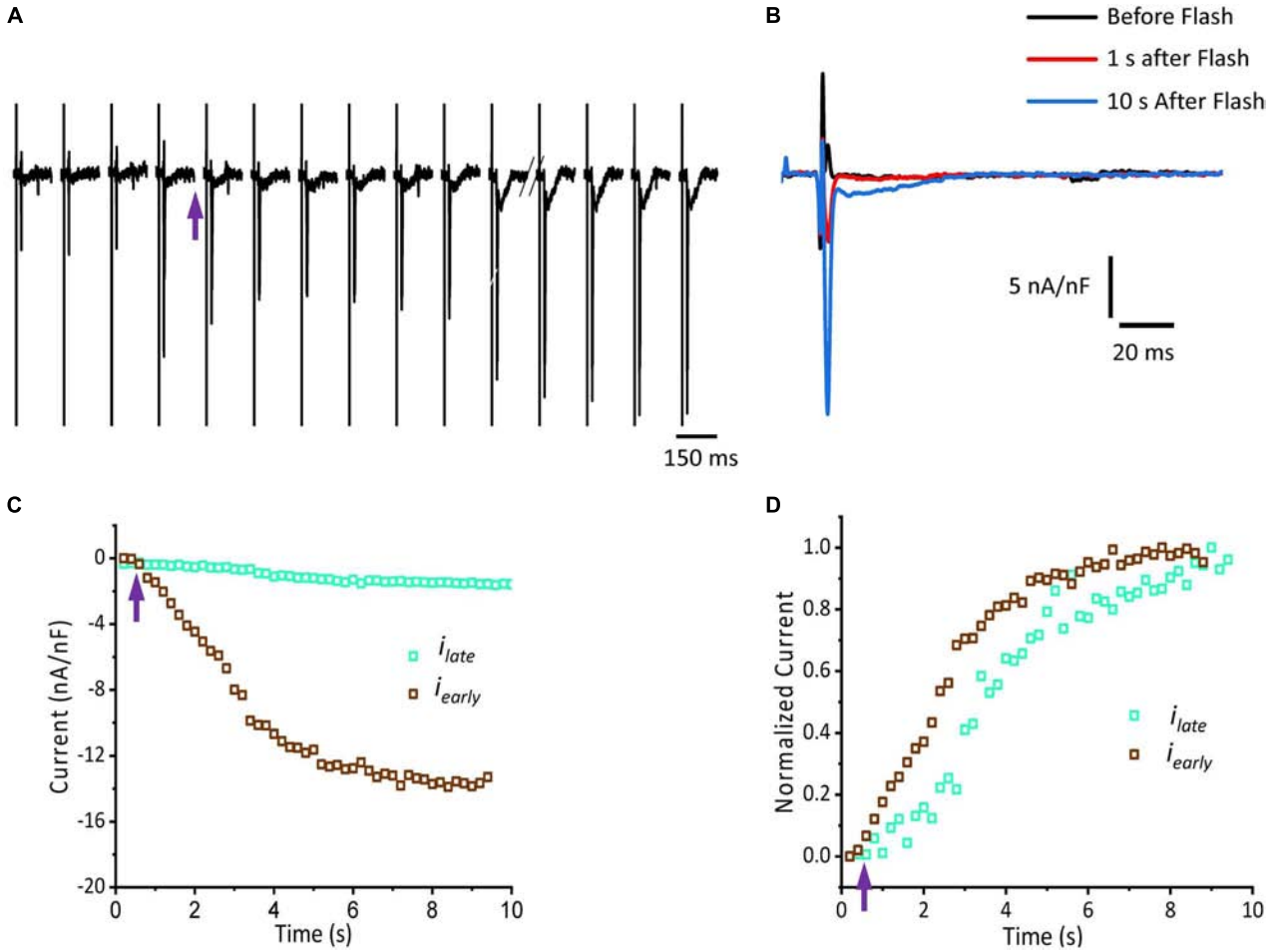

FIGURE 6 | cAMP modulates the time course of Ca^{2+}-driven currents. **(A)** Ionic currents recorded during consecutive cardiac cycles before and after the photolysis of caged cAMP. **(B)** Ionic currents induced by cAMP taken from **(A)** at the indicated time points (traces black, red, and blue) are overlapped to demonstrate the effect in amplitude for both i_{early} and i_{late} components. **(C)** Current amplitude peaks of i_{early} and i_{late} as a function of time before and after the photolysis of caged cAMP. **(D)** Normalized data from **(C)** re-plotted as a function of time. Purple arrow indicates the time of the UV pulse (cAMP uncaging).

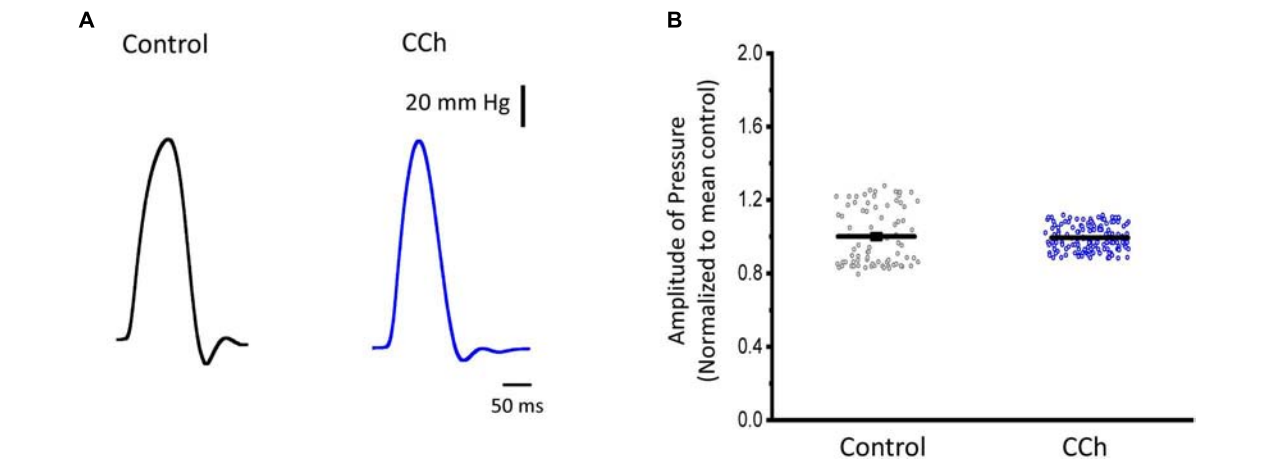

FIGURE 7 | Cholinergic stimulation does not modify the left ventricular developed pressure. **(A)** Representative traces of the left ventricular pressure before (black) and after 5 μM carbachol (CCh; blue). **(B)** Data of the normalized amplitude of the developed pressure before and after carbachol. Means ± SEM are represented as the solid horizontal lines, $N = 3$ hearts.

TABLE 2 | Carbachol effects on Ca^{2+} transient kinetics and AP durations.

Carbachol effects on Ca^{2+} transient kinetics				
Condition	**RT (ms)**	**TP (ms)**	**HD (ms)**	**FT (ms)**
Endo Control	8.32 ± 0.06 (*n* = 676)	12.07 ± 0.08 (*n* = 734)	54.37 ± 0.25 (*n* = 832)	76.45 ± 0.30 (*n* = 764)
Endo CCh	8.06 ± 0.06 (*n* = 706)*	12.63 ± 0.08 (*n* = 738)*	55.49 ± 0.29 (*n* = 808)*	79.34 ± 0.34 (*n* = 806)*
Endo CCh + Atropine	8.75 ± 0.05 (*n* = 545)*	13.08 ± 0.10 (*n* = 697)*	63.27 ± 0.25 (*n* = 586)*	82.80 ± 0.36 (*n* = 583)*
Epi Control	6.78 ± 0.07 (*n* = 302)	11.70 ± 0.12 (*n* = 367)	53.97 ± 0.25 (*n* = 462)	78.47 ± 0.39 (*n* = 456)
Epi CCh	7.05 ± 0.07 (*n* = 321)*	11.83 ± 0.14 (*n* = 341)	55.32 ± 0.19 (*n* = 520)*	81.26 ± 0.43 (*n* = 448)*
Epi CCh + Atropine	7.78 ± 0.15 (*n* = 93)*	12.16 ± 0.17 (*n* = 357)	58.96 ± 0.23 (*n* = 368)*	84.90 ± 0.61 (*n* = 347)*
Carbachol effects on AP durations				
Condition	**APD30 (ms)**	**APD half phase 2 (ms)**	**APD90 (ms)**	
Endo Control	7.41 ± 0.14 (*n* = 264)	81.53 ± 0.31 (*n* = 239)	82.61 ± 0.41 (*n* = 269)	
Endo CCh	6.88 ± 0.11 (*n* = 269)*	52.65 ± 0.18 (*n* = 211)*	65.65 ± 0.20 (*n* = 240)*	
Endo CCh + Atropine	8.69 ± 0.12 (*n* = 440)*	67.42 ± 0.16 (*n* = 443)*	82.47 ± 0.22 (*n* = 443)	
Epi Control	3.24 ± 0.11 (*n* = 425)	68.90 ± 0.15 (*n* = 581)	81.62 ± 0.18 (*n* = 426)	
Epi CCh	3.22 ± 0.12 (*n* = 442)	52.15 ± 0.19 (*n* = 544)*	65.89 ± 0.27 (*n* = 405)*	
Epi CCh + Atropine	3.08 ± 0.27 (*n* = 612)*	66.05 ± 0.17 (*n* = 628)*	79.46 ± 0.18 (*n* = 629)*	

*Endo, endocardium; Epi, epicardium; CCh, carbachol; RT, rise time; TP, time to peak; HD, half duration; FT, fall time. APD, AP durations measured at 30, half phase 2, and 90% repolarization. *Kolmogorov–Smirnov test, $p < 0.01$, $N = 5$.*

and epicardial AP parameters from five hearts. Carbachol did not alter APD30 in epicardium, but had a very modest effect on the endocardial layer (6.9 ± 1.16%). Interestingly, the APD half phase 2 (endocardium 33.4 ± 0.62%; epicardium 24.9 ± 0.42%) and APD90 (endocardium 20.1 ± 0.68%; epicardium 19.4 ± 0.43%), were significantly reduced by the muscarinic stimulation. An interesting effect by the addition of atropine in the presence of carbachol was the recovery of the tested parameters. The APD half phase 2 in endocardium recovered to 90.0 ± 1.12% and the epicardium to 95.7 ± 0.29%. The APD90 for endocardium and epicardium recovered 106.6 ± 0.67% and 100.8 ± 0.26% respectively, from the control values. This suggests that atropine, aside from blocking carbachol's action, may also be blocking an intrinsic, existing cholinergic tone in the isolated heart that modulates the time course of the ventricular AP. Moreover, the fact that carbachol clearly modified both APD half phase 2 and APD90 without changing the kinetic properties of Ca^{2+} transients indicates that the Ca^{2+} influx that triggers Ca^{2+} induced Ca^{2+} release may not occur during phase 2. To further explore this possibility, we then evaluated the properties of Ca^{2+} currents driven by its own AP, when the heart was exposed to a parasympathetic drive. Indeed, the decrease of APD half phase 2 with carbachol could be due to a decrease in the amplitude of L-type Ca^{2+} currents. For example, a reduction in the L-type Ca^{2+} current will lead to a decrease in the Ca^{2+} released from the SR. In turn, this will result in less activation of the NCX in its forward mode. To test this scenario, we evaluated the effect of carbachol on the time course of the L-type Ca^{2+} current during an evoked AP. In **Figures 10A,B**, we recorded the epicardial Ca^{2+}-driven currents that were activated by the photolysis of nifedipine before and after carbachol perfusion. **Figure 10C** shows the superposition of two Ca^{2+}-driven current traces before and after the carbachol perfusion. The Ca^{2+}-driven currents displayed an i_{early} and i_{late} component, but they were not affected by the presence of carbachol. **Figure 10D** shows that carbachol did not significantly modify the amplitude of i_{early}.

Since carbachol did not induce changes in the amplitude of L-type Ca^{2+} currents, we examined if a repolarizing outward current (associated with the cholinergic stimulation) was involved in the shortening of the APD half phase 2. Although it is well established in the atrium that the current of an acetylcholine (ACh) activated potassium channel, I_{KACh}, can severely affect the AP repolarization, the role of this current in the ventricle is still a matter of debate. The role of the I_{KACh} was evaluated by perfusing the hearts with tertiapin, a bee venom that can block with high affinity GIRK1/GIRK2 hetero-tetramers (Hashimoto et al., 2006). GIRK1/GIRK2 hetero-tetramers form the pore of the inward rectifying K^+ channels responsible for I_{KACh}. The perfusion of tertiapin prevented the carbachol shortening of the AP in the epicardium **Table 3** and **Figure 11**. **Figure 11A** illustrates that in the presence of tertiapin, 5 μM carbachol is not able to produce any visible change in the kinetics of the electrically recorded APs. However, in the absence of tertiapin, 5 μM carbachol modified APD half phase 2 and APD90 (**Figure 11B**). The summarized epicardial AP data (**Figure 11D**; $N = 5$ hearts) shows tertiapin induced statistically significant differences in all of the AP phases (5.2 ± 0.38% for APD30, 0.8 ± 0.56% for APD half phase 2 and 0.5 ± 0.02% for APD90). Although these differences are statistically significant, the magnitude of the change is so small (see **Table 3**) that we do not consider that these changes will have any physiological effect. Interestingly, in the presence of tertiapin, carbachol was not able to induce the same shortening effect, as in the absence of tertiapin, on the total AP duration (APD half phase 2 and APD90, 3 ± 0.71% and 5.3 ± 0.19%, respectively). To corroborate that tertiapin was blocking the carbachol effect, we perfused the heart

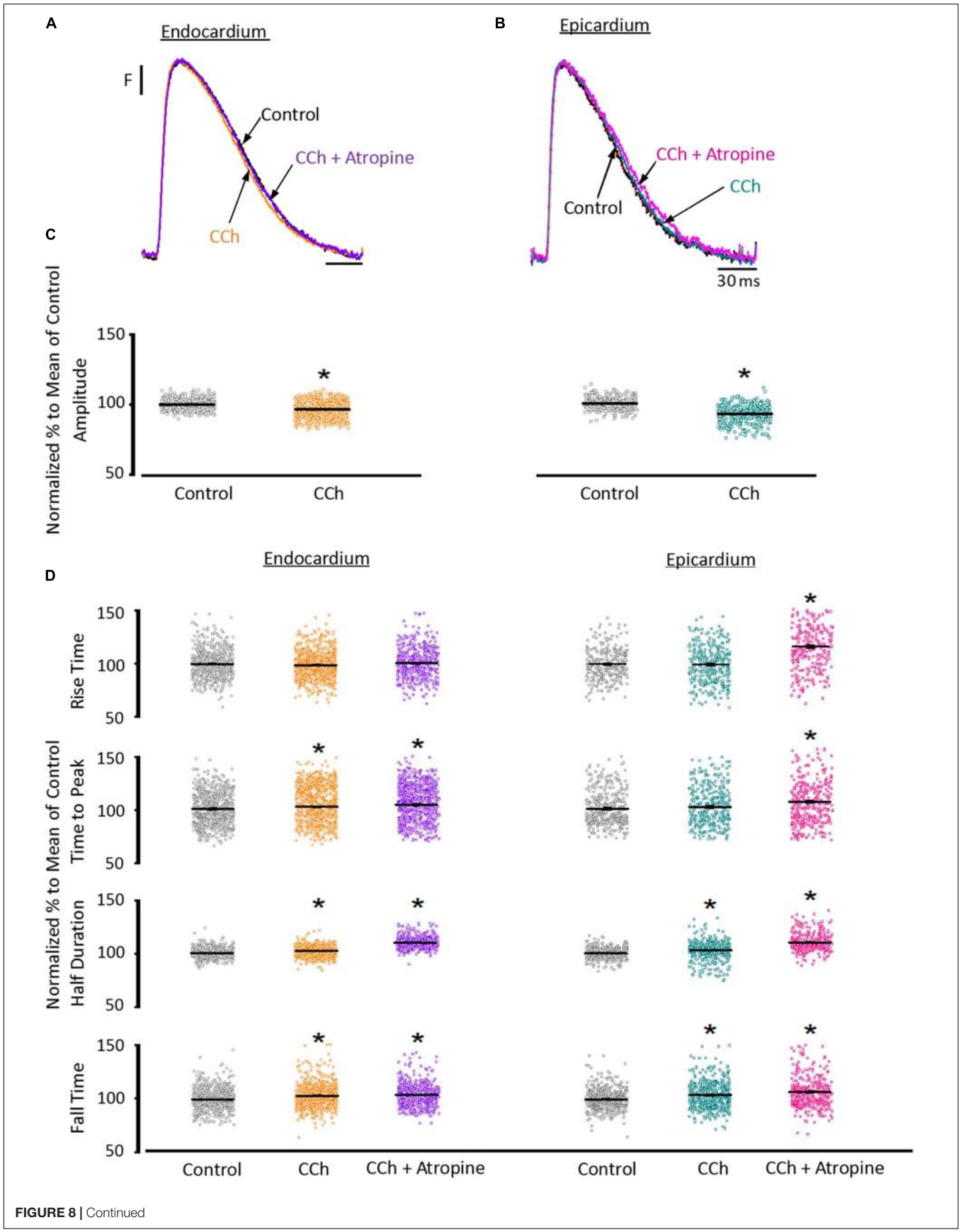

FIGURE 8 | Continued

FIGURE 8 | Cholinergic stimulation has a low impact on the Ca^{2+} transients in endocardium and epicardium. **(A)** Normalized fluorescent Ca^{2+} transients recorded, simultaneously, from endocardium and **(B)** epicardium using Rhod-2 and the pulsed local field fluorescence microscopy technique before and after 5 μM carbachol (CCh) and in the presence of both carbachol and 40 μM atropine. Overlapping Ca^{2+} transients were normalized to their maximum fluorescence. **(C)** Summary of the normalized amplitude of the Ca^{2+} transient changes, from the endocardium (circles) and epicardium (squares), before and after carbachol. **(D)** Data showing the kinetic changes in the normalized Ca^{2+} transients before and after carbachol, and after carbachol plus atropine. Means ± SEM are represented as the solid horizontal lines. *$p < 0.01$, $N = 5$ hearts.

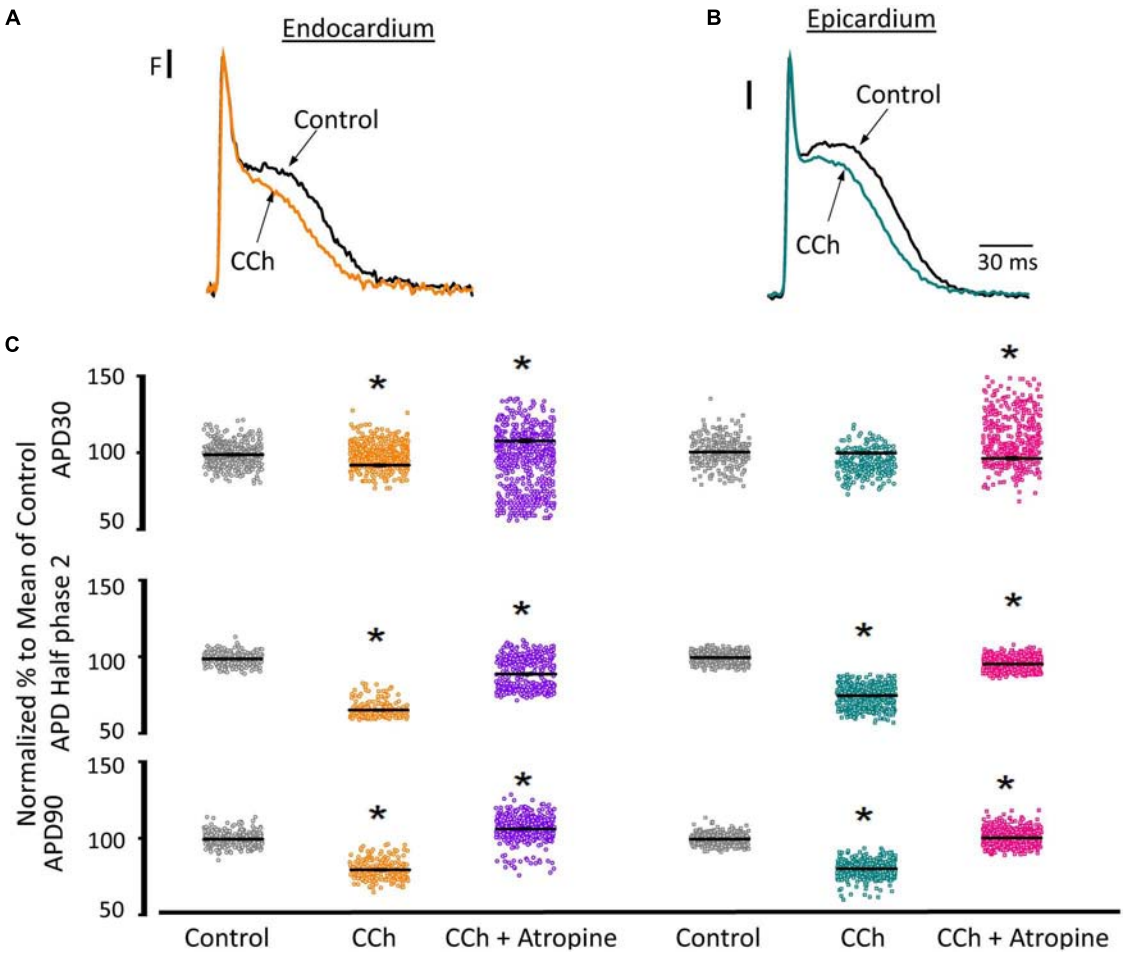

FIGURE 9 | Cholinergic stimulation modifies overall AP morphology in endocardium and epicardium. **(A)** Normalized APs recorded optically with Di-8-ANEPPS from the endocardium and **(B)** epicardium before and after perfusion with 5 μM carbachol (CCh). **(C)** Summary of the normalized APD30, APD half phase 2 and APD90 changes from the endocardium (circles) and epicardium (squares), before and after carbachol, and after carbachol plus atropine. Means ± SEM are represented as the solid horizontal lines. *$p < 0.01$, $N = 5$ hearts.

with carbachol after tertiapin was washed out (**Figures 11B,E**). Carbachol significantly modified APD30 (5.9 ± 0.42%) above control and decreased both APD half phase 2 (12.4 ± 0.22%) and APD90 (9.9 ± 0.19%). These results were consistent with the ones reported in **Figure 9C**. Overall, these results suggest that the AP shortening produced by a cholinergic stimulation is due to the activation of I_{KACh} instead of a Ca^{2+}-driven mechanism. Finally, we evaluated if in the perfused heart, there is a tonic release of acetylcholine from the postganglionic parasympathetic terminals located in the ventricular wall. **Figure 11C** shows that 40 μM atropine prolongs the late repolarization of the epicardial AP. Indeed, although the increase in APD half phase 2 (6.0 ± 0.11%) and APD90 (4.9 ± 0.02%) are not prominent, the increase is statistically significant and reflects a change >5 ms (**Table 3** and **Figure 11F**). This result indicates that it is likely that an intrinsic parasympathetic tone is present in the isolated heart and can slightly decrease the duration of ventricular APs.

DISCUSSION

Although, there is a substantial body of experimental information on sympathetic and parasympathetic regulation of the electrical and mechanical properties of the heart, there is

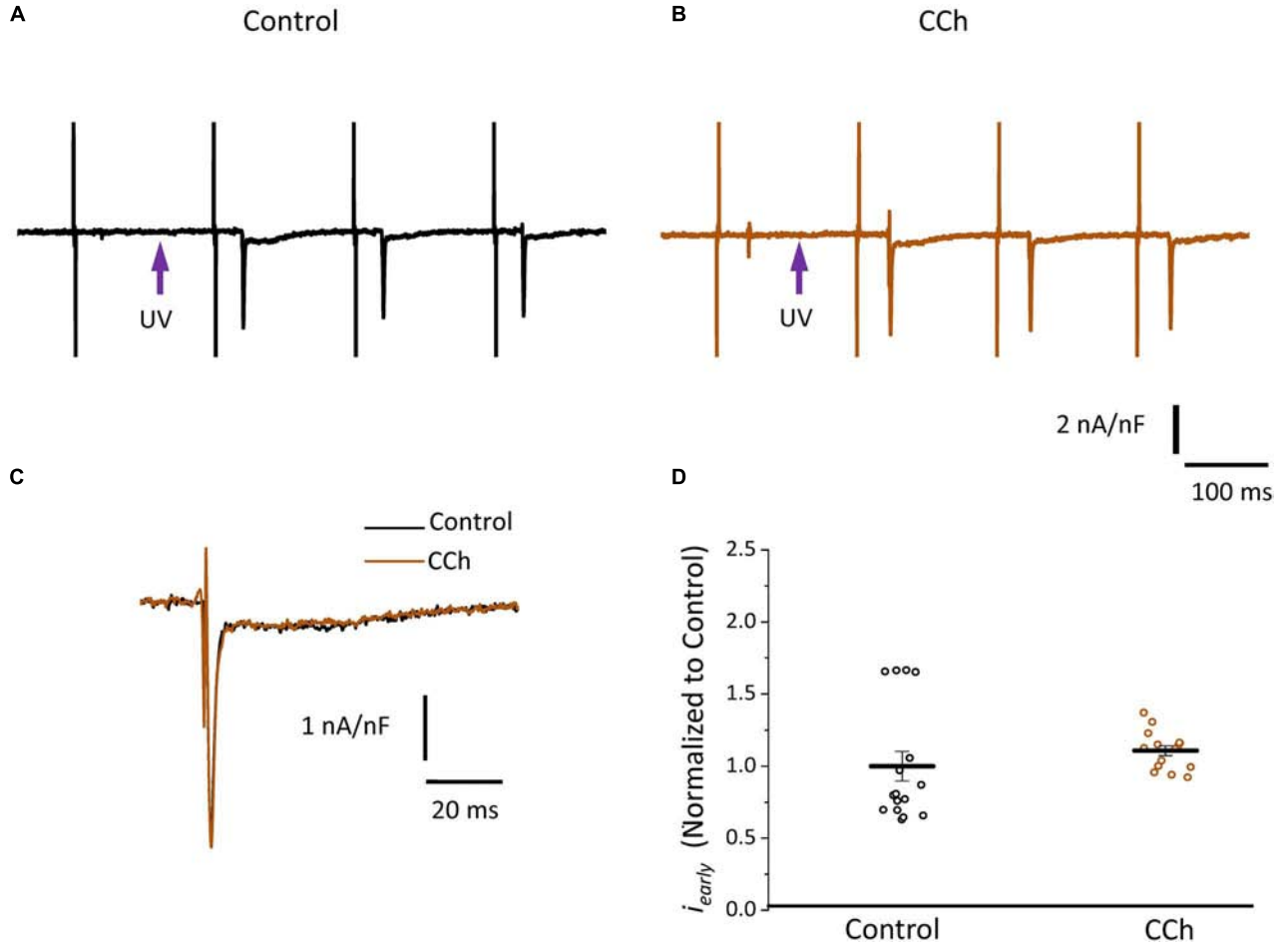

FIGURE 10 | Cholinergic stimulation does not modify L-type Ca^{2+} currents in the absence of a sympathetic drive. **(A)** Representative traces of Ca^{2+}-driven currents recorded after the local photolysis of nifedipine using the Loose Patch Photolysis technique showing i_{early} and i_{late} components under control conditions and **(B)** in the presence of 5 μM carbachol (CCh). **(C)** Overlapping traces of Ca^{2+}-driven currents before (black) and after cholinergic stimulation (brown). **(D)** Normalized data of the peak values of i_{early}, before and after carbachol.

no conclusive evidence of how autonomic driven changes affects the relationship between contractility and excitability in the mouse heart. Neither is it known how sympathetic and parasympathetic nervous system regulate those properties across the ventricular wall. In this study, we investigated how either β-adrenergic or muscarinic cholinergic agonists regulate the time course of ventricular APs and how these electrical changes correlate with the left ventricular pressure, Ca^{2+} transients, and Ca^{2+}-driven currents at the whole-heart level. Our results indicate that in the mouse heart the influx of Ca^{2+} that triggers the ECC happens during AP phase 1 and not phase 2, contrary to what occurs in larger mammals (Boyett, 1986; Antzelevitch et al., 1991; Qu et al., 2013). Indeed, in isolated mice hearts, sympathetic stimulation reduced the rate of repolarization and increased the amplitude of epicardial Ca^{2+} currents. The increase in Ca^{2+} influx drives an increase in the amplitude of Ca^{2+} transients both in the endocardium and the epicardium that finally produces an increase in the developed pressure. In contrast, parasympathetic stimulation dramatically reduced the duration of phase 2 without inducing major changes in Ca^{2+} currents, Ca^{2+} transients and developed pressure indicating that the Ca^{2+} signaling involved in controlling the ECC does not occur during the AP phase 2.

β-Adrenergic Stimulation Across the Ventricular Wall Regulate Ca^{2+}-Driven Mechanisms

It is well known that β-adrenergic stimulation will accelerate the heart rate (chronotropism), and the higher systemic demands will be met by increasing the systolic pressure (inotropism) as well as the rate of relaxation (lusitropism) of the developed pressure. In our mouse model, exposure to isoproterenol generated an increase in the left ventricular developed pressure (**Figure 1**). This increase in inotropism resulted because of an increase in the amplitude of cytosolic Ca^{2+} transients in both endocardial and epicardial layers (**Figure 2**). Although we found no significant changes in the expression of β-adrenergic and muscarinic

TABLE 3 | Tertiapin, carbachol, and atropine effects on AP durations.

Condition	APD30 (ms)	APD half phase 2 (ms)	APD90 (ms)
Epi Control	2.47 ± 0.01 (*n* = 650)	48.63 ± 0.10 (*n* = 650)	60.72 ± 0.08 (*n* = 649)
Epi Tertiapin	2.62 ± 0.01 (*n* = 650)*	48.36 ± 0.15 (*n* = 643)*	60.46 ± 0.12 (*n* = 650)*
Epi Tertiapin + CCh	3.24 ± 0.02 (*n* = 602)*	50.21 ± 0.19 (*n* = 642)*	64.03 ± 0.15 (*n* = 641)*
Epi Control (after Tertiapin + CCh washout)	2.39 ± 0.01 (*n* = 423)	53.89 ± 0.27 (*n* = 582)	67.18 ± 0.28 (*n* = 582)
Epi CCh	2.64 ± 0.02 (*n* = 393)*	47.54 ± 0.18 (*n* = 432)*	62.08 ± 0.27 (*n* = 431)*
Epi Control	2.58 ± 0.01 (*n* = 720)	60.71 ± 0.41 (*n* = 719)	70.19 ± 0.45 (*n* = 720)
Epi Atropine	2.61 ± 0.01 (*n* = 566)*	67.33 ± 0.45 (*n* = 566)*	75.19 ± 0.58 (*n* = 566)*

*Epi, epicardium; CCh, carbachol. APD, AP durations measured at 30, half phase 2, and 90% repolarization. *Kolmogorov–Smirnov test, $p < 0.01$, $N = 5$.*

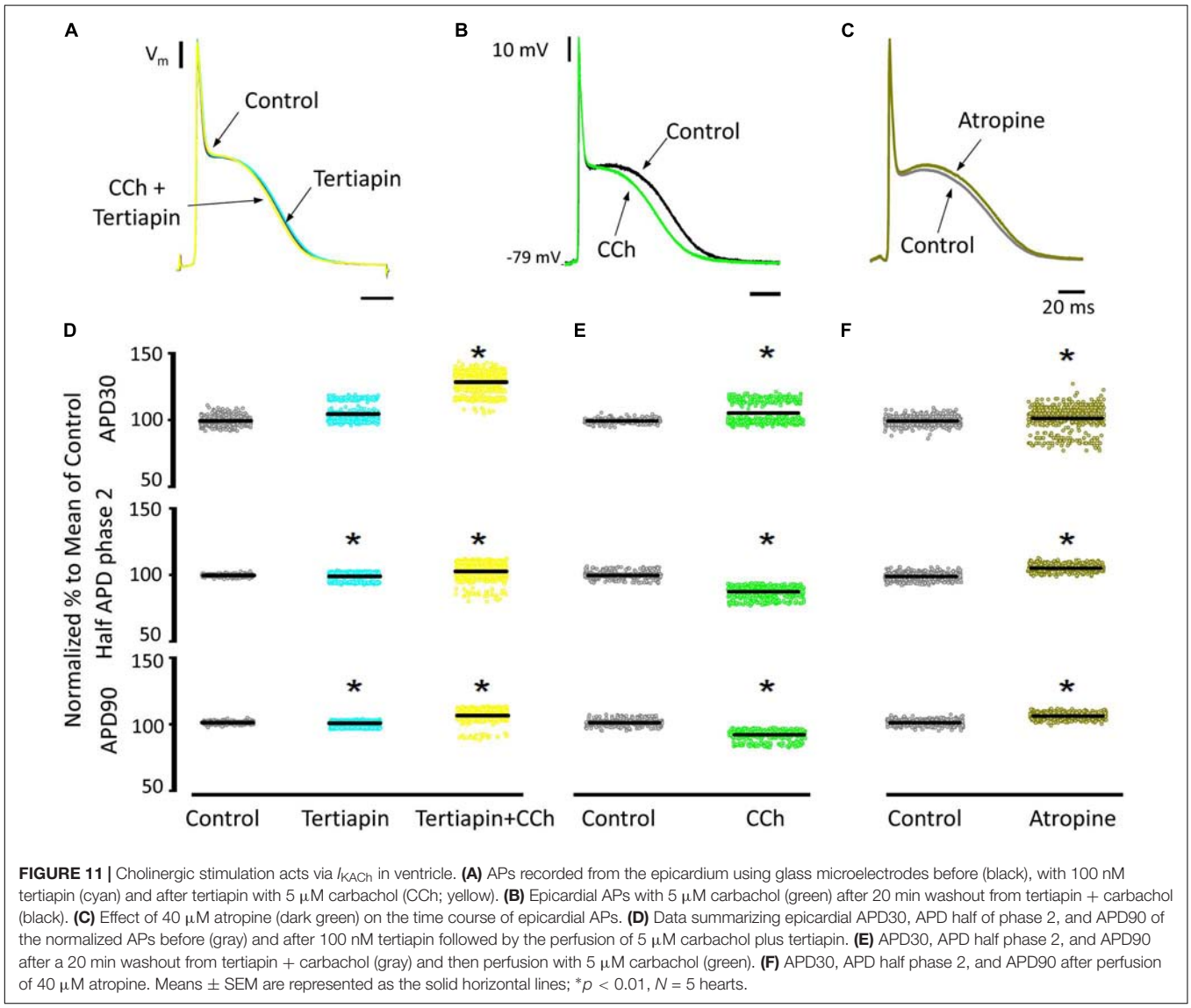

FIGURE 11 | Cholinergic stimulation acts via I_{KACh} in ventricle. **(A)** APs recorded from the epicardium using glass microelectrodes before (black), with 100 nM tertiapin (cyan) and after tertiapin with 5 μM carbachol (CCh; yellow). **(B)** Epicardial APs with 5 μM carbachol (green) after 20 min washout from tertiapin + carbachol (black). **(C)** Effect of 40 μM atropine (dark green) on the time course of epicardial APs. **(D)** Data summarizing epicardial APD30, APD half of phase 2, and APD90 of the normalized APs before (gray) and after 100 nM tertiapin followed by the perfusion of 5 μM carbachol plus tertiapin. **(E)** APD30, APD half phase 2, and APD90 after a 20 min washout from tertiapin + carbachol (gray) and then perfusion with 5 μM carbachol (green). **(F)** APD30, APD half phase 2, and APD90 after perfusion of 40 μM atropine. Means ± SEM are represented as the solid horizontal lines; *$p < 0.01$, $N = 5$ hearts.

receptors between the endocardial and the epicardial layer, there were differences in the expression of downstream targets (**Figure 3**). For example, there was a higher expression of SERCA in the epicardial layer. This molecular difference correlates well with the recorded shorter half durations and fall times of Ca^{2+} transients with isoproterenol, in this layer (**Figure 2** and **Table 1**). In addition, the higher expression of RyR2 in the epicardium can explain the faster activation of Ca^{2+} transients and the larger β-adrenergic modulation of the rise time in this layer (Mattiazzi et al., 2015).

There are intrinsic functional differences in the sympathetic regulation of the endocardial and epicardial APs. The differences are imposed by the differential expression of ionic channels in endocardium versus epicardium as reflected by their respective AP morphologies (Antzelevitch et al., 1991; Antzelevitch and Fish, 2001; Abd Allah et al., 2012). Indeed, in **Figure 3** we showed a higher expression of Kv4.3 in the epicardial layer. The higher expression of this K^+ channel explains the faster rate of repolarization of AP phase 1 in epicardium. In addition, β-adrenergic stimulation affected the AP's morphology by increasing the duration of the AP phase 1 and the amplitude of phase 2 across the ventricular wall (**Figure 4**). One possibility that may explain the increase in the AP phase 1 duration is a reduction in the amplitude of a repolarizing current, such as I_{to}. There are few reports of β-adrenergic regulation of I_{to}. Some experimental evidence (Nakayama et al., 1989; Setién et al., 2013) showed that the catecholamine-induced phosphorylation of the transient outward current (I_{to}) components increased the amplitude of this fast repolarizing current. This possibility is unlikely to occur in our experimental conditions. Increase of I_{to}, would accelerate instead of slowing the repolarization rate of phase 1. In contrast, a reduction of the amplitude of I_{to} by norepinephrine and alpha adrenoceptor stimulation has been reported in healthy rat ventricular myocytes (Ravens et al., 1989; Gallego and Casis, 2001) which may explain our results. However, this is very unlikely in our experiments because isoproterenol is a β-adrenergic and not an α-adrenergic agonist at the concentrations used here. In either scenario, the increase in the duration of phase 1 (APD30) is most likely a consequence of the competition between I_{to} and the inward L-type Ca^{2+} current (López Alarcón et al., 2019). Indeed, a β-adrenergic increase of the L-type Ca^{2+} current (i.e., by PKA phosphorylation) during phase 1 will maintain a depolarization of this phase for a longer time, increasing APD30. Additionally, in the presence of nifedipine, the effect of isoproterenol on APD30 was smaller (**Figure 5A**). Altogether, these results support the idea that the increase in duration of AP phase 1 correlates well with larger L-type Ca^{2+} currents under isoproterenol stimulation. These findings agree with previous experiments from our group in which we showed that the transmembrane Ca^{2+} influx that triggers Ca^{2+}-induced Ca^{2+}-released (CICR) enters during phase 1 (Ramos-Franco et al., 2016).

A final proof of concept was to demonstrate that isoproterenol mediates an increase of the amplitude of the L-type Ca^{2+} current during phase 1. Indeed, we corroborated that under β-adrenergic stimulation there is an increase in the amplitude of the L-type Ca^{2+} current during phase 1 (**Figure 5**). This could result in (1) the decrease of the rate of AP repolarization during phase 1, and (2) the depolarization induced by the increase in the L-type Ca^{2+} current will further activate L-type Ca^{2+} channels with the enlargement of this Ca^{2+} current. Interestingly, in the presence of a submaximal concentration of nifedipine, isoproterenol increased the duration of phase 2. This effect can be attributed to an increase in the amplitude of the Ca^{2+} transients as shown in **Figure 2**. The most likely possibility is that an increase in the amplitude of the Ca^{2+} transient will induce a larger activation of the NCX in the forward mode as previously suggested (Ferreiro et al., 2012). The validity of this hypothesis was assessed in **Figure 5B** where we found an increase in the fast and early inward current (i_{early}) through the L-type Ca^{2+} channels and a significant increase in the amplitude of the late NCX current as reflected by i_{late}. These results suggest that changes in the electrical excitability induced by the β-adrenergic stimulation across the ventricular wall are highly mediated through a Ca^{2+}-driven mechanism.

As we showed, the sympathetic branch of the ANS can induce mechanical changes in the intact heart by altering the underlying plasma membrane Ca^{2+} currents and consequently, Ca^{2+} release from the SR. However, PKA activation can affect other targets. For example, PLN (Toyofuku et al., 1993; Frank and Kranias, 2000), a protein that regulates the activity of SERCA can be phosphorylated on residue S16 (Chu et al., 2000; Valverde et al., 2006). This phosphorylation will relieve the inhibitory effect PLN has on SERCA, that will result in increased contractility (Luo et al., 1994). On the other hand, RyR2 can be phosphorylated by PKA in the residues S2030 (Huke and Bers, 2008) and S2808 (Obayashi et al., 2006; Chen-Izu et al., 2007). This phosphorylation can increase the RyR2 open probability. However, it is not fully established that the RyR2 phosphorylation by itself will increase contractility mostly because of the changes produced in the intra-SR Ca^{2+} content as a consequence of the interplay between release and recapture (Eisner et al., 2004). Although it is accepted that the phosphorylation of these targets will modify Ca^{2+} release from the SR, the timing of the PKA induced phosphorylation is unknown. Specifically, it is unclear which phosphorylated target will have a faster effect on the ECC process. **Figure 6** clearly showed that under a global increase in cAMP concentration the L-type Ca^{2+} current is the first transport mechanism that is activated by PKA. However, this may not be the case *in vivo*, due to the documented compartmentation of cAMP resulting from localized cyclic nucleotide phosphodiesterase (PDE) activity (Nikolaev et al., 2006; Leroy et al., 2008). In our experimental conditions (cAMP cell loading), we assumed a homogeneous cellular distribution of cAMP. Based on this, we propose that PKA phosphorylation of the L-type Ca^{2+} channels has a dual effect. Immediately after phosphorylation, the increase in L-type Ca^{2+} current will increase Ca^{2+} release from the SR. Consequently, the increase in the intracellular Ca^{2+} will promote a larger uptake of Ca^{2+} into the SR mediated by SERCA. Finally, the phosphorylation of PLN will induce a later increase in the intra-SR Ca^{2+} content that will further increase SR Ca^{2+} release.

Cholinergic Stimulation Across the Ventricular Wall Did Not Alter Ca^{2+} Dynamics

Although the sympathetic branch of the ANS produced mechanical changes in the intact heart by altering the underlying Ca^{2+} currents, the cholinergic stimulation did not. Interestingly, the left ventricular pressure showed no changes when exposed to carbachol (**Figure 7**). However, there were minor changes in the amplitude of the Ca^{2+} transients in both endocardium and epicardium (**Figure 8**). Carbachol induced some statistically

significant changes in most of the kinetic parameters of Ca^{2+} transients, but these changes were never larger than 4% (**Figure 8D**). This suggest that although parasympathetic regulation has a negative inotropic effect on the cardiac function at the whole animal level, in the Langendorff perfused heart, we were unable to observe any substantial effect in contractility. One difference between the intact animal and the isolated perfused heart relies on the fact that, in the perfused heart, we do not have an intrinsic systemic sympathetic drive. Indeed, in the intact animal, the binding of acetylcholine to muscarinic receptors will activate a G_i protein that will exert an inhibitory effect on AC, antagonizing the stimulatory effect of the β-AR coupled to a G_s protein. However, in the isolated heart, if G_s is not activating AC, the activation of a G_i will not produce changes in the intracellular cAMP levels. Finally, this would explain why we did not observe any major negative inotropic action of carbachol in the perfused heart in the absence of a sympathetic drive.

Cholinergic Stimulation Modifies Endocardial and Epicardial Cardiac Excitability

Recently, it was shown that vagal innervation exists in the ventricle, but it is 80% less innervated than atria (Coote, 2013). Parasympathetic action on the AP's waveform has been mostly evaluated in atrial and nodal myocytes (sinus and atrio-ventricular). In both cell types, acetylcholine induces an increase in the AP repolarization rate mediated by a K^+ current activated by acetylcholine (I_{KACh}; Engelstein et al., 1994; Corey et al., 1998; Wickman et al., 1999; Choisy et al., 2012). There was a general belief that this mechanism is absent in the ventricle (Coote, 2013). Recently, immunofluorescence studies have shown the presence of G-protein-coupled inward rectifier K^+ proteins in mouse, rat, and human ventricle (Liang et al., 2014). Here, we found that, in a mouse ventricle, carbachol had a significant effect on AP repolarization rate (**Figure 9**). The APD half phase 2 and the APD90 were reduced in both the endocardial and the epicardial layers, with a modest effect on APD30. Furthermore, atropine, an antagonist of M2 muscarinic receptors, was able to prevent the effect of carbachol indicating that this effect was mediated by a muscarinic receptor.

Interestingly, Litovsky and Antzelevitch (1990) reported that acetylcholine had little if any effect in canine ventricular endocardium but a concentration-dependent biphasic effect in epicardium. Specifically, acetylcholine induced an APD50 prolongation at 0.1 and 1 μM and a reduction at 10 μM. The discrepancy with our findings could be explained by the difference in species (canine vs. murine) and tissue preparation (ventricular wedges vs. whole heart). Another difference is that these authors found no significant effects on APD30 in either layer (Litovsky and Antzelevitch, 1990). Even though our APD30 results showed a significant difference only for the endocardium, the change induced by carbachol was of 530 ± 250 μs (**Table 2**). This difference is 4 times smaller than the increase that we observed in APD30 when the heart was perfused with isoproterenol (**Table 1**). The fact that carbachol had a profound effect on the AP morphology but minor effects on contractility and Ca^{2+} currents, supports the idea that Ca^{2+}influx, that determine the CICR, does not occur during AP phase 2.

Cholinergic Stimulation Across the Ventricular Wall Was Mediated via I_{KACh}

In general, there are two main hypotheses to explain the muscarinic actions on AP repolarization rate: (1) inhibitory effect on the Ca^{2+} influx through L-type Ca^{2+} channels or (2) an agonistic effect on a cationic outward current. In principle, the muscarinic effect on the L-type Ca^{2+} is very unlikely because, as we showed, there were no effects on the developed pressure and very minor effects (3.5 ± 0.35% in the endocardium, and 7.5 ± 0.58% in epicardium) on the amplitude of the Ca^{2+} transients in the presence of carbachol. Even more, this first hypothesis was discarded when epicardial Ca^{2+} currents were not affected by carbachol (**Figure 10**). The second scenario where the increase in the rate of AP repolarization is mediated by the activation of an outward K^+ current was tested in **Figure 11**. When the hearts were perfused simultaneously with carbachol and the I_{KACh} blocker (tertiapin) a small shortening of the total duration of the AP was observed. Moreover, this apparent blocking effect was corroborated when the same hearts were perfused with carbachol after tertiapin was washed out (**Figure 11**). Together these results suggest that, in the mouse ventricle, cholinergic-mediated changes in the AP morphology are driven by I_{KACh}.

CONCLUSION

In conclusion, our results indicate that: (1) in both endocardium and epicardium, the increase in contractility by isoproterenol was driven by an increase in the amplitude of intracellular Ca^{2+} currents triggered during the AP phase 1; (2) PKA phosphorylates L-type Ca^{2+} channels before the SR Ca^{2+} release activates NCX current; (3) cholinergic stimulation by carbachol decreased the duration of the late AP repolarization. However, this cholinergic stimulation did not substantially modify *per se* the intracellular Ca^{2+} signals when compared with β-adrenergic stimulation; (4) cholinergic stimulation decreased the total duration of the ventricular AP through activation of I_{KACh}.

In summary, the results presented here demonstrate that, in a mouse heart, β-adrenergic input acts across the ventricular wall by modulating the L-type Ca^{2+} currents that occur in phase 1 but not phase 2 of the APs. In contrast, a cholinergic input does not directly modulate Ca^{2+} dynamics, but rather alters inward rectifier potassium channels in the isolated heart.

ETHICS STATEMENT

Mice were maintained in accordance to the National Institutes of Health Guide for the Care and Use of Laboratory Animals (NIH Publication No. 85–23, Revised 1996) and the Institutional Animal Care and Use Committee guidelines of the University of California Merced (Protocol # 2008–201).

AUTHOR CONTRIBUTIONS

AE and JR-F designed the research. YA-S, AR, MA, AE, and JR-F performed the research. YA-S, AR, AE, and JR-F analyzed the data. YA-S, AE, and JR-F wrote the manuscript.

FUNDING

This work was supported by grants from the NIH (R01 HL-084487 to AE and R01 GM-111397 to JR-F).

ACKNOWLEDGMENTS

We thank Alicia Mattiazzi, Fabiana Scornik, and Michael Fill for their valuable feedback on the manuscript.

SUPPLEMENTARY MATERIAL

The Supplementary Material for this article can be found online at: https://www.frontiersin.org/articles/10.3389/fphys.2019.00773/full#supplementary-material

REFERENCES

Abd Allah, E. S. H., Aslanidi, O. V., Tellez, J. O., Yanni, J., Billeter, R., Zhang, H., et al. (2012). Postnatal development of transmural gradients in expression of ion channels and Ca2+-handling proteins in the ventricle. *J. Mol. Cell. Cardiol.* 53, 145–155. doi: 10.1016/j.yjmcc.2012.04.004

Aguilar-Sanchez, Y., Fainstein, D., Mejia-Alvarez, R., and Escobar, A. L. (2017). Local field fluorescence microscopy: imaging cellular signals in intact hearts. *J. Vis. Exp* 121:e55202. doi: 10.3791/55202

Antzelevitch, C., and Fish, J. (2001). Electrical heterogeneity within the ventricular wall. *Basic Res. Cardiol.* 96, 517–527.

Antzelevitch, C., Sicouri, S., Litovsky, S. H., Lukas, A., Krishnan, S. C., Di Diego, J. M., et al. (1991). Heterogeneity within the ventricular wall. *Electrophysiology and pharmacology of epicardial, endocardial, and M cells*. *Circ. Res.* 69, 1427–1449.

Boyett, M. R. (1986). Current concepts on the electrophysiology of the myocardium. *J. Perinat. Med.* 14, 349–354.

Breitwieser, G. E., and Szabo, G. (1988). Mechanism of muscarinic receptor-induced K+ channel activation as revealed by hydrolysis-resistant GTP analogues. *J. Gen. Physiol.* 91, 469–493.

Brum, G., Osterrieder, W., and Trautwein, W. (1984). Beta-adrenergic increase in the calcium conductance of cardiac myocytes studied with the patch clamp. *Pflugers Arch.* 401, 111–118.

Chen-Izu, Y., Ward, C. W., Stark, W., Banyasz, T., Sumandea, M. P., Balke, C. W., et al. (2007). Phosphorylation of RyR2 and shortening of RyR2 cluster spacing in spontaneously hypertensive rat with heart failure. *Am. J. Physiol. Heart Circ. Physiol.* 293, H2409–H2417. doi: 10.1152/ajpheart.00562.2007

Choisy, S. C. M., James, A. F., and Hancox, J. C. (2012). Acute desensitization of acetylcholine and endothelin-1 activated inward rectifier K+ current in myocytes from the cardiac atrioventricular node. *Biochem. Biophys. Res. Commun.* 423, 496–502. doi: 10.1016/j.bbrc.2012.05.148

Chu, G., Lester, J. W., Young, K. B., Luo, W., Zhai, J., and Kranias, E. G. (2000). A single site (Ser16) phosphorylation in phospholamban is sufficient in mediating its maximal cardiac responses to beta -agonists. *J. Biol. Chem.* 275, 38938–38943. doi: 10.1074/jbc.M004079200

Clapham, D. E., and Kim, D. (1989). G protein activation mechanisms of the cardiac K+ channel, iK.ACh. *Soc. Gen. Physiol. Ser.* 44, 55–68.

Cohn, J. N. (1989). Sympathetic nervous system activity and the heart. *Am. J. Hypertens* 2, 353S–356S.

Collins, J. H., Kranias, E. G., Reeves, A. S., Bilezikjian, L. M., and Schwartz, A. (1981). Isolation of phospholamban and a second proteolipid component from canine cardiac sarcoplasmic reticulum. *Biochem. Biophys. Res. Commun.* 99, 796–803.

Coote, J. H. (2013). Myths and realities of the cardiac vagus. *J. Physiol.* 591, 4073–4085. doi: 10.1113/jphysiol.2013.257758

Corey, S., Krapivinsky, G., Krapivinsky, L., and Clapham, D. E. (1998). Number and stoichiometry of subunits in the native atrial G-protein-gated K+ channel, IKACh. *J. Biol. Chem.* 273, 5271–5278.

Dilly, K. W., Rossow, C. F., Votaw, V. S., Meabon, J. S., Cabarrus, J. L., and Santana, L. F. (2006). Mechanisms underlying variations in excitation-contraction coupling across the mouse left ventricular free wall: heterogeneous EC coupling in heart. *J. Physiol.* 572, 227–241. doi: 10.1113/jphysiol.2005.102020

Eisner, D. A., Díaz, M. E., O'Neill, S. C., and Trafford, A. W. (2004). Physiological and pathological modulation of ryanodine receptor function in cardiac muscle. *Cell Calcium* 35, 583–589. doi: 10.1016/j.ceca.2004.01.012

Engelstein, E. D., Lippman, N., Stein, K. M., and Lerman, B. B. (1994). Mechanism-specific effects of adenosine on atrial tachycardia. *Circulation* 89, 2645–2654.

Evans, D. B. (1986). Modulation of cAMP: mechanism for positive inotropic action. *J. Cardiovasc. Pharmacol.* 8(Suppl. 9), S22–S29.

Ferreiro, M., Petrosky, A. D., and Escobar, A. L. (2012). Intracellular Ca^{2+} release underlies the development of phase 2 in mouse ventricular action potentials. *Am. J. Physiol. Heart Circ. Physiol.* 302, H1160–H1172. doi: 10.1152/ajpheart.00524.2011

Frank, K., and Kranias, E. G. (2000). Phospholamban and cardiac contractility. *Ann. Med.* 32, 572–578. doi: 10.3109/07853890008998837

Gallego, M., and Casis, O. (2001). Regulation of cardiac transient outward potassium current by norepinephrine in normal and diabetic rats. *Diabetes Metab. Res. Rev.* 17, 304–309.

Hashimoto, N., Yamashita, T., and Tsuruzoe, N. (2006). Tertiapin, a selective IKACh blocker, terminates atrial fibrillation with selective atrial effective refractory period prolongation. *Pharmacol. Res.* 54, 136–141. doi: 10.1016/j.phrs.2006.03.021

Hayes, J. S., and Mayer, S. E. (1981). Regulation of guinea pig heart phosphorylase kinase by cAMP, protein kinase, and calcium. *Am. J. Physiol.* 240, E340–E349. doi: 10.1152/ajpendo.1981.240.3.E340

Henning, R. J. (1992). Vagal stimulation during muscarinic and beta-adrenergic blockade increases atrial contractility and heart rate. *J. Auton. Nerv. Syst.* 40, 121–129.

Hildebrandt, J. D., Sekura, R. D., Codina, J., Iyengar, R., Manclark, C. R., and Birnbaumer, L. (1983). Stimulation and inhibition of adenylyl cyclases mediated by distinct regulatory proteins. *Nature* 302, 706–709.

Hiltunen, J. O., Laurikainen, A., Airaksinen, M. S., and Saarma, M. (2000). GDNF family receptors in the embryonic and postnatal rat heart and reduced cholinergic innervation in mice hearts lacking ret or GFRalpha2. *Dev. Dyn. Off. Publ. Am. Assoc. Anat* 219, 28–39.

Huke, S., and Bers, D. M. (2008). Ryanodine receptor phosphorylation at Serine 2030, 2808 and 2814 in rat cardiomyocytes. *Biochem. Biophys. Res. Commun.* 376, 80–85. doi: 10.1016/j.bbrc.2008.08.084

Katz, A. M. (1967). Regulation of cardiac muscle contractility. *J. Gen. Physiol.* 50(Suppl.), 185–196.

Kornyeyev, D., Petrosky, A. D., Zepeda, B., Ferreiro, M., Knollmann, B., and Escobar, A. L. (2012). Calsequestrin 2 deletion shortens the refractoriness of Ca2+ release and reduces rate-dependent Ca2+-alternans in intact mouse hearts. *J. Mol. Cell. Cardiol.* 52, 21–31. doi: 10.1016/j.yjmcc.2011.09.020

Kornyeyev, D., Reyes, M., and Escobar, A. L. (2010). Luminal Ca(2+) content regulates intracellular Ca(2+) release in subepicardial myocytes of intact beating mouse hearts: effect of exogenous buffers. *Am. J. Physiol. Heart Circ. Physiol.* 298, H2138–H2153. doi: 10.1152/ajpheart.00885.2009

Krebs, E. G. (1972). Protein kinases. *Curr. Top. Cell. Regul.* 5, 99–133.

Kurachi, Y., Ito, H., Sugimoto, T., Katada, T., and Ui, M. (1989). Activation of atrial muscarinic K+ channels by low concentrations of beta gamma subunits of rat brain G protein. *Pflugers Arch.* 413, 325–327.

Lee, W. C., and Shideman, F. E. (1959). Role of myocardial catecholamines in cardiac contractility. *Science* 129, 967–968.

Leroy, J., Abi-Gerges, A., Nikolaev, V. O., Richter, W., Lechêne, P., Mazet, J.-L., et al. (2008). Spatiotemporal dynamics of beta-adrenergic cAMP signals and L-type Ca2+ channel regulation in adult rat ventricular myocytes: role of phosphodiesterases. *Circ. Res.* 102, 1091–1100. doi: 10.1161/CIRCRESAHA.107.167817

Liang, B., Nissen, J. D., Laursen, M., Wang, X., Skibsbye, L., Hearing, M. C., et al. (2014). G-protein-coupled inward rectifier potassium current contributes to ventricular repolarization. *Cardiovasc. Res.* 101, 175–184. doi: 10.1093/cvr/cvt240

Lindemann, J. P., and Watanabe, A. M. (1985). Muscarinic cholinergic inhibition of beta-adrenergic stimulation of phospholamban phosphorylation and Ca2+ transport in guinea pig ventricles. *J. Biol. Chem.* 260, 13122–13129.

Litovsky, S. H., and Antzelevitch, C. (1990). Differences in the electrophysiological response of canine ventricular subendocardium and subepicardium to acetylcholine and isoproterenol. *A direct effect of acetylcholine in ventricular myocardium*. *Circ. Res.* 67, 615–627.

López Alarcón, M. M., Rodríguez de Yurre, A., Felice, J. I., Medei, E., and Escobar, A. L. (2019). Phase 1 repolarization rate defines Ca2+ dynamics and contractility on intact mouse hearts. *J. Gen. Physiol.* 151, 771–785. doi: 10.1085/jgp.201812269

Luo, W., Grupp, I. L., Harrer, J., Ponniah, S., Grupp, G., Duffy, J. J., et al. (1994). Targeted ablation of the phospholamban gene is associated with markedly enhanced myocardial contractility and loss of beta-agonist stimulation. *Circ. Res.* 75, 401–409.

Marks, A. R. (2013). Calcium cycling proteins and heart failure: mechanisms and therapeutics. *J. Clin. Invest.* 123, 46–52. doi: 10.1172/JCI62834

Mattiazzi, A., Argenziano, M., Aguilar-Sanchez, Y., Mazzocchi, G., and Escobar, A. L. (2015). Ca2+ Sparks and Ca2+ waves are the subcellular events underlying Ca2+ overload during ischemia and reperfusion in perfused intact hearts. *J. Mol. Cell. Cardiol.* 79, 69–78. doi: 10.1016/j.yjmcc.2014.10.011

Mejía-Alvarez, R., Manno, C., Villalba-Galea, C. A., del Valle Fernández, L., Costa, R. R., Fill, M., et al. (2003). Pulsed local-field fluorescence microscopy: a new approach for measuring cellular signals in the beating heart. *Pflugers Arch* 445, 747–758. doi: 10.1007/s00424-002-0963-961

Mundiña de Weilenmann, C., Vittone, L., de Cingolani, G., and Mattiazzi, A. (1987). Dissociation between contraction and relaxation: the possible role of phospholamban phosphorylation. *Basic Res. Cardiol.* 82, 507–516.

Nakayama, T., Palfrey, C., and Fozzard, H. A. (1989). Modulation of the cardiac transient outward current by catecholamines. *J. Mol. Cell. Cardiol.* 21(Suppl. 1), 109–118.

Nerbonne, J. M., and Kass, R. S. (2005). Molecular Physiology of Cardiac Repolarization. *Physiol. Rev.* 85, 1205–1253. doi: 10.1152/physrev.00002.2005

Nikolaev, V. O., Bünemann, M., Schmitteckert, E., Lohse, M. J., and Engelhardt, S. (2006). Cyclic AMP imaging in adult cardiac myocytes reveals far-reaching beta1-adrenergic but locally confined beta2-adrenergic receptor-mediated signaling. *Circ. Res.* 99, 1084–1091. doi: 10.1161/01.RES.0000250046.69918.d5

Obayashi, M., Xiao, B., Stuyvers, B. D., Davidoff, A. W., Mei, J., Chen, S. R. W., et al. (2006). Spontaneous diastolic contractions and phosphorylation of the cardiac ryanodine receptor at serine-2808 in congestive heart failure in rat. *Cardiovasc. Res.* 69, 140–151. doi: 10.1016/j.cardiores.2005.07.010

Osterrieder, W., Brum, G., Hescheler, J., Trautwein, W., Flockerzi, V., and Hofmann, F. (1982). Injection of subunits of cyclic AMP-dependent protein kinase into cardiac myocytes modulates Ca2+ current. *Nature* 298, 576–578.

Qu, Z., Xie, L.-H., Olcese, R., Karagueuzian, H. S., Chen, P.-S., Garfinkel, A., et al. (2013). Early afterdepolarizations in cardiac myocytes: beyond reduced repolarization reserve. *Cardiovasc. Res.* 99, 6–15. doi: 10.1093/cvr/cvt104

Ramos-Franco, J., Aguilar-Sanchez, Y., and Escobar, A. L. (2016). Intact heart loose patch photolysis reveals ionic current kinetics during ventricular action potentials. *Circ. Res.* 118, 203–215. doi: 10.1161/CIRCRESAHA.115.307399

Ravens, U., Wang, X. L., and Wettwer, E. (1989). Alpha adrenoceptor stimulation reduces outward currents in rat ventricular myocytes. *J. Pharmacol. Exp. Ther.* 250, 364–370.

Rysevaite, K., Saburkina, I., Pauziene, N., Vaitkevicius, R., Noujaim, S. F., Jalife, J., et al. (2011). Immunohistochemical characterization of the intrinsic cardiac neural plexus in whole-mount mouse heart preparations. *Heart Rhythm* 8, 731–738. doi: 10.1016/j.hrthm.2011.01.013

Setién, R., Alday, A., Diaz-Asensio, C., Urrutia, J., Gallego, M., and Casis, O. (2013). Mechanisms responsible for the trophic effect of beta-adrenoceptors on the I(to) current density in type 1 diabetic rat cardiomyocytes. *Cell. Physiol. Biochem.* 31, 25–36. doi: 10.1159/000343346

Suko, J., Maurer-Fogy, I., Plank, B., Bertel, O., Wyskovsky, W., Hohenegger, M., et al. (1993). Phosphorylation of serine 2843 in ryanodine receptor-calcium release channel of skeletal muscle by cAMP-, cGMP- and CaM-dependent protein kinase. *Biochim. Biophys. Acta* 1175, 193–206.

Toyofuku, T., Kurzydlowski, K., Tada, M., and MacLennan, D. H. (1993). Identification of regions in the Ca(2+)-ATPase of sarcoplasmic reticulum that affect functional association with phospholamban. *J. Biol. Chem.* 268, 2809–2815.

Valdivia, H. H., Kaplan, J. H., Ellis-Davies, G. C., and Lederer, W. J. (1995). Rapid adaptation of cardiac ryanodine receptors: modulation by Mg2+ and phosphorylation. *Science* 267, 1997–2000.

Valverde, C. A., Kornyeyev, D., Ferreiro, M., Petrosky, A. D., Mattiazzi, A., and Escobar, A. L. (2010). Transient Ca2+ depletion of the sarcoplasmic reticulum at the onset of reperfusion. *Cardiovasc. Res.* 85, 671–680. doi: 10.1093/cvr/cvp371

Valverde, C. A., Mundiña-Weilenmann, C., Reyes, M., Kranias, E. G., Escobar, A. L., and Mattiazzi, A. (2006). Phospholamban phosphorylation sites enhance the recovery of intracellular Ca2+ after perfusion arrest in isolated, perfused mouse heart. *Cardiovasc. Res.* 70, 335–345. doi: 10.1016/j.cardiores.2006.01.018

Wickman, K., Krapivinsky, G., Corey, S., Kennedy, M., Nemec, J., Medina, I., et al. (1999). Structure, G protein activation, and functional relevance of the cardiac G protein-gated K+ channel, IKACh. *Ann. N. Y. Acad. Sci.* 868, 386–398.

Conflict of Interest Statement: The authors declare that the research was conducted in the absence of any commercial or financial relationships that could be construed as a potential conflict of interest.

frontiers in Physiology

REVIEW
published: 23 January 2020
doi: 10.3389/fphys.2019.01630

Unbalance Between Sarcoplasmic Reticulum Ca^{2+} Uptake and Release: A First Step Toward Ca^{2+} Triggered Arrhythmias and Cardiac Damage

Marilén Federico[1†], Carlos A. Valverde[1†], Alicia Mattiazzi[1] and Julieta Palomeque[1,2]*

[1] Centro de Investigaciones Cardiovasculares "Dr. Horacio E. Cingolani", CCT-La Plata/CONICET, Facultad de Cs. Médicas, Universidad Nacional de La Plata, La Plata, Argentina, [2] Centro de Altos Estudios en Ciencias Humanas y de la Salud, Universidad Abierta Interamericana, Buenos Aires, Argentina

OPEN ACCESS

Edited by:
Maria Fernandez-Velasco,
La Paz University Hospital, Spain

Reviewed by:
Sandor Gyorke,
The Ohio State University,
United States
Agustín Guerrero-Hernández,
Center for Research and Advanced Studies (CINVESTAV), Mexico

***Correspondence:**
Julieta Palomeque
jpalomeque@ciclaplata.org.ar;
pa.lomeque@hotmail.com

[†]These authors have contributed equally to this work

Specialty section:
This article was submitted to Membrane Physiology and Membrane Biophysics, a section of the journal Frontiers in Physiology

Received: 28 August 2019
Accepted: 24 December 2019
Published: 23 January 2020

Citation:
Federico M, Valverde CA, Mattiazzi A and Palomeque J (2020) Unbalance Between Sarcoplasmic Reticulum Ca^{2+} Uptake and Release: A First Step Toward Ca^{2+} Triggered Arrhythmias and Cardiac Damage. Front. Physiol. 10:1630. doi: 10.3389/fphys.2019.01630

The present review focusses on the regulation and interplay of cardiac SR Ca^{2+} handling proteins involved in SR Ca^{2+} uptake and release, i.e., SERCa2/PLN and RyR2. Both RyR2 and SERCA2a/PLN are highly regulated by post-translational modifications and/or different partners' proteins. These control mechanisms guarantee a precise equilibrium between SR Ca^{2+} reuptake and release. The review then discusses how disruption of this balance alters SR Ca^{2+} handling and may constitute a first step toward cardiac damage and malignant arrhythmias. In the last part of the review, this concept is exemplified in different cardiac diseases, like prediabetic and diabetic cardiomyopathy, digitalis intoxication and ischemia-reperfusion injury.

Keywords: sarcoplasmic reticulum Ca^{2+}-ATPase, ryanodine receptor 2, arrhythimas, phospholamban, apoptosis, diabetic myocardiopathy, isquemia-reperfusión

INTRODUCTION

Cardiovascular diseases are the leading cause of morbidity and mortality worldwide, being Ca^{2+} mishandling one of the most striking abnormalities in the setting of a wide spectrum of pathologies, including cardiac hypertrophy, heart failure, DCM, and I/R damage. Indeed, alterations that constitute the hallmark of these diseases, like contractile dysfunction, cardiac arrhythmias or cell death are in great part a reflection of the impairment in Ca^{2+} handling and the altered function of the SR, a pivotal responsible of Ca^{2+} cycling within cardiac myocytes.

The purpose of this review is: (1) To summarize the regulation of the main cardiac SR Ca^{2+} handling proteins involved in SR Ca^{2+} uptake and release, i.e., SERCA2a/PLN and RyR2. Both proteins are highly regulated by additional partners' proteins and/or PTMs that may increase or decrease their activity. (2) To describe how the disruption of the interplay among these proteins

Abbreviations: β-ARS, β-adrenergic stimulation; AGEs, advanced glycation end products; AP, action potential; Ca^{2+}, calcium; CaM, calmodulin; CaMKII, Ca^{2+}-calmodulin dependent Kinase II; CASQ2, calsequestrin; CPA, cyclopiazonic acid; DAD, delay afterdepolarizations; DCM, diabetic cardiomyopathy; EAD, early afterdepolarizations; ECC, excitation contraction coupling; ER, endoplasmic reticulum; HRC, histidine-rich Ca^{2+}binding protein; I/R, ischemia/reperfusion; MCU, mitochondrial Ca^{2+} uniporter; Na^{+}, sodium; NCX, Na^{+}/Ca^{2+} exchanger; NO, nitric oxide; $ONOO^{-}$, peroxynitrite; P_0, open probability; PKA, protein kinase A; PLN, phospholamban; PP1, type 1 phosphatase; PTM, post-translational modification; RNS, reactive nitrogen species; ROS, reactive oxygen species; RyR2, ryanodine receptor 2; SERCA2a, sarcoplasmic reticulum Ca^{2+}-ATPase; SR, sarcoplasmic reticulum; SUMO1, small ubiquitin-like modifier type 1; T2DM, type 2 diabetes mellitus.

may constitute a key determinant of Ca^{2+} triggered arrhythmias and cardiac damage. (3) To recapitulate experimental evidence in which alterations of the balance between these key players contribute to SR Ca^{2+} mishandling with the ensuing production of Ca^{2+} triggered arrhythmias and cell death in different cardiac diseases.

EXCITATION-CONTRACTION COUPLING

Cardiomyocyte excitation-contraction coupling (ECC) is the process that links membrane depolarization, at the surface cell level, with myofilament interaction that drives contraction, inside the cell. Ca^{2+} ions are the link between the two processes (**Figure 1**).

REGULATION OF CA^{2+} HANDLING PROTEINS INVOLVED IN SR CA^{2+} UPTAKE AND RELEASE

The SR orchestrates the ECC, being Ca^{2+} ions the main players. Ryanodine Receptors 2 (RyR2) and SERCA2a are highly and precisely regulated by several proteins and kinases, which allow a fine-tuned synchronization of Ca^{2+} cycling and therefore of cardiac contraction and relaxation processes. We will mention here several key modulators and PTMs of these two main proteins. For a further review see for instance (Kranias and Hajjar, 2012; Haghighi et al., 2014; Mattiazzi and Kranias, 2014; Eisner et al., 2017; Meissner, 2017; Santulli et al., 2017a,b).

Regulation of SR Ca^{2+} Uptake

SERCa2a Post-translational Modifications

Redox regulations appear to play an important role in SERCA2a function, both in health and disease. In cardiac myocytes it has been shown that oxidative stress reduces contractility with depletion of SR Ca^{2+} stores, due to SERCA2a inhibition (Morris and Sulakhe, 1997; Xu et al., 1997; Kaplan et al., 2003; Kuster et al., 2010). Indeed, several pathologies like metabolic syndrome (Balderas-Villalobos et al., 2013) or atherosclerosis (Cohen and Adachi, 2006), which are associated with an increase in oxidative stress, reduced SERCA2a activity and contractility.

Nitric oxide activates SERCA2a activity by a cGMP-independent pathway which involves the direct modification of reactive thiol groups on the protein, not only of vascular smooth muscle but also of cardiac and skeletal muscle. On its own, NO is a weak SH-group oxidant. However, in the presence of O_2^- it results in an increased $ONOO^-$ production. Under physiological conditions, the $ONOO^-$ produced may react with the thiol groups of proteins producing S-nitrosylation and S-gluthationylation of cysteine residues. S-gluthationylation increases the activity of the pump. The SERCA2a residue mainly involved in this reaction is the reactive thiol group Cys^{674} (Adachi et al., 2004). However, an exacerbated increase of $ONOO^-$ nitrosylates the hydroxyl groups of SERCA2a, producing impairment of cardiac relaxation (Braun et al., 2019).

Sarcoplasmic reticulum Ca^{2+}-ATPase is also regulated by the SUMO1 (sumoylation), by AGEs (glycation) and by acetylation/deacetylation processes. SERCA2a sumoylation appears to prolong the lifetime of SERCA2a as well as to increase its intrinsic activity by SUMO1 binding to Lys480 and Lys585 residues. Indeed, increasing SUMO1 expression restores SERCA2a levels, improves hemodynamic performance, and reduces mortality in heart failure (Kho et al., 2011). AGEs complexes can compromise the pump activity by altering the structural movements required for translocating Ca^{2+} from the cytosol to the lumen of the SR (Bidasee et al., 2004). Finally, recent experiments indicated that the acetylation of SERCA2a at K492 site was significantly increased in heart failure (HF) in association with a reduction of SIRT1, a class III histone deacetylase. Acetylation of K492 significantly diminished SERCA2a activity, possibly by interfering with the binding of ATP. Activation of SIRT1 restored SERCA2a activity. This strategy may, therefore, be useful for HF treatment (Gorski et al., 2019).

PLN Post-translational Modifications and the PLN Interactome

Undoubtedly, the main regulator of SERCA2a activity is PLN (Tada et al., 1975). PLN is a small protein (52 amino acid residues) that binds to and allosterically inhibits SERCA2a (MacLennan and Kranias, 2003). Dephosphorylated PLN reduces the affinity of SERCA2a for Ca^{2+} whereas PLN phosphorylation increases SERCA2a pump activity. There are two PLN phosphorylation sites that are physiologically relevant: Ser^{16} residue, phosphorylated by PKA and Thr^{17} site, phosphorylated by the Ca^{2+}-calmodulin-dependent protein kinase II (CaMKII) (**Figure 2A**). Phosphorylation of these sites increases the affinity of SERCA2a for Ca^{2+} and the rate of SR Ca^{2+} uptake. This, in turn, leads to increases in SR Ca^{2+} load, SR Ca^{2+} release and myocardial contractility (Lindemann et al., 1983; Lindemann and Watanabe, 1985; Mundina de Weilenmann et al., 1987; Mundina-Weilenmann et al., 1996).

The status of PLN phosphorylation, as is the case of any other protein, depends on the dynamic balance between the activity of kinases and phosphatases that phosphorylate and dephosphorylate the protein, respectively. PP1, is the major SR phosphatase that specifically dephosphorylates PLN (Steenaart et al., 1992). Inhibition of PP1 results in increased phosphorylation of PLN and SERCA2a activation (Haghighi et al., 2015; **Figure 2A**). During β-ARS, PKA phosphorylates PLN at Ser^{16} site and simultaneously inhibits PP1 through the PKA dependent phosphorylation of two additional proteins, inhibitor-1 (I-1) and the small heat shock protein 20 (Hsp20) (Qian et al., 2011). Under β-ARS, PLN-Thr^{17} site is also phosphorylated by CaMKII activation due to the increase in intracellular Ca^{2+} and the inhibition of PP1, produced by the activity of PKA. In contrast, phosphorylation of Thr^{17} of PLN does not occur when only intracellular Ca^{2+} was increased without PKA activation, which is necessary to inhibit PP1 (Mundina-Weilenmann et al., 1996).

Post-translational modification of phospholamban by reactive oxygen and nitrogen species (ROS and RNS, respectively) may

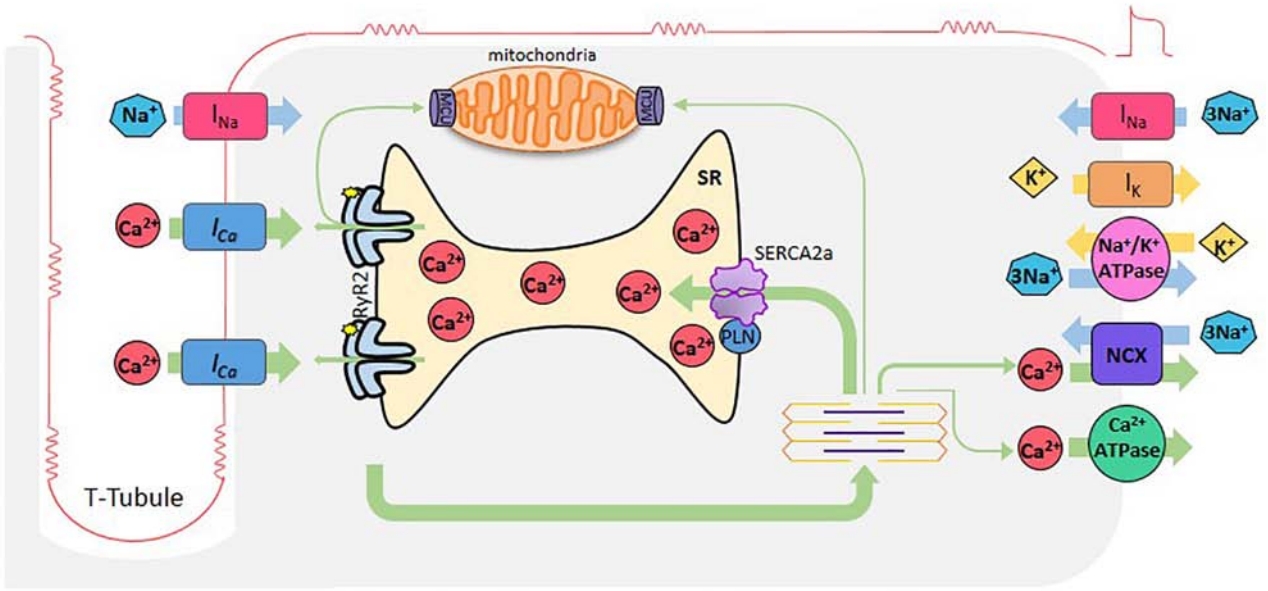

FIGURE 1 | Cardiac excitation-contraction coupling. When cardiomyocytes are reached by an AP, depolarization of the plasma membrane by Na^+ entry (I_{Na}), induces the opening of L-type Ca^{2+} channels. Ca^{2+} entering through these channels (Ca^{2+} current, I_{Ca}), induces Ca^{2+} release by the RyR2s (Ca^{2+}-induced-Ca^{2+}-release), which subsequently activates myofilaments for muscle contraction. Relaxation occurs when SR -Ca^{2+} ATPase (SERCA2a) reuptakes Ca^{2+}, lowering cytosolic Ca^{2+} concentration in combination with Ca^{2+} extrusion via the Na^+- Ca^{2+} exchanger (NCX) working in reverse mode and the sarcolemma Ca^{2+}-ATPase. Mitochondria also participate taking and extruding Ca^{2+} from the cytosol during Ca^{2+} cycle. Green arrows depict Ca^{2+} fluxes.

also influence SR Ca^{2+} uptake (Bigelow and Squier, 2005; Froehlich et al., 2008; Lancel et al., 2009; Ha et al., 2011). Among these PTM it is interesting to mention the one-electron reduction product of NO, nitroxyl (HNO). This molecule has received special attention not only as a possible signaling molecule in the cardiovascular system but also as a potential therapeutic strategy for HF treatment due to its positive inotropic and lusitropic effects in normal and failing canine hearts (Paolocci et al., 2001, 2003; Sivakumaran et al., 2013). PLN played a central role in these effects of HNO, by enhancing SERCA2a activity (Froehlich et al., 2008). Moreover, it has been suggested that S-nitrosylation of PLN at Cys^{36} and Cys^{41} modulates the PLN-dependent regulation of SERCA2a during β-ARS, i.e., S-nitrosylation of PLN is required for stabilization of the pentameric form of PLN, and consequent SERCA2a activation (Irie et al., 2015). Several additional regulatory proteins are associated with PLN and SERCA2a and contribute to the control of SR Ca^{2+}-transport. These include the hematopoietic lineage cell-specific protein-1 (HS-1) associated protein X-1 (HAX1), a ∼35 kDa protein, which was identified forming a complex with HS-1 in lymphocytes (Suzuki et al., 1997), the intra-luminal histidine-rich Ca^{2+} binding protein (HRC), which has been shown to interact with both SERCA2a and triadin on the SR luminal side (see below and **Figure 2C**) and S100A1 on the cytosolic side (Kiewitz et al., 2003). Ca^{2+}-dependent S100A1 binding to SERCA2a results in an increased enzymatic activity which is associated with enhanced SR Ca^{2+} uptake and load (Most et al., 2001; Kiewitz et al., 2003; Kettlewell et al., 2005). As will be discussed below, HRC and S100A1 also interact and regulate RyR2 and SR Ca^{2+} release (Völkers et al., 2007; for review, see Haghighi et al., 2014; Kranias and Hajjar, 2017; Arvanitis et al., 2018).

Regulation of SR Ca^{2+} Release

Ryanodine receptor 2 is the largest ion channel known in nature and one of the most relevant Ca^{2+} handling proteins. RyR forms a homotetrameric assembly comprising four monomers of 565 kDa each (Van Petegem, 2015). There are three mammalian isoforms that share 65% sequence identity: RyR1, predominantly expressed in skeletal muscle; RyR2, the cardiac isoform and RyR3, expressed in several tissues including the brain (Capes et al., 2011). While at the cytosolic portion, the channel contains multiple regulatory domains, such as binding sites for energy sensors (ATP, ADP, and AMP) (**Figure 2B**), and inorganic phosphate, metabolites such as pyruvate, fatty acids and polyamines, and ions (Mg^{2+}, H^+, and Cl^-, not shown in the Figure for the sake of clarity) (Zucchi and Ronca-Testoni, 1997; Fill and Copello, 2002; Meissner, 2004); the Ca^{2+} binding site is located in the core domain of the channel just above the transmembrane domain an involves de carboxyl-terminal domain region (Murayama et al., 2018). This complex is also regulated and modulated by a diverse array of RyR2-interacting proteins which involve PKA, CaMKII, phosphatases (i.e., phosphatase 1 and 2A), and phosphodiesterase (PDE4D) which are tethered to the channel and held near their target sites by means of anchoring proteins (Marks, 2002; Lehnart et al., 2005). This allows for a tight and spatially confined homeostatic regulation of the balance between RyR2 phosphorylation and phosphatase dependent dephosphorylation.

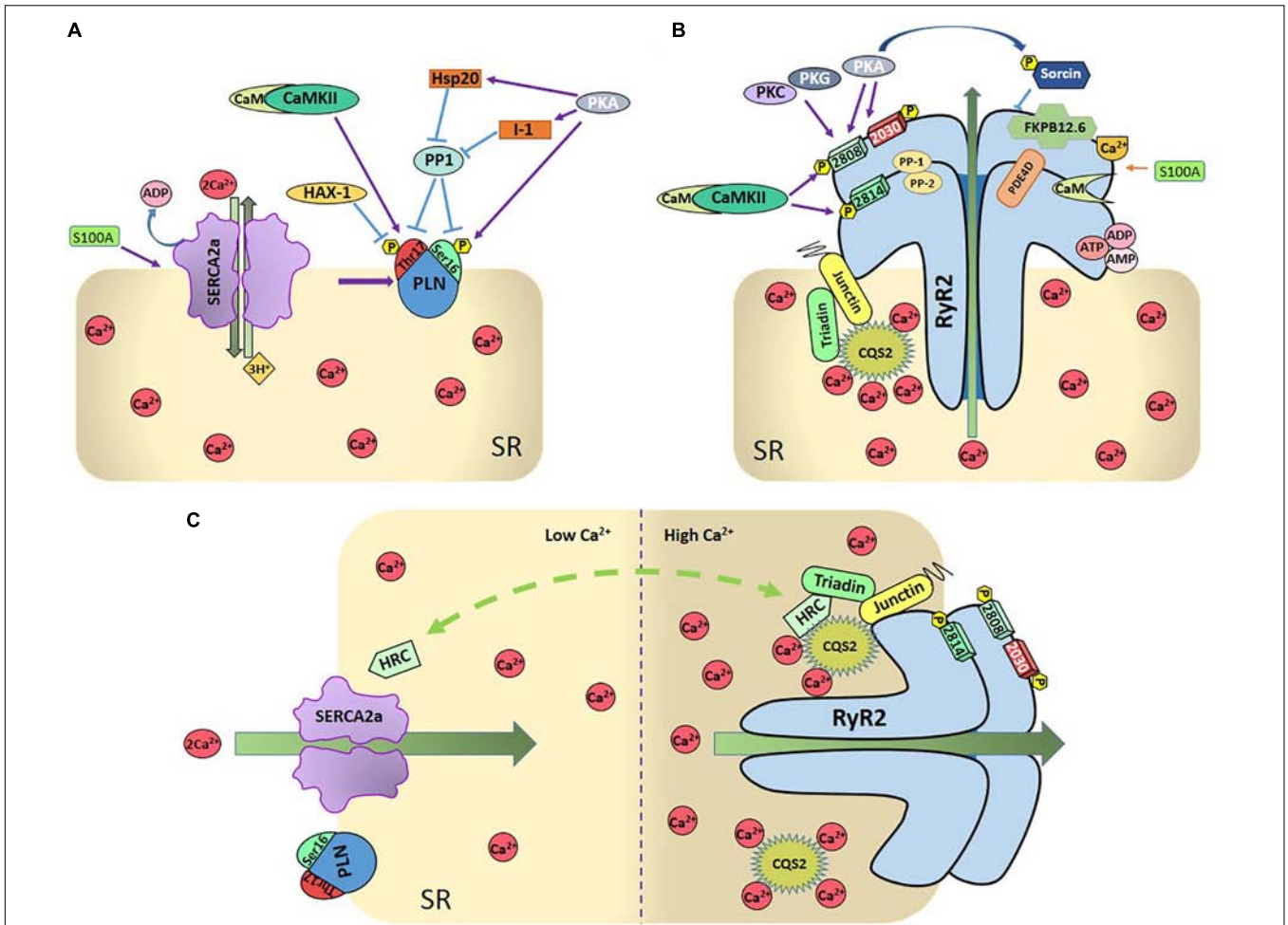

FIGURE 2 | (A) Regulation of SR-Ca^{2+} uptake. SR- Ca^{2+} uptake takes place through the SR- Ca^{2+} ATPase (SERCA2a), being PLN the main regulatory protein of SERCA2a. PLN can be phosphorylated by PKA at Ser^{16} residue and by Ca^{2+}-calmodulin-dependent protein kinase (CaMKII) at Thr^{17} site. Protein phosphatase 1 (PP1) dephosphorylates both sites. Either one or both phosphorylation sites relieve PLN inhibition on SERCA2a. Several other proteins regulate SERCA2 either directly, like S100A or Sumo1, or indirectly, through the regulation of PLN (like the hematopoietic lineage cell-specific protein-1 (HS-1) associated protein X-1 (Hax-1), the Heat-shot protein 20 (Hsp20), and the inhibitor 1 (I-1). As described in the text, PLN and SERCA2a are also regulated by redox processes and SERCA by acetylation and glycation (Not shown in the Figure for the sake of clarity). **(B)** Regulation of SR-Ca^{2+} release: SR-Ca^{2+} release occurs mainly through the RyR2 which are also highly regulated. CaMKII phosphorylates RyR2 at Ser2814 and S2808 sites and PKA at Ser2808 and 2030 sites. Ser2808 is also target of protein-kinase C (PKC) and protein-kinase G (PKG). PP1 and PP2 are the phosphatases that dephosphorylate RyR2. Other regulatory proteins are sorcin, S-100 at the cytosolic side, FKB12.6 and calmodulin (Cm), bounded to RyR2, CASQ2, triadin, and juntin at the cytosolic site. Phosphodiesterase (PDE), ions, and nucleoside phosphates (AMP, ADP, and ATP) are also bounded to RyR2. **(C)** Dual role of HRC: The intra-luminal protein histidine-rich calcium binding protein (HRC) interacts with SERCA2a as well as with triadin in a Ca^{2+}-dependent fashion, increasing RyR2 Ca^{2+} release and SERCA2a Ca^{2+}-uptake when Ca^{2+} increases in SR.

Post-translational Modifications of RyR2

Phosphorylation is possibly the most studied and controversial PTM modification of RyR2. Phosphorylation of the channel modulates the effect of Ca^{2+} on the RyR2 without having the inherent ability to open or close the channel *per se* (Camors and Valdivia, 2014). Until now three phosphorylation sites in the RyR2 have been identified: Ser^{2808}, Ser^{2814}, and Ser^{2030} (**Figure 2B**). Serine 2808 (Ser^{2808}, mouse, and Ser2809 in human and canine RyR2 nomenclature) was first described by Witcher and collaborators as a CaMKII site (Witcher et al., 1991). Further in-depth studies of this phospho-site indicated that Ser^{2808} is a target for PKA, CaMKII and possibly PKG (Jiang et al., 2002; Rodriguez et al., 2003; Stange et al., 2003; Currie et al., 2004; Ai et al., 2005; Xiao et al., 2005; Carter et al., 2006; Kohlhaas et al., 2006; Ferrero et al., 2007; Huke and Bers, 2008; MacDonnell et al., 2008; Fischer et al., 2013). Experiments by Marx et al. (2000) indicated that PKA-dependent phosphorylation of RyR2 at Ser^{2808} site under β-ARS, increases P_0 and SR Ca^{2+} release. However, this contention was not supported by different studies and the functional meaning of this phosphorylation is not clear yet (Xiao et al., 2006; Ferrero et al., 2007; Huke and Bers, 2008). This is in part due to the fact that most studies found that Ser^{2808} is constitutively phosphorylated under basal conditions (Jiang et al., 2002; Rodriguez et al., 2003; Carter et al., 2006; Ferrero et al., 2007; Huke and Bers, 2008), generating doubts about the relevance of "extra" phosphorylation on this site. Moreover, it

was also showed that RyR2s were hyperphosphorylated in failing hearts from humans and dogs at Ser^{2809}, which was attributed at least in part to a decrease in the amount of PP1 associated to RyR2 (Marx et al., 2000; Wehrens et al., 2006). However, several subsequent experiments by other groups failed to reproduce these findings (Li et al., 2002), turning the attention to serine 2814 (Ser^{2814}) site as the primary phosphorylation site responsible for SR Ca^{2+} leak and arrhythmogenic events in HF (Li et al., 2002; Respress et al., 2012). The role of Ser^{2808} phosphorylation was further complicated by the finding that both, minimum and maximum RyR2 phosphorylation at Ser^{2808}, increase RyR2 activity, suggesting a U-shaped of RyR2 activity according to the PKA phosphorylation level (Carter et al., 2006). A clear revision of these controversial results is given by Bers (Bers, 2012) and Camors and Valdivia (Camors and Valdivia, 2014).

Ser^{2814} site was described by Wehrens et al. (2004) as a CaMKII site and further evidence confirmed that this site seems to be exclusively phosphorylated by CaMKII. In single-channel experiments, the P_0 of the RyR2s was generally found to be increased upon phosphorylation by CaMKII (Lokuta et al., 1995; Wehrens et al., 2004; Yang et al., 2007). In line with these results, either activation or overexpression of CaMKII was associated with the positive inotropic effect of β-ARS (Ferrero et al., 2007), an increase of Ca^{2+} spark frequency (Guo et al., 2006) and the susceptibility to arrhythmias (Maier et al., 2003; Dybkova et al., 2011; Respress et al., 2012; Mazzocchi et al., 2016; Valverde et al., 2019). In contrast, animals in which Ser^{2814} was replaced by Alanine (S2814A mice) were protected from arrhythmias and cardiac dysfunction induced by several diseases (van Oort et al., 2010; Di Carlo et al., 2014; Mazzocchi et al., 2016).

Serine 2030 (Ser^{2030}) was characterized as a PKA phosphorylation site using classical phospho-epitope mapping (Xiao et al., 2005). Whereas in quiescent cardiac myocytes the RyR2 appears to be completely unphosphorylated (Huke and Bers, 2008), this site has been suggested as the major phosphorylation site in RyR2 responding to PKA activation upon β-ARS in normal and failing hearts (Xiao et al., 2006). In this context, it has recently been described that phosphorylation of RyR2 at Ser^{2030} is required for a complete effect of β-ARS (Potenza et al., 2019) in mouse lines with genetic ablation of this site (RyR2-S2030A).

Interestingly, recent work reports crystal structures of the RyR2 phosphorylation domain with the PKA catalytic subunit (PKAc), showing Ser^{2808} captured within the active site of PKA. The results further demonstrated that the addition of a phosphomimetic at the CaMKII site (S2814D), results in structural changes in the RyR2 phosphorylation domain that enhance the interaction with PKAc. These findings strongly suggest that phosphorylation of Ser^{2814} site may affect the activity of PKA and impact on Ser^{2808}, i.e., nearby phosphorylation sites might influence one each other (Haji-Ghassemi et al., 2019). This possible interaction among the different residues sharing the phosphorylation "hotspot" region of RyR2, might clarify previous controversial findings on the role of Ser^{2808} site on different physiological and disease situations. Since RyR2 phosphorylation by PKA and CaMKII may not be independent, the authors suggest that the phosphorylation status of Ser^{2808} may be altered in studies that have used S2814D mice. Of note, in contrast with this prediction, previous experiments indicate that isoproterenol-induced phosphorylation of RyR2-Ser^{2808} site did not vary when isoproterenol was administrated in the absence and presence of a CaMKII inhibitor (KN-93), to avoid the simultaneous phosphorylation of Ser^{2814} residue (Ferrero et al., 2007), i.e., phosphorylation of Ser^{2814} did not influence the extent of phosphorylation of Ser^{2808} site. However, the isoproterenol concentration used in these experiments was rather high and may not allow any further PKA-dependent phosphorylation of this site. Therefore, it would be important to perform similar experiments in the presence of lower isoproterenol concentrations to investigate the possible influence of Ser^{2814} phosphorylation on the isoproterenol-induced phosphorylation of Ser^{2808} site predicted by the crystal structure studies.

The role of phosphatases activity on RyR2 phosphorylation was recently emphasized. It was shown that PP1 activation counteracts the increased kinase activity in human heart failure reducing SR Ca^{2+} leak as well as cellular arrhythmias without significant changes in SR Ca^{2+} load and contractility (Fischer et al., 2018).

Oxidative conditions generally increase the RyR2 P_0, while reducing agents do the opposite (Marengo et al., 1998; Xu et al., 1998; Salama et al., 2000; Sun et al., 2008). The functional consequence of a moderate cellular oxidative/nitrosative stress could result in an immediate enhancement of Ca^{2+} release from the SR in response to a given physiological trigger. However, severe oxidative stress can cause irreversible and persistent activation of RyR2s (Xu et al., 1998), increasing SR Ca^{2+} leak. It has been reported that NADPH oxidase 2 (NOX2) is the predominant isoform expressed in T-tubules and SR membranes of adult cardiomyocytes. Therefore, it is strategically positioned to modulate the activity of the RyR2s. ROS produced by NOX2 stimulates SR Ca^{2+} release via at least two pathways: direct oxidation or S-glutathionylation of RyR2s or indirectly through CaMKII activation (Palomeque et al., 2009), followed by phosphorylation of the RyR2s. In healthy cardiac muscle neuronal nitric oxide synthase (nNOS) is mainly located in the SR membrane, linked to the RyR2s, which would favor direct RyR2 nitrosation. The role of this PTM of RyR2 on cardiac ECC has been previously reviewed (Lim et al., 2008; Gonzalez et al., 2009).

The RyR2 Complex

Ryanodine receptor 2 modulation has been shown to involve also several key proteins (**Figure 2B**), most importantly CASQ2. CASQ2 not only acts as a Ca^{2+} buffer, but it also mediates the responsiveness of the RyR2 channel to luminal Ca^{2+} by serving as a Ca^{2+} sensor (Gyorke et al., 2004; Gyorke and Terentyev, 2008). This function is effective through protein-protein interactions, with junctin and triadin (Zhang et al., 1997; Shin et al., 2000). However, a direct interaction between CASQ2 and RyR2 has recently been described (Handhle et al., 2016). Junctin is a 26 kDa transmembrane protein forming a complex with triadin, CASQ2, and RyR2. It has been proposed that junctin is in direct contact with RyR2 and works as an anchor for CASQ2 (Zhang et al., 1997; Gyorke et al., 2004).

Calstabin 2 or FKBP12.6, is a peptidyl-prolyl cis/trans-isomerase of 12.6 kDa, associated with RyR2 with a stoichiometry of 4:1 (**Figure 2B**). The role of FKBP12.6 has been a matter of controversy for over the past two decades (Kaftan et al., 1996; Timerman et al., 1996; Barg et al., 1997; Marks, 2000; Doi et al., 2002; Jiang et al., 2002; Stange et al., 2003; Wehrens et al., 2003; Xiao et al., 2007; Guo et al., 2010). FKBP12.6 has been considered as RyR2 "stabilizer," since some results indicate that FKBP12.6 dissociation from RyR2 produces RyR2 sub-conductance states and increase the Po of the channel. However, other piece of evidence indicates that FKBP12.6 failed to show any effect of FKBP12.6 on RyR2 gating. The recent identification of FKB12 binding site on RyR2 may help to understand the controversial matters encompassing the FKBP-RyR2 interactions. FKBP12 binds to RyR2 with lower affinity than FKBP12.6, but has a higher cardiac expression level (Jeyakumar et al., 2001). Recent results revealed that only 20% of RyR2 proteins are associated with FKBP12.6 in myocytes (Guo et al., 2010) which could explain why RyR2 is unaffected in FKBP12.6-KO mice (Xiao et al., 2007). Acute overexpression of FKBP12 in adult rabbit ventricular myocytes showed a reduction in the gain of ECC and a decrease in Ca^{2+} spark frequency, suggesting that FKBP12 reduces RyR2 sensitivity to cytosolic Ca^{2+}(Seidler et al., 2007). In contrast, more recent results show that FKBP12 activates the RyR2 and competes with FKBP12.6. The last study, would suggest that rather than a direct stabilization of the channel, an increase in FKBP12.6-RyR2 binding competes with FKBP12 at the same binding site and blunts the activation of RyR2 promoted by FKBP12 (Galfre et al., 2012).

Apo-Calmodulin or Ca^{2+}-free CaM has an inhibitory effect on RyR2 channel. The Ca^{2+}-bound CaM is named Ca^{2+}-CaM. Although Ca^{2+}-CaM is the usual form that binds to target proteins, CaM can also bind to RyR2. CaM shifts the Ca^{2+}-dependence of RyR2 activation to higher Ca^{2+} concentrations (Fruen et al., 2000; Balshaw et al., 2001; Yamaguchi et al., 2005). The role of CaM on RyR2 regulation was highlighted by results that indicate that mutations in CaM are associated with RyR2-mediated cardiac arrhythmias (Nomikos et al., 2014; Sondergaard et al., 2017). High resolution cryo-electron microscopy recently provided new insights into the modulation of RyR2 channel gating by CaM (Gong et al., 2019). These data indicate that Ca^{2+}-CaM changes RyR2 conformation differently under different situations. Whereas Ca^{2+}-CaM can reverse RyR2 opening by Ca^{2+} and PCB95, a potent channel opener (Samso et al., 2009), it cannot counteract the activation of the channel by a mixture of Ca^{2+}, ATP and caffeine. These results emphasize that the P_0 of RyR2 is critically determined by a strict balance between different activators and inhibitors of the channel (Van Petegem, 2019).

Several proteins that interact with SERCA2a regulating SR Ca^{2+} uptake, also modify the RyR2 function. As already mentioned, the HRC protein is not only associated with SERCA2a but also with triadin. The interaction of HRC with triadin increases with increasing Ca^{2+} concentration (Sacchetto et al., 1999; Arvanitis et al., 2007). This interaction is believed to modulate RyR2 function and SR Ca^{2+} release by conferring refractoriness to SR Ca^{2+} release. In turn, HRC-SERCA2a interaction is also Ca^{2+}-dependent. In this case, the maximal HRC-SERCA2a association occurs at low Ca^{2+} concentration and diminishes with increasing Ca^{2+} concentrations (Arvanitis et al., 2007). The different Ca^{2+} dependence of the interaction HRC-SERCA2a and HRC-triadin determines the HRC effects on SR Ca^{2+} handling (**Figure 2C**): At low SR Ca^{2+}, HRC interacts with SERCA2a inhibiting SR Ca^{2+} uptake. When SR Ca^{2+} concentration increases, HRC dissociates from SERCA2a and enhances its binding to triadin, regulating SR Ca^{2+} release (for review, see Arvanitis et al., 2018).

Sorcin is a 22 kDa penta-EF hand Ca^{2+}-binding protein expressed in many tissues, including the heart. Single-channel studies indicated that when applied to the cytoplasmic region of RyR2s, sorcin inhibits RyR2 activity in a dose-dependent manner by prolonging the mean close time without modifying single-channel conductance, an effect that is abrogated when sorcin is phosphorylated by PKA. More recent experiments (Farrell et al., 2003) demonstrated that sorcin significantly inhibits both the spontaneous activity of RyR2s in quiescent cells and the Ca^{2+} current (I_{Ca})-triggered activity of RyR2s. Moreover, it decreased the amplitude of the Ca^{2+} transient without affecting the amplitude or kinetics of I_{Ca}, reducing the "gain" of ECC mechanism. Sorcin seems to be a key RyR2-associated protein under stress conditions since its ablation displayed a significantly higher incidence of cardiac arrhythmias and sudden death in sorcin-KO mice when subjected to acute or chronic stress challenge (Chen et al., 2018). It has also been shown that sorcin increases SR Ca^{2+} uptake (Matsumoto et al., 2005) and interacts with NCX (Zamparelli et al., 2010) and L-type Ca^{2+} channels (LTCC) (Fowler et al., 2008). All these interactions point to an important role of this protein in ECC regulation.

Also, as in the case of SERCA2a, S100A1 modulates RyR2 function under both diastolic and systolic conditions (Kiewitz et al., 2003; Most et al., 2004; Völkers et al., 2007, Volkers et al., 2010). Most et al. (2004), first demonstrated that addition of S100A1 to isolated SR vesicles resulted in diminished ^{3}H-ryanodine ([^{3}H]Ry) binding to RyR2 at free Ca^{2+} concentrations of about 150 nM, while a significantly increased [^{3}H]Ry binding occurred at Ca^{2+} concentrations greater than 300 nM. Hypothesizing a reduced RyR2 P_0 at diastolic cytoplasmic Ca^{2+} levels, S100A1 would reduce SR Ca^{2+} leak in quiescent cardiomyocytes (Völkers et al., 2007). Moreover, S100A1 increases fractional SR Ca^{2+} release in voltage-clamped rabbit cardiomyocytes, suggesting that S100A1 enhances the ECC gain under systolic conditions (Kettlewell et al., 2005).

Cytosolic and Luminal Ca^{2+} Regulation of RyR2

Both cytosolic and luminal Ca^{2+} regulate RyR2. It has long been known that the release of SR Ca^{2+} in cardiac muscle during ECC is graded by the amount of activating Ca^{2+} outside the SR by the Ca^{2+}-induced Ca^{2+} release (CICR) process (Fabiato and Fabiato, 1977). Experimental evidence suggested the presence of high and low affinity Ca^{2+} binding sites in the cytosolic region of RyR2 and luminal Ca^{2+}-binding sites, whose luminal occupancy depends on SR Ca^{2+} load (Fabiato and Fabiato, 1979; Shannon et al., 2000). RyR2s are normally closed at low cytosolic Ca^{2+} (100–200 nM); channel activity is maximal at 10–100 μM cytosolic Ca^{2+}, while elevating cytosolic

Ca^{2+} beyond this point leads to a reduction in P_0 (Xu and Meissner, 1998). This biphasic behavior implies there are at least two classes of Ca^{2+} binding sites: high-affinity activation and low-affinity inactivation sites. The P_0 steep dependence of RyR2 on cytoplasmic Ca^{2+}, which typically exhibits Hill coefficients of 2–4 (Sitsapesan and Williams, 1994) indicates that RyR2 activation resulted from cooperative involvement of one high-affinity (∼1 μM) Ca^{2+} binding site on each subunit of the homotetrameric channel (Zahradnik et al., 2005). RyR2s also possess two inhibitory sites in their cytoplasmic domains with Ca^{2+} affinities of the order of 1 μM and 1 mM. Mg^{2+} competes with Ca^{2+} at these sites to inhibit RyR2s (for instance, see Laver, 2018).

In 1994, Sitsapesan and Williams were the first to show that luminal Ca^{2+} could directly activate RyR2 (Sitsapesan and Williams, 1994). Since then, different type of evidence supports the notion that luminal Ca^{2+} controls RyR2 function (i.e., Bassani et al., 1995; Gyorke and Gyorke, 1998; Shannon et al., 2000; Kong et al., 2007; Gyorke and Terentyev, 2008). Two different mechanisms have been proposed to explain luminal Ca^{2+} regulation of RyR2: The "feed-through" hypothesis suggests that luminal Ca^{2+} acts on its own cytosolic Ca^{2+} binding site during or after Ca^{2+} passage through an open RyR2 (Herrmann-Frank and Lehmann-Horn, 1996; Xu and Meissner, 1998). A second mechanism proposes that luminal Ca^{2+} regulation of RyR2 is mediated by a Ca^{2+} sensing mechanism inside the SR (Gyorke and Gyorke, 1998; Ching et al., 2000; Jiang et al., 2007; Gyorke and Terentyev, 2008). Although CASQ2, may serve as a key SR luminal Ca^{2+} sensor (Gyorke et al., 2004), experiments in CASQ2-null mice (Knollmann et al., 2006) and in purified native and recombinant RyR2s that lack CASQ2 (Xu and Meissner, 1998; Kong et al., 2007), indicate that RyR2s are also regulated by a luminal Ca^{2+} sensing mechanism that does not require CASQ2. Indeed, a point mutation in RyR2 (RyR2-E4872A) which eliminates Ca^{2+} regulation by luminal but not by cytosolic Ca^{2+} was recently identified (Chen et al., 2014). Structural analysis, at near-atomic resolution, suggests that in addition to E4872, the E4878 residue may also be involved in luminal Ca^{2+} activation of RyR2 (Peng et al., 2016), although the precise mechanism by which each of these different sites promotes luminal Ca^{2+} activation of RyR2 is not clear yet.

HOW CAN THE DISRUPTION OF THE NORMAL INTERPLAY AMONG SR CA^{2+} HANDLING PROTEINS EVOKE CA^{2+} TRIGGERED ARRHYTHMIAS AND APOPTOSIS?

The normal interplay among the different proteins responsible for the release and reuptake of Ca^{2+} by the SR is regulated by different mechanisms as reviewed above. This regulation may be altered and evolve toward different types of cardiac disorders, which include arrhythmias and cell death through apoptotic and necrotic processes. Therefore, regulation and/or alteration of SR Ca^{2+} handling proteins (for instance by phosphorylation, redox changes or mutations), have received great attention from physiologists and clinicians. We will describe below two main consequences of the unbalance of SR Ca^{2+} uptake and release, i.e., Ca^{2+} triggered arrhythmias and cellular apoptosis and necroptosis, with a main focus on those produced by PTM of Ca^{2+} handling proteins.

Ca^{2+} Triggered Arrhythmias

Mechanisms

As stated above, RyR2s are highly regulated molecules. Genetic or PTM of RyR2 are a main cause of Ca^{2+} triggered arrhythmias, i.e., arrhythmias that are originated due to abnormal Ca^{2+} handling.

Triggered activity describes impulse initiation that is dependent on the so-called afterdepolarizations, which are oscillations in membrane potential that follow the primary depolarization phase (0) of an AP. Afterdepolarizations are divided into early and delayed afterdepolarizations, EAD, and DAD, respectively. EADs are defined as a slowing or reversal of normal repolarization that occurs before completion of AP, usually in phases 2 and 3 of human AP, whereas DADs occur after AP completion (**Figure 3**). These mechanisms may produce sustained arrhythmias by reentry circuits (Anderson, 2007). EADs occurs usually in the setting of prolonged repolarization and are classically attributed to reactivation of I_{Ca} (January and Riddle, 1989; Nuss et al., 1999). However, a second major current that facilitates EADs formation is NCX. Indeed, experimental evidence indicates that these two currents act synergistically to generate EADs, with their relative contributions varying under specific conditions (Weiss et al., 2010). The late component of the Na^+ current (I_{Na}), has been recognized as an important player to set up the conditions for EADs, by producing SR Ca^{2+} overload, via the reduction of repolarization reserve and the increase in intracellular Na^+ concentration. In addition, experimental evidence and modeling studies indicate that EADs may directly arise from Na^+ channel reactivation (Horvath et al., 2013; Sato et al., 2017; **Figure 3A**).

Delay afterdepolarizations are caused by spontaneous Ca^{2+} releases from the SR (Bers, 2006). Under conditions of SR Ca^{2+} overload and/or in circumstances which sensitize the RyR2s, the Ca^{2+} released by a group of RyR2 activates neighboring RyR2, in such a way that Ca^{2+} propagates in a regenerative way traveling along the myocytes in a saltatory fashion from sarcomere to sarcomere (Cheng et al., 1996). Ca^{2+} waves have substantial arrhythmogenic potential, since they may trigger Ca^{2+} activated currents, such as the NCX current (I_{NCX}). This promotes a transient Na^+ current (It_i), that depolarizes cell membrane and may eventually trigger a spontaneous AP (Bers, 2006), which is referred to as triggered AP, leading to spontaneous contraction (Spencer and Sham, 2003; Fujiwara et al., 2008; Mazzocchi et al., 2016; **Figure 3B**).

When referring to a multicellular tissue, e.g., whole heart, spontaneous Ca^{2+} releases synchronized in a small group of cells is not enough for triggering an AP. 3D modeling (Xie et al., 2010) estimated that about 800,000 cells are required to trigger a premature ventricular complex, being able to bring

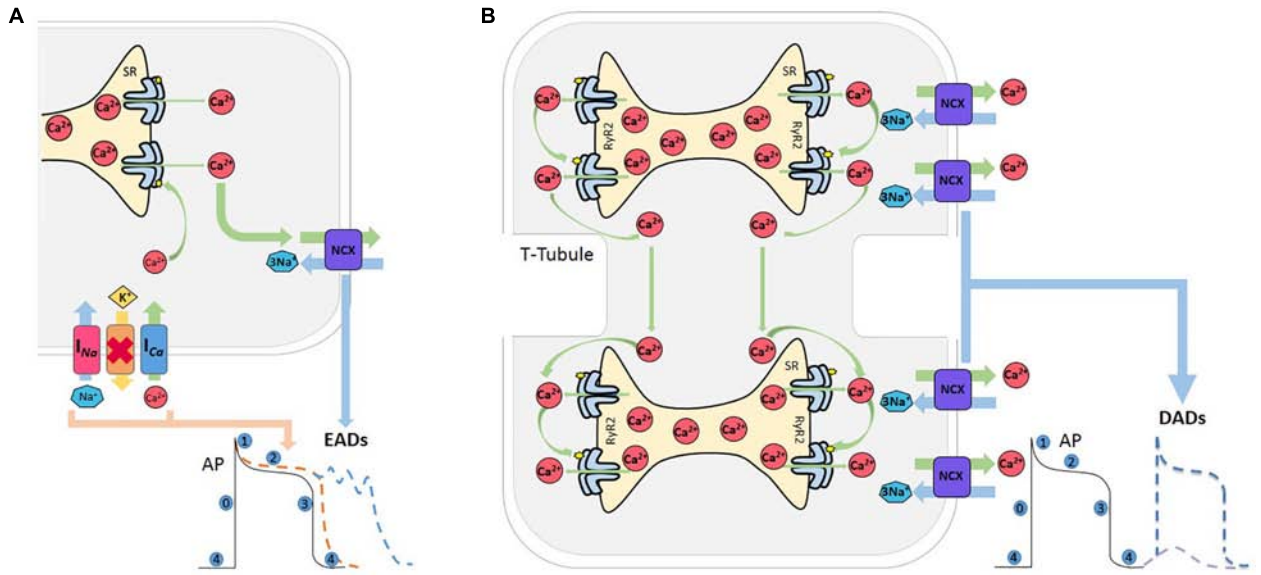

FIGURE 3 | Afterdepolarizations. **(A)** Reactivation of L-type Ca^{2+} current (I_{Ca}) during prolongation of the AP, mainly during phase 2 or 3, increases the propensity for EADs. The Na^{+}-Ca^{2+} current (NCX) also meets the criterion needed for the positive feedback required for an EAD to occur. Both currents can act synergistically facilitating EAD formation, and thus increasing the probability of an EAD-triggered AP. Red cross indicates inhibition of K^{+} channels. **(B)** Various conditions which increase SR-Ca^{2+} and/or sensitize RyR2 can induce spontaneous Ca^{2+} release from the SR. When this release achieves certain critical mass, Ca^{2+} can induce a saltatory propagation along cell sarcomeres, known as Ca^{2+} waves, which in turn activates the NCX that extrude 2 Ca^{2+} and enter 3 Na^{+}, depolarizing the cell membrane and producing a delay after depolarization (DAD). If this depolarization attains the excitability threshold, a spontaneous AP occurs.

the sink (adjacent tissue in basal conditions) to its activation threshold. A sort of synchronization mechanism must exist for EADs and DADs to overcome the source-sink mismatch. Normally, in an intact tissue, the source-sink mismatch is the main mechanism protecting the heart against spontaneous Ca^{2+} release-induced arrhythmias.

The Threshold Concept

In the context of Ca^{2+} triggered arrhythmias, an intriguing issue to consider is the SR Ca^{2+} *threshold*. As mentioned above, spontaneous SR Ca^{2+} leak can occur in the absence of membrane depolarization. It has long been known that several conditions that increase SR Ca^{2+} load increase SR Ca^{2+} waves and spontaneous contractions (Orchard et al., 1983; Stern et al., 1983; Wier et al., 1987). Diaz et al. (1997) showed that increasing extracellular Ca^{2+} in quiescent cells produced spontaneous Ca^{2+} release associated with increased SR Ca^{2+} content (Diaz et al., 1997). Once spontaneous Ca^{2+} release arose, further increase in extracellular Ca^{2+} did not affect SR Ca^{2+} content because of the proportional increase in SR Ca^{2+} leak. The authors conclude "It appears there is a maximum level of SR Ca^{2+} content, perhaps because spontaneous release results when the content reaches a threshold"(Diaz et al., 1997). Due to its dependence on the SR Ca^{2+} store, this depolarization–independent SR Ca^{2+} release has been called "Store Overload-Induced Ca^{2+} Release (SOICR)"(Jiang et al., 2004). It has been further shown that the threshold level also depends on the activity of RyR2. One important premise of this mechanism is that ". . .once a threshold level of SR Ca^{2+} content is reached, SOICR occurs"(Jiang et al., 2004). More recent experiments by Belevych et al. (2012) challenged the idea of *immediacy* that encompasses the last concept. These authors demonstrated that SR Ca^{2+} leak occurs with a substantial time delay after the attainment of diastolic SR Ca^{2+} level, i.e., the attainment of a certain SR Ca^{2+} level is not sufficient for spontaneous Ca^{2+} release and waves generation. The time factor is necessary. Interestingly, the post-refilling refractory period was shorter in myocytes from infarcted hearts than in control myocytes, even though the rate of SR Ca^{2+} content recovery after the stimulus-induced SR Ca^{2+} release was similar. Based on these and other results (Sobie et al., 2005), it was concluded that the probability of spontaneous Ca^{2+} triggering also depends on the recovery of RyR2 from refractoriness (time and Ca^{2+} store–dependent properties of RyR2). In post-infarction myocytes the post-refilling refractory period was reduced, an effect attributed to CaMKII phosphorylation and redox modifications of RyR2. **Figure 4** schematizes a possible interpretation of the experimental results.

Ca^{2+}-Induced Apoptosis and Necroptosis

It is generally accepted that mitochondria are at the central stage of cell death (Finkel, 2001; Dorn and Maack, 2013; Pan et al., 2013). Indeed, numerous recent investigations revealed the mitochondria are effectors of programed apoptosis or necrosis and sources of damaging ROS.

Mitochondria are organelle in close association with the SR. This proximity allows a cross-talk between mitochondria and SR which is extremely valuable under normal conditions:

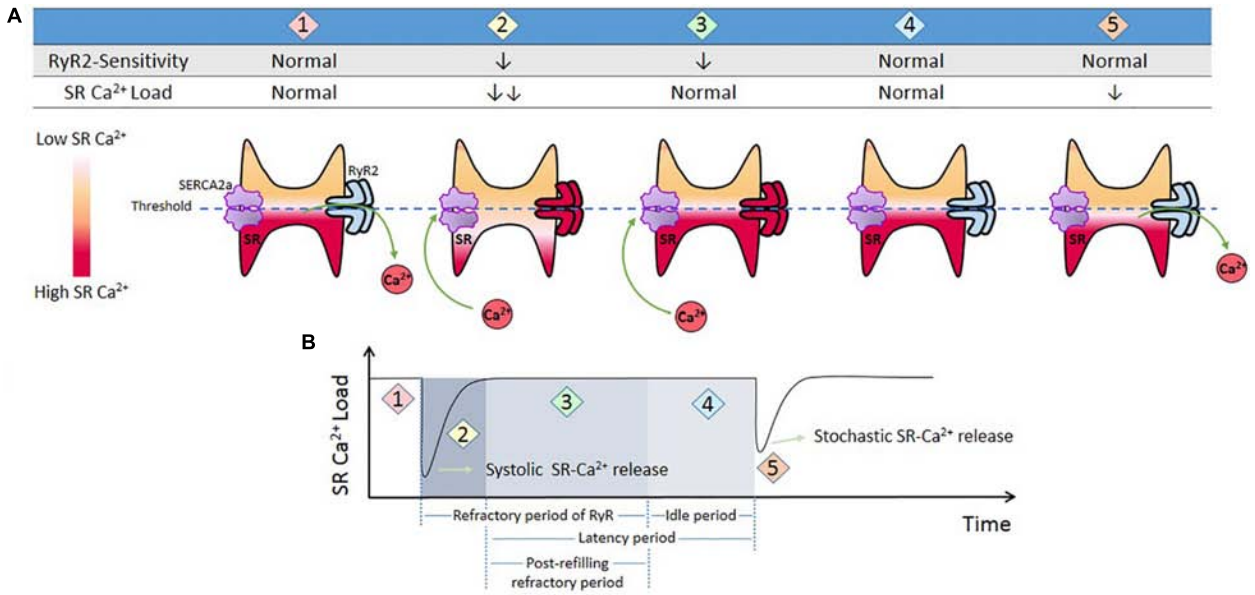

FIGURE 4 | Threshold concept. **(A)** Cartoon that represents different conditions of RyR2 sensitivity and SR-Ca^{2+} load during Ca^{2+} release from SR. When the cell triggers a Ca^{2+} transient (1), SR Ca^{2+} load diminishes and RyR2s enter in a refractory period (2). SR Ca^{2+} uptake produces SR Ca^{2+} recovery (3). During this period there are no spontaneous releases, i.e., RyR2 remained refractory in spite of the fact that SR level has recovered completely (SR *threshold*). This period is followed by what has been named an "idle" period, by Belevych et al., 2012, (4) in which, after SR-Ca^{2+} load and RyR2s recovering, a stochastic activation of RyR2 may trigger a spontaneous release. **(B)** Schematic representation of time dependent changes of SR Ca^{2+} t (1 and 2), and refractoriness (2 and 3) after a stimulus-induced Ca^{2+} transient. (4) "Idle" period during which a spontaneous SR-Ca^{2+} release occurs. We called *post-refilling refractory period* to the period of time needed for refractoriness to recover after SR Ca^{2+} *threshold* was reached.

Mitochondrial ATP production is crucial for modulation of oxidative phosphorylation and therefore essential to maintain myocyte activity, including SR Ca^{2+} cycling, contraction, and relaxation (Denton, 2009). The physical contact between SR membranes and mitochondria are known as sarco/endoplasmic reticulum (SR/ER)/mitochondria microdomains or mitochondria-associated SR/ER membranes (MAMs). A sufficient local Ca^{2+} concentration may be achieved in specialized microdomains created by the close association of mitochondria and the SR/ER (Szabadkai et al., 2003). In these microdomains, cytosolic Ca^{2+} is predicted to transiently rise to micromolar concentrations, consequently allowing significant Ca^{2+} uptake via the MCU. Physical proximity and functional interplay between mitochondria and SR is maintained in part through tethering of these two organelles by different linkers that may contribute to either decrease or maintain the physical gap between the SR and the mitochondria. For an extensive review see Csordas et al. (2018). On the other hand, perturbation of Ca^{2+} handling may alter mitochondrial-SR Ca^{2+} crosstalk and excessive Ca^{2+} can go to the mitochondria which may contribute to apoptosis and necroptosis in different diseases. Stress conditions that lead to Ca^{2+} or ROS overload trigger mPTP opening, i.e., the mitochondrial membrane becomes permeable to any molecule less than 1.5 kDa in size. Consequent dissipation of the membrane potential ($\Delta\Psi m$) leads to mitochondrial membrane depolarization, failure to produce ATP and release of mitochondrial proteins such as cytochrome c, which initiate cell death pathways (Bernardi and Di Lisa, 2015). Importantly, it has been shown that mitochondria-initiated cell death is one main mechanism in HF (Nakayama et al., 2007).

The Interplay Between SR Ca^{2+} Uptake and Leak

As discussed above, the properties of RyR2 are a main factor in determining the magnitude of SR Ca^{2+} leak. However, can an increase in RyR2 P_0, increase SR Ca^{2+} leak by itself? Experiments by Venetucci et al., clearly demonstrated that the potentiation of RyR2 produces only a transient increase in SR Ca^{2+} leak, because once SR Ca^{2+} leak initiates, SR Ca^{2+} load decreases below the threshold for SR Ca^{2+} leak (Venetucci et al., 2007). Only a simultaneous enhancement of SR Ca^{2+} uptake would be able to maintain the necessary level of SR Ca^{2+} content to attain the threshold for SR Ca^{2+} leak. This conclusion is in agreement with clinical facts showing that patients with catecholaminergic polymorphic ventricular tachycardia (CPVT) due to RyR2 mutation only suffer arrhythmias after β-ARS. Experiments performed in S2814D myocytes, in which Ser^{2814} was mutated to aspartic acid and behaves as pseudo constitutively phosphorylated (van Oort et al., 2010), also showed that an increase in the P_0 of RyR2 produced by CaMKII phosphorylation was not able to evoke an SR Ca^{2+} leak higher than the one observed in wild type (WT) myocytes unless they are challenged by increasing extracellular Ca^{2+} or β-ARS (Mazzocchi et al., 2016).

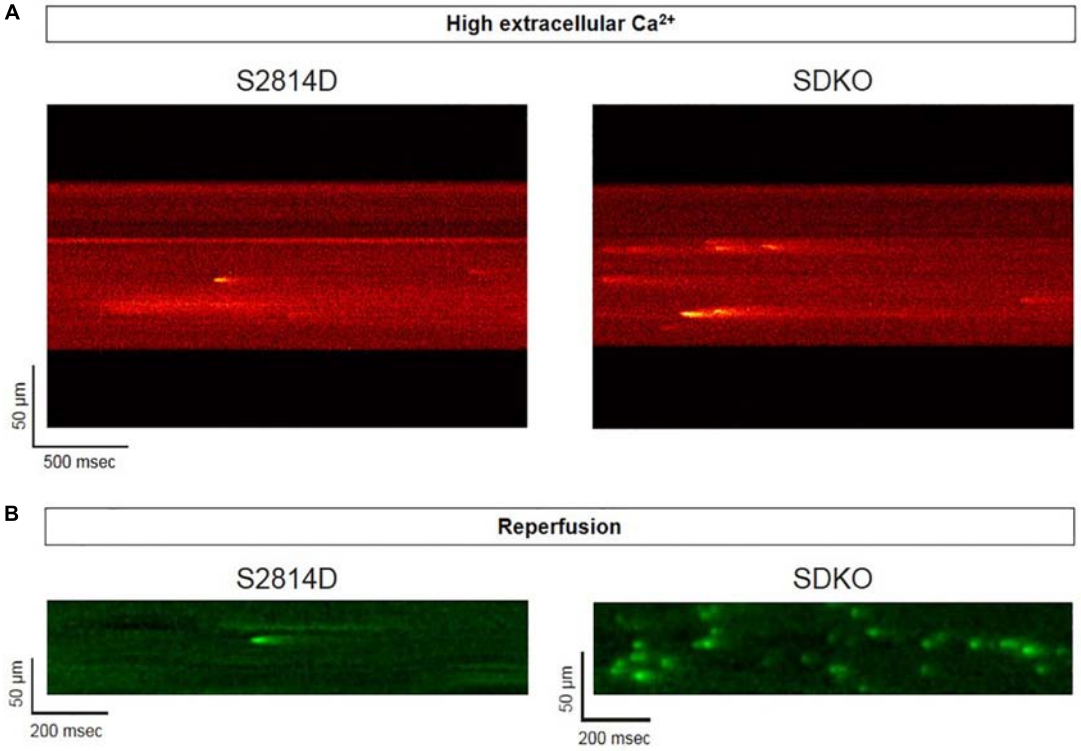

FIGURE 5 | Confocal assessment of spontaneous Ca^{2+} release. **(A)** Representative confocal images showing that Ca^{2+} spark frequency is higher in isolated cardiomyocytes from SDKO mice in comparison to S2814D myocytes (unpublished confocal microscopy records representative of overall data shown in Mazzocchi et al., 2016). **(B)** Similar results were obtained in fluo-4 loaded intact isolated hearts from S2814D and SDKO mice under a confocal microscope, during reperfusion of the hearts submitted to a period of ischemia (unpublished confocal microscopy records representative of overall data shown in Valverde et al., 2019). In both examples, ablation of PLN increases Ca^{2+} spark frequency respect to hearts from S2814D mice.

Sarcoplasmic reticulum Ca^{2+} leak is also critically dependent on SR Ca^{2+} load. As stated above, SR Ca^{2+} overload triggers spontaneous Ca^{2+} release via the activation of the RyR2 luminal Ca^{2+} sensor (Gyorke and Terentyev, 2008). Therefore, the potential effect of increasing SR Ca^{2+} load on Ca^{2+} triggered arrhythmias, seems obvious. However, PLN knock-out mice (PLNKO), which have a fully loaded SR, have not proven to be prone to arrhythmias under basal conditions (Santana et al., 1997). Although at first sight these results might suggest that the increase in SR Ca^{2+} load *per se* does not increase arrhythmia propensity, several studies have provided evidence that the increase in SR Ca^{2+} load produced by PLN ablation does produce a dramatic increase SR Ca^{2+} leak (Santana et al., 1997; Huser et al., 1998; Mazzocchi et al., 2016). Unexpectedly, it hardly evokes SR Ca^{2+} waves (Huser et al., 1998; Mazzocchi et al., 2016). **Figure 5A** shows the results of experiments performed in S2814D mice. As discussed above, this mutation confers the hearts a high propensity to SR Ca^{2+} waves and arrhythmias when submitted to stress (van Oort et al., 2010), and in double mutant mice resulting from cross-breeding S2814D mice with PLNKO mice, to increase SR Ca^{2+} reuptake (SDKO mice) (Mazzocchi et al., 2016; Valverde et al., 2019). In the presence of high extracellular Ca^{2+}, the frequency of Ca^{2+} sparks and SR Ca^{2+} leak were higher in SDKO than in S2814D myocytes, consistent with the overall higher SR Ca^{2+} load in SDKO cells (Mazzocchi et al., 2016). Similar results were obtained when SR Ca^{2+} load was increased in both strains subjected to an I/R protocol (Mazzocchi et al., 2016; Valverde et al., 2019; **Figure 5B**). Unexpectedly, whereas S2814D myocytes displayed full propagating Ca^{2+} waves when exposed to high extracellular Ca^{2+} (**Figure 6A**) or I/R (**Figure 6B**), SDKO myocytes mostly show non-propagating Ca^{2+} events, known as mini-waves. Thus, in spite of the higher SR Ca^{2+} leak observed in SDKO myocytes vs. S2814D, the proportion of fully propagating events in SDKO myocytes was significantly less (Mazzocchi et al., 2016). This seeming paradox can be clarified by the acknowledgment that two main factors intervene in the production of arrhythmogenic Ca^{2+} waves: 1. Increased SR Ca^{2+} leak and 2. Cytosolic Ca^{2+} wave propagation.

An increase in SR Ca^{2+} leak associated with a decrease in propagating SR Ca^{2+} waves indicates a limitation in cytosolic Ca^{2+} diffusion (**Figure 7**). PLN ablation interrupts cell-wide propagating Ca^{2+} waves, converting them into non-propagated events, like mini-waves or groups of Ca^{2+} sparks (Huser et al., 1998; Mazzocchi et al., 2016; Valverde et al., 2019), supporting the contention that by decreasing cytosolic Ca^{2+}, PLN ablation would increase cytosolic Ca^{2+} buffer capacity, hampering Ca^{2+} wave propagation and preventing the arrhythmogenic susceptibility produced by an enhanced SR Ca^{2+} load. Further

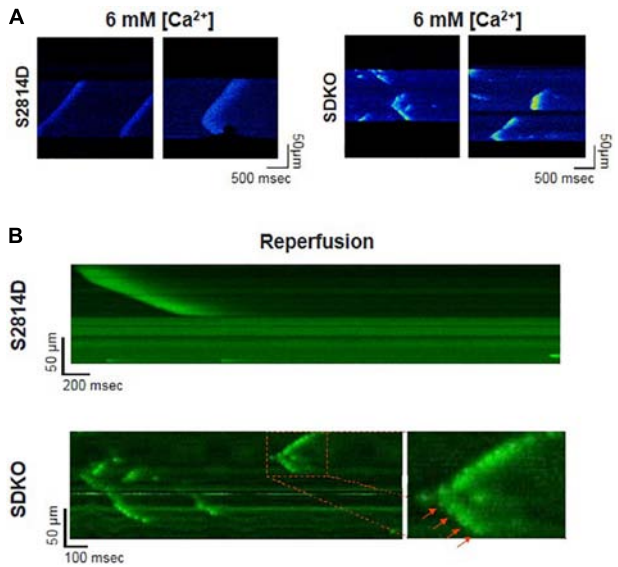

FIGURE 6 | Confocal assessment of spontaneous SR Ca^{2+} waves. **(A)** Representative confocal images showing Ca^{2+} waves in isolated cardiomyocytes from S2814D myocytes (left panel) when exposed to 6 mM extracellular Ca^{2+}. When SDKO isolated myocytes are exposed to the same condition, they exhibit miniwaves instead of full propagating Ca^{2+} waves (Reproduced with permission from Mazzocchi et al., 2016). **(B)** Representative confocal images of epicardial Ca^{2+} waves in S2814D and SDKO intact isolated hearts during reperfusion after an ischemic period. SDKO hearts display fragmented Ca^{2+} waves or mini-waves. Red arrows indicate a series of mini-events conserving a Ca^{2+} wave pattern (reproduced with permission from Valverde et al., 2019).

support to this idea is given by the experiments in which decreasing SR Ca^{2+} uptake by the SERCA2a inhibitor CPA, converts non-propagating mini-waves into full propagating Ca^{2+} waves (Valverde et al., 2019). These results indicate therefore that an increase in SR Ca^{2+} content does increase the propensity to arrhythmias. However, the mechanism by which the increase in SR Ca^{2+} occurred may conspire against the arrhythmogenic effect of the high SR Ca^{2+} load, i.e., an enhancement of SR Ca^{2+} sequestration, if high enough, would increase SR Ca^{2+} load and leak but also preclude Ca^{2+} wave propagation (Huser et al., 1998; Mazzocchi et al., 2016; Valverde et al., 2019).

In contrast, the increase in SR Ca^{2+} leak evoked by increasing SR Ca^{2+} uptake was unable to prevent but rather enhanced heart attack. It was speculated that increasing SR Ca^{2+} uptake was not efficient to hamper the excessive flow of SR Ca^{2+} to the mitochondria, aggravating cardiac damage (Valverde et al., 2019).

Experimental Evidence

In the following sections, we will give experimental evidence that highlight the importance of Ca^{2+} handling misbalance in the production of Ca^{2+} triggered arrhythmias and cell death. Although the mechanisms of cardiac arrhythmias and apoptosis/necroptosis are usually multifactorial, we will concentrate on experimental examples that emphasize the role of PTM of SR Ca^{2+} handling proteins. When possible, the interplay between Ca^{2+} uptake and release in determining arrhythmias and cardiac damage will be also discussed.

Abnormal RyR2 Regulation in the Development of Diabetic Cardiomyopathy

The current typical definition of DCM comprises structural and functional abnormalities of the myocardium in diabetic patients independently of other risk factors, as coronary artery disease or hypertension (Aneja et al., 2008). DCM is the last stage of cardiac damage in Type 1 and 2 Diabetes Mellitus (T1DM and T2DM, respectively) and of metabolic syndrome associated with insulin resistance. The subcellular mechanisms involved in this last stage of DCM have been discussed in several previous reviews (Bugger and Abel, 2014; Cox and Marsh, 2014; Fuentes-Antras, Picatoste et al. 2015, Fuentes-Antras, Picatoste et al. 2015). Most of them concluded that mayor alterations of Ca^{2+} handling, protein expressions, and activities in overt DCM mimic those of HF from different etiologies, including a decrease in SERCA2a activity, SR Ca^{2+} load, systolic Ca^{2+}, rate of Ca^{2+} decay, and increase in SR Ca^{2+} leak (Lebeche et al., 2008). Protein glycosylation (Clark et al., 2003) and oxidized CaMKII are significantly up-regulated in the DCM (Jay et al., 2006), therefore CaMKII activation and RyR2 phosphorylation has been proposed as a potential mechanism of heart failure, ventricular arrhythmias and apoptosis in this disease (Daniels et al., 2015). In rats with T2DM, the opening of mPTP in ventricular myocytes was shown to be mainly influenced by the increased ROS and decreased ATP content. It was suggested that Ca^{2+} mishandling due to the slow rate of SR Ca^{2+} uptake could play a role in increasing mPTP opening that might further exacerbate mitochondrial dysfunction and induce cell death (Riojas-Hernandez et al., 2015). Moreover, ROS derived from hyperglycemia trigger myocardial apoptosis by

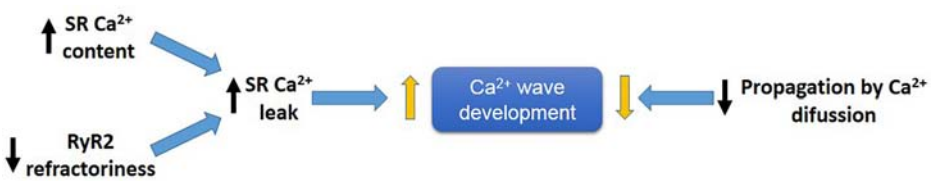

FIGURE 7 | Main factors developing arrhythmogenic Ca^{2+} waves. An increase in SR-Ca^{2+} content and/or a decrease in RyR2 refractoriness favor SR-Ca^{2+} leak and Ca^{2+} wave generation, meanwhile a decrease in propagation of Ca^{2+} by diffusion (e.g., like that produce by PLN ablation), will prevent Ca^{2+} wave propagation by conversion of Ca^{2+} waves into non-propagable Ca^{2+} miniwaves.

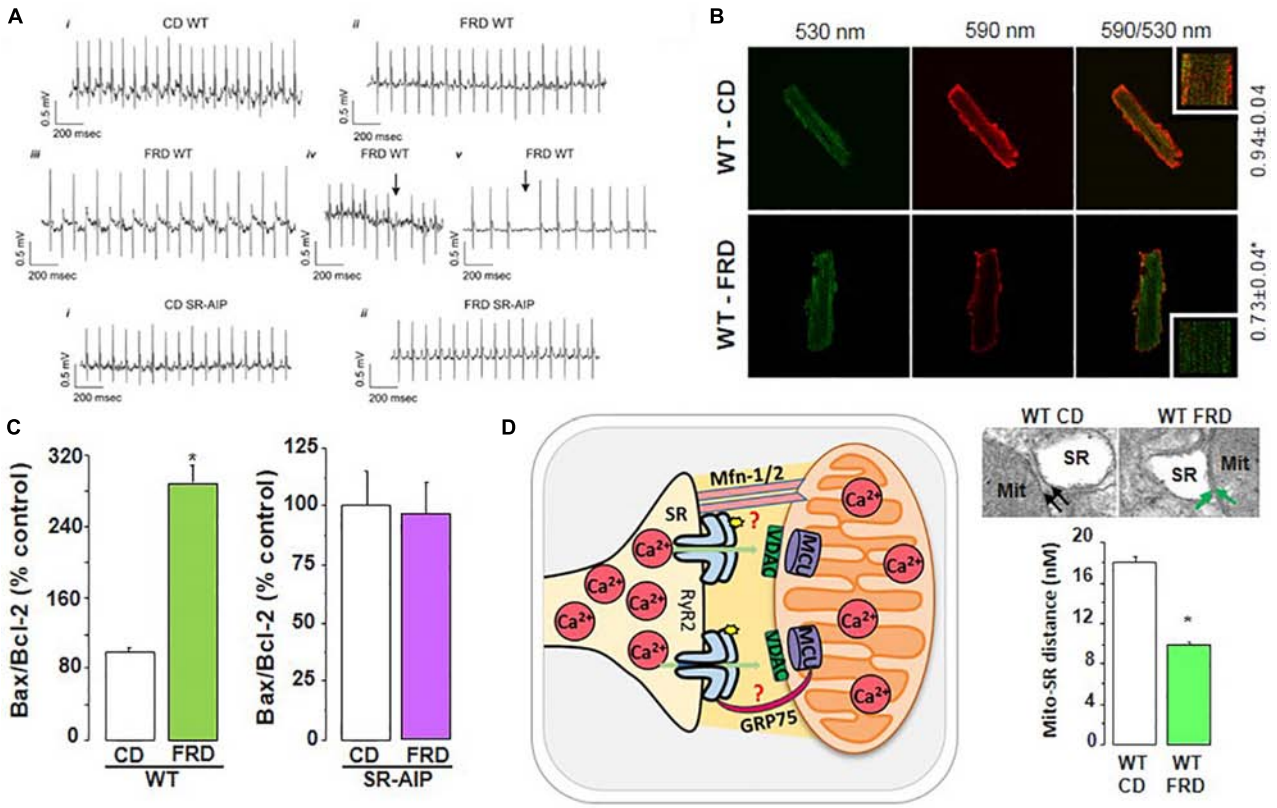

FIGURE 8 | RyR2 dysregulation in DCM development. **(A)** Representative ECG recordings showing that fructose-rich diet (FRD) induces cardiac arrhythmias in WT but not in SR-AIP mice (CD, control diet). WT mice exhibit bradycardia (ii), bidirectional tachycardia (iii), ventricular ectopic beats (iv, arrow), and AV block (v, arrow) when treated with FRD. **(B)** FRD deteriorates mitochondria membrane potential, as shown by an increase in JC-1 green/red fluorescence ratio. **(C)** This alteration in FRD mitochondria is in accordance with a higher apoptotic ratio (Bax/Bcl-2 proteins), which can be prevented in mice expressing the CaMKII inhibitory peptide at the SR level (SR-AIP). **(D)** Histological samples (upper right) show a closer distance between mitochondria and SR in FRD vs. CD treated mice, which might be due to an alteration in structural proteins involved in SR-mitochondria communication. The cartoon in the left side of **(D)** represents this SR-mito interaction (reproduced with permission from Federico et al., 2017). *$p < 0.05$.

mitochondrial cytochrome c release and consequent activation of the caspase-3 pathway (Cai et al., 2002). Although the underlying mechanism of cell death in DCM is not clear yet, these results suggest that a possible pathway underlying apoptosis in DMC is linked to Ca^{2+} mishandling and mitochondrial-SR Ca^{2+} crosstalk, as described above (For further review about the role of mitochondria on cardiac arrhythmogenesis in DCM see (El Hadi et al., 2019).

Much less is known about Ca^{2+} handling and mishandling and the potential occurrence of arrhythmias and apoptosis in the first stages of this disease, in which subclinical events develop for years before the clear emergence of HF symptoms. A possible cause for this lack of information may lie in the poor diagnosis of this stage of the disease and in the different models used to study prediabetic molecular events (King, 2012; Graham and Schuurman, 2015; King and Bowe, 2016). Indeed, the results that reveal the underlying mechanisms of the pathogenesis of DCM, are different according to the model, the degree of evolution of the disease before reaching DCM and the gender explored. Examples of conflicting results at the level of Ca^{2+} handling and particularly of RyR2 are observed in the metabolic syndrome model, (db/db mice), which lacks leptin receptors (Chen et al., 1996). In male db/db mouse hearts, the levels of RyR2 were found to be depressed and the RyR2 phosphorylation at the CaMKII site was not altered. However, RyR2 phosphorylation at the PKA site was found to be increased (Pereira et al., 2006, 2014). Intriguingly, db/db female mouse hearts showed no changes in RyR2 expression associated with a decrease in PKA and CaMKII RyR2 phosphorylation sites (Pereira et al., 2014). In a model of fructose-rich diet (FRD) applied to male rats and mice, our laboratory has described that this hypercaloric diet, which also induces insulin resistance, increases CaMKII activation and RyR2 dysfunction due to Ser^{2814} phosphorylation (Sommese et al., 2016; Federico et al., 2017). On the other hand, experiments *in vitro* revealed that during acute hyperglycemia, RyR2 activity can also be altered. Hyperglycemia leads to *O*-Glc-NAcylation of proteins such as CaMKII. Erickson et al. elegantly showed that the acute increase of glucose or *O*-linked N-acetylglucosamine is directly responsible for CaMKII-dependent diastolic RyR2 Ca^{2+} leak and SR Ca^{2+} load depletion in hyperglycemia (Erickson et al., 2013). Additionally, we recently demonstrated that in an early diabetic stage, prevention of CaMKII activation by ROS avoided

SR Ca^{2+} leak evoked by CaMKII-dependent phosphorylation of RyR2 (Sommese et al., 2016). Thus, the available results indicate that a main disturbance of Ca^{2+} handling in prediabetic hearts occurs at the level of RyR2 phosphorylation with the consequent increase in SR Ca^{2+} leak and the possibility of triggered arrhythmias and cell death. Indeed, during prediabetic states, the risk of cardiovascular events is already increased and myocardial abnormalities might appear before the diagnosis of T2DM. These alterations are thought to root irregularities at the cardiac myocyte level, ultimately contributing to structural and functional anomalies observed in DCM (Hajat et al., 2004). Actually, in the mouse model of impaired glucose tolerance (IGT) mentioned above (FRD-induced insulin resistance), we found serious cardiac disorders (Sommese et al., 2016; Federico et al., 2017). The fact that this model lacks the more frequent co-morbidities of DCM, supports the metabolic origin of the alterations at the cell level. These animals develop remarkable cardiac remodeling (Sommese et al., 2016). Also, ventricular myocytes exhibit cardiac arrhythmogenic events leading to ventricular arrhythmias which can be prevented in transgenic mice expressing the CaMKII inhibitor AIP targeted to the SR membranes, avoiding phosphorylation of SR proteins (PLN and RyR2) by CaMKII (SR-AIP mice) (**Figure 8**). Moreover, a ROS scavenger as tempol could avoid RyR2 phosphorylation and SR Ca^{2+} leak, preventing the arrhythmogenic pattern of the prediabetic cells (Sommese et al., 2016). Of note, the increase in RyR2 phosphorylation observed in FRD myocytes decreases SR Ca^{2+} content. This decrease occurs in spite of the increase in SERCA2a activity which contributes to preserving SR Ca^{2+} load. This increase, which may be due to the CaMKII-dependent increase in Thr^{17} phosphorylation of PLN, would contribute to avoiding a further decrease in SR Ca^{2+} load but would also favor SR Ca^{2+} leak and arrhythmogenic Ca^{2+} waves.

Apoptosis is also an early sign of myocardial dysfunction in the evolution of the diabetic disease, preceding the increase in collagen which may lead to structural and irreversible alterations (Federico et al., 2017). We described a cascade of events initiated by a CaMKII-induced increase in SR Ca^{2+} leak which is linked to mitochondrial membrane depolarization and cardiac damage. A particularly striking finding was the CaMKII-induced remodeling of SR-mitochondria microdomains. The latter would strongly support SR–mitochondria dialogue, facilitating Ca^{2+} drain to the mitochondria and cell death, in the scenario of an increased SR Ca^{2+} leak (Federico et al., 2017). The elucidation of the intracellular signaling pathway of this altered SR-mitochondria relationship would further contribute to the knowledge of DCM molecular alterations. Further investigations are needed to examine the proteins involved in the SR-mitochondria communication (like mitofusin-2, Mfn2, and the chaperone glucose-related protein 75, GRP-75), a completely unexplored field in this disease.

Ca^{2+} Triggered Arrhythmias Induced by Digitalis Intoxication

Cardiac glycosides have been used for the treatment of HF over the last 200 years due to their inotropic properties (Altamirano et al., 2006; Gonano et al., 2011). Although many doubts about their safety in HF treatment have emerged mainly at the end of the last millennium, it is still considered a valuable cardiac tool in some particular scenarios (see for review Whayne, 2018). Unfortunately, these compounds have a very narrow therapeutic range due to their toxic effects that include an enhanced propensity to arrhythmias. The arrhythmic effects of cardiac glycosides have been traditionally attributed to an increase in SR Ca^{2+} load which, by leading to an increase in Ca^{2+} leak, would evoke cytosolic Ca^{2+} waves and triggered arrhythmias (Wier and Hess, 1984; Fujiwara et al., 2008; Eisner et al., 2009; Weiss et al., 2011). More recent experiments indicated that a change in RyR2 may be also involved in cardiac glycosides–induced arrhythmias. Experiments by Gyorke's group (Ho et al., 2011) indicate that the arrhythmogenic effect of cardiotonic glycosides is linked to NOX2-dependent ROS release from mitochondria. The increase in ROS was initially thought to produce RyR2 thiol oxidation that would increase the sensitivity of the channel to luminal Ca^{2+}, thus lowering the critical SR Ca^{2+} content at which spontaneous Ca^{2+} waves occur (Terentyev et al., 2008). However, simultaneous experiments by Gonano et al., indicated that ouabain-induced arrhythmias requires CaMKII activation: Chronic administration or high–toxic doses of ouabain administered acutely, increased CaMKII activity in mouse hearts (Gonano et al., 2011). Moreover, inhibition of CaMKII was able to prevent spontaneous contractions in isolated myocytes and arrhythmias in intact mouse hearts, without affecting ouabain inotropic action. These experiments also showed that CaMKII phosphorylates both, RyR2 and PLN, which would increase SR Ca^{2+} leak and SERCA2a activity. Although this later effect would add to the increase in SR Ca^{2+} load resulting from Na^{+}-K^{+}-ATPase inhibition, these experiments concluded that CaMKII-dependent PLN phosphorylation might not contribute to ouabain–induced increase in SR Ca^{2+} content and inotropic effect since they were of similar magnitude in the absence and presence of CaMKII inhibition. However, since CaMKII dependent phosphorylation of RyR2 was also inhibited, it might be that the resultant similar SR Ca^{2+} load observed after CaMKII inhibition was due to the prevention of SR Ca^{2+} leak. Moreover, the fact that CaMKII inhibition prevents arrhythmias without affecting the ouabain-induced increase in SR Ca^{2+} load would suggest that the increase in SR Ca^{2+} content produced by the drug is not enough to reach the necessary *threshold* to trigger, by itself, ouabain-induced arrhythmias (Gonano et al., 2011). An increase in RyR2 sensitivity is needed.

The role of CaMKII-dependent induced increase in SR Ca^{2+} leak and ventricular arrhythmias was later confirmed by experiments by Gyorke's group, which revealed that replacement of Ser^{2814} site of RyR2 by Ala -a non-phosphorylatable amino acid-prevents ouabain-induced Ca^{2+} leak and arrhythmias. These results definitively confirmed that phosphorylation, rather than RyR2 oxidation, was required for the increase in channel spontaneous activity and arrhythmogenesis in the context of digitalis toxicity. Instead, the increase in ROS would contribute to CaMKII activation that in turn produces the observed RyR2 phosphorylation (Palomeque et al., 2009; Ho et al., 2014).

Importantly, other studies have shown that mitochondria are also involved in the toxic and arrhythmogenic effects

of cardiotonic glycosides. The results of these investigations indicate that ouabain-induced increase in cytoplasmic Na^+ compromises mitochondrial energetics and redox balance by blunting mitochondrial Ca^{2+} accumulation. Improving mitochondrial Ca^{2+} retention by inhibition of mitochondrial NCX, can mitigate these effects, suppress Ca^{2+}-triggered arrhythmias and improve the positive inotropic effects of cardiac glycosides (Liu et al., 2010).

Abnormal Ca^{2+} Handling in Ischemia/Reperfusion

Ischemic heart disease is a leading cause of mortality worldwide. Cardiac ischemia reduces cardiac output and promotes arrhythmias and cell death. Reperfusion therapies are the standard treatment for patients suffering myocardial infarction, however, re-establishing blood flow is associated with additional cell damage (I/R injury), and exacerbating the effect of the preceding ischemia. Indeed, it was shown that reperfusion may trigger life-threatening arrhythmias, accounting for up to half of the total I/R-induced infarcts (Braunwald and Kloner, 1985; Yellon and Hausenloy, 2007; Said et al., 2011; Garcia-Dorado et al., 2012). Although the factors contributing to I/R injury are complex (see for review (Murphy and Steenbergen, 2008). I/R injury constitutes another example in which experimental evidence reveals that disturbed Ca^{2+} handling and mitochondria ROS production are main responsible for reperfusion arrhythmias and cardiac damage (Valverde et al., 2006, 2010; Mattiazzi et al., 2015; Bagheri et al., 2016). The increase in cytosolic Ca^{2+} during ischemia was associated with an enhancement of SR Ca^{2+} load (Valverde et al., 2010), which is released at the onset of reperfusion and produces an abrupt rise in cytosolic Ca^{2+} (Ca^{2+} *bump*) and the consequent decrease in SR Ca^{2+} content and Ca^{2+} transient. Moreover, a major mechanism for the ischemia-induced increase in diastolic Ca^{2+} is an increase in the frequency of Ca^{2+} sparks which may switch to arrhythmogenic Ca^{2+} waves during reperfusion (Mattiazzi et al., 2015).

Reactive oxygen species/reactive nitrogen species are generated during reperfusion by several different cellular sources, being the mitochondria the more important one. Mitochondrial Ca^{2+} overload and subsequently ROS production trigger mitochondrial permeability transition pore and ROS production via ROS-induced ROS release mechanisms (Zorov et al., 2000). Both, Ca^{2+} mishandling and ROS production set an ideal intracellular milieu for activation of CaMKII, which play a main role in I/R arrhythmias, apoptosis, and necroptosis. *Ex vivo* and *in vivo* experiments described an increase in phosphorylated-CaMKII (p-CaMKII) and oxidized-CaMKII (ox-CaMKII) at the onset of reperfusion (Said et al., 2011; Becerra et al., 2016), which was associated to a significant increase in the phosphorylation of Thr^{17} site and RyR2 Ser^{2814} (Vittone et al., 2002; Salas et al., 2010; Ling et al., 2013), as well as redox changes of RyR2 (Becerra et al., 2016). Reperfusion arrhythmias are largely dependent on SR Ca^{2+} leak evoked by these PTM of RyR2 (Said et al., 2008; Becerra et al., 2016). In this scenario the role played by a substantial increase in SR Ca^{2+} uptake was similar to that observed in stress-induced Ca^{2+}-triggered arrhythmias, i.e., increasing SR Ca^{2+} uptake by PLN ablation protects against reperfusion arrhythmias. This protection was achieved by alteration of Ca^{2+} wave propagation, which were transformed in non-arrhythmogenic mini-waves and reconverted in full Ca^{2+} waves in the presence of SERCA2a inhibition (Figure 6C; Valverde et al., 2019). Of note, PLN ablation is equivalent to a situation of permanent maximal PLN phosphorylation as stated above. In ischemic reperfused WT hearts, PLN phosphorylation is highly but transiently increased at the onset of reperfusion (Vittone et al., 2002; Said et al., 2008). Under these conditions, we did not observe Ca^{2+} mini-waves (Valverde et al., 2010). This would mean that Thr^{17} phosphorylation at the onset of reperfusion is unable to prevent SR Ca^{2+} waves progression. In contrast, it might help to increase SR Ca^{2+} load and maintain SR Ca^{2+} leak. This contention is supported by experiments in which hearts were subjected to a short I/R protocol to produce stunning. In the stunned heart, the transient phosphorylation of Thr^{17} of PLN is essential for contractile recovery upon reperfusion, even though phosphorylation of RyR2 also occurs and induces reperfusion arrhythmias (Said et al., 2003, 2011).

After a prolonged ischemic period, reperfusion evokes irreversible cardiac injury. Under these conditions, myocytes die by apoptosis, autophagy, and necrosis. The rise in Ca^{2+} during I/R leads to mitochondrial Ca^{2+} accumulation, which is greatly favored by the close association between mitochondria and SR and constitutes a main event in the initiation of cell death (Rizzuto and Pozzan, 2006). Experimental evidence consistently indicates that CaMKII inhibition is protective in the irreversible I/R injury (Zhang et al., 2005; Vila-Petroff et al., 2007; Salas et al., 2010). Although the mechanisms for myocardial protection by CaMKII inhibition are still unclear, one of the CaMKII deleterious pathway in I/R certainly involves the SR and the mitochondria (Vila-Petroff et al., 2007; Salas et al., 2010; Valverde et al., 2010; Joiner et al., 2012). In previous experiments, we showed that I/R damage was diminished in hearts from S2814A mice. Conversely, in the hearts of S2814D mice (constitutively pseudo-phosphorylated), cardiac damage increased (Di Carlo et al., 2014). A decrease in the expression of RyR2 described in I/R (Salas et al., 2010), compatible with a degradation/damage of these channels (Pedrozo et al., 2010) and changes in RyR2 activity induced by redox alterations, may contribute to increase SR Ca^{2+} leak (Hidalgo et al., 2004; Said et al., 2011; Di Carlo et al., 2014). These alterations in RyR2 would add to the deleterious action of RyR2 phosphorylation favoring the increase in mitochondria Ca^{2+} content and greatly contributing to necroptosis and apoptosis in reperfusion cardiac damage (Salas et al., 2010; Di Carlo et al., 2014). This cascade would be further stimulated by the increase in CaMKII-dependent phosphorylation of MCU described by Joiner, Koval et al.(Joiner et al., 2012). However, recent experiments do not support a relevant role of CaMKII for mitochondrial Ca^{2+} uptake in cardiac myocytes at least under physiological conditions (Nickel et al., 2019).

As stated above, the transient increase in CaMKII-dependent PLN phosphorylation plays a beneficial role in the stunned heart. The role of PLN phosphorylation in I/R injury is less clear. After prolonged ischemia, we showed that preventing PLN

phosphorylation exacerbates the functional and structural heart damage after myocardial infarction, suggesting that CaMKII-dependent phosphorylation of PLN observed during reperfusion favors post-ischemic recovery and protects from I/R cardiac damage (Di Carlo et al., 2014). However, the fact that I/R does produce cardiac damage indicates that even being beneficial, CaMKII-dependent PLN phosphorylation results insufficient to counteract the effect of simultaneous detrimental mechanisms that take place during I/R. On the other hand, several groups have tested the effects of increasing SR Ca^{2+} uptake on cardiac damage during I/R injury, by different maneuvers. The outcome of these experiments is controversial. For instance, Yang et al. (2006) demonstrated that the protective effect of chronic CaMKII inhibition in AC3I mice was lost when they were interbred with PLNKO mice and submitted to myocardial infarction, supporting a detrimental effect of enhancing of SR Ca^{2+} uptake. Similar results were obtained in our laboratory. The ablation of PLN in SDKO mice increases Ca^{2+} leak upon reperfusion (**Figure 6A**). This increase was associated with an increase in infarct size and mitochondrial dysfunction. Therefore, these experiments demonstrated that an important increase in SR Ca^{2+} uptake as that produced by PLN ablation, was able to prevent reperfusion arrhythmias, but failed to prevent, and even enhance, cardiac damage (Valverde et al., 2019). The important increase in SR Ca^{2+} uptake would favor the unbalance between SR Ca^{2+} uptake and leak, promoting mitochondrial Ca^{2+} overload and cell death. Other studies demonstrated that accelerating SR Ca^{2+} uptake by different means (i.e., overexpressing SERCA1a, with higher kinetics than SERCA2a, or expressing a repressor of PLN activity, PP1 H-1), alleviated post-ischemic cardiac injury (Talukder et al., 2007, 2008; Nicolaou et al., 2009a), supporting a beneficial effect of accelerating SR Ca^{2+} uptake. These controversial results seem not to arise from species differences since most of the experiments mentioned above referred to rodents. It is possible that the final beneficial or detrimental outcome of increasing SR Ca^{2+} uptake might tightly depend on the extent of Ca^{2+} uptake and SR Ca^{2+} load achieved during ischemia and at the onset of reperfusion. For instance, moderate increases in SR Ca^{2+} content have been associated with beneficial effects (Nicolaou et al., 2009b), whereas more important increases, like those expected in PLNKO mice, were associated with detrimental actions (Valverde et al., 2019).

Is RyR2 Activation Always Detrimental?

We have previously associated the increase in RyR2 activation, for instance by CaMKII-dependent phosphorylation, with cardiac damage and arrhythmias due to exacerbated diastolic SR Ca^{2+} leak, as discussed above. However, it is important to bear in mind that potentiation of RyR2 activity persists during systole and enhances systolic fractional Ca^{2+} release, bringing the heart to a new state of higher efficiency. This would allow the heart to maintain a given contractility despite a decrease in SR Ca^{2+} content or to enhance contractility if SR Ca^{2+} content is simultaneously preserved (for further discussion, see Lascano et al., 2017).

CONCLUDING REMARKS

The normal interplay among the proteins involved in SR Ca^{2+} uptake and release is a main determinant of the regular beat to beat contractile function of cardiac myocytes. Regulation and deregulation of these proteins are crucial to understanding the balance between SR Ca^{2+} uptake and leak, responsible for SR Ca^{2+} content and myocardial contractility, as well as its unbalance, which determines an excess of SR Ca^{2+} leak, able to produce arrhythmias and cardiac damage. Post-translational enhancements of SR Ca^{2+} uptake have a beneficial effect resulting in a detectable increase in contractility when the unbalance between SR Ca^{2+} uptake and leak favors the uptake. This is the case of PLNKO mice and stunned hearts. When SR Ca^{2+} leak is increased by the enhancement of RyR2 activity, the increase in SR Ca^{2+} uptake may not be enough to counteract SR Ca^{2+} leak, resulting in two opposite effects: (a) beneficial, by opposing to SR Ca^{2+} leak and rescuing at least in part SR Ca^{2+} load and contractility; (b) detrimental, because the increase in SR Ca^{2+} load would favor SR Ca^{2+} leak, arrhythmias, and cardiac damage. Interestingly, a greatly exacerbated increase in SR Ca^{2+} uptake, as that produced by PLN ablation, does contribute to increasing SR Ca^{2+} leak and cardiac damage by incrementing SR Ca^{2+} load and leak. Paradoxically, and in spite of the exacerbated SR Ca^{2+} leak, this increase may prevent Ca^{2+} triggered arrhythmias, by a different mechanism, i.e., diminishing cytosolic Ca^{2+} and avoiding Ca^{2+} wave propagation. Post-translational activation of RyR2 activity would produce a deleterious effect by increasing SR Ca^{2+} leak and predisposing to cardiac damage and arrhythmias. When this modification occurs only at the level of SR Ca^{2+} release/leak, the short-lived enhancement of SR Ca^{2+} leak may produce a decrease in contractility due to the decrease in SR Ca^{2+} load, without any further detrimental effect. Moreover, the increased activity of RyR2 during systole tends to preserve contractility, even at lower SR Ca^{2+} loads. The detrimental effect of RyR2 activation (i.e., arrhythmias and cardiac damage) can only take place when it occurs associated to an increase in SR Ca^{2+} uptake, able to maintain SR Ca^{2+} leak. This is the typical case of Ser2814D myocytes, with constitutive pseudo-phosphorylation of RyR2 at the CaMKII site.

AUTHOR CONTRIBUTIONS

JP and AM generated the idea. JP, AM, MF, and CV wrote the manuscript, designed, and edited the figures.

FUNDING

This work was supported by PICT 2015-3009 (FONCyT, Argentina) and PS-1 (UAI, Argentina) to JP, PICT 2015-3210 (FONCyT, Argentina) to CV, and PICT 2524 (FONCyT, Argentina) and PIP 0305 (CONICET, Argentina) to AM. MF is a doctoral fellow from CONICET.

REFERENCES

Adachi, T., Weisbrod, R. M., Pimentel, D. R., Ying, J., Sharov, V. S., Schoneich, C., et al. (2004). S-Glutathiolation by peroxynitrite activates SERCA during arterial relaxation by nitric oxide. *Nat. Med.* 10, 1200–1207. doi: 10.1038/nm1119

Ai, X., Curran, J. W., Shannon, T. R., Bers, D. M., and Pogwizd, S. M. (2005). Ca2+/calmodulin-dependent protein kinase modulates cardiac ryanodine receptor phosphorylation and sarcoplasmic reticulum Ca2+ leak in heart failure. *Circ. Res.* 97, 1314–1322. doi: 10.1161/01.res.0000194329.41863.89

Altamirano, J., Li, Y., DeSantiago, J., Piacentino, V. III, Houser, S. R., and Bers, D. M. (2006). The inotropic effect of cardioactive glycosides in ventricular myocytes requires Na+-Ca2+ exchanger function. *J. Physiol.* 575(Pt 3), 845–854. doi: 10.1113/jphysiol.2006.111252

Anderson, M. E. (2007). Multiple downstream proarrhythmic targets for calmodulin kinase II: moving beyond an ion channel-centric focus. *Cardiovasc. Res.* 73, 657–666. doi: 10.1016/j.cardiores.2006.12.009

Aneja, A., Tang, W. H., Bansilal, S., Garcia, M. J., and Farkouh, M. E. (2008). Diabetic cardiomyopathy: insights into pathogenesis, diagnostic challenges, and therapeutic options. *Am. J. Med.* 121, 748–757. doi: 10.1016/j.amjmed.2008.03.046

Arvanitis, D. A., Vafiadaki, E., Fan, G. C., Mitton, B. A., Gregory, K. N., Del Monte, F., et al. (2007). Histidine-rich Ca-binding protein interacts with sarcoplasmic reticulum Ca-ATPase. *Am. J. Physiol. Heart Circ. Physiol.* 293, H1581–H1589.

Arvanitis, D. A., Vafiadaki, E., Johnson, D. M., Kranias, E. G., and Sanoudou, D. (2018). The histidine-rich calcium binding protein in regulation of cardiac rhythmicity. *Front. Physiol.* 9:1379. doi: 10.3389/fphys.2018.01379

Bagheri, F., Khori, V., Alizadeh, A. M., Khalighfard, S., Khodayari, S., and Khodayari, H. (2016). Reactive oxygen species-mediated cardiac-reperfusion injury: mechanisms and therapies. *Life Sci.* 165, 43–55. doi: 10.1016/j.lfs.2016.09.013

Balderas-Villalobos, J., Molina-Munoz, T., Mailloux-Salinas, P., Bravo, G., Carvajal, K., and Gomez-Viquez, N. L. (2013). Oxidative stress in cardiomyocytes contributes to decreased SERCA2a activity in rats with metabolic syndrome. *Am. J. Physiol. Heart Circ. Physiol.* 305, H1344–H1353. doi: 10.1152/ajpheart.00211.2013

Balshaw, D. M., Xu, L., Yamaguchi, N., Pasek, D. A., and Meissner, G. (2001). Calmodulin binding and inhibition of cardiac muscle calcium release channel (ryanodine receptor). *J. Biol. Chem.* 276, 20144–20153. doi: 10.1074/jbc.m010771200

Barg, S., Copello, J. A., and Fleischer, S. (1997). Different interactions of cardiac and skeletal muscle ryanodine receptors with FK-506 binding protein isoforms. *Am. J. Physiol.* 272(5 Pt 1), C1726–C1733.

Bassani, J. W., Yuan, W., and Bers, D. M. (1995). Fractional SR Ca release is regulated by trigger Ca and SR Ca content in cardiac myocytes. *Am. J. Physiol.* 268(5 Pt 1), C1313–C1319.

Becerra, R., Roman, B., Di Carlo, M. N., Mariangelo, J. I., Salas, M., Sanchez, G., et al. (2016). Reversible redox modifications of ryanodine receptor ameliorate ventricular arrhythmias in the ischemic-reperfused heart. *Am. J. Physiol. Heart Circ. Physiol.* 311, H713–H724. doi: 10.1152/ajpheart.00142.2016

Belevych, A. E., Terentyev, D., Terentyeva, R., Ho, H. T., Gyorke, I., Bonilla, I. M., et al. (2012). Shortened Ca2+ signaling refractoriness underlies cellular arrhythmogenesis in a postinfarction model of sudden cardiac death. *Circ. Res.* 110, 569–577. doi: 10.1161/CIRCRESAHA.111.260455

Bernardi, P., and Di Lisa, F. (2015). The mitochondrial permeability transition pore: molecular nature and role as a target in cardioprotection. *J. Mol. Cell Cardiol.* 78, 100–106. doi: 10.1016/j.yjmcc.2014.09.023

Bers, D. M. (2006). Altered cardiac myocyte Ca regulation in heart failure. *Physiology* 21, 380–387. doi: 10.1152/physiol.00019.2006

Bers, D. M. (2012). Ryanodine receptor S2808 phosphorylation in heart failure: smoking gun or red herring. *Circ. Res.* 110, 796–799. doi: 10.1161/circresaha.112.265579

Bidasee, K. R., Zhang, Y., Shao, C. H., Wang, M., Patel, K. P., Dincer, U. D., et al. (2004). Diabetes increases formation of advanced glycation end products on Sarco(endo)plasmic reticulum Ca2+-ATPase. *Diabetes Metab. Res. Rev.* 53, 463–473. doi: 10.2337/diabetes.53.2.463

Bigelow, D. J., and Squier, T. C. (2005). Redox modulation of cellular signaling and metabolism through reversible oxidation of methionine sensors in calcium regulatory proteins. *Biochim. Biophys. Acta* 1703, 121–134. doi: 10.1016/j.bbapap.2004.09.012

Braun, J. L., Hamstra, S. I., Messner, H. N., and Fajardo, V. A. (2019). SERCA2a tyrosine nitration coincides with impairments in maximal SERCA activity in left ventricles from tafazzin-deficient mice. *Physiol. Rep.* 7, e14215. doi: 10.14814/phy2.14215

Braunwald, E., and Kloner, R. A. (1985). Myocardial reperfusion: a double-edged sword? *J. Clin. Invest.* 76, 1713–1719. doi: 10.1172/jci112160

Bugger, H., and Abel, E. D. (2014). Molecular mechanisms of diabetic cardiomyopathy. *Diabetologia* 57, 660–671. doi: 10.1007/s00125-014-3171-6

Cai, L., Li, W., Wang, G., Guo, L., Jiang, Y., and Kang, Y. J. (2002). Hyperglycemia-induced apoptosis in mouse myocardium: mitochondrial cytochrome C-mediated caspase-3 activation pathway. *Diabetes Metab. Res. Rev.* 51, 1938–1948. doi: 10.2337/diabetes.51.6.1938

Camors, E., and Valdivia, H. H. (2014). CaMKII regulation of cardiac ryanodine receptors and inositol triphosphate receptors. *Front. Pharmacol.* 5:101. doi: 10.3389/fphar.2014.00101

Capes, E. M., Loaiza, R., and Valdivia, H. H. (2011). Ryanodine receptors. *Skelet Muscle* 1:18. doi: 10.1186/2044-5040-1-18

Carter, S., Colyer, J., and Sitsapesan, R. (2006). Maximum phosphorylation of the cardiac ryanodine receptor at serine-2809 by protein kinase a produces unique modifications to channel gating and conductance not observed at lower levels of phosphorylation. *Circ. Res.* 98, 1506–1513. doi: 10.1161/01.res.0000227506.43292.df

Chen, H., Charlat, O., Tartaglia, L. A., Woolf, E. A., Weng, X., Ellis, S. J., et al. (1996). Evidence that the diabetes gene encodes the leptin receptor: identification of a mutation in the leptin receptor gene in db/db mice. *Cell* 84, 491–495. doi: 10.1016/s0092-8674(00)81294-5

Chen, W., Wang, R., Chen, B., Zhong, X., Kong, H., Bai, Y., et al. (2014). The ryanodine receptor store-sensing gate controls Ca2+ waves and Ca2+-triggered arrhythmias. *Nat. Med.* 20, 184–192. doi: 10.1038/nm.3440

Chen, X., Weber, C., Farrell, E. T., Alvarado, F. J., Zhao, Y. T., Gomez, A. M., et al. (2018). Sorcin ablation plus beta-adrenergic stimulation generate an arrhythmogenic substrate in mouse ventricular myocytes. *J. Mol. Cell Cardiol.* 114, 199–210. doi: 10.1016/j.yjmcc.2017.11.017

Cheng, H., Lederer, M. R., Lederer, W. J., and Cannell, M. B. (1996). Calcium sparks and [Ca2+]i waves in cardiac myocytes. *Am. J. Physiol.* 270(1 Pt 1), C148–C159.

Ching, L. L., Williams, A. J., and Sitsapesan, R. (2000). Evidence for Ca(2+) activation and inactivation sites on the luminal side of the cardiac ryanodine receptor complex. *Circ. Res.* 87, 201–206. doi: 10.1161/01.res.87.3.201

Clark, R. J., McDonough, P. M., Swanson, E., Trost, S. U., Suzuki, M., Fukuda, M., et al. (2003). Diabetes and the accompanying hyperglycemia impairs cardiomyocyte calcium cycling through increased nuclear O-GlcNAcylation. *J. Biol. Chem.* 278, 44230–44237. doi: 10.1074/jbc.m303810200

Cohen, R. A., and Adachi, T. (2006). Nitric-oxide-induced vasodilatation: regulation by physiologic s-glutathiolation and pathologic oxidation of the sarcoplasmic endoplasmic reticulum calcium ATPase. *Trends Cardiovasc. Med.* 16, 109–114. doi: 10.1016/j.tcm.2006.02.001

Cox, E. J., and Marsh, S. A. (2014). A systematic review of fetal genes as biomarkers of cardiac hypertrophy in rodent models of diabetes. *PLoS One* 9:e92903. doi: 10.1371/journal.pone.0092903

Csordas, G., Weaver, D., and Hajnoczky, G. (2018). Endoplasmic reticulum-mitochondrial contactology: structure and signaling functions. *Trends Cell. Biol.* 28, 523–540. doi: 10.1016/j.tcb.2018.02.009

Currie, S., Loughrey, C. M., Craig, M. A., and Smith, G. L. (2004). Calcium/calmodulin-dependent protein kinase IIdelta associates with the ryanodine receptor complex and regulates channel function in rabbit heart. *Biochem. J.* 377(Pt 2), 357–366. doi: 10.1042/bj20031043

Daniels, L., Bell, J. R., Delbridge, L. M., McDonald, F. J., Lamberts, R. R., and Erickson, J. R. (2015). The role of CaMKII in diabetic heart dysfunction. *Heart Fail. Rev.* 20, 589–600. doi: 10.1007/s10741-015-9498-3

Denton, R. M. (2009). Regulation of mitochondrial dehydrogenases by calcium ions. *Biochim. Biophys. Acta* 1787, 1309–1316. doi: 10.1016/j.bbabio.2009.01.005

Di Carlo, M. N., Said, M., Ling, H., Valverde, C. A., De Giusti, V. C., Sommese, L., et al. (2014). CaMKII-dependent phosphorylation of cardiac ryanodine receptors regulates cell death in cardiac ischemia/reperfusion injury. *J. Mol. Cell Cardiol.* 74, 274–283. doi: 10.1016/j.yjmcc.2014.06.004

Diaz, M. E., Trafford, A. W., O'Neill, S. C., and Eisner, D. A. (1997). Measurement of sarcoplasmic reticulum Ca2+ content and sarcolemmal Ca2+ fluxes in isolated rat ventricular myocytes during spontaneous Ca2+ release. *J. Physiol.* 501(1 Pt 1), 3–16. doi: 10.1111/j.1469-7793.1997.003bo.x

Doi, M., Yano, M., Kobayashi, S., Kohno, M., Tokuhisa, T., Okuda, S., et al. (2002). Propranolol prevents the development of heart failure by restoring FKBP12.6-mediated stabilization of ryanodine receptor. *Circulation* 105, 1374–1379. doi: 10.1161/hc1102.105270

Dorn, G. W. II, and Maack, C. (2013). SR and mitochondria: calcium cross-talk between kissing cousins. *J. Mol. Cell Cardiol.* 55, 42–49. doi: 10.1016/j.yjmcc.2012.07.015

Dybkova, N., Sedej, S., Napolitano, C., Neef, S., Rokita, A. G., Hunlich, M., et al. (2011). Overexpression of CaMKIIdeltac in RyR2R4496C+/- knock-in mice leads to altered intracellular Ca2+ handling and increased mortality. *J. Am. Coll. Cardiol.* 57, 469–479. doi: 10.1016/j.jacc.2010.08.639

Eisner, D. A., Caldwell, J. L., Kistamas, K., and Trafford, A. W. (2017). Calcium and excitation-contraction coupling in the heart. *Circ. Res.* 121, 181–195.

Eisner, D. A., Kashimura, T., O'Neill, S. C., Venetucci, L. A., and Trafford, A. W. (2009). What role does modulation of the ryanodine receptor play in cardiac inotropy and arrhythmogenesis? *J. Mol. Cell Cardiol.* 46, 474–481. doi: 10.1016/j.yjmcc.2008.12.005

El Hadi, H., Vettor, R., and Rossato, M. (2019). Cardiomyocyte mitochondrial dysfunction in diabetes and its contribution in cardiac arrhythmogenesis. *Mitochondrion* 46, 6–14. doi: 10.1016/j.mito.2019.03.005

Erickson, J. R., Pereira, L., Wang, L., Han, G., Ferguson, A., Dao, K., et al. (2013). Diabetic hyperglycaemia activates CaMKII and arrhythmias by O-linked glycosylation. *Nature* 502, 372–376. doi: 10.1038/nature12537

Fabiato, A., and Fabiato, F. (1977). Calcium release from the sarcoplasmic reticulum. *Circ. Res.* 40, 119–129.

Fabiato, A., and Fabiato, F. (1979). Calcium and cardiac excitation-contraction coupling. *Annu. Rev. Physiol.* 41, 473–484. doi: 10.1146/annurev.ph.41.030179.002353

Farrell, E. F., Antaramian, A., Rueda, A., Gomez, A. M., and Valdivia, H. H. (2003). Sorcin inhibits calcium release and modulates excitation-contraction coupling in the heart. *J. Biol. Chem.* 278, 34660–34666. doi: 10.1074/jbc.m305931200

Federico, M., Portiansky, E. L., Sommese, L., Alvarado, F. J., Blanco, P. G., Zanuzzi, C. N., et al. (2017). Calcium-calmodulin-dependent protein kinase mediates the intracellular signalling pathways of cardiac apoptosis in mice with impaired glucose tolerance. *J. Physiol.* 595, 4089–4108. doi: 10.1113/JP273714

Ferrero, P., Said, M., Sanchez, G., Vittone, L., Valverde, C., Donoso, P., et al. (2007). Ca2+/calmodulin kinase II increases ryanodine binding and Ca2+-induced sarcoplasmic reticulum Ca2+ release kinetics during beta-adrenergic stimulation. *J. Mol. Cell Cardiol.* 43, 281–291. doi: 10.1016/j.yjmcc.2007.05.022

Fill, M., and Copello, J. A. (2002). Ryanodine receptor calcium release channels. *Physiol. Rev.* 82, 893–922. doi: 10.1152/physrev.00013.2002

Finkel, E. (2001). The mitochondrion: is it central to apoptosis? *Science* 292, 624–626. doi: 10.1126/science.292.5517.624

Fischer, T. H., Eiringhaus, J., Dybkova, N., Saadatmand, A., Pabel, S., Weber, S., et al. (2018). Activation of protein phosphatase 1 by a selective phosphatase disrupting peptide reduces sarcoplasmic reticulum Ca(2+) leak in human heart failure. *Eur. J. Heart Fail.* 20, 1673–1685. doi: 10.1002/ejhf.1297

Fischer, T. H., Herting, J., Tirilomis, T., Renner, A., Neef, S., Toischer, K., et al. (2013). Ca2+/calmodulin-dependent protein kinase II and protein kinase a differentially regulate sarcoplasmic reticulum Ca2+ leak in human cardiac pathology. *Circulation* 128, 970–981. doi: 10.1161/CIRCULATIONAHA.113.001746

Fowler, M. R., Colotti, G., Chiancone, E., Smith, G. L., and Fearon, I. M. (2008). Sorcin modulates cardiac L-type Ca2+ current by functional interaction with the alpha1C subunit in rabbits. *Exp. Physiol.* 93, 1233–1238. doi: 10.1113/expphysiol.2008.043497

Froehlich, J. P., Mahaney, J. E., Keceli, G., Pavlos, C. M., Goldstein, R., Redwood, A. J., et al. (2008). Phospholamban thiols play a central role in activation of the cardiac muscle sarcoplasmic reticulum calcium pump by nitroxyl. *Biochemistry* 47, 13150–13152. doi: 10.1021/bi801925p

Fruen, B. R., Bardy, J. M., Byrem, T. M., Strasburg, G. M., and Louis, C. F. (2000). Differential Ca(2+) sensitivity of skeletal and cardiac muscle ryanodine receptors in the presence of calmodulin. *Am. J. Physiol. Cell Physiol.* 279, C724–C733.

Fuentes-Antras, J., Picatoste, B., Gomez-Hernandez, A., Egido, J., Tunon, J., and Lorenzo, O. (2015). Updating experimental models of diabetic cardiomyopathy. *J. Diabetes Res.* 2015:656795. doi: 10.1155/2015/656795

Fuentes-Antras, J., Picatoste, B., Ramirez, E., Egido, J., Tunon, J., and Lorenzo, O. (2015). Targeting metabolic disturbance in the diabetic heart. *Cardiovasc. Diabetol.* 14:17. doi: 10.1186/s12933-015-0173-8

Fujiwara, K., Tanaka, H., Mani, H., Nakagami, T., and Takamatsu, T. (2008). Burst emergence of intracellular Ca2+ waves evokes arrhythmogenic oscillatory depolarization via the Na+-Ca2+ exchanger: simultaneous confocal recording of membrane potential and intracellular Ca2+ in the heart. *Circ. Res.* 103, 509–518. doi: 10.1161/CIRCRESAHA.108.176677

Galfre, E., Pitt, S. J., Venturi, E., Sitsapesan, M., Zaccai, N. R., Tsaneva-Atanasova, K., et al. (2012). FKBP12 activates the cardiac ryanodine receptor Ca2+-release channel and is antagonised by FKBP12.6. *PLoS One* 7:e31956. doi: 10.1371/journal.pone.0031956

Garcia-Dorado, D., Ruiz-Meana, M., Inserte, J., Rodriguez-Sinovas, A., and Piper, H. M. (2012). Calcium-mediated cell death during myocardial reperfusion. *Cardiovasc. Res.* 94, 168–180. doi: 10.1093/cvr/cvs116

Gonano, L. A., Sepulveda, M., Rico, Y., Kaetzel, M., Valverde, C. A., Dedman, J., et al. (2011). Calcium-calmodulin kinase II mediates digitalis-induced arrhythmias. *Circ. Arrhythm. Electrophysiol.* 4, 947–957. doi: 10.1161/CIRCEP.111.964908

Gong, D., Chi, X., Wei, J., Zhou, G., Huang, G., Zhang, L., et al. (2019). Modulation of cardiac ryanodine receptor 2 by calmodulin. *Nature* 572, 347–351. doi: 10.1038/s41586-019-1377-y

Gonzalez, D. R., Treuer, A., Sun, Q. A., Stamler, J. S., and Hare, J. M. (2009). S-Nitrosylation of cardiac ion channels. *J. Cardiovasc. Pharmacol.* 54, 188–195. doi: 10.1097/FJC.0b013e3181b72c9f

Gorski, P. A., Jang, S. P., Jeong, D., Lee, A., Lee, P., Oh, J. G., et al. (2019). Role of SIRT1 in modulating acetylation of the sarco-endoplasmic reticulum Ca(2+)-ATPase in heart failure. *Circ. Res.* 124, e63–e80. doi: 10.1161/CIRCRESAHA.118.313865

Graham, M. L., and Schuurman, H. J. (2015). Validity of animal models of type 1 diabetes, and strategies to enhance their utility in translational research. *Eur. J. Pharmacol.* 759, 221–230. doi: 10.1016/j.ejphar.2015.02.054

Guo, T., Cornea, R. L., Huke, S., Camors, E., Yang, Y., Picht, E., et al. (2010). Kinetics of FKBP12.6 binding to ryanodine receptors in permeabilized cardiac myocytes and effects on Ca sparks. *Circ. Res.* 106, 1743–1752. doi: 10.1161/CIRCRESAHA.110.219816

Guo, T., Zhang, T., Mestril, R., and Bers, D. M. (2006). Ca2+/Calmodulin-dependent protein kinase II phosphorylation of ryanodine receptor does affect calcium sparks in mouse ventricular myocytes. *Circ. Res.* 99, 398–406. doi: 10.1161/01.res.0000236756.06252.13

Gyorke, I., and Gyorke, S. (1998). Regulation of the cardiac ryanodine receptor channel by luminal Ca2+ involves luminal Ca2+ sensing sites. *Biophys. J.* 75, 2801–2810. doi: 10.1016/s0006-3495(98)77723-9

Gyorke, I., Hester, N., Jones, L. R., and Gyorke, S. (2004). The role of calsequestrin, triadin, and junctin in conferring cardiac ryanodine receptor responsiveness to luminal calcium. *Biophys. J.* 86, 2121–2128. doi: 10.1016/s0006-3495(04)74271-x

Gyorke, S., and Terentyev, D. (2008). Modulation of ryanodine receptor by luminal calcium and accessory proteins in health and cardiac disease. *Cardiovasc. Res.* 77, 245–255. doi: 10.1093/cvr/cvm038

Ha, K. N., Masterson, L. R., Hou, Z., Verardi, R., Walsh, N., Veglia, G., et al. (2011). Lethal Arg9Cys phospholamban mutation hinders Ca2+-ATPase regulation and phosphorylation by protein kinase. *Proc. Natl. Acad. Sci. U.S.A.* 108, 2735–2740. doi: 10.1073/pnas.1013987108

Haghighi, K., Bidwell, P., and Kranias, E. G. (2014). Phospholamban interactome in cardiac contractility and survival: a new vision of an old friend. *J. Mol. Cell Cardiol.* 77, 160–167. doi: 10.1016/j.yjmcc.2014.10.005

Haghighi, K., Pritchard, T. J., Liu, G. S., Singh, V. P., Bidwell, P., Lam, C. K., et al. (2015). Human G109E-inhibitor-1 impairs cardiac function and promotes

arrhythmias. *J. Mol. Cell Cardiol.* 89(Pt B), 349–359. doi: 10.1016/j.yjmcc.2015.10.004

Hajat, C., Tilling, K., Stewart, J. A., Lemic-Stojcevic, N., and Wolfe, C. D. (2004). Ethnic differences in risk factors for ischemic stroke: a European case-control study. *Stroke* 35, 1562–1567. doi: 10.1161/01.str.0000131903.04708.b8

Haji-Ghassemi, O., Yuchi, Z., and Van Petegem, F. (2019). The cardiac ryanodine receptor phosphorylation hotspot embraces PKA in a phosphorylation-dependent manner. *Mol. Cell.* 75, 39–52 e4. doi: 10.1016/j.molcel.2019.04.019

Handhle, A., Ormonde, C. E., Thomas, N. L., Bralesford, C., Williams, A. J., Lai, F. A., et al. (2016). Calsequestrin interacts directly with the cardiac ryanodine receptor luminal domain. *J. Cell Sci.* 129, 3983–3988.

Herrmann-Frank, A., and Lehmann-Horn, F. (1996). Regulation of the purified Ca2+ release channel/ryanodine receptor complex of skeletal muscle sarcoplasmic reticulum by luminal calcium. *Pflugers. Arch.* 432, 155–157. doi: 10.1007/s004240050117

Hidalgo, C., Bull, R., Behrens, M. I., and Donoso, P. (2004). Redox regulation of RyR-mediated Ca2+ release in muscle and neurons. *Biol. Res.* 37, 539–552.

Ho, H. T., Liu, B., Snyder, J. S., Lou, Q., Brundage, E. A., Velez-Cortes, F., et al. (2014). Ryanodine receptor phosphorylation by oxidized CaMKII contributes to the cardiotoxic effects of cardiac glycosides. *Cardiovasc. Res.* 101, 165–174. doi: 10.1093/cvr/cvt233

Ho, H. T., Stevens, S. C., Terentyeva, R., Carnes, C. A., Terentyev, D., and Gyorke, S. (2011). Arrhythmogenic adverse effects of cardiac glycosides are mediated by redox modification of ryanodine receptors. *J. Physiol.* 589(Pt 19), 4697–4708. doi: 10.1113/jphysiol.2011.210005

Horvath, B., Banyasz, T., Jian, Z., Hegyi, B., Kistamas, K., Nanasi, P. P., et al. (2013). Dynamics of the late Na(+) current during cardiac action potential and its contribution to afterdepolarizations. *J. Mol. Cell Cardiol.* 64, 59–68. doi: 10.1016/j.yjmcc.2013.08.010

Huke, S., and Bers, D. M. (2008). Ryanodine receptor phosphorylation at Serine 2030, 2808 and 2814 in rat cardiomyocytes. *Biochem. Biophys. Res. Commun.* 376, 80–85. doi: 10.1016/j.bbrc.2008.08.084

Huser, J., Bers, D. M., and Blatter, L. A. (1998). Subcellular properties of [Ca2+]i transients in phospholamban-deficient mouse ventricular cells. *Am. J. Physiol.* 274, H1800–H1811.

Irie, T., Sips, P. Y., Kai, S., Kida, K., Ikeda, K., Hirai, S., et al. (2015). S-Nitrosylation of calcium-handling proteins in cardiac adrenergic signaling and hypertrophy. *Circ. Res.* 117, 793–803. doi: 10.1161/CIRCRESAHA.115.307157

January, C. T., and Riddle, J. M. (1989). Early afterdepolarizations: mechanism of induction and block. a role for L-type Ca2+ current. *Circ. Res.* 64, 977–990. doi: 10.1161/01.res.64.5.977

Jay, D., Hitomi, H., and Griendling, K. K. (2006). Oxidative stress and diabetic cardiovascular complications. *Free Radic. Biol. Med.* 40, 183–192. doi: 10.1016/j.freeradbiomed.2005.06.018

Jeyakumar, L. H., Ballester, L., Cheng, D. S., McIntyre, J. O., Chang, P., Olivey, H. E., et al. (2001). FKBP binding characteristics of cardiac microsomes from diverse vertebrates. *Biochem. Biophys. Res. Commun.* 281, 979–986. doi: 10.1006/bbrc.2001.4444

Jiang, D., Chen, W., Wang, R., Zhang, L., and Chen, S. R. (2007). Loss of luminal Ca2+ activation in the cardiac ryanodine receptor is associated with ventricular fibrillation and sudden death. *Proc. Natl. Acad. Sci. U.S.A.* 104, 18309–18314. doi: 10.1073/pnas.0706573104

Jiang, D., Xiao, B., Yang, D., Wang, R., Choi, P., Zhang, L., et al. (2004). RyR2 mutations linked to ventricular tachycardia and sudden death reduce the threshold for store-overload-induced Ca2+ release (SOICR). *Proc. Natl. Acad. Sci. U.S.A.* 101, 13062–13067. doi: 10.1073/pnas.0402388101

Jiang, M. T., Lokuta, A. J., Farrell, E. F., Wolff, M. R., Haworth, R. A., and Valdivia, H. H. (2002). Abnormal Ca2+ release, but normal ryanodine receptors, in canine and human heart failure. *Circ. Res.* 91, 1015–1022. doi: 10.1161/01.res.0000043663.08689.05

Joiner, M. L., Koval, O. M., Li, J., He, B. J., Allamargot, C., Gao, Z., et al. (2012). CaMKII determines mitochondrial stress responses in heart. *Nature* 491, 269–273. doi: 10.1038/nature11444

Kaftan, E., Marks, A. R., and Ehrlich, B. E. (1996). Effects of rapamycin on ryanodine receptor/Ca(2+)-release channels from cardiac muscle. *Circ. Res.* 78, 990–997. doi: 10.1161/01.res.78.6.990

Kaplan, P., Babusikova, E., Lehotsky, J., and Dobrota, D. (2003). Free radical-induced protein modification and inhibition of Ca2+-ATPase of cardiac sarcoplasmic reticulum. *Mol. Cell. Biochem.* 248, 41–47.

Kettlewell, S., Most, P., Currie, S., Koch, W. J., and Smith, G. L. (2005). S100A1 increases the gain of excitation-contraction coupling in isolated rabbit ventricular cardiomyocytes. *J. Mol. Cell Cardiol.* 39, 900–910. doi: 10.1016/j.yjmcc.2005.06.018

Kho, C., Lee, A., Jeong, D., Oh, J. G., Chaanine, A. H., Kizana, E., et al. (2011). SUMO1-dependent modulation of SERCA2a in heart failure. *Nature* 477, 601–605. doi: 10.1038/nature10407

Kiewitz, R., Acklin, C., Schafer, B. W., Maco, B., Uhrik, B., Wuytack, F., et al. (2003). Ca2+ -dependent interaction of S100A1 with the sarcoplasmic reticulum Ca2+ -ATPase2a and phospholamban in the human heart. *Biochem. Biophys. Res. Commun.* 306, 550–557. doi: 10.1016/s0006-291x(03)00987-2

King, A., and Bowe, J. (2016). Animal models for diabetes: understanding the pathogenesis and finding new treatments. *Biochem. Pharmacol.* 99, 1–10. doi: 10.1016/j.bcp.2015.08.108

King, A. J. (2012). The use of animal models in diabetes research. *Br. J. Pharmacol.* 166, 877–894. doi: 10.1111/j.1476-5381.2012.01911.x

Knollmann, B. C., Chopra, N., Hlaing, T., Akin, B., Yang, T., Ettensohn, K., et al. (2006). Casq2 deletion causes sarcoplasmic reticulum volume increase, premature Ca2+ release, and catecholaminergic polymorphic ventricular tachycardia. *J. Clin. Invest.* 116, 2510–2520.

Kohlhaas, M., Zhang, T., Seidler, T., Zibrova, D., Dybkova, N., Steen, A., et al. (2006). Increased sarcoplasmic reticulum calcium leak but unaltered contractility by acute CaMKII overexpression in isolated rabbit cardiac myocytes. *Circ. Res.* 98, 235–244. doi: 10.1161/01.res.0000200739.90811.9f

Kong, H., Wang, R., Chen, W., Zhang, L., Chen, K., Shimoni, Y., et al. (2007). Skeletal and cardiac ryanodine receptors exhibit different responses to Ca2+ overload and luminal ca2+. *Biophys. J.* 92, 2757–2770. doi: 10.1529/biophysj.106.100545

Kranias, E. G., and Hajjar, R. J. (2012). Modulation of cardiac contractility by the phospholamban/SERCA2a regulatome. *Circ. Res.* 110, 1646–1660. doi: 10.1161/CIRCRESAHA.111.259754

Kranias, E. G., and Hajjar, R. J. (2017). The phospholamban journey 4 decades after setting out for ithaka. *Circ. Res.* 120, 781–783. doi: 10.1161/circresaha.116.310007

Kuster, G. M., Lancel, S., Zhang, J., Communal, C., Trucillo, M. P., Lim, C. C., et al. (2010). Redox-mediated reciprocal regulation of SERCA and Na+-Ca2+ exchanger contributes to sarcoplasmic reticulum Ca2+ depletion in cardiac myocytes. *Free Radic. Biol. Med.* 48, 1182–1187. doi: 10.1016/j.freeradbiomed.2010.01.038

Lancel, S., Zhang, J., Evangelista, A., Trucillo, M. P., Tong, X., Siwik, D. A., et al. (2009). Nitroxyl activates SERCA in cardiac myocytes via glutathiolation of cysteine 674. *Circ. Res.* 104, 720–723. doi: 10.1161/CIRCRESAHA.108.188441

Lascano, E., Negroni, J., Vila Petroff, M., and Mattiazzi, A. (2017). Impact of RyR2 potentiation on myocardial function. *Am. J. Physiol. Heart Circ. Physiol.* 312, H1105–H1109. doi: 10.1152/ajpheart.00855.2016

Laver, D. R. (2018). Regulation of the RyR channel gating by Ca(2+) and Mg(2). *Biophys. Rev.* 10, 1087–1095. doi: 10.1007/s12551-018-0433-4

Lebeche, D., Davidoff, A. J., and Hajjar, R. J. (2008). Interplay between impaired calcium regulation and insulin signaling abnormalities in diabetic cardiomyopathy. *Nat. Clin. Pract. Cardiovasc. Med.* 5, 715–724. doi: 10.1038/ncpcardio1347

Lehnart, S. E., Wehrens, X. H., Reiken, S., Warrier, S., Belevych, A. E., Harvey, R. D., et al. (2005). Phosphodiesterase 4D deficiency in the ryanodine-receptor complex promotes heart failure and arrhythmias. *Cell* 123, 25–35. doi: 10.1016/j.cell.2005.07.030

Li, Y., Kranias, E. G., Mignery, G. A., and Bers, D. M. (2002). Protein kinase a phosphorylation of the ryanodine receptor does not affect calcium sparks in mouse ventricular myocytes. *Circ. Res.* 90, 309–316. doi: 10.1161/hh0302.105660

Lim, G., Venetucci, L., Eisner, D. A., and Casadei, B. (2008). Does nitric oxide modulate cardiac ryanodine receptor function? implications for excitation-contraction coupling. *Cardiovasc. Res.* 77, 256–264. doi: 10.1093/cvr/cvm012

Lindemann, J. P., Jones, L. R., Hathaway, D. R., Henry, B. G., and Watanabe, A. M. (1983). beta-Adrenergic stimulation of phospholamban phosphorylation and Ca2+-ATPase activity in guinea pig ventricles. *J. Biol. Chem.* 258, 464–471.

Lindemann, J. P., and Watanabe, A. M. (1985). Phosphorylation of phospholamban in intact myocardium. Role of Ca2+-calmodulin-dependent mechanisms. *J. Biol. Chem.* 260, 4516–4525.

Ling, H., Gray, C. B., Zambon, A. C., Grimm, M., Gu, Y., Dalton, N., et al. (2013). Ca2+/Calmodulin-dependent protein kinase II delta mediates myocardial ischemia/reperfusion injury through nuclear factor-kappaB. *Circ. Res.* 112, 935–944. doi: 10.1161/CIRCRESAHA.112.276915

Liu, T., Brown, D. A., and O'Rourke, B. (2010). Role of mitochondrial dysfunction in cardiac glycoside toxicity. *J. Mol. Cell Cardiol.* 49, 728–736. doi: 10.1016/j.yjmcc.2010.06.012

Lokuta, A. J., Rogers, T. B., Lederer, W. J., and Valdivia, H. H. (1995). Modulation of cardiac ryanodine receptors of swine and rabbit by a phosphorylation-dephosphorylation mechanism. *J. Physiol.* 487(Pt 3), 609–622. doi: 10.1113/jphysiol.1995.sp020904

MacDonnell, S. M., Garcia-Rivas, G., Scherman, J. A., Kubo, H., Chen, X., Valdivia, H., et al. (2008). Adrenergic regulation of cardiac contractility does not involve phosphorylation of the cardiac ryanodine receptor at serine 2808. *Circ. Res.* 102, e65–e72.

MacLennan, D. H., and Kranias, E. G. (2003). Phospholamban: a crucial regulator of cardiac contractility. *Nat. Rev. Mol. Cell Biol.* 4, 566–577. doi: 10.1038/nrm1151

Maier, L. S., Zhang, T., Chen, L., DeSantiago, J., Brown, J. H., and Bers, D. M. (2003). Transgenic CaMKIIdeltaC overexpression uniquely alters cardiac myocyte Ca2+ handling: reduced SR Ca2+ load and activated SR Ca2+ release. *Circ. Res.* 92, 904–911. doi: 10.1161/01.res.0000069685.20258.f1

Marengo, J. J., Hidalgo, C., and Bull, R. (1998). Sulfhydryl oxidation modifies the calcium dependence of ryanodine-sensitive calcium channels of excitable cells. *Biophys. J.* 74, 1263–1277. doi: 10.1016/s0006-3495(98)77840-3

Marks, A. R. (2000). Cardiac intracellular calcium release channels: role in heart failure. *Circ. Res.* 87, 8–11. doi: 10.1161/01.res.87.1.8

Marks, A. R. (2002). Ryanodine receptors, FKBP12, and heart failure. *Front. Biosci.* 7:d970–d977. doi: 10.2741/a822

Marx, S. O., Reiken, S., Hisamatsu, Y., Jayaraman, T., Burkhoff, D., Rosemblit, N., et al. (2000). PKA phosphorylation dissociates FKBP12.6 from the calcium release channel (ryanodine receptor): defective regulation in failing hearts. *Cell* 101, 365–376. doi: 10.1016/s0092-8674(00)80847-8

Matsumoto, T., Hisamatsu, Y., Ohkusa, T., Inoue, N., Sato, T., Suzuki, S., et al. (2005). Sorcin interacts with sarcoplasmic reticulum Ca(2+)-ATPase and modulates excitation-contraction coupling in the heart. *Basic Res. Cardiol.* 100, 250–262. doi: 10.1007/s00395-005-0518-7

Mattiazzi, A., Argenziano, M., Aguilar-Sanchez, Y., Mazzocchi, G., and Escobar, A. L. (2015). Ca2+ Sparks and Ca2+ waves are the subcellular events underlying Ca2+ overload during ischemia and reperfusion in perfused intact hearts. *J. Mol. Cell Cardiol.* 79, 69–78. doi: 10.1016/j.yjmcc.2014.10.011

Mattiazzi, A., and Kranias, E. G. (2014). The role of CaMKII regulation of phospholamban activity in heart disease. *Front. Pharmacol.* 5:5. doi: 10.3389/fphar.2014.00005

Mazzocchi, G., Sommese, L., Palomeque, J., Felice, J. I., Di Carlo, M. N., Fainstein, D., et al. (2016). Phospholamban ablation rescues the enhanced propensity to arrhythmias of mice with CaMKII-constitutive phosphorylation of RyR2 at site S2814. *J. Physiol.* 594, 3005–3030. doi: 10.1113/JP271622

Meissner, G. (2004). Molecular regulation of cardiac ryanodine receptor ion channel. *Cell Calcium* 35, 621–628. doi: 10.1016/j.ceca.2004.01.015

Meissner, G. (2017). The structural basis of ryanodine receptor ion channel function. *J. Gen. Physiol.* 149, 1065–1089. doi: 10.1085/jgp.201711878

Morris, T. E., and Sulakhe, P. V. (1997). Sarcoplasmic reticulum Ca(2+)-pump dysfunction in rat cardiomyocytes briefly exposed to hydroxyl radicals. *Free Radic. Biol. Med.* 22, 37–47. doi: 10.1016/s0891-5849(96)00238-9

Most, P., Bernotat, J., Ehlermann, P., Pleger, S. T., Reppel, M., Borries, M., et al. (2001). S100A1: a regulator of myocardial contractility. *Proc. Natl. Acad. Sci. U.S.A.* 98, 13889–13894. doi: 10.1073/pnas.241393598

Most, P., Pleger, S. T., Volkers, M., Heidt, B., Boerries, M., Weichenhan, D., et al. (2004). Cardiac adenoviral S100A1 gene delivery rescues failing myocardium. *J. Clin. Invest.* 114, 1550–1563. doi: 10.1172/jci21454

Mundina de Weilenmann, C., Vittone, L., de Cingolani, G., and Mattiazzi, A. (1987). Dissociation between contraction and relaxation: the possible role of phospholamban phosphorylation. *Basic Res. Cardiol.* 82, 507–516. doi: 10.1007/bf01907220

Mundina-Weilenmann, C., Vittone, L., Ortale, M., de Cingolani, G. C., and Mattiazzi, A. (1996). Immunodetection of phosphorylation sites gives new insights into the mechanisms underlying phospholamban phosphorylation in the intact heart. *J. Biol. Chem.* 271, 33561–33567. doi: 10.1074/jbc.271.52.33561

Murayama, T., Ogawa, H., Kurebayashi, N., Ohno, S., Horie, M., and Sakurai, T. (2018). A tryptophan residue in the caffeine-binding site of the ryanodine receptor regulates Ca(2+) sensitivity. *Commun. Biol.* 1:98. doi: 10.1038/s42003-018-0103-x

Murphy, E., and Steenbergen, C. (2008). Ion transport and energetics during cell death and protection. *Physiology* 23, 115–123. doi: 10.1152/physiol.00044.2007

Nakayama, H., Chen, X., Baines, C. P., Klevitsky, R., Zhang, X., Zhang, H., et al. (2007). Ca2+- and mitochondrial-dependent cardiomyocyte necrosis as a primary mediator of heart failure. *J. Clin. Invest.* 117, 2431–2444. doi: 10.1172/jci31060

Nickel, A. G., Kohlhaas, M., Bertero, E., Wilhelm, D., Wagner, M., Sequeira, V., et al. (2019). CaMKII does not control mitochondrial Ca(2+) uptake in cardiac myocytes. *J. Physiol.* [Epub ahead of print].

Nicolaou, P., Hajjar, R. J., and Kranias, E. G. (2009a). Role of protein phosphatase-1 inhibitor-1 in cardiac physiology and pathophysiology. *J. Mol. Cell Cardiol.* 47, 365–371. doi: 10.1016/j.yjmcc.2009.05.010

Nicolaou, P., Rodriguez, P., Ren, X., Zhou, X., Qian, J., Sadayappan, S., et al. (2009b). Inducible expression of active protein phosphatase-1 inhibitor-1 enhances basal cardiac function and protects against ischemia/reperfusion injury. *Circ. Res.* 104, 1012–1020. doi: 10.1161/CIRCRESAHA.108.189811

Nomikos, M., Thanassoulas, A., Beck, K., Vassilakopoulou, V., Hu, H., Calver, B. L., et al. (2014). Altered RyR2 regulation by the calmodulin F90L mutation associated with idiopathic ventricular fibrillation and early sudden cardiac death. *FEBS Lett.* 588, 2898–2902. doi: 10.1016/j.febslet.2014.07.007

Nuss, H. B., Kaab, S., Kass, D. A., Tomaselli, G. F., and Marban, E. (1999). Cellular basis of ventricular arrhythmias and abnormal automaticity in heart failure. *Am. J. Physiol.* 277, H80–H91. doi: 10.1152/ajpheart.1999.277.1.H80

Orchard, C. H., Eisner, D. A., and Allen, D. G. (1983). Oscillations of intracellular Ca2+ in mammalian cardiac muscle. *Nature* 304, 735–738. doi: 10.1038/304735a0

Palomeque, J., Rueda, O. V., Sapia, L., Valverde, C. A., Salas, M., Petroff, M. V., et al. (2009). Angiotensin II-induced oxidative stress resets the Ca2+ dependence of Ca2+-calmodulin protein kinase II and promotes a death pathway conserved across different species. *Circ. Res.* 105, 1204–1212. doi: 10.1161/CIRCRESAHA.109.204172

Pan, X., Liu, J., Nguyen, T., Liu, C., Sun, J., Teng, Y., et al. (2013). The physiological role of mitochondrial calcium revealed by mice lacking the mitochondrial calcium uniporter. *Nat. Cell Biol.* 15, 1464–1472. doi: 10.1038/ncb2868

Paolocci, N., Katori, T., Champion, H. C., St John, M. E., Miranda, K. M., Fukuto, J. M., et al. (2003). Positive inotropic and lusitropic effects of HNO/NO- in failing hearts: independence from beta-adrenergic signaling. *Proc. Natl. Acad. Sci. U.S.A.* 100, 5537–5542. doi: 10.1073/pnas.0937302100

Paolocci, N., Saavedra, W. F., Miranda, K. M., Martignani, C., Isoda, T., Hare, J. M., et al. (2001). Nitroxyl anion exerts redox-sensitive positive cardiac inotropy in vivo by calcitonin gene-related peptide signaling. *Proc. Natl. Acad. Sci. U.S.A.* 98, 10463–10468. doi: 10.1073/pnas.181191198

Pedrozo, Z., Sanchez, G., Torrealba, N., Valenzuela, R., Fernandez, C., Hidalgo, C., et al. (2010). Calpains and proteasomes mediate degradation of ryanodine receptors in a model of cardiac ischemic reperfusion. *Biochim. Biophys. Acta* 1802, 356–362. doi: 10.1016/j.bbadis.2009.12.005

Peng, W., Shen, H., Wu, J., Guo, W., Pan, X., Wang, R., et al. (2016). Structural basis for the gating mechanism of the type 2 ryanodine receptor RyR2. *Science* 354:aah5324. doi: 10.1126/science.aah5324

Pereira, L., Matthes, J., Schuster, I., Valdivia, H. H., Herzig, S., Richard, S., et al. (2006). Mechanisms of [Ca2+]i transient decrease in cardiomyopathy of db/db

type 2 diabetic mice. *Diabetes Metab. Res. Rev.* 55, 608–615. doi: 10.2337/diabetes.55.03.06.db05-1284

Pereira, L., Ruiz-Hurtado, G., Rueda, A., Mercadier, J. J., Benitah, J. P., and Gomez, A. M. (2014). Calcium signaling in diabetic cardiomyocytes. *Cell Calcium* 56, 372–380. doi: 10.1016/j.ceca.2014.08.004

Potenza, D. M., Janicek, R., Fernandez-Tenorio, M., Camors, E., Ramos-Mondragon, R., Valdivia, H. H., et al. (2019). Phosphorylation of the ryanodine receptor 2 at serine 2030 is required for a complete beta-adrenergic response. *J. Gen. Physiol.* 151, 131–145. doi: 10.1085/jgp.201812155

Qian, J., Vafiadaki, E., Florea, S. M., Singh, V. P., Song, W., Lam, C. K., et al. (2011). Small heat shock protein 20 interacts with protein phosphatase-1 and enhances sarcoplasmic reticulum calcium cycling. *Circ. Res.* 108, 1429–1438. doi: 10.1161/CIRCRESAHA.110.237644

Respress, J. L., van Oort, R. J., Li, N., Rolim, N., Dixit, S. S., deAlmeida, A., et al. (2012). Role of RyR2 phosphorylation at S2814 during heart failure progression. *Circ. Res.* 110, 1474–1483. doi: 10.1161/CIRCRESAHA.112.268094

Riojas-Hernandez, A., Bernal-Ramirez, J. D., Rodriguez-Mier, F. E., Morales-Marroquin, E. M., Dominguez-Barragan, C., Borja-Villa, I., et al. (2015). Enhanced oxidative stress sensitizes the mitochondrial permeability transition pore to opening in heart from zucker Fa/fa rats with type 2 diabetes. *Life Sci.* 141, 32–43. doi: 10.1016/j.lfs.2015.09.018

Rizzuto, R., and Pozzan, T. (2006). Microdomains of intracellular Ca2+: molecular determinants and functional consequences. *Physiol. Rev.* 86, 369–408. doi: 10.1152/physrev.00004.2005

Rodriguez, P., Bhogal, M. S., and Colyer, J. (2003). Stoichiometric phosphorylation of cardiac ryanodine receptor on serine 2809 by calmodulin-dependent kinase II and protein kinase. *J. Biol. Chem.* 278, 38593–38600. doi: 10.1074/jbc.m301180200

Sacchetto, R., Turcato, F., Damiani, E., and Margreth, A. (1999). Interaction of triadin with histidine-rich Ca(2+)-binding protein at the triadic junction in skeletal muscle fibers. *J. Muscle Res. Cell Motil.* 20, 403–415.

Said, M., Becerra, R., Palomeque, J., Rinaldi, G., Kaetzel, M. A., Diaz-Sylvester, P. L., et al. (2008). Increased intracellular Ca2+ and SR Ca2+ load contribute to arrhythmias after acidosis in rat heart. Role of Ca2+/calmodulin-dependent protein kinase II. *Am. J. Physiol. Heart Circ. Physiol.* 295, H1669–H1683. doi: 10.1152/ajpheart.00010.2008

Said, M., Becerra, R., Valverde, C. A., Kaetzel, M. A., Dedman, J. R., Mundina-Weilenmann, C., et al. (2011). Calcium-calmodulin dependent protein kinase II (CaMKII): a main signal responsible for early reperfusion arrhythmias. *J. Mol. Cell Cardiol.* 51, 936–944. doi: 10.1016/j.yjmcc.2011.08.010

Said, M., Vittone, L., Mundina-Weilenmann, C., Ferrero, P., Kranias, E. G., and Mattiazzi, A. (2003). Role of dual-site phospholamban phosphorylation in the stunned heart: insights from phospholamban site-specific mutants. *Am. J. Physiol. Heart Circ. Physiol.* 285, H1198–H1205.

Salama, G., Menshikova, E. V., and Abramson, J. J. (2000). Molecular interaction between nitric oxide and ryanodine receptors of skeletal and cardiac sarcoplasmic reticulum. *Antioxid. Redox. Signal.* 2, 5–16. doi: 10.1089/ars.2000.2.1-5

Salas, M. A., Valverde, C. A., Sanchez, G., Said, M., Rodriguez, J. S., Portiansky, E. L., et al. (2010). The signalling pathway of CaMKII-mediated apoptosis and necrosis in the ischemia/reperfusion injury. *J. Mol. Cell Cardiol.* 48, 1298–1306. doi: 10.1016/j.yjmcc.2009.12.015

Samso, M., Feng, W., Pessah, I. N., and Allen, P. D. (2009). Coordinated movement of cytoplasmic and transmembrane domains of RyR1 upon gating. *PLoS Biol.* 7:e85. doi: 10.1371/journal.pbio.1000085

Santana, L. F., Kranias, E. G., and Lederer, W. J. (1997). Calcium sparks and excitation-contraction coupling in phospholamban-deficient mouse ventricular myocytes. *J. Physiol.* 503(Pt 1), 21–29. doi: 10.1111/j.1469-7793.1997.021bi.x

Santulli, G., Lewis, D. R., and Marks, A. R. (2017a). Physiology and pathophysiology of excitation-contraction coupling: the functional role of ryanodine receptor. *J. Muscle Res. Cell Motil.* 38, 37–45. doi: 10.1007/s10974-017-9470-z

Santulli, G., Nakashima, R., Yuan, Q., and Marks, A. R. (2017b). Intracellular calcium release channels: an update. *J. Physiol.* 595, 3041–3051. doi: 10.1113/JP272781

Sato, D., Clancy, C. E., and Bers, D. M. (2017). Dynamics of sodium current mediated early afterdepolarizations. *Heliyon* 3:e00388. doi: 10.1016/j.heliyon.2017.e00388

Seidler, T., Loughrey, C. M., Zibrova, D., Kettlewell, S., Teucher, N., Kogler, H., et al. (2007). Overexpression of FK-506 binding protein 12.0 modulates excitation contraction coupling in adult rabbit ventricular cardiomyocytes. *Circ. Res.* 101, 1020–1029. doi: 10.1161/circresaha.107.154609

Shannon, T. R., Ginsburg, K. S., and Bers, D. M. (2000). Potentiation of fractional sarcoplasmic reticulum calcium release by total and free intra-sarcoplasmic reticulum calcium concentration. *Biophys. J.* 78, 334–343. doi: 10.1016/s0006-3495(00)76596-9

Shin, D. W., Ma, J., and Kim, D. H. (2000). The asp-rich region at the carboxyl-terminus of calsequestrin binds to Ca(2+) and interacts with triadin. *FEBS Lett.* 486, 178–182. doi: 10.1016/s0014-5793(00)02246-8

Sitsapesan, R., and Williams, A. J. (1994). Regulation of the gating of the sheep cardiac sarcoplasmic reticulum Ca(2+)-release channel by luminal Ca2+. *J. Membr. Biol.* 137, 215–226.

Sivakumaran, V., Stanley, B. A., Tocchetti, C. G., Ballin, J. D., Caceres, V., Zhou, L., et al. (2013). HNO enhances SERCA2a activity and cardiomyocyte function by promoting redox-dependent phospholamban oligomerization. *Antioxid. Redox. Signal.* 19, 1185–1197. doi: 10.1089/ars.2012.5057

Sobie, E. A., Song, L. S., and Lederer, W. J. (2005). Local recovery of Ca2+ release in rat ventricular myocytes. *J. Physiol.* 565(Pt 2), 441–447. doi: 10.1113/jphysiol.2005.086496

Sommese, L., Valverde, C. A., Blanco, P., Castro, M. C., Rueda, O. V., Kaetzel, M., et al. (2016). Ryanodine receptor phosphorylation by CaMKII promotes spontaneous Ca(2+) release events in a rodent model of early stage diabetes: the arrhythmogenic substrate. *Int. J. Cardiol.* 202, 394–406. doi: 10.1016/j.ijcard.2015.09.022

Sondergaard, M. T., Liu, Y., Larsen, K. T., Nani, A., Tian, X., Holt, C., et al. (2017). The Arrhythmogenic calmodulin p.Phe142 leu mutation impairs C-domain Ca2+ binding but not calmodulin-dependent inhibition of the cardiac ryanodine receptor. *J. Biol. Chem.* 292, 1385–1395. doi: 10.1074/jbc.M116.766253

Spencer, C. I., and Sham, J. S. (2003). Effects of Na+/Ca2+ exchange induced by SR Ca2+ release on action potentials and afterdepolarizations in guinea pig ventricular myocytes. *Am. J. Physiol. Heart Circ. Physiol.* 285, H2552–H2562.

Stange, M., Xu, L., Balshaw, D., Yamaguchi, N., and Meissner, G. (2003). Characterization of recombinant skeletal muscle (Ser-2843) and cardiac muscle (Ser-2809) ryanodine receptor phosphorylation mutants. *J. Biol. Chem.* 278, 51693–51702. doi: 10.1074/jbc.m310406200

Steenaart, N. A., Ganim, J. R., Di Salvo, J., and Kranias, E. G. (1992). The phospholamban phosphatase associated with cardiac sarcoplasmic reticulum is a type 1 enzyme. *Arch. Biochem. Biophys.* 293, 17–24. doi: 10.1016/0003-9861(92)90359-5

Stern, M. D., Kort, A. A., Bhatnagar, G. M., and Lakatta, E. G. (1983). Scattered-light intensity fluctuations in diastolic rat cardiac muscle caused by spontaneous Ca++-dependent cellular mechanical oscillations. *J. Gen. Physiol.* 82, 119–153. doi: 10.1085/jgp.82.1.119

Sun, J., Yamaguchi, N., Xu, L., Eu, J. P., Stamler, J. S., and Meissner, G. (2008). Regulation of the cardiac muscle ryanodine receptor by O(2) tension and S-nitrosoglutathione. *Biochemistry* 47, 13985–13990. doi: 10.1021/bi8012627

Suzuki, Y., Demoliere, C., Kitamura, D., Takeshita, H., Deuschle, U., and Watanabe, T. (1997). HAX-1, a novel intracellular protein, localized on mitochondria, directly associates with HS1, a substrate of Src family tyrosine kinases. *J. Immunol.* 158, 2736–2744.

Szabadkai, G., Simoni, A. M., and Rizzuto, R. (2003). Mitochondrial Ca2+ uptake requires sustained Ca2+ release from the endoplasmic reticulum. *J. Biol. Chem.* 278, 15153–15161. doi: 10.1074/jbc.m300180200

Tada, M., Kirchberger, M. A., and Katz, A. M. (1975). Phosphorylation of a 22,000-dalton component of the cardiac sarcoplasmic reticulum by adenosine 3':5'-monophosphate-dependent protein kinase. *J. Biol. Chem.* 250, 2640–2647.

Talukder, M. A., Kalyanasundaram, A., Zhao, X., Zuo, L., Bhupathy, P., Babu, G. J., et al. (2007). Expression of SERCA isoform with faster Ca2+ transport properties improves postischemic cardiac function and Ca2+ handling and decreases myocardial infarction. *Am. J. Physiol. Heart Circ. Physiol.* 293, H2418–H2428.

Talukder, M. A., Kalyanasundaram, A., Zuo, L., Velayutham, M., Nishijima, Y., Periasamy, M., et al. (2008). Is reduced SERCA2a expression detrimental or beneficial to postischemic cardiac function and injury? evidence from

heterozygous SERCA2a knockout mice. *Am. J. Physiol. Heart Circ. Physiol.* 294, H1426–H1434. doi: 10.1152/ajpheart.01016.2007

Terentyev, D., Gyorke, I., Belevych, A. E., Terentyeva, R., Sridhar, A., Nishijima, Y., et al. (2008). Redox modification of ryanodine receptors contributes to sarcoplasmic reticulum Ca2+ leak in chronic heart failure. *Circ. Res.* 103, 1466–1472. doi: 10.1161/CIRCRESAHA.108.184457

Timerman, A. P., Onoue, H., Xin, H. B., Barg, S., Copello, J., Wiederrecht, G., et al. (1996). Selective binding of FKBP12.6 by the cardiac ryanodine receptor. *J. Biol. Chem.* 271, 20385–20391.

Valverde, C. A., Kornyeyev, D., Ferreiro, M., Petrosky, A. D., Mattiazzi, A., and Escobar, A. L. (2010). Transient Ca2+ depletion of the sarcoplasmic reticulum at the onset of reperfusion. *Cardiovasc. Res.* 85, 671–680. doi: 10.1093/cvr/cvp371

Valverde, C. A., Mazzocchi, G., Di Carlo, M. N., Ciocci Pardo, A., Salas, N., Ragone, M. I., et al. (2019). Ablation of phospholamban rescues reperfusion arrhythmias but exacerbates myocardium infarction in hearts with Ca2+/calmodulin kinase II constitutive phosphorylation of ryanodine receptors. *Cardiovasc. Res.* 115, 556–569. doi: 10.1093/cvr/cvy213

Valverde, C. A., Mundina-Weilenmann, C., Reyes, M., Kranias, E. G., Escobar, A. L., and Mattiazzi, A. (2006). Phospholamban phosphorylation sites enhance the recovery of intracellular Ca2+ after perfusion arrest in isolated, perfused mouse heart. *Cardiovasc. Res.* 70, 335–345. doi: 10.1016/j.cardiores.2006.01.018

van Oort, R. J., McCauley, M. D., Dixit, S. S., Pereira, L., Yang, Y., Respress, J. L., et al. (2010). Ryanodine receptor phosphorylation by calcium/calmodulin-dependent protein kinase II promotes life-threatening ventricular arrhythmias in mice with heart failure. *Circulation* 122, 2669–2679. doi: 10.1161/CIRCULATIONAHA.110.982298

Van Petegem, F. (2015). Ryanodine receptors: allosteric ion channel giants. *J. Mol. Biol.* 427, 31–53. doi: 10.1016/j.jmb.2014.08.004

Van Petegem, F. (2019). Slaying a giant: structures of calmodulin and protein kinase a bound to the cardiac ryanodine receptor. *Cell Calcium* 83:102079. doi: 10.1016/j.ceca.2019.102079

Venetucci, L. A., Trafford, A. W., and Eisner, D. A. (2007). Increasing ryanodine receptor open probability alone does not produce arrhythmogenic calcium waves: threshold sarcoplasmic reticulum calcium content is required. *Circ. Res.* 100, 105–111. doi: 10.1161/01.res.0000252828.17939.00

Vila-Petroff, M., Salas, M. A., Said, M., Valverde, C. A., Sapia, L., Portiansky, E., et al. (2007). CaMKII inhibition protects against necrosis and apoptosis in irreversible ischemia-reperfusion injury. *Cardiovasc. Res.* 73, 689–698. doi: 10.1016/j.cardiores.2006.12.003

Vittone, L., Mundina-Weilenmann, C., Said, M., Ferrero, P., and Mattiazzi, A. (2002). Time course and mechanisms of phosphorylation of phospholamban residues in ischemia-reperfused rat hearts. dissociation of phospholamban phosphorylation pathways. *J. Mol. Cell. Cardiol.* 34, 39–50. doi: 10.1006/jmcc.2001.1488

Völkers, M., Loughrey, C. M., Macquaide, N., Remppis, A., DeGeorge, BR. Jr., Wegner, F. V., et al. (2007). S100A1 decreases calcium spark frequency and alters their spatial characteristics in permeabilized adult ventricular cardiomyocytes. *Cell Calcium* 41, 135–143. doi: 10.1016/j.ceca.2006.06.001

Volkers, M., Rohde, D., Goodman, C., and Most, P. (2010). S100A1: a regulator of striated muscle sarcoplasmic reticulum Ca2+ handling, sarcomeric, and mitochondrial function. *J. Biomed. Biotechnol.* 2010, 178614. doi: 10.1155/2010/178614

Wehrens, X. H., Lehnart, S. E., Huang, F., Vest, J. A., Reiken, S. R., Mohler, P. J., et al. (2003). FKBP12.6 deficiency and defective calcium release channel (ryanodine receptor) function linked to exercise-induced sudden cardiac death. *Cell* 113, 829–840. doi: 10.1016/s0092-8674(03)00434-3

Wehrens, X. H., Lehnart, S. E., Reiken, S., Vest, J. A., Wronska, A., and Marks, A. R. (2006). Ryanodine receptor/calcium release channel PKA phosphorylation: a critical mediator of heart failure progression. *Proc. Natl. Acad. Sci. U.S.A.* 103, 511–518. doi: 10.1073/pnas.0510113103

Wehrens, X. H., Lehnart, S. E., Reiken, S. R., and Marks, A. R. (2004). Ca2+/calmodulin-dependent protein kinase II phosphorylation regulates the cardiac ryanodine receptor. *Circ. Res.* 94, e61–e70.

Weiss, J. N., Garfinkel, A., Karagueuzian, H. S., Chen, P. S., and Qu, Z. (2010). Early afterdepolarizations and cardiac arrhythmias. *Heart Rhythm* 7, 1891–1899. doi: 10.1016/j.hrthm.2010.09.017

Weiss, J. N., Nivala, M., Garfinkel, A., and Qu, Z. (2011). Alternans and arrhythmias: from cell to heart. *Circ. Res.* 108, 98–112. doi: 10.1161/CIRCRESAHA.110.223586

Whayne, T. F. Jr. (2018). Clinical Use of Digitalis: a State of the art review. *Am. J. Cardiovasc. Drugs* 18, 427–440. doi: 10.1007/s40256-018-0292-1

Wier, W. G., Cannell, M. B., Berlin, J. R., Marban, E., and Lederer, W. J. (1987). Cellular and subcellular heterogeneity of [Ca2+]i in single heart cells revealed by fura-2. *Science* 235, 325–328. doi: 10.1126/science.3798114

Wier, W. G., and Hess, P. (1984). Excitation-contraction coupling in cardiac Purkinje fibers. effects of cardiotonic steroids on the intracellular [Ca2+] transient, membrane potential, and contraction. *J. Gen. Physiol.* 83, 395–415. doi: 10.1085/jgp.83.3.395

Witcher, D. R., Kovacs, R. J., Schulman, H., Cefali, D. C., and Jones, L. R. (1991). Unique phosphorylation site on the cardiac ryanodine receptor regulates calcium channel activity. *J. Biol. Chem.* 266, 11144–11152.

Xiao, B., Jiang, M. T., Zhao, M., Yang, D., Sutherland, C., Lai, F. A., et al. (2005). Characterization of a novel PKA phosphorylation site, serine-2030, reveals no PKA hyperphosphorylation of the cardiac ryanodine receptor in canine heart failure. *Circ. Res.* 96, 847–855. doi: 10.1161/01.res.0000163276.26083.e8

Xiao, B., Zhong, G., Obayashi, M., Yang, D., Chen, K., Walsh, M. P., et al. (2006). Ser-2030, but not Ser-2808, is the major phosphorylation site in cardiac ryanodine receptors responding to protein kinase a activation upon beta-adrenergic stimulation in normal and failing hearts. *Biochem. J.* 396, 7–16. doi: 10.1042/bj20060116

Xiao, J., Tian, X., Jones, P. P., Bolstad, J., Kong, H., Wang, R., et al. (2007). Removal of FKBP12.6 does not alter the conductance and activation of the cardiac ryanodine receptor or the susceptibility to stress-induced ventricular arrhythmias. *J. Biol. Chem.* 282, 34828–34838. doi: 10.1074/jbc.m707423200

Xie, Y., Sato, D., Garfinkel, A., Qu, Z., and Weiss, J. N. (2010). So little source, so much sink: requirements for afterdepolarizations to propagate in tissue. *Biophys. J.* 99, 1408–1415. doi: 10.1016/j.bpj.2010.06.042

Xu, K. Y., Zweier, J. L., and Becker, L. C. (1997). Hydroxyl radical inhibits sarcoplasmic reticulum Ca(2+)-ATPase function by direct attack on the ATP binding site. *Circ. Res.* 80, 76–81. doi: 10.1161/01.res.80.1.76

Xu, L., Eu, J. P., Meissner, G., and Stamler, J. S. (1998). Activation of the cardiac calcium release channel (ryanodine receptor) by poly-S-nitrosylation. *Science* 279, 234–237. doi: 10.1126/science.279.5348.234

Xu, L., and Meissner, G. (1998). Regulation of cardiac muscle Ca2+ release channel by sarcoplasmic reticulum lumenal Ca2+. *Biophys. J.* 75, 2302–2312. doi: 10.1016/s0006-3495(98)77674-x

Yamaguchi, N., Xu, L., Pasek, D. A., Evans, K. E., Chen, S. R., and Meissner, G. (2005). Calmodulin regulation and identification of calmodulin binding region of type-3 ryanodine receptor calcium release channel. *Biochemistry* 44, 15074–15081. doi: 10.1021/bi051251t

Yang, D., Zhu, W. Z., Xiao, B., Brochet, D. X., Chen, S. R., Lakatta, E. G., et al. (2007). Ca2+/calmodulin kinase II-dependent phosphorylation of ryanodine receptors suppresses Ca2+ sparks and Ca2+ waves in cardiac myocytes. *Circ. Res.* 100, 399–407. doi: 10.1161/01.res.0000258022.13090.55

Yang, Y., Zhu, W. Z., Joiner, M. L., Zhang, R., Oddis, C. V., Hou, Y., et al. (2006). Calmodulin kinase II inhibition protects against myocardial cell apoptosis in vivo. *Am. J. Physiol. Heart Circ. Physiol.* 291, H3065–H3075.

Yellon, D. M., and Hausenloy, D. J. (2007). Myocardial reperfusion injury. *N. Engl. J. Med.* 357, 1121–1135.

Zahradnik, I., Gyorke, S., and Zahradnikova, A. (2005). Calcium activation of ryanodine receptor channels–reconciling RyR gating models with tetrameric channel structure. *J. Gen. Physiol.* 126, 515–527. doi: 10.1085/jgp.200509328

Zamparelli, C., Macquaide, N., Colotti, G., Verzili, D., Seidler, T., Smith, G. L., et al. (2010). Activation of the cardiac Na(+)-Ca(2+) exchanger by sorcin via the interaction of the respective Ca(2+)-binding domains. *J. Mol. Cell Cardiol.* 49, 132–141. doi: 10.1016/j.yjmcc.2010.03.003

Zhang, L., Kelley, J., Schmeisser, G., Kobayashi, Y. M., and Jones, L. R. (1997). Complex formation between junctin, triadin, calsequestrin, and the ryanodine receptor. proteins of the cardiac junctional sarcoplasmic reticulum membrane. *J. Biol. Chem.* 272, 23389–23397. doi: 10.1074/jbc.272.37.23389

Zhang, R., Khoo, M. S., Wu, Y., Yang, Y., Grueter, C. E., Ni, G., et al. (2005). Calmodulin kinase II inhibition protects against structural heart disease. *Nat. Med.* 11, 409–417. doi: 10.1038/nm1215

Zorov, D. B., Filburn, C. R., Klotz, L. O., Zweier, J. L., and Sollott, S. J. (2000). Reactive oxygen species (ROS)-induced ROS release: a new phenomenon accompanying induction of the mitochondrial permeability transition in cardiac myocytes. *J. Exp. Med.* 192, 1001–1014.

Zucchi, R., and Ronca-Testoni, S. (1997). The sarcoplasmic reticulum Ca2+ channel/ryanodine receptor: modulation by endogenous effectors, drugs and disease states. *Pharmacol. Rev.* 49, 1–51.

Conflict of Interest: The authors declare that the research was conducted in the absence of any commercial or financial relationships that could be construed as a potential conflict of interest.

Advantages of publishing in Frontiers

OPEN ACCESS
Articles are free to read for greatest visibility and readership

FAST PUBLICATION
Around 90 days from submission to decision

HIGH QUALITY PEER-REVIEW
Rigorous, collaborative, and constructive peer-review

TRANSPARENT PEER-REVIEW
Editors and reviewers acknowledged by name on published articles

Frontiers
Avenue du Tribunal-Fédéral 34
1005 Lausanne | Switzerland

Visit us: www.frontiersin.org
Contact us: info@frontiersin.org | +41 21 510 17 00

REPRODUCIBILITY OF RESEARCH
Support open data and methods to enhance research reproducibility

DIGITAL PUBLISHING
Articles designed for optimal readership across devices

FOLLOW US
@frontiersin

IMPACT METRICS
Advanced article metrics track visibility across digital media

EXTENSIVE PROMOTION
Marketing and promotion of impactful research

LOOP RESEARCH NETWORK
Our network increases your article's readership